



**Bruno Alexandre
Abreu Silva**

**Caracterização e Modelação do Comportamento
Reológico de Nanofluidos**

**Rheological Characterization and Modelling of CNT
Nanofluids**



**Bruno Alexandre
Abreu Silva**

**Caracterização e Modelação do Comportamento
Reológico de Nanofluidos**

Tese apresentada à Universidade de Aveiro para cumprimento dos requisitos necessários à obtenção do grau de Doutor em Sistemas Energéticos e Alterações Climáticas, realizada sob a orientação científica da Doutora Mónica Sandra Abrantes de Oliveira Correia, Professor Auxiliar do Departamento de Engenharia Mecânica da Universidade de Aveiro e coorientação do Doutor Nelson Amadeu Dias Martins Professor Auxiliar do Departamento de Engenharia Mecânica da Universidade de Aveiro

Apoio financeiro da FCT e do FSE no âmbito do III Quadro Comunitário de Apoio.



Universidade de Aveiro Departamento de Engenharia Mecânica
Ano 2018

**Bruno Alexandre
Abreu Silva**

**Rheological Characterization and Modelling of CNT
Nanofluids**

“The true sign of intelligence is not knowledge but imagination” Albert Einstein

o júri

presidente

Prof. Doutor Vitor António Ferreira da Costa
professor catedrático da Universidade de Aveiro

Prof. Doutor João Miguel Amorim Novais Costa Nóbrega
professor associado da Universidade do Minho

Prof. Doutor Abel Gomes Martins Ferreira
professor associado da Faculdade de Engenharia da Universidade do Porto

Prof. Doutor António Gil D'Orey de Andrade Campos
professor auxiliar da Universidade de Aveiro

Prof. Doutora Mónica Sandra Abrantes de Oliveira Correia
professor auxiliar da Universidade de Aveiro

agradecimentos

I express my gratitude to my supervisors Doctor Mónica Oliveira and Nelson Martins, assistant professors at the Department of Mechanical Engineering from the University of Aveiro, for their support and guidance.

I am also very grateful to Doctor Alexandra Fonseca and Doctor Bruno Lamas, for their assistance during the nanofluids engineering and empirical characterization.

In addition, I want to express my sincere acknowledge to Dra. Helena Nogueira, and Dra. Celeste Azevedo from University of Aveiro for their support with the spectroscopic studies (FTIR), to Dra. Sandra Magina from University of Aveiro for her support with the thermo gravimetric analysis (TGA), to Joana Catarina Mendes from Instituto de Telecomunicações (IT) from University of Aveiro and to Eng. Pedro Prazeres for his assistance with the analytical centrifuge measurements.

I also acknowledge Fundação para a Ciência e Tecnologia (FCT) and Fundo Social Europeu (FSE), for the financial support through the individual grant (SFRH/BD/95356/2013)

Finally, I am very grateful for my wonderful Parents, Vasco and Fátima Silva for the continuous and unconditional love and support. I could not have come thus far without you.

palavras-chave

Nanofluidos, reologia, viscosidade, nanotubos de carbono de múltiplas paredes; estabilidade coloidal; fluidos térmicos avançados

resumo

A sustentabilidade energética é um dos principais desafios para o século XXI. A tecnologia intrínseca à Desta forma, as técnicas de produção, transporte e distribuição de energia necessita de uma maior eficiência energéticas associada, tendo todos os sistemas energéticos um papel fundamental na industria. O transporte de energia sob a forma de calor é normalmente efectuado por recurso a sistemas de convecção forçada, sendo a sua eficiência limitada pela área de troca de calor e/ou pelas propriedades do fluido operante. Deste modo, o desenvolvimento e caracterização de novos fluidos detentores de maior eficiência de permuta assume maior importância, dadas as aplicações em várias áreas de engenharia, nomeadamente a defesa, a exploração espacial, transportes, ou qualquer outro sistema onde a miniaturização acoplada a um elevado grau de transferência de calor seja necessária.

Os nanofluidos surgem no sentido de dar resposta a estes desafios, contribuindo para o desenvolvimento mais sustentável da sociedade. Contudo, a falta de uma técnica padrão para a sua preparação, associada ao conhecimento empírico das suas propriedades termofísicas e suportado por modelos físico-matemáticos devidamente validados, são sérios entraves à adoção desta tecnologia por parte da indústria.

Neste trabalho, estudou-se de forma sistemática a viscosidade de nanofluidos de base aquosa aditivados com nanotubos de carbono de múltiplas paredes, tendo em vista o desenvolvimento de um modelo físico-matemático capaz de descrever o comportamento reológico destes fluidos. Com este objetivo, produziram-se nanofluidos com elevada estabilidade coloidal, tendo-se dado particular ênfase à reprodutibilidade e rigor da técnica utilizada para a sua produção.

Por recurso a um desenho de experiências, foi desenvolvido um plano experimental, tendo o mesmo resultado numa base de dados de propriedades termofísicas em função de fatores de controlo previamente identificados, nomeadamente fluido base, temperatura, taxa de corte, tamanho, concentração dos nanotubos de carbono de múltiplas paredes. A análise paramétrica levada a efeito, permitiu concluir que os fatores de controlo que têm uma maior influência sobre o comportamento reológico do nanofluido são a concentração de nanopartículas, a taxa de corte, a temperatura e por fim o tamanho das partículas. Tendo por base todos estes resultados, foi desenvolvido e validado um modelo físico-matemático capaz de determinar a viscosidade dinâmica e o comportamento reológico de nanofluidos.

keywords

Nanofluids, rheology, viscosity, multi-walled carbon nanotubes, colloidal stability and advanced heat transfer fluids.

abstract

Energy sustainability is one of the major challenges for the twenty-first century. Intrinsic technology for energy production, transmission and distribution requires a higher associated energy efficiency, with all energy systems playing a key role in industry. The transport of energy in the form of heat is usually accomplished by means of forced convection systems, its efficiency being limited by the area of heat exchange and/or by the properties of the working fluid. In this way, the development and characterization of new fluids with higher exchange efficiency is of greater importance, given the applications in several engineering areas, namely defense, space, transportation, or any other system where miniaturization coupled with high degree of heat transfer is required.

Nanofluids arise in order to respond to these challenges, contributing to the more sustainable development of society. However, the lack of a standard technique for its preparation, coupled with the empirical knowledge of its thermo-physical properties, supported by duly validated physic-mathematical models, are serious obstacles to the adoption of this technology by the industry. In this work, the viscosity of MWCNTs (Multi Walled Carbon Nanotubes) water-based nanofluids was systematically studied, in order to develop a physic-mathematical model capable of describing the rheological behavior of these fluids. With this perspective, nanofluids with colloidal stability were produced, with particular emphasis on the reproducibility and accuracy of the technique used for their production.

By using DOE (Design of Experiment), an experimental plan was developed. The latter enable to gather a database of thermo-physical properties as a function of previously identify control factors, namely: base fluid, temperature, shear rate, and MWCNTs size and concentration. The parametric analysis carried out has allowed to established that the control factors that have a greater influence on the rheological behavior of the nanofluid are the concentration of nanoparticles, the shear rate, the temperature and, finally, the particle size. Based on all these results, a physic-mathematical model was developed and validated to determine the dynamic viscosity and rheological behavior of nanofluids.

Table of Contents

TABLE OF CONTENTS	1
LIST OF FIGURES.....	3
LIST OF TABLES.....	5
NOMENCLATURE.....	7
CHAPTER 1 - INTRODUCTION.....	13
1.1 THESIS BACKGROUND & MOTIVATION	13
1.2 STATEMENT OF THE PROBLEM AND GENERAL OBJECTIVES.....	17
1.3 LITERATURE REVIEW	17
1.4 THESIS SPECIFIC OBJECTIVES AND RESEARCH QUESTIONS.....	73
1.5 THESIS CONTRIBUTION	74
1.6 THESIS ORGANIZATION	77
CHAPTER 2 - DISPERSIONS.....	79
2.1 OVERVIEW.....	79
2.2 DEFINITION OF A FLUID	80
2.3 FLUID KINEMATICS.....	81
2.4 RHEOLOGICAL MODELS.....	86
2.5 RHEOLOGY OF COLLOIDS.....	90
2.6 RHEOLOGY OF SUSPENSIONS: MEASUREMENT OF THE MACROSCOPIC PROPERTIES.....	94
2.7 CHAPTER CONCLUSIONS.....	103
CHAPTER 3 - MWCNTS BASED NANOFLUIDS ENGINEERING	105
3.1 INTRODUCTION	105
3.2 STABILITY MECHANISMS OF NANOFLUIDS.....	107
3.3 DESIGN OF EXPERIMENTS	117
3.4 SURFACE MODIFICATION TECHNIQUES	122

3.5	SIZE DISTRIBUTION EVALUATION.....	127
3.6	STABILITY INTEGRITY EVALUATION	128
3.7	CHAPTER CONCLUSIONS	131
CHAPTER 4 - EXPERIMENTAL DETERMINATION OF NANOFUIDS PROPERTIES .		133
4.1	LONG-TERM MWCNTS NANOFUIDS QUALITY ASSESSMENT.....	133
4.2	STRUCTURAL INTEGRITY.....	133
4.3	NANOFUIDS DENSITY EVALUATION	142
4.4	BRIEF DISCUSSION	148
4.5	CHAPTER CONCLUSIONS.....	148
CHAPTER 5 - EXPERIMENTAL ASSESSMENT OF NANOFUIDS RHEOLOGICAL PROPERTIES.....		151
5.1	OVERVIEW.....	151
5.2	NANOFUIDS VISCOSITY MEASUREMENTS.....	151
5.3	NANOFUIDS EFFECTIVE VISCOSITY.....	158
5.4	RHEOLOGY MODELLING OF MWCNTS NANOFUIDS.....	168
5.5	CHAPTER CONCLUSIONS.....	183
CHAPTER 6 - CONCLUSIONS		185
6.1	CONCLUSIONS.....	186
6.2	FUTURE WORK.....	192
REFERENCES.....		195
APPENDIX		219

List of Figures

Figure 1.1 - Typical rheological behaviour for fluids: (a) shear stress as a function of shear rate; (b) viscosity as a function of shear rate.....	30
Figure 1.2 - Schematic 2D representation: (a) Concentric Cylinders; (b) Cone and Plate; (c) Parallel-Plate.....	34
Figure 1.3 - Rheology behaviour of nanofluids composed by aggregates with strong and weak attraction forces [159].....	40
Figure 1.4 - Suspension structure/viscosity as a function of shear rate [159].....	41
Figure 1.5 - Classical models summary for the same concentration at 300 K.....	53
Figure 1.6 - Spherical models predicted viscosity for a suspension of 30% Ethylene Glycol-Water and different concentrations of nanoparticles at 300 K.....	63
Figure 1.7 - Non-Spherical models predicted viscosity for a suspension of 30% Ethylene Glycol-Water and different concentrations of nanoparticles at 300 K.....	64
Figure 1.8 - Summary of the experimental data available on the open literature for nanofluids.....	76
Figure 2.1 - Particle motion in shear and extensional flows.....	81
Figure 2.2 - Three-dimensional stress state: definition of the stress tensor components.....	83
Figure 2.3 - Schematic of a one dimension unidirectional flow.....	84
Figure 2.4 - Schematic representation of the interactions of particle with shear flow....	91
Figure 3.1 - Schematic microstructure representation: (a) diluted; (b) semi-diluted; (c) percolation like structure.....	106
Figure 3.2 - Distortion of flow streamlines around a settling particle and forces acting.....	111
Figure 3.3 - SEM image of (a) Bulk MWCNTs and (b) Functionalized MWCNTs.....	127
Figure 3.4 - Schematic representation of the measuring principle of the LUMiSizer Stability Analyser.....	131
Figure 4.1 - FTIR spectrum for bulk and functionalized D20-40 L1-2 MWCNTs.....	135
Figure 4.2 - Zeta Potential of the studies samples.....	136
Figure 4.3 - Schematic representation of the methodology used to assess the size evaluation of the MWCNTs.....	137
Figure 4.4 - Diameter distribution of the D20-40 L1-2.....	138
Figure 4.5 - Length distribution of the D20-40 L1-2.....	139

Figure 4.6 – Proposed model for the diameter (a) and length (b) of functionalized MWCNTs.	141
Figure 4.7 – Transmission Profile of the sample D20-40 L1-2 in 30EG+DW with (a) 0,25% vol. (b) 0,75%vol and (c) 1,5%vol of MWCNTs at 500 G's.	145
Figure 4.8 – Settling velocity as a function of the RCF for the nanoparticle D20-40 L1-2	146
Figure 4.9 – Settling velocity for all the nanofluids study for RCF=1 (a) DW+30EG (b) DW+60EG.	147
Figure 5.1 – Schematic Representation of the flow between two concentric cylinders	152
Figure 5.2 – Viscosity Calibration Curve for (a) 30%EG + DW and (b) 60EG + DW.	155
Figure 5.3 – Base fluid shear rate as a function of shear rate for (a) 30EG+DW and (b) 60EG+DW	157
Figure 5.4 – Main effects of the MWCNTs aspect ratio on the experimental viscosity...	162
Figure 5.5 – Main Effects of the MWCNTs (a) length and (b) diameter	163
Figure 5.6 – Main effects of the volume fraction on the experimental visocsity	164
Figure 5.7 – Main Effects of the base fluid in the experimental viscosity	165
Figure 5.8 – Main effects of the temperature in the experimental viscosity.....	166
Figure 5.9 – Main effects of the applied shear rate in the experimental viscosity.....	167
Figure 5.10 – Main effect analysis of the volume fraction of MWCNTs for different shear rates.	173
Figure 5.11 – Main effect of the relative viscosity as a function of the shear rate and the MWCNTs volume fraction.	174
Figure 5.12 – Effect of the MWCNTs volume fraction on the Reynolds number.....	175
Figure 5.13 – Main effects of the volume fraction of MWCNTs for different temperatures.	176
Figure 5.14 – Inverse Schmidt as a function of the temperature	177
Figure 5.15 – Scatter chart of the proposed model and experimental data.....	181
Figure 5.16 – Relation between the proposed model and other models for non-spherical nanoparticles.	183

List of Tables

Table 1.1 – Thermal and transport properties of conventional working fluids @ 295 K [1].....	14
Table 1.2 - Literature survey of some characteristics concerning the engineering of CNTs nanofluids and stability evaluation.....	25
Table 1.3 - Proposed Mechanisms for the viscosity of nanofluids	38
Table 1.4 – Viscosity Model Summary.....	52
Table 1.5 – Summary of the effective viscosity models and respective control parameters	65
Table 1.6 – Summary of experimental studies of viscosity of spherical particles based nanofluids.....	66
Table 1.7 – Summary of experimental studies of viscosity of non-spherical particles based nanofluids.....	70
Table 1.8 – Summary of the effective viscosity models and respective proposed mechanisms	75
Table 2.1 – Power-Law index values for some non-Newtonian fluids	89
Table 2.2 – Variable affecting the rheology of MWCNTs	100
Table 3.1 – Expected relation of the control factor on the mechanisms governing the rheology	117
Table 3.2 – Nanoparticles characteristics and selected geometries.....	118
Table 3.3 – Control factors and their range of setting for the experiments	120
Table 3.4 – Nanoparticles and base fluid quantities for the preparation of the samples	125
Table 4.1 – Weight loss ratio for bulk and functionalized MWCNTs at 320 and 1000 K.	134
Table 4.2 – Sample Size distribution from SEM images	139
Table 4.3 – Geometrical properties of the measured MWCNTs	140
Table 4.4 – Adjustments factors for the exponential regression for the diameter, length and aspect ratio.....	140
Table 4.5 – Predicted geometrical properties of the MWCNTs.....	142
Table 4.6 – MWCNTs nanofluid density measurements @ 305 K	143
Table 4.7 – LUMiSizer Stability analyser measuring conditions	143
Table 5.1 - Viscosity accuracy intervals for the selected spindle/speed configuration.	154

Table 5.2 – Theoretical and experimental viscosity achieved in the experimental apparatus.....	156
Table 5.3 – Average and maximum results obtained experimentally for each MWCNT geometry.....	160
Table 5.4 – Multi factor analysis of variance (ANOVA) of the experimental viscosity ...	161
Table 5.5 – Fitness estimators of some models available in the literature to the experimental results.....	182

Nomenclature

A	Area [m ²]
Q	Heat [W]
H	Convection Coefficient [W/m ² K]
T	Temperature [K]
Nu	Nusselt Number
K	Thermal Conductivity [W/mK]
L	Length [m]
Re	Reynolds Number
Pr	Prandtl Number
HVT	Hydrodynamic Viscosity Theory
CNT	Carbon Nanotube
MWCNT	Multi Walled Carbon Nanotube
SWCNT	Single Walled Carbon Nanotube
Al ₂ O ₃	Alumina / Aluminium Oxide
TiO ₂	Titania / Titanium Oxide
Cu	Copper
CuO	Copper Oxide
DW	Distilled Water
EG	Ethylene Glycol
EO	Engine Oil
DWCNT	Double Walled Carbon Nanotube
CCVD	Catalytic Chemical Vapour Deposition
COOH	Carboxylic Groups
EDL	Electric Double Layer
TGA	Thermogravimetric Analysis
SEM	Scanning Electron Microscope
TEM	Transmission Electron Microscope
PG	Polyethylene Glycol
HSM	High Speed Mixer
MS	Mechanical Stirrer
BM	Ball Mixing
US	Ultrasound

HPH	High Pressure Homogenizer
UV	Ultraviolet Spectroscopy
VE	Visual Evaluation
UH	Ultrasound Homogenizer
UB	Ultrasound Bath
MS	Mechanical Stirring
Gly	Glycerine
SO	Silicone Oil
AT	Acid Treatment
PT	Plasma Treatment
TA	Turbidity analysis
ASTM	American Society for Testing Materials
ISO	International Standards Organization
a, d, r	Particle Radius
k	Conductivity (Electrical or Thermal)
F	Axial Ratio
k_b	Boltzmann's Constant
C_f	Crowding Factor
H	Interparticle Distance
k_e	Einstein Constant
k_h	Huggin's Constant
Ni	Nickle
V_B	Brownian Velocity
d_f	Equivalent Diameter
M	Molecular Weight
N	Avogadro number
T	Time
G	Gravity Acceleration
t^*	Reduce Time
Pe	Peclet Number
D_S	Equivalent Diameter
D_r	Diffusion Coefficient
Sc	Schmidt Number
F_B	Buoyancy Force
F_G	Gravitational Force
F_R	Resistance or Friction Force

V_{Sed}	Sedimentation Velocity
V_{Stokes}	Stokes Settling Velocity
V_{hind}	Hindering Settling Velocity
F_{hind}	Hindrance Function
D_{Volume}	Volume Equivalent Diameter
$D_{Surface}$	Surface Equivalent Diameter
D_{Stokes}	Stokes Equivalent Diameter
DOE	Design of Experiments
HNO ₃	Nitric Acid
H ₂ SO ₄	Sulphuric Acid
m	Mass [kg]
AR	Aspect Ratio
e	Electronic charge

Greek Simbols

ζ	Electro Kinetic Potential (Zeta Potential)
$\sigma, \sigma_{ij}, \tau_{ij}$	Shear [Pa]
$\gamma, \dot{\gamma}$	Strain Rate [s ⁻¹]
μ	Viscosity [mPa.s or cPs]
ϕ	Volume Fraction
ϵ	Dielectric Constant
u	Geometric Constant
ϕ_{max}	Packing Fraction Maximum
ϕ^*	Shape Depended Critical Volume Fraction
ρ	Density
δ	Distance Between Adjacent Particles
ϕ_H	Hydrodynamic Volume Fraction
δ_{ij}	Kronecker Delta

Subscripts

eff	Effective
bf, BF	Base Fluid
max	Maximum

p	Particle
np	Nanoparticle
B	Brownian
nf	Nanofluid
rel	Relative
MWCNT	Multi Walled Carbon nanotube
Sed	Sedimentation

Chapter 1 - Introduction

1.1 Thesis Background & Motivation

Humankind is the first known species depending on technology to maintain and improve its living standard. Current days technology development trends emphasise increasingly efficient and miniaturized systems and tools. As miniaturization progresses, thermal-energy management technologies face additional challenges, many times playing a serious constrains or even a restrictive role on the development and dematerialization of these systems and processes. The improvement of the heat transfer intensification in engineering systems is, therefore, detrimental to achieve a higher level of technology development. A known example is the continuous miniaturization of electronic devices, which increases the demand for new, compact and more efficient heat transfer technologies, being the latter a major limitation to the continuous development of this technological area. It is a fact that heat transfer is one of the major hindrances to increase performance of many of these systems and devices. In most cases, heat transfer is accomplished through forced convection systems, which require a fluid (e.g. water, air, oil) as exchange media. This phenomenon (energy movement) obeys to *Newton's law of cooling (Eq.1.1)*, which states that the improvement of heat transfer can be achieved through: the increase of the heat transfer area (A); the increase of the temperature difference (ΔT); or by increasing the convective heat transfer coefficient (h) [1].

$$Q = h \cdot A \cdot \Delta T \qquad \text{Eq. 1.1}$$

As increasing the exchange surface area or the temperature difference may not be possible, due to miniaturization or material constraints. Nevertheless, new technologies are being sought, such as: heat pipes, micro-channel heat exchangers, phase-change materials, metallic foams, among others [2]. Other technologies attempt to increase the overall convective heat transfer coefficient (Eq. 1.2), which is the ratio between the *Nusselt number (Nu)* and the

thermal conductivity (k) by the characteristic length of the heat transfer exchanging surface (L).

$$h = \frac{Nu K}{L} \quad \text{Eq. 1.2}$$

Enhancing the heat transfer coefficient can be achieved by increasing the thermal conductivity of the operant fluid or by increasing the pumping velocity. The latter, results in an increase of the *Nusselt* number (Nu) that is a function of the *Reynolds* number (Re) and the *Prandtl* number (Pr), or in other words, a function of the fluid properties and the ratio of inertial to viscous forces. Thus, regardless the adopted technology, these systems will always be limited by the thermal and transport properties of the working fluid. Heat transfer intensification can thus be achieved by optimizing the thermal properties with a minimum penalty to the transport properties of the heat transfer fluids.

Table 1.1, presents some thermal and transport properties of conventional working fluids and some solid materials. As it can be depicted, fluids present a considerably lower thermal conductivity than solid materials. It became clear, then, that a mixture between highly conductive solid particles and conventional fluids could improve the overall heat transfer capability.

Table 1.1 – Thermal and transport properties of conventional working fluids @ 295 K [1]

Properties		Fluids				Solids		
		Air	Water	Ethylene Glycol	Oil	Copper	Aluminium	Carbon Nanotubes
Thermal Conductivity	[W/m.K]	0,0116	0,613	0,252	0,145	401	237	3000
Viscosity	[Pa.s]	1,7E-5	0,001	0,016	0,999	---	---	---
Density	[g/cm ³]	1205	0,997	1,114	0,890	8,933	2,702	2,100
Specific Heat	[kJ/kg.K]	1,005	4,179	2,415	1,868	385	903	0,71

In fact, particulate suspensions can be widely found in nature, it was in the XIX century that Maxwell conducted an empirical work in an attempt to increase the conductivity of liquids, by suspending millimetre and micrometre sized particles in fluids {Maxwell:2014va}. Since then, many studies have been devoted to evaluate and tailor the properties of these systems.

In 1906, Einstein derived the well-known viscosity equation and presented a relationship to describe the effective contribution of rigid spheres on the viscosity of dilute suspensions [5]. The Hydrodynamic Viscosity Theory (*HVT*) emerged from this work, establishing a connexion between the dissipation of the mechanical energy into heat (solvent), subtracting the energy dissipation in the portion of particles (solute) [6].

As the theory of Einstein only reflects on diluted suspensions of non-interacting spherical particles, several models were proposed to extend the HVT. These upgraded models add to the HVT the effect produced by non-diluted concentrations of particles, particles interactions, particle orientation percolation network behaviour and particles Brownian motion [5], [7]-[10].

The incorporation of millimetre and micrometre sized particles in suspensions have been widely used in industry. However, the latter present rapid sedimentation due to their high specific length, causing a fast decay of the engineered properties, increase pressure drop and can clog channels [3], [4], [11].

In 1991, Iijima [12] opened up a new era in material science with the discovery of carbon nanotubes (CNTs). Since then, many researchers used this new material to develop new functional composite materials with advanced and tailored properties. The word *Nanofluid* was first used by Choi to describe an innovative class of suspensions for heat transfer applications [13]. They have reported that the dispersion of small concentrations of nano-sized particles in a base fluid, lead to significant improvements on the effective thermal conductivity, with low penalty on the pressure drop. Since then, many theoretical and empirical researchers gained interest on this new class of colloids for heat transfer intensification. Subsequently, properly engineered thermal nanofluids detain the following advantages [14]:

- Tailored properties, including thermal conductivity, viscosity, specific heat and density.
- Low pressure drop penalty
- Higher dispersion stability and a lower particle clogging
- Possibility to be introduced both in miniaturized or conventional thermal systems

In tandem with thermal conductivity, viscosity is one of the most studied properties in nanofluid technology. However, investigations regarding the rheological behaviour of carbon based nanofluids are very scarce, when compared to other types of nanoparticles [15]-[19]. Nevertheless, some theories have been recently proposed in an attempt to model the rheological behaviour of these next generation engineering fluids, but, apparently, without success [20], [21]. As expected, the dissimilarity between theoretical premises and also the different methodologies from synthesis to characterization among research groups, cause unrelated results, therefore, contributing to a lack of confidence on the effective transport properties prediction.

As previously stated, nanofluids are suspensions of particles having at least one dimension less than 100nm in conventional fluids. At this scale, particles exhibit unique physical properties from the corresponding bulk materials. Also, the large surface area (>300% than microparticles) increases the surface-to-volume making the production of stable suspensions possible [22], [23]. Furthermore, the large density number and surface structure (20% of their atoms near the surface) allows nanoparticles to absorb and transfer heat more efficiently [24].

The distinctive features of nanofluids show great promise as the next-generation of heat transfer fluids. Unlike suspensions containing larger particles, nanofluids require low volume concentrations ($\leq 2\%$) of nanoparticles to significantly improve heat transfer efficiency, while increasing the stability and reducing the severe clogging problem [22], [23]. Moreover, the potential market for nanofluids applications is estimated over 1,7 Billion Euros per year worldwide and growing [25].

Besides water, energy will become the most important commodity for humankind., therefore, any technology capable of receiving, storing and/or transport energy in a sustainable and efficient fashion, will be of great interest. The successful employment of nanofluids will be detrimental to support the current trends towards system miniaturization, while improving the energy efficiency in industrial systems and processes.

1.2 Statement of the Problem and General objectives

In the known literature, investigations regarding the rheological behaviour of suspensions of carbon-based nanofluids are scarce. Moreover, the models proposed for predicting the viscosity and consequently the rheological behaviour of nanofluids are not consensual and lack the acceptable level of accuracy for engineering purposes.

Nevertheless, from the limited experimental results available from other researchers, it is known that the effective viscosity of nanofluids may depend upon several parameters, including nanoparticle geometry and spatial distribution, their concentration, temperature, base fluid type and density and also the shear stress. However, given the lack of a comprehensive empirical assessment of this property (viscosity), emphasis must be given to the study of this particular field and promising research line.

A comprehensive experimental investigation, supported by a well-designed parametric study is a pre-condition to identify the mechanisms responsible for the rheological behaviour in nanofluids. More, these empirical results will enable the development and validation of a general physical model, capable of evaluating the effective viscosity and rheological behaviour of nanofluids.

So, it is of utmost importance the development of a complete property database supported by reliable predictive models of nanofluids properties. Such information is essential to accelerate the introduction of nanofluids in industrial applications, since it will reduce the need for a strong support of experimental work.

1.3 Literature Review

In the following Sections, it is presented a literature survey covering all subjects from the preparation of nanofluids, their colloidal stability and the most important investigations concerning viscosity and rheological behaviour of nanofluids.

1.3.1 Nanofluids Engineering

As previously mentioned, nanofluids are suspensions of nanoparticles in conventional fluids. Regarding its final application, these can have tailored properties, with the appropriate nanoparticle geometry and concentration.

Over the years, several types of nanoparticles have been used for the production of nanofluids. Among them, the most common are Alumina (Al_2O_3), Titania (TiO_2), Copper (Cu) and Copper Oxide (CuO) and Carbon nanotubes (CNT), dispersed in base fluids like distilled water (DW), ethylene glycol (EG), mixtures of water and ethylene glycol and engine oil (EO).

Carbon Nanotubes discovered by Iijima [12] in 1991, are a novel graphitic material with hexagonal carbon atoms arranged in a cylindrical fashion into a tubular structure. Their huge aspect ratio along with their unique structure, exhibit extraordinary mechanical, electrical and thermal properties [12]. Nanotubes can be categorized as single-walled (SWCNT), double-walled (DWCNT) or multi-walled carbon nanotubes (MWCNT).

Since its discovery, the production of CNTs passed from a few grams to industrial grade CNTs produced in tonnes. This production upgrade was possible due to a method of production named catalytic chemical vapour deposition (CCVD). Through this method, it is possible to grow nanotubes on substrates, enabling uniform, large-scale production with the highest-quality [26]. Other techniques include arc-discharge, laser ablation, pyrolysis and plasma vapour deposition [26].

The production of nanofluids is the first and most critical step in any experimental investigation, regarding suspensions of solid nanoparticles. This can be achieved by several approaches, although they can be widely classified as the single-step and the two-step method. In the latter, the nanoparticles, nanotubes or nanorods are, firstly, produced by mechanical or chemical procedures and then dispersed in the fluid medium [27].

One-Step Method

The one-step method consists in the synthesis of the nanoparticles directly in the base fluid. In this method, all the preparation process (drying,

storage) is avoided. Additionally, the stability of the suspension is increased, since the agglomeration of nanoparticles is minimized. However, this method present some drawbacks, it is only compatible with low pressure fluids and the production cost are higher, when compared with the two-step method [27], [28].

Eastman et al. [29] used the one-step method to disperse copper nanoparticles into ethylene-glycol. The obtained nanofluid presented a good dispersion with little agglomeration. In 2004, Zhu et al. [30] proposed a method, which consist on reducing a mixture of copper sulphate pentahydrate ($\text{CuSO}_4 \cdot 5\text{H}_2\text{O}$) with sodium hypophosphite ($\text{NaH}_2\text{PO}_2 \cdot \text{H}_2\text{O}$) in ethylene glycol under microwave irradiation.

The submerged arc nanoparticle synthesis system (SANSS) is another technique to produce nanofluids. This technique was used by Yo et al. [31] to produced Cu nanofluids. Mineral oil-based nanofluids containing silver nanoparticles was prepared by Bonnemann et al. [32] using this method. The suspensions were stable for about one month.

As seen, the one-step approach mainly advantage, is the production of nanofluids with low nanoparticles agglomeration. However, there are several disadvantages in this method. The most relevant is that the residual reactants are left in the nanofluid, contaminating the suspension. Moreover, just dielectric fluids and certain type of nanoparticles can be used to produce nanofluids and when compared with the two-step method, further described ahead, this method is more expensive.

Two-Step Method

As the name implies, the two-step method consist in two phases, the nanoparticles are firstly produced as dry powders and then dispersed into a fluid through mechanical agitation process.

This method is by far the most widely used to prepare nanofluids. This relies on the fact that, the production of dry powders of nanoparticles has already been scaled up to industrial quantities, reducing its price. However, as the one-step method, this also presents some disadvantages, such as: dry nanoparticles powder have the tendency to form agglomerates due to the high surface area and surface activity [33]. In order to overcome these issues

dispersants are normally used. Nevertheless, these can be a liability, since it can affect the properties of the colloid. Additionally, the use of surfactants in high temperature applications is also a big concern, since the surfactant tend to degrade [33]. Nevertheless, CNTs based nanofluids are typically synthesised by this technique [34].

Dispersion and Suspension Integrity techniques

Ever since its discovery, researchers have pursued a technique to produce a homogeneous and stable suspension of nanoparticles in a fluid matrix [12].

Despite some achievements, increasing the wettability of nanoparticles, especially CNT, and overcoming the interparticle van der Waals attraction forces still proves to be extremely challenging. Moreover, a homogeneous dispersion of nanoparticles not necessarily signifies a stable suspension, since nanoparticles will always tend to agglomerate. In this regard, the engineering of a nanofluid involves disentangling individual nanoparticles, but also prevents its re-aggregation.

This issue lead some researchers to study this subject in detail, since the improper preparation of a nanofluid can lead to erratic results [29], [35]. Moreover, order to prevent re-aggregation and/or sedimentation of nanoparticles, it is of utmost importance to increase the repulsive forces between them. The latter may be achieved by attaching functionalized groups on the surface of the nanoparticles, through covalent or non-covalent techniques and thereby increasing its solubility in solvents, such as water and ethylene glycol [23], [36], [37]. Recently, several reviews have outlined the role of these techniques to increase the solubilisation and colloidal stability of CNTs [38], [39].

Surface Modification Techniques

Particle agglomeration may be prevented by balancing the interparticle interaction forces through electrostatic or steric repulsion [40]. Steric repulsion is the most common method to balance the interparticle interaction forces, and can be employed through chemical methods. These methods can be categorized in non-covalent and covalent functionalization techniques.

For CNTs based nanofluids, covalent functionalization appears to be the most promising technique for refluxing CNTs, in what stabilization, dispersibility

and long shelf life is concerned [41]. This technique has the peculiarity of introducing covalent-bonds, such as carboxylic (COOH) groups, on the sidewalls of nanotubes. However, in order to be successful a highly reactive reagent has to be used [37]. Moreover, the oxidising reagent has to be chosen regarding the CNTs final application, since different reagents ratios will modify the properties of CNTs in distinctive ways. For thermal applications and polar fluids, the most common technique is to reflux CNTs in strong acid mixtures, such sulphuric and nitric acids. This oxidising treatment has the peculiarity of introducing carboxylic groups (COOH) into the wall of CNTs, while simultaneously removing impurities originated from the CNT production [36]. However, if not properly assessed, this technique may damage the CNTs surface, reducing the CNTs length and decreasing the spatial distribution ratio [42].

In the case of non-covalent functionalization, the use of surfactants and polymers also called dispersion agents, such as Potassium hydroxide, deacetylation, Triton x-100, gum Arabic, sodium dodecyl benzene sulfonate (SDBS), sodium dodecylsulfate (SDS), cetyltrimethylammoniumbromide and hemadecyltrimethylammonium bromide (CTAB) are normally used [34], [43]. It is acknowledged that surfactants produce an envelop around the CNTs, which increase their wettability, but also affect the interaction between CNTs, and as a consequence, penalizing the thermal conductivity, increasing the viscosity and hence affecting the thermal performance of nanofluids. Moreover, the use of surfactants for high temperature applications is also a big concern, since it may lead to the degradation of some surfactants and the formation of foams [34], [44].

Electrostatic repulsions may be induced by mechanical methods, such as ultrasonication, high speed shearing or ball milling [45]. These methods place electric double layers on the nanoparticle surface which, when particles approach each other, interact, leading to repulsion [46]. However, as it will be demonstrated in the next sections, these methods are normally used as a supplement to the chemical functionalization.

Dispersion Techniques

As it was mentioned earlier, for the preparation of a stable dispersion it is of utmost importance to overcome the cohesive energy associated to nanoparticles bundles and also to increase the repulsions between particles. This can be achieved by applying mechanical agitation methods, such as ultrasonication, [47], [48] high-shear mixing and high-pressure homogenizer [49].

Dispersion by ultrasonication relies on a physical phenomenon known as cavitation (i.e. the rapid and continuum formation and collapse of a bubble that is formed in a liquid [39]). This bubble implosion induces the rise of local temperature up to $\sim 4730^{\circ}\text{C}$ (5003 K) and pressures of a few hundred atmospheres, resulting in the propagation of microscopic shock waves [50]. These extreme conditions give rise to free radicals and the energy produced is sufficient to overcome the van der Waals attraction forces between CNTs [29]. However, this violent phenomenon, if not properly controlled, can damage the nanoparticles with higher impact to non-spherical particles as CNTs, modifying its unique properties.

Hilding et al., have studied this effect on multi-walled carbon nanotubes, and reported that MWCNT became shorter and thinner when subjected to high ultrasonication periods. The authors have also discovered that for long sonication times the tube length tends to a fixed saturation value [23]. Thus, to engineer CNTs nanofluids, it is desirable to pursue the best relationship between reducing damage and entanglement of CNTs, while increasing their dispersibility in the fluid matrices.

Huang et al. developed a correlation capable of quantifying the energy density required to separate raw CNTs networks. They have reported that the required energy is a function of the CNT geometry, viscosity of the dispersion medium as well as the characteristics of the ultrasound device [39]. The aptness of converting electric energy into mechanical energy by an ultrasonic instrument (ex. Ultrasonic bath, horn/tip), relies on several parameters which have a direct influence on the quality of the dispersion, where the ultrasound intensity, power, frequency, amplitude and time interval are the most critical. However, the external pressure and temperature are also important, since they will affect the

viscosity and surface tension of liquids, disturbing the capability of the cavitation to disentangle the CNTs [51]. To obtain reproducible results, it is of utmost importance to keep these parameters consistent.

The separation of CNT agglomerates can also be achieved by a shear flow induced by a vane, a magnetic stirrer or by ball milling. Usually, the shear mixing is used as a complement to the ultrasonication process or for suspensions of CNTs in high viscous media. Moreover, shear flow parameters (time and rotation speed) are more controllable resulting in better reproducible CNTs dispersions when compared to those obtained by ultrasonication. However, this technique is more common on polymer suspensions, since the high viscosity prevents the effectiveness of the cavitation phenomena of ultrasonication [35].

The high-pressure homogenizer is the least used technique to suspend nanoparticles in fluids. This method comprises several physical phenomena to disperse the nanoparticles in fluidic media, such as: high hydrostatic pressure, cavitation, shear stress, turbulence and temperature. Fedele et al. [52], investigated the effect of different preparation techniques on the stability of single walled carbon nanohorns. They have concluded that the use of a high-pressure homogeniser was the most effective method to obtain a stable suspension over the ball-milling and sonication. However, little information can be found concerning this technique for dispersing CNTs in fluidic matrices.

Stability evaluation techniques

A stable nanofluid is characterised by three factors: low-agglomeration, low sedimentation and high structural integrity. Prior to any empirical characterization, nanofluids must, therefore, fulfil these requirements. It is recognized that the morphological structural evaluation of nanofluids is detrimental, in order to reduce any noise factors, which could lead to inconsistent results. However, a large number of scientific research neglects this evaluation, as it can be depicted from Table 1.2 for CNTs nanofluids.

In this section, it is presented a survey of the most common methods for the evaluation of each stability factors.

In order to guarantee the low-agglomeration or high repulsivity between adjacent nanoparticles, the electrokinetic potential forces or Zeta potential (ζ)

must be assessed. When nanoparticles are dispersed in polar liquids an electric double layer (EDL) between the surface of the nanoparticle and the bulk liquid is spontaneously developed. The EDL is formed in order to neutralize the charged colloid and, in turn, causes an electrokinetic potential between the two phases. This electrical potential, which is related to the mobility of the nanoparticles, is called the zeta potential [53]. In general, colloidal systems with low zeta potential ($<25\text{mV}$) are considered unstable, with attraction forces exceeding the repulsion forces, tending to flocculate. In contrast, high zeta potential ($>40\text{mV}$) indicates that particles are electrically stabilized, and repulsive forces dominate [54].

The structural integrity and thermal behaviour of nanoparticles can be evaluated by a Thermogravimetric Analysis (TGA). Through the evaluation of the weight-loss of a substance subjected to a controlled temperature variation in an inert atmosphere, it is possible to assess its structural integrity. This technique should be assessed in order to address the endurance of nanoparticles for high temperature applications [55].

Sedimentation evaluation is normally achieved by two methods, photography and spectrophotometry. The first is portraying as the most simple and less precise method. It consists in taking photographs to test tubes filled with a nanofluid for a constant time interval, until sedimentation occurs [54]. This approach, despite giving some qualitative information, has some drawbacks, such as the long period observation and the vulnerability to external disturbances (e.g. vibrations), which can influence the results. For the second method a spectrophotometer is commonly used. These instruments measure the absorption or reflectance by the substance, when subjected to an electromagnetic spectrum. This absorption measurement is based on the Beer-Lambert law, which postulates a linear relationship between the absorbance and the concentration of an absorber [56]. Furthermore, as the supernatant nanoparticles settles the concentration in the nanofluid will vary and through a mathematical formulation it is possible to express the relative concentration of the sample over time, assessing its stability [57]. However, these devices have the same drawbacks as the first method and are not suitable for high concentrations of nanoparticles since they require sample dilution.

Recently, a new technology developed by LUM GmbH (LUMiSizer) has been revolutionizing the stability assessment of suspensions. This multisampler analytical centrifuge with programmable acceleration profiles and temperature, employs the innovative STEP® technology (Space and Time Extinction Profiles), to assess the intensity of transmitted light as a function of time and position over the entire sampler container. The presence of centrifugal forces compels the particle to migrate resulting in a variation of the supernatant particle concentration and corresponds to the local and temporal variations of the transmission. These transmission profiles are representative of particle separation and the degree of dispersion, i.e. dispersion quality [41].

From Table 1.2, it can clearly be seen, that the preparation and quality evaluation of a CNT suspension must fulfil at least five fundamental steps: Firstly, a surface modification technique must be applied to the bulk CNTs increasing its wettability. Secondly, the treated CNTs are dispersed in the fluidic matrices by mechanical agitation. Thirdly, a SEM and/or TEM examination is required, to assess the structural integrity and dispersibility of CNTs, after the dispersion process. Fourthly, a Zeta potential analysis should be made to assess the repulsivity between adjacent CNTs. The fifth and final step, is a shelf life analysis in order to assess the suspension longevity. Despite this information being available in the open literature, very few researchers fulfil all these steps, being the shelf life of nanofluids the most neglected one and very often determined only by qualitative methodologies.

Table 1.2 - Literature survey of some characteristics concerning the engineering of CNTs nanofluids and stability evaluation

Base Fluid	Nano-particle	Stabilization		Dispersion		Shelf Life	REFERENCE
		Methods	Evaluation	Methods	Evaluation		
DW	SWCNT	Surfactant	ZP, VE	HPH	-	>15 days	Fedele et al. [58]
DW	Carbon Powder	AT	ZP	UH	TEM	-	Han et al. [59]
Gly - Water	CNF	-	-	UH	SEM	-	Xu et al. [60]
Gly - Water	CNF	AT	-	UH	SEM	-	Xu et al. [60]

Water	CNT	AT	-	-	SEM, TEM	Many months	Shaffer et al.	[61]
DW	CNT	Surfactant	UV	UH, HPH	-	-	Walvekar et al.	[62]
DW	CNT	Surfactant	VE	UH	TEM	2 months	Ko et al.	[63]
Water	MWCNT	Surfactant	ZP	UH	TEM	2 months	Madni et al.	[64]
DW	MWCNT	Surfactant	VE	UH	SEM, TEM	1 month	Ding et al.	[65]
DW	MWCNT	Surfactant	VE	UH, MS	-	45 days	Phuoc et al.	[66]
DW	MWCNT	Surfactant	VE	UH, MS	TEM	-	Halefadi et al.	[67]
DW	MWCNT	AT	UV	UH; MS	SEM	-	Abreu et al.	[68]
EG - DW	MWCNT	AT	UV	UH, MS	SEM	100 Hours	Lamas et al.	[69]
DW	MWCNT	AT	UV	UH	SEM	-	Oliveira et al.	[70]
EG - DW	MWCNT	AT	LUM, ZP	UH, MS	SEM	>2 years for 0,25 vol and >50 years for 1,5%vol	Lamas et al.	[41]
Water	MWCNT	AT	-	-	TEM, SEM	Up to 1 Year	Kinloch et al.	[71]
DW	MWCNT	Surfactant	-	UH	TEM	Several weeks	Garg et al.	[36]
EG	MWCNT	AT	-	UH	-	-	Han et al.	[59]
EG	MWCNT	Surfactant	-	MS, UH	SEM	-	Liu et al.	[72]
EG	MWCNT	Surfactant	-	MS, UH	SEM	-	Liu et al.	[72]
Engine oil	MWCNT	Surfactant	UV	MS, UH	SEM	-	Liu et al.	[73]
DW, EG, EO	MWCNT	-	UV	UH	SEM	Up to 800h	Hwang et al.	[74]
EG	MWCNT	Surfactant	-	UH, MS	-	-	Ruan et al.	[75]
DW	MWCNT	Surfactant	VE	UH	TEM	Up to 10 days	Yousefi et al.	[76]
DW	MWCNT	Surfactant	VE	UH	TEM	Several months	Halefadi et al.	[67]
DW	MWCNT	AT	VE	UH	SEM	Several months	Amrollahi et al.	[77]
SO	MWCNT	AT+Surfactant	-	MS	TEM	-	Chen et al.	[78]
DW	MWCNT	AT	ZP, VE	US	SEM	Several weeks	Talaei et al.	[79]
DW	MWCNT	AT	ZP	UH	TEM	Two months	Xie et al.	[80]
Oil	SWCNT	-	SEM	UH	VE	-	Vakili et al.	[81]
Oil	MWCNT	Surfactant	-	UH	SEM	-	Yang et al.	[82]
DW	MWCNT, Carbon	AT+Surfactant	VE	UH	-	One Week	Vander et al.	[83]

black							
DW	SWCNH	Surfactant	ZP	-	SEM	>18 days	Bobbo et al. [84]
DW	MWCNT	Surfactant	-	UH	SEM	3 weeks	Meibodi et al. [85]
DW, EG, Gly	MWCNT	AT	-	UH	TEM	Many months	Chen et al. [86]
SO	MWCNT	Surfactant	-	UH	-	-	Chen et al. [87]
EG	MWCNT	AT	ZP	UH	SEM	-	Xie et al. [88]
PVA - GLY	MWCNT	AT	VE	UH	SEM, TEM	-	Wang et al. [89]
DW	SWCNT	Surfactant	VE	UH	-	-	Wensel et al. [90], [91]
DW	CNT	AT	VE	UH	-	7 days	Badu et al. [91]
DW	MWCNT	AT, Surfactant	-	UH	TEM, SEM	-	Kim et al. [92]
Alkali Eutetic	MWCNT	Surfactant	-	UH	TEM, SEM	-	Jo et al. [15]
DW-EG	MWCNT	Surfactant	VE	UH	TEM	-	Ruan et al. [93]
DW-EG	SWCNT	AT	VE	UH	-	-	Glover et al. [94]
PAO	MWCNT	AT	-	UH	-	-	Shaikh et al. [95]
DW	MWCNT	-	VE	UH, HPH	TEM	10 days	Gomez et al. [96]
DW	SWCNT	Surfactant	UV, VE, ZP	UH	TEM	30 days	Said et al. [97]
DW	CNT	Surfactant	-	UH, MS	-	-	Soma et al. [98]
Oil	MWCNT	-	-	MS, UB, UH	-	-	Kasaeian et al. [99]
Water	MWCNT	Surfactant	-	MS, UB	-	2 days	Tabari et al. [100]
Water	MWCNT	Surfactant	-	MS, US	-	-	Rashmi et al. [101]
DW	MWCNT	AT	-	UB	-	-	Liu et al. [102]
DW	CNT	AT, Surfactant	ZP	UB, UH	-	3 days	Nasiri et al. [34]
DW	CNT	AT	-	UB	-	-	Lotfi et al. [103]
DW	CNT	AT	VE	UH	TEM	>3 days	Su et al. [104]
DW	MWCNT	Surfactant	VE	UH	-	20 days	Shanbedi et al. [105]
DW	MWCNT	Surfactant	VE	MS, UH	-	1 month	Wusiman et al. [106]
Oil	MWCNT	-	VE	MS, UB	-	5 days	Ashtiani et al. [107]
DW	MWCNT	Surfactant	-	UH	-	-	Meyer et al. [10]
DW	DWCNT	AT	VE	MS, UH	-	1 week	Hemmat et al. [108]
DW, EG, PG	MWCNT	PT	VE	UB	-	8 months	Hordy et al. [109]
EG-DW	MWCNT	Surfactant	ZP, VE, UV	HPH, MS, UH	-	2 weeks	Teng et al. [49]
EO	MWCNT	AT, Surfactant	VE	BM	-	720h	Zare et al. [110]
DW-EG	MWCNT	AT, Surfactant	ZP	MS, UH	-	-	Hungthang et al. [111]
DW	MWCNT	AT	-	UH	-	-	Chougule et al. [112]

							al.	
DW	MWCNT	AT	-	UH	SEM	-	Amiri et al.	[113]
DW	MWCNT	Surfactant	-	MS	SEM	-	Estelle et al.	[114]
DW	MWCNT	Surfactant	-	UH	SEM	-	Piratheepan et al.	[115]
DW	Carbon	-	-	-	-	-	Kim et al.	[116]
DW	SWCNT	AT	-	UH	-	-	Park et al.	[117]
DW	MWCNT	Surfactant	UV	MS, UB	SEM	40 days	Rashmi et al.	[118]
DW - GLY	MWCNT	Surfactant	VE	MS	SEM	12h	Steele et al.	[119]
Oil	MWCNT	-	VE	MS, UH	-	24h	Derakhan et al.	[120]
DW	MWCNT	Surfactant	VE	Uh	SEM	1 day	Lee et al.	[16]
Oil	MWCNT	AT	-	UB	-	-	Behesti et al.	[121]
DW	CNT	AT	VE	UB	-	Months	Badu et al.	[122]
DW-EG	MWCNT	Surfactant	VE	MS, UH	SEM	3 months	Kumaresan badu et al.	[123]
Oil	MWCNT	-	-	MS, UH	-	-	Tagmouti et al.	[124]
DW	MWCNT	Surfactant	-	UH	TEM	-	Sadri et al.	[125]
EG	MWCNT	AT	VE	UH	TEM	Two months	Meng et al.	[126]
DW	MWCNT	Surfactant	UV, ZP	UH	TEM	>48 hours	Mondragon et al.	[127]
DW	MWCNT	Surfactant	-	UH	SEM	-	Estelle et al.	[19]

DW - Deionize water EG - Ethylene Glycol EO - Engine oil PG - Propylene glycol Gly - Glycerine SO - Silicone Oil AT - Acid treatment PT - Plasma treatment MS - Mechanical stirring BM - Ball milling UB - Ultrasounds bath UH - Ultrasounds homogenizer HPH - High-pressure homogenizer UV - Ultraviolet/visual spectroscopy ZP - Zeta potential VE - Visual evaluation TA - Turbidity analyses LUM - STEP technology

The dispersibility evaluation can only be characterized by a Transmission or Scanning Electron Microscopy (TEM and SEM) [41], [60], [128]. However, both techniques present one major limitation, the fact that they both require the samples to be dried and exposed to vacuum before they can be analysed. This may induce changes in the samples morphology and, therefore, one can never be sure whether the test sample is representative of the original sample [36]. Furthermore, in the same test sample it is possible to have distinct results. In this regard, conclusions based only on TEM or SEM images have to be withdrawn very carefully.

1.3.2 Rheology

The characterization of the rheological behaviour of materials is defined by the general term rheometry, while the term viscometry is typically used to defined measurements of viscosity. However, independent of the rheological behaviour of the fluid, the measurement of two fundamental characteristics always plays a central role: viscosity as a function of a shear rate, and viscoelastic properties as a function of frequency.

The classical understanding of the rheology of liquids originates from the “Theorem XXXIX” of Newton. Newton introduced the terms “*defectus lubricitatus*” and “*atritus*”, which in modern terms means “internal friction” and “viscosity”. Newton proposed a fundamental hypothesis which delineates the viscous behaviour of nearly all common fluids: “The resistance which arises from the lack of lubricity in the parts of a fluid, other things being equal, is proportional to the velocity by which the parts of the fluid are being separated from each other” [129]. In other words, viscosity (μ) is the property of a fluid that relates applied stress (σ) to the resulting strain rate ($\dot{\gamma}$):

$$\sigma = \mu \cdot \dot{\gamma} \quad \text{Eq. 1.3}$$

Liquids that obey linearly to this viscous-flow theory are designated *Newtonian liquids*, meaning that its viscosity is independent of the imposed shear rate. Fluids which do not obey to Eq. 1.3, are designated *non-Newtonian* [130]. In Figure 1.2, it can be depicted the general shape of the flow curves representing: (a) the variation of shear stress with shear rate and (b) the variation of viscosity with shear rate.

Non-Newtonian fluids are mainly categorized as pseudoplastic or dilatant fluids. Pseudoplastic fluids present shear-thinning flow behaviour, i.e. the viscosity of the fluid will decrease with increasing shear rate and even with time. Dilatant fluids are characterized by a shear thickening flow behaviour, i.e. as shear rate increases so does the fluid viscosity [129]. For the cases where fluid viscosity will change with a time period and under constant shear rate, these can be categorized as thixotropic fluids, where viscosity will decrease with time, or

as rheopxy fluids, where the fluid viscosity will increase with time. Both thixotropy and rheopxy fluids may occur for any of the previously flow behaviours identified [129].

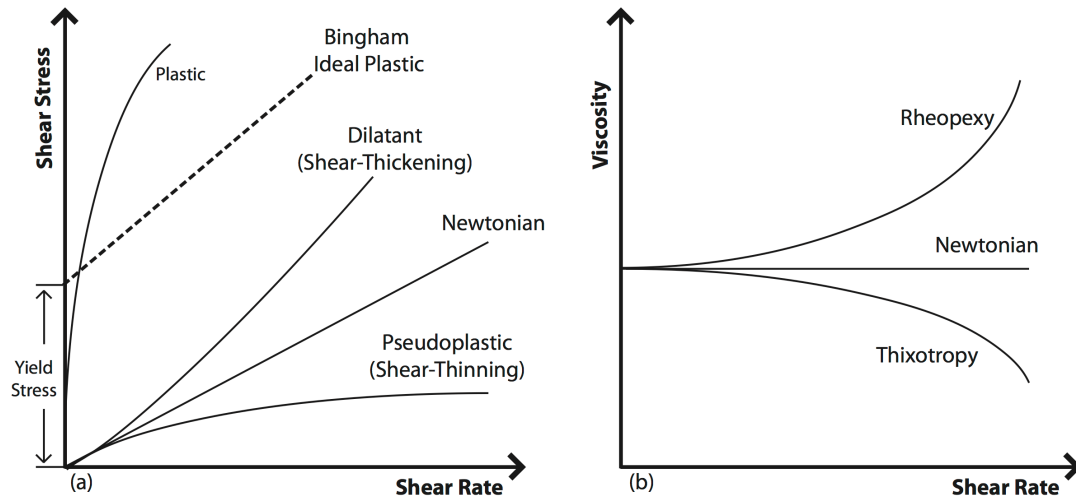


Figure 1.1 - Typical rheological behaviour for fluids: (a) shear stress as a function of shear rate; (b) viscosity as a function of shear rate.

A yield stress is a common phenomenon that occurs in some materials. This phenomenon is characterized by a solid-like behaviour at rest or at low stress, starting to flow only when the applied external forces overcome the internal structural forces. A rheological behaviour where an *apparent yield stress* can be observed is not uncommon in fluids, in dispersions or emulsions. Nevertheless, these materials often show a drastic change of viscosity at a certain shear stress interval [131].

The rheological behaviour of a fluid can have a profound effect on the selection of the ideal experimental technique to determine its viscosity. In the following section, it will be discussed some of the parameters that influence the rheological behaviour of fluids.

1.3.3 Viscosity Parameters

Viscosities, as well as thermal conductivity, are the most studied properties of nanofluids. The first measures the resistance of a fluid against a deformation, and it is of utmost importance to guarantee the flowability of nanofluids in forced convection energetic systems. The second represents the ability of a substance to conduct heat, and is directly related with the thermal effectiveness of fluids. It is, therefore, crucial to enable the use of nanofluids as advanced thermal fluids and it will require a full understanding and characterization of the influence of nanoparticles on the properties, with respect to conventional thermal fluids.

Viscosity determination often functions as a technique through which other characteristics of a material can be obtained. However, the fluid viscosity is very sensible to many external and internal factors, as it will be discussed further ahead, hence to compare two results in a measuring series, all parameters must be kept the same.

Temperature

The viscosity of a fluid is strongly dependent on the temperature, since it will affect the molecular interactions and the microstructure of the fluid, hence affecting the intrinsic viscosity [129]. A precise control of the fluid temperature is essential to properly evaluate the fluid viscosity, but also to establish a comparison between different fluids.

Shear rate

In nature completely Newtonian fluids are rare, making non-Newtonian fluids to be the rule rather than the exception. It is, therefore, crucial to include the effects of shear rate in any viscosity evaluation. Thus, it is necessary to make viscosity measurements at several shear rates, in order to detect any irregular rheological behaviour [132].

Material composition

The stability of a fluid during viscosity measurements is essential to guarantee the accuracy, but also the reproducibility and the actual viscosity of

the material that is being measured. Also, the homogeneity of the sample can have a profound effect on the rheological behaviour and on the consistency of the viscosity measurement [132].

Previous History

The history of a material should also be taken into consideration, especially in fluids sensitivity to heat and ageing. Special attention should be taken when materials exhibiting thixotropic behaviour, since they are very sensitive to prior history. Therefore, storage and sample preparation should be designed in such a way to minimize any undesirable effect on the viscosity measurement [131], [132].

Dispersions

The stability and homogeneity of dispersions can have a drastic effect on the viscosity measurements. These multi-phase materials, consisting of at least one solid material can be affected by the factors discussed above and also by: the state of aggregation, the size of aggregates, how adherent are the aggregate particles and the geometry of the particles [132]. Therefore, when measuring the viscosity of dispersions, one must have special precautions to ensure that the data acquired is not erroneous.

1.3.4 Experimental Methods of Viscosity Evaluation

In order to address the rheological properties of materials two types of rheometers can be used, according to the flow type: simple shear and/or extensional flow rheometers. Instruments used to measure the viscosity of liquids can be broadly classified into the following categories [133]:

- Rotational viscometers
- Capillary viscometers
- Falling ball viscometers
- Vibrational viscometers

When addressing the rheological properties of materials two approaches are possible: *absolute* or *relative* measurements. The absolute methods are based on direct measurement of the shear rate and shear stress, and viscosity is calculated as a ratio of these quantities, see Eq. 1.3. Relative methods of viscosity measurements are based on comparisons with a standard fluid with known properties.

Next, it is presented an extended survey on the different types of rheometers used to evaluate the viscosity of fluids. The working principle, the advantages and the disadvantages of each type will also be discussed.

Rotational Rheometers

Rotational rheometers are by far the most common instruments used to characterize materials in steady and oscillatory shear flow. The measuring principle of these rheometers are based on measuring the rate of rotation of a solid shape in a viscous medium when a known torque or force is applied. These instruments are ideal to study the rheological behaviour of non-Newtonian fluids. However, when compared to other types, they are less accurate especially for Newtonian liquids. Nevertheless, these rheometers can perform multiple measurements in steady state conditions, different shear rates, continuous measurements as a function of temperature, time and rate of shear [133].

This type of rheometers can be divided into three different types according to the design configuration, as it can be depicted from Figure 1.2:

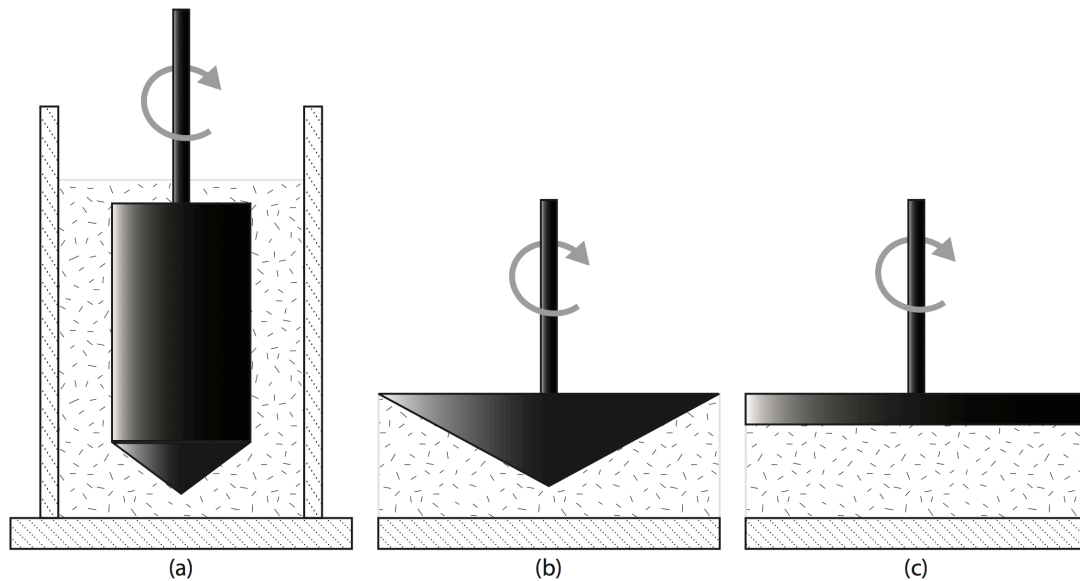


Figure 1.2 - Schematic 2D representation: (a) Concentric Cylinders; (b) Cone and Plate; (c) Parallel-Plate.

Concentric Cylinders

As it can be depicted from Figure 1.2 (a), the concentric cylinder system is composed by an outer cylinder (cup) and an inner cylinder (bob). This system can have two modes of operation: the Couette mode, where the cup rotates while the bob is stationary; the Searle mode, where the cup is stationary and the bob rotate. The gap between the two concentric cylinders should be small enough to enables a constant shear rate and a constant film thickness [133]. This type of measuring systems is specially suitable for low-viscous liquids due to the large contact area and for high shear rates the sample can not be expelled from the container [131]. Moreover, this type of system is especially recommended for suspensions, but this will be discussed in detailed in section 1.3.5. For that reason many researchers [36], [127], [134]-[137] adopted this method.

Cone and Plate

As it can be depicted from Figure 1.2 (b), the sample is contained in the space between a large apex cone and a flat surface normal to its axis. These types of viscometers are probably the most common instruments for studying the rheological properties of non-Newtonian fluids. Nevertheless, this geometry can have a number of problems, such as viscous heating in the cone and plate due to

friction, inertial forces that tend to pull the plates together and can generate a secondary flow that increases the torque [133]. Even so, many researchers [15], [47], [71], [96], [138]-[141] used this method.

Parallel Plates

As it is shown in Figure 1.2 (c) the parallel plates work in a similar fashion to the cone and plate geometry. However, by controlling the gap between plates, this system allows measurements of suspensions with large particles. Also, by operating at small gaps high shear rates can be obtained while minimizing errors due to secondary flows [131]. However, this system is not advised for suspensions, since any sedimentation or particle migration will affect the viscosity measurements [131]. Nevertheless, several researchers [142]-[146] used these equipments. For instance, Aladag et al. [143] studied the rheological behaviour of alumina and CNT - water nanofluids with this type of equipment.

Capillary Rheometer

A capillary rheometer is composed by a piston that drives the sample to flow at a constant velocity through a capillary tube. A pressure transducer measures the pressure drop along the capillary and through the flow-rate the shear stress, shear rate and the viscosity are evaluated. However, determining the viscosity of non-Newtonian fluids on these instruments can be very challenging, due to sources of errors such as the entrance effects of the capillary flow, slippage at the walls, and viscous heating effects. These problems could be even more pronounced for high concentration suspensions. Nevertheless, these instruments have some advantages such as the fact: that can sustained high shear conditions, high process temperatures and due to the closed configuration solvent evaporation and edge effects that can be avoided [131]. Many researchers [93], [147]-[155] have reported experimental studies with capillarity viscometers. For instant, Yu et al. [156], measured the effective viscosity of nanofluids composed by alumina and polyalphaolefin, and Ruan et al. [93] for multiwalled-carbon nanotubes dispersed in water and ethylene glycol.

Falling Ball Viscometer

The falling ball viscometer, is composed by a vertical glass tube in which a sphere of known size and density is allowed to descend through the liquid. After a period of initial acceleration the ball reaches a constant terminal velocity, the viscous resistance to motion is equal to the difference in density between the sphere and the fluid. This principle of operation is known as the Stocks law [131]. The main source of errors of these viscometers is related to the wall effect. Also, these viscometers are more suitable for transparent Newtonian liquids. However, some researchers [157], [158] used this method for determine the viscosity of nanofluids.

Vibrational Viscometer

The vibrational viscometers are best suited for on-line measurements of viscosity. These instruments are normally used in some industries such as the petrochemical industry, where maintaining the quality of the product is crucial. By measuring the power required to maintaining the electromechanical resonator at constant amplitude, the viscosity is determined. Despite the versatility of these instruments, there is little information regarding its usage to measure the viscosity of suspensions [133].

1.3.5 Standards

As previously stated, several techniques, instruments and control variables have been widely used to determine the viscosity and rheological behaviour of nanofluids. However, for replication proposes, experimental assessments obtained with different instruments must respect the general test methods based on methodologies provided by the *International Standards Organization (ISO)*, *American Society for Testing and Materials (ASTM)* or any other standard organization. Despite that, most authors have reported the use use of equipment that does not comply with international standards. The experimental methodology is commonly chosen based on the experience of the author, without any specific or standardized guidance. The latter, finds its

justification in the lack of international standardization specific developed for the determination of suspensions viscosity with nanoscale particles.

Nevertheless, there are several international standards that could be adopted for the viscosity evaluation of liquids and suspensions, which could be adopted to nano-scale suspensions. These are: ISO 3219:1995 -*"Plastics - Polymers/resins in the liquid state or as emulsions or dispersions -Determination of viscosity using a rotational viscometer with defined shear state"*; ASTM D445-06 *"Standard test methods for kinematic viscosity of transparent and opaque liquids"*; ASTM D2196-05 *"Standard test methods for rheological properties of non-Newtonian materials by rotational viscometer"*. These standards, contain all the specifications that should be satisfied in any rheological characterization.

1.3.6 Suspension Rheology Mechanisms

As per the definition of the American Society of Rheology, rheology is "The science of the flow and deformation to all forms of matter". Suspensions rheology can exhibit a wide range of mechanical behaviour from Hookian elastic behaviour to Newtonian fluid behaviour [159]. As previously stated, most researchers reported an increase on the viscosity of nanofluids with nanoparticle concentration. This lays on a fact that, the presence of nanoparticles in a fluid will disturb the energy dissipation related to the hydrodynamic interactions between the liquid and the nanoparticle. In order to understand the rheological behaviour of a suspension, one must first address the nature of the nanoparticles in the suspension, i.e. if the nanoparticles interact with neighbouring particles, if the nanoparticles are aggregated into clusters, if the surface forces are attractive or repulsive and also the size and shape of the nanoparticle. Moreover, the experimental methodology and conditions will also affect the rheological behaviour of nanofluids. Based on these premises, some theories have been formulated in an attempt to describe the rheological behaviour of nanofluids. From these, it is highlighted the nanoparticles clustering or aggregation, the particle-particle and particle-fluid hydrodynamic interaction and orientation of nanoparticles under shear conditions.

In Table 1.3 summarises the main researchers that proposed the mechanisms to explain the rheological behaviour of nanofluids.

Table 1.3 - Proposed Mechanisms for the viscosity of nanofluids

Proposed Mechanisms	Researchers
Nanoparticles Aggregation/Percolation	[15], [19], [82], [125], [142], [148], [160]-[170]
Hydrodynamic Interactions	[161], [171]
Nanoparticle Orientation	[142], [160], [161]

Aggregation / Percolation

The nanoparticle network structure is one of the proposed mechanisms to explain the rheological behaviour of nanofluids. Nanoparticles dispersed in a fluid can present two forms: aggregates and separate single nanoparticles. Also, the network structure can be categorized into two groups: nanoparticle separation and nanoparticle interconnection. The first one refers to the separation of individual nanoparticles. The second refers to the interconnection between clusters and separated nanoparticles or simply separated nanoparticles, which form percolation networks. Still, both types of suspensions exhibit distinctly rheological behaviours [160].

Most researchers agree that as the concentration of nanoparticles increases, so it does the nanoparticles clusters and that could lead to the formation of percolation networks. These structures offer resistance to the deformation, hence contributing to the growth of the effective viscosity of nanofluids [125], [142], [160]-[163]. However, according to Fan et al. [160] these structures are very sensitive to shear forces, interparticle interactions and nanoparticle size and geometry. Additionally, the suspension regime (i.e. diluted, semi-diluted or concentrated) plays a crucial role on the formation of aggregates and percolation networks. According to Mueller et al. and Hobbie et al. [161], [165], in dilute suspensions where the interaction between particles are rare, the formation of agglomerates and percolation networks becomes less likely to occur. In contrast, in semi-dilute and concentrated suspensions the particle-particle contact becomes more pronounced and more likely to form aggregates and percolation networks.

Regarding non-spherical particles, such as CNTs, several authors have suggested that the elongated geometry of CNTs allows the formation of local percolation networks [81], [160], [164]. Through the measurement of the effective viscosity, Yearsley et al. [164] found experimentally that carbon black powders and CNTs nanofluids exhibit similar rheological behaviours. However, CNTs nanofluids have an extremely lower percolation threshold than carbon black nanofluids, ten times lower. These results have shown, that the suspension viscosity depends not only on the size of the agglomerates, but also on the packing density of the aggregates. The latter are more pronounced for CNTs suspensions, since these long and often bent nanoparticles could not pack easily within agglomerates, comparatively to spherical particles agglomerates.

Timofeeva et al. [172] experimentally verified that the viscosity of Al_2O_3 nanofluids is strongly dependent on nanoparticle geometries, aspect ratios and concentration. The authors claim, that for cylindrical type suspensions, the critical volume fraction where nanoparticles start to interact is 1,56 %vol., forming clusters of nanoparticles. This results in shear thinning behaviour and higher viscosities.

In order to study the behaviour of the structural network of CNTs water based nanofluids under shearing forces, Estellé et al. [19] conducted a series of empirical test from a shear rate of 0 to 1600 s^{-1} . The author's claim, that for low shear rate the effective viscosity increased due to the breakdown of the structural network, while for high shear rates a well-defined shear thinning was observed.

Moreover, the viscosity of an aggregated nanofluid is also a function of the magnitude of the attraction between the nanoparticles. Martin Rhodes [159], empirically demonstrated that as the electric double layer (EDL) increases so does the zeta potential, thus reducing the overall attraction. As a result, the shear thinning behaviour is less pronounced and the nanofluid microstructure is broken down into smaller clusters, reducing the overall viscosity. In Figure 1.3 it can be depicted an illustration of this phenomena.

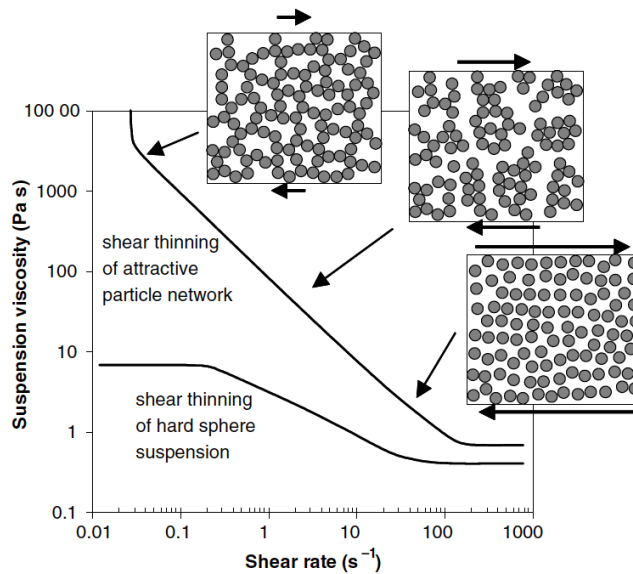


Figure 1.3 - Rheology behaviour of nanofluids composed by aggregates with strong and weak attraction forces [159].

Hydrodynamic Interaction

On any suspension of solid particles there will always exist hydrodynamic interactions between the particles and the fluid. These interactions can be categorized in three types: particle-fluid interactions; hydrodynamic particle-particle interaction; and particle-particle interaction. The particle-fluid interaction occurs at very low particle volume fractions (diluted regime). In this regime, the suspended particles are so distant from each other that the interactions between neighbouring particles are negligible. For this case, the viscosity enhancement is caused by the extra work that the fluid has to do flowing around the particle. The hydrodynamic particle-particle interaction occurs when neighbouring particles are closed enough to interact hydrodynamically. Pairs or higher multiples of particles rotate together, distorting the flow and increasing the viscosity. At slightly higher particle concentration, the distance between particles becomes so small that the fluid is forced to pass on the small gaps between particles, resulting in a shear thinning behaviour [161], [173].

In the pioneering work of Einstein [5], he assumed that the distance between particles is far enough that they do not interact. In contrast, Batchelor [8] extended the analysis to include higher volume fractions. However, for

concentrated suspensions where particle-particle hydrodynamic interactions become more significant, both Einstein and Batchelor analysis fails to predict the suspension viscosity [159].

In the case of suspensions at rest and at low shear rate, Brownian motion dominates over the hydrodynamic interactions. However, as shear rate increases the hydrodynamic interaction overcomes the Brownian motion [159]. In this case, the suspension viscosity is lower than the viscosity of the same volume fraction with randomized structure, see Figure 1.4

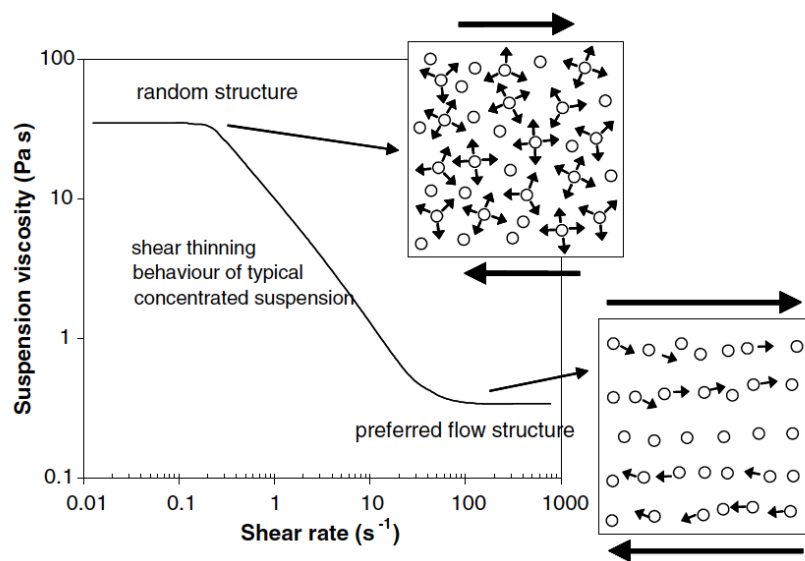


Figure 1.4 - Suspension structure/viscosity as a function of shear rate [159]

Mueller et al. [161] conducted an extensive investigation on the rheological behaviour of five suspensions with different geometries, materials and aspect ratio. The empirical data has shown, that nanofluids with different geometry and aspect ratio of nanoparticles can have different rheological behaviours. These results, suggested that as the volume fraction and aspect ratio increases, so does the interaction between neighbouring particles affecting the nanofluid microstructure. They have, therefore, concluded that the rheological behaviour of nanofluids is directly related with the degree of separation between particles, i.e. the degree of interaction between neighbouring particles.

Cristina et al. [173] conducted an analytical investigation based on the hydrodynamic interactions between two-body and three-body and its

contribution on the viscosity of a diluted suspension. Based on a multiple scattering theory, they have concluded that the empirical correlations available on the literature are in reasonable agreement with their calculation of the hydrodynamic interaction between three particles.

Nanoparticle Orientation

The alignment of nanoparticles in the direction of shearing flows has been studied throughout the history [9], [161], [174]. One of the first works related to the orientation of suspended particles under a shear force, was studied by Jeffery [9]. He has theorized that solid particles suspended in a fluid and subjected to shearing forces would drift to the orientations that offer the least consumption of energy, i.e. the particles align to the direction that offer least friction. In order to test this theory, Taylor [175] conducted a series of empirical investigations on suspensions of aluminium ellipsoids and water-glass solutions. They have concluded effectively that the particles assume a defined orientation in relation to fluid motion.

In a similar fashion, non-spherical particles as CNTs, will tend to align to the shearing flow direction, reducing the nanoparticle drag coefficient and, therefore, resulting in the decreased of the suspension effective viscosity [176]. The latter was verified by Fan et al. [177] for suspensions of MWCNT in vinyl ester. Moreover, the authors claim that the Brownian motion does not have any effect on the orientation of MWCNTs. Yu et al. [156] studied the effect on the viscosity and pressure drop of spherical and non-spherical Al_2O_3 nanoparticles, under different flow conditions. The empirical results have shown that the pressure drop of the nanofluids is higher than the base fluid, an expected result since the viscosity is also higher. Moreover, they have observed that non-spherical nanofluids presented a shear thinning behaviour and a lower friction factor, which they have attributed to the alignment of the nanoparticles under shear rate.

As it has been highlighted, the orientation of particles suspended in a fluid is more pronounced for non-spherical particles. Let's consider a particle suspended in a fluid, the forces acting on the particle can be expressed as the sum of: Brownian force, interaction potential, drag force, the buoyancy and the

gravitational force. These forces dominate for cylindrical particles compared with spherical particles, with special emphasis to the drag force [178]. As the nanoparticles align in the direction of the shearing force, shear-thinning behaviour is more likely to happen due to the reduction of the particle drag force.

Moreover, the suspension regime (dilute, semi-dilute or concentrate) plays a crucial role on the rheological behaviour of nanofluids. Similarly, the nanoparticle orientation under shearing forces is also affected by the suspension regime, nanoparticle aspect ratio and base fluid viscosity.

1.3.7 Rheological Models

The rheology of a colloid encompasses the measurement of its viscosity with respect to shearing forces. The term "dynamic viscosity or shear viscosity" expresses the ability of a fluid system to dissipate imposed shear energy, or in other words, it expresses the fluid resistance to shearing flows. Throughout the years, several investigations endeavour to find a mechanism capable of explaining how colloidal suspensions dissipate shearing energies. Despite these efforts, to date, there is no universally accepted model capable of predicting, with precision, the viscosity of nanoscale colloidal suspensions.

Nevertheless, researchers agree that the rheological properties are strongly related to the nanofluid microstructure. When analysing a nanoparticle suspended in a base fluid, this is in constant random motion due to the influence of several forces such as: Brownian motion (Langevin force), the viscous resistance (Stokes Drag Force), intermolecular van der Waals forces (dispersion forces, repulsion), and electrostatic interactions between particles and the suspension medium (Coulomb forces). However, predicting the contribution of these forces on nanofluid viscosity is not straightforward, since it depends on many factors, such as: volume concentration, particle geometry, size and aspect ratio, particle size distribution (PSD), particle-particle interaction, particle agglomerations, electric double layer (ELD), base fluid density and polarity, electromagnetic and electroviscous dispersion energy, and pH level [10], [179].

In the next section it will be presented an extended survey of the theoretical models available in the literature. These, are characterized by classical models, models of nanofluids of spherical particles, and models of nanofluids of non-spherical particles. The models are presented in a chronology manner.

Classical Models

The classical models are generally based on the fundamental work developed by Einstein [5]. By analysing the viscosity of diluted suspension of shard spheres and based on the internal friction exerted on the spheres, Einstein proposed the first available model for the viscosity of colloidal systems, Eq. 1.4. The model predicts the effective viscosity (μ_{eff}) of a suspension, by correlating the dynamic viscosity of the base fluid (μ_{bf}), with a particle geometric constant $[\eta]=2, 5$ and the solid volume fraction ϕ .

$$\mu_{eff} = \mu_{bf}(1 + [\eta] \phi) \quad \text{Eq. 1.4}$$

The main limitation of Einstein model is that it only applies for suspensions with uncharged spherical shape particles and sufficiently diluted suspensions ($\phi \leq 0,02$), so the particles do not interact between them. To address these constrains, numerous models [8], [9], [173], [180]-[191] were developed in an attempt to extend Einstein model. Despite the peculiarities of each model, no single model is able to predict the effective viscosity for any particle geometry and concentration.

An almost identical model to the Einstein model, was proposed by Hatschek [186], given by Eq. 1.5

$$\mu_{eff} = \mu_{bf}(1 + 4,5 \phi) \quad \text{Eq. 1.5}$$

Despite the similarities to Einstein, this model was developed empirically by Harrison to predict the effective viscosity of suspensions of spherical particles up to 30% in volume.

In contrast with Einstein uncharged particles, Smoluchowski [180] proposed a model (Eq. 1.6) to predict an increase in the effective viscosity of a suspension due to the electrostatic potential on the particles.

$$\mu_{eff} = \mu_{bf} \left[1 + 2,5 \phi \left(1 + \frac{1}{\mu_{bf} a^2 \sigma} \left(\frac{\zeta \varepsilon}{2\pi} \right)^2 \right) \right] \quad \text{Eq. 1.6}$$

where ε is the dielectric constant of water, a^2 the radius of the solid particle, σ the electric conductivity of the electrolyte and ζ is the electro-kinetic potential (zeta potential) of the charged particles. However, he did not disclose how he obtained this formula.

Jeffrey [9], extended Einstein work for suspensions of solid ellipsoidal particles. Based on the same principal of energy dissipation, due to internal friction, the proposed model disagrees very little from Einstein model. However, the geometric constant (η) was provided with two limits (minimum and maximum), regarding the ellipticity of the spheroids. The proposed model is given by:

$$\mu_{eff} = \mu_{bf} (1 + \eta \phi) \quad \text{Eq. 1.7}$$

where, η is given by the ellipticity of the particle (2,0 for prolate and 2,061 for oblate spheroids). It may be remarked that, when the ellipticity tends to zero (i.e. a spherical particle), Jeffrey model (Eq. 1.7) agrees well with Einstein model $\eta = 2,5$. Additionally, the author suggested that particles would tend to adopt a specific orientation with respect to the motion of the surrounding fluid. This orientation would correspond to a smallest friction force.

In order to test Jeffrey hypothesis (Eq. 1.7), Taylor [175] conducted a series of experiments on a suspension of aluminium ellipsoids and a water-glass solution. He concluded that ellipsoid particles immersed in a solution do, in fact, assume a certain defined orientation in relation to the fluid motion, as predicted by Jeffrey [9].

In 1932, Burgers [192] conducted an extensive investigation on the contribution that particle shape, orientation and Brownian movement have on

the effective viscosity of a colloidal suspension. The author proposed two models regarding the following cases: For the case of oriented ellipsoidal particles the model is given by:

$$\mu_{eff} = \mu_{bf} \left(1 + \left(\frac{4\pi L^3 n}{3 \left(\log_2 \frac{L}{d} - 1,50 \right)} \right) \phi \right) \quad \text{Eq. 1.8}$$

For the case of sufficiently effective Brownian movement in oriented ellipsoidal particles, the model is given by:

$$\mu_{eff} = \mu_{bf} \left(1 + \left(\frac{\frac{L^2}{d^2}}{\left(\log \frac{L}{d} - 0,81 \right)} \right) \frac{1}{15} \phi \right) \quad \text{Eq. 1.9}$$

where L , and d , are the cylindrical length and equatorial radius, respectively.

In line with Smoluchowski [180] assumptions, Krasny-Ergen [193] proposed a model for the effective viscosity through the recalculation of the electrokinetic potential. The proposed model is given by:

$$\mu_{eff} = \mu_{bf} \left[1 + 2,5 \phi \left(1 + \frac{1}{\mu_{bf} a^2 \sigma} \frac{3}{2} \left(\frac{\zeta \varepsilon}{2\pi} \right)^2 \right) \right] \quad \text{Eq. 1.10}$$

where ε is the dielectric constant of water, a^2 the radius of the solid particle, σ the electric conductivity of the electrolyte and ζ is the electro-kinetic potential (zeta potential) of the charged particles. However, these two models Eq. 1.6 and Eq. 1.10 assumed that all the suspended particles are spherical and the electric double layer (EDL) thickness to be smaller than the particle diameter.

Bull [194], was the first to conduct a series of empirical tests to determine the contribution of the electroviscous effect on the effective viscosity of egg albumin. His results have suggested that the effective viscosity varies with the square of the electrophoretic mobility. When comparing the empirical data with Smoluchowski [180] and Krasny-Ergen [193] models, he has discovered that

both models over-predict the suspension viscosity. Thus, he has proposed the following model for the specific viscosity at the isoelectric point,

$$\frac{\mu_s}{\phi} = 0,0112 \frac{\mu_e}{\sqrt{k}} \quad \text{Eq. 1.11}$$

where μ_s is the specific viscosity, μ_e the electrophoric mobility and k the electric conductivity.

Later, Simha [195] extended the work of Einstein and Jeffrey and proposed a model based on the magnitude of the Péclet number (Pe), i.e., the ratio between the rate of strain to the rotational diffusion of the particle. According to the author, for high Péclet numbers, the motion of the particles is a purely hydrodynamic case and therefore Jeffrey model can be accepted. In contrast, as Pe tends to zero, the thermal motion of the particles are so intensive that the macroscopic flow is no longer able to align the ellipsoids. When this happens, one must consider the effects of Brownian motion. The model is given by:

$$\mu_{eff} = \mu_{bf} \left(1 + \left(\frac{f^2}{15(\log_2 f - 1,5)} + \frac{f^2}{5(\log_2 f - 0,5)} + \frac{14}{15} \right) \phi \right) \quad \text{Eq. 1.12}$$

this model is valid for an axial ratio of $f \gg 1$ for rigid rods, resulting in an increased viscosity due to the Brownian motion contribution. Moreover, this model can only be applied for the case of a laminar Couette flow.

Vand [181], studied how collisions between adjacent particles contribute to the viscosity of suspensions. He has stated that the collision process would be affected by the strength of the Brownian motion, by the attraction/repulsion forces and primarily due to the concentration. The proposed model only considers the simplest case, i.e. no attraction/repulsion forces and no Brownian motion. Moreover, the model considers collisions between doublets (two particles), triplets or more particles, and also the corresponding shape factor. The model is given by:

$$\begin{aligned} \mu_{eff} = \mu_{bf} & (1 + k_1\phi \\ & + \left[\frac{1}{2!} k_1(k_1 + 2Q) + r_2(k_2 - k_1) \right] \phi^2 + \dots) \end{aligned} \quad \text{Eq. 1.13}$$

where $k_1=2,5$ is Einstein shape factor of single spheres, $k_2=3,175$ is the shape factor of collision doublets, $r_2=4$ is the collision time constant and $Q=0,609$ is the hydrodynamic interaction constant. The Eq. 1.13 can then be written as:

$$\mu_{eff} = \mu_{bf} (1 + 2,5\phi + 7,349\phi^2 + \dots) \quad \text{Eq. 1.14}$$

Ten years after Bull [194] publication, Booth [196] recalculated the electroviscous effect and modified Smoluchowski model. The proposed model (Eq. 1.15) was capable of predicting the experimental data of Bull [194] with a higher accuracy,

$$\mu_{eff} = \mu_{bf} \left[1 + 2,5\phi \left(1 + \sum_1^{\infty} b_n \left(\frac{e\zeta}{k_b T} \right)^n \right) \right] \quad \text{Eq. 1.15}$$

where e is the electronic charge, ζ is the electro-kinetic potential, k_b is the Boltzmann's constant and T the absolute temperature.

As it could be seen, Einstein, Jeffrey, Burgers, Vand and Simha, they all proved that the effective viscosity is influenced by the particle geometry and concentration. In order to experimentally corroborate Einstein model, Ward et al. [197] conducted a series of experiments with rigid polymer microspheres in an aqueous solution. They concluded that the relative viscosity are independent of the rate of shear up to a concentration of 30%, independent of the absolute size of the spheres and viscosity of the suspending liquid, but dependent on the particle size distribution (PSD). The results have shown that for a PSD of 1:1 to 3:1, Einstein geometric constant (η) varies from approximately 4 to 1,9, respectively. Einstein, constant (2,5) was obtained for a ratio of 1,5:1. Additionally, these results have also corroborated the work developed by Vand [181].

In 1951, Mooney [185] proposed a model mainly based on empirical results of rigid spherical particles. The effective viscosity of the suspension is a function of the space-crowding effect (crowding factor) between adjacent particles. For the case of a mono-dispersed suspension, the model is given by:

$$\begin{aligned} \mu_{eff} &= \mu_{bf} \exp\left(\frac{\eta\phi}{1 - k\phi}\right) \Leftrightarrow \\ \Leftrightarrow \mu_{eff} &= \mu_{bf} \left(1 + \eta\phi + \left(\eta C_f + \frac{\eta^2}{2}\right)\phi^2 \right. \\ &\quad \left. + \left(\eta C_f^2 + C_f \eta^2 \frac{\eta^3}{6}\right)\phi^3\right) \end{aligned} \quad \text{Eq. 1.16}$$

where $\eta=2,5$ and C_f is the crowding factor for specific densely packed spheres. The crowding factor must be determined regarding the distribution of diameters of the suspended particles, but from a purely geometric argument $1,35 < k < 1,91$. One year later, Roscoe [182] demonstrated that the effective viscosity of a suspension containing spherical particles of diverse sizes and valid for all concentrations can be described by Eq. 1.17:

$$\mu_{eff} = \mu_{bf} (1 - \phi)^{-2,5} \quad \text{Eq. 1.17}$$

However, for the case of spherical suspensions of equally size and for high concentration, the structure on the fluid is arranged in such a way that results in the formation of packed aggregates. When this happens, the effective concentration increases and the proposed model can be expressed as:

$$\mu_{eff} = \mu_{bf} (1 - 1,35 \phi)^{-2,5} \quad \text{Eq. 1.18}$$

It has to be noted, that as the suspension become more diluted (lower concentration) both these models Eq. 1.17 and Eq. 1.18 are reduced to Einstein model (Eq. 1.4). Later, Krieger et al. [191] also considered the structuring of mono-dispersed systems as proposed by Mooney [185] and Roscoe [182]. The proposed model could be expressed as:

$$\mu_{eff} = \mu_{bf} \left(1 - \frac{\phi}{\phi_{max}}\right)^{-\phi_{max}[\eta]} \quad \text{Eq. 1.19}$$

where $\eta=2,5$, ϕ_{max} is the packing fraction (i.e the maximum concentration at which flow can occur), which varies from 0,495 to 0,54 in motionless conditions and 0,605 at high shear rates. However, in nature, mono-dispersed colloidal suspensions do not exist, therefore the aforementioned models may not be applied to practical situations. Later, Frankel et al. [189], applied an asymptotic technique and modified Krieger model (Eq. 1.19) and suggested the following expression:

$$\mu_{eff} = \mu_{bf} \left[\frac{9 \left(\left(\frac{\phi}{\phi_{max}} \right)^{\frac{1}{3}} \right)}{1 - \left(\frac{\phi}{\phi_{max}} \right)^{\frac{1}{3}}} \right] \quad \text{Eq. 1.20}$$

A different approach was considered by Batchelor [8]. He considered a colloidal suspension where individual particles interact with each other, and demonstrated that the particles hydrodynamic interactions as well as the Brownian motion affect the velocity and bulk stress in the suspension. The proposed model is given by:

$$\mu_{eff} = \mu_{bf} (1 + 2,5\phi + b\phi^2) \quad \text{Eq. 1.21}$$

where the coefficient b depends on the strength of the Brownian motion, which varies from 6,2 for strong or 7,6 for weak Brownian motion.

Leal et al. [198] expand the work developed by Jeffery [9] and Simha [195] on the effect of the particle axial ratio in a zero Reynolds numbers shear flow. The proposed model for the effective viscosity is a function of the particle axial ratio (f) and Péclet number and is given by:

$$\mu_{eff} = \begin{cases} \mu_{bf} \left[1 + \left(2 + \frac{0,312f}{\ln(f) - 1,5} \right) \phi \right] & (f \rightarrow \infty) \\ \mu_{bf} [1 + (3,183 - 1,792f)\phi] & (f \rightarrow 0) \end{cases} \quad \text{Eq. 1.22}$$

In 1981, Graham [188] suggested that the energy dissipation rate in a suspension, is due to particle interaction and energy dissipation as the fluid flow around the particle. Based on this assumption, the author proposed the following model:

$$\mu_{eff} = \mu_{bf} \left[1 + \frac{5}{2} \phi + \frac{9}{4} \left(\frac{1}{1 + \frac{h}{2a}} \right) \left[\frac{1}{\frac{h}{a}} - \frac{1}{1 + \frac{h}{a}} - \frac{1}{\left(1 + \frac{h}{a} \right)^2} \right] \right] \quad \text{Eq. 1.23}$$

where h is the interparticle distance and a is the particle radius. Despite being in the limits his formula is close to Einstein (dilute suspension) and Frankel et al. [189] (concentrated suspension), and is valid over the entire concentration range.

One of the last proposed models prior to the discovery of nanofluids came from Cristina et al. [173]. They have studied the contribution from hydrodynamic interactions on the effective viscosity of dilute suspensions of three hard spheres. The proposed model incorporates two types of interaction between particles, hydrodynamic interactions due to the influence of the particle movement on another particles and direct interactions due to interparticles forces. The model can be expressed as:

$$\mu_{eff} = \mu_{bf} (1 + 2,5\phi + 4,68\phi^2 + 6,40\phi^3 + \dots) \quad \text{Eq. 1.24}$$

Viscosity classic models summary

Throughout this survey, it was found that many theories were developed in an attempt to explain the effective viscosity of colloids. From the proposed mechanisms, the authors tend to highlight the internal friction, the particle

orientation, the electroviscous effect and the crowding effect. In Table 1.4 it can be depicted a synopsis of the proposed mechanisms.

Table 1.4 – Viscosity Model Summary

Researchers	Proposed Models						
	Internal Friction	Particle Collision	Particle Orientation	Size Distribution	Brownian Motion	Electroviscous Effects	Crowding Effect
Einstein [5]	X						
Hatschek [186]	X						
Smoluchowski [180]						X	
Jeffrey [9]	X						
Burgers [192]	X		X		X		
Krasny-Ergen [193]						X	
Bull [194]						X	
Simha [195]			X				
Vand [181]		X					
Booth [196]						X	
Ward et al. [197]				X			
Mooney [185]							X
Roscoe [182]							X
Krieger et al. [191]							X
Frankel et al. [189]							X
Batchelor [8]	X		X				
Leal et al. [198]					X		

Although a century has passed since Einstein theory, there is still a huge debate on the effective mechanisms that governs the viscosity of suspensions.

As it can be seen, most classical models are based on a relation between the viscosity of the base fluid and particle concentration. Moreover, when tested, these models give distinct results that can be depicted from Figure 1.5.

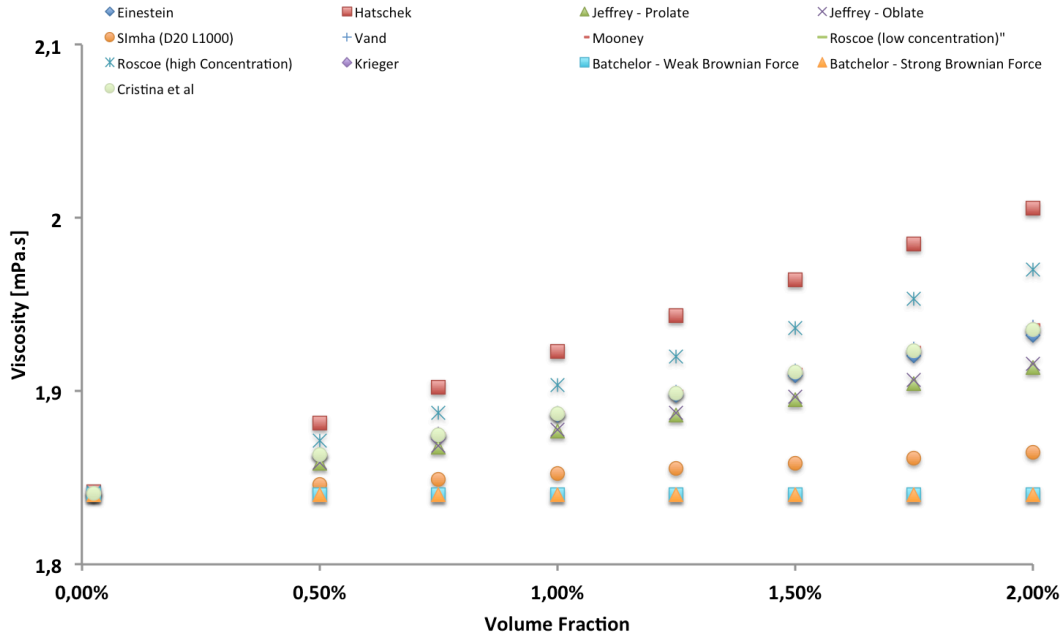


Figure 1.5 – Classical models summary for the same concentration at 300 K.

Models for nanofluids with spherical particles

Nanometric sized particles suspensions were first introduced by Eastman [199] in 1995. However, just in 1999 Liu et al. [137] proposed one of the first viscosity model for suspensions of nanoparticles. They have suggested that the viscosity of a suspension is a relation of the hydrodynamic interactions between particle and the liquid medium, particle-particle interaction and Brownian forces. The model can be expressed as:

$$\mu_{eff} = \mu_{bf} \left[\left(1 - \frac{\phi}{\phi_{max}}\right)^{-2} + \left(k_e - \frac{2}{\phi_{max}}\right) \phi + \left(k_h - \frac{6}{\phi_{max}^2}\right) \phi^2 \right] \quad \text{Eq. 1.25}$$

where $k_e = 2,5$ is the Einstein constant, k_h is the Huggin's constant and is a function of the flow strength, i.e. $k_h = 6$ when the flow is weak and $k_h = 7, 1$ when is strong. Also, the packing limit particle volume fraction ϕ_{max} is flow dependent being $\phi_{max} = 0, 64$ when the flow is weak and the particle orientation is randomly and $\phi_{max} = 0, 71$ when the flow is strong, since the particles will fill the spaces otherwise inaccessible with weak flows. In the same year Bicerano et al. [200]

conducted an exhaustive investigation on the viscosity of dispersions on the dilute, semi-dilute and concentrated regimes. They have developed a model based on the hydrodynamics and electrostatics relationship between particles and the liquid medium. The predicted model Eq. 1.26, was effective for dilute, semi-dilute and concentrate suspensions.

$$\mu_{eff} = \mu_{bf}(1 + 2,5\phi + k_H\phi^2 + \dots) \quad \text{Eq. 1.26}$$

where μ_{bf} is the intrinsic viscosity, and k_H is the Huggins coefficient. As mentioned, Huggins coefficient is a measure of interparticle interaction and Brownian motion. Also, k_H is very sensitive to particle aspect ratio and also to solvent type. They have, therefore, developed a general equation that is capable of predicting the effective viscosity over all concentration regimes and particle shape. The proposed model can be expressed has:

$$\mu_{eff} = \mu_{bf} \left(\left[1 - \frac{\phi}{\phi^*} \right]^{-2} \left[1 - 0,4 \left(\frac{\phi}{\phi^*} \right) + 0,34 \left(\frac{\phi}{\phi^*} \right)^2 \right] \right) \quad \text{Eq. 1.27}$$

where ϕ^* is the shape dependent critical volume fraction and for mono-dispersed spheres $\phi^* \approx 0,64$.

Tseng et al. [201] conducted a series of empirical investigations on nanofluids with spherical nanoparticles of Nickel (Ni) and Titanium dioxide (TiO₂). Based on experimental data, they have concluded that the particle network was flocculated having a fractal nature. They have, therefore, developed a model based on the nature of the nanoparticle fractal structure, as follows:

$$\mu_{eff} = \mu_{bf}(0,4513exp^{0,6965\phi}), \quad \text{for Ni} \quad \text{Eq. 1.28}$$

$$\mu_{eff} = \mu_{bf}(13,47exp^{35,98\phi}), \quad \text{for TiO}_2 \quad \text{Eq. 1.29}$$

A year later, Maiga et al. [202] correlated the empirical data from Wang et al. [203] and by performing a least-square curve fitting proposed the following models:

$$\mu_{eff} = \mu_{bf}(1 + 7,3\phi + 123\phi^2), \quad \text{for water} - Al_2O_3 \quad \text{Eq. 1.30}$$

$$\mu_{eff} = \mu_{bf}(1 - 0,19\phi + 306\phi^2), \text{ for ethylene glycol} - Al_2O_3 \quad \text{Eq. 1.31}$$

Kulkarni et al. [204] conducted an extensive empirical study on the rheological behaviour of aqueous dispersions of copper oxide (CuO) nanoparticles. Since viscosity is strongly temperature dependent, they have proposed a model where the effective nanofluid viscosity is a function of temperature and particle volume fraction. The model is valid for volume fractions ranging from 0,05 to 0,15%vol and is given by:

$$\ln(\mu_{eff}) = A\left(\frac{1}{T}\right) - B \quad \text{Eq. 1.32}$$

where T is the temperature and A and B are polynomials given by:

$$A = 20587\phi^2 + 15857\phi + 1078,3 \quad \text{Eq. 1.33}$$

$$B = -107,12\phi^2 + 53,548\phi + 2,8715 \quad \text{Eq. 1.34}$$

However, models based on the relation between effective viscosity with the volume fraction and temperature can only be applied for suspensions with the same base fluid and nanoparticle.

Chen et al. [205], suggested that the effective viscosity of nanofluids depends only on the concentration of nanoparticles. Furthermore, they have considered the aggregation of nanoparticles as the governing factor on the rheological behaviour of nanofluids. From this study, they have proposed the following model:

$$\mu_{eff} = \mu_{bf}(1 + 10,6\phi + 10,6\phi^2) \quad \text{Eq. 1.35}$$

On the same year, Praveen et al. [206] proposed another model based on empirical results for nanofluids containing CuO nanoparticles and a mixture of water and ethylene glycol. The model considers that the viscosity of the nanofluid is a function of the temperature and volume fraction, as it follows:

$$\text{Log}(\mu_{eff}) = A \exp^{-BT} \quad \text{Eq. 1.36}$$

where T is the temperature in Kelvin and A, B are coefficients related with the volume fraction (0 to 6.12% vol) as:

$$A = 1,8375\phi^2 - 29,643\phi + 165,56 \quad \text{Eq. 1.37}$$

$$B = 4E^{-6}\phi^2 - 0,001\phi + 0,0186 \quad \text{Eq. 1.38}$$

As it can be depicted, this model is in a similar form to Kulkarni [204] model and, therefore, has the same limitations (i.e it can only be applied to this type of nanofluid).

Another empirical investigation developed by Nguyen et al. [207] for $\text{Al}_2\text{O}_3\text{-H}_2\text{O}$ nanofluids, postulated that the growth off the effective viscosity over nanoparticle concentration, is directly related to the strength of the internal viscous shear stresses. Additionally, they have demonstrated that nanoparticles size and temperature also have influence on the viscosity, proposing four models:

$$\mu_{eff} = \mu_{bf}(0,904 \exp^{0,1483\phi}) \text{ for } 47\text{nm} \quad \text{Eq. 1.39}$$

$$\mu_{eff} = \mu_{bf}(1 + 0,025\phi + 0,015\phi^2) \text{ for } 36\text{nm} \quad \text{Eq. 1.40}$$

and the temperature dependence,

$$\mu_{eff} = \mu_{bf}(1,125 - 0,0007T) \text{ for } 1\%vol \quad \text{Eq. 1.41}$$

$$\mu_{eff} = \mu_{bf}(2,1275 - 0,0215\phi + 0,0002\phi^2) \text{ for } 4\%vol \quad \text{Eq. 1.42}$$

where T is the fluid temperature in °C.

Masoumi et al. [208] suggested that the Brownian motion has an important contribution to the apparent viscosity. Though an empirical and theoretical analysis, they deduced that the apparent viscosity is a function of size, density and nanoparticle volume fraction, temperature and base fluid physical properties. Furthermore, the author claims that this model is capable of predicting the effective viscosity for other nanofluids, such as: CuO-H₂O, CuO-EG, TiO₂-EG, CuO-EG+H₂O and Al₂O₃-H₂O. The model can be expressed as:

$$\mu_{eff} = \mu_{bf} + \frac{\rho_p V_B d_p^2}{72C\delta} \quad \text{Eq. 1.43}$$

where ρ_p is the particle density, δ is the distance between adjacent particles, V_B is the Brownian velocity, d_p is the particle diameter. V_B , δ and C are defined as:

$$\delta = \sqrt[3]{\frac{\pi}{6\phi}} d_p \quad \text{Eq. 1.44}$$

$$V_B = \frac{1}{d_p} \sqrt{\frac{18 K_b T}{\pi \rho_p d_p}} \quad \text{Eq. 1.45}$$

$$C = \mu_{bf}^{-1} [(c_1 d_p + c_2) \rho + c_3 d_p + c_4] \quad \text{Eq. 1.46}$$

where c_1 a c_4 are determined experimentally. It should be noted, that for comparative purposes the determination of these constants, as described by the authors, would not be feasible to other nanofluids.

The same hindrance could be founded on the model developed by Duangthongsuk et al. [209]. The proposed model is similar to Batchelor [8] model (Eq. 1.21). However, no conclusion is made regarding the contribution of the Brownian motion as Batchelor did. The correlation is given by:

$$\mu_{eff} = \mu_{bf}(a + b\phi + c\phi^2) \quad \text{Eq. 1.47}$$

where a , b and c are constants determined empirically by curve fitting for three different temperatures.

Similarly, Sahoo et al. [210], provided an empirical model for Al₂O₃ nanofluids based on volume fraction and temperature. The proposed correlation is able to predict the effective viscosity in both low (238 - 273K) and high (273-363K) temperature regimes and can be expressed as:

$$\mu_{eff} = A \exp\left(\frac{B}{T} + C\phi\right) \quad \text{Eq. 1.48}$$

where T is the absolute temperature in K and A, B and C were obtained by curve fitting the experimental data.

Phuoc et al. [211], conducted a series of experiments to study the shear rate viscosity dependence on Fe₂O₃ - H₂O nanofluids. They have suggested that an effective viscosity model must account for the effects that an imposed shear rate has on the suspension percolation network. From this study they have proposed the following model:

$$\mu_{eff} = \mu_{bf} + \left(\frac{k \exp^{n\phi}}{\gamma}\right)^{0,5} \left[(k \exp^{n\phi})^{0,5} + 2\mu_{bf}^{0,5} \right] \quad \text{Eq. 1.49}$$

where k and n were determined through linear fitting the experimental data.

Chandrasekar et al. [212] re-analysed the effective viscosity of suspensions based on Noni [136] model. For a given particle size, the model can be expressed as it follows:

$$\mu_{eff} = \mu_{bf} \left(1 + 6 \left(\frac{\phi}{1 - \phi} \right)^n \right) \quad \text{Eq. 1.50}$$

where the constants $b=5300$ and $n=2,8$ are influenced by the electromagnetic effects between phases (Liquid - Solid). These were empirically determined for Al₂O₃ - H₂O nanofluids, at room temperature. Likewise, Hosseini et al. [213] proposed a different model for the same suspension of Al₂O₃ in water. Contrary to other authors, they have deduced that the effective viscosity cannot only be a function of volume fraction and base fluid viscosity, but it also has to take into

consideration the contribution of nanoparticles size, effect of the capping layer and temperature. The authors have proposed the following model:

$$\mu_{eff} = \mu_{bf} \exp \left[m + \alpha \left(\frac{T}{T_0} \right) + \beta(\phi_H) + \gamma \left(\frac{d}{1+r} \right) \right] \quad \text{Eq. 1.51}$$

where $m=0,72$ depends on the system properties, i.e. the solid nanoparticles, the base fluid and their interaction, the constants α , β and γ were empirically determined and T , $T_0=25^\circ\text{C}$ are the suspension temperature and reference temperature, respectively. In order to account for particle interaction, especially for high concentration regimes, the hydrodynamic volume fraction (ϕ_H) has to be evaluated:

$$\phi_H = \phi \left[\frac{d + 2s}{d} \right]^3 \quad \text{Eq. 1.52}$$

where d is the particle diameter and $s=1\text{E-}9$ is the thickness of the capping layer.

In 2010, Godson et al. [214] proposed a model for aqueous suspensions of silver nanoparticles. Despite their demonstration on the influence of Brownian motion and thermophoresis on the thermal conductivity, little information is given regarding the mechanisms governing the effective viscosity. Nevertheless, through a quadratic linearization of the volume fraction, they have proposed the following model:

$$\mu_{eff} = \mu_{bf} (1,005 + 0,497\phi - 0,1146\phi^2) \quad \text{Eq. 1.53}$$

Corcione et al. [215] developed an empirical correlation considering the experimental data obtained by several authors [216]. The author claims that the model provides a good agreement with the experimental results, within a 1,84% standard deviation. The model is given by:

$$\mu_{eff} = \mu_{bf} \left(\frac{1}{1 - 34,87 \left(\frac{d_p}{d_f} \right)^{-0,3} \phi^{1,03}} \right) \quad \text{Eq. 1.54}$$

where d_f is the equivalent diameter of a base fluid molecule and is given by:

$$d_f = 0,1 \left(\frac{6M}{N \pi \rho_{bf}} \right)^{\frac{1}{3}} \quad \text{Eq. 1.55}$$

in which M is the molecular weight of the base fluid, N is the Avogadro number and ρ_{bf} is the mass density of the base fluid at 293K.

In the same year, Abareshi et al. [217] fit their Fe_3O_3 - glycerol nanofluid experimental data, into the Vogel-Fulcher-Tammann (Eq.1) [218]. The proposed correlation is as follows:

$$\mu_{eff} = \mu_{bf} A \exp \left(\frac{B}{T - T_0} \right) \quad \text{Eq. 1.56}$$

where A and T_0 are fitting constants and B is related with the free activation energy of the fluid. As the authors did not suggest any responsible mechanisms for the viscosity enhancement, the empirical determined constants make this model impractical for other type of nanofluids. Even so, for the same nanoparticles, Colla et al. [219] proposed a correlation in a similar form to Batchelor (Eq. 1.21) as follows:

$$\mu_{eff} = \mu_{bf} (1 + a\phi + b\phi^2) \quad \text{Eq. 1.57}$$

where the parameters $a=18,64$ and $b=248,3$ were regressed basing on extensive experimental data. Also, Sundar et al. [171] suggested a model for these type of nanoparticles expressed as:

$$\mu_{eff} = \mu_{bf} \left(1 + \frac{\phi}{12,5}\right)^{6,356} \quad \text{Eq. 1.58}$$

Nevertheless, both authors [171], [219] did not suggested any mechanism capable of explaining the observed results. In the same manner, Bobbo et al. [84] also proposed a equation similar to Batchelor model, as:

$$\mu_{eff} = \mu_{bf}(1 + 0,36838\phi + 1,74486\phi^2) \quad \text{Eq. 1.59}$$

More recently, Heyhat et al. [220] proposed a correlation considering only the effect of volume fraction for water based Al_2O_3 nanofluids. Despite no governing mechanism was suggested, the curve-fit model is expressed as:

$$\mu_{eff} = \mu_{bf} \exp\left(\frac{5,989\phi}{0,278 - \phi}\right) \quad \text{Eq. 1.60}$$

For concentration regimes of 0,01 to 5% vol. of alumina dispersed in water, Sekhar et al. [168] proposed a model by curve fitting the experimental data. The model is given by:

$$\mu_{eff} = \mu_{bf} \left[0,935 \left(1 + \frac{T_{nf}}{70}\right)^{0,5602} \left(1 + \frac{d_p}{80}\right)^{-0,05915} \left(1 + \frac{\phi}{100}\right)^{10,51} \right] \quad \text{Eq. 1.61}$$

where the above correlation is valid for $13 < d_p < 100$ [nm] and $20 < T_{nf} < 70$ °C.

Recently, Esfe et al. [221] developed an experimental investigation on Zinc Oxide (ZnO) nanoparticles suspended in Ethylene glycol. The proposed model, results from the regression of viscosity data for different temperatures and solid concentrations. However, no governing mechanism has suggested to explain the experimental observations. The proposed model can be expressed as:

$$\mu_{eff} = \mu_{bf}(0,9118 \exp(5,49\phi - 0,00001359T^2) + 0,0303 \ln(T)) \quad \text{Eq. 1.62}$$

where T and Φ is the nanofluid temperature and volume fraction, respectively.

Models for nanofluids with non-spherical or elongated particles

Previously it was highlighted that, Jeffrey, Einstein, Burgers, Vand have established the contribution of particle geometry on the viscosity of suspensions. It is, therefore, critical to establish alternative formulations for suspensions of non-spherical particles. The most studied non-spherical particles are carbon nanotubes (CNT). However, very few viscosity models here proposed for these tubular shape particles with a high aspect ratio.

In 2012, Vakili-Nezhaad et al. [81] empirically investigated the effective viscosity of single walled carbon nanotubes (SWCNT) in Lubricant oil. Although the authors did not experimentally prove it, they suggested that the discrepancies found between theoretical and empirical models could be attributed to particles aggregations and the formation of percolation networks between nanotubes. Notwithstanding, they have proposed two models based on the experimental data:

$$\mu_{eff} = (1048 - 30,3T + 0,2T^2) \text{ for } 0,1\% \text{ wt.} \quad \text{Eq. 1.63}$$

$$\mu_{eff} = \mu_{bf}(1 + 1,59\phi - 16,36\phi^2 + 50,4\phi^3) \text{ for } T = 298 \text{ K} \quad \text{Eq. 1.64}$$

In the same year, Bobbo et al. [84] proposed a model based on experimental data for SWCNT and water. Although the authors did not suggest any possible mechanism to explain the nanofluid viscosity enhancement, the model is in a similar fashion to Batchelor model (Eq. 1.21) and is given by:

$$\mu_{eff} = \mu_{bf}(1 - 0,50438\phi + 1,74486\phi^2) \quad \text{Eq. 1.65}$$

Nanofluids viscosity models summary

During the conducted survey, it was found that there are several models specially developed to predict the effective viscosity of nanofluids. However, very few authors have suggested which intrinsic mechanisms are responsible for theirs experimental observations. Moreover, the majority of the studied authors, proposed their models based on the regression of empirical results, and,

therefore, limiting their models to a specific nanofluid, temperature and concentration.

In Figure 1.6, it can be depicted the predictions presented by some models for spherical particles, with respect to the same base fluid and nanoparticle size and geometry. As it can be seen, some discrepancies can be found between models. Moreover, some models predict viscosities inferior to that of the base fluid. This can be explained since some models do not consider the effect of the base fluid viscosity and also because some models were developed through empirical data regression.

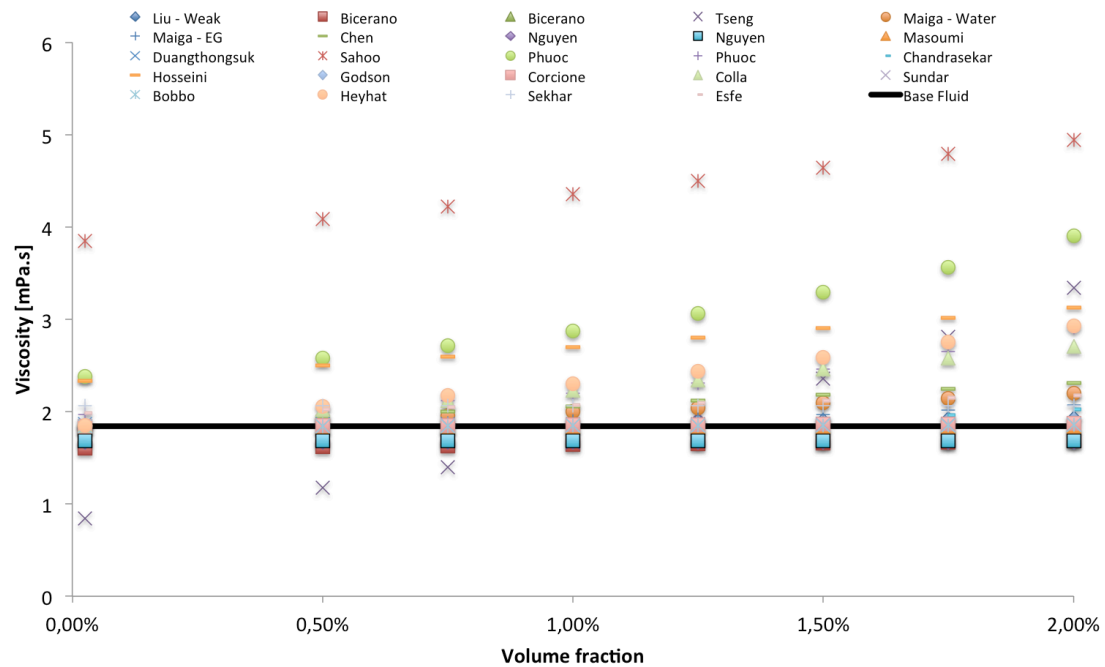


Figure 1.6 - Spherical models predicted viscosity for a suspension of 30% Ethylene Glycol-Water and different concentrations of nanoparticles at 300 K

In contrast with the large number of predictive models for nanofluids with spherical particles, non-spherical particles, such as CNT, has received very little attention. In Figure 1.7 it is represented the predicted viscosity given by Vakili-Nezhaad et al. [81] and Bobbo et al. [84] models. As it can be depicted, both models show a linear relationship between the effective viscosity and the nanoparticle volume fraction. Furthermore, the differences between each model are less than 2%. Moreover, just Vakili-Nezhaad et al. [81] have suggested that

the discrepancies found when applying spherical models to predicted the viscosity of CNTs nanofluids, could be attributed to particle aggregation and to the formation of percolation networks.

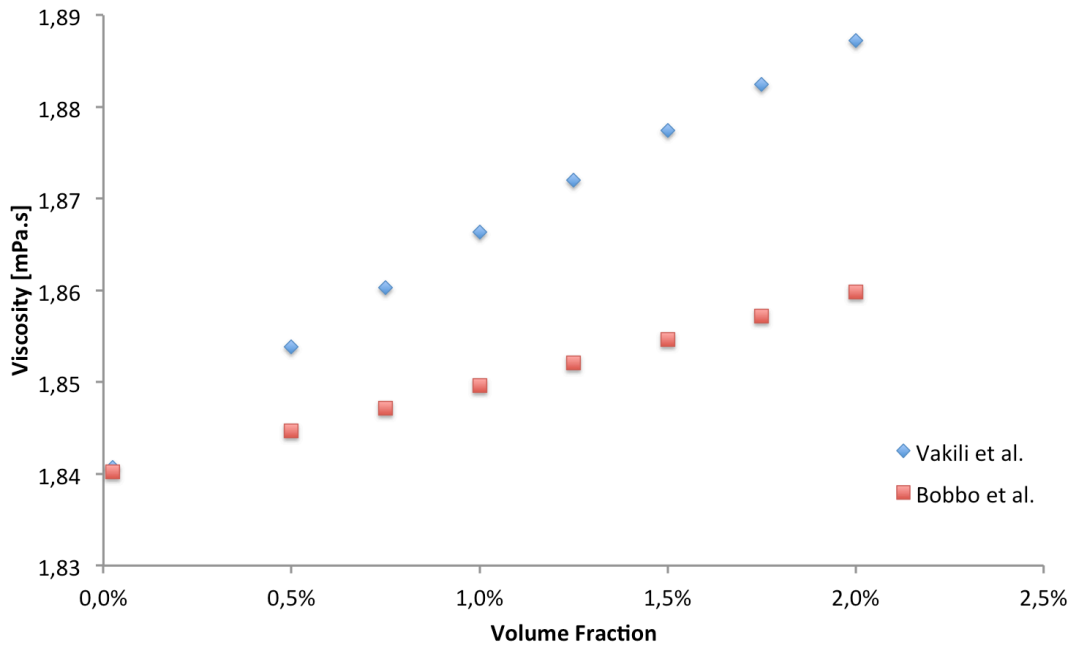


Figure 1.7 - Non-Spherical models predicted viscosity for a suspension of 30% Ethylene Glycol-Water and different concentrations of nanoparticles at 300 K

As it can be depicted from Table 1.5, almost all authors take into consideration the effect of nanoparticle volume fraction and base fluid viscosity on their models. This was expected, since colloidal particles move in response to fluid motion. By reacting to the local velocity of the fluid, colloidal particles experience hydrodynamic interaction, and higher volume fractions lead to more hydrodynamic interactions, which then result on a higher viscosity. Despite this long-recognized ubiquity, quantifying the influence of hydrodynamic interactions on colloidal systems is still challenging. This problem relies on the fact that hydrodynamic interactions are sensitive to nanoparticles shape and size, the existence of agglomerates or percolation networks and base fluid properties.

Table 1.5 – Summary of the effective viscosity models and respective control parameters

	References	% Vol.	Critical Volume Fraction	Temperature	Base Fluid Viscosity	Nanoparticle Size	Shear Rate	Camping Layer
Spherical Particles	Liu et al. [137]	X	X		X			
	Bicerano et al. [200]	X	X		X			
	Tseng et al. [201]	X			X			
	Maiga et al. [222]	X			X			
	Kulkarni et al. [204]	X		X				
	Chen et al. [205]	X						
	Praveen et al. [206]	X		X				
	Nguyen et al. [207]	X		X	X	X		
	Masoumi et al. [208]	X		X	X	X		
	Duangthongsuk et al. [209]	X			X			
	Sahoo et al. [210]	X		X				
	Phuoc et al. [211]	X			X		X	
	Chandrasekar et al. [212]	X			X			
	Hosseini et al. [213]	X		X	X	X		X
	Godson et al. [214]	X				X		
	Corcione et al. [215]	X				X	X	
	Abareshi et al. [217]	X			X	X		
	Colla et al. [219]	X				X		
	Sundar et al. [171]	X				X		
	Bobbo et al. [84]	X				X		
	Heyhat et al. [220]	X				X		
	Sekhar et al. [168]	X			X	X	X	
Esfe et al. [221]	X			X	X			
Non-Spherical particles	Vakili-Nezhaad et al. [81]	X			X			
	Bobbo et al. [84]	X			X			

The most surprising fact is that, very few authors have suggested any theory or mechanism to explain their empirical observations regarding the viscosity of nanofluids, (see Table 1.3). Nevertheless, the authors highlighted the Brownian motion, the particle agglomeration, formation of percolation networks, the interparticle interaction and the hydrodynamic interaction. In Table 1.5 it is summarized the derived predicted models and theirs underlying respective mechanisms.

1.3.8 Experimental Studies

Throughout the years, several types of nanoparticles have been used to alter the thermo-physical properties of conventional fluids. These new type of

heat transfer fluids or nanofluids, are strongly related to the fluid microstructure, and, therefore, can be categorized regarding the nature of the nanoparticles, i.e. metallic, metallic oxide and non-metallic, or through their shape, (quasi-) spherical and non-spherical (elongated). Moreover, nanoparticles suspended in a fluid are influenced by several forces such as: Brownian motion, viscous resistance (Stokes drag force), intermolecular van der Waals interaction (interparticles interactions, particle-fluid interaction) and electrostatic forces (interactions between ions and dipoles) [172].

Next, it is presented a survey of some empirical studies regarding the viscosity of nanofluids. The intent of this survey is to identify the proposed mechanisms responsible for the rheological behaviour of nanofluids.

Nanofluids with Spherical Nanoparticles

Copper oxide (CuO), alumina (Al₂O₃) and titania (TiO₂) are by far the most used nanoparticles for the production of nanofluids. This relies on the fact that these nanoparticles are less expensive and chemically stable. In Table 1.6, it is represented a summary of empirical investigations, for some types of nanoparticles.

Table 1.6 – Summary of experimental studies of viscosity of spherical particles based nanofluids.

Researchers	Particle	Diameter	Base Fluid	Dispersion Method	Volume Fraction	Temperature	Max Relative viscosity	Rheological behaviour
		[nm]			[% vol.]	[K]		
Non-Covalent Functionalization								
Pak and Cho [216]	Al ₂ O ₃	13	DW	HSM	1 - 10	298	3	Shear Thinning > 3%vol.
Pak and Cho [216]	TiO ₃	27	DW	HSM	1 - 10	298	200	Shear Thinning >10% vol.
Noni et al. [136]	Al ₂ O ₃	1200	DW	MS	2 – 24	298	350	Shear Thinning
Tseng et al. [223]	TiO ₃	7 – 20	DW	BM	5 – 12	298	1200	Shear Thinning
Kulkarni et al. [204]	CuO	29	DW	MS – US	5 – 15	278 – 323	-	Shear Thinning
Chevalier et al. [149]	SiO ₂	35 – 190	Etanol	MS	1,1 – 7	-	1,9	Newtonian
Chen et al. [145]	TiO ₃	25	EG	US	0 – 8 %wt.	293 – 333	20	Newtonian
Namburu et al. [206]	CuO	29	60:40 /	MS, US	1 – 6,12	238 – 323	4,6	Newtonian

EG:DW								
Garg et al. [224]	Cu		EG	US	0,6 – 1,5	298	-	Shear Thinning
Masoumi et al. [208]	Al ₂ O ₃	13, 28	DW	-	1 – 5	-	2,6	
Duangthongnuk et al. [209]	TiO ₃	21	DW	MS, US	0,2 – 2,0	288 – 308	1,15	
Sahoo et al. [210]	Al ₂ O ₃	53	60:40 / EG:DW	US	1 -10	238 – 363	4	Shear Thinning T< 273 K Newtonian T>273 K
Houseini et al. [213]	Al ₂ O ₃	36	DW	-	1 – 9,1	238 – 293	5,1	-
Abareshi et al. [217]	Fe ₂ O ₃	5	Glycerol	US	0,25 – 0,75	305 – 343	-	Shear Thinning
Colla et al. [219]	Fe ₂ O ₃	67	DW	US	5 – 20 %wt.	298 – 343	2,72	Newtonian
Heyhat et al. [220]	Al ₂ O ₃	40	DW	US	0,1 – 2	298 – 333	1,65	
Vakili et al. [225]	TiO ₃	25	DW	US	0,5 – 1,5	294	-	-
Suganthi et al. [226]	ZnO	35 – 40	PG	US	0,5 – 2	301 – 413	1,1	Newtonian
Covalent Functionalization								
Tseng et al. [201]	Ni	300	Terpicol / Dispersant	BM	3 – 10	298	540	Shear Thinning
Nguyen et al. [207]	Al ₂ O ₃	36, 47	DW / Dispersant	MS	1 -13	294 - 348	5,5	-
Phuoc et al. [211]	Fe ₂ O ₃	20 - 40	DW / Dispersant	MS, US	1 – 4	298	-	Shear Thinning
Kole et al. [169]	CuO	40	Gear Oil / Dispersant	MS	0,5 – 2,5	273 – 353	3	Shear Thinning
Bobbo et al. [84]	TiO ₃	21	DW / Dispersant	HPH	0,01 – 1% wt.	283 – 353	-	Newtonian
Suganthi et al. [167]	ZnO	136 – 140	DW / Dispersant	US	0,25 – 2	283 – 323	1,17	-
Sekhar et al. [168]	Al ₂ O ₃	47	DW / Dispersant	-	0,01 – 1	293 – 323	1,33	-

DW – Dionized Water, EG – Ethylene Glicol, PG – Polyethylene, HSM – High Speed Mixer, MS – Mechanical Stirrer, BM – Ball Mixing, US – Ultrasound, HPH – High Pressure Homogenizer.

Most researchers covered by this survey, reported an increase of the effective viscosity with the volume fraction and a decrease with increasing temperature. Moreover, it can be depicted from Table 1.6 that shear thinning (i.e. viscosity decreases with shear rate) is the most common rheological phenomena in suspensions. However, this phenomenon is not yet fully understood. Some authors attribute this to the disentanglement of nanoparticles clusters due to shearing forces, while others to the alignment of the nanoparticles with the shear direction.

In contrast with most authors, Suganthi et al. [226] observed that the relative viscosity, for a temperature range of 301-383 K and 0 - 2% vol., is lower

than one, i.e. the addition of nanoparticles decrease the effective viscosity. They have attributed this distinctive phenomenon, to the weakening of the intermolecular hydrogen bond between the nanoparticles and the base fluid.

One of the first empirical works regarding the viscosity of nanofluids was made by Pak and Cho [216]. They have measured the effective viscosity of Al_2O_3 and TiO_2 dispersed in water for various volume fractions. Despite the Newtonian nature of the base fluid, the experimental results depicted a shear thinning behaviour for concentrations over 3% for Al_2O_3 and 10% for TiO_2 . However, when comparing the absolute viscosity for the same volume fraction, the Al_2O_3 suspension presented an increase of 200 times over the base fluid viscosity, while the TiO_2 suspension increase was only 3 times higher. The authors suggested that this significant increment may be attributed to the viscoelectric effect, i.e. the particle effective radius is much larger than its radius. Moreover, the irregular shape of the particle and also a rough surface may have contributed to the viscosity increment. Also, Tseng et al. [223] studied the effective viscosity of TiO_2 suspended in water. They have reported a thixotropy behaviour for suspensions with volume fractions over 10%, which they attribute to the existence of particles clusters and interparticle interaction. Other authors also suggested this aggregate like structured to explained the non-Newtonian behaviour of nanofluids [149], [167], [205], [211].

Namburu et al. [206] studied the effective viscosity of CuO nanoparticles suspended in a mixture of 60% Ethylene glycol and 40% of water. They have stated that the nanofluid exhibit a Newtonian behaviour over the entire volume fraction and temperatures. An identical result has obtained by Garg et al. [224] for Cu nanoparticles in Ethylene glycol.

Masoumi et al. [208] investigated the influence of the temperature, nanoparticle diameter, volume fraction and base fluid properties on the effective viscosity of a suspension of Al_2O_3 in water and Ethylene glycol. Their results effectively demonstrate that: the nanofluid viscosity increases with the nanoparticle diameter and volume fraction increment, is directly related with base fluid properties and also that the nanoparticles Brownian motion influences the nanofluid viscosity. A similar investigation was carried out by Wang et al.

[148] for SiO₂ nanoparticles suspended in water. They report a viscosity increment with decreasing nanoparticle diameter and with increasing pH level.

In order to resolve the inconsistencies found on the literature, several worldwide researchers reported on a benchmark designed as the *International Nanofluid Property Benchmark Exercise* (INPBE). Ten different nanofluids were distributed in four sets to participants in the program. The samples viscosities were measured through different approaches, but in general there were agreement ($\pm 20\%$) between different laboratories. However, the researchers did not disclose the temperature in which the tests were conducted, making impossible to compare their results with other investigations. Moreover, they have attributed the shear thinning behaviour of some nanofluids to the flow-induced perturbation of particle positions, i.e. the rate of particle displacement is given by the shear rate and by Brownian motion. Therefore, as the nanoparticle positions are disturbed by the induced-flow at a faster rate than they can recover by thermal fluctuations, the viscosity of the suspension becomes shear-rate dependent [227].

Despite the huge international effort to understand the rheological behaviour of spherical nanoparticles suspensions, there is still some controversy regarding the mechanisms that govern the rheology of colloids.

Nanofluids with Non-Spherical Nanoparticles

Non-spherical particles such as carbon nanotubes (CNTs) have attained much attention from the scientific community, mainly due to the high thermal conductivity of these nanoparticles. However, a small amount of scientific reports, when compared with thermal conductivity, can be found regarding the rheological behaviour of nanofluids with non-spherical nanoparticles. In Table 1.7, it is presented a summary of some empirical investigations regarding the viscosity of non-spherical nanofluids.

Table 1.7 – Summary of experimental studies of viscosity of non-spherical particles based nanofluids

Researchers	Particle	Diameter	Length	Base Fluid	Dispersion Method	Volume Fraction	Temperature	Max Relative viscosity	Rheological behaviour
		[nm]	[µm]			[% vol.]	[K]		
Non-Covalent Functionalization									
Indhuja et al. [18]	MWCNT	10	5 – 15	DW	US	0,14 – 0,24	301 – 333	1,23	-
Lee et al. [16]	MWCNT	10 – 60	0,5 – 50	DW	US	1	-	-	-
Chen et al. [228]	MWCNT	30 – 50	20	EG, Gly, SO	US	0,2 – 1	293 – 333	-	Newtonian
Bobbo et al. [84]	SWCNT	60	-	DW	HPH	0,0048 – 0,48	283 – 353	1,26	Newtonian
Kumaresan et al. [123]	MWCNT	30 – 50	10 – 20	30:70 EG:DW	MS, US	0,15 – 0,45	273 – 313	3,25	-
Teng et al. [49]	MWCNT	20 – 30	10 – 30	50:50 EG:DW	Ms, US	0,1 – 0,8% wt	373 – 368	1,1	-
Rashmi et al. [118]	MWCNT	-	-	DW	-	0,01% wt	298 – 333	0,81	Shear Thinning
Ruan et al. [93]	MWCNT	10 – 30	10 – 30	DW, EG	US	0,05 – 0,24	293	1,3	Shear Thinning
Ding et al. [65]	MWCNT	-	-	DW	MS	0,1 – 0,5	-	7,5	Shear Thinning
Yang et al. [82]	MWCNT	-	-	Oil	US	0,04 – 0,34	298	-	Shear Thinning
Ko et al. [63]	MWCNT	-	-	DW	US	0,14	-	-	Shear Thinning
Phuoc et al. [66]	MWCNT	20 – 30	10 – 30	DW	US	0,4 – 1,4	-	-	Shear Thinning
Said et al. [97]	SWCNT	1 – 2	1 – 3	DW	US	0,1 – 0,3	298 – 333	1,39	-
Soma et al. [229]	CNT	20 – 30	-	DW	MS, US	0,2 – 0,8	303 – 333	1,27	Shear Thinning
Aladag et al. [143]	MWCNT	9000	200	DW	-	1% wt	275 – 283	-	Shear Thinning
Sadri et al. [125]	MWCNT	20 – 30	10 – 30	DW	US	0,5% wt	288 – 313	-	Shear Thinning
Estellè et al. [67]	MWCNT	9	15	DW	-	0,55	293	-	Shear Thinning
Covalent Functionalization									
Timofeeva et al. [172]	Al ₂ O ₃	9 – 40	9 – 80	50:50 EG:DW	MS, US	1 – 8,4	298	-	Newtonian / Shear Thinning
Vakili et al. [81]	SWCNT2	2	10 – 15	Oil	Ms, US	0,01 – 0,2% wt	298 – 373	1,14	-
Beheshti et al. [121]	MWCNT	10 – 20	30	Oil	US	0,001 – 0,01% wt	293 – 353	0,98	Newtonian
Derakhshan et al. [230]	MWCNT	5 – 20	1 – 10	Oil	MS, US	0,031 – 0,125	293 – 373	1,24	Newtonian
Gomez et al. [231]	MWCNT	15 – 80	8 – 20	DW	US	0,12 – 0,24	278 – 298	1,16	-
Chougule et al. [112]	MWCNT	20 – 30	3 – 8	DW	US	0,15 – 1	293 – 353	1,3	-
Ko et al. [63]	MWCNT	-	-	DW	-	0,06 – 0,22	-	-	Shear Thinning
Oliveira et al. [70]	MWCNT	50 – 80	10 – 20	DW	MS, US	0,25 – 2,5	298 – 318	-	Shear Thinning
Han et al. [59]	Carbon Power	50 – 500	-	DW	US	4,4 – 7,7	298 – 323	-	Shear Thinning
Kinloch et al. [71]	MWCNT	11	9100	DW	US	0,4 – 11	298	-	Shear Thinning

DW – Dionized Water, EG – Ethylne Glicol, PG – Polyethylene, HSM – High Speed Mixer, MS – Mechanical Stirrer, BM – Ball Mixing, US – Ultrasound, HPH – High Pressure Homogeneizer.

As it can be depicted from Table 1.7, almost all researchers reported a viscosity increment with volume fraction and decrease with the temperature rise. Moreover, the shear thinning behaviour is much common for non-spherical particle than for spherical. However, like for spherical nanoparticles, this phenomenon is not fully understood. Still, a large number of mechanisms have been proposed to clarify this behaviour. It is described by the literature that the viscosity of a nanofluid critically depends upon size, geometry and aspect ratio of the nanoparticles, volume fraction, particle-particle interaction, base fluid density and polarity [66], [172].

The effect of pH level, nanoparticle shape and dimension was part of the investigation carried out by Timofeeva et al. [172] for Al_2O_3 nanofluids. One of the objectives of this study was, to verify how the pH level affected the particle-particle interaction. The experimental data has shown that pH level is directly proportional to nanofluid viscosity, i.e. the higher the pH level the higher the viscosity. They have attributed this phenomenon to the intensification of repulsion forces between particles at low pH level, resulting in weaker particle-particle interactions and in a lower viscosity. Moreover, they have demonstrated that the rheological behaviour is a function of particle shape and aspect ratio, i.e. the viscosity is higher for platelet-like and smaller aspect ratio nanoparticles. Also, as the volume fraction reaches $>3\%$ vol. these nanofluids present a shear thinning effect.

Ma et al. [142] studied the influence of chemically treated and untreated CNTs on the apparent viscosity as a function of shear rate. In this study, it was found that both types of nanofluids were shear thinned, but for the same concentration the untreated CNT suspension has shown a significant larger viscosity than the chemically treated CNTs. Similar observations were made by Xu et al. [60] and Rahatekar et al. [163]. Both authors optically observed an aggregate microstructure for the untreated CNTs suspensions.

Another insight that may contribute to the discrepancy found between empirical investigations is the synthesis of the nanofluids. Despite the majority of researchers using ultrasounds to disperse the nanoparticles in the base fluid, there is no consensus regarding the time or energy that should be supplied to the mixtures. To tackle this issue Ruan et al. [75] studied the effect of ultrasonication

on the rheological properties of CNTs. The objective of this study has to evaluate if the preparation of a nanofluid with ultrasounds equipment affected the viscosity of nanofluids. The authors reported that at a fixed shear rate, the viscosity of the nanofluid increased with sonication time until a maximum (40minute sonication time). Afterwards, it decreases gradually until for long sonication times it approaches the viscosity of the based fluid. The authors attributed these effects to the decreased of clusters sizes with sonication time. Thus, the energy induced in the suspension must be carefully chosen.

Nevertheless, some divergence in results were reported by Beheshti et al. [121]. They claim that the dispersion of MWCNTs in a fluid decreased the viscosity of the solution. They attribute this phenomenon to the increase of the lubricating property between fluid layers and consequently viscosity decreases. Also, Rashmi et al. [118] reported that theirs nanofluids have a lower viscosity than water. However, this situation occurs due to the presence of Gum Arabic (dispersant), which reduces the overall viscosity of the base fluid.

1.3.9 Discussion and Major conclusions

From the conducted survey it is possible to claim that the addition of solid particles in fluids modifies its intrinsic properties. Despite the large number of empirical and theoretical work in colloidal science, there is still a huge discussion regarding the effects of dispersed nanoparticles on the transport and thermal properties of nanofluids.

Additionally, it was possible to notice the existence of a large discrepancy between similar empirical investigations. This may be explained by the lack of an appropriate standardised synthesis methodology to disperse nanoparticles in fluids. It is, therefore, fundamental the development of an optimized and standardized methodology capable of producing stable, long-term suspensions stabilities. The latter has to take into consideration all the parameters, from the nanoparticle production method to the energy required to disperse the nanoparticles in the fluid.

Several authors reported anomalous viscosities enhancements in nanofluids and rheological behaviours that cannot be explained by classical theories. Despite the several new theories that have been proposed, there is still a lack of agreement between research groups regarding the intrinsic mechanisms governing its rheology. Moreover, prior to any study regarding the rheological behaviour of nanofluids, a complete database covering all the thermal and transport properties of MWCNTs nanofluids must be evaluated. This is very important since from the literature survey it was possible to verify that the rheological behaviour of nanofluids are sensible to several parameters such as, base fluid density, particle density, nanoparticle dimensions, etc.

1.4 Thesis Specific Objectives and Research Questions

The main objective of this work is to develop and characterize multi-walled carbon nanotubes based nanofluids for thermal engineering purposes. Moreover, this work comes in continuation of a previously work developed by Lamas entitled “Nanofluids development and characterization for heat exchanging intensification”.

It is a fact, that the addition of conductive solid nanoparticles to conventional fluids modifies its thermal and transport capabilities. However, nanofluid preparation is not problem-free and requires a precise and specific methodology to ensure a long-term stability. This feature is essential to guarantee that the transport properties of the suspension remains constant during the experimental tests, but even more important to promote the adoption of this nanotechnology by the industry. To accomplish the latter, the first objective of this work is to optimize and validate a methodology specially designed to synthesize long-term suspensions of carbon-based nanofluids.

For the second objective of this work, it is intended to identify the inherent mechanisms responsible for the rheological behaviour of nanofluids. In addition, a predictive model for the effective viscosity of nanofluids will be designed and experimentally validated. To this end, on a first analysis, a complete design of experiments capable of evaluating the rheological behaviour

of nanofluids will be achieved. Secondly, a thorough experimental parametric analysis where special emphasis is given to the nanoparticle size, volume fraction, temperature, shear rate and base fluid type will be carried out.

The proposed research work contributes to the worldwide scientific knowledge answering to the following questions:

1. What is the optimized methodology to achieve long-term MWCNTs based nanofluids for heat transfer applications?
2. What are the most important inherent physical mechanisms responsible for the effective viscosity of nanofluids and their rheological behaviour?
3. It is possible to predict the effective viscosity of MWCNTs based nanofluids through a general physical-mathematical model?

The absolute aim of this research work is the development and validation of a physical based mathematical model, capable of predicting the effective viscosity of MWCNTs based nanofluids under different experimental conditions. The development of a complete property database regarding the thermal and transport properties of nanofluids will be fundamental to contribute to the dissemination of this nanotechnology in engineering applications.

1.5 Thesis Contribution

Nanofluids are a new class of fluids engineered by dispersing nano-scale size materials in a base fluid. In the past few years, many researchers have claimed that the addition of nanoparticles in the base fluid significantly alters the thermo-physical properties of the base fluid. As expected, these abnormal results lead to a growing scientific interest in nanosized suspensions. Actually, there is still a large debate concerning the intrinsic mechanisms that govern the transport properties of these types of suspensions.

Table 1.8 – Summary of the effective viscosity models and respective proposed mechanisms

	References	Proposed Mechanisms				
		Brownian Motion	Particle Agglomeration	Percolation Network	Hydrodynamic interaction	Interparticle Interaction
Spherical Particles	Liu et al. [137]	X			X	
	Bicerano et al. [200]				X	
	Tseng et al. [201], [223]		X			
	Maiga et al. [232]					
	Kulkarni et al. [204]					
	Chen et al. [205]		X			
	Praveen et al. [206]					
	Nguyen et al. [207]					
	Masoumi et al. [208]	X				
	Duangthosuk et al. [209]					
	Sahoo et al. [210]					
	Phuoc et al. [211]					
	Chandraskar et al. [212]					
	Hosseini et al. [213]					X
	Godson et al. [214]					
	Corcione et al. [215]					
	Abareshi et al. [217]					
	Colla et al. [219]					
	Sundar et al. [233]					
	Bobbo et al. [84]					
	Heyhat et al. [220]					
	Sekhar et al. [168]					
	Esfe et al. [221]					
Non-Spherical particles	Vakili-Nezhaad et al. [81]		X	X		
	Bobbo et al. [84]					

Despite the large number of scientific papers available in the literature, the divergences on empirical results and the publication of several predictive models with different premises, has led to unrelated effects. This has contributed to a growing noise, but with a possible simple explanation. This noise might be attributed to the preparation techniques, unsatisfactory sample characterization or the lack of a standardized methodology for nanofluid characterization. In general, researchers neglect the characterization of particles geometry, phase distribution, stability evaluation as well as the methodology used to disperse the

nanoparticles on the base fluid. Moreover, to successfully ensure the application of nanofluids as an effective heat transfer fluid, it is definitely important to ensure a long-term colloidal stability. The conducted survey revealed that it is broadly accepted that MWCNTs are the most promising nanoparticle for advanced heat transfer fluids. These nanofluids have the lowest volume fraction and consequently a lower relative viscosity, as it can be depicted from Figure 1.8. The latter is an important parameter, since lower viscosity results in lower pumping power and less pressure losses.

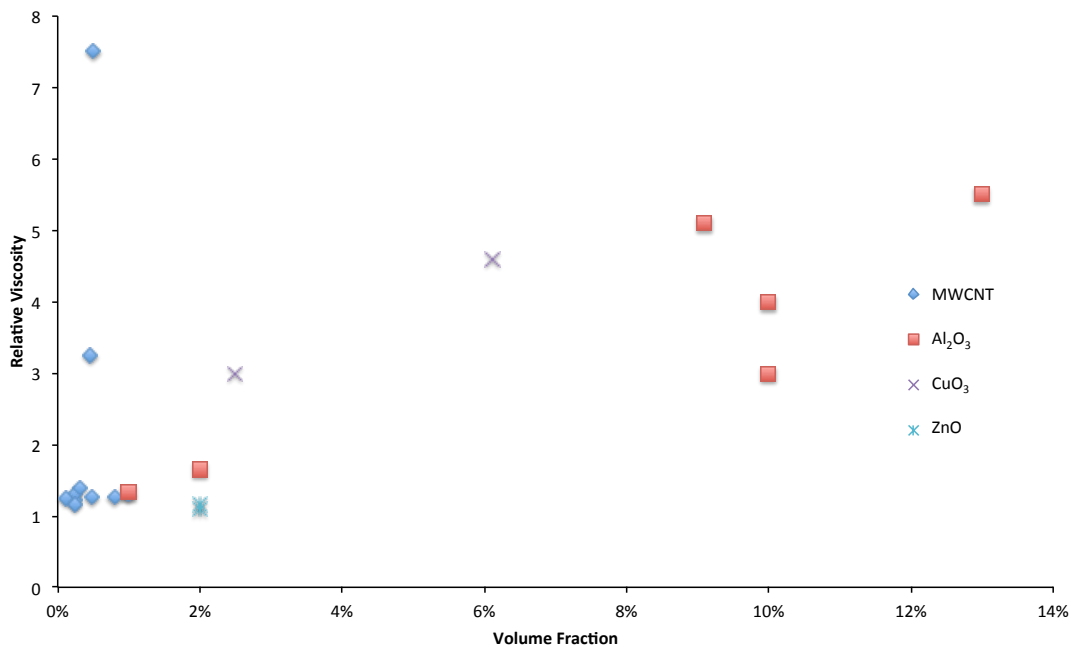


Figure 1.8 - Summary of the experimental data available on the open literature for nanofluids

This research aims to contribute to the development and characterization of the rheological behaviour of long-term MWCNTs based nanofluids. The samples are properly characterized, enabling a better inference on the transport properties mechanisms governing the viscosity of nanofluids. A physical prediction model for the effective viscosity of nanofluids is also developed and experimentally validated. It is expected that the acquired experimental and theoretical results contribute to the scientific knowledge that will be available for future work, both fundamental and at an engineering level.

1.6 Thesis Organization

In Chapter 1 an overview of the relevant literature on the synthesis and transport properties characterization of nanofluids is presented, including experimental and theoretical models. Also, the objectives and the main challenges were also outlined. In Chapter 2 some fundamental concepts of fluid mechanics and colloidal rheology are revised in detail. In addition, a correlation for evaluating the rheological behaviour of nanofluids is proposed. Based on these results, Chapter 3 deals with the methods and materials that were used to prepare and characterized the transport and thermal properties of the samples. In Chapter 4, the obtained experimental results for evaluating the intrinsic properties of the samples are discussed. Finally, in Chapter 5 it is presented the methodology used to assess the rheological behaviour of MWCNTs nanofluids. In addition, the prediction correlation is empirically validated. In Chapter 6 the major conclusions and future research objectives are given. In the annexes it is presented the experimental results for all the tested samples, the methodology to ascertain the experimental error, a business plan for a product based on this technology and the submitted patent.

Chapter 2 - Dispersions

2.1 Overview

The determination of the rheological behaviour of dispersions is very important for many industrial applications, from quality control, to the prediction of pumpability and pourability, and to ascertain the procedure in which a material can be processed and handle. Thus, rheology helps describe the mechanical behaviour of materials as a function of stress, strain, temperature and pressure, i.e. rheology studies the deformation and the flow of a material when it is subjected to an external force. Moreover, the interrelation between some materials properties and its rheological behaviour can be used to ascertain changes on the microstructure of suspensions, colour and density.

As verified on Chapter 1, a considerable amount of work has been developed to study the rheology of suspension. Despite, the mechanics of microfluids being well understood, the intrinsic nature of nanoparticles introduces unknown phenomena to the suspensions that have not yet been fully described by theoretical studies.

For colloidal dispersions, the rheological property of interest is the viscosity. However, in order to determine this property and probe some knowledge about the rheology and microstructure of suspensions, a flow must be induced, therefore the assessment of variables such as: Shear rate, shear stress and their variation with time becomes mandatory. Moreover, the thermal energy of the system also plays an important role requiring evaluation. However, solving this multivariable phenomenon introduces a certain complexity and special techniques must be employed to develop a model capable of dealing with the appropriate representation of the suspension rheology.

This Chapter is divided in four sections. In the first section, it is presented a description and mathematical formulation of continuous mechanics. The latter aims at presenting the physics underling the rheology of a material. In the second section, a detailed description of the rheological behaviour of fluids and some of the models that capture these features are presented. On the third section, an extensive survey on mathematical models and theories proposed by

several authors on the rheological behaviour of suspensions is carried out. In the fourth and final section it is presented the adopted methodology for developing a model capable of predicting the rheological behaviour of MWCNTs suspensions.

2.2 Definition of a Fluid

Most substances can be categorized in two states, solid and fluid. A *solid* can be describe as having a preferred shape, which when is subjected to a shear stress that will deform but then springs back to its original state. By definition a *fluid* is a substance that continually deforms (flow) under an applied force [234]. These are conventionally classified as either liquid or gases. Thus, a *fluid* describes the mechanical behaviour of a liquid or a gas. Still, any type of matter at any phase can be deformed.

A *flow* can be divided in two classes, shear and extensional flow. In a simple shear flow, fluid elements flow over or past each other, while in extensional (or elongation, or stretching) flow, fluid elements flow towards or away from each other, see Figure 2.1 [235]. Thus, the gradient of the velocity at which the fluid layers move past each other is called shear rate while the force creating the flow is called shear stress. Although the differences between solid and fluid elements, they behave similarly under the action of a compressive normal stress.

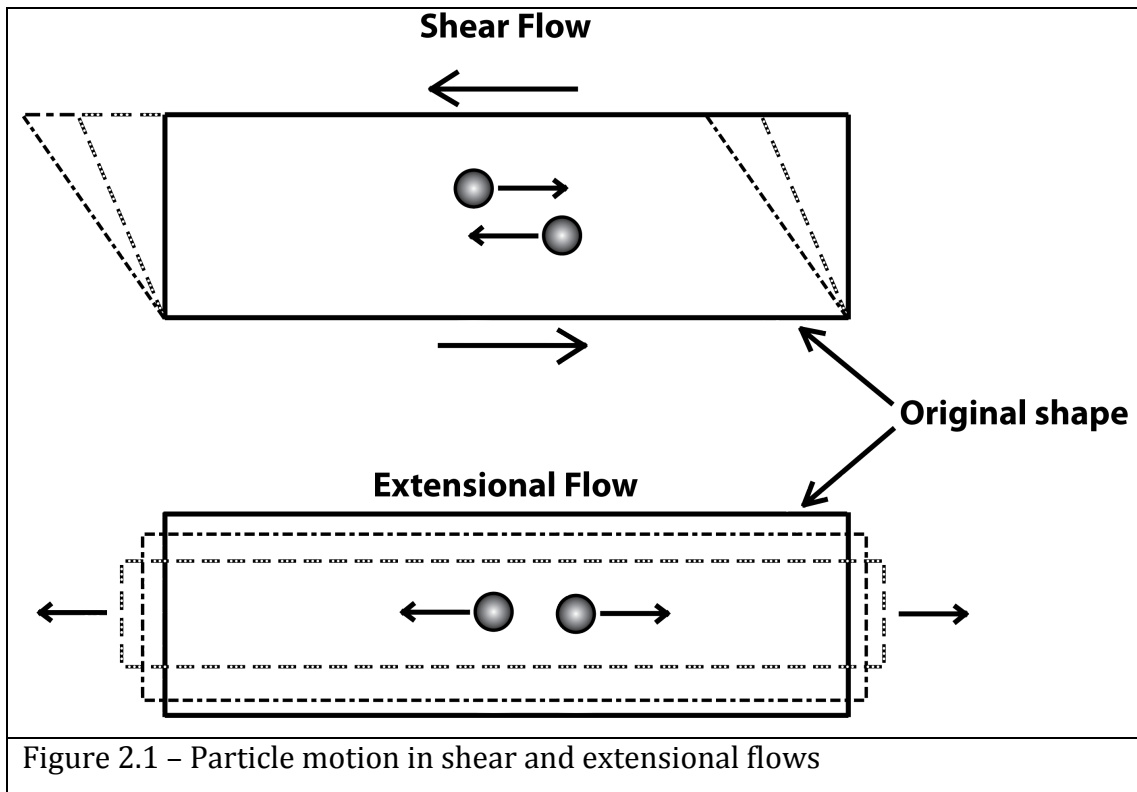


Figure 2.1 – Particle motion in shear and extensional flows

Both fluid and solid materials are composed of a large number of inter-related molecules in constant motion, therefore, at a microscopic scale, matter is discontinuous or discrete. Through the kinetic theory or via statistical mechanics it is possible to describe the behaviour of a fluid by studying the motion of its molecules. However, *Fluid mechanics* normally deals with flow at a macroscopic level, which is the average manifestation of molecular motion. Since the length and time scales are much larger than the associated molecular size and vibration, the bulk properties of a liquid fluid are completely continuous in the fluid structure. Thus, the fluid can be approximated as a continuum medium [234]. Under these circumstances, one can assume that bulk properties are approximately constant and any statistical variation of these can be neglected.

2.3 Fluid Kinematics

Fluid mechanics is a branch of continuum mechanics that deals with the deformation of fluids under an external force (fluid flow). The next section sets forth the mathematical model used to describe the dynamics of continuum fluid.

More information regarding the fundamental assumptions that underlie continuum fluid can be found in [129], [236].

The classical prediction models for the viscosity of fluids originate from the pioneer work of Sir. *Isaac Newton*, published in 1687. Newton essentially proposed that the shear stress (σ) is a function of the viscosity and the rate of strain ($d\gamma/dt$) [237]:

$$\tau = \mu \frac{d\gamma}{dt} \quad \text{Eq. 2.1}$$

However, it was not until the 18th century that Navier and Stokes independently developed a theory for a Newtonian viscous fluid, known as the Navier-Stokes equation. This, form the basis for what is known as Newtonian Fluid Mechanics [237].

With the development of new fluids, it became clear that many fluids could not be described by Newton's premises. Thus, a new scientific discipline known as *non-Newtonian* Fluids Mechanics was created. These fluids have viscosities that increase or decrease with shear. So, a non-Newtonian fluid can be characterized as one whose behaviour cannot be described by the Navier-Stokes equations [237].

Considering a simple steady shear flow, in which the material flows unidirectional (see Figure 2.1), any external force regardless of the origin when applied to a body leads to either the movement of the body or to the distortion of its initial shape. This force creates a dynamic situation in the body, which is characterized by an applied stress (σ). Therefore, the complete characterization of the stress requires the identification of two vectors: a force and a normal surface area, to which the vector is applied. The physical objects determined in such manners are called *tensors*. These, describe the linear relationships between the normal direction vector of a plane and the local stress density on that plane, or in other words, the stress is a value of the tensor nature, see Figure 2.2 [235].

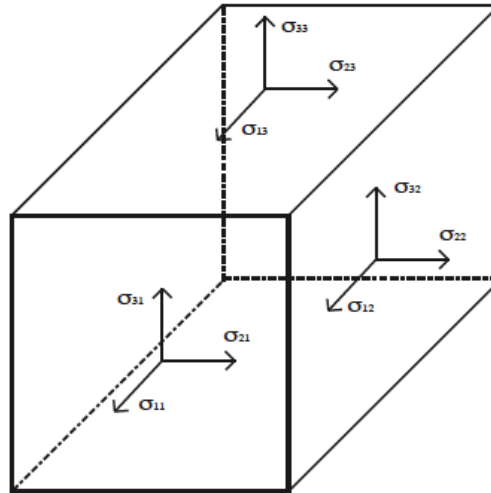


Figure 2.2 – Three-dimensional stress state: definition of the stress tensor components.

The force (\mathbf{F}) applied at any surface may not be constant, and can be oriented along different directions. The force vector can be decomposed into three components, one perpendicular (*normal stress*), and two tangential (*shear stress*) components to the selected cross-area (ΔS). Moreover, the selected cross area can also be arbitrary, and can be expressed by a vector \mathbf{n} . Therefore, the combination of the force and cross section vector is defined as the *stress* at any orientation reference. However, for practical applications, each vector should be decomposed into its three projections on coordinate axes, x_1, x_2, x_3 . In Figure 2.2, it can be depicted all the components of the stress tensor acting on each surface. So, the nine components that characterize the normal and tangential stress can be written on the form of a matrix.

$$T = \sigma = \begin{bmatrix} \sigma_{11} & \sigma_{12} & \sigma_{13} \\ \sigma_{21} & \sigma_{22} & \sigma_{23} \\ \sigma_{31} & \sigma_{32} & \sigma_{33} \end{bmatrix} \quad \text{Eq. 2.2}$$

It may, therefore, be said that the values of the stress tensor components depend on the orientation of the selected cross-area.

Consider now a steady, one-dimension unidirectional flow, as represented on Figure 2.3,

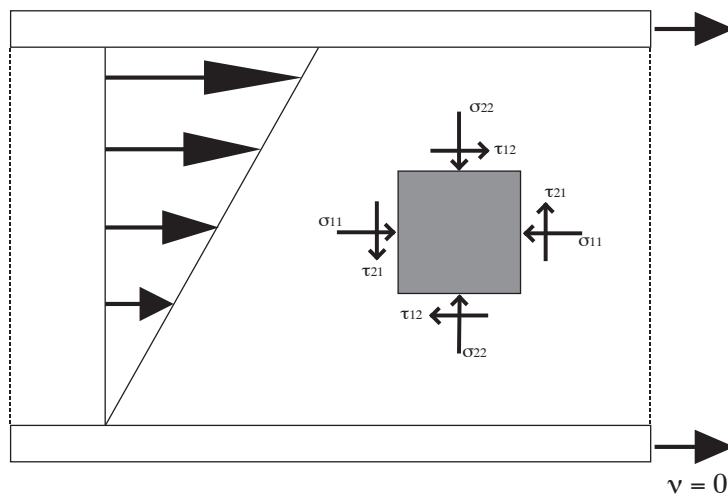


Figure 2.3 – Schematic of a one dimension unidirectional flow

the distribution of stresses throughout a body can be described by the equilibrium equations, which in the case of the central point can be formulated as:

$$\sigma_{ij} = \sigma_{ji}$$

This implies that the stress state at a specific point is completely defined by six values: three shear stresses (τ) and three normal stresses (σ). So, the stress matrix can be written as:

$$\sigma = \begin{bmatrix} \sigma_{11} & \tau_{12} & \tau_{13} \\ & \sigma_{22} & \tau_{23} \\ & & \sigma_{33} \end{bmatrix} \quad \text{Eq. 2.3}$$

For a fluid in static equilibrium, the stress tensor consists of an isotropic or pressure part (p) and an deviatoric or viscous part (τ), which resists relative to motion:

$$\sigma_{ij} = -p\delta_{ij} + \tau_{ij} \quad \text{Eq. 2.4}$$

where δ_{ij} is called a *(Kronecker delta)*, and represents the unit tensor,

$$\delta_{ij} = \begin{cases} 1, & i = j \\ 0, & i \neq j \end{cases} \Leftrightarrow \delta_{ij} = \begin{bmatrix} 1 & 0 & 0 \\ 0 & 1 & 0 \\ 0 & 0 & 1 \end{bmatrix} \equiv \mathbf{I} \quad \text{Eq. 2.5}$$

The extra stresses τ_{ij} come from the relative motion of fluid particles and is represented by elements in the extra stress matrix T' :

$$T' = \tau_{ij} = \begin{bmatrix} \tau_{11} & \tau_{12} & \tau_{13} \\ \tau_{21} & \tau_{22} & \tau_{23} \\ \tau_{31} & \tau_{32} & \tau_{33} \end{bmatrix} \quad \text{Eq. 2.6}$$

So, in matrix notation Eq. 2.4 becomes:

$$\begin{bmatrix} \sigma_{11} & \sigma_{12} & \sigma_{13} \\ \sigma_{21} & \sigma_{22} & \sigma_{23} \\ \sigma_{31} & \sigma_{32} & \sigma_{33} \end{bmatrix} = \begin{bmatrix} -p & 0 & 0 \\ 0 & -p & 0 \\ 0 & 0 & -p \end{bmatrix} + \begin{bmatrix} \tau_{11} & \tau_{12} & \tau_{13} \\ \tau_{21} & \tau_{22} & \tau_{23} \\ \tau_{31} & \tau_{32} & \tau_{33} \end{bmatrix} \quad \text{Eq. 2.7}$$

or in index notation becomes,

$$\sigma_{ij} = -p\delta_{ij} + \tau_{ij} \Leftrightarrow T = -p\mathbf{1} + T' \quad \text{Eq. 2.8}$$

In summary, fluids can be *ideal* or *inviscid* if the viscosity is null otherwise, they are named *viscous*. Viscous fluids can be classified into *generalized Newtonian* and *non-Newtonian* fluids. The first is characterized by having a linear relationship between the shear stress and the shear rate. A Non-Newtonian fluid can have different relationships between the shear stress and shear rate, as can be depicted in Figure 1.1. The later, have a large number of industrial applications from paints, solutions and melts to suspensions and polymeric liquids.

It was also demonstrated that an incompressible, one-dimensional unidirectional flows might be analytically solved by simplifying the Navier-Stokes equations. However, *bidirectional* or *tridirectional* flows can rarely be solved analytically. The nonlinearities introduced by the convective terms make it very difficult to find an analytical solution [234]. Nevertheless, these complex

systems may be solved by computational numerical models, using finite elements differences.

In the following section, a survey on some theoretical and empirical models developed to characterize the rheological behaviour of fluids, will be presented.

2.4 Rheological Models

Rheological models were developed from the fundamental concepts of fluid mechanics and may be grouped under three categories: empirical, theoretical and structural. These models were very useful to provide guidelines to understand the role of the percolation structure and how it changes with fluid properties. For convenience, these models will be divided in *Newtonian* and *non-Newtonian* models.

2.4.1 Newtonian Fluids

As described on Chapter 1, Newtonian fluids follow *Newton's law of viscosity* which states that the viscous stress tensor T' is proportional to the strain rate tensor $\dot{\gamma}$,

$$T' = 2\mu\dot{\gamma} = \mu[\nabla v + (\nabla v)^T] \quad \text{Eq. 2.9}$$

When there is relative motion of fluid particles, the stress tensor T' , the velocity gradient tensor ∇v and the strain rate tensor $\dot{\gamma}$ are not zero,

$$\dot{\gamma} \equiv \frac{1}{2}[\nabla v + (\nabla v)^T] \quad \text{Eq. 2.10}$$

where μ is a proportional constant, which is called dynamic viscosity or, simply viscosity. Therefore, the stress tensor T can be written as:

$$T = -p1 + \mu[\nabla v + (\nabla v)^T] \quad \text{Eq. 2.11}$$

Finally, the Newtonian model is described by the equation:

$$[\nabla v + (\nabla v)^T] = \frac{\tau}{\mu} \quad \text{Eq. 2.12}$$

For the case of a *zero order fluid*, i.e. an inviscid fluid, where the molecules are only subjected to the influence of Brownian motion, the resulting stress tensor become,

$$T = -pI \quad \text{Eq. 2.13}$$

2.4.2 Non-Newtonian Fluid

As envisaged in Chapter 1, *non-Newtonian* fluids are characterized by a viscosity that is a function of the rate of strain tensor $\dot{\gamma}$, more precisely the viscosity is a function of the second invariant of $\dot{\gamma}$, $\mu = \mu(II_{\dot{\gamma}})$. If the fluid viscosity is a decreasing function of $II_{\dot{\gamma}}$, the fluid presents a *shear thinning* behaviour; when the opposite is true, the fluid is said to be *shear thickening*.

This interesting phenomenon leads many researchers to modify *Newton's* equation in an attempt to characterize the non-Newtonian behaviour of some fluids. Some of the most widely used models are described as follows,

(A) Bingham plastic fluids, these are generalized Newtonian fluids that exhibit a yield stress. The material flows only when the applied shear stress (τ) exceeds the finite yield stress (τ_0) [238]. Therefore, the viscosity function may be presented as:

$$\begin{cases} \tau = \tau_0 + \eta\dot{\gamma}, & \tau > \tau_0 \\ \tau = 0, & \tau \leq \tau_0 \end{cases} \quad \text{Eq. 2.14}$$

This equation describes the shear stress/shear rate behaviour of many shear-thinning materials at low shear rates. Additionally, the value of τ_0 depends on the shear rate ranges used for the extrapolation procedure.

(B) A Herschel-Bulkley fluid is a generalization of the Bingham fluid, where, upon deformation, the viscosity is either shear thinning or shear thickening [234].

$$\tau = \tau_0 + k\dot{\gamma}^n \quad \text{Eq. 2.15}$$

When $\tau_0 = 0$, Eq. 2.15 is reduced to the *power fluid model*, whereas when $n = 1$ Eq. 2.16 is reduced to the Bingham model. More, when $\tau_0 = 0$ and $n = 1$, Eq. 2.17 become the *Newton* equation.

(C) Casson fluid can be defined as a shear thinning liquid which is assumed to have an infinitive viscosity at zero shear rate and a yield stress [239]. This model is used to address the rheological behaviour of many paints and printing ink formulations [240]:

$$\sqrt{\tau} = \sqrt{\tau_0} + \sqrt{k\dot{\gamma}} \quad \text{Eq. 2.18}$$

(D) Power Law fluid can also be described as a shear thinning fluid (if $n < 1$) that has an infinitive viscosity at rest and zero as the shear rate approaches infinity and is given by:

$$\tau = k\dot{\gamma}^n \quad \text{Eq. 2.19}$$

where k is the consistency index and n is the shear thinning index if $n < 1$. These can be evaluated by fitting experimental data. The viscosity at a given shear rate can be calculated as:

$$\mu = \frac{\tau}{\dot{\gamma}} = k\dot{\gamma}^{n-1} \quad \text{Eq. 2.20}$$

Although, this model is more versatile than the Bingham model, it is also more suitable for non-Newtonian systems over two or three decades of shear rate. For high shear rates, this model describes the viscosity as a constant value. In Table 2.1 it is shown some typical index values for non-Newtonian fluids are presented [240].

Table 2.1 – Power-Law index values for some non-Newtonian fluids

Fluids	k (Pa.sⁿ)	n	Shear rate range (s⁻¹)
Polymer melt	10000	0,6	10 ² -10 ⁴
Lubricating Grease	1000	0,1	10 ⁻¹ -10 ³
Tooth-past	300	0,3	10 ⁰ -10 ³
Skin Cream	250	0,1	10 ⁰ -10 ²
Molten Chocolate	50	0,5	10 ⁻¹ -10 ¹
Pen Ink	10	0,85	10 ⁰ -10 ³

It is acknowledged that the nature of non-Newtonian system is directly linked to the applied rate of shear. However, some non-Newtonian fluids subjected to a shear rate may result in different values of stress at a fix time interval. When this phenomenon occurs, the viscosity becomes time-dependent. This effect known as *thixotropy*, results from the spatial rearrangement of particles or molecules when subjected to a flow field. More, this behaviour can also be explained by the adjustment of the percolation network due to the breaking of weak bonds, alignment of the particles and the collision of particles to form aggregates [237]. Thixotropy like fluids, are characterized by a decrease of viscosity with time, or "negative thixotropy" when viscosity increases with time.

As seen, theoretical models were developed from the fundamental concepts of fluid mechanics and it has been of utmost importance to provide guidelines to understand the role of the molecular percolation structure. Other models, such as the *Power law* were deduced from extensive experiments on fluid flow. Finally, the Structure models are derived from considerations and kinetics change in the percolation structure. One such model is that of Casson

(Eq. 2.18), that has been used extensively for the characterization of paints and other suspensions.

2.5 Rheology of colloids

In the literature, it can be found many descriptions to define a colloid. According to the International Union of Pure and Applied Chemistry (IUPAC) a colloidal dispersion can be defined as a system in which particles of “colloidal size” (at least one dimension in the size range 1 nm to 1 μm) are dispersed in a continuous phase. More, a colloidal dispersion can be classified concerning their size, size distribution and shape.

The rheology of particles dispersed in a fluidic matrix has been intensely investigated in the last hundred years. However, due to the many body character of suspensions, understanding the rheology of these systems is extremely complex. Thus, for the characterization of such complex system, one has to grasp the contribution of each individual mechanism that disturb the suspension microstructure, such as hydrodynamic forces, particles interaction and Brownian motion [241].

As it was mentioned earlier, the first known model to predict the effective viscosity of suspensions was developed by Einstein. He used the *Effective Medium Theory* (EMT) to predict the relative viscosity of uncharged and diluted suspensions of spherical particles [242]-[244]. The EMT was developed from a set of physical models used to describe the effective properties of suspensions. These are based on the averaged properties of each individual material that constitute the composite. Nevertheless, by solving suitable average equations, the EMT captures some of the multi-particle effects [245].

Despite well defined, the Einstein model only considers the contribution of each individual material of the composite, neglecting the contribution of geometry, orientation, interaction and microstructures arrangement of the particles. However, it has been shown that in most suspensions interaction between particles cannot be neglected. Some models [8], [173], [181], [246]-[248] began to take into account the hydrodynamic interactions between

particle-particle, particle-fluid and how these affect the overall viscosity of the system.

As it can be depicted from Figure 2.4, for a given volume fraction, under the percolation threshold, the hydrodynamics interactions between particles become very important, as the disturbance of the fluid around one particle interacts with neighbouring particles. Such behaviour becomes more and more important from the transition to non-diluted structure arrangements, i.e. as the particle concentration increase [241].

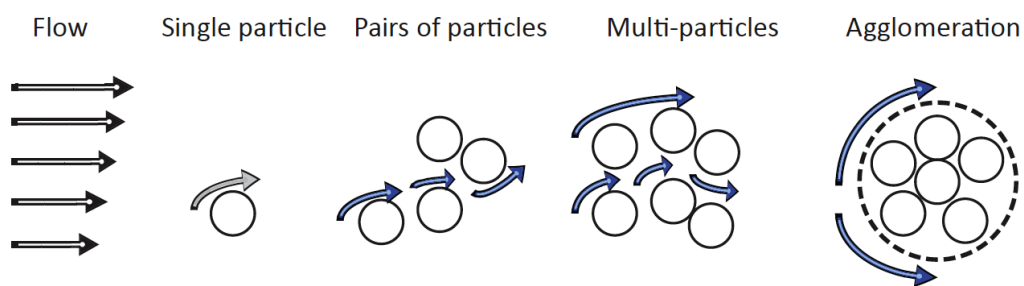


Figure 2.4 – Schematic representation of the interactions of particle with shear flow

In order to overcome the limitation of the EMT, Bruggeman [249] proposed a theory know as the (*Differential Effective Medium Theory (DEMT)*). Since then, several modifications to this theory have been made in order to extend it to larger filling fractions. The *DEMT* is based in considering a progressive addition of particles to the solution [247]. Mendoza et al. [247], proposed a model to extend Einstein equation based on the *DEMT*. They concluded that, in order to account for the hydrodynamic interactions between particles in simple shear flow, the Fokker-Planck equation for a single-particle has to be extended for a N-particles distribution function, obeying the multivariate Fokker-Planck or Smoluchowski equations [180].

Another important contribution to the study particles interactions was made by Vand [181], who point out the importance of collisions between particles. He found out that even at the diluted regime, an appreciable number of collisions between doublets or pairs of particles occur. Thus, a certain amount of

liquid is trapped between the particles increasing the concentration of the suspension and, therefore, contributing to an increased of the overall viscosity.

In 1993, Sandstrom [250] proposed a complex model for concentrate suspensions of rod-like particles. He assumed that for high concentrations particle-particle contacts are inevitable, affecting the orientation state and hence the suspension viscosity. Therefore, he considered an interparticle contact force, as a linear lubrication force. Servais et al. extend the work of Sandstrom [250] assuming that beside the lubrication force a friction force and a normal force of electrostatic origin must be considered [251].

Later, Le Corre et al. [252] proposed a completely different approach for modelling the suspension rheology. They have used a homogenization method for periodic discrete structures, to predict the influence of the particles volume fraction and orientation on the resulting macroscopic rheological behaviour. Recently, Ma et al. [253] concluded that a simple orientation model based on a Fokker-Planck equation, failed to capture the steady shear viscosity for untreated CNT suspensions. They have proposed an "aggregation/orientation" model, which gathers the orientation model with the aggregation modelling within the Fokker-Planck equation. However, this model is limited to low CNTs volume fractions. More recently, Chinesta [254] developed a model for CNTs suspensions in epoxy. He proposed a two-scale model that takes into account the contribution of kinematics of particle clusters and of individual particles constituting the clusters.

As it was reported, a large number of theories with different approaches have been proposed. In the case of low concentration suspensions most models predict with some degree of precision the rheological behaviour of suspensions. However, as soon as the concentration increases, interparticles interactions and particles clusters (aggregation/disaggregation) occur, resulting in discrepancies between empirical data and the theoretical models. However, a model able to capture the well-known shear thinning and normal stress in all concentration regimes of MWCNTs suspensions is still missing. Nevertheless, two distinct approaches can clearly be identified, the direct numerical simulations (DNS) and the kinetic theories. The first, can be used to track a rod population which moves with the suspending fluid and the orientation of the particles depends on the

velocity gradient. Despite the well-defined physics at the microscale, DNS requires large computational times. Kinetic theories are used to describe suspensions at the mesoscopic level. The main advantage of these approaches lies in their capability to address macroscopic systems while keeping the fine physics for describing the microstructure and its time evolution [241], [255]-[257]. The microstructure is defined from a probability distribution function that depends on the physical space, time and conformational coordinates. Similarly to the DNS approaches, the kinetic theories also required a large computational time.

Brief Conclusion

It can clearly be stated that a few theories have been proposed in an attempt to describe the rheological behaviour of suspensions. Despite the fact the mechanics of dilute and semi-dilute suspensions are well understood, the multi-body interactions of nanofluids makes the mathematics extremely complicated even for just a few particles. Nevertheless, rheologists employed computer simulations to gain more insight to the understanding of suspensions mechanics and rheology [258]-[260]. Still, most theories neglect the molecular nature of the medium in which the colloidal material are dispersed, leading to “anomalous” hydrodynamics problems.

Moreover, the flows regime was assumed to be in the laminar regime, so that distinct layers of material would pass each other without intermixing. However, in many industrial applications especially for heat transfer equipment turbulent flows predominate. In these flows, eddy currents, swirls, and vortices start to develop causing an intermixing of the distinctive fluid layers, leading to oscillations in fluid motion. In turbulent flow, the viscosity shows an apparent increase with shear rate. This means that part of the stress is used to increase the number of eddies rather than to increase the flow of the fluid. However, a constitutive equation relating the rheological properties of a fluid in terms of shear variables and the contribution of the structural parameters (percolation networks), which determine its mechanical response under laminar and turbulent flows is still missing. The difficulties in the integration are based, firstly, on the fact that these equations, unlike most partial differential equations

in physics, are nonlinear. This implies that solutions that have been found cannot be “superimposed” to form a new solution, as it is the case with linear systems. Secondly the system is of a very high order, arising from the coupling of equations and from the high derivatives that appear in the viscous terms.

2.6 Rheology of Suspensions: Measurement of the Macroscopic Properties

A rheological model is a prediction of the mechanical response of a fluid when subjected to an external force, which has to adapt to the structural properties of the continuum medium. For that reason, knowledge on the rheological properties of a dispersed system is a prerequisite for increasing the effectiveness of the predictive model.

As it was mentioned earlier, to prone the rheological behaviour of a fluid a flow must be applied and the medium properties should be fully assessed. Thus, sets of dimensionless numbers were developed in order to characterize the behaviour of a fluid flow. The most important dimensionless numbers of fluids mechanics are the *Reynolds number* (Re), the *Stokes number* (St) and the *Peclet number* (Pe). The Reynolds number is an estimation of the inertia effects of a particle, i.e. the ratio between the inertial forces to viscous forces.

$$Re = \frac{\rho v D}{\mu} \quad \text{Eq. 2.21}$$

The Stokes number is crucial in suspensions since it characterizes the behaviour of particles suspended in a fluid flow.

$$St = \frac{\rho g L^2}{\mu \bar{u}} \quad \text{Eq. 2.22}$$

These dimensionless numbers, Re and St , were developed based on the equations of conservation of momentum. Finally, the Peclet number is a dimensionless group that represents the ratio between the shear force and the

Brownian force, or in other words, the ratio of order due to shearing and disorder due to Brownian motion.

$$Pe = \frac{\dot{\gamma}}{D_r} = \frac{\mu_{bf} a^3 \dot{\gamma}}{k_B T} \quad \text{Eq. 2.23}$$

where, D_r is the rotational diffusion coefficient, k_B is Boltzmann's constant, T is the absolute temperature, $\dot{\gamma}$ is shear rate, and a is a particle shape factor. Thus, one can deduce that the presence of particles will affect the flow behaviour from linear sheared to non-linear due to the hydrodynamic interactions between particles. Thus, to study the rheological behaviour of a fluid, one has to take into consideration both the properties of continuous and dispersed phase, as well as the interactions within and between both phases [261].

2.6.1 Properties

As per definition, *Properties* are a value that describes a state of a physical system. These can be *extensive* if they depend on the amount of fluid or otherwise *intensive*. Therefore, temperature, pressure and density are intensive properties, while volume, mass, weight and internal energy are extensive.

It is a fact that temperature changes the internal energy of any fluidic system. In many cases, viscosity shows an exponential reduction with temperature rise, e.g. water viscosity decreases 3% per degree. In contrast, non-Newtonian fluids can have multiple behaviours. In the simplest case, the variation of the internal energy may reflect a change on the continuous phase viscosity. Therefore, the properties of an incompressible homogeneous fluid have to be measured as a function of temperature and to a much lesser extent, as a function of pressure. However, as it will be demonstrated on the next section, in complex fluids like dispersions the thermal energy enhancement affects the interparticle interaction and the percolation network, changing the overall viscosity.

As it has been highlighted, a large number of dependent and independent variables affect the rheology of suspensions, resulting it all in a large volume of data. However, correlating the different variables and identifying the trends and rates of change is sometimes extremely difficult. Moreover, the complexity of

some fluidic systems makes it almost impossible to solve the governing equations analytically.

Another possible alternative to get some insight of the rheological behaviour is to use *approximation methods*. The latter, allows for the simplification of the governing equations, leading to an analytical solution of the truncated form of the governing equations, or in other words to the development of approximate solutions. The postulation of those solutions is described next.

2.6.2 Dimensional Analysis

A *dimensional analysis* is a technique based on Buckingham Π - theorem. Although this is credited to E. Buckingham it was first proposed by Lord Rayleigh in his book "The theory of sound" [262]. This theorem is based on the rule of *dimensional homogeneity*, which states that an equation expresses a proper relationship between variables if it will be dimensionally homogeneous. Baring that in mind, a dimensional analysis results in a number of dimensionless groups, which characterizes the ratio of the various influence parameters. These allows for the estimation of the physical relevant phenomena or the irrelevance of the influence parameters. Nevertheless, a dimensional analysis only gives some information about the general form of the relation between the variables. The exact form of the correlation must be determined by a truly empirical study of the unknown variables.

Although the Π - theorem enables to reduce the number of experimental variables and group them into a dimensionless form, this analysis also has some additional benefits. First, it allows the reduction of experimental time, by grouping previously unrelated variables. Secondly, it helps the design of experiments since it suggests variables to be discarded, reducing the complexity of the physical problem. Finally, it provides *scaling laws* that allow the prediction from a small model to a large model.

Next it will be presented a dimensional analysis carried out by Krieger et al [263] to assess the empirical-based correlation regarding the rheology of colloidal suspensions.

2.6.3 Rheological Equation of State

Krieger et al [263], considered that the rheological behaviour of a suspension is a general function of several system parameters:

$$\mu = f(r_p, \rho_p, \Phi, \mu_{bf}, \rho_{bf}, kT, \dot{\gamma}, t) \quad \text{Eq. 2.24}$$

where, the continuum medium properties are the base fluid viscosity μ_{bf} and density ρ_{bf} . The particles properties are the average equivalent radius of the particle r_p (for multi-sized particles), their concentration Φ and density ρ_p and, whenever Brownian movement is significant, a thermal energy variable kT , where k is the Boltzmann's constant and T the temperature. Finally, the shear variables shear rate $\dot{\gamma}$ and time t . All the nine variables that constitute this equation can be expressed in terms of the three basic units of mass, length and time (MLT). Thus, according to the principles of dimensional analysis Eq. 2.24 they can be reduced to form six (9-3=6) dimensionless groups. Following the methodology of Krieger [263], the six independent groups consist of:

Relative Viscosity	$\mu_{rel} = \frac{\mu_{nf}}{\mu_{bf}}$	Eq. 2.25
--------------------	---	----------

Relative density	$\rho_{rel} = \frac{\rho_p}{\rho_{bf}}$	Eq. 2.26
------------------	---	----------

Volume Fraction (Sphere)	$\phi^* = \frac{4\pi n r_p^3}{3}$	Eq. 2.27
--------------------------	-----------------------------------	----------

Reduced time	$t^* = \frac{t kT}{\mu_{bf} r_p^3}$	Eq. 2.28
--------------	-------------------------------------	----------

Reduced Shear Stress (Peclet Number)	$Pe_{\dot{\gamma}} = \frac{6\pi r_p^3 \dot{\gamma} \mu_{bf}}{kT}$	Eq. 2.29
---	---	----------

Reduced Energy (Reynolds Number)	$Re_{\dot{\gamma}} = \frac{r_p^2 \dot{\gamma} \rho_{bf}}{\mu_{bf}}$	Eq. 2.30
-------------------------------------	---	----------

Therefore, the equations of state in the reduced form become:

$$\mu_{rel} = f(t^*, \rho_{rel}, \Phi^*, Re_{\dot{\gamma}}, Pe_{\dot{\gamma}}) \quad \text{Eq. 2.31}$$

Eq. 2.31 may be further reduced regarding the defined state conditions, i.e. for a steady-state system the reduced time may be neglected ($t^* \rightarrow 0$), then Eq. 2.31 become:

$$\mu_{rel} = f(\rho_{rel}, \Phi^*, Re_{\dot{\gamma}}, Pe_{\dot{\gamma}}) \quad \text{Eq. 2.32}$$

As it was mention earlier, the final form of the function must be found either theoretically or through an extensive empirical analysis of the process. Krieger et al. assumed that for a steady shear state ($t^* \rightarrow 0$) of neutrally buoyant ($\rho_{rel} \rightarrow 0$) and for laminar flow conditions ($Re_{\tau} \rightarrow 0$), equation Eq. 2.31 become a function of the volume fraction and reduced shear stress:

$$\mu_{rel} = f(\Phi, Pe_{\dot{\gamma}}) \quad \text{Eq. 2.33}$$

However, as it can be depicted in Chapter 1 most proposed correlations are only a function of the volume fraction ϕ neglecting both Reynolds ($Re_{\tau} \leq 10^{-3}$) and the Peclet Number of the system ($Pe_{\dot{\gamma}} \geq 10^{-3}$). Therefore, the governing equation becomes,

$$\mu_{rel} = f(\Phi) \quad \text{Eq. 2.34}$$

However, it should be noted that only for highly diluted suspension, the relative viscosity only depends on the volume fraction of particles [263].

In summary, the approximation techniques are very useful to simplify the governing equations and develop an approximated solution. These solutions can have many forms based on the flow characteristics and boundary conditions. Nevertheless, it seems reasonable to conclude that suspensions may have multiple rheological phenomena regarding the state condition.

2.6.4 Proposed Model

A solution to assess the rheological behaviour can be achieved through the use of a combination of mathematical analysis and experimental data. However, this system may be difficult to define without proper insight. Thus, a dimensional analysis seems to be a viable solution. The approach employed in this work is to choose the simplest system, which might be capable of exhibiting some of the rheological phenomena of interest, and then apply a dimensional analysis to find the dimensionless groups, which must appear in the rheological equation. Afterwards, by supplementing this knowledge with known empirical rheological data of MWCNTs nanofluids, an analytical relationship can be developed allowing for the computation work to be carried out.

Following the methodology described on the previously section, the first step for conducting an experiment would be to decide on the variables of interest that affect the rheological behaviour of colloidal suspensions. However, it should be noted not to overdo the number of independent variables, since these have to be characterized empirically, without compromising the precision. Considering a steady flow of an incompressible fluid with MWCNTs suspended in a continuous Newtonian medium, the viscosity of the suspension will depend on the viscosity of the medium (μ_{bf}), the particle equivalent diameter (D_S) and volume fraction (ϕ), the densities of the MWCNTs (ρ_{MWCNT}) and base fluid (ρ_{bf}), the shear rate ($\dot{\gamma}$) or shear stress (τ), time (t) and the temperature (T). The latter, besides its effect on the μ_{bf} it will also influence the Brownian motion of MWCNTs. Therefore, to quantify the contribution of the temperature on the Brownian motion, the temperature must be multiplied by the Boltzmann constant (k_B). The following general relation for the dependence of the relative viscosity:

$$\mu_{nf} = f(\phi, \mu_{bf}, D_S, \rho_{MWCNT}, \rho_{bf}, \dot{\gamma} \text{ or } \tau, k_B T, t) \quad \text{Eq. 2.35}$$

Now, is possible to reduce the dimensionality in terms of mass, length and time (M, L, T), as can be depicted from Table 2.2:

Table 2.2 – Variable affecting the rheology of MWCNTs

Symbol	Meaning	Dimensionality
(μ_{nf})	Nanofluid Viscosity	$ML^{-1}T^{-1}$
(μ_{bf})	Base fluid Viscosity	$ML^{-1}T^{-1}$
(D_S)	Equivalent Diameter	L
(ρ_{MWCNT})	MWCNTs Density	ML^{-3}
(ρ_{bf})	Base Fluid Density	ML^{-3}
$(\dot{\gamma})$	Shear Rate	T^{-1}
(τ)	Shear Stress	$ML^{-1}T^{-2}$
(ϕ)	Volume Fraction	---
(t)	Time	T
$(k_B T)$	Thermal Energy	ML^2T^{-2}

The second step in the dimensionless analysis is to evaluate the required number of Π (π_i) terms. In other words, Eq. 2.35 can be substitute by the following equation expressing it as a function of a smaller number of non-dimensional groups:

$$\mu_{nf} = f(\pi_1, \pi_2, \pi_3 \dots \pi_m) \quad \text{Eq. 2.36}$$

For the case under study and based on the principles of dimensional analysis, the nine-variables represent on Table 2.2 can be expressed in terms of the three basic units of mass, length and time. Hence, based on the principles of dimensional analysis, Eq. 2.35 can be reduced to $9-3 = 6$ dimensional groups.

The third step is to select non-repeating variables from the original list, that you can be combined with each of the remaining variables to form a Π term. In order to study the mechanical phenomena of colloidal suspensions, three variables were chosen, μ_{bf} , ρ_{bf} and kT . These comprise a complete, dimensionally independent subset of the nine independent variables. Moreover, the dimension of any of these three cannot be made up of the dimensions of the other two. However, it should be noted that other variables could be selected,

leading to different dimensionless numbers. The remaining independent variables $\phi, \rho_{MWCNT}, \dot{\gamma}$ or τ, t can, however, be made up of those μ_{bf}, ρ_{bf} and kT as follows. It should be noted that the shear stress τ was chosen rather than the shear rate $\dot{\gamma}$.

Relative Viscosity	$\Pi_1 = \mu_{rel} = \frac{\mu_{nf}}{\mu_{bf}}$	Eq. 2.37
Relative density	$\Pi_2 = \rho_{rel} = \frac{\rho_p}{\rho_{bf}}$	Eq. 2.38
Volume Fraction	$\Pi_3 = \phi^* = \phi$	Eq. 2.39
Reduced time	$\Pi_4 = t^* = \frac{t \mu_{bf}}{\rho_{bf} r_p^2}$	Eq. 2.40
Reduced Shear Stress	$\Pi_5 = \tau^* = \frac{\tau \rho_{bf} r_p^2}{\mu_{bf}^2}$	Eq. 2.41
Reduced Energy	$\Pi_6 = kT^* = \frac{kT \rho_{bf}}{\mu_{bf}^2 r_p}$	Eq. 2.42

The final step in a *dimensional analysis* is to express the final form of the equation as a relationship among Π 's terms. Using the premises of the Buckingham's theorem, the relative viscosity of a colloidal suspension is a function of:

$$\Pi_1 = f(\Pi_2, \Pi_3, \Pi_4, \Pi_5, \Pi_6) \quad \text{Eq. 2.43}$$

Or

$$\mu_{rel} = f(\phi, \rho_{rel}, t^*, \tau^*, k_B T^*) \quad \text{Eq. 2.44}$$

Or

$$\mu_{rel} = f\left(\frac{\rho_p}{\rho_{bf}}, \phi, \frac{t \mu_{bf}}{\rho_{bf} r_p^2}, \frac{\tau \rho_{bf} r_p^2}{\mu_{bf}}, \frac{kT \rho_{bf}}{\mu_{bf}^2 r_p}\right) \quad \text{Eq. 2.45}$$

Now it is possible to look for relationships among the subsets of variables. As it was mentioned earlier, the Reynolds number is undoubtedly the most famous dimensionless parameter in fluid mechanics. From Eq. 2.45 it can be depicted that the reduced shear stress has the same relationship as the Reynolds number, i.e. the ratio between the inertial forces ($\tau \rho_{bf} r_p^2$) to the viscous force (μ_{bf}). Similarly, the reduced energy (Π_6) has the same relationship as the inversed Schmidt number (Sc^{-1}). This dimensionless number plays a crucial role in mass transfer, since it represents the ratio between the ability of a fluid to transport momentum by molecular means to the ability of that fluid to transport species by molecular means, and it is represented as it follows:

$$Sc = \frac{v}{D_r} = \frac{\mu_{bf}}{k_B T \rho_{bf}} \quad \text{Eq. 2.46}$$

where v is the *kinematic viscosity* and D_r is the diffusion coefficient. This dimensionless number can also be represented as the ratio between the Peclet number to Reynolds number. Thus, the Schmidt number is the relation between the imposed shear and Brownian forces to inertial forces. Therefore, Eq. 2.45 can be represented as:

$$\mu_{rel} = f(\rho_{rel}, \phi, \frac{t \mu_{bf}}{\rho_{bf} r_p^2}, Re_\tau, Sc^{-1}) \quad \text{Eq. 2.47}$$

Nevertheless, the exact form of the solution is unknown. However, one can now conclude that the rheological behaviour of a colloidal suspension is a function of the buoyancy effects (density), the MWCNTs inertial effects (Re), the concentration of MWCNTs (ϕ), the suspensions kinematic viscosity over time and the transport properties of the fluid (Sc). In order to investigate the exact form of Eq. 2.47 one has to empirically determine the individual properties

identified by of Eq. 2.47. Therefore, of Eq. 2.47 would serve as a guide to a systematic experimental procedure for uncovering the unknown variables and functions.

2.7 Chapter Conclusions

Despite rheology is considered to be a relative young science, it has received a great deal of attention over the last one hundred years. The development of new fluids like suspensions contributes even more to this growth. These tailored fluids lead industrial systems to adopt this technology. However, fluid customization requires an intrinsic knowledge on the thermal and transport properties of fluids and how these affect its rheological behaviour. Classical rheological models failed to capture the intrinsic nature of suspensions, since it does not take into account the interparticle interactions common to this type of fluids. With the development of colloidal suspensions, these interactions become even more important. This has lead to the development of many complex theories in an attempt to describe the rheological behaviour of suspensions. However, the complexity of some fluidic systems makes it almost impossible to solve the governing equation analytically.

For the reasons above stated, a model capable of describing the rheological behaviour of these multi-body systems is still missing. As it was highlighted, many purely mathematical models were proposed to characterize these fluids. Despite the complicated mathematics these only consider simple laminar flows. However, in many industrial applications especially for heat transfer equipment turbulent flows predominate. In these flows, eddy currents, swirls, and vortices start to develop causing an intermixing of the distinctive fluid layers, leading to oscillations in fluid motion and requiring other parameters to be considered.

As such, it was proposed a methodology to develop a model based on approximation techniques. The latter allow for the organization in a truncated form of the fine physics influencing the rheological behaviour of colloidal suspensions. Nevertheless, the final form of the equation has to be determined through model-fit with intensive empirical work. However, one can now

conclude that the rheological behaviour of a colloidal suspension is a function of the buoyancy effects (density), the MWCNTs inertia effects (Re), the concentration of MWCNTs (ϕ), the suspensions kinematic viscosity over time and the transport properties of the fluid (Sc). The next Chapter comprises a description on the experimental work conducted to evaluate the thermal and transport properties of MWCNTs suspensions.

Chapter 3 - MWCNTs Based Nanofluids Engineering

3.1 Introduction

Nanofluids, this word coined by Eastman in the last decade of the past century, is used to describe dispersions of solid nanoparticles in conventional fluids.

As it was emphasised in Chapter 1, studies of dispersions of solid nanoparticles in fluids are quite common. Among the several types of nanoparticles, MWCNTs are referred as one of the most promising nanomaterial in what heat transfer intensification is concerned. The cylindrical and highly elongated geometry of these nanoparticles enables a higher degree of spatial distribution. Moreover, the nanoparticle distribution alters the system microstructure, which may increase the overall suspension viscosity, as described by the *effective medium theory* (EMT). However, viscosity increase could contribute to undesirable effects for heat transfer applications, such as: increasing the pressure loss and required systems pumping power. It is therefore, of utmost importance to acquire more knowledge in what concerns the rheological behaviour of MWCNTs based nanofluids.

It is a fact that nanofluids properties strongly depend upon the properties of each individual phase, the spatial distribution of the nanoparticles and the interactions between phases. As stated by the *effective medium theory*, the contribution of each individual phase on the thermo-physical properties of the system is a function of nanoparticle concentration. As the particle concentration increases a point known as the percolation threshold is reached, and a continuous network is formed [264]. However, this network strongly depends on the spatial distribution and nanoparticle geometry. Moreover, the spatial distribution of nanoparticles dispersed in a fluid is very difficult to assess, and it is largely transient regarding external stimulus. Also, this is especially true if the suspended nanoparticles are in the form of clusters, or submitted to an applied shear. Initial attempts to explain the lower percolation threshold of nanoparticles with larger aspect ratio, such MWCNTs, were based on the

excluded volume theory developed by Balberg et al. [265]. This theory defines that the excluded volume of an object, is defined as the region of space into which the centre of another similar object is not allowed to enter if overlapping of these two is to be avoided [266].

In colloidal science, there are three main microstructure morphologies: a) Diluted, b) Non-diluted and c) Percolation like structure, see Figure 3.1

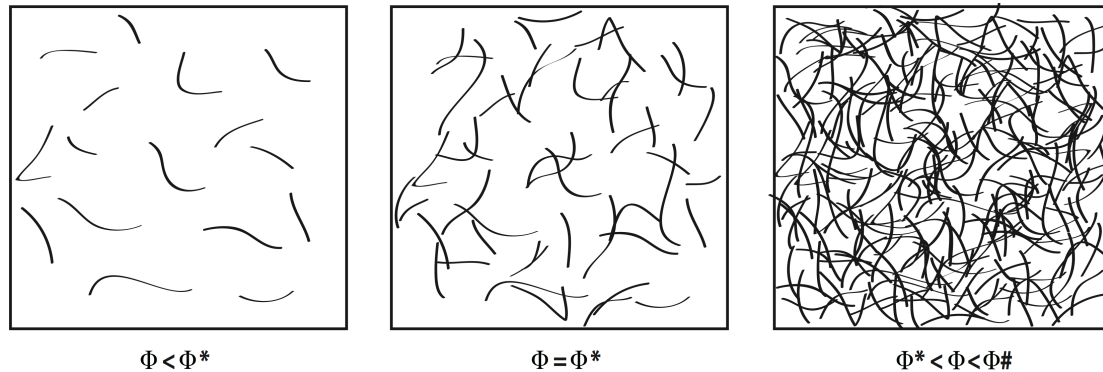


Figure 3.1 - Schematic microstructure representation: (a) diluted; (b) semi-diluted; (c) percolation like structure.

In simple terms, Percolation theory is a standard model for a structurally disordered system, as explained by Broadbent and Hammersley pioneers of this theory [267]. The diluted regime is characterized by a volume fractions Φ inferior to the percolation threshold Φ^* , where the particles in a control volume are totally isolated from each other. The non-diluted regime is reached when the volume fraction equals the percolation threshold concentration. The concentrated or percolation like structure is characterized by a volume fraction superior to the percolation threshold concentration, that forms a spanning cluster that connects both sides of the representative control volume [264].

The percolation threshold of a nanofluids strongly depends on many factors, such as: mean aspect ratio, the length polydispersity, the bending flexibility and tortuosity of the nanoparticle, as well as interactions between them and the fluid matrix [268], this is even more pronouncing for tube-like nanoparticles. Also, it is well established, that the percolation threshold decreases in inverse proportion to their aspect ratio [265], which make MWCNTs the most suitable particles for the development of advanced heat transfer fluids.

Based on this fact, the central issue is how to produce a nanofluid with enhanced heat transfer capacities and with the lowest possible loading of MWCNTs.

Despite the large number of investigations regarding MWCNTs nanofluids, the production of nanofluids is still not problem-free. The major challenge is to produce a nanofluid with thermo-physical properties that remained constant, or with negligible variation over time. To attain the latter, it is of utmost importance to ensure a great level of effectiveness, which lies mainly in the stability and quality of the suspension over time.

3.2 Stability Mechanisms of Nanofluids

Life cycle management is of increasing interest and importance to prone the application of MWCNTs nanofluids for real applications. Moreover, the colloidal stability has a huge influence on the transport and thermo-physical properties of any suspension. It should be noted that a colloid is defined as a microscopic material dispersed throughout a continuous medium with a dispersed-phase diameter of approximately 1 μm to 1 nm. Therefore, high aspect ratio and large contact area between the nanoparticles and dispersing medium play a central role, on what stability of a colloid is concerned. This means that the colloidal stability and also the system as a whole, is significantly affected by the interparticle interactions [269].

This leads to the following question, what is a stable fluid? In colloidal and interfacial science, the term stable or unstable is used to describe the balance of various interaction forces acting on the nanoparticle, such as van der Waals attraction, electric double-layer repulsion and steric interaction. These interactions forces were described at a fundamental level in the well known DLVO theory from Deryaguin and Landau [270] and Verwey and Overbeek [271]. In the frame of the DLVO theory, the interactions between colloid particles are defined by the summation of two independent interactions: a repulsive electrostatic force, which arises due to charges on the particle surface, and an attractive van der Waals force due to the solid particle cores [272]. The potential energies of these interactions will determine the phase behaviour and the kinetics of agglomeration in colloidal dispersions.

Controlling the agglomeration of nanoparticles in a nanofluid has become the primary issue for the initial research of nanofluids. Moreover, it is of major importance to assess the stability and dispersion of the nanoparticles in the liquid medium in order to exploit their potential benefits and applications [54].

An overview of these interactions are given bellow and this is followed by establishing the conditions of stable /unstable suspensions.

3.2.1 Aggregation

Aggregation of colloidal particles occurs when particle surfaces come in contact with each other and interactions allows for particle aggregation. Moreover, the rate of aggregation is in general determined by the frequency of interparticle collisions. However, when contact occurs it may result in attachment or repulsion. These phenomena can be understood in the context of DLVO theory. The DLVO theory combines the quantification of the energy due to the overlap of van der Waals forces (V_A) and the electrostatic repulsion forces (V_R) as a function of the distance (H) between pairs of nanoparticles. The sum of these forces is called the net interaction energy (V_T) [46]. This value will determine the ability of the nanoparticles to agglomerate or to repel, and is directly linked to the surface potential and electrolyte concentration [46].

The van der Waals interaction forces arise from the interaction of induced dipoles in the molecules of two opposing bodies. Due to the long-range characteristics of this force, it can act between the bodies and reach several nanometers across. In contrast to the EDL repulsion nature, the van der Waals force is always attractive and does not depend on the electrolyte concentration on solution [272].

The electric double layer (EDL) occurs when a surface with ionized groups is placed in a polar medium. The EDL consists of charged surface and the corresponding oppositely charged ions. The presence of the EDL is very important, since the more particles repel each other, more stable is the solution [273]. Furthermore, for agglomeration to occur the balance between forces must have an attractive nature, otherwise the particles may collide but will not

agglomerate [274]. On the other hand, the higher the repulsion forces the higher will be the stability of the dispersion. An important feature of the agglomeration/repulsion rate is that, for the case of nanofluids for thermal application, the thermo-physical properties can change significantly with the degree of aggregation [166], therefore, the higher the rate of dispersion, the higher the probability of homogeneous thermo-physical properties. As a result, a barrier potential must be developed to prevent agglomeration. Thus, two methods are widely used to prevent agglomeration of particles: electrostatic repulsion and steric exclusion.

In nanofluids research, the electrostatic repulsions are usually applied through mechanical processes, such as intense ultrasonication, ball milling or high speed shearing [275], [276]. However, it should be noted that electrostatic stabilization is limited by the following facts [277]:

- It is a kinetic stabilization
- It is only applicable to dilute systems
- It is not applicable to electrolyte sensitive systems
- It is almost impossible to re-disperse the agglomerated particles
- It is difficult to apply to multiple phase systems

The Steric stabilisation, also called polymeric stabilization, is the most common method of stabilisation in nanofluid research. Such repulsive forces are achieved by the particle absorption of polymers (non-covalent) and/or active species (covalent). The steric effect of polymer dispersant, or surfactant, envelope the nanoparticle forming chemical bonds between the surface atoms and polymer molecules. This method does offer several advantages over the electrostatic stabilization [277]:

- It is a thermodynamic method, the particles are always re-dispersible
- It can be applied to high concentration systems
- It is not electrolyte sensitive
- It is suitable to apply to multiple phase systems

Nevertheless, non-Covalent functionalization may influence negatively the effective thermo-physical properties of nanofluids, since it forms an interfacial layer between the two phases. Moreover, Nguyen et al. [278] found that when these type of nanofluids were submitted to heat and cooling cycles, the nanoparticles agglomerated, suggesting a degradation of the surfactant. Moreover, when submitted to external forces the surfactant can be separate from the base fluid, since this is not covalently attached to the nanoparticle surface. Covalent functionalization is another type of steric stabilization. In contrast to the non-Covalent, this one enduringly bond active species to the nanoparticle surface.

3.2.2 Sedimentation

Sedimentation represents the rate of separation between two-phase materials, which can occur under the influence of gravity and/or an external force. More, sedimentation can be an indicator of the state of aggregation, since aggregation produces larger and heavier clusters of nanoparticles, which then cause a more rapid sedimentation. The settling velocity of sediment particles, also known as the terminal or fall velocity, is the key parameter to assess the shelf life of a suspension [279].

The separation by sedimentation in a colloid only occurs when an external force is applied, such as gravity or centrifugal forces. Moreover, there will be a relative motion between the particles and the suspending fluid unless the density of the nanoparticles and the dispersion medium is the same. For the case when interactions between the two phases are strong, the system forms a single-phase non-Newtonian fluid. This means that the nanoparticles in contact with the fluid form a gel and become captured within the fluid network [280]. Therefore, if a stable and homogeneous suspension is desired, then a proper methodology is required to prevent this relative motion. On the other hand, motion of nanoparticles in a fluid is the basis of all separation process [280]. Based on these facts, the motion of nanoparticles should be under control for proper and efficient operations of the processes. The key parameters that affect the velocity of nanoparticles dispersed in a Newtonian fluid are, the

nanoparticles geometry, base fluid viscosity, interaction forces between particles and the forces acting on the nanoparticle.

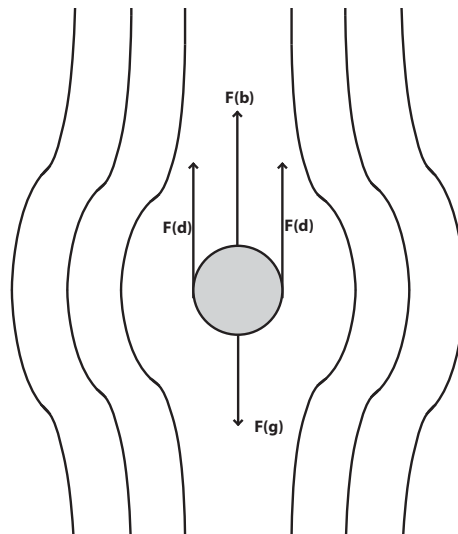


Figure 3.2 - Distortion of flow streamlines around a settling particle and forces acting

The hydrodynamic interactions between the particle and the fluid should be taken up first, before other analyses of the forces acting on the nanoparticle. This means that the drag force acting on the nanoparticle or the equivalently hydrodynamic Stokes Law, is of prime importance [281]. Stokes model [281] for a spherical particle falling in a fluid, can be derived from the force equilibrium (see Figure 3.2) as follows:

$$F_B - F_G + F_R = 0 \quad \text{Eq. 3.1}$$

where F_B is the buoyancy force acting on the particle,

$$F_B = \frac{4}{3} \pi R^3 \rho_{BF} g \quad \text{Eq. 3.2}$$

and the F_G is the gravitational force,

$$F_G = \frac{4}{3} \pi R^3 \rho_p g \quad \text{Eq. 3.3}$$

and F_R is the resistance force or friction force exerted by the fluid medium

$$F_R = 6 \pi \mu R V_{Sed} \quad \text{Eq. 3.4}$$

where V_{Sed} is the settling velocity of the particle. Stokes settling velocity or terminal velocity can be evaluated as follows,

$$V_{Stokes} = \frac{2 (\rho_p - \rho_{BF}) g R^2}{9 \mu_{BF}} \quad \text{Eq. 3.5}$$

However, this model has some limitations, such as: it was derived for a single particle motion and nanofluids normally have more than one, it does not take into account disturbances that occur due to interparticle interaction, and it can only be applied to spherical particles.

As it was mentioned, for the case of multi-particle systems the hydrodynamic interactions (collision/repulsion) between nanoparticles have to be taken into consideration [282], [283]. As a result, hindered sedimentation occurs and settling velocity decreases. For this case, to assess the settling velocity one must introduce in Stokes equation the so-called hindrance function $F_{hind}(\Phi)$.

$$V_{hind} = V_{Stokes} \cdot F_{hind}(\phi) \quad \text{Eq. 3.6}$$

where V_{Stokes} is the Stokes settling velocity defined in Equation 1.5.

Over the years, several models have been proposed to assess the hindrance function. Robinson modified the Stokes law and used the apparent viscosity μ_{nf} and apparent density ρ_{nf} of the suspension in place of the properties of the base fluid to give [284]

$$V_{HindRobinson} = \frac{K (\rho_p - \rho_{nf}) g D^2}{\mu_{BF}} \quad \text{Eq. 3.7}$$

where $K=(1/18)$ is a proportionality constant and “D” is the equivalent diameter of particles.

Later, Steinour and Hawksley interpreted in a different way Robinson's hypothesis. They have proposed a correlation, which takes into account the slip velocity between the particles and the suspending fluid, as follows:

$$V_{HindSteinor} = \frac{(\rho_p - \rho_{nf})(1 - \phi) g D^2}{18 \mu_{BF}} \quad \text{Eq. 3.8}$$

Winterwerp proposed a model accounting for the buoyancy effects, increased viscosity effects and return flow [285], as follows:

$$f_{Hind_{Winterwerp}} = \frac{(1 - \phi_{bf})(1 - \phi_p)}{1 + 2,5\phi} \quad \text{Eq. 3.9}$$

Schaflinger correlation, relates the base fluid viscosity, colloidal viscosity and the volume fraction, as follows:

$$f_{Hind_{Schaflinger}} = \frac{\mu_{bf}(1 - \phi_p)}{\mu(\phi)} \quad \text{Eq. 3.10}$$

which depends on the volume fraction Φ and on the concentration dependence viscosity $\eta(\phi)$ [286], [287], and Richardson-Zaki [288] function is given as,

$$f_{Hind_{Zaki}} = (1 - \phi)^n \quad \text{Eq. 3.11}$$

where, $n=4,65$ was established on the base of numerous empirical datum.

Moreover, Anestis et al. proposed the *theory of kinematic waves and shocks*. The latter states that, if the dispersion viscosity law is known, the sedimentation kinematics of nanoparticles at an arbitrary volume fraction under a given centrifugal force may be theoretically described [289], [290]. They have proposed the following correlation for the hindrance function [289]:

$$f_{Hind_{Anestis}} = \frac{(1 - \phi_p)^2}{\mu(\phi)} \quad \text{Eq. 3.12}$$

Despite the large number of correlations, full understanding of the settling kinetics is still precluded by substantial empirical and theoretical challenges. The intricacies brought by the hydrodynamic interactions between particles and solvent counterflow, leads to a diverging expression for the settling velocity. Yet, most researchers agree that during phase separation, the

sedimentation rate of a single particle is always higher than in a multi-particle system. Batchelor [291] empirically concluded that a suspension containing 3% volume fraction of spheres has an average settling velocity 20% lower than that predicted by Stokes law, due to the hydrodynamic interactions.

As it was highlighted, the geometry of a nanoparticle has a major influence on the rate of sedimentation. For instance, the drag force acting on an elongated particle such MWCNTs, is much higher than on a spherical particle, due to the superior cross section area, therefore, the deviation from a spherical shape is quantified by shape factors. One of the most widely used shape factors was proposed by Corey [292] (csf) and is given by:

$$csf = \frac{c}{(ab)^{0.5}} \quad \text{Eq. 3.13}$$

where a, b and c are the longest, intermediate and short axes of the nanoparticles and is assumed to be an ellipsoid.

Yu et al. [293], studied the sedimentation rate of MWCNT under a centrifugal force. They have concluded that in order to use the Stokes Law, they have to consider that CNTs were spherical, and the equivalent diameter of CNTs was calculated as:

$$d = \sqrt{ab} \quad \text{Eq. 3.14}$$

where a and b are the diameter and length of CNTs. In the literature there are many other correlations to assess the equivalent diameter of particles, some of the most important *equivalent diameters* are:

- Volume-equivalent

$$D_{Volume} = \left(\frac{6}{\pi} V_p \right)^{1/3} \quad \text{Eq. 3.15}$$

- Surface-equivalent (diameter of a sphere with the same surface as the particle)

$$D_{Surface} = \left(\frac{6}{\pi} S_p \right)^{1/2} \quad \text{Eq. 3.16}$$

- Stokes-equivalent (diameter of a sphere with the same final settling velocity)

$$D_{Stokes} = \sqrt{\frac{18 \mu V_{Sed}}{(\rho_{np} - \rho_{BF}) g}} \quad \text{Eq. 3.17}$$

For the purpose of this work the surface equivalent diameter was selected.

The orientation state of MWCNTs also plays a crucial role on the sedimentation rate. The orientation of the nanoparticles is always changing due to fluctuations of the fluid viscosity or due to an imposed external force. As a result, the drag coefficient of the nanoparticle will change over time. Furthermore, the elongated geometry of MWCNTs reduces the distance between particles, increasing the influence produced by the displacement of the fluid and by interparticle interactions and collisions. Sedimentation that has these characteristics is designed as hindered settling [177], [294].

3.2.3 Long-Term Nanofluids Engineering

It has been demonstrated that the synthesis of long-term stable and homogeneous suspensions it is of utmost importance to fully prompt the thermo and transport physical properties of nanofluids. However, in order to maintain particle spatial distribution, it is necessary to guarantee the structural integrity of the nanoparticles, with a low probability of agglomeration and no sedimentation.

Since the unique properties of nanoparticles originate from their size, especially MWCNTs, it is widely understood that nanofluids with agglomerates will behave differently from well dispersed ones [295]. For that reason, especial attention should be given to reduce the degradation of the MWCNTs structure. Moreover, as it was identified on Section 1.3.1, the stability of dispersions is also influenced by other factors, such as: nanoparticles characteristics, surface properties and solution chemistry (pH level, concentration, ionic strength) [295].

Furthermore, the nanoparticles aggregation may lead to an increases on the effective viscosity of nanofluids, especially for low shear velocities [296]. Also, the rheological behaviour of suspensions may change from a Newtonian to a shear thinning behaviour, just due to the presence of agglomerates. As a result, it is of utmost importance to ensure the homogeneity within the samples, while reducing any noise factor that can affect the physical properties evaluation.

However, when MWCNTs are dispersed in a polar solvent that they spontaneously tend to agglomerate into bundles with varying lengths and diameters. This occurs due to the hydrophobic nature of MWCNTs structure and the high surface-to-volume ratio, resulting in strong van der Waals attraction forces [277]. It becomes, therefore, necessary to overcome these attractions forces while increasing the solubilisation of MWCNTs [297]. The latter may be achieved throw functionalization of the surface of the MWCNT by covalent and non-covalent techniques. The most common covalent functionalization is chemical oxidation, which consists in refluxing the MWCNTs in strong acids such as nitric and/or sulphuric acids. This technique attaches oxygenated functional groups, such as carboxylic (-COOH) and alcohol groups (-OH), into the side wall of MWCNTs [80], [298]. More, these groups have both polar characteristics, which contribute to increase the wettability of MWCNTs and also the solubility in polar solvents.

Both covalent and non-covalent techniques have advantages and disadvantages. In the case of covalent functionalization, the main disadvantage is that it can cause the shorting of the MWCNTs, altering the spatial distribution of the solution. This chemical oxidation has to be precisely controlled to reduce any defects caused on the MWCNTs [299]. Functionalization must ideally occur at the ends of the MWCNTs, as side wall functionalization has been shown to disrupt the tube structure causing it to lose some intrinsic electronic, mechanical and thermal capabilities [300], [301].

In order to prompt MWCNTs based nanofluids as the next generation of advanced heat transfer fluids, these have to fulfil certain characteristics, such as: the nanofluid has to be homogeneous, with negligible agglomeration and no sedimentation, over long periods of time. Only then will be possible to guarantee the long-term homogeneity of the transport physical properties.

3.3 Design of Experiments

The main objective of the experiments is to assess the rheological behaviour and the mechanisms governing the effective viscosity of MWCNTs based nanofluids. To this end, a proper *design of experiments* (DOE)} is developed in an attempt to understand the mechanisms proposed in the published literature.

The conducted literature review on Chapter 1 suggested that the effective viscosity and rheological behaviour of nanofluids, may be explained through the hydrodynamic interactions, the Brownian motion, nanoparticle orientation, viscous resistance (drag force) and percolation and agglomeration of the nanoparticles. In order to assess the contribution of each mechanisms and simplify its analysis, the dimensional analysis conducted in Chapter 2 identified that there are seven main control factors that may influence the rheological behaviour, these are: (1) MWCNTs geometries and density, volume fraction, the base fluid viscosity and density, the temperature and the shear rate. It should be noted that a control factor of an experiment is a controlled independent variable. In Table 3.1, it is presented a summary of the expected relationship between the identified control factors and the mechanisms proposed in the open literature.

Table 3.1 – Expected relation of the control factor on the mechanisms governing the rheology

Control Factors	Brownian Motion	Nano-Layer Structure	Nanoparticle Orientation	Viscous Resistance	Hydrodynamic Interactions	Spatial Distribution
Nanoparticle Geometry	X	X	X	X	X	X
Volume Fraction	X	X		X	X	X
Base Fluid Temperature	X	X		X		
Shear Rate	X		X			X

As it can be seen, the Brownian motion of the particles depends on several parameters such as: base fluid viscosity, temperature, and geometry of the nanoparticles. This will affect the drag coefficient, volume fraction and also the shear rate since at higher shear rates the Brownian motion may become

neglected. The formation of a nano-layer around a particle also affects the viscosity of the suspension, due to the enhancement of the particle surface area, which causes more resistance to flow. The latter is affected by the nanoparticle geometry, volume fraction, and by the base fluid, since different base fluid densities will produce distinct nano-layer thicknesses. Moreover, the orientation of the nanoparticles, the hydrodynamic interactions and the spatial distribution also depends on the nanoparticle geometry and volume fraction.

It appears, therefore, that the MWCNTs geometries present the most intriguing impact on the effective viscosity and rheological behaviour of colloidal suspensions. In order to study this behaviour, six different MWCNTs geometries were selected for the present study. The properties of the selected MWCNTs are described in Table 3.2

Table 3.2 – Nanoparticles characteristics and selected geometries

MWCNTs Nomenclature	Ash [wt%]	Purity [%]	ρ_{MWCNT} [kg/m³]	Aspect Ratio
D20-40 L1-2	<3,0	>97	2160	50
D20-40 L5-15	<3,0	>97	2160	333
D20-40 L10-30	<1,5	>95	2160	667
D50-80 L10-20	<1,5	>95	2160	231
D60-100L1-2	<3,0	>97	2160	19
D60-100 L5-15	<3,0	>97	2160	125

These six particles can be grouped into two average diameters, $d_p=30$ (D20-40) and $d_p=80$ (D60-100); and three average length distributions, $L_p=1500$, $L_p=10000$ and $L_p=15000$. The selection of these nanoparticles was made in order to cover a broad diameters and lengths interval. All of the selected particles were produced by catalysed chemical vapour deposition (CCVD).

Moreover, the discrepancies verified between empirical investigations regarding the linearity or non-linear behaviour of nanofluids viscosities with volume fractions, were also investigated. To that extent, five volume fractions were selected, namely: 0,25; 0,5; 0,75; 1,0; 1,5 %vol. These concentrations were chosen based on the facts that, the viscosity of nanofluids increases considerably with the volume fraction, as pointed out on the literature review.

The selection of the base fluids was made based on the fact that the properties of the liquid medium may induce a significant difference, especially in the case of the Brownian motion and the orientation of the nanoparticles under a shear flow. More, heat transfer fluids have some degree of freezing protection, low corrosion and lubricant properties. This is commonly achieved through the addition of ethylene glycol to an aqueous solution. For the above-mentioned reasons, two distinct base fluids composed by a mixture of deionized water with 30%DW+30EG and 60%DW+60EG of ethylene glycol, were selected.

It is a fact that the rheological behaviour of solutions is strongly dependent on the temperature. It is also known that a temperature rise will result in an enhancement of the internal energy, resulting in a decreased of the medium viscosity. Hence, six temperatures were selected: 283; 293; 298; 303; 313 and 323 K. The upper limit temperature represents the limit to ensure the accuracy of the viscosities measurements.

As it was pointed out, most researchers suggested that nanofluids have a shear thinning nature, which means that the viscosity strongly depends on the imposed shear rate. It is known that, as the shear rate increases the forces acting on the suspended particles will cause the particles to migrate and orientate in the direction of the flow lines. Thus, seven shear rates were selected: 92,4; 132; 171; 211,2; 250,8; 290,4 and 330 s⁻¹.

In Table 1.3 is summarized the control factors selected for the study and their respective degrees of freedom. The literature review clearly highlights that the lack of a standardized production methodology may be one of the reasons that have contributed to noise factors and to the discrepancies between empirical research groups. Due to this fact, a factorial design may hinder the results contributing to reduce noise factors. To ensure a higher degree of inference over the experimental results, a full factorial design of experiments was selected to carry out the work here presented. In this, all levels of each factor are combined with every remaining one. This means that the problem results in 2940 experimental data points ($6 \times 2 \times 5 \times 7 \times 7 = 2940$), i.e. (ABCDE).

Table 3.3 – Control factors and their range of setting for the experiments

Control Factor	MWCNTs	Base Fluid	Volume Fraction [vol. %]	Temperature [K]	Shear Rate [s ⁻¹]
	A	B	C	D	E
Level 1	D20-40 L1-2	30EG+DW	0,25	283	92
Level 2	D20-40 L5-15	60EG + DW	0,5	293	132
Level 3	D20-40 L10-30		0,75	298	171
Level 4	D50-80 L10-20		1,0	303	211
Level 5	D60-100L1-2		1,5	313	251
Level 6	D60-100 L5-15			323	290
Level 7				333	330
Degrees of Freedom	5	1	4	6	6

The three basic principles of a Design of Experiments (DOE) are [302]:

Randomization - when randomizing the experimental runs, the sequence helps to eliminate effects of unknown or uncontrolled variables. However, as it will be discussed in Section 5, the randomization of the measurements at the various temperatures and shear rates may be conditioned by the experimental apparatus.

Blocking - when it is too costly or impossible to randomize a factor, blocking allows for increasing the precision. Thus, the design is blocked by the factors such as temperature and shear rate, allowing to decrease the number of experimental runs to 60. Through this procedure, the total number of nanofluids (ABC) is reduced as well as the total time for the experimental measurements.

Replication - when replicating an entire experiment can help to identify any source of experimental variance sources or to identify uncertainties. If the number of experiences is too short this will result in a lack of precision of the experimental results, and if it is too high, time and resources will be wasted for minimal gain. Therefore, the calculation of the sample size is crucial for an efficient design of experiments.

3.3.1 Multivariable Analysis Methodology

Multivariable analysis is a statistical analysis performed to several measurements in order to ascertain the correlation between control factors. Thus, the goal of any multivariable approach is to untangle the overlapping information provided by correlated variables. For the purpose of this work, the multivariable analysis will reveal the interactions between control factors, validating the proposed mechanisms and to ascertain the effective properties of the nanofluids.

The correlation between control factors occurs when the relationship between a single dependent control factor is affected by the outcome of two or more independent control factors. Thus, the behaviour of the output control factor and control factor interaction can be described through the *main effect* analysis [302]. The latter, results in comparisons of the marginal means of each factor. Moreover, it enables a graphical representation that shows the change in response occurring by means of a change in the level of the observed factor [302]. The main effect can be expressed as:

$$\text{main effect} = \overline{X_{cf_n}} \quad \text{Eq. 3.18}$$

where X_{cf_n} in the experimental data means when the control factor (cf) is at level n, and X is the overall or "grand mean" of the experimental result under analysis [303]. A *main effect* is said to occur when the differences between the levels of a control factor are different from zero, otherwise no effect of any level occurs between the two controlled factors.

In order to receive more information about the background of the experimental results, the *analysis of variance (ANOVA)* was applied. The latter, enables the investigation of the statistical significance of the main effects and two or more-factor interactions, or in other words, the ANOVA will assess which control factor has the greatest impact on the experimental viscosity.

The procedure works by comparing the variance between control factors means versus the variance within the control factors, as a way of determining whether the groups are all part of one large population or separate populations

with different characteristics. Moreover, for the design of experiments with a factorial nature, when the null hypothesis is true $H_{0,cf}$, then one cannot conclude that there are any differences among these control factors. The null hypothesis is expressed as:

$$H_{0,C}: \overline{X_{C1}} = \overline{X_{C2}} = \dots = \overline{X_{Cn}} \quad \text{Eq. 3.19}$$

In contrast, if the null hypothesis is not true, i.e. the alternative hypothesis $H_{1,cf}$, then one can conclude that at least one of the levels means is different and, therefore, the control factor has a significant impact on the experimental results. The alternative hypothesis can be expressed as:

$$H_{0,C}: \overline{X_{C1}} \neq \overline{X_{C2}} \neq \dots \neq \overline{X_{Cn}} \quad \text{Eq. 3.20}$$

For the purpose of this work, the statistical analysis of the effective viscosity was performed for the effective viscosity ratio, due to the selected base fluids present distinct viscosities. Through this analysis, the effect of the incorporation of the MWCNTs on the effective viscosity can be assessed, and independently of the viscosity of the selected base fluid. This interpretation is in line with the majority of the prediction models.

3.4 Surface Modification Techniques

As discussed in Chapter 1, a higher wettability of MWCNTs can be achieved by two distinct methods: the covalent and non-covalent functionalization. The covalent functionalization is achieved by oxidative treatments that attach oxygenated functional groups on the surface of the MWCNTs. This technique presents some advantages over the use of surfactants (non-covalent) especially for thermal transport applications.

There are several methodologies to perform a covalent functionalization of the MWCNTs. However, during the present research, the oxidative method proposed by Esumi et al. [298] was adopted. This method may be summarized as it follows:

1. In a hood, pristine MWCNTs were weighted and transferred to a 5L beaker;
2. A 1:3 volume ratio of nitric acid (HNO_3) and sulphuric acid (H_2SO_4) are added to the pristine MWCNTs, until it performs a ratio of 40ml of acid per gram of MWCNTs, as suggested by several authors [88], [111], [298], [304];
3. The mixture is then heated to 413 K and stirred for 30 minutes;
4. Subsequently, the mixture is allow to cool down naturally for 24 hours;
5. The mixture is then diluted in distilled water and centrifuge until the MWCNTs were completely sediment. This washing process is repeated until a pH level of ± 5 is reached. At this step, the carboxylic bounds are already bonded to the MWCNT surface, being impossible to reach a pH level of ± 7 ;
6. The cleaned MWCNTs were then dried at 373 K in an oven, in order to remove all the remaining water and a hard pellet is formed.
7. Finally, the dried MWCNT were powdered with an analytical miller and stored in a desiccator to avoid any gain of moisture.

The above steps were carefully repeated for all the six different geometries of MWCNTs.

3.4.1 Functionalization Evaluation

To evaluate if the functionalization was properly inferred and to identify the functional groups attached to the MWCNTs surface, a Fourier Transform Infrared Spectroscopy (FTIR) was performed in pristine and functionalized MWCNTs. This technique consists in shining the samples with a beam of light containing multiple frequencies and in measuring the ratio of light absorbed by the sample. The FTIR measurements were performed in a Bruncker Tensor-27 spectrometer in the range of 400 to 4000 cm^{-1} . Due to the high absorption of

MWCNTs, they were mixed with potassium bromide (KBr) and pellets were prepared. The results of this analysis will be shown in Chapter 4.

3.4.2 Dispersion Methodology

In order to accomplish the production of the long-term nanofluids and properly disperse the MWCNTs in the liquid medium, first the base fluid was prepared. Next, the chosen volume fraction of MWCNTs was obtained through the following correlation,

$$\phi = \frac{m_{MWCNT} \rho_{MWCNT}}{m_{MWCNT} \rho_{MWCNT} + V_{BF}} \cdot 100 \quad \text{Eq. 3.21}$$

Based on the previously correlation two approaches could be made: one can establish the volume fraction desired and calculate the amount of base fluid; or one can establish a fixed volume of base fluid and calculate the mass of MWCNTs. The first approach can induce some noise factors, since the volume of base fluid to be measured can become decimal or centesimal, therefore, the second approach was adopted. The total volume of base fluid V_{bf} was fixed to 50 ml and the total mass of MWCNTs was calculated. In Table 1.5, it is represented the chosen volume fractions of the tested nanofluids and the respective mass of MWCNTs. In Appendix A, it is provided the mathematical formulation for the experimental volume fraction error.

However, in order to achieve a homogeneous dispersion of MWCNTs in the base fluid, one must first overcome the cohesive energy associated to the MWCNTs bundles.

The following steps describe the methodology adopted to the production of the long-term MWCNTs based nanofluid.

Table 3.4 – Nanoparticles and base fluid quantities for the preparation of the samples

Base Fluid	ϕ [%]	V_{DW} [ml]	V_{EG} [ml]	m_{MWCNT} [g]
30%EG+70%DW	0,25	35	15	0,271
	0,5	35	15	0,543
	0,75	35	15	0,816
	1,00	35	15	1,091
	1,5	35	15	1,645
60%EG+40%DW	0,25	20	30	0,271
	0,5	20	30	0,543
	0,75	20	30	0,816
	1,00	20	30	1,091
	1,5	20	30	1,645

This methodology has been patented in order to provide a standard methodology and, once adopted, it is believed to reduce the discrepancies found between empirical investigations hence reducing the noise factors.

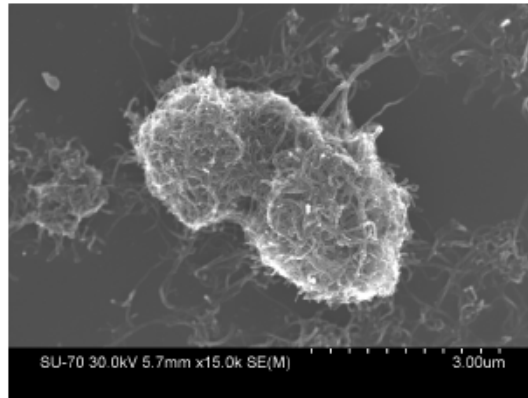
1. The amount of MWCNTs for a desired volume fraction is weighted with a high-precision balance $\partial m=0,001g$ see Table 1.5;
2. With a graduated pipette $\partial V=0,1ml$ the volume of each base fluid is measured;
3. The MWCNTs are then added to the base fluid;
4. This mixture is mechanical agitated with a magnetic stirrer and sonicated with a low intensity cavitation probe (Bioblock Scientific Vibra-Cell 750). The cavitation phenomena releases large amounts of energy to the sample, and if not properly controlled could induce damages to the MWCNTs structure. To prevent the latter, the imposed energy was maintained constant at 250 J/ml.
5. In order to maintain the temperature of the sample during the sonication process, the sample was cooled in a cold-water bath.

It has been reported by several authors, that covalent functionalization can effectively eliminate the majority of impurities present on bulk MWCNTs, but also tends to damage the structural integrity of nanotubes, creating defects in the graphene layers, hence reducing the nanotube length [305]-[307]. The structural

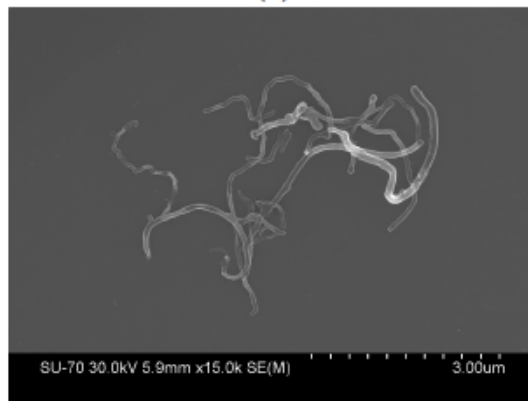
integrity of the MWCNTs and the size distribution should be evaluated and compared with that announced by the manufacturers.

3.4.3 Dispersion Evaluation

As it was mentioned earlier, in order to achieve a homogeneous dispersion of MWCNTs in the base fluid, one must first overcome the cohesive energy associated with the MWCNTs bundles. Evaluating the degree of dispersion in a suspension could be assessed by indirect measurements, such as TEM and SEM. However, both techniques present one major limitation, since the samples have to be dried and exposed to vacuum before they can be analysed. Thus, any conclusion regarding the degree of dispersion must be made carefully, since one cannot be sure if the test sample is representative of the entire sample. Nevertheless, as it can be depicted from the SEM images (Figure 3.3), it is perceptible that the bulk MWCNTs are highly entangled and, in contrast, the functionalized MWCNTs are well dispersed.



(a)



(b)

Figure 3.3 – SEM image of (a) Bulk MWCNTs and (b) Functionalized MWCNTs

3.5 Size Distribution Evaluation

As it was mentioned in Chapter 2, the geometrical properties of the suspended nanoparticles have a major impact on the viscosity of the samples. Moreover, the functionalization and dispersion techniques enabled the production of well-dispersed homogeneous suspensions of MWCNTs. However, it is recognised that these techniques can damage the surface of the MWCNTs as well as dramatically reduce its lengths [23]. The size distribution evaluation should, therefore be addressed and compared with that announced by the manufacturer.

There are many techniques and instrumentation to ascertain the size distribution of bulk and functionalized MWCNTs. Techniques such as nuclear magnetic resonance (NMR), Dynamic light scattering (DLS), UV-Vis spectroscopy, laser diffraction, microscopy (SEM/TEM) that can be applied to analyse such

particles. However, the cylindrical shape of MWCNTs impose a certain challenge in addressing its geometrical properties [308], [309]. Thus, a selection of an appropriate methodology to assess the two-dimensional size distributions of the dispersed MWCNTs is of utmost importance.

In this work, the size distributions of the MWCNTs were determined through a scanning electron microscope (SEM) Hitachi SU-70. The six geometries of MWCNTs were dispersed on a highly diluted fashion in a solution of ethanol. Next, these suspensions were deposited over the sample's holder and a sputter coating of carbon was performed to ensure that the samples are electron conductive. The length and diameter distribution for the six oxidized MWCNTs was obtained manually measurements, with the assistance of a free image editor, (GIMP 2.8). In an attempt to minimize the human error, approximately eighty MWCNTs randomly taken in several SEM images were measured. It is assumed that the size distributions have a normal distribution, enabling the estimation of confidence interval and standard error. Also, this method lies on the fact that these images are projected on a 2D plane.

Moreover, this technique enables the verification of the structural integrity of the MWCNTs, i.e. length reduction, and the maintenance of tubular shape. The mathematical formulation to estimate the 95% confidence interval can be found in Appendix B.

3.6 Stability Integrity Evaluation

The stability of nanofluids implies that these have to preserve its properties for large periods of time with negligible variations. However, as it was pointed out in Chapter 1, a long-term stable MWCNTs nanofluid has to detain:

- Low-Agglomeration
- Low-Sedimentation
- High Structural Integrity

However, achieving all of these requirements is very challenging, since to enhance one can sometimes jeopardized another. In the following paragraphs a description of the techniques used to evaluate these factors will be presented.

3.6.1 MWCNTs Agglomeration Evaluation

The agglomeration state of MWCNTs is directly linked with the surface properties [310]. These properties can be manipulated through functionalization techniques, as it was previously described. In order to identify the functional groups attached to the MWCNT surface, a Fourier Transform Infrared Spectroscopy (FTIR) was performed. Due to the highly absorbance properties of MWCNTs, these had to be mixed with KBr and pellets were prepared. These measurements were made in a Bruker Tensor-27 spectrometer in the 400 to 4000 cm^{-1} range. Each spectrum is the mean of 3 measurements with a resolution of 4 cm^{-1} .

Additionally, the feasibility of forming stable non-agglomerate suspensions is further supported by the electrostatic repulsion forces. These forces also known as electrostatic potential or Zeta Potential, were evaluated in a Malvern ZS Nano S Analyser at 293,15 K. Predominantly, suspensions with an absolute zeta potential higher than 30 mV or less than -30 mV are generally considered to represent sufficient mutual repulsions to ensure the stability and low agglomeration of the MWCNTs [54], [311]. General speaking, the higher the absolute value of Zeta potential, the more stable the system will be.

3.6.2 MWCNTs Sedimentation Evaluation

As it was mentioned on Chapter 1, the evaluation of the rate of sedimentation could be achieved through several methods, being the most common the sedimentation photograph and the UV-visible spectrophotometry.

The sedimentation photograph method consists in taking photography's of a test-tube filled with nanofluid at a constant time period. In a qualitative fashion it is possible to determine the sedimentation rate of the nanoparticles [54]. The UV-visible spectrophotometer measures the absorption profiles of the nanofluid when subjected to an electromagnetic spectrum. The sedimentation rate can be evaluated based on the Beer-Lambert law that relates the absorption profiles with the variation of concentration [312]. However, both these methods have two major drawbacks, the long time measuring period required to the

nanoparticles to sediment and the sensibility of this measurement to external perturbations like vibrations [57].

To reduce the identified noise factors, a novel technique that employs centrifugal fields to evaluate the phase separation rate was used. The LUMiSizer 6120 Stability analyser, subjected the samples to different centrifugal fields (RCF - Centrifugal acceleration/earth acceleration) while measuring the intensity of the transmitted light as a function of time and the position over the entire sampler holder (for details refer to www.lum-gmbh.com) [313]. As it can be depicted from Figure 3.4, as the particles migrate due to the centrifugal force, this results in a variation of the local particle concentration, resulting in a local and temporal variation of the transmission light. This feature enables the evaluation of the phase separation rate for each RCF. The integrated software allows the recording of each individual transmission profile and the slope of each profile is directly related to the stability of the fluid [313]. Zero slope means that no change in the particle concentration occurs over time, meaning that the dispersion is stable. In contrast, the higher the slope the more unstable the sample is. Furthermore, if the de-mixing velocity is proportional for a given RCF, the sedimentation behaviour can be extrapolated to gravity conditions (RCF=1) and shelf life can be predicted [313]. When compared with other methods, this technique is a great improvement, since it does not require sampler dilution and, therefore, it takes into account all nanoparticles interaction.

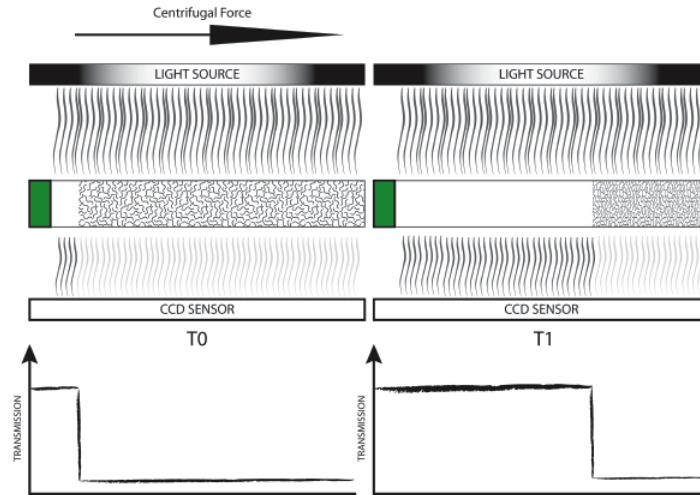


Figure 3.4 – Schematic representation of the measuring principal of the LUMiSizer Stability Analyser

3.6.3 MWCNTs Structural Integrity Evaluation

The structural integrity of the functionalized MWCNTs can be achieved through the analysis of SEM/TEM images. However, in order to evaluate the stability of the MWCNTs when subjected to thermal variations a Thermogravimetric analysis (TGA) was performed. The TGA measures the weight-lost of the sample as a function of the temperature. The measurements were performed in a SETSYS Setaram DSC-TG from 293 to 1023 K with a heating rate of 10 K/min and under an inert atmosphere of nitrogen. The adoption of this gas instead of an oxidative atmosphere, ensuring more reliable measurements, and also minimization of the risk of MWCNTs decomposition to occur due to oxidative reaction with the functionalized groups.

3.7 Chapter Conclusions

Nanofluid engineering is the first and most important step in an experimental characterization. However, dispersing nanoparticles in a fluid medium is still a complex process. The intricate nature of MWCNTs induces the formation of clusters, and its proper dispersion in a fluidic medium is not always as easy as it seems. Nonetheless, several chemical and mechanical techniques were proposed in an attempt to disentangle the MWCNTs bundles and promote a

homogeneously dispersed suspension. However, if not properly controlled these dispersion techniques can induce damage to the tube surface, altering its structural integrity and its properties. For the production of a long-term MWCNTs nanofluid, one must guarantee that the dispersion has a low agglomeration, a low sedimentation ratio and a high structural integrity.

In the next chapter, it is presented the results obtained from the techniques here identified and that were used to evaluate the long-term stability and structural integrity of the produced MWCNTs nanofluids.

Chapter 4 - Experimental Determination of Nanofluids

Properties

4.1 Long-Term MWCNTs Nanofluids Quality Assessment

In the conducted survey on Chapter 3, it was identified that a nanofluid can have three possible forms of instability: nanoparticle structural integrity; nanoparticle agglomeration; and sedimentation. To ensure a long-term nanofluid and to evaluate the rheology of MWCNTs dispersions, one must first evaluate the quality of the dispersion (low-agglomeration and low-sedimentation). Moreover, the mechanical technique employed to disentangle the MWCNTs clusters can cause damages on the structure of MWCNTs, thus as previously identify on Chapter 2, the MWCNTs dimensions play a crucial role on the rheological behaviour of suspensions and needs to be properly assess, and require proper assessment.

In this section it will present the results obtained on the quality analysis conducted to the MWCNTs nanofluids under study.

4.2 Structural Integrity

The structural integrity of the MWCNTs may be degraded, especially when subjected to hard temperature gradients. In order to evaluate the structural integrity of the MWCNTs a thermo-gravimetric analyser (SETSYS Evolution) from SETARAM Instrumentation was used. Both bulk and functionalized MWCNTs were analysed for temperatures ranging from 293 to 1023 K at 10 K/minute.

In Table 4.1, it can be depicted the weight ratio of both bulk and functionalized MWCNTs. As it can be seen, the bulk MWCNTs are thermally stable, since very little weight loss ratio was recorded (4%). In contrast, the functionalized MWCNTs present a linear weight reduction (up to 16%). Nevertheless, there is no apparent decomposition temperature set point, which means that the weight reduction can be associated to the presence of impurities

resulting from the functionalization process. Similar results were found for all the samples tested (see Appendix F).

Table 4.1 – Weight loss ratio for bulk and functionalized MWCNTs at 320 and 1000 K.

MWCNT	Bulk		Functionalized	
	320 K	1000 K	320 K	1000 K
	Weight loss [%]			
D20-40 L1-2	0	0,56	0,65	10,45
D20-40 L5-15	1,74	4,68	1,17	15,29
D20-40 L10-30	0,15	0,78	0,87	9,61
D60-100 L1-2	0,34	1,47	0,38	5,71
D60-100 L5-15	0,79	3,58	1,05	16,63
D50-80 L10-20	0	0,53	0,73	11,82

4.2.1 Probability of Repulsion / Agglomeration

As envisaged in the Chapter 3, in order to maintain the stability of a nanofluid, one must guarantee that the nanoparticles do not flocculate after being dispersed in the base fluid. In this regard, to increase the probability of repulsion the MWCNTs were covalently functionalized.

In order to identify the functional groups attached to the MWCNTs, a Fourier Transform Infrared Spectroscopy (FTIR) was performed in both bulk and functionalized MWCNTs. The FTIR spectrum is illustrated in Figure 4.1, here one can see vertical lines representing the wavelength of: the wavenumber near 3450 and 1060 cm^{-1} , which is a characteristic of the hydroxyl group O - H assigned to the carboxylic groups (O=C - OH or C - OH) [34], [314]; the peak near 1700 and 1150 cm^{-1} are linked to the C=O and C - O stretching of the carboxylic groups (-COOH), respectively [315]. The peak near 1580 cm^{-1} is assigned to the FTIR active phonon mode of the MWCNTs [316]. These results have clearly shown that the hydroxyl and carboxylic groups have been properly introduced to the MWCNTs surface. Similar results were found in all the samples tested.

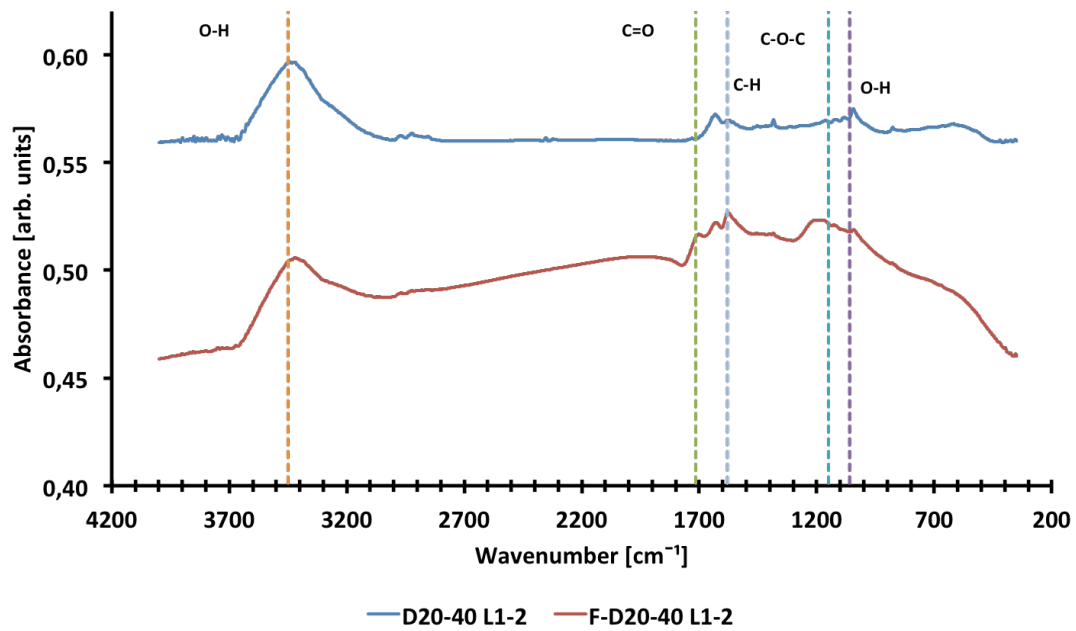


Figure 4.1 – FTIR spectrum for bulk and functionalized D20-40 L1-2 MWCNTs.

The presence of functionalized groups on the surface of the MWCNTs, it is not enough to guarantee the repulsion between particles. The development of an electrical double layer around each particle, capable of increasing the concentration of ions of opposite charges, is very important to form a stable entity between the nanoparticles and the base fluid. This boundary is known as the surface of hydrodynamic shear or slipping plane. The potential that exists at this boundary is called the Zeta Potential. However, zeta potential cannot be directly measured, it has to be estimated through theoretical models. These models are based on the fact that, charged particles in a suspension can be set in motion by the action of an electric field. The velocity acquired by the particles due to the presence of the electric field is called the electrophoretic mobility (EM) [317]. As the electric potential of the nanoparticle increases so does the velocity or electrophoretic mobility. Based on this premise, Henry proposed a following correlation [318],[319]:

$$u_e = \frac{2 \varepsilon_0 D \zeta}{3 \mu_{bf}} f(k, a) \quad \text{Eq. 4.1}$$

where ϵ_0 is the permittivity of a vacuum, D is the dielectric constant of the base fluid, u_e is the electrophoretic mobility and μ_{bf} is the base fluid viscosity. If the particles are small relatively to the electric double layer then $f(\kappa, a)=1$, if the particles are larger than the EDL then $f(\kappa, a)=1,5$ and Eq. 4.1 becomes the Smoluchowski equation [317].

It should be noted that samples measured by this technique have to be optically transparent and, therefore, depending on the optical properties of the nanoparticles, it requires the sample to be diluted. Nevertheless, the inter-facial equilibrium between the MWCNTs surface and the base fluid are independent of the concentration of MWCNTs, and, therefore, the Zeta potential would be the same for all the volume fractions considered [320]. Thus, all tested samples here diluted to a $\varphi = 0,02\%$ vol., and five runs were performed for each sample, enabling to verify the repeatability of the measurements and estimate the average value and respective uncertainty.

The dielectric constant and refractive index considered for the base fluids are 61,08 / 1,389 and 71,59 / 1,364 for DW+60EG and DW+30EG, respectively [321]-[323].

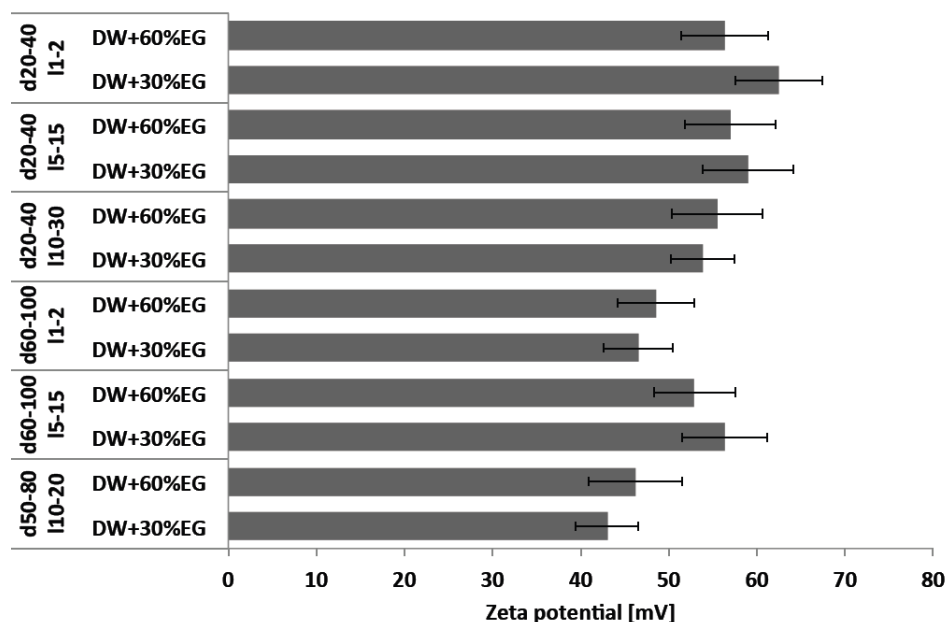


Figure 4.2 – Zeta Potential of the studies samples

As it can be depicted from Figure 4.2, all tested samples present a Zeta Potential superior to 40 mV, suggesting an excellent particle repulsion ($>40\text{mV}$), i.e. low probability of agglomeration. Moreover, it can also be seen that the variation of the base fluid, nanoparticle geometry and concentration present a similar Zeta potential, meaning that the EDL is constant regarding these parameters. The uncertainties were calculated through the methodology presented in Appendix D.

4.2.2 MWCNTs Size Distribution Measurement and Analysis

As it could be seen throughout Chapter 3, the preparation methodology used to produce nanofluids can cause damage to the surface and size distribution of the MWCNTs. The size of MWCNTs was, therefore evaluated by analysing SEM images, as it can be depicted from Figure 4.3. However, it should be noted that this techniques uses projected 2D images of a 3D structure, which induces some unknown inaccuracy on the measurements. Nevertheless, this is the best technique to assess the length and diameter for tube-like suspensions.

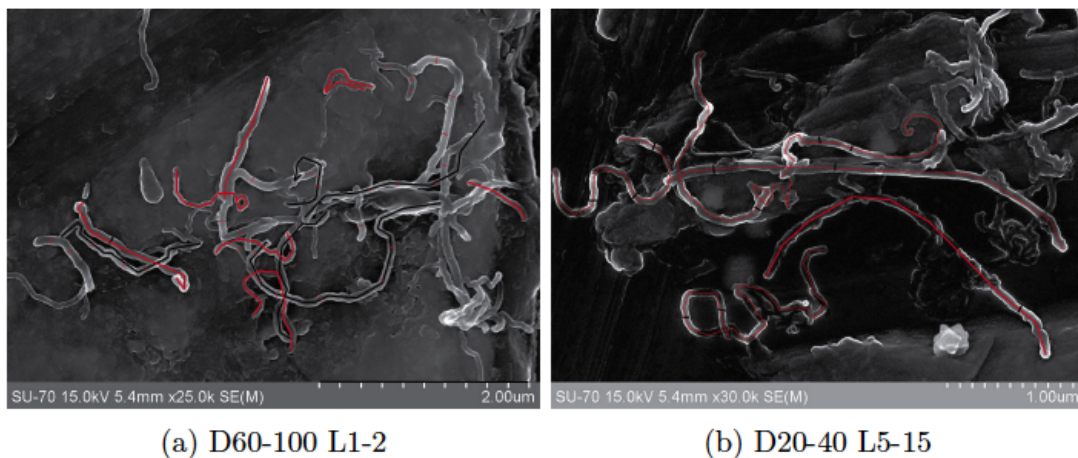


Figure 4.3 – Schematic representation of the methodology used to assess the size evaluation of the MWCNTs

Hilding et al. conducted an empirical study to address the effect of different ultrasonication techniques on the size distribution of MWCNTs. They have concluded that as the nanoparticles fragment to smaller sizes, less of the

applied energy results in fragmentation. Moreover, they have found that the length and diameter distributions are better described by *log-normal* distribution, since it has a greater fraction of higher length scales than Gaussian distributions [23].

During this study, for each MWCNT geometry, at least five images were analysed to obtain the largest number of MWCNTs lengths and diameters and, therefore, increasing the accuracy. In line with Hilding [23], the size distribution for all the MWCNTs geometries were fitted by a *log-normal* distribution, with a confidence level of 95%. In Figure 4.4, it can be depicted the log-normal curve for the length and diameter measurements for the nanofluid D20-40 L1-2. Similar results (Appendix E) were obtained for all the nanofluid samples tested. From these results, it was possible to evaluate the mod diameter and length, as well as the confidence level of 95%, for all the studied MWCNTs.

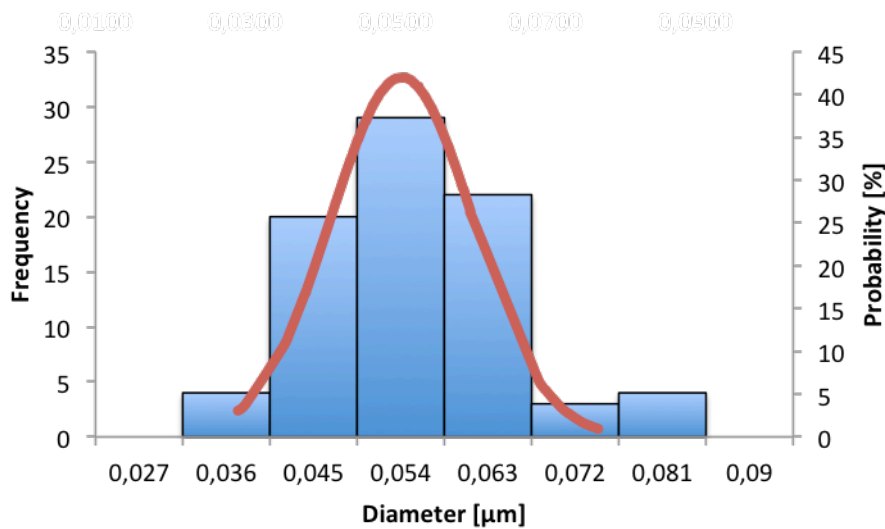


Figure 4.4 –Diameter distribution of the D20-40 L1-2

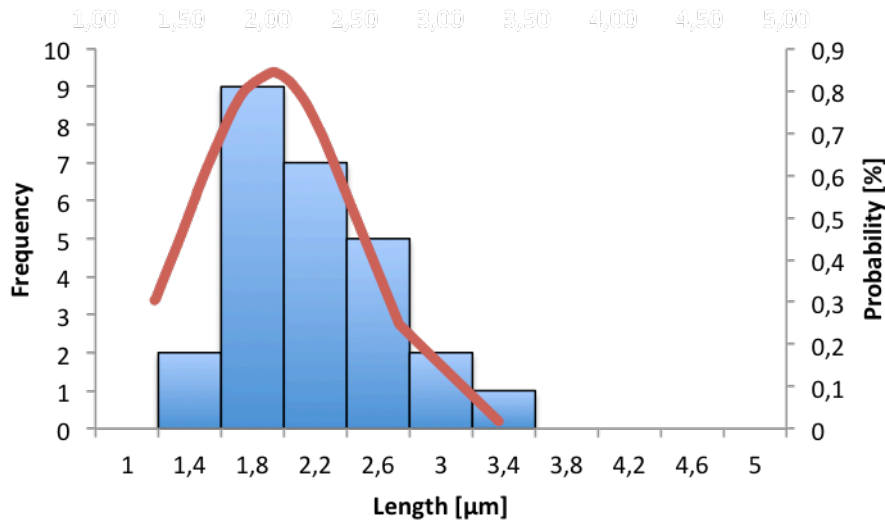


Figure 4.5 –Length distribution of the D20-40 L1-2

In Table 4.2, it can be depicted the results from the size distribution for the experimentally measured MWCNTs. The uncertainty and confidence level of the means were calculated as describe in Appendix A.

Table 4.2 – Sample Size distribution from SEM images

MWCNT	Diameter			Length		
	d_{np} [nm]	Δd_{np} [nm]	95% C. I.	l_{np} [nm]	Δl_{np} [nm]	95% C. I.
D20-40 L1-2	48,8	1,2	[47 ; 50]	1689	72,5	[1616 ; 1762]
D20-40 L5-15	54,5	1,4	[53 ; 56]	2731	85,7	[2645 ; 2817]
D20-340 L10-30	48,6	1,2	[47 ; 50]	2765	91,9	[2674 ; 2857]
D60-100 L1-2	57,9	1,4	[56 ; 59]	1603	84,3	[1519 ; 1687]
D60-100 L5-15	87,2	2,0	[85 ; 89]	2742	129,7	[2613 ; 2871]
D50-80 L10-20	54,3	1,4	[53 ; 56]	3103	91,9	[3011 ; 3195]

As it would be expected, the MWCNTs were damaged during the production process. Despite the MWCNTs diameter remain similar to those supplied by the manufacturer, the length is the most affected by the production methodology, decreasing in average 49% of its original length.

Table 4.3 – Geometrical properties of the measured MWCNTs

MWCNT	Diameter	Length	Aspect Ratio
	d_{np}	l_{np}	(l_{np}/d_{np})
D20-40 L1-2	48,8	1689	34,6
D20-40 L5-15	54,5	2731	50,1
D20-40 L10-30	48,6	2765	56,9
D60-100 L1-2	57,9	1603	27,7
D60-100 L5-15	87,2	2742	31,4
D50-80 L10-20	54,3	3103	57,2

Taking into consideration that the production methodology is the same for all the samples, as described in Section 2, one can assume that the final geometrical dimensions of the nanoparticle depends on the initial dimensions of the MWCNTs. Based on this assumption, is now possible to develop a predictive model to evaluate the geometrical properties of the suspended MWCNTs. In Eq. 4.2 it is presented an exponential regression to predict both magnitude of the diameter and length of the MWCNTs based on the dimensions disclosed by the manufacturers. It should be noted that the predictive model passes through the origin.

$$Y = a(b - e^{-cx}) \quad \text{Eq. 4.2}$$

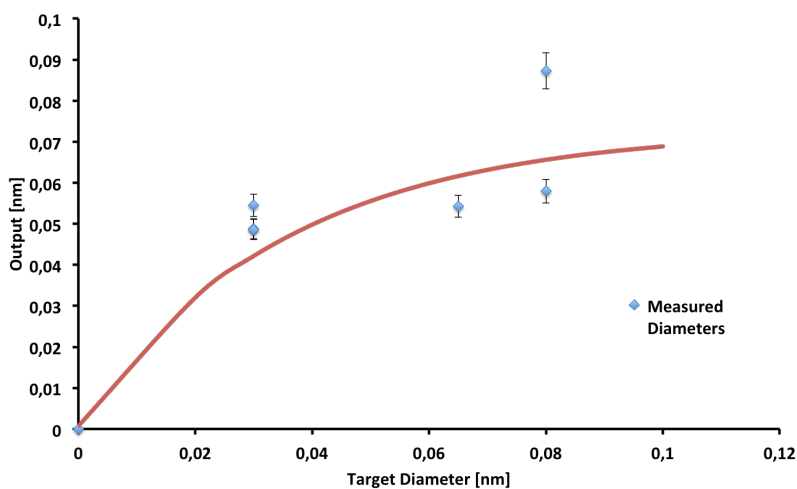
where Y is the variable to be predicted and a to c are the adjustments factors shown in Table 4.4

Table 4.4 – Adjustments factors for the exponential regression for the diameter, length and aspect ratio

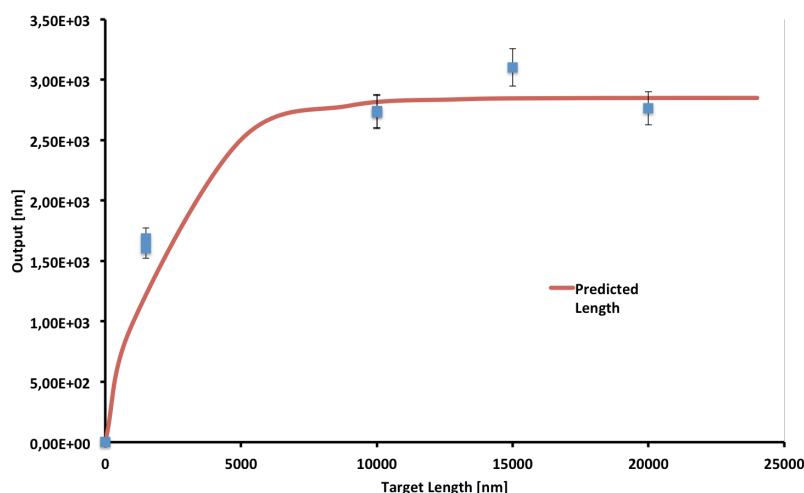
Adjustment Factors	Diameter	Length
a	1,32E-15	2,85E03
b	3,54E00	1,00E00
c	2,83E01	4,22E-04

In Figure 4.6 it can be depicted the results achieved through the regression model. The data presents an acceptable correlation with the

statistical result and, therefore this can be used to predict the final dimensions of the MWCNTs.



(a)



(b)

Figure 4.6 – Proposed model for the diameter (a) and length (b) of functionalized MWCNTs.

It should be noted that this technique presents some limitations in what nanoparticles dimensions assessment is concerned and any conclusion must be made carefully. Some of these limitations are related to the almost impossible task of taking SEM pictures to individual MWCNTs. From the SEM pictures it can be observed that the MWCNTs overlap each other, therefore measuring any

dimension in the picture will result in some degree of error. Nevertheless, this is the best technique capable of assessing the geometrical dimensions of non-spherical nanoparticles [324]. In Table 4.5, it is presented the geometrical properties that will be used in this work.

Table 4.5 – Predicted geometrical properties of the MWCNTs

MWCNT	Diameter	Length	Aspect Ratio
	d_{np}	l_{np}	(l_{np}/d_{np})
D20-40 L1-2	42,2	2850	68
D20-40 L5-15	42,2	1950	46
D20-40 L10-30	42,2	1963	47
D60-100 L1-2	61,6	2081	21
D60-100 L5-15	65,6	1401	30
D50-80 L10-20	65,6	1954	34

4.3 Nanofluids Density Evaluation

As identified on the dimensional analysis, nanofluids density plays an important role on the evaluation of the fluid dynamics. For this reason the density of some MWCNTs nanofluids were measured. There are several techniques capable of evaluating the density of nanofluids. However, the most widely used technique by the petroleum and chemical industries is the oscillating U-tube. The latter consists of a hollow U-shape glass tube that is electronically excited at a determined oscillation frequency. Then, as the vibration passes through the sample a group of sensors receive the oscillating signals and determine the period of oscillation. As the frequency of the oscillation of the U-tube is influenced by the mass, it is possible to determine the density of the sample.

The density of the MWCNTs nanofluids were measured by a U-tube digital density meter (densitometer) DDM 2910 from Rudolph Research Analytical. This densitometer was designed to meet the standards of the petroleum industry as well as chemical industrial laboratories. The measured samples were maintained at a constant temperature and five measurements of each nanofluids were taken.

In order to reduce the experimental work, two types of MWCNTs and three concentrations were chosen. In Table 4.6 it is represented the average measured density of each MWCNT nanofluid at 305 K

Table 4.6 – MWCNTs nanofluid density measurements @ 305 K

Base Fluid	Density g/cm ³					
	30EG+DW			60EG+DW		
	0,25%	0,75%	1,5%	0,25%	0,75%	1,5%
D60-100 L1-2 AR 28	1,046	1,052	1,067	1,082	1,088	1,098
D50-80 L10-20 AR 57	1,047	1,054	1,066	1,082	1,088	1,093

As it can be depicted, the MWCNTs nanofluids density increases with the volume fraction and also with aspect ratio. This may be an indication that as the MWCNTs geometry increases the percolation networks becomes more densely packed, affecting the overall fluid density.

4.3.1 Phase Separation

As envisaged in Chapter 3, the phase separation rate of the engineered MWCNTs nanofluids was evaluated by the LUMiSizer 6120 Stability analyser. For cost reduction purposes, three volume fractions were selected (0,25; 0,5 and 1,5% vol.) and tested at a controlled temperature (293 K) at three different centrifugal forces (see Table 4.7).

Table 4.7 – LUMiSizer Stability analyser measuring conditions

Velocity	RCF	Time Step
[RPM]	[G's]	[s]
1990	500	200
2800	1000	100
4000	2000	50

In Figure 4.7 it is represented a series of transmission profiles for the nanofluid D20-40 L1-2 in DW+30EG with 0,25% vol. subjected to a centrifugal force of a) 500, b) 1000 and c) 2000 G's. From the first profile (see Figure 1.6 a)) it can be depicted the position of the interface immediately after the centrifugation process begins (20s) and the last one after fourteen hours. Also, there is no significant change in the shape of the profiles, which implies that the suspension contains mono-dispersed nanoparticles [290]. The transmission profile of the remaining samples can be found in Appendix D.

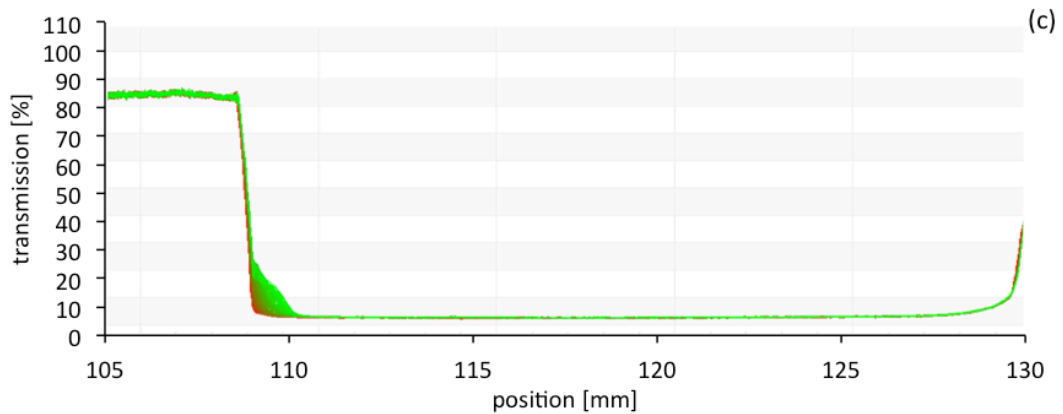
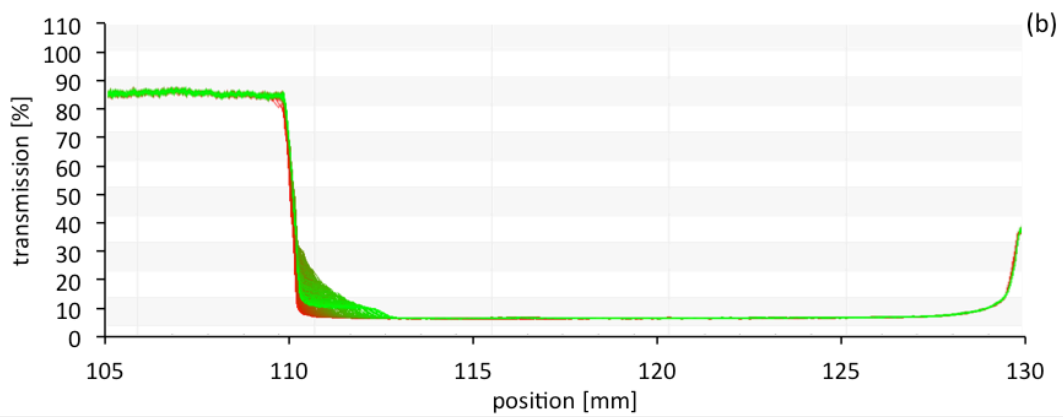
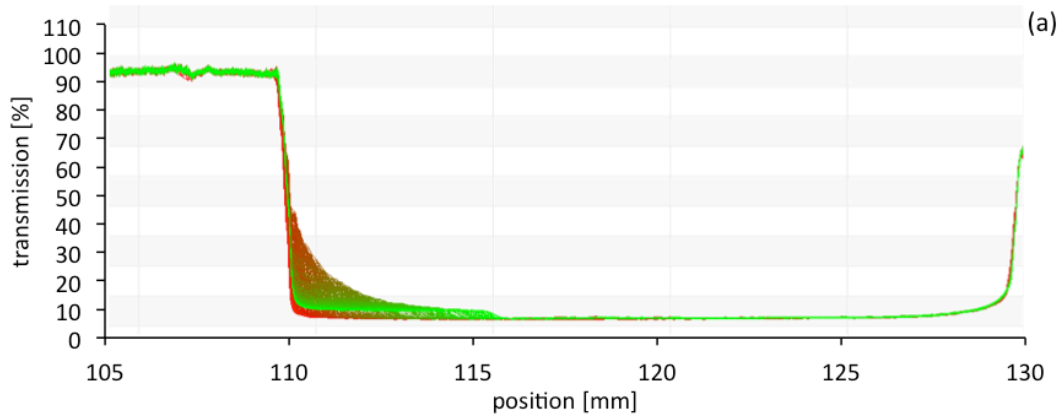


Figure 4.7 – Transmission Profile of the sample D20-40 L1-2 in 30EG+DW with (a) 0,25% vol. (b) 0,75%vol and (c) 1,5%vol of MWCNTs at 500 G's.

Moreover, by comparing the slop between the first and last profile for the different RCF, one can conclude that as RCF increases so does the transmission, i.e. the settling velocity increases with RCF. These results are in consonance with the *Stokes law of continuity* for the dispersed phase. However, it should be stressed that *Stokes law* is only valid for non-interacting particles subjected to a

Reynolds number inferior to 1 ($Re < 1$). In Figure 4.8, it is represented the average settling velocity as a function of RCF for the D20-40 L1-2 and for each base fluid.

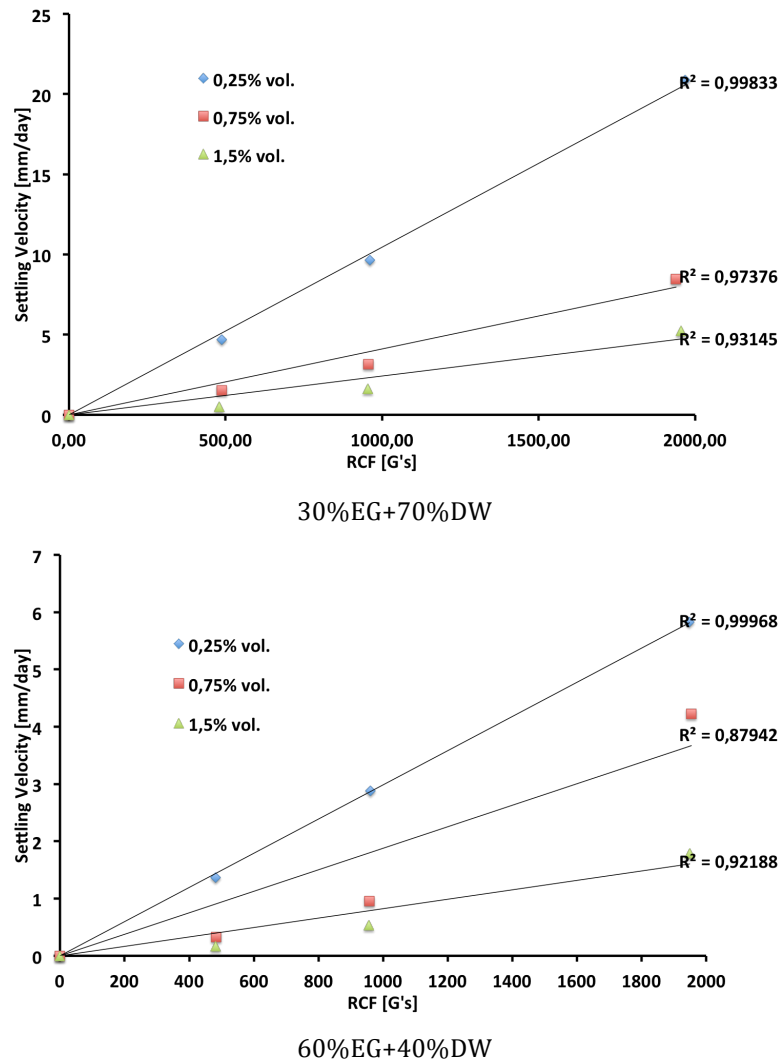
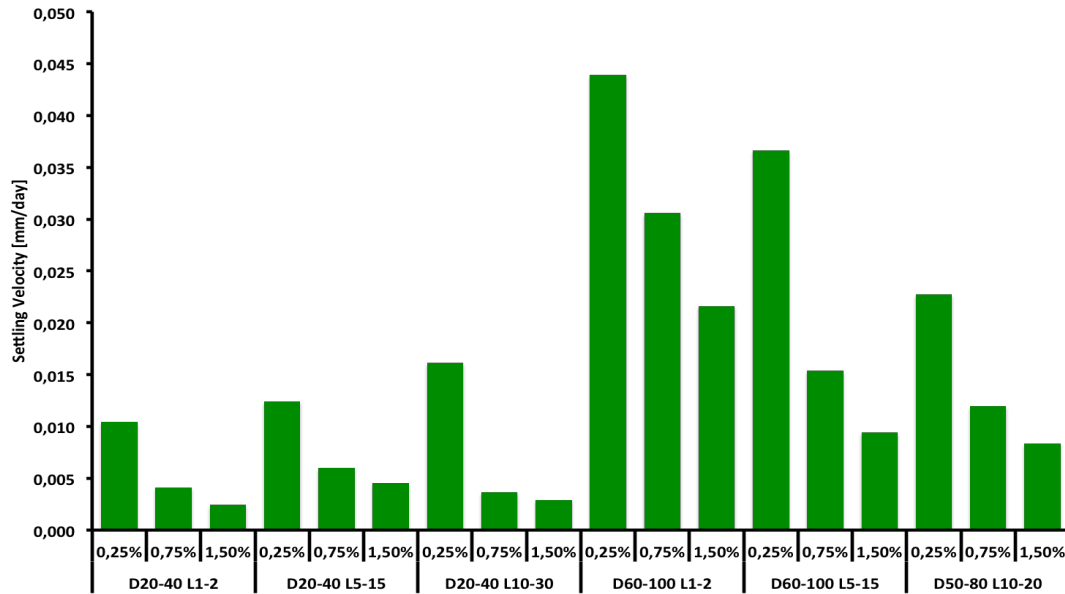
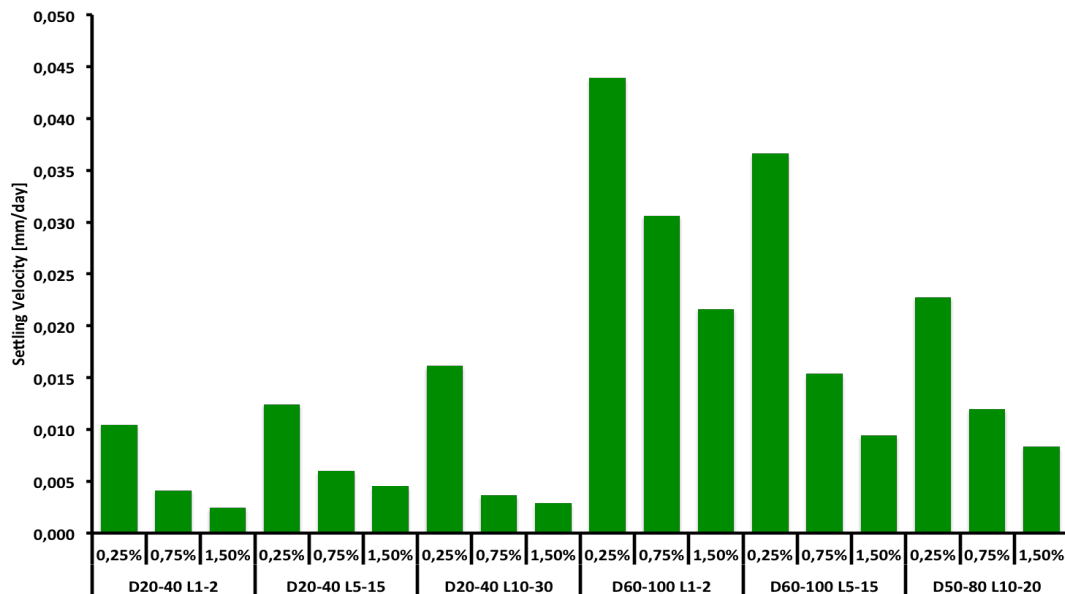


Figure 4.8 – Settling velocity as a function of the RCF for the nanoparticle D20-40 L1-2

As it can be depicted, the settling velocity profile presents a linear fashion for all the MWCNT concentrations and base fluids. It should be noted that these regressions intercept the origin, since it is assumed that no sedimentation can occur if the centrifugal force is null. Thus, it is now possible to extrapolate the settling velocity to the earth gravitational field ($RCF=1G$) as represented in Figure 4.9. The results have shown that the production of a stable, long shelf life nanofluid is possible.



(a) 30%EG + 70%DW



(b) 60%EG + 40%DW

Figure 4.9 – Settling velocity for all the nanofluids study for RCF=1 (a) DW+30EG (b) DW+60EG.

As it was mentioned in Chapter 2, for high concentrations of MWCNTs hydrodynamic interactions (collision/repulsion) between nanoparticles have to be taken into consideration [282], [283]. As a result, hindered sedimentation

occurs and settling velocity decreases. Based on Stokes law, the terminal velocity is the difference between weight and buoyancy or in other words, the relation between density and viscosity effects. In order to properly test Stokes law and other proposed correlations, some of the variables identified in the dimensional analysis require evaluation. The comparison between the different models and the settling velocity determined by the Lumisizer will be established in Chapter 5.

4.4 Brief Discussion

So far, it was verified that the tested nanofluids present negligible probability of agglomeration and phase separation. In addition, despite the high reduction in the length distribution of the MWCNTs the nanoparticle seems to present low damage structure and acceptable thermal stability.

4.5 Chapter Conclusions

Throughout the analysis conducted on this Chapter, one can conclude that the functionalization techniques attached the desired carboxylic groups to the sidewalls of the pristine MWCNTs. Through this, it is expected the enhancement of the MWCNTs wettability due to the creation of a hydrophilic envelop. The TGA revealed that the chemical treatment produced some changes on the MWCNTs. Nevertheless, this is only noticeable for high temperatures (>1000 K). For the temperatures projected to the evaluation of the viscosity, the TGA variation is minimal and can, therefore be neglected.

Even so, the mechanical dispersion technique used along with the functionalization process present a major drawback, which is the reduction of the MWCNTs length. The latter results in an enhancement of the viscosity for the same volume fraction, as it will be depicted on the next chapter. However, this is not desirable since an enhancement on the viscosity will imply an enhancement on the pressure drop resulting in a higher pumping energy. The ideal thermal nanofluid should present long-term effective properties and the optimal concentration of MWCNTs, which enhances the ability for transferring heat with little penalty in pressure drop. In the next Chapter, it will be presented the

experimental results obtained for the evaluation of the rheological behaviour of the nanofluids.

Chapter 5 - Experimental Assessment of Nanofluids

Rheological Properties

5.1 Overview

In this chapter an experimental assessment to the rheological properties identified in Chapter 2 for the MWCNTs based nanofluids is performed. As previously highlighted, viscosity is the most important property in rheology science, therefore an experimental apparatus for assertively measure the effective viscosity of the engineered nanofluids, is here proposed. In the chapter, the experimental procedure undertaken is also described in detail and prior to further measurements particular attention was given to the experimental repeatability of the base fluids measurements, where a maximum deviation from the theoretical values of 15,5% for viscosity and 3,4% for density, was observed. Given the high number of experimental observations, a statistical analysis is delineated in an attempt to easily verify the existence of some of the recent theories suggested to explain the observed rheological behaviour. Moreover, the settling velocity evaluated in Chapter 4 will be compared with postulated correlations from the literature to ascertain the validity of such postulations.

5.2 Nanofluids Viscosity Measurements

The literature survey presented in Chapter 1 highlighted several techniques to assess the viscosity of suspensions. However, as it was previously mentioned there is no standardized methodology to assess the viscosity of nanofluids. Despite that, the effective viscosity of the produced liquid samples was assessed with the orientation of the International Organization for Standardization (*ISO*) and from the German Institute for Standardization (*DIN*), more particularly from ISO 3219:1995 - "*Plastics, Polymers/resins in the liquid state or as emulsions or dispersions - Determination of viscosity using a rotational viscometer with defined shear rate*", and the DIN 53019 - "*Viscometry Measurement of viscosities and flow curves by means of rotational viscometers*".

These standards specify a methodology to determine the viscosity at a defined shear rate by means of rotational viscometers.

The effective viscosity of the nanofluids was measured by means of a rotational rheometer with concentric cylinders geometry, namely a Brookfield LV DVIII-Ultra rheometer. The temperatures identified in the DOE were guaranteed through a thermal bath (Brookfield TC-550) within an accuracy of $\pm 0,1^{\circ}\text{C}$. The overall experimental setup is schematically represented in Figure 5.1. It should be noted that this technique assumes that the measured properties are isotropic.

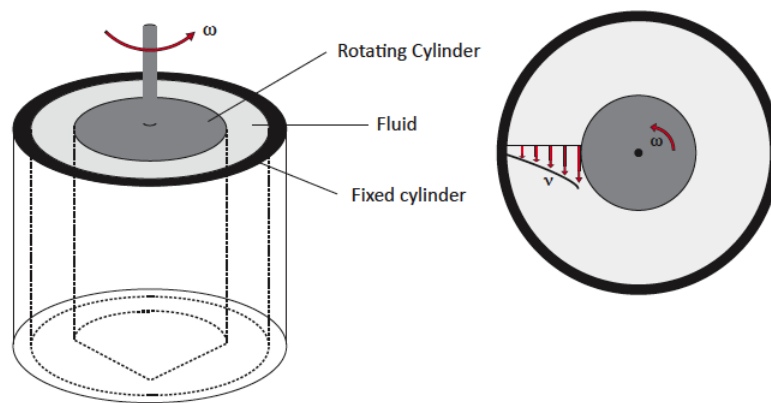


Figure 5.1 – Schematic Representation of the flow between two concentric cylinders

As it can be depicted from Figure 5.1, the sampler container (Small Sampler Adapter (SSA)) consists of a cylindrical sample chamber (SC4) that fits into a flow jacket, which is then connected to the thermal bath. According to the manufacturer, the sampler shaft requires exactly 6,7ml of nanofluid to ensure that the spindle is completely covered. The spindle geometry was selected based on the requirements set forth in DIN 53019-1, namely: that the ratio between the spindle radius (R_b) and the sample chamber radius (R_c) is equal to $R_b/R_c > 0,91$. Thus, the cylindrical spindle SC4-18 with a diameter of 17,48 mm and a length of 35,53mm was chosen.

The rheometer is automatically controlled and the data collected with Rheocalc32 Software. Each nanofluid was measured in ascending temperature and shear rate. Before each measurement, a five minutes interval was taken, in order for sample to reach apparent equilibrium. The measurements are taken at

each minute until it reaches 20 readings per temperature per shear rate. The following steps describe the methodology adopted for the characterization of the rheological behaviour of the prepared nanofluids:

- Ensure the rheometer is properly levelled;
- The AutoZero is performed every time the equipment is turned ON;
- Select the appropriate spindle;
- Introduction of 6,7ml of nanofluid into the sample chamber;
- Introduce the spindle into the sample chamber and attach the spindle to the coupling nut;
- Load the Rheocalc32 program;
- Turn on the thermal bath;
- Start the measurements.

It was previously referred that, the agglomeration and sedimentation of nanoparticles can affect the viscosity measurements, since this will cause a gradient in the nanoparticles volume fraction, requiring a greater force to dissipate the solid component of the dispersion. Moreover, when aggregates are sheared these could result in a shear-thinning phenomena due to the destruction of the agglomerates. A good colloidal stability is the only means to ensure that such a phenomenon does not occur. The latter is the sole premise of this work and it is believed that all the steps were taken to attain it

5.2.1 Experimental Apparatus Calibration

The experimental apparatus was calibrated with both standard calibration fluids and base fluids, following the directives proposed by the DIN 53019. The accuracy of the DVIII rheometer is guaranteed to be within $\pm 2\%$ of the full-scale range of the selected spindle/speed combination. The accuracy of the system is, therefore, established, by the following equation and it is summarized in Table 5.1,

$$Accuracy = 1\% \cdot TK \cdot SMC \cdot \frac{10000}{RPM} \quad \text{Eq. 5.1}$$

where $TK=0,09373$ is the torque constant and $SMC=3,2$ is the spindle constant.

Table 5.1 - Viscosity accuracy intervals for the selected spindle/speed configuration

Speed [RPM]	Accuracy	
	1%	2%
	[mPa.s]	
70	0,428	0,857
100	0,300	0,600
130	0,231	0,461
160	0,187	0,375
190	0,158	0,316
220	0,136	0,273
250	0,120	0,240

As it can be depicted, the accuracy of the system increases with the rotational speed. Moreover, to minimize any sources of error, the manufacturer suggests that the measurements should be taken for a torque superior to 10%. Thus, the rotation speeds were selected based on these directives.

In rotational viscometers with concentric cylinders, the shear stress (τ) and the shear rate ($\dot{\gamma}$) are not constant in the measuring gap between the internal and external cylinders, but decrease from the inside outwards (see Figure 5.1). For that reason, the DIN 53019 suggests that a representative shear stress (τ_{rep}) that is the mean of the shear stress at the outer and inner cylinders, should be considered. These correlations are given by:

$$\tau_{rep} = \frac{1 + \delta^2}{2\delta^2} \cdot \frac{M}{2 \pi R_i^2 L c_L} \quad \text{Eq. 5.2}$$

And

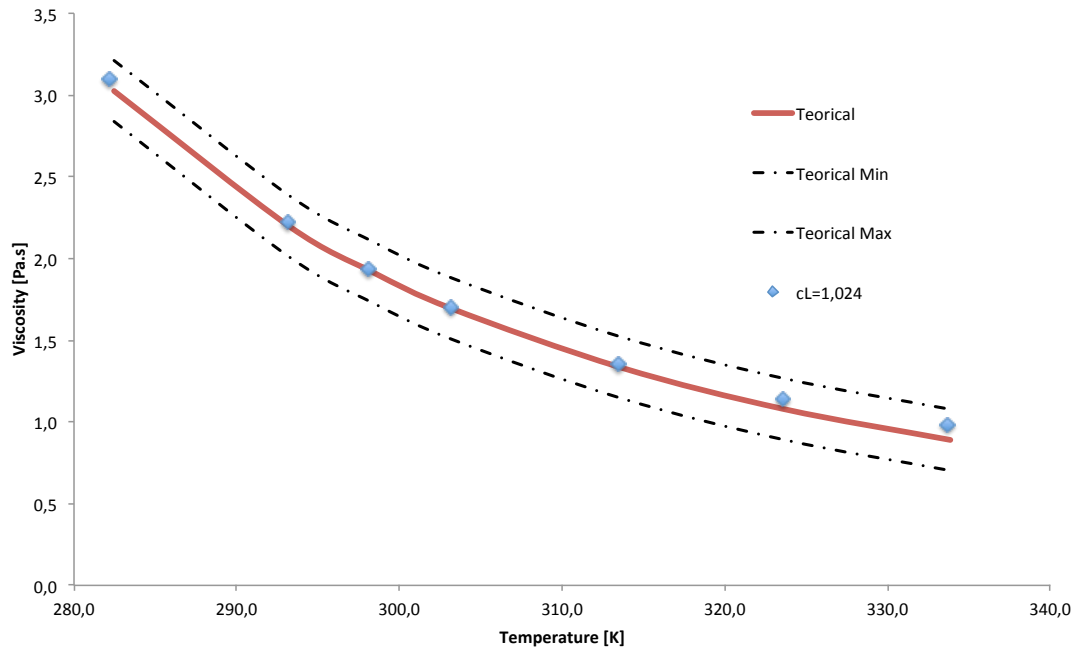
$$\dot{\gamma}_{rep} = \frac{1 + \delta^2}{\delta^2 - 1} \cdot \Omega \quad \text{Eq. 5.3}$$

And

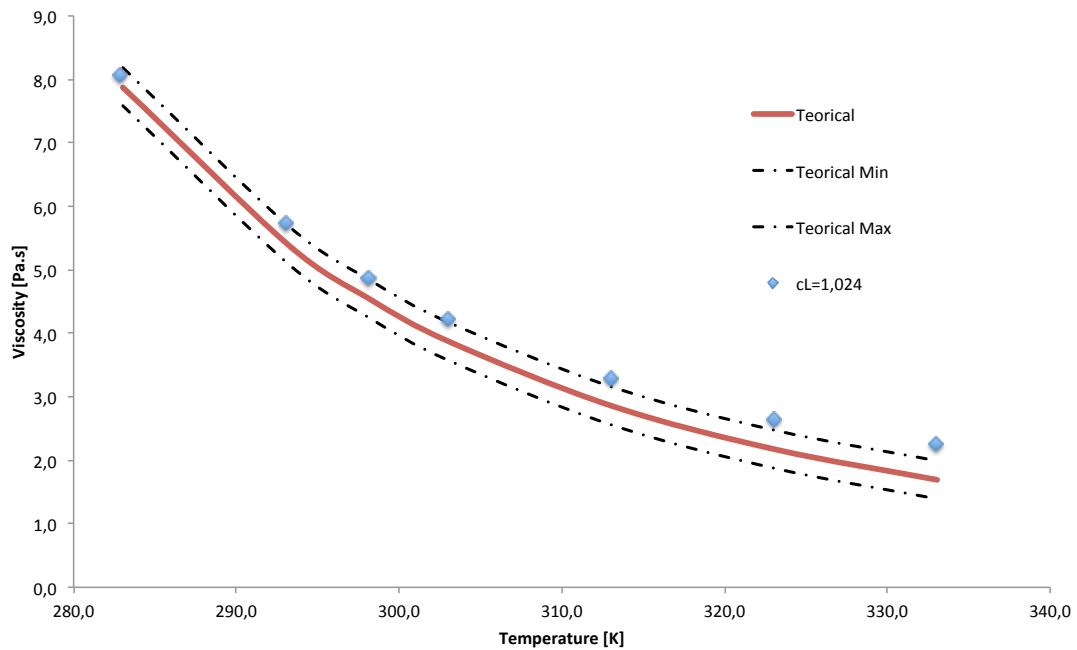
$$\eta_{rep} = \frac{\delta^2 - 1}{2 \delta^2} \cdot \frac{1}{2 \pi R_i^2 L c_L} \cdot \frac{M}{\Omega} \quad \text{Eq. 5.4}$$

where δ is the radius ratio between the outer (R_a) and inner (R_i) cylinder, $\delta = R_a/R_i$, Ω is the angular velocity and c_L is the end face correction factor, that for standard geometries is 1,1. Despite the selected spindle complying with some of the recommendations of DIN 53019 it fails in some others. To take that into

account, the end face correction factor needs to be experimentally determined. The average c_L for the selected shear rates and for a viscosity range from 0,450 - 36 mPa.s is equal to 1,024. The results for the calibration with both base fluids are illustrated in Figure 5.2, and summarized in Table 1.2.



(a) 30%EG+DW



(b) 60%EG+DW

Figure 5.2 – Viscosity Calibration Curve for (a) 30%EG + DW and (b) 60EG + DW.

As it can be depicted from Figure 5.2, the variation between experimental and theoretical results reaches a maximum of 15,5% for 60% EG at 323 K. Nevertheless, this deviation lay's between the declared 1% (dash lines) of the full-scale range of the spindle/speed configuration, suggesting a very good repeatability.

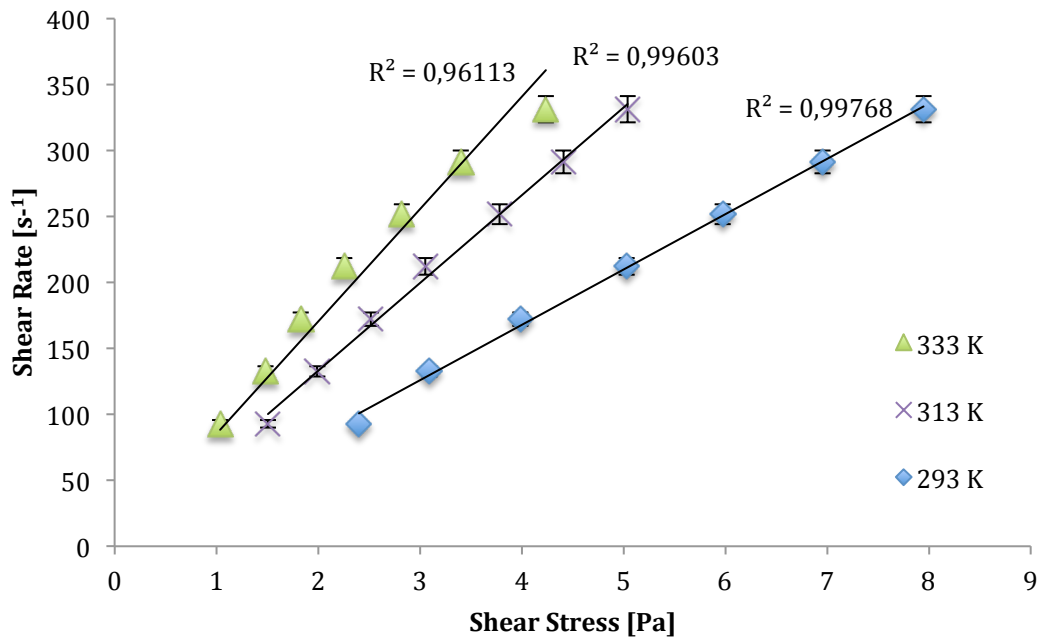
Table 5.2 – Theoretical and experimental viscosity achieved in the experimental apparatus

Base Fluid		30EG+DW						
Temperature	[K]	283	293	298	303	313	323	333
$\eta_{Theoretical}$	[mPa.s]	3,023	2,192	1,912	1,689	1,333	1,079	0,891
$\bar{\eta}$	[mPa.s]	3,101	2,221	1,930	1,702	1,359	1,139	0,980
$\Delta\bar{\eta}$	[mPa.s]	0,003	0,009	0,003	0,004	0,005	0,005	0,007
Variation	[%]	2,6	1,3	0,9	0,8	1,9	5,6	10

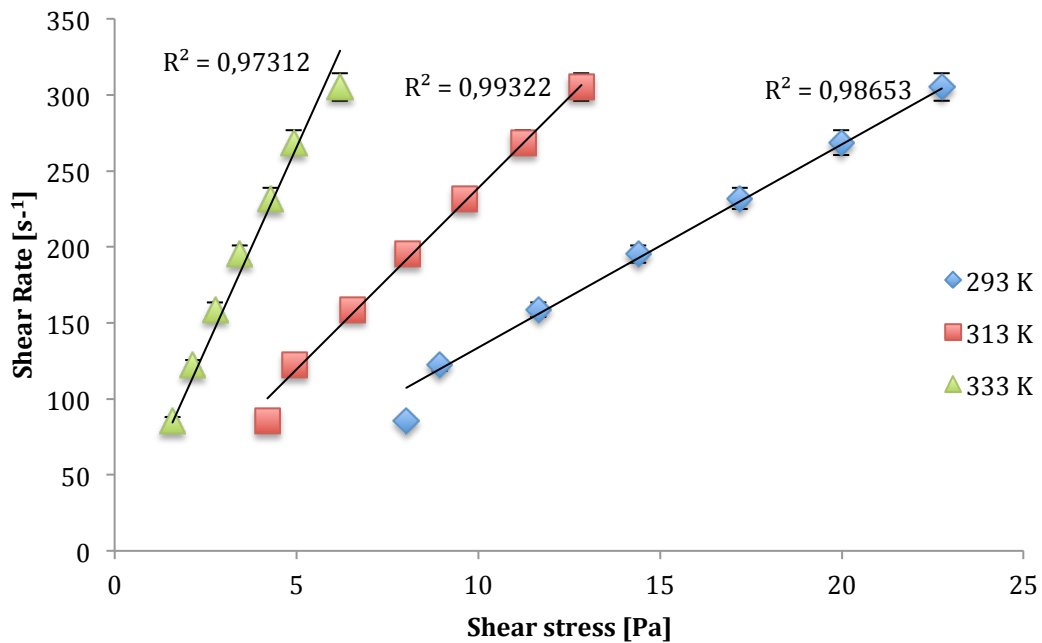
Base Fluid		60EG+DW						
Temperature	[K]	283	293	298	303	313	323	333
$\eta_{Theoretical}$	[mPa.s]	8,375	5,351	4,499	3,832	2,800	2,138	1,662
$\bar{\eta}$	[mPa.s]	8,038	5,292	4,497	3,902	3,008	2,348	1,918
$\Delta\bar{\eta}$	[mPa.s]	0,004	0,000	0,002	0,004	0,006	0,007	0,014
Variation	[%]	4,0	1,1	0,0	1,8	7,4	9,8	15,4

5.2.2 Base Fluid Effective Viscosity

The first step in the experimental procedure is to verify the effective viscosity of the base fluids and identify its rheological nature. To that end, the evaluation of the effective viscosity of the base fluids was conducted for several temperatures and for several shears rates. The results are presented in Figure 5.3.



(a)



(b)

Figure 5.3 – Base fluid shear rate as a function of shear rate for (a) 30EG+DW and (b) 60EG+DW

As it can be depicted, the relation between the shear rate and the shear stress is linear for both base fluids. These results suggest that the base fluids

used for the production of the MWCNTs nanofluids present a Newtonian behaviour for all the temperatures tested. This was an expected result since both fluids (ethylene glycol and water) present a Newtonian behaviour.

5.3 Nanofluids Effective Viscosity

This section describes the experimental results obtained for the viscosity of MWCNTs nanofluids, with the objective of determining empirically the functional form of the rheology equation of state. Statistical techniques were applied to ascertain the relationships between the empirical variables.

5.3.1 Multivariable Statistical Analysis Methodology

As envisaged in Chapter 3, the empirical viscosity evaluation was programmed with a full factorial design. Thus, given the large amount of experimental data (2940 observations), a multi variable statistical analysis is performed. The experimental results are exposed in detail in Appendix J, in the form of thermodynamic tables and figures.

This statistical analysis allows for ascertaining which and how much the control factors (identify in the DOE) produce a significant impact on the effective viscosity. Moreover, through the interactions among control factors assessment, it is possible to find out which of the correlations proposed during the dimensional analysis have a more significant impact on the relative viscosity and on the rheological behaviour of MWCNTs nanofluids. This section describes the multivariable analysis carried out on the experimental relative viscosity, with the objective of determining empirically for MWCNTs dispersions the functional form of the rheological equation of state..

As it was previously seen, a control factor interaction occurs when the relationship among two or more variables have some effect on the dependent variable. The main effect, then, occurs when the mean difference between the levels of a control factor are statistically significant to the overall mean. Moreover, through the main effect analysis, it is possible to assess the statistical contribution of each individual control factor and also to graphically represent the results. This is very useful since it allows for a rather quick and efficient way

to visualize the effects of each parameter. It should be stated that the main effect of each individual control factor is assessed.

In order to determine whether the differences between means have any statistical significance, one has to verify the null hypothesis. If the null hypothesis $H_{0,C}$ is verified, this signifies that the mean of each parameter is constant and there is no relationship between two quantities, i.e. it does not significantly affect the experimental results.

$$H_{0,C}: \overline{X_{C1}} = \overline{X_{C2}} = \dots = \overline{X_{Cn}} \quad \text{Eq. 5.5}$$

In contrast, the alternative hypothesis assumes that if the difference between averages is not null, then the control factor has a significant effect on the experimental results.

$$H_{0,C}: \overline{X_{C1}} \neq \overline{X_{C2}} \neq \dots \neq \overline{X_{Cn}} \quad \text{Eq. 5.6}$$

Furthermore, the selected base fluids present distinct viscosities. Thus, the statistical analysis was performed regarding the relative viscosity (considering the base fluid as reference), i.e. $X = \mu_{nf} / \mu_{bf}$. Through this methodology it is identified the viscosity variations produced by the incorporation of the MWCNTs, independently on the magnitude of the viscosity of the base fluids.

5.3.2 Analysis of the Experimental Viscosity of Nanofluids

Until now, it was shown that the production of stable, long-term nanofluids is possible. Through a standardized production methodology, it was possible to ensure the reduction of noise effects and, therefore, improving the statistical inference from the results. The effective viscosity of the produced MWCNTs nanofluids was measured and the rheological behaviour was characterized.

As it was expected, the presence of MWCNTs increases the effective viscosity changing the rheological nature of the base fluids. The experimental

results are exposed in detail in Appendix E, in the form of thermodynamic tables and figures.

As it was suggested by the rheometer supplier, the viscosity measurements should be taken for a torque ratio superior to 10%. Below this limit, the measurements relative error increases from 1% to 10%. This can be an issue for less viscous fluid or at higher temperatures. However, as it will be seen further ahead, this issue is statistically negligible.

In Table 5.3, shows the experimental average and maximum results for the obtained viscosity, for each MWCNTs studied. It is important to notice that the minimum enhancement on the effective viscosity was verified when testing the MWCNTs with highest aspect ratio, and vice-versa. These results are a first indication that the geometrical properties of the MWCNTs affect the effective viscosity.

Table 5.3 – Average and maximum results obtained experimentally for each MWCNT geometry

Nanoparticle Geometry	Average		Maximum	
	η_{nf}/η_{bf}	$\eta_{nf} - \eta_{bf}$	η_{nf}/η_{bf}	$\eta_{nf} - \eta_{bf}$
D50-80 L10-20 AR 57	1,218	0,0007	1,684	0,0055
D20-40 L10-30 AR 57	1,310	0,0009	2,085	0,0087
D20-40 L5-15 AR 50	1,440	0,0013	2,102	0,0097
D20-40 L1-2 AR 35	1,309	0,0009	2,175	0,0061
D60-100 L5-15 AR 31	1,370	0,0011	2,472	0,0118
D60-100 L1-2 AR 28	1,319	0,0010	2,182	0,0095

AR – Aspect Ratio

As it was mentioned previously, an analysis of variance (ANOVA) was performed in order to verify which control factors detain the greatest effect on the experimental viscosity. A significant level of $\alpha = 0,05$ was chosen. This indicates that it exists a risk of 5% on concluding that a difference exists when there is no actual difference. Also, from the ANOVA one can get the F-statistic. The latter, is a value that indicates if the means between two populations are

significantly different. Through the comparison of the F-statistic with the tabulated F-critical, it is possible to reject or validate the null hypothesis, i.e., if $F\text{-statistical} > F\text{-critical}$ then the null hypothesis is false or the alternative hypothesis is true, and vice-versa. Additionally, the p value that indicates the probability of the obtained results may have happened by chance, is also determined.

In Table 5.4 it is presented the ANOVA from the experimental viscosity data. As it can be depicted, all the control factors: the nanoparticles volume fraction, base fluid, shear rate and geometry present a F-statistical higher than the F-critical. For these factors, one can conclude that the null hypothesis is false or the alternate hypothesis is true. Thus, the variations of these control factors significantly affect the viscosity of the nanofluids. This is an expectable result since the dimensional analysis conducted in Chapter 2 shows that the dimensions of the nanoparticles have some influence on the rheological behaviour of colloids.

Table 5.4 – Multi factor analysis of variance (ANOVA) of the experimental viscosity

Control Factor	SST	DOF	Variance	F-Test	F-Critical	Contribution
Volume Fraction	6333	4	6,43	146,5	2,39	40,2%
Shear Rate	3291	6	1,17	34,6	2,12	20,89%
Temperature	2966	6	0	319,6	2,12	18,83%
Base Fluid	3142	1	0	23,14	3,86	19,95%
Geometry	18,69	5	0,14	560,93	2,37	0,12%

Through ANOVA it was possible to identify which control factors present a higher statistically significance interaction. However, to provide further information regarding the intrinsic mechanisms governing the rheology of the tested samples, one must evaluate the main effect of each control factors and control factors interactions identified by the proposed correlation Eq. 2.62. As it

can be verified, the MWCNTs geometry have influence on the effective viscosity of nanofluids, nevertheless it is a rather small contribution.

As envisaged in Chapter 1, the aspect ratio is one of the most important parameters affecting the nanofluid viscosity.

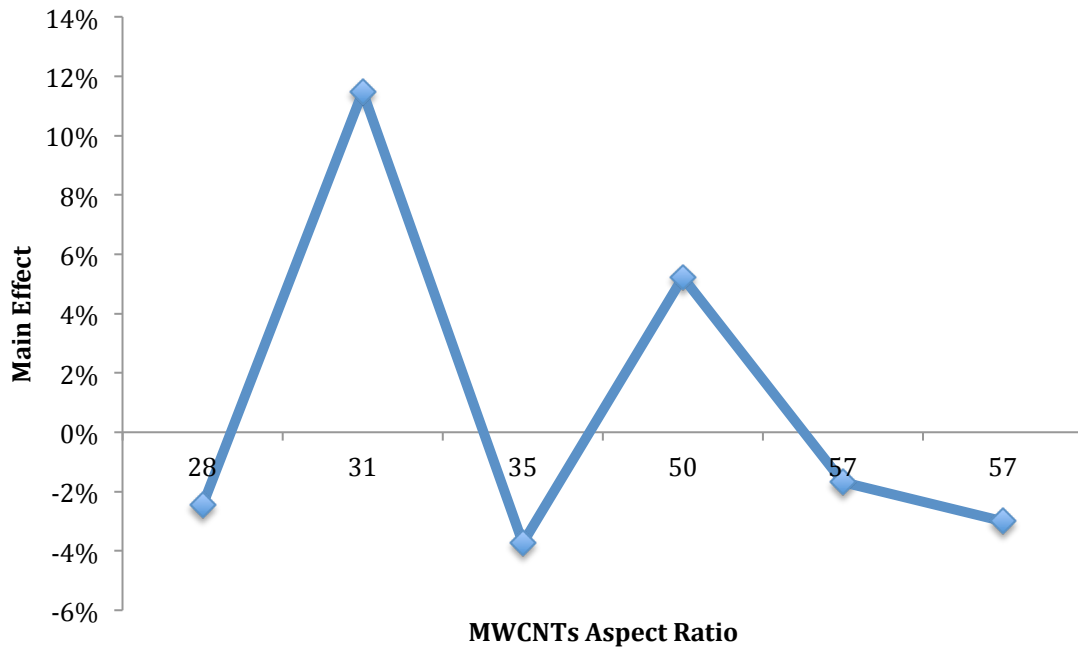
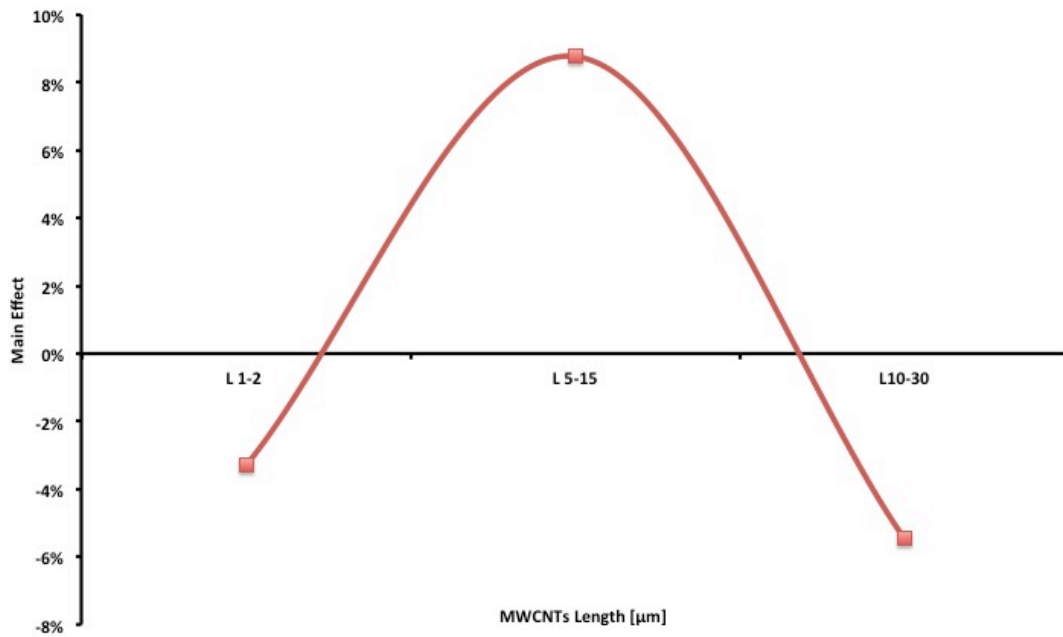
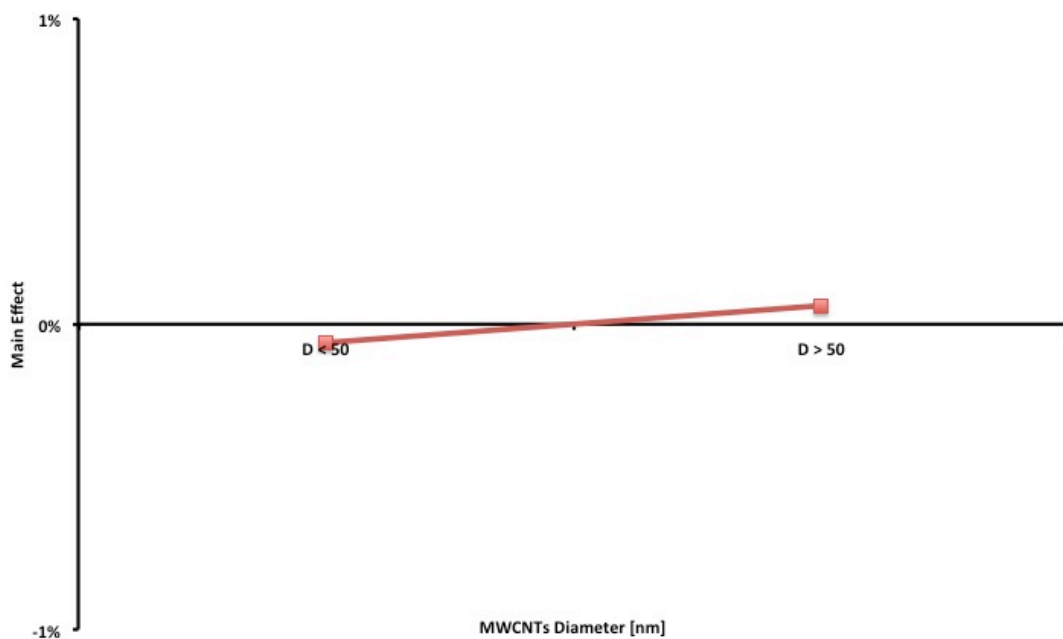


Figure 5.4 – Main effects of the MWCNTs aspect ratio on the experimental viscosity

In Figure 5.4, it is shown the main effect of the MWCNTs aspect ratio on the viscosity. As it can be depicted, the experimental viscosity ratio enhancement is inversely proportional to the aspect ratio (i.e. the higher the aspect ratio the less it influences the viscosity). Such behaviour may be attributed to a decrease in magnitude of interparticle stresses or in other words, due to the higher spatial distribution through the medium for an arbitrary volume fraction. Despite some researchers reported contradictory results, especially for spherical particles, see [207], authors like [148] reported similar results, i.e. viscosity enhancement with decreasing particle size. However, the interaction effects with other control factors may produce different results.



(a)



(b)

Figure 5.5 – Main Effects of the MWCNTs (a) length and (b) diameter

As it can be depicted in Figure 5.5(a), the contribution of the MWCNTs length to the overall viscosity shows a maximum for the interval 5-15 μm. Moreover, the MWCNTs diameter has no significant contribution to the experimental viscosity, see Figure 5.5(b).

In Figure 5.6, it can be depicted the main effect of the volume fraction on the experimental viscosity. The latter suggests a slight non-linear relationship between the volume fraction and the effective viscosity ratio. Nevertheless, several researchers reported similar observations [47], [81], [325]-[328], i.e. the measured nanofluid viscosity increases with particle loading. These expected results, taking into account most proposed prediction models, suggest that the interactions between particles have an important contribution to the overall nanofluid viscosity, even for these small volume fractions. These results compelled, even more, that the spatial distribution and the interparticles interactions have a great impact in the experimental viscosity.

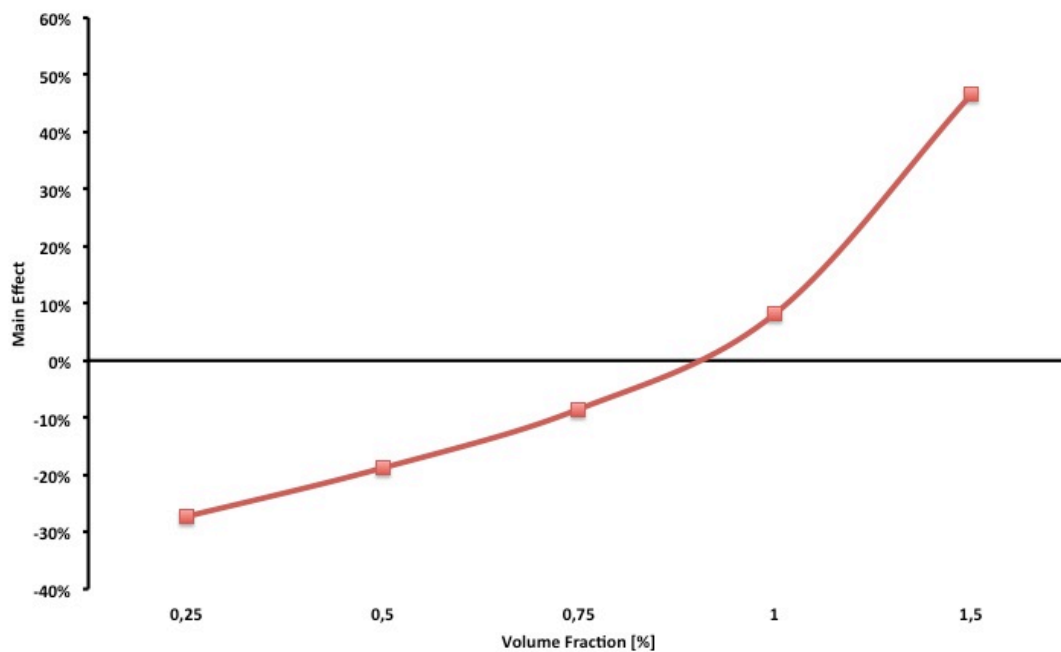


Figure 5.6 – Main effects of the volume fraction on the experimental viscosity

From Figure 5.7, the base fluid presents a negligible contribution to the effective nanofluid viscosity. Again, it should be noted that these analysis are conducted for the viscosity ratio (μ_{nf} / μ_{bf}), diminishing the effect of the magnitude of the base fluid original viscosity. The observed behaviour may suggest that, the interparticle and hydrodynamic interactions may induce some impact on the experimental results. The slight decrease in the viscosity enhancement ratio for 60EG+DW may be explained by a lower surface

wettability of the MWCNTs, leading to a lower contribution to the overall viscosity.

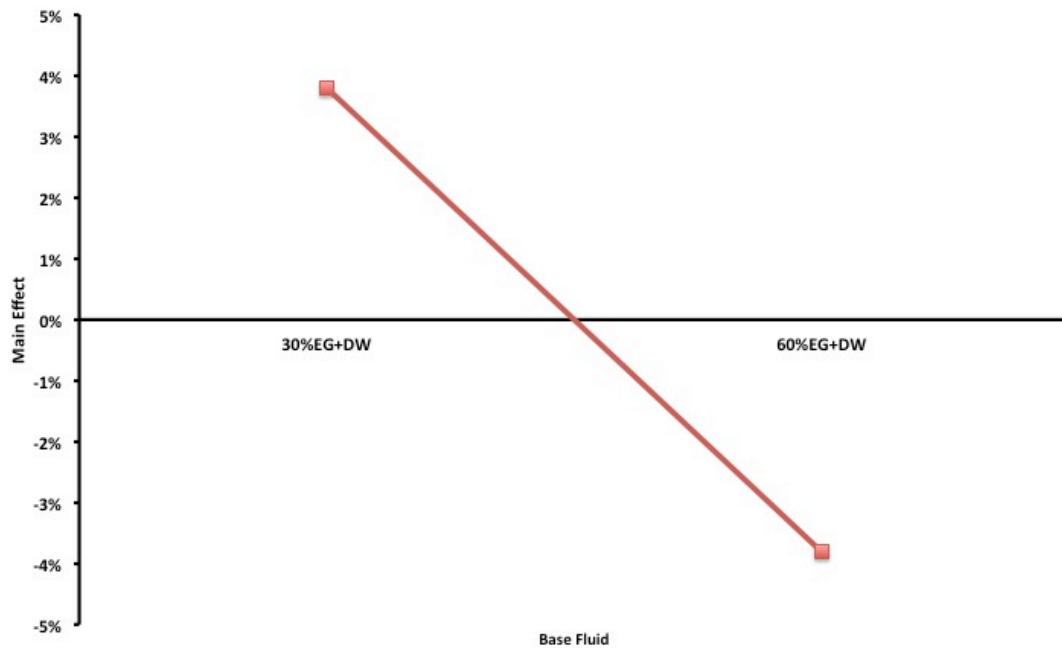


Figure 5.7 – Main Effects of the base fluid in the experimental viscosity

In line with ANOVA, the analysis to the main effect of the control factors revealed that the temperature has no significant impact on the experimental viscosity, as can be depicted from Figure 5.8. With the exception of the lowest temperature (283 K) all the remaining temperatures have negligible contribution on the experimental viscosity. Nevertheless, since the temperature main effect does not account for the contribution of the continuous medium viscosity, this trend may be explained due to a reduction of the inter-molecular cohesive forces between the fluid and the MWCNTs.

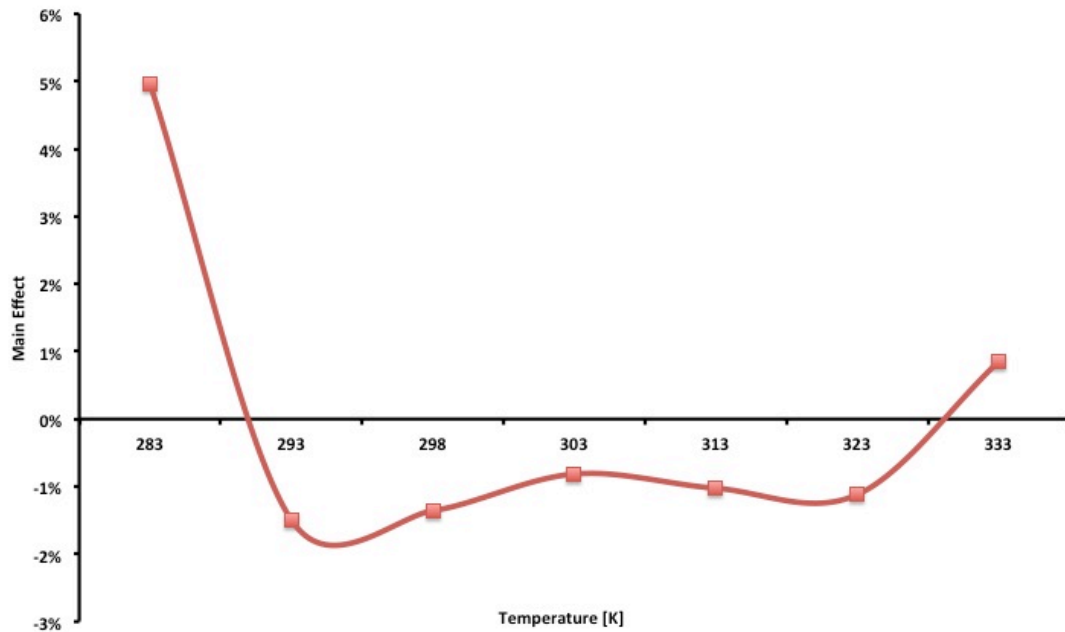


Figure 5.8 – Main effects of the temperature in the experimental viscosity

Similar to the volume fraction main effect, the shear rate main effect (Figure 5.9) also has a non-linear trend. As it was seen, a variety of structures and networks can be formed in a suspension. However, under shear forces, these networks can be broken into smaller units. Moreover, as the spindle rotates at low shear rates, the structure of the MWCNTs changes temporarily, aligning in the direction of increasing shear rate. As the shear rates increases, the maximum amount of shear ordering is attained, the aggregates are broken down decreasing the friction and hence the viscosity. This is also an indication of a shear-thinning effect common in colloidal suspensions. Similar results were obtained by several researchers [46], [60], [125], [142], [329]. Still, one cannot neglect that these control factors may produce some interactions with the other control factors.

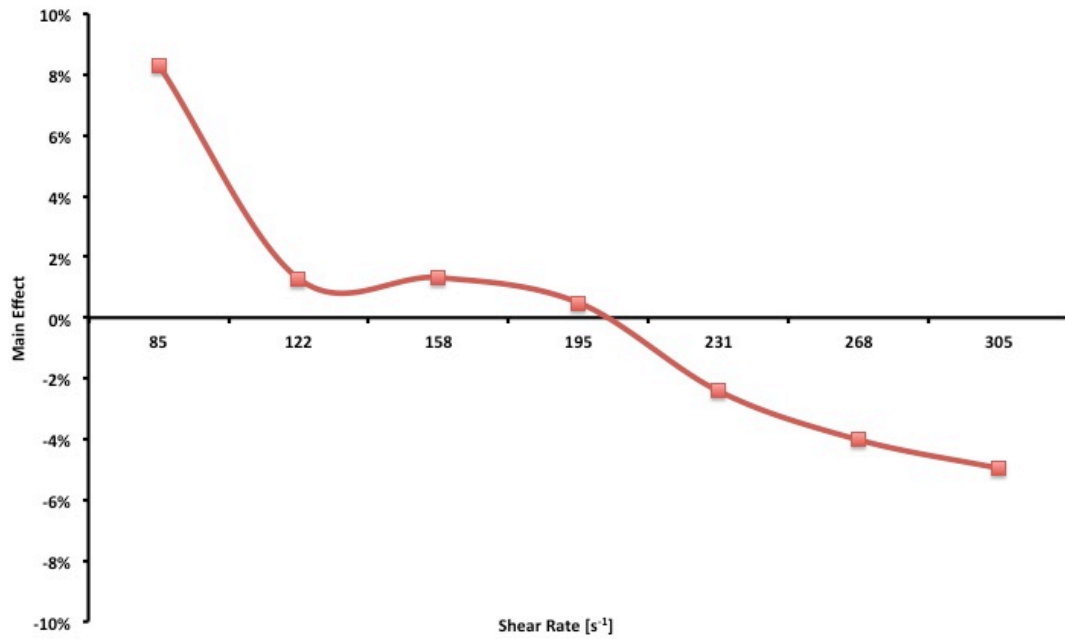


Figure 5.9 – Main effects of the applied shear rate in the experimental viscosity

Brief Conclusions

The results presented in the previous section enable to state that some control factors identified in the dimensional analysis have some influence in the effective viscosity. The statistical analysis of the experimental results suggested that the effective viscosity depends on the geometrical properties of the MWCNTs, especially on its length. This may be explained due to the variation on the spatial distribution of the MWCNTs in the base fluid. Moreover, as the volume fraction of the MWCNTs increases so does the effective viscosity. However, this enhancement presents a non-linear trend. The latter may indicate that as the concentration regime changes from diluted to concentrate, the hydrodynamic interactions solely cannot explain this behaviour and the interaction between particles have to be taken into consideration. The temperature has little influence on the viscosity except for the lowest temperature. This was expected since the major contribution of temperature is on changing the base fluid viscosity and since the main effect analysis was conducted for the effective viscosity this contribution cannot be depicted. Also, the Brownian motion is directly linked to the thermal diffusivity, which is a

function of the temperature. One can, therefore, conclude that the contribution due to Brownian motion can be neglected. As it was seen in the survey on Chapter 1, most colloidal suspensions present a shear thinning behaviour, i.e. a decrease of viscosity with shear rate. This behaviour was observed on the shear rate main effect analysis.

Based on these results, one can conclude that MWCNTs nanofluids viscosity depends on the effective length and concentration of nanoparticles, on the applied shear rate and on the temperature.

Nevertheless, there seems to be no evidence of some of the intriguing mechanisms suggested by some authors, namely Brownian and nanoparticles agglomeration/percolation. The latter was excluded by the measurement of the Zeta potential of the samples, reported in the Section 4.2.1. However, for high shear rates the percolation networks may become extremely dense, resulting in anomalous behaviours. Nevertheless, the main effect analysis only indicate the significant influencing factors, it cannot be used to obtain a valid relationship between experimental and control factors. To this end, the model of the effective viscosity of the MWCNTs nanofluids has to be developed through dimensional analysis with regression-fit the experimental data. In the following section the development of the effective viscosity model will be presented.

5.4 Rheology modelling of MWCNTs nanofluids

Viscosity plays a major role in determining the pumping power requirements of any heat exchanger. However, determining the effective viscosity of nanofluids is still a complex problem. Einstein's model (Eq. 1.4) showed that the viscosity of colloidal suspensions of spherical particles increases linearly as the volume fraction of suspended particles increases. More, Jeffrey (Eq. 1.7), Krieger and Dougherty (Eq. 1.19) and Batchelor (Eq. 1.21) all modified Einstein equation to model the effect of particle interaction and volume fraction on the effective viscosity of suspensions. However, colloidal suspensions present intrinsic behaviours, like shear thinning. Therefore, the effects of particle size, temperature and shear rate must be accountable. However, this multivariable

analysis, induce a huge complexity in the development of a predictive model for the effective viscosity.

As it was seen on Chapter 2, a solution to assess the rheological behaviour can be achieved through the use of a combination of mathematical analysis and experimental data. The rheological equation of state is a relation giving the rheological properties of the fluid in terms of shear variables and of those structural parameters, which determine its mechanical behaviour. To this end, a dimensional analysis was developed. The approach employed in this work is to choose the simplest system, which might be capable of exhibiting some of the rheological phenomena of interest, and then apply a dimensional analysis to find the dimensionless groups, which must appear in the rheological equation. Afterwards, by supplementing this knowledge with known empirical rheological data of MWCNTs nanofluids, an analytical relationship can be developed allowing for the computation to be conducted.

Dimensional Analysis

Following the methodology described on Chapter 2, the first step for conducting an experiment would be to decide on the variables of interest that affect the rheological behaviour of colloidal suspensions. However, particular attention should be given to not overdo the number of independent variables, since these have to be characterized empirically. Considering a steady flow of an incompressible fluid with MWCNTs suspended in a continuous Newtonian medium, the viscosity of the suspension will depend on the viscosity of the medium (η_{bf}), the particle equivalent diameter (D_S) and volume fraction (ϕ), the densities of the MWCNTs (ρ_{MWCNT}) and base fluid (ρ_{bf}), the shear rate ($\dot{\gamma}$) or shear stress (τ), time (t) and the temperature (T). The latter, besides its effect on the base fluid viscosity (η_{bf}) it will also influence the Brownian motion of MWCNTs. Therefore, to quantify the contribution of the temperature on the Brownian motion, the temperature must be multiplied by the Boltzmann constant (k_B). The following general relation for the dependence of the relative viscosity is:

$$\eta_{nf} = f(\phi, \eta_{bf}, D_S, \rho_{MWCNT}, \rho_{bf}, \dot{\gamma} \text{ or } \tau, k_B T, t) \quad \text{Eq. 5.7}$$

Now, it is possible to reduce the dimensionality in terms of mass, length and time (M, L, T), as demonstrated in Table Table 2.2

The second step in the dimensionless analysis is to evaluate the required number of Π (π_i) terms. In other words, Eq. 5.7 can be substituted by the following equation expressing it as a function of a smaller number of non-dimensional groups:

$$\eta_{nf} = f(\pi_1, \pi_2, \pi_3 \dots \pi_m) \quad \text{Eq. 5.8}$$

For the case under study and based on the principles of dimensional analysis, the nine-variables presented on Table 2.2 it can be expressed in terms of the three basic units of mass, length and time. Hence, based on the principles of dimensional analysis, Eq. 5.7 it can be reduced to $9-3 = 6$ dimensional groups.

The third step is to select non-repeating variables from the original list, that one can combine with each of the remaining variables to form a Π term. In order to study the mechanical phenomena of colloidal suspensions, three variables were chosen, η_{bf}, ρ_{bf} and kT . These comprise a complete and dimensionally independent subset of the nine independent variables. Moreover, the dimension of any of these three cannot be made up of the dimensions of the other two. However, it should be noted that other variables could be selected, leading to different dimensionless numbers. The remaining independent variables $\phi, \rho_{MWCNT}, \dot{\gamma}$ or τ, t can, however, be made up of those μ_{bf}, ρ_{bf} and kT as it follows. It should be noted that the shear stress τ was chosen rather than the shear rate $\dot{\gamma}$.

$$\text{Relative Viscosity} \quad \Pi_1 = \mu_{rel} = \frac{\mu_{nf}}{\mu_{bf}} \quad \text{Eq. 5.9}$$

$$\text{Relative density} \quad \Pi_2 = \rho_{rel} = \frac{\rho_p}{\rho_{bf}} \quad \text{Eq. 5.10}$$

$$\text{Volume Fraction} \quad \Pi_3 = \phi^* = \phi \quad \text{Eq. 5.11}$$

$$\text{Reduced time} \quad \Pi_4 = t^* = \frac{t \mu_{bf}}{\rho_{bf} r_p^2} \quad \text{Eq. 5.12}$$

$$\begin{array}{l} \text{Reduced Shear} \\ \text{Stress} \end{array} \quad \Pi_5 = \tau^* = \frac{\tau \rho_{bf} r_p^2}{\mu_{bf}^2} \quad \text{Eq. 5.13}$$

$$\text{Reduced Energy} \quad \Pi_6 = kT^* = \frac{kT \rho_{bf}}{\mu_{bf}^2 r_p} \quad \text{Eq. 5.14}$$

The final step in a *dimensional analysis* is to express the final form of the equation as a relationship among Π 's terms. Using the premises of the Buckingham's theorem, the relative viscosity of a colloidal suspension is a function of:

$$\Pi_1 = f(\Pi_2, \Pi_3, \Pi_4, \Pi_5, \Pi_6) \quad \text{Eq. 5.15}$$

or

$$\eta_{rel} = f(\phi, \rho_{rel}, t^*, \tau^*, k_B T^*) \quad \text{Eq. 5.16}$$

or

$$\mu_{rel} = f\left(\frac{\rho_p}{\rho_{bf}}, \phi, \frac{t \mu_{bf}}{\rho_{bf} r_p^2}, \frac{\tau \rho_{bf} r_p^2}{\mu_{bf}}, \frac{kT \rho_{bf}}{\mu_{bf}^2 r_p}\right) \quad \text{Eq. 2.45}$$

Now it is possible to look for relationships among the subsets of variables. As it was mentioned, the Reynolds number is undoubtedly the most famous dimensionless parameter in fluid mechanics. From Eq. 2.45 it can be depicted that the reduced shear stress has the same relationship as the Reynolds number, i.e. the ratio between the inertial forces ($\tau \rho_{bf} r_p^2$) to the viscous force (μ_{bf}). Similarly, the reduced energy (Π_6) has the same relationship as the inversed Schmidt number (Sc^{-1}). This dimensionless number plays a crucial role in mass transfer. It represents the ratio between the ability of a fluid to transport momentum by molecular means to the ability of that fluid to transport species by molecular means, i.e. the relation between the viscous diffusion rate to nanoparticle diffusion rate and it is represented as it follows:

$$Sc = \frac{\nu}{D_r} = \frac{\mu_{bf}}{k_B T \rho_{bf}} \quad \text{Eq. 5.17}$$

where ν is the *kinematic viscosity* and D_r is the diffusion coefficient. This dimensionless number can also be represented as the ratio between the Peclet

number to Reynolds number. Thus, the Schmidt number is the relation between the imposed shear and Brownian forces to inertial forces. Therefore, Eq. 2.45 can be represented as:

$$\eta_{rel} = f(\rho_{rel}, \phi, \frac{t \mu_{bf}}{\rho_{bf} r_p^2}, Re_{\tau}, Sc^{-1}) \quad \text{Eq. 5.18}$$

Nevertheless, the exact form of the solution is unknown. However, one can now conclude that the rheological behaviour of a colloidal suspension is a function of the buoyancy effects (density), the MWCNTs inertia effects (Re), the concentration of MWCNTs (ϕ), the suspensions kinematic viscosity over time and the transport properties of the fluid (Sc).

In order to investigate the exact form of Eq. 5.18 one has first to empirically determine the individual properties identified by Eq. 2.45 or through theoretical analysis of the flow process. Nevertheless, this equation can be simplified considering some flow process characteristics:

- Neutrally buoyance condition, i.e. a condition in which the MWCNTs have the same average density as the density of the fluid in which it is suspended. In these condition the relative density tends to one ($\rho_{nf}/\rho_{bf} \rightarrow 1$). This condition was verified during the stability evolution of Section 1.4, in which most nanofluids present a shelf life of over two years. Based on these results one can conclude that the suspended MWCNTs are in a neutrally buoyance state.
- Steady Shear State, i.e. a condition under which a fluid is sheared continuously in one direction during the duration of a rheometric experiment. The empirical evaluation of the viscosity of the MWCNTs nanofluids was conducted under constant shear rate. Therefore, the reduce time tends to $t^* \rightarrow \infty$. The equation of state in reduced form become:

$$\mu_{rel} = f(\phi, \frac{\tau \rho_{bf} r_p^2}{\mu_{bf}}, \frac{kT \rho_{bf}}{\mu_{bf}^2 r_p}) \quad \text{Eq. 5.19}$$

Or

$$\mu_{rel} = f(\phi, Re_{\tau}, Sc^{-1}) \quad \text{Eq. 5.20}$$

This is the corresponding-state principle. This means that the nanofluids rheology is a function of the inertial forces, the mass diffusivity and the concentration of the MWCNTs. To evaluate the final form of the correlation, one must evaluate the relation between these control factors on the effective viscosity of the MWCNTs nanofluids. The next section describes the experimental results with the objective of determining the functional form of the rheological equation of state.

5.4.2 Analysis to the Experimental Viscosity

In order to develop the final form of the equation Eq. 5.20, a main effect analysis between these control factors is conducted. The effects of the concentration of MWCNTs on the relative viscosity for different values of shear rate is represented in Figure 5.10.

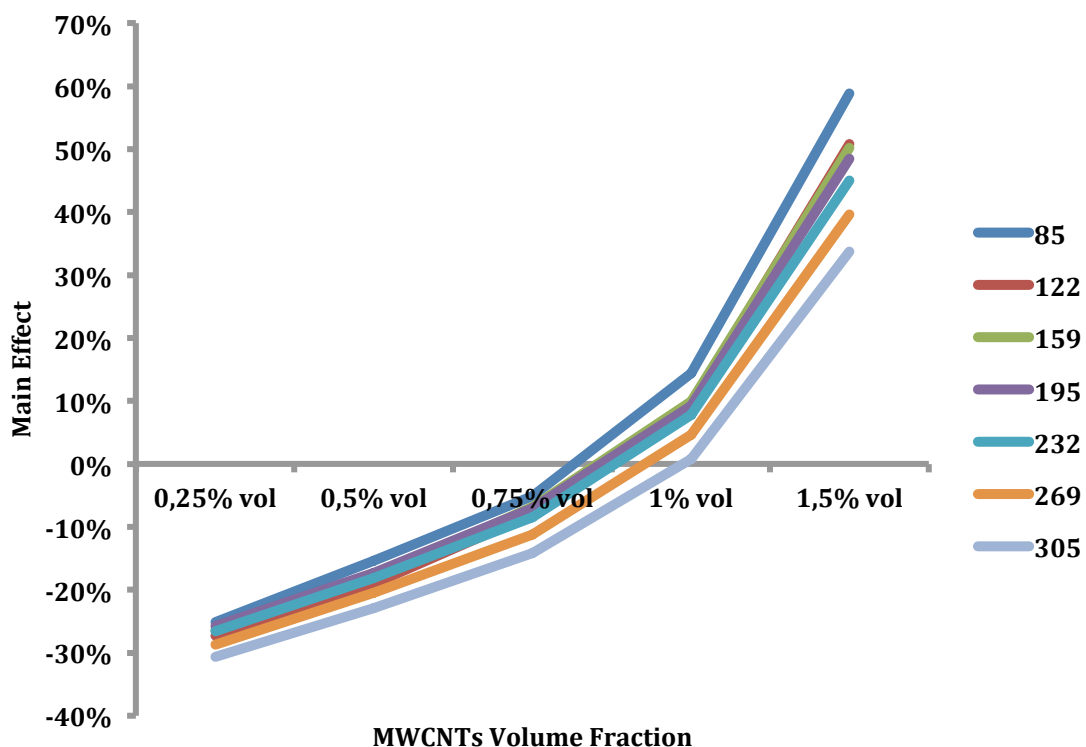


Figure 5.10 – Main effect analysis of the volume fraction of MWCNTs for different shear rates.

As it can be depicted from Figure 5.10, as the concentration of the MWCNTs increases so does its contribution on the relative viscosity. However, as

the shear rate increases this contribution is less pronounced. This leads to the conclusion that MWCNTs nanofluids are non-Newtonian and present a shear thinning behaviour as previously depicted in Figure 5.9. This behaviour can be attributed to many factors such as: at low shear rates, particle diffusion is significant and particles occupy a larger effective volume than at high shear rates, leading to a larger viscosity. For higher shear rates, the pressure also increases leading to a decrease of the minimum possible distance between MWCNTs as they flow. The latter, leading to a reduction of the suspensions viscosity as function of the imposed shear. Moreover, this reduction can also be attributed to the disagglomeration of the nanotube clustering, as suggested by other authors [47], [330], despite all efforts carried out to reduce clustering, during nanofluids preparation. Another explanation might also be the re-alignment of the MWCNTs with the direction of the shearing force, resulting in a less viscous fluid. Garg et al. and Nanda et al. have reported similar results [36], [224]. This intriguing result is linked to a decrease on the hydrodynamic resistances of the MWCNTs under flow. Moreover, for higher content of MWCNTs these resistances increase leading to a stronger shear thinning behaviour, as it can be seen in Figure 5.11.

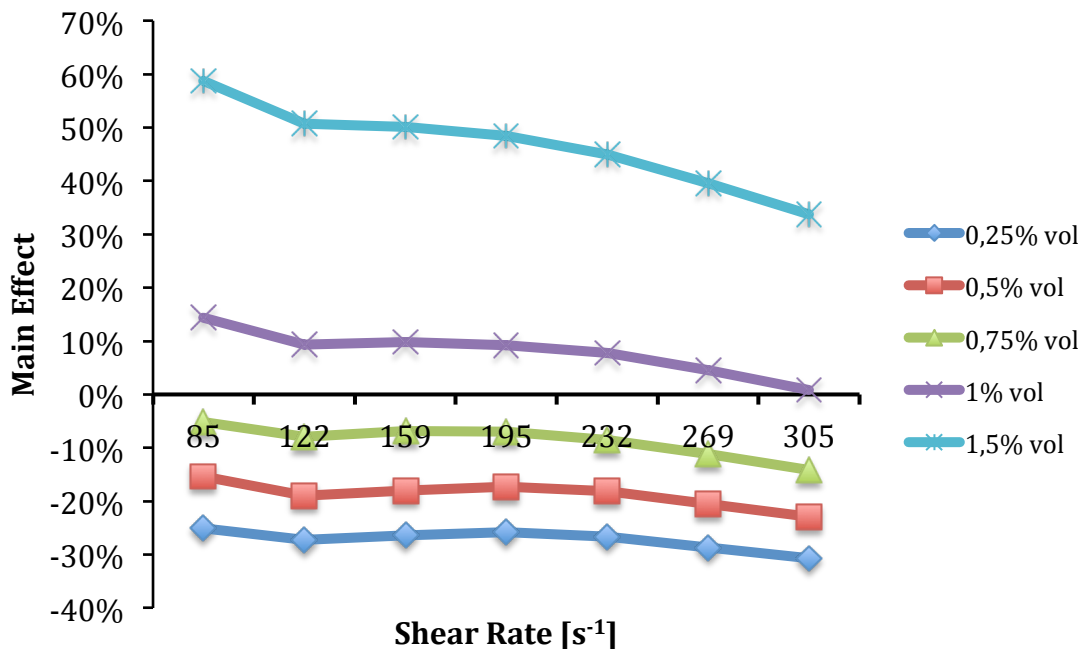


Figure 5.11 – Main effect of the relative viscosity as a function of the shear rate and the MWCNTs volume fraction.

Based on these results, it is expected that the Reynolds number increases with the concentration of MWCNTs, and that can be depicted in Figure 5.12.

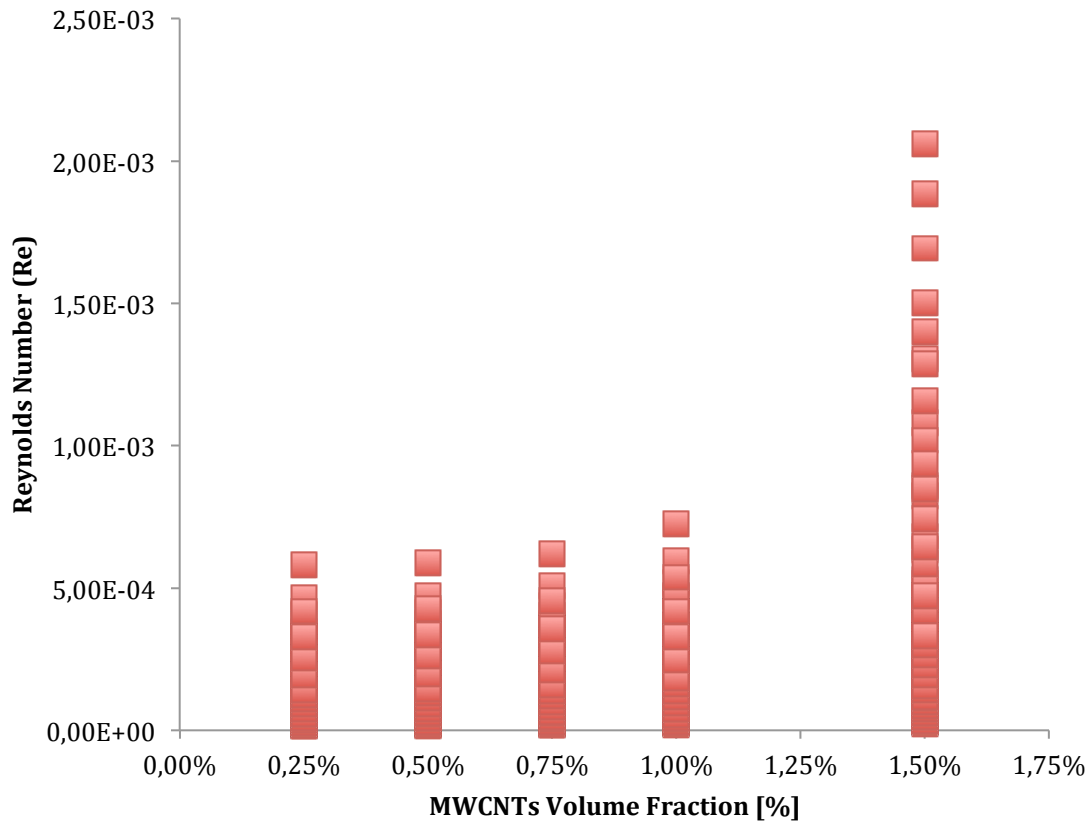


Figure 5.12 – Effect of the MWCNTs volume fraction on the Reynolds number.

In a similar fashion to Figure 5.10, the main effect analysis of the evolution of the effective viscosity with the volume fraction of MWCNTs for different temperatures (Figure 5.13) also demonstrate a non-linear increase of viscosity with volume fraction. However, the influence of the temperature enhancement can only be depicted for the higher concentrations of MWCNTs. This enhancement may be attributed to an increase of the thermophoretic force of the MWCNTs leading to a higher contribution on the nanofluids viscosity. Although the thermophoretic forces are weak forces and have a negligible effect on larger particles, it becomes the dominant force for sub-micron particles [331]. This, increases the nanoparticles random velocity leading to decreases in the

inter-molecular forces between base fluid and MWCNTs resulting in a lower viscosity [332], [333].

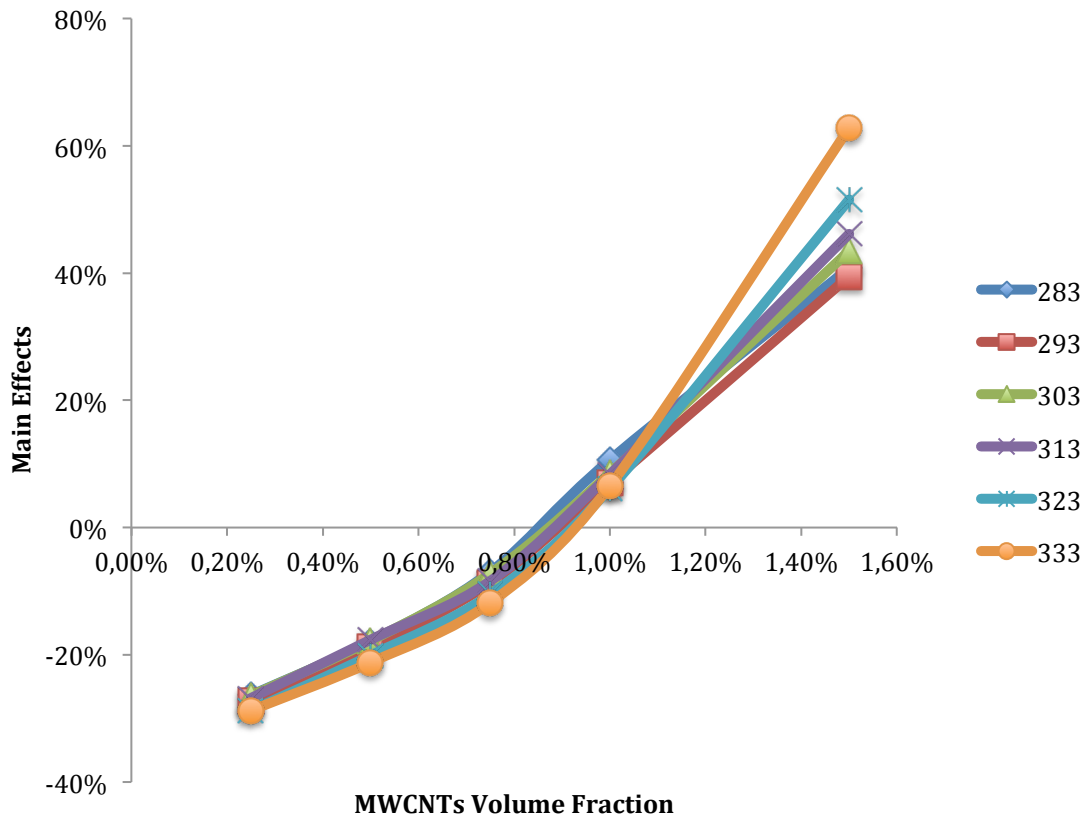


Figure 5.13 – Main effects of the volume fraction of MWCNTs for different temperatures.

Based on these results it is expected that the prescribed Schmidt number, which is the physical relation between the relative thicknesses of the hydrodynamic layer to nanoparticles diffusion rate, will decrease with increasing temperature. However, the dimensional analysis concluded that the relative viscosity is a function of the inverse Schmidt number. It is, therefore, expected an increase of the inverse Schmidt number with temperature, as it can be depicted from Figure 5.14.

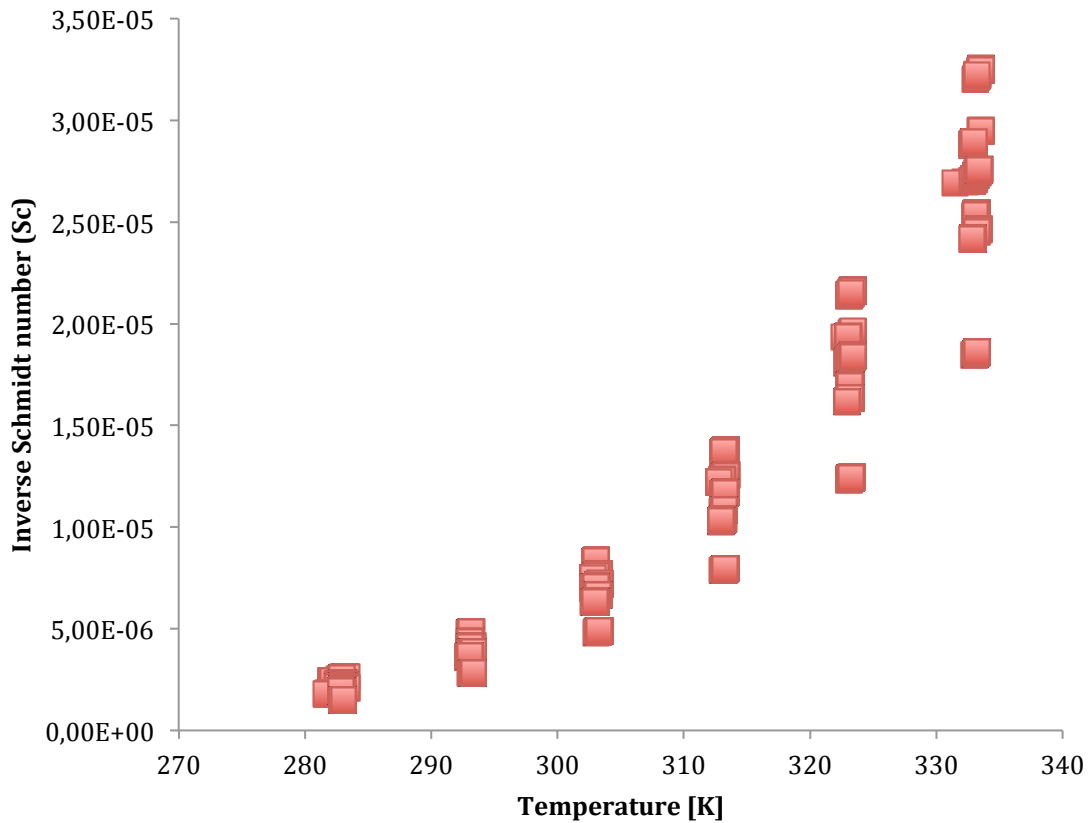


Figure 5.14 – Inverse Schmidt as a function of the temperature

The behaviour identified on Figure 5.14 means that the contribution due to the MWCNTs diffusion rate increases with temperature as the hydrodynamic interaction between the fluid molecules and the MWCNTs become weaker. However, when comparing the values from Figure 5.13 and Figure 5.14 one can conclude that the contribution from the hydrodynamic inertia (Re) is several orders of magnitude higher than the contribution due to diffusion. Thus the major contribution on the effective viscosity of MWCNTs nanofluids occurs from the inertia forces caused by the presence of the MWCNTs.

Brief Conclusions

It is a fact that most researchers and the experimental data confirms that the rheological behaviour of MWCNTs nanofluids has a shear-thinning nature. This rheological behaviour can be attributed to the alignment of the MWCNTs in the shear direction, to the disentanglement of the MWCNTs clusters or to the

spatial distribution of the nanoparticles in the fluidic matrix. Moreover, with increasing volume fraction the relative viscosity presents a non-linear behaviour, suggesting that the relative nanofluids viscosity is influenced by the concentration regime. A rheological model capable of capturing these behaviours has, therefore, to correlate the MWCNTs inertial forces with the MWCNTs concentration and their shear dependence.

5.4.3 Modelling the Rheology of MWCNTs nanofluids

As it was seen through Chapter 1, several models have been proposed to correlate the low shear volume fraction dependence viscosity $\eta(\phi)$. However, any model claiming utility beyond the dilute regime must incorporate the maximum packing volume fraction (ϕ_m) [334]. Interpretation of the maximum volume fraction has varied with time and circumstances in which it is being applied. At present, it is regarded as a variable corresponding to a given collection of particles under given conditions of flow and it is believed to be a representation of the actual structure of suspensions [334], [335]. Thus, ϕ_m reflects the state of the nanoparticles percolation network, so it represents indirectly their microstructure and their resistance to breakup. This variable is a function of the particle shape, particle size and spatial distribution. The physical rationale is that at low shear stress, the ϕ_m is caused by the random initial orientations of the nanoparticles and microstructure, while for high shear stresses values, nanoparticle orientation, nanoparticle spatial density (i.e. particle migration to fit voids), interparticle interactions and the breakup of microstructures, causes changes in the ϕ_m [334]. In order to account for the variation on the nanofluid microstructure, one has to consider the contribution of the variation of the packing volume fraction with the imposed shear $\phi_m(\tau)$.

In order to obtain the shear-dependent ϕ_m , of a concentrate suspension, some correlations have been proposed see [191], [336], [337]. Following the original equation of Krieger and Dougherty [191],

$$\mu_{rel} = \left(1 - \frac{\phi}{\phi_m}\right)^{-\eta\phi_m} \quad \text{Eq. 5.21}$$

where $(-\eta\phi_m)$ is 0,63 and depends on shear stress. In the literature, different values for $(-\eta\phi_m)$ are available. Kalidasan et. al. proposed that the (ϕ_m) of rod shape like MWCNTs, that have a poor space filling, a value of 0,3 [338]. However, they did not disclosure how they have reached this value. Nevertheless, these values vary according to concentration, shear conditions and nanoparticle geometry and were proposed based on linearization of experimental data. This value has to be obtained by trial and error and by means of least-squares fitting of experimental data [335]. Thus, for a dispersion of MWCNTs in a mixture of water and ethylene glycol it is proposed that the variation of the percolation network (microstructure) is a function of the dimensionless shear stress, as follows:

$$\phi_m = \phi^{\tau_{AD}} \quad \text{Eq. 5.22}$$

where,

$$\tau_{AD} = \frac{\mu_{bf} \dot{\gamma}}{\tau} \quad \text{Eq. 5.23}$$

Based on the proposed model for the packing volume fraction (Eq. 5.22), one can conclude that some degree of shear-induced ordering occurs.

In a similar fashion, the shear-dependent intrinsic viscosities and exponents can also be found by least squares fitting of experimental data. However, modelling this multivariable problem is very difficult. Recently, some special statistical techniques were applied such as, artificial neural networks in an attempt to model the rheological behaviour of nanofluids. Despite the high accuracy of these methods it leads to correlations with many constants, which make them only suitable for those nanofluids, see [339], [340].

The model here proposed was developed based on the contribution of each control factor identified in the dimensional analysis and by fitting the experimental data of MWCNTs nanofluids. Nevertheless, this model has to be capable of capturing the contribution from the inertial forces, how these forces affect the percolation network and its response to the imposed shear.

Using non-linear regression modelling, the function f in Eq. 5.19 is expressed as follows:

$$\frac{\mu_{nf}}{\mu_{bf}} = \left(1 + K \left(\left(\frac{\tau \rho_{bf} r_p^2}{\mu_{bf}^2} \right)^{-1} \left(\frac{kT \rho_{bf}}{\mu_{bf}^2 r_p} \right)^{-1} \phi \right)^{n_1} \phi_m^{n_2} \right) \quad \text{Eq. 5.24}$$

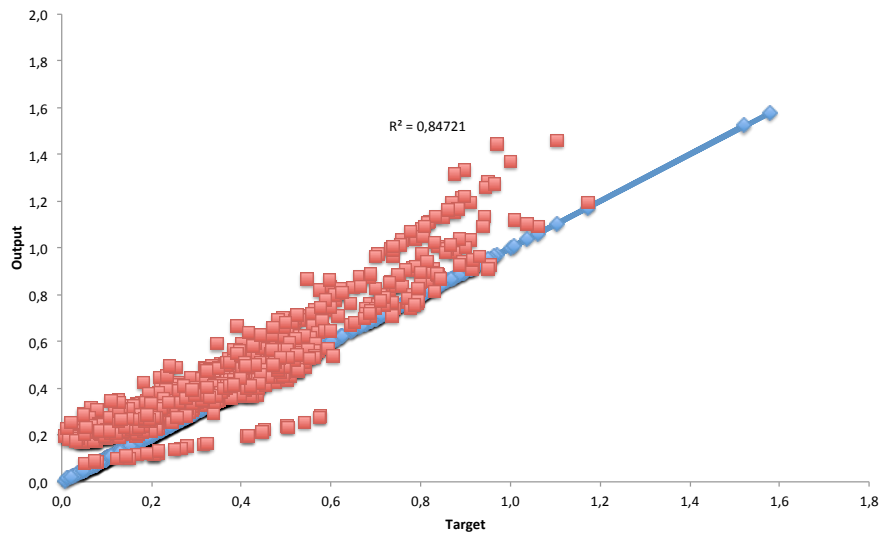
where 0,142 and $n_2 = -2,52$ are the correlation coefficient and $K = 1,7E-5$ is a consistency index. The final form of Eq. 5.24 is as follows,

$$\frac{\mu_{nf}}{\mu_{bf}} = \left(1 + 1,7E - 5 \left(\left(\frac{\tau \rho_{bf} r_p^2}{\mu_{bf}^2} \right)^{-1} \left(\frac{kT \rho_{bf}}{\mu_{bf}^2 r_p} \right)^{-1} \phi \right)^{0,142} \phi_m^{-2,52} \right) \quad \text{Eq. 5.25}$$

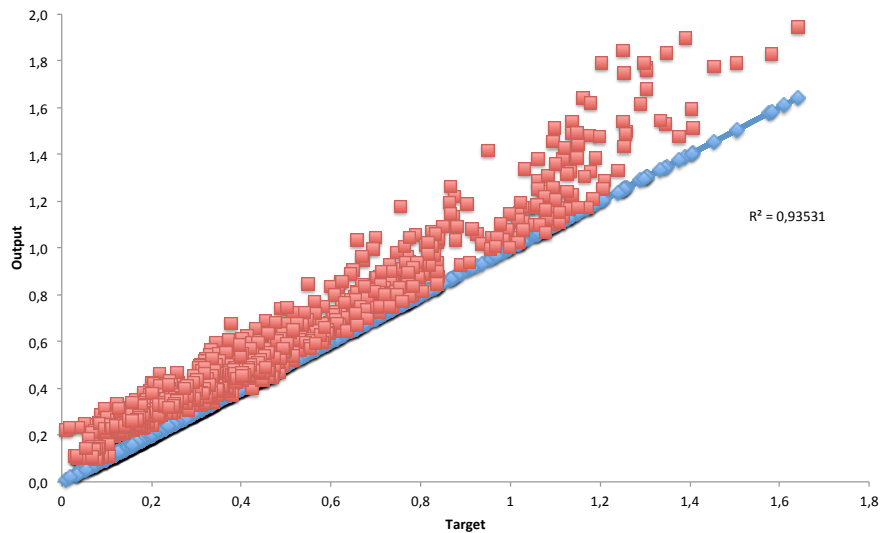
This model was developed based on a *power-law model* and is valid for any type of nanoparticle geometry and length, base fluid, temperature or shear conditions.

In Figure 5.15, it is shown the scatter chart of the proposed model with the experimental viscosity, also in terms of effective viscosity. As this is a multivariable problem, the chart is represented by means of *output* and *target*, were the outputs are the obtained results, both experimental and analytical, being the target the analytical. The experimental results are, therefore, the dispersed points, and the proposed model is the straight line of slope 1.

The Person's correlation R^2 of the proposed model for the base fluids 30EG+DW and 60EG+DW is 0,84 and 0,93, respectively. Moreover, the mean square error (*mse*) was estimated for both base fluids and a value of 0,013 and 0,017 was found. This value is an estimator of the accuracy of the predictive model regarding the experimental results. Thus, the smaller the *mse*, the better the results fit to the model [341].



(a) 30%EG + DW



(b) 60%EG + DW

Figure 5.15 – Scatter chart of the proposed model and experimental data

In general, it was shown that the proposed model is capable of predicting the effective viscosity of long-term MWCNTs nanofluids. Furthermore, it was also shown that the structural morphology of the prepared nanofluids agrees with the correlations considered for the development of the model. Moreover, many of the predictive models available were developed and validated with modest experimental data, which are in general, poorly characterized regarding the nanoparticles size distribution, degree of stability and transport and thermal

properties of the base fluid and nanoparticles. This is a characteristic that distinguishes this study from the remaining ones available in the literature. In addition, this study used a large amount of experimental data, with a special focus on the effect of the nanoparticle geometry, volume fraction and how the nanofluids react to an imposed shear. These were proven statically as the parameters with the greatest impact on the effective viscosity.

Table 5.5 – Fitness estimators of some models available in the literature to the experimental results.

Estimator	Proposed Model	Phuoc et al.	Hosseini et al.	Bobbo et al.
R²	0,91	0,29	0,04	0,63
MSE	0,015	0,36	0,86	0,53
Average Fractional Error	26%	55%	77%	64%
Standard Deviation of Error	18%	23%	88%	23%

In Table 5.5 and Figure 5.16, it is compared the fitness estimators of some predictive models available in the open literature. As it can be depicted, the predictive models proposed by other researchers seems to worse represent the experimental data of the MWCNTs nanofluids. The mean squared Eq. 1.1 and Person’s correlation diverges from the experimental viscosity (slope 1) by several orders of magnitude. As such, the major contribution of this study was the development and calibration of a more generalist predictive model for the effective viscosity of nanofluids.

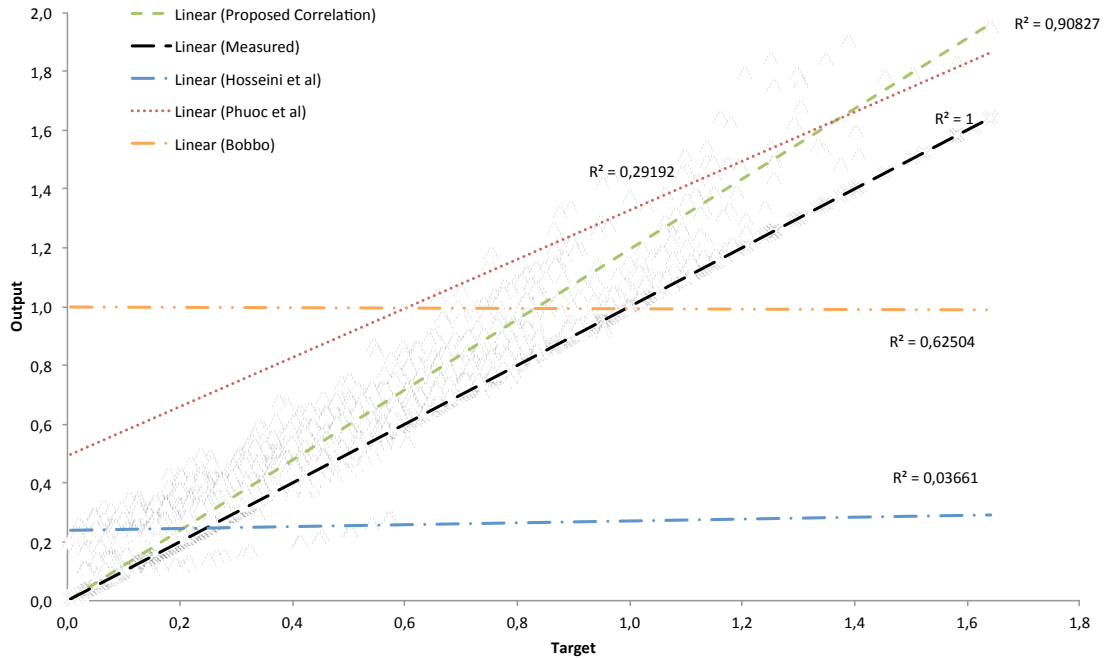


Figure 5.16 – Relation between the proposed model and other models for non-spherical nanoparticles.

5.5 Chapter Conclusions

In this Chapter, it was provided the experimental apparatus for the determination of nanofluids effective viscosity. The effective viscosity of the MWCNTs nanofluids was achieved through concentric cylinders, namely Brookfield DV-III Rheometer, which provided a maximum deviation of 15,5% from the theoretical values for the base fluids. The experimental results revealed a maximum enhancement of 147% for the nanoparticles with one of the smallest aspect ratio distributions and a volume fraction of 1,5%. A delineated control factor interaction provides the ability to verify the correlation between variables identified on the dimensionless analysis. It was found that MWCNTs based nanofluids present an anomalous enhancement of the effective viscosity, when compared with the predictions from classical theories. The proposed model for predicting the rheological behaviour of MWCNTs nanofluids seems to fit to the experimental results, with an average fractional error of 26%. Nevertheless, this error is within the 2% deviation announced by the manufacturer. In addition, the

statistical analysis shows that the effective viscosity strongly depends on the MWCNTs aspect ratio and volume fraction and on the imposed shear.

Chapter 6 - Conclusions

The main objective of this work was the development and characterization of multi-walled carbon nanotubes based nanofluids for thermal engineering purposes. It is scientifically proven that the addition of solid nanoparticles to conventional fluids modifies their thermal and transport capabilities. It was concluded that a nanofluid, with high colloidal stability, would preserve the transport and thermal properties constant for long periods of time. This feature is essential to promote the adoption of this nanotechnology by the specialized industry. It should, however, be mentioned, that the adopted preparation methodology of these suspensions leads to the reduction of the MWCNTs length, which induces modifications on the rheological behaviour of the nanofluid.

The intrinsic mechanism responsible for the rheological behaviour of this type of nanofluids was not properly identified. The rheological behaviour of MWCNTs suspensions is a multivariable function, which is influenced, among others, by the shear-imposed conditions. Nevertheless, it was possible to propose and validate a predictive model for the dynamic viscosity or shear viscosity of MWCNTs suspensions. The rheological characterization of the MWCNTs nanofluids was achieved through an experimental parametric analysis, revealing a strong dependence on nanoparticle volume fraction and imposed shear, with a maximum enhancement of 147% for the smallest aspect ratio nanoparticles ($AR=31$). Moreover, it was identified that the MWCNTs suspensions present a shear-thinning nature, which is attributed to the response of the suspension microstructure (percolation network) to the external stimulus.

Along the doctoral programme, several contacts and meetings were developed with engineering and manufacturing companies incorporating and/or prescribing heat transfer fluids in everyday products. Most of them demonstrated a strong and genuine interest in this project results. As a result of that, despite not initially identified as a project objective, the development of a

technology-transfer plan was assumed as an additional and important objective of this doctoral plan. A complete business plan was developed and it can be found in Appendix K.

6.1 Conclusions

This research work focuses on the development and characterization of MWCNTs nanofluids for heat transfer applications. The conducted survey on the available open literature revealed that the addition of small amounts of solid nanoparticles to conventional fluids modifies its transport and thermal properties. The latter also revealed that there are no standardized production methodologies, which, in addition to a considerable lack of intrinsic features evaluation, may be the cause for the discrepancies between research groups, both at an experimental and theoretical level.

Among the several thermo-physical properties of nanofluids, thermal conductivity and viscosity are still the most studied ones. The latter was suggested to have distinct and intrinsic behaviours since it seems to be unpredictable by the classical theories. A considerable amount of different type of nanoparticles can be found in the literature, divided into non-spherical (prolate) or spherical particles. From experimental and theoretical results, it is evident that elongated nanoparticles, such as MWCNTs provide the highest known thermal conductivity enhancement. However, the prolate geometry of the MWCNTs can increase the viscosity of the suspensions leading to pressure drops that can jeopardize the overall efficiency of the heat transfer system. For that reason, an optimization process aiming a low-pressure penalty (low viscosity) and a high thermal conductivity enhancement must be conducted. Such results are of utmost importance for the appropriate development of enhanced heat transfer nanofluids while keeping the energy consumption (pumping) to a minimum.

Despite rheology being still a young science, the viscosity is a very important property, and many classical rheological models for heterogeneous systems were developed based on the pioneering work of Einstein, developed more than a century ago. In this work, homogeneously dispersed spherical

particles through the medium at diluted concentrations, in which the interparticle interactions were neglected were considered. Later, several authors like Jeffrey, Simha and Taylor extended Einstein energy dissipation model, enabling the prediction of this property to ellipsoidal particles and higher volume fractions. More recently, Vand developed a model that accounts for the contribution of spherical particle collisions. However, this model is only valid for single or doublets pairs of particles.

In an attempt to describe the rheological behaviour of nanofluids, a few theories were suggested in addition to the classical ones, however, most of them were developed for diluted and semi-dilute suspensions, failing to capture the interparticle interaction and particle clusters (aggregation/disaggregation) common in concentrated suspensions. In fact, a model able to capture the shear-thinning nature of suspensions in all concentration regimes is still missing. Two distinct approaches can be clearly identified, the direct numerical simulations (DNS) and the kinetic theories. However, the multi-body interactions of nanofluids made the mathematics extremely complicated even for just a few particles. Still, most theories neglect the molecular nature of the medium, leading to “anomalous” hydrodynamics problems. Moreover, in most industrial heat transfer systems turbulent flows predominate, causing eddy currents, swirls and vortices. Therefore, a constitutive model relating the rheological molecular nature of the fluid medium in terms of shear variables and the contribution of the structural parameters (nanoparticle percolation networks) that determines its mechanical response under laminar and turbulent conditions is still missing. As such, the Buckingham Theorem methodology was used to support the development of an experimental programme aiming a parametric analysis of the fluid viscosity as a function of several input parameters. The latter allows for the organization of the fine physics influencing the rheological behaviour of colloidal suspensions in an aggregated form. This procedure allowed to conclude that the rheological behaviour of a colloidal suspension is a function of the buoyancy effects (density), the MWCNTs inertia effects (Reynolds number), the concentration of MWCNTs (ϕ), the suspensions kinematic viscosity over time and the transport properties of the fluid (Schmitt number).

The survey suggested that the disagreement between research groups might have resulted from different sample preparation techniques, poor colloidal stability and the lack of a standardized methodology to ascertain the rheology of nanofluids. To the present date, the literature does not present a consensual and robust preparation methodology capable of long-term colloidal stabilities. The study here presented contributes to the definition of a standardized preparation technique capable of long-term standing nanofluids. The term industrial nanofluid should represent a dispersion of nanoparticles in a base fluid, able of operating at all temperatures and flow conditions, with negligible probability of agglomeration or phase separation. These requisites ensure persistence thermal and transport properties and, particularly important for the correct assessment of the nanofluid thermal properties.

From a well-defined design of experiments (DOE), a total number of sixty (60) different MWCNTs based nanofluids were estimated and prepared through the optimized production methodology. These sixty nanofluids are the result of a full factorial arrangement of 6 MWCNTs geometries, dispersed in 2 different aqueous solutions of ethylene glycol at 5 volume fractions.

The MWCNTs were functionalized through an oxidation of the sidewalls of the MWCNTs with strong acid mixtures. This allows the formation of carboxylic groups as confirmed by the Fourier transform infrared spectroscopy. However, as confirm by the SEM image analysis, the MWCNTs length revealed an intensive reduction, in relation to that announced by the manufacturer. This is a major drawback for the conducted research since the results revealed that the MWCNTs length had a huge impact on the rheological properties of the nanofluids. It is, therefore, anticipated the requirement for even more refinement of the functionalization and dispersion technique here used. Nevertheless, the thermo-gravimetric analysis revealed that the functionalized MWCNTs present a negligible structural damage for the tested temperatures.

To evaluate the colloidal stability and guarantee their long shelf life stability, the produced MWCNTs nanofluids were subjected to a proper stability evaluation. To ensure a repulsive force between adjacent nanoparticles, a Zeta potential analysis was conducted. The results showed a Zeta potential superior to $>40\text{mV}$, suggesting an excellent particle repulsion or in other words a low

probability for nanoparticle agglomeration. Moreover, the samples were subjected to intensive centrifugal forces to evaluate the phase separation rate. The results have shown that the produced MWCNTs nanofluids present a self-life superior to two years, meaning an excellent colloidal stability.

To assess its rheological behaviour, the effective viscosities of MWCNTs nanofluids were tested at 7 temperatures and under 7 shear rates, performing 2940 experimental observations. It was observed a maximum dynamic viscosity enhancement (i.e. relative to the base fluid) of 147% for a 1,5% volume fraction for one of the smallest aspect ratios. The experimental results revealed that the effective dynamic viscosity strongly depended upon the volume fraction and imposed shear rate is the distribution of the MWCNTs length the less important feature. The latter may be explained since the final MWCNTs lengths are relatively similar between nanoparticles, when compared with its original (by the manufacturer) lengths differences. Therefore, any conclusion regarding the contribution of the size distribution must be made carefully. Nevertheless, the results have shown a higher viscosity increase for the nanoparticle with the smallest aspect ratio.

In a similar trend, temperatures have little influence on the MWCNTs percolation viscosity contribution (relative viscosity). This was expected since the major contribution of temperature is on changing the base fluid viscosity. Nevertheless, the Brownian motion is directly related to the thermal diffusivity that is a function of temperature, therefore, one can conclude that the contribution due to Brownian forces can be neglected. Moreover, there seems to be no evidence of some of the intriguing mechanisms suggested by some authors, namely Brownian motion and nanoparticle agglomeration. Except for high shear rates and concentrations, when the percolation networks become more densely packed, resulting in some anomalous behaviours.

Given the lack of a predictive model for the effective viscosity of suspensions of non-spherical nanoparticles that capture the inertial contribution of the percolations networks and the alignment of the nanoparticles with shearing forces, a model was proposed based on extensive experimental data and dimensional analysis techniques. The proposed model considers both the contribution of the inertial forces of the MWCNTs percolation network and of the

medium, the nanoparticle geometry, and how all of these interact with shearing forces.

Nevertheless, due to the deficit of experimental research on the magnitude of the fine physic dynamics of nano-scale percolation networks under shear conditions, it was assumed an adjustment parameter for the non-Newtonian power law model. Even so, the experimental results present satisfactory adjustment with the new model, suggesting that the rheological behaviour of nanofluids may be predicted through classical theories, after a proper upgrade to account for the contribution of the inertial forces of the percolation networks. It was verified that the magnitude of the overall inertial forces of the suspension is a limitation since it increases the fluidic resistance of the nanofluid. The 2940 experimental observations were predicted with a maximum fractional error lower than 10% leading to the conclusion that the proposed model is valid and can be applied to assess the rheological behaviour of homogeneous dispersions of MWCNTs, at any volume fraction. However, for unstable dispersions, this model may fail to predict its rheological behaviour, which is not a major limitation since these are not of great value for engineering applications.

In summary, the developed research programme provided evidence to answer the questions raised in the objectives of the thesis:

1. What is the most appropriate methodology to achieve long-term MWCNTs based nanofluids for heat transfer applications?

A stable nanofluid or a colloid means that the suspensions of the nanoparticles in the fluid medium remain constant over time. It must also imply the ability to preserve its engineered thermal and transport properties, with negligible variation over the required duty cycle. Therefore, it is of utmost importance that the nanoparticles present low probability of agglomeration and phase separation. In addition, it is detrimental to optimize the geometrical integrity of the nanoparticle, since it contributes to the rheological behaviour of the colloid.

2. What are the most important inherent physical mechanisms responsible for the effective viscosity of nanofluids and their rheological behaviour?

The experimental results have shown that the parameters that contribute for the rheology of MWCNTs nanofluids are: the size of the nanoparticles, its volume fraction and the base fluid properties, since these are associated to the spatial distribution, hence contributing to the interaction between the percolation network and the base fluid; and the shearing forces that are being applied to the system, since these will influence the spatial and percolation distribution. Furthermore, it was seen that the effective viscosity of these mixtures is limited (i.e. higher viscosity results in higher pump energy) to the inertial resistance of the MWCNTs network.

3. Is it possible to predict the effective viscosity of MWCNTs based nanofluids through a general physical-mathematical model?

It was verified that to stable nanofluids that respect the structural morphology envisaged, the effective viscosity could be predicted by a general physical-mathematical model. The latter was designed as an upgraded power law model, considering both inertial contributions of the nanoparticle network and the base medium, the nanoparticle geometry, the volume fraction and how these are influenced by an opposing shearing force. Given the lack of theoretical formalism for assessing the dynamics between colloidal systems vs shear forces, it was verified that the proposed model predicts the effective dynamic viscosity of nanofluids with a maximum fractional error of 10%.

As a result of the developed research programme, it was possible to confirm, empirically, that the addition of MWCNTs to conventional heat transfer fluids influences its thermal and transport properties. However, this technology has to be tailored to fit applications such as conductive inks; aqueous additives for

enhancing other materials properties; protective films; and as an advanced solar absorption fluid (solar collectors). The now complete thermo-physical property database enables the development of customized advanced nanofluids regarding its final application.

The academic and industrial fuzz created over the last years for more sustainable and energy friendly platform technologies, like the nanofluids, lead to the development of a Patent “Stable carbon nanofluid, obtaining methods and uses thereof”. However, due to previously publication in international scientific journals led to the decline of this patent. An example of the patent can be found in Appendix K.

6.2 Future Work

The conducted research work was able to successfully answer all the original proposed research questions. Nevertheless, additional questions and research ideas were revealed as a natural result of the developed work.

For future work it is of utmost importance to develop a nanofluid production methodology capable of inferring long-term stabilities with a low penalty to the MWCNTs geometrical dimensions, especially its length. This may be achieved by applying different functionalization techniques. Accordingly, to the proposed predictive model, the incorporation of longer MWCNTs would produce a stronger enhancement on the effective viscosity and a distinctive rheological behaviour. This is of utmost importance since depending on its industrial application the incorporation of a more viscous or more shear-thinning nanofluid will have distinctive impacts on the effectiveness of the system. Unfortunately this effect was not completely verified due to the limitations associated with the adopted production methodology.

In addition, it is of utmost importance to deeply study the mechanisms associated with the dynamics of the percolation networks of MWCNTs under shear conditions and how these affect the overall hydrodynamic resistance of the system. From previous research works, it becomes clear that the hydrodynamic interaction between the solid and liquid phase of the colloidal system depends:

on the base fluid thermal and transport properties, on the geometrical properties of the nanoparticle and how these affect the density of the percolation networks. However, given the divergences reported in the open literature, other mechanisms must be identified and modelled. Therefore, the development of analytical models capable of modelling the dynamics of individual and percolation-like MWCNTs is also of utmost importance, in order to complete the present study.

Finally, the developed database of thermal and transport properties makes possible to develop tailored made advanced heat transfer fluids, envisage their application and predict the efficiency of the system overall gain.

References

- [1] F. P. Incropera, D. P. DeWitt, T. L. Bergman, and A. S. Lavine, *Fundamentals of heat and mass transfer; 6th ed.* New York, NY: Wiley, 2007.
- [2] Z. Anxionnaz, M. Cabassud, C. Gourdon, and P. Tochon, "Heat exchanger/reactors (HEX reactors): Concepts, technologies: State-of-the-art," *Chemical Engineering and Processing: Process Intensification*, vol. 47, no. 12, pp. 2029–2050, Nov. 2008.
- [3] J. C. Maxwell, *A Treatise on Electricity and Magnetism V1 (1881)*. 2014.
- [4] "Heat transfer characteristics of nanofluids: a review," vol. 46, no. 1, pp. 1–19, Dec. 2006.
- [5] A. Einstein, *Berichtigung zu meiner Arbeit: "Eine neue Bestimmung der Moleküldimensionen."* 1911.
- [6] K. Toda and H. Furuse, "Extension of Einstein's viscosity equation to that for concentrated dispersions of solutes and particles," *Journal of Bioscience and Bioengineering*, vol. 102, no. 6, pp. 524–528, Dec. 2006.
- [7] B. M. Haines and A. L. Mazzucato, "A Proof of Einstein's Effective Viscosity for a Dilute Suspension of Spheres," *SIAM Journal on Mathematical Analysis*, vol. 44, no. 3, pp. 2120–2145, 2012.
- [8] G. K. Batchelor, "The effect of Brownian motion on the bulk stress in a suspension of spherical particles," *J. Fluid Mech.*, vol. 83, no. 1, pp. 97–117, Nov. 1977.
- [9] G. B. Jeffery, "The Motion of Ellipsoidal Particles Immersed in a Viscous Fluid," *Proceedings of the Royal Society of London A: Mathematical, Physical and Engineering Sciences*, vol. 102, no. 715, pp. 161–179, Nov. 1922.
- [10] J. P. Meyer, S. A. Adio, M. Sharifpur, and P. N. Nwosu, "The viscosity of nanofluids: a review of the theoretical, empirical and numerical models," *Heat Transfer Engineering*, pp. 00–00, Jun. 2015.
- [11] R. L. Hamilton and O. K. Crosser, "Thermal conductivity of heterogeneous two-component systems," *Industrial & Engineering chemistry fundamentals*, vol. 1, no. 3, pp. 187–191, 1962.
- [12] S. Iijima, "Helical microtubules of graphitic carbon," *Nature*, vol. 354, no. 6348, pp. 56–58, 1991.
- [13] S. Choi, "Enhancing thermal conductivity of fluids with nanoparticles," *Developments and Applications of Non-Newtonian Flows. FED-vol. 231/MD-vol. 66*, p. 99, 1995.
- [14] D. Wen, G. Lin, S. Vafaei, and K. Zhang, "Review of nanofluids for heat transfer applications," *Particuology*, vol. 7, no. 2, pp. 141–150, May 2009.
- [15] B. Jo and D. Banerjee, "Viscosity measurements of multi-walled carbon nanotubes-based high temperature nanofluids," *Materials Letters*, vol. 122, pp. 212–215, May 2014.
- [16] J. Lee, Y.-J. Yoon, J. K. Eaton, K. E. Goodson, and S. J. Bai, "Analysis of oxide (Al₂O₃, CuO, and ZnO) and CNT nanoparticles disaggregation effect on the thermal conductivity and the viscosity of nanofluids," *Int. J. Precis. Eng. Manuf.*, vol. 15, no. 4, pp. 703–710, Apr. 2014.

- [17] S. Halelfadl, P. Estellé, B. Aladag, N. Doner, and T. Maré, "Viscosity of carbon nanotubes water-based nanofluids: Influence of concentration and temperature," *International Journal of Thermal Sciences*, vol. 71, pp. 111–117, Aug. 2013.
- [18] I. A. S. K S, M. S, and R. K S, "Viscosity and thermal conductivity of dispersions of gum arabic capped MWCNT in water: Influence of MWCNT concentration and temperature," *Journal of the Taiwan Institute of Chemical Engineers*, vol. 44, no. 3, pp. 474–479, May 2013.
- [19] P. Estellé, S. Halelfadl, N. Doner, and T. Maré, "Shear History Effect on the Viscosity of Carbon Nanotubes Water-based Nanofluid," *CNANO*, vol. 9, no. 2, pp. 225–230, Apr. 2013.
- [20] V. Y. Rudyak, "Viscosity of Nanofluids. Why It Is Not Described by the Classical Theories," *ANP*, vol. 2, no. 3, pp. 266–279, 2013.
- [21] B. Abreu, A. Válega, B. Lamas, A. Fonseca, N. Martins, and M. Oliveira, "On the Assessment of Viscosity Variability by Nanofluid Engineering: A Review," *J Nanofluids*, vol. 5, no. 1, pp. 23–36, Mar. 2016.
- [22] P. Keblinski, J. EASTMAN, and D. CAHILL, "Nanofluids for thermal transport," *Materials Today*, vol. 8, no. 6, pp. 36–44, Jul. 2005.
- [23] J. Hilding, E. A. Grulke, Z. George Zhang, and F. Lockwood, "Dispersion of Carbon Nanotubes in Liquids," *Journal of Dispersion Science and Technology*, vol. 24, no. 1, pp. 1–41, Feb. 2003.
- [24] S. Ebrahimi, A. Gavili, I. Hadi, J. Sabbaghzadeh, M. Lajevardi, and T. D. Isfahani, *New Class of Coolants: Nanofluids*. 2010.
- [25] R. Taylor, S. Coulombe, T. Otanicar, P. Phelan, A. Gunawan, W. Lv, G. Rosengarten, R. Prasher, and H. Tyagi, "Small particles, big impacts: A review of the diverse applications of nanofluids," *J. Appl. Phys.*, vol. 113, no. 1, p. 1301, Jan. 2013.
- [26] T. Yamabe, K. Fukui, and K. Tanaka, *The Science and Technology of Carbon Nanotubes*, 1st ed. Elsevier, 1999.
- [27] D. Zhang, L. Shi, J. Fang, X. Li, and K. Dai, "Preparation and modification of carbon nanotubes," *Materials Letters*, vol. 59, no. 29, pp. 4044–4047, Dec. 2005.
- [28] Y. Li, J. A. E. Zhou, S. Tung, E. Schneider, and S. Xi, "A review on development of nanofluid preparation and characterization," *Powder Technology*, vol. 196, no. 2, pp. 89–101, Oct. 2009.
- [29] J. A. Eastman, S. U. S. Choi, S. Li, W. Yu, and L. J. Thompson, "Anomalously increased effective thermal conductivities of ethylene glycol-based nanofluids containing copper nanoparticles," *Appl. Phys. Lett.*, vol. 78, no. 6, p. 718, Mar. 2001.
- [30] H.-T. Zhu, Y.-S. Lin, and Y.-S. Yin, "A novel one-step chemical method for preparation of copper nanofluids," *J Colloid Interface Sci*, vol. 277, no. 1, pp. 100–103, Sep. 2004.
- [31] C.-H. Lo, T.-T. Tsung, and L.-C. Chen, "Shape-controlled synthesis of Cu-based nanofluid using submerged arc nanoparticle synthesis system (SANSS)," *Journal of Crystal Growth*, vol. 277, no. 1, pp. 636–642, Apr. 2005.
- [32] H. Bönnemann, S. S. Botha, B. Bladergroen, and V. M. Linkov, "Monodisperse copper- and silver-nanocolloids suitable for heat-conductive fluids," *Appl. Organometal. Chem.*, vol. 19, no. 6, pp. 768–

773, 2005.

- [33] W. Y. A. H. Xie, "Review Article A Review on Nanofluids: Preparation, Stability Mechanisms, and Applications," pp. 1–17, Sep. 2011.
- [34] A. Nasiri, M. Shariaty-Niasar, A. Rashidi, A. Amrollahi, and R. Khodafarin, "Effect of dispersion method on thermal conductivity and stability of nanofluid," *Experimental Thermal and Fluid Science*, vol. 35, no. 4, pp. 717–723, Apr. 2011.
- [35] Y. Y. Huang and E. M. Terentjev, "Dispersion and rheology of carbon nanotubes in polymers," *Int J Mater Form*, vol. 1, no. 2, pp. 63–74, 2008.
- [36] P. Garg, J. L. Alvarado, C. Marsh, T. A. Carlson, D. A. Kessler, and K. Annamalai, "An experimental study on the effect of ultrasonication on viscosity and heat transfer performance of multi-wall carbon nanotube-based aqueous nanofluids," *International Journal of Heat and Mass Transfer*, vol. 52, no. 21, pp. 5090–5101, Oct. 2009.
- [37] A. Hirsch, "Functionalization of Single-Walled Carbon Nanotubes," *Angewandte Chemie International Edition*, vol. 41, no. 11, pp. 1853–1859, Jun. 2002.
- [38] O. V. Kharissova, B. I. Kharisov, and E. G. de Casas Ortiz, "Dispersion of carbon nanotubes in water and non-aqueous solvents," *RSC Adv.*, vol. 3, no. 47, pp. 24812–41, 2013.
- [39] Y. Y. Huang and E. M. Terentjev, "Dispersion of Carbon Nanotubes: Mixing, Sonication, Stabilization, and Composite Properties," *Polymers*, vol. 4, no. 4, pp. 275–295, Dec. 2012.
- [40] Botha and S. Senara, "SYNTHESIS AND CHARACTERIZATION OF NANOFLUIDS FOR COOLING APPLICATIONS," pp. 1–182, Mar. 2008.
- [41] B. Lamas, B. Abreu, A. Fonseca, N. Martins, and M. Oliveira, "Long-Term MWCNTs Nanofluids toward Heat Transfer Capability Improvement," *J. Phys. Chem. C*, vol. 117, no. 24, pp. 12826–12834, Jun. 2013.
- [42] K. Balasubramanian and M. Burghard, "Chemically Functionalized Carbon Nanotubes," *Small*, vol. 1, no. 2, pp. 180–192, Mar. 2005.
- [43] T. Yousefi, F. Veisy, E. Shojaeizadeh, and S. Zinadini, "An experimental investigation on the effect of MWCNT-H₂O nanofluid on the efficiency of flat-plate solar collectors," *Experimental Thermal and Fluid Science*, vol. 39, no. C, pp. 207–212, Jun. 2012.
- [44] L. Vaisman, H. D. Wagner, and G. Marom, "The role of surfactants in dispersion of carbon nanotubes," *Adv. Colloid Interf. Sci.*, vol. 128, no. 0, pp. 37–46, Feb. 2006.
- [45] S. K. Das, S. U. Choi, W. Yu, and T. Pradeep, *Nanofluids*, 1st ed. Wiley-Interscience, 2007.
- [46] T. Tadros, *General Principles of Colloid Stability and the Role of Surface Forces*. Weinheim, Germany: Wiley-VCH Verlag GmbH & Co. KGaA, 2011, pp. 1–22.
- [47] S. Halelfadl, T. Maré, P. Estellé, and N. Mohd-Ghazali, "Experimental Investigation of Rheological Behavior and Pressure Drop of Aqueous Suspensions of Carbon Nanotubes in a Horizontal Tube," *Procedia Engineering*, vol. 56, pp. 344–349, 2013.
- [48] "Long-Term MWCNTs Nanofluids toward Heat Transfer Capability Improvement," vol. 117, no. 24, pp. 12826–12834, Dec. 2012.
- [49] T.-P. Teng and C.-C. Yu, "Heat dissipation performance of MWCNTs

- nano-coolant for vehicle," *Experimental Thermal and Fluid Science*, vol. 49, pp. 22–30, Sep. 2013.
- [50] A. Gedanken, "Sonochemistry and its application to nanochemistry," *CURRENT SCIENCE-BANGALORE*, vol. 85, no. 12, pp. 1720–1722, 2003.
- [51] S. Berliner, *Application of ultrasonic processors*. International Biotechnology Laboratory, 1984.
- [52] L. Fedele, L. Colla, S. Bobbo, S. Barison, and F. Agresti, "Experimental stability analysis of different water-based nanofluids," *Nanoscale Res Lett*, vol. 6, no. 1, p. 300, Apr. 2011.
- [53] H. Hu, A. Yu, E. Kim, B. Zhao, M. E. Itkis, E. Bekyarova, and R. C. Haddon, "Influence of the Zeta Potential on the Dispersability and Purification of Single-Walled Carbon Nanotubes," *J. Phys. Chem.*, vol. 109, no. 23, pp. 11520–11524, Feb. 2013.
- [54] X. Li, D. Zhu, and X. Wang, "Evaluation on dispersion behavior of the aqueous copper nano-suspensions.," *J Colloid Interface Sci*, vol. 310, no. 2, pp. 456–463, Jul. 2007.
- [55] D. López-González, M. Fernandez-Lopez, J. L. Valverde, and L. Sanchez-Silva, "Thermogravimetric-mass spectrometric analysis on combustion of lignocellulosic biomass," *Bioresource Technology*, vol. 143, no. 0, pp. 562–574, Sep. 2013.
- [56] R. Sturgeon, *Spectrochemical analysis: James D. Ingle Jr and Stanley R. Crouch. XV+ 590 pp. Prentice Hall, Englewood Cliffs, NJ (1988). Price (US) \$52.00. ISBN 0-13 1988.*
- [57] Y. Hwang, J.-K. Lee, J.-K. Lee, Y.-M. Jeong, S.-I. Cheong, Y.-C. Ahn, and S. H. Kim, "Production and dispersion stability of nanoparticles in nanofluids," *Powder Technology*, vol. 186, no. 2, pp. 145–153, Aug. 2008.
- [58] L. Fedele, L. Colla, S. Bobbo, S. Barison, and F. Agresti, "Experimental stability analysis of different water-based nanofluids," *Nanoscale Res Lett*, vol. 6, no. 1, pp. X1–8, 2011.
- [59] D. Han, Z. Meng, D. Wu, C. Zhang, and H. Zhu, "Thermal properties of carbon black aqueous nanofluids for solar absorption," *Nanoscale Res Lett*, vol. 6, no. 1, p. 457, Jul. 2011.
- [60] J. Xu, S. Chatterjee, K. W. Koelling, Y. Wang, and S. E. Bechtel, "Shear and extensional rheology of carbon nanofiber suspensions," *Rheol Acta*, vol. 44, no. 6, pp. 537–562, May 2005.
- [61] M. Shaffer, X. Fan, and A. H. Windle, "Dispersion and packing of carbon nanotubes," *Carbon*, vol. 36, no. 11, pp. 1603–1612, 1998.
- [62] R. Walvekar, I. A. Faris, and M. Khalid, "Thermal conductivity of carbon nanotube nanofluid-Experimental and theoretical study," *Heat Trans. Asian Res.*, vol. 41, no. 2, pp. 145–163, Jan. 2012.
- [63] G. H. Ko, K. Heo, K. Lee, D. S. Kim, C. Kim, Y. Sohn, and M. Choi, "An experimental study on the pressure drop of nanofluids containing carbon nanotubes in a horizontal tube," *International Journal of Heat and Mass Transfer*, vol. 50, no. 23, pp. 4749–4753, Nov. 2007.
- [64] I. Madni, C.-Y. Hwang, S.-D. Park, Y.-H. Choa, and H.-T. Kim, "Mixed surfactant system for stable suspension of multiwalled carbon nanotubes," *Colloids and Surfaces A: Physicochemical and Engineering Aspects*, vol. 358, no. 1, pp. 101–107.
- [65] Y. Ding, H. Alias, D. Wen, and R. A. Williams, "Heat transfer of aqueous

- suspensions of carbon nanotubes (CNT nanofluids)," *International Journal of Heat and Mass Transfer*, vol. 49, no. 1, pp. 240–250, Jan. 2006.
- [66] T. X. Phuoc, M. Massoudi, and R.-H. Chen, "Viscosity and thermal conductivity of nanofluids containing multi-walled carbon nanotubes stabilized by chitosan," *International Journal of Thermal Sciences*, vol. 50, no. 1, pp. 12–18, Jan. 2011.
- [67] S. Halelfadl, T. Maré, P. Estellé, and N. Mohd-Ghazali, "Experimental Investigation of Rheological Behavior and Pressure Drop of Aqueous Suspensions of Carbon Nanotubes in a Horizontal Tube," *Procedia Engineering*, vol. 56, pp. 344–349, 2013.
- [68] B. Abreu, B. Lamas, A. Fonseca, N. Martins, and M. S. A. Oliveira, "Experimental characterization of convective heat transfer with MWCNT based nanofluids under laminar flow conditions," *Heat Mass Transfer*, vol. 50, no. 1, pp. 65–74, Jan. 2014.
- [69] B. C. Lamas, A. Fonseca, F. A. M. M. Gonçalves, A. G. M. Ferreira, I. M. A. Fonseca, S. Kanagaraj, N. Martins, and M. S. A. Oliveira, "EG/CNTs Nanofluids Engineering and Thermo-Rheological Characterization," *JNanoR*, vol. 13, pp. 69–74, Mar. 2011.
- [70] M. S. Oliveira, N. Martins, S. Kanagaraj, J. Ponmozhi, F. Gonçalves, A. Ferreira, and I. Fonseca, "Thermodynamic and transport properties of CNT- water based nanofluids," *JNanoR*, vol. 11, pp. 101–106, 2010.
- [71] I. A. Kinloch, S. A. Roberts, and A. H. Windle, "A rheological study of concentrated aqueous nanotube dispersions," *Polymer*, vol. 43, no. 26, pp. 7483–7491, 2002.
- [72] M.-S. Liu, M. Ching-Cheng Lin, I.-T. Huang, and C.-C. Wang, "Enhancement of thermal conductivity with carbon nanotube for nanofluids," *International Communications in Heat and Mass Transfer*, vol. 32, no. 9, pp. 1202–1210, 2005.
- [73] M. Liu, Y. Yang, T. Zhu, and Z. Liu, "Chemical modification of single-walled carbon nanotubes with peroxytrifluoroacetic acid," *Carbon*, vol. 43, no. 7, pp. 1470–1478, Jun. 2005.
- [74] Y. J. Hwang, Y. C. Ahn, H. S. Shin, C. G. Lee, G. T. Kim, H. S. Park, and J. K. Lee, "Investigation on characteristics of thermal conductivity enhancement of nanofluids," *CURRENT APPLIED PHYSICS*, vol. 6, no. 6, pp. 1068–1071, Oct. 2006.
- [75] B. Ruan and A. M. Jacobi, "Ultrasonication effects on thermal and rheological properties of carbon nanotube suspensions," *Nanoscale Res Lett*, vol. 7, no. 1, p. 127, 2012.
- [76] T. Yousefi, F. Veisy, E. Shojaeizadeh, and S. Zinadini, "An experimental investigation on the effect of MWCNT-H₂O nanofluid on the efficiency of flat-plate solar collectors," *Experimental Thermal and Fluid Science*, vol. 39, no. C, pp. 207–212, May 2012.
- [77] A. Amrollahi, A. M. Rashidi, and M. E. Meibodi, "Convection heat transfer of functionalized MWNT in aqueous fluids in laminar and turbulent flow at the entrance region," *CORD Conference Proceedings*, pp. 439–440, Oct. 2010.
- [78] H. Chen, S. Witharana, Y. Jin, C. Kim, and Y. Ding, "Predicting thermal conductivity of liquid suspensions of nanoparticles (nanofluids) based on rheology," *Particuology*, vol. 7, no. 2, pp. 151–157, Apr. 2009.

- [79] Z. Talaei, A. R. Mahjoub, A. M. Rashidi, A. Amrollahi, and M. E. Meibodi, "The effect of functionalized group concentration on the stability and thermal conductivity of carbon nanotube fluid as heat transfer media," *International Communications in Heat and Mass Transfer*, vol. 38, no. 4, pp. 513–517, May 2011.
- [80] H. Xie, H. Lee, W. Youn, and M. Choi, "Nanofluids containing multiwalled carbon nanotubes and their enhanced thermal conductivities A1 -," *J. Appl. Phys.*, vol. 94, no. 8, p. 4967, 2003.
- [81] G. Vakili-Nezhaad and A. Dorany, "Effect of Single-Walled Carbon Nanotube on the Viscosity of Lubricants," *Energy Procedia*, vol. 14, no. 0, pp. 512–517, 2012.
- [82] Y. Yang, E. A. Grulke, Z. G. Zhang, and G. Wu, "Thermal and rheological properties of carbon nanotube-in-oil dispersions," *J. Appl. Phys.*, vol. 99, no. 1, p. 4307, Jun. 2006.
- [83] R. L. Vander Wal, S. D. Mozes, and V. Pushkarev, "Nanocarbon nanofluids: morphology and nanostructure comparisons," *Nanotechnology*, vol. 20, no. 10, p. 105702, Feb. 2009.
- [84] S. Bobbo, L. Fedele, A. Benetti, L. Colla, M. Fabrizio, C. Pagura, and S. Barison, "Viscosity of water based SWCNH and TiO₂nanofluids," *Experimental Thermal and Fluid Science*, vol. 36, pp. 65–71, Jan. 2012.
- [85] M. E. Meibodi, M. Vafaie-Sefti, A. M. Rashidi, A. Amrollahi, M. Tabasi, and H. S. Kalal, "The role of different parameters on the stability and thermal conductivity of carbon nanotube/water nanofluids," *International Communications in Heat and Mass Transfer*, vol. 37, no. 3, pp. 319–323, Mar. 2010.
- [86] L. Chen, H. Xie, Y. Li, and W. Yu, "Nanofluids containing carbon nanotubes treated by mechanochemical reaction," *Thermochimica Acta*, vol. 477, no. 1, pp. 21–24, Oct. 2008.
- [87] L. Chen, H. Xie, W. Yu, and Y. Li, "Rheological Behaviors of Nanofluids Containing Multi-Walled Carbon Nanotube," *Journal of Dispersion Science and Technology*, vol. 32, no. 4, pp. 550–554, Mar. 2011.
- [88] H. Xie and L. Chen, "Adjustable thermal conductivity in carbon nanotube nanofluids," *Physics Letters A*, vol. 373, no. 21, pp. 1861–1864, May 2009.
- [89] B. Wang, W. Lou, X. Wang, and J. Hao, "A gel-sol transition phenomenon of oxidation multi-walled carbon nanotubes-glycerol nanofluids induced by polyvinyl alcohol," *New J. Chem.*, vol. 36, no. 5, pp. 1273–1279, 2012.
- [90] J. Wensel, B. Wright, D. Thomas, W. Douglas, B. Mannhalter, W. Cross, H. Hong, J. Kellar, P. Smith, and W. Roy, "Enhanced thermal conductivity by aggregation in heat transfer nanofluids containing metal oxide nanoparticles and carbon nanotubes," *Appl. Phys. Lett.*, vol. 92, no. 2, p. 023110, 2008.
- [91] K. Babu and T. S. Prasanna Kumar, "Effect of CNT concentration and agitation on surface heat flux during quenching in CNT nanofluids," *International Journal of Heat and Mass Transfer*, vol. 54, no. 1, pp. 106–117, 2011.
- [92] N.-J. Kim, S.-S. Park, S. H. Lim, and W. Chun, "A study on the characteristics of carbon nanofluids at the room temperature (25°C),"

- International Communications in Heat and Mass Transfer*, vol. 38, no. 3, pp. 313–318, Mar. 2011.
- [93] B. Ruan and A. M. Jacobi, “Heat transfer characteristics of multiwall carbon nanotube suspensions (MWCNT nanofluids) in intertube falling-film flow,” *International Journal of Heat and Mass Transfer*, vol. 55, no. 11, pp. 3186–3195, May 2012.
- [94] B. Glover, K. W. Whites, H. Hong, A. Mukherjee, and W. E. Billups, “Effective electrical conductivity of functional single-wall carbon nanotubes in aqueous fluids,” *Synthetic Metals*, vol. 158, no. 12, pp. 506–508, Jul. 2008.
- [95] S. Shaikh, K. Lafdi, and R. Ponnappan, “Thermal conductivity improvement in carbon nanoparticle doped PAO oil: An experimental study,” *J. Appl. Phys.*, vol. 101, no. 6, p. 064302, 2007.
- [96] A. O. Cárdenas Gómez, A. R. K. Hoffmann, and E. P. Bandarra Filho, “Experimental evaluation of CNT nanofluids in single-phase flow,” *International Journal of Heat and Mass Transfer*, vol. 86, pp. 277–287, Jul. 2015.
- [97] Z. Said, R. Saidur, M. A. Sabiha, N. A. Rahim, and M. R. Anisur, “Thermophysical properties of Single Wall Carbon Nanotubes and its effect on exergy efficiency of a flat plate solar collector,” *Solar Energy*, vol. 115, pp. 757–769, May 2015.
- [98] K. Soma and S. C. Babu J, “Factors Influencing the Rheological Behavior of Carbon Nanotube Water-Based Nanofluid,” *Fullerenes, Nanotubes and Carbon Nanostructures*, vol. 23, no. 8, pp. 750–754, Dec. 2014.
- [99] A. Kasaeian, S. Daviran, R. D. Azarian, and A. Rashidi, “Performance evaluation and nanofluid using capability study of a solar parabolic trough collector,” *Energy Conversion and Management*, vol. 89, pp. 368–375, Jan. 2015.
- [100] Z. T. Tabari and S. Z. Heris, “Heat Transfer Performance of Milk Pasteurization Plate Heat Exchangers Using MWCNT/Water Nanofluid,” *Journal of Dispersion Science and Technology*, vol. 36, no. 2, pp. 196–204, Sep. 2014.
- [101] W. Rashmi, A. F. Ismail, M. Khalid, A. Anuar, and T. Yusaf, “Investigating corrosion effects and heat transfer enhancement in smaller size radiators using CNT-nanofluids,” *Journal of Materials Science*, vol. 49, no. 13, pp. 4544–4551, Apr. 2014.
- [102] Z. H. Liu, X. F. Yang, G. S. Wang, and G. L. Guo, “Influence of carbon nanotube suspension on the thermal performance of a miniature thermosyphon,” *International Journal of Heat and Mass Transfer*, vol. 53, no. 9, pp. 1914–1920, 2010.
- [103] R. Lotfi, A. M. Rashidi, and A. Amrollahi, “Experimental study on the heat transfer enhancement of MWNT-water nanofluid in a shell and tube heat exchanger,” *International Communications in Heat and Mass Transfer*, vol. 39, no. 1, pp. 108–111, Jan. 2012.
- [104] G. Balasubramanian, S. Sen, and I. K. Puri, “Shear viscosity enhancement in water-nanoparticle suspensions,” *Physics Letters A*, vol. 376, no. 6, pp. 860–863, Jan. 2012.
- [105] M. Shanbedi, S. Zeinali Heris, M. Baniadam, and A. Amiri, “The Effect of Multi-Walled Carbon Nanotube/Water Nanofluid on Thermal

- Performance of a Two-Phase Closed Thermosyphon," *Experimental Heat Transfer*, vol. 26, no. 1, pp. 26–40, Jan. 2013.
- [106] K. Wusiman, H. Jeong, K. Tulugan, H. Afrianto, and H. Chung, "Thermal performance of multi-walled carbon nanotubes (MWCNTs) in aqueous suspensions with surfactants SDBS and SDS," *International Communications in Heat and Mass Transfer*, vol. 41, pp. 28–33, Feb. 2013.
- [107] D. Ashtiani, M. A. Akhavan-Behabadi, and M. F. Pakdaman, "An experimental investigation on heat transfer characteristics of multi-walled CNT-heat transfer oil nanofluid flow inside flattened tubes under uniform wall temperature condition," *International Communications in Heat and Mass Transfer*, vol. 39, no. 9, pp. 1404–1409, Nov. 2012.
- [108] M. Hemmat Esfe, S. Saedodin, O. Mahian, and S. Wongwises, "Heat transfer characteristics and pressure drop of COOH-functionalized DWCNTs/water nanofluid in turbulent flow at low concentrations," *International Journal of Heat and Mass Transfer*, vol. 73, pp. 186–194, Jun. 2014.
- [109] N. Hordy, D. Rabilloud, J.-L. Meunier, and S. Coulombe, "High temperature and long-term stability of carbon nanotube nanofluids for direct absorption solar thermal collectors," *Solar Energy*, vol. 105, pp. 82–90, Jul. 2014.
- [110] E. N. Zare, M. M. Lakouraj, P. N. Moghadam, and R. Azimi, "Novel polyfuran/functionalized multiwalled carbon nanotubes composites with improved conductivity: Chemical synthesis, characterization, and antioxidant activity," *Polym Compos*, vol. 34, no. 5, pp. 732–739, Feb. 2013.
- [111] B. Hung Thang, L. Dinh Quang, N. Manh Hong, P. H. Khoi, and P. N. Minh, "Application of Multiwalled Carbon Nanotube Nanofluid for 450 W LED Floodlight," *Journal of Nanomaterials*, vol. 2014, no. 2, pp. 1–6, 2014.
- [112] S. S. Chougule and S. K. Sahu, "Heat transfer and friction characteristics of Al₂O₃/water and CNT/water nanofluids in transition flow using helical screw tape inserts – a comparative study," *Chemical Engineering and Processing: Process Intensification*, vol. 88, pp. 78–88, Feb. 2015.
- [113] A. Amiri, M. Shanbedi, H. Amiri, S. Z. Heris, S. N. Kazi, B. T. Chew, and H. Eshghi, "Pool boiling heat transfer of CNT/water nanofluids," *Applied Thermal Engineering*, vol. 71, no. 1, pp. 450–459, Oct. 2014.
- [114] P. Estellé, S. Halelfadl, and T. Maré, "Lignin as dispersant for water-based carbon nanotubes nanofluids: Impact on viscosity and thermal conductivity," *International Communications in Heat and Mass Transfer*, vol. 57, pp. 8–12, Oct. 2014.
- [115] M. Piratheepan and T. N. Anderson, "An experimental investigation of turbulent forced convection heat transfer by a multi-walled carbon-nanotube nanofluid," *International Communications in Heat and Mass Transfer*, vol. 57, pp. 286–290, Oct. 2014.
- [116] S. Kim, H. Chung, H. Jeong, B. Lee, B. Ochirkhuyag, J. Lee, and H. Choi, "The study of heat transfer for nanofluid with carbon nano particle in an exhaust gas recirculation (EGR) cooler," *Heat Mass Transfer*, vol. 49, no. 7, pp. 1051–1055, May 2013.

- [117] S.-S. Park and N.-J. Kim, "A study on the characteristics of carbon nanofluid for heat transfer enhancement of heat pipe," *Renewable Energy*, vol. 65, pp. 123–129, May 2014.
- [118] W. Rashmi, M. Khalid, A. F. Ismail, R. Saidur, and A. K. Rashid, "Experimental and numerical investigation of heat transfer in CNT nanofluids," *Journal of Experimental Nanoscience*, vol. 10, no. 7, pp. 545–563, Oct. 2013.
- [119] A. Steele, I. S. Bayer, and E. Loth, "Pipe flow drag reduction effects from carbon nanotube additives," *Carbon*, vol. 77, pp. 1183–1186, 2014.
- [120] M. M. Derakhshan, M. A. Akhavan-Behabadi, and M. Ghazvini, "Rheological Characteristics, Pressure Drop, and Skin Friction Coefficient of MWCNT–Oil Nanofluid Flow Inside an Inclined Microfin Tube," *Heat Transfer Engineering*, vol. 36, no. 17, pp. 1436–1446, Apr. 2015.
- [121] A. Beheshti, M. Shanbedi, and S. Z. Heris, "Heat transfer and rheological properties of transformer oil-oxidized MWCNT nanofluid," *J Therm Anal Calorim*, vol. 118, no. 3, pp. 1451–1460, Aug. 2014.
- [122] K. Babu and T. S. P. Kumar, "Optimum CNT Concentration and Bath Temperature for Maximum Heat Transfer Rate during Quenching in CNT Nanofluids," *Journal of ASTM International*, vol. 9, no. 5, p. 104442, 2012.
- [123] V. Kumaresan and R. Velraj, "Experimental investigation of the thermo-physical properties of water–ethylene glycol mixture based CNT nanofluids," *Thermochimica Acta*, vol. 545, pp. 180–186, Oct. 2012.
- [124] S. Tagmouti, S. E. Bouzit, L. C. Costa, M. P. F. Graça, and A. Outzourhit, "Impedance Spectroscopy of Nanofluids based on Multiwall Carbon Nanotubes," *Spectroscopy Letters*, vol. 48, no. 10, pp. 761–766, Jul. 2015.
- [125] R. Sadri, G. Ahmadi, H. Togun, M. Dahari, S. N. Kazi, E. Sadeghinezhad, and N. Zubir, "An experimental study on thermal conductivity and viscosity of nanofluids containing carbon nanotubes," vol. 9, no. 1, pp. 1–16, Mar. 2014.
- [126] Z. Meng, D. Wu, L. Wang, H. Zhu, and Q. Li, "Carbon nanotube glycol nanofluids: Photo-thermal properties, thermal conductivities and rheological behavior," *Particuology*, vol. 10, no. 5, pp. 614–618, Oct. 2012.
- [127] R. Mondragón, C. Segarra, R. Martínez-Cuenca, J. E. Juliá, and J. C. Jarque, "Experimental characterization and modeling of thermophysical properties of nanofluids at high temperature conditions for heat transfer applications," *Powder Technology*, vol. 249, no. 0, pp. 516–529, Nov. 2013.
- [128] Y. Wang, Z. Iqbal, and S. Mitra, "Rapidly Functionalized, Water-Dispersed Carbon Nanotubes at High Concentration," *J. Am. Chem. Soc.*, vol. 128, no. 1, pp. 95–99, Feb. 2013.
- [129] F. M. White, *Viscous Fluid Flow*. McGraw-Hill Science, Engineering & Mathematics, 1991.
- [130] A. I. A. Malkin, A. Y. Malkin, and A. I. Isayev, *Rheology: Concepts, Methods & Applications*. ChemTec Pub., 2006.
- [131] N. Willenbacher and K. Georgieva, *Rheology of Disperse Systems*. Weinheim, Germany: Wiley-VCH Verlag GmbH & Co. KGaA, 2013, pp. 7–

49.

- [132] B. E. Laboratories, *More Solutions to Sticky Problems: A Guide to Getting More from Your Brookfield Viscometer*. The Laboratory, 1995.
- [133] D. S. Viswanath, T. Ghosh, D. H. L. Prasad, N. V. K. Dutt, and K. Y. Rani, *Viscosity of Liquids*. Dordrecht: Springer Science & Business Media, 2007.
- [134] J. P. Meyer, T. J. McKrell, and K. Grote, "The influence of multi-walled carbon nanotubes on single-phase heat transfer and pressure drop characteristics in the transitional flow regime of smooth tubes," *International Journal of Heat and Mass Transfer*, vol. 58, no. 1, pp. 597–609, Mar. 2013.
- [135] W. J. Tseng and C. H. Wu, "Aggregation, rheology and electrophoretic packing structure of aqueous Al₂O₃ nanoparticle suspensions," *Acta Materialia*, vol. 50, no. 15, pp. 3757–3766, 2002.
- [136] A. De Noni Jr, D. E. Garcia, and D. Hotza, "A modified model for the viscosity of ceramic suspensions," *Ceramics International*, vol. 28, no. 7, pp. 731–735, 2002.
- [137] S. Liu, "Particle dispersion for suspension flow," *Chemical Engineering Science*, vol. 54, no. 7, pp. 873–891, Apr. 1999.
- [138] G. Żyła, A. Witek, and M. Cholewa, "Viscosity of diethylene glycol-based Y₂O₃ nanofluids," *Journal of Experimental Nanoscience*, vol. 10, no. 6, pp. 458–465, Oct. 2013.
- [139] A. K. Tiwari, P. Ghosh, and J. Sarkar, "Heat transfer and pressure drop characteristics of CeO₂/water nanofluid in plate heat exchanger," *Applied Thermal Engineering*, pp. 1–38, May 2013.
- [140] H. J. Choi, T. M. Kwon, and M. S. Jhon, "Effects of shear rate and particle concentration on rheological properties of magnetic particle suspensions," *Journal of Materials Science*, vol. 35, no. 4, pp. 889–894, 2000.
- [141] R. J. Johnson and R. Pitchumani, "Characterization of the Rheology and Cure Kinetics of Epoxy Resin with Carbon Nanotubes," *Frontiers in Heat and Mass Transfer*, vol. 1, no. 1, 2010.
- [142] A. W. K. Ma, F. Chinesta, and M. R. Mackley, "The rheology and modeling of chemically treated carbon nanotubes suspensions," *J. Rheol.*, vol. 53, no. 3, p. 547, 2009.
- [143] B. Aladag, S. Halelfadl, N. Doner, T. Maré, S. Duret, and P. Estellé, "Experimental investigations of the viscosity of nanofluids at low temperatures," *Applied Energy*, vol. 97, pp. 876–880, Sep. 2012.
- [144] S. Abbasi, P. J. Carreau, A. Derdouri, and M. Moan, "Rheological properties and percolation in suspensions of multiwalled carbon nanotubes in polycarbonate," *Int J Mater Form*, vol. 48, no. 2, pp. 943–959, Jul. 2008.
- [145] H. Chen, W. Yang, Y. He, Y. Ding, L. Zhang, C. Tan, A. A. Lapkin, and D. V. Bavykin, "Heat transfer and flow behaviour of aqueous suspensions of titanate nanotubes (nanofluids)," *Powder Technology*, vol. 183, no. 1, pp. 63–72, Feb. 2008.
- [146] Y. Ding, H. Alias, D. Wen, and R. A. Williams, "Heat transfer of aqueous suspensions of carbon nanotubes (CNT nanofluids)," *International Journal of Heat and Mass Transfer*, vol. 49, no. 1, pp. 240–250, Feb.

2006.

- [147] F. Su, X. Ma, and Z. Lan, "The effect of carbon nanotubes on the physical properties of a binary nanofluid," *Journal of the Taiwan Institute of Chemical Engineers*, vol. 42, no. 2, pp. 252–257, Mar. 2011.
- [148] T. Wang, M. Ni, Z. Luo, C. Shou, and K. Cen, "Viscosity and aggregation structure of nanocolloidal dispersions," *Chin. Sci. Bull.*, vol. 57, no. 27, pp. 3644–3651, Sep. 2012.
- [149] J. Chevalier, O. Tillement, and F. Ayela, "Rheological properties of nanofluids flowing through microchannels," *Appl. Phys. Lett.*, vol. 91, no. 23, p. 233103, 2007.
- [150] K. B. Anoop, T. Sundararajan, and S. K. Das, "Effect of particle size on the convective heat transfer in nanofluid in the developing region," *International Journal of Heat and Mass Transfer*, vol. 52, no. 9, pp. 2189–2195, May 2009.
- [151] Y. Yang, Z. G. Zhang, E. A. Grulke, W. B. Anderson, and G. Wu, "Heat transfer properties of nanoparticle-in-fluid dispersions (nanofluids) in laminar flow," *International Journal of Heat and Mass Transfer*, vol. 48, no. 6, pp. 1107–1116, Apr. 2005.
- [152] T. Yiamsawas, A. S. Dalkilic, O. Mahian, and S. Wongwises, "Measurement and Correlation of the Viscosity of Water-Based Al₂O₃ and TiO₂ Nanofluids in High Temperatures and Comparisons with Literature Reports," *Journal of Dispersion Science and Technology*, p. 130306111702006, Apr. 2013.
- [153] S.-Q. Zhou, R. Ni, and D. Funfschilling, "Effects of shear rate and temperature on viscosity of alumina polyalphaolefins nanofluids," *J. Appl. Phys.*, vol. 107, no. 5, p. 054317, 2010.
- [154] D. López-González, J. L. Valverde, P. Sánchez, and L. Sanchez-Silva, "Characterization of different heat transfer fluids and degradation study by using a pilot plant device operating at real conditions," *Energy*, vol. 54, pp. 240–250, May 2013.
- [155] D. Kim, Y. Kwon, Y. Cho, C. Li, S. Cheong, Y. Hwang, J. Lee, D. Hong, and S. Moon, "Convective heat transfer characteristics of nanofluids under laminar and turbulent flow conditions," *CURRENT APPLIED PHYSICS*, vol. 9, no. S, pp. e119–e123, Apr. 2009.
- [156] L. Yu, D. Liu, and F. Botz, "Laminar convective heat transfer of alumina-polyalphaolefin nanofluids containing spherical and non-spherical nanoparticles," *Experimental Thermal and Fluid Science*, vol. 37, no. C, pp. 72–83, Jan. 2012.
- [157] J. Yu, B. Tonpheng, G. Gröbner, and O. Andersson, "Thermal properties and transition studies of multi-wall carbon nanotube/nylon-6 composites," *Carbon*, vol. 49, no. 14, pp. 4858–4866, Nov. 2011.
- [158] R. L. Powell, "Rheology of suspensions of rodlike particles," *Journal of Statistical Physics*, vol. 62, no. 5, pp. 1073–1094, Apr. 1991.
- [159] M. J. Rhodes, *Introduction to Particle Technology*. John Wiley & Sons, 2013.
- [160] Z. Fan and S. G. Advani, "Rheology of multiwall carbon nanotube suspensions," *Journal of Rheology (1978-present)*, vol. 51, no. 4, pp. 585–604, 2007.
- [161] S. Mueller, E. W. Llewellyn, and H. M. Mader, "The rheology of

- suspensions of solid particles,” presented at the Proceedings of the Royal Society A: Mathematical, 2009, vol. 466, no. 2116, pp. 1201–1228.
- [162] G. R. Vakili-Nezhaad and A. Dorany, “INVESTIGATION OF THE EFFECT OF MULTIWALLED CARBON NANOTUBES ON THE VISCOSITY INDEX OF LUBE OIL CUTS,” *Chemical Engineering Communications*, vol. 196, no. 9, pp. 997–1007, May 2009.
- [163] S. S. Rahatekar, “Optical microstructure and viscosity enhancement for an epoxy resin matrix containing multiwall carbon nanotubes,” *J. Rheol.*, vol. 50, p. 599, n/a 2006.
- [164] K. M. Yearsley, M. R. Mackley, F. Chinesta, and A. Leygue, “The rheology of multiwalled carbon nanotube and carbon black suspensions,” *J. Rheol.*, vol. 56, no. 6, pp. 1465–27, 2012.
- [165] E. K. Hobbie and D. J. Fry, “Rheology of concentrated carbon nanotube suspensions,” *J. Chem. Phys.*, vol. 126, no. 12, pp. 124907–8, 2007.
- [166] R. Prasher, D. Song, J. Wang, and P. Phelan, “Measurements of nanofluid viscosity and its implications for thermal applications,” *Appl. Phys. Lett.*, vol. 89, no. 13, pp. 133108–4, 2006.
- [167] K. S. Suganthi and K. S. Rajan, “Temperature induced changes in ZnO–water nanofluid: Zeta potential, size distribution and viscosity profiles,” *International Journal of Heat and Mass Transfer*, vol. 55, no. 25, pp. 7969–7980, Dec. 2012.
- [168] Y. R. Sekhar and K. V. Sharma, “Study of viscosity and specific heat capacity characteristics of water-based Al₂O₃ nanofluids at low particle concentrations,” *Journal of Experimental Nanoscience*, vol. 10, no. 2, pp. 86–102, May 2013.
- [169] M. Kole and T. K. Dey, “Effect of aggregation on the viscosity of copper oxide–gear oil nanofluids,” *International Journal of Thermal Sciences*, vol. 50, no. 9, pp. 1741–1747, Jan. 2011.
- [170] S. M. S. Murshed, K. C. Leong, and C. Yang, “Investigations of thermal conductivity and viscosity of nanofluids,” *International Journal of Thermal Sciences*, vol. 47, no. 5, pp. 560–568, Jun. 2008.
- [171] L. S. Sundar, M. K. Singh, and A. C. M. Sousa, “Investigation of thermal conductivity and viscosity of Fe₃O₄ nanofluid for heat transfer applications,” *International Communications in Heat and Mass Transfer*, vol. 44, no. C, pp. 7–14, May 2013.
- [172] E. V. Timofeeva, J. L. Routbort, and D. Singh, “Particle shape effects on thermophysical properties of alumina nanofluids,” *J. Appl. Phys.*, vol. 106, no. 1, p. 4304, Jul. 2009.
- [173] C. U. Thomas and M. Muthukumar, “Three-body hydrodynamic effects on viscosity of suspensions of spheres,” *J. Chem. Phys.*, vol. 94, no. 7, pp. 5180–11, 1991.
- [174] L. Tian, G. Ahmadi, Z. Wang, and P. K. Hopke, “Transport and deposition of ellipsoidal fibers in low Reynolds number flows,” *Journal of Aerosol Science*, vol. 45, no. C, pp. 1–18, Mar. 2012.
- [175] G. I. Taylor, “The Motion of Ellipsoidal Particles in a Viscous Fluid,” *Proceedings of the Royal Society of London A: Mathematical, Physical and Engineering Sciences*, vol. 103, no. 720, pp. 58–61, Apr. 1923.
- [176] E. K. Hobbie, H. Wang, H. Kim, C. C. Han, E. A. Grulke, and J. Obrzut, “Optical measurements of structure and orientation in sheared carbon-

- nanotube suspensions," vol. 74, no. 3, pp. 1244–1250, Apr. 2003.
- [177] Z. Fan and S. G. Advani, "Characterization of orientation state of carbon nanotubes in shear flow," *Polymer*, vol. 46, no. 14, pp. 5232–5240, Jun. 2005.
- [178] S. Savithiri, A. Pattamatta, and S. K. Das, "Scaling analysis for the investigation of slip mechanisms in nanofluids," *Nanoscale Res Lett*, vol. 6, no. 1, p. 471, Jul. 2011.
- [179] P. N. N. M. S. N. T. J P Meyer, "Parametric Analysis of Effective Viscosity Models for Nanofluids," pp. 1–9, Aug. 2012.
- [180] M. von Smoluchowski, "Theoretische Bemerkungen über die Viskosität der Kolloide," *Kolloid-Zeitschrift*, vol. 18, no. 5, pp. 190–195, 1916.
- [181] V. Vand, "Viscosity of Solutions and Suspensions. I. Theory," *J. Phys. Chem.*, vol. 52, no. 2, pp. 277–299, Feb. 1948.
- [182] R. Roscoe, "The viscosity of suspensions of rigid spheres," *British Journal of Applied Physics*, vol. 3, no. 8, pp. 267–269, Aug. 1952.
- [183] H. C. Brinkman, "The Viscosity of Concentrated Suspensions and Solutions," *Journal of Chemical Physics*, vol. 20, p. 571, Apr. 1952.
- [184] G. I. Taylor, "The Viscosity of a Fluid Containing Small Drops of Another Fluid," *Proceedings of the Royal Society of London A: Mathematical, Physical and Engineering Sciences*, vol. 138, no. 834, pp. 41–48, Oct. 1932.
- [185] M. Mooney, "The viscosity of a concentrated suspension of spherical particles," *Journal of Colloid Science*, vol. 6, no. 2, pp. 162–170, 1951.
- [186] E. Hatschek, "The general theory of viscosity of two-phase systems," *Trans. Faraday Soc.*, vol. 9, pp. 80–13, 1913.
- [187] T. S. Lundgren, "Slow flow through stationary random beds and suspensions of spheres," *J. Fluid Mech.*, vol. 51, no. 2, pp. 273–299, Mar. 2006.
- [188] A. L. Graham, "On the viscosity of suspensions of solid spheres," *Appl. Sci. Res.*, vol. 37, no. 3, pp. 275–286, 1981.
- [189] N. A. Frankel and A. Acrivos, "On the viscosity of a concentrated suspension of solid spheres," *Chemical Engineering Science*, vol. 22, no. 6, pp. 847–853, 1967.
- [190] "Concentration Dependence of the Viscosity of High Polymer Solutions. I," *J. Phys. Soc. Jpn.*, vol. 5, no. 1, pp. 4–8, Jan. 1950.
- [191] I. M. Krieger and T. J. Dougherty, "A Mechanism for Non-Newtonian Flow in Suspensions of Rigid Spheres," *J. Rheol.*, vol. 3, no. 1, pp. 137–152, Mar. 1959.
- [192] J. M. Burgers, "On the Motion of Small Particles of Elongated Form. Suspended in a Viscous Liquid," in *Selected Papers of J. M. Burgers*, no. 9, F. T. M. Nieuwstadt and J. A. Steketee, Eds. Dordrecht: Springer Netherlands, 1938, pp. 209–280.
- [193] W. Krasny-Ergen, "Untersuchungen über die Viskosität von Suspensionen und Lösungen. 2. Zur Theorie der Elektroviskosität," *Kolloid-Zeitschrift*, vol. 74, no. 2, pp. 172–178, 1936.
- [194] H. B. Bull, "The electroviscous effect in egg albumin solutions," *Trans. Faraday Soc.*, vol. 35, pp. 80–5, 1940.
- [195] R. Simha, "The Influence of Brownian Movement on the Viscosity of Solutions," *The Journal of Physical Chemistry*, vol. 44, no. 1, pp. 25–34,

- 1940.
- [196] F. Booth, "The Electroviscous Effect for Suspensions of Solid Spherical Particles," presented at the Proceedings of the Royal Society of London. Series A, 1950, vol. 203, no. 1, pp. 533–551.
- [197] S. G. Ward and R. L. Whitmori, "Studies of the viscosity and sedimentation of suspensions Part 2. - The viscosity and sedimentation of suspensions of rough powders," *British Journal of Applied Physics*, vol. 1, no. 1, pp. 325–328, Dec. 1950.
- [198] L. G. Leal and E. J. Hinch, "The effect of weak Brownian rotations on particles in shear flow," *J. Fluid Mech.*, vol. 46, no. 4, pp. 685–703, n/a 1971.
- [199] J. A. Eastman, U. S. Choi, S. Li, L. J. Thompson, and S. Lee, "Enhanced Thermal Conductivity through the Development of Nanofluids," *MRS Proc.*, vol. 457, p. 3, Mar. 2011.
- [200] J. BICERANO, J. F. DOUGLAS, and D. A. BRUNE, "Model for the Viscosity of Particle Dispersions," *Journal of Macromolecular Science, Part C: Polymer Reviews*, vol. 39, no. 4, pp. 561–642, Sep. 1999.
- [201] W. Tseng and C. N. Chen, "Effect of polymeric dispersant on rheological behavior of nickel-terpineol suspensions," *Materials Science and Engineering: A*, vol. 347, no. 1, pp. 145–153, 2003.
- [202] S. E. B. Maïga, C. T. Nguyen, N. Galanis, and G. Roy, "Heat transfer behaviours of nanofluids in a uniformly heated tube," *Superlattices and Microstructures*, vol. 35, no. 3, pp. 543–557, Mar. 2004.
- [203] X. Wang, X. Xu, and S. U. S. Choi, "Thermal conductivity of nanoparticle-fluid mixture," *J. Thermophys. Heat Transfer*, vol. 13, no. 4, pp. 474–480, 1999.
- [204] D. P. Kulkarni, D. K. Das, and G. A. Chukwu, "Temperature Dependent Rheological Property of Copper Oxide Nanoparticles Suspension (Nanofluid)," *J. Nanosci. Nanotech.*, vol. 6, no. 4, pp. 1150–1154, Apr. 2006.
- [205] H. Chen, Y. Ding, Y. He, and C. Tan, "Rheological behaviour of ethylene glycol based titania nanofluids," *Chemical Physics Letters*, vol. 444, no. 4, pp. 333–337, Aug. 2007.
- [206] P. K. Namburu, D. P. Kulkarni, D. Misra, and D. K. Das, "Viscosity of copper oxide nanoparticles dispersed in ethylene glycol and water mixture," *Experimental Thermal and Fluid Science*, vol. 32, no. 2, pp. 397–402, Nov. 2007.
- [207] C. T. Nguyen, F. Desgranges, N. Galanis, G. Roy, T. Maré, S. Boucher, and H. Angue Mintsa, "Viscosity data for Al₂O₃-water nanofluid—hysteresis: is heat transfer enhancement using nanofluids reliable?," *International Journal of Thermal Sciences*, vol. 47, no. 2, pp. 103–111, Feb. 2008.
- [208] N. Masoumi, N. Sohrabi, and A. Behzadmehr, "A new model for calculating the effective viscosity of nanofluids," *J. Phys. D: Appl. Phys.*, vol. 42, no. 5, p. 055501, Mar. 2009.
- [209] W. Duangthongsuk and S. Wongwises, "Measurement of temperature-dependent thermal conductivity and viscosity of TiO₂-water nanofluids," *Experimental Thermal and Fluid Science*, vol. 33, no. 4, pp. 706–714, Apr. 2009.

- [210] B. C. Sahoo, R. S. Vajjha, R. Ganguli, G. A. Chukwu, and D. K. Das, "Determination of Rheological Behavior of Aluminum Oxide Nanofluid and Development of New Viscosity Correlations," *Petroleum Science and Technology*, vol. 27, no. 15, pp. 1757–1770, Oct. 2009.
- [211] T. X. Phuoc and M. Massoudi, "Experimental observations of the effects of shear rates and particle concentration on the viscosity of Fe₂O₃-deionized water nanofluids," *International Journal of Thermal Sciences*, vol. 48, no. 7, pp. 1294–1301, Jan. 2009.
- [212] M. Chandrasekar, S. Suresh, and A. C. Bose, "Experimental investigations and theoretical determination of thermal conductivity and viscosity of Al₂O₃/water nanofluid," *Experimental Thermal and Fluid Science*, vol. 34, no. 2, pp. 210–216, 2010.
- [213] S. Masoud Hosseini, A. R. Moghadassi, and D. E. Henneke, "A new dimensionless group model for determining the viscosity of nanofluids," *J Therm Anal Calorim*, vol. 100, no. 3, pp. 873–877, Mar. 2010.
- [214] L. Godson, B. Raja, D. M. Lal, and S. Wongwises, "Experimental Investigation on the Thermal Conductivity and Viscosity of Silver-Deionized Water Nanofluid," *Experimental Heat Transfer*, vol. 23, no. 4, pp. 317–332, Sep. 2010.
- [215] M. Corcione, "Empirical correlating equations for predicting the effective thermal conductivity and dynamic viscosity of nanofluids," *Energy Conversion and Management*, vol. 52, no. 1, pp. 789–793, Jan. 2011.
- [216] B. C. Pak and Y. I. Cho, "HYDRODYNAMIC AND HEAT TRANSFER STUDY OF DISPERSED FLUIDS WITH SUBMICRON METALLIC OXIDE PARTICLES," *Experimental Heat Transfer*, vol. 11, no. 2, pp. 151–170, Apr. 1998.
- [217] M. Abareshi, S. H. Sajjadi, S. M. Zebarjad, and E. K. Goharshadi, "Fabrication, characterization, and measurement of viscosity of α -Fe₂O₃-glycerol nanofluids," *Journal of Molecular Liquids*, vol. 163, no. 1, pp. 27–32, Sep. 2011.
- [218] A. Takeuchi, H. Kato, and A. Inoue, "Vogel–Fulcher–Tammann plot for viscosity scaled with temperature interval between actual and ideal glass transitions for metallic glasses in liquid and supercooled liquid states," *Intermetallic*, vol. 18, no. 4, pp. 406–411, Jan. 2010.
- [219] L. Colla, L. Fedele, M. Scattolini, and S. Bobbo, "Water-Based Fe₂O₃ Nanofluid Characterization: Thermal Conductivity and Viscosity Measurements and Correlation," *Advances in Mechanical Engineering*, vol. 4, no. 0, pp. 674947–674947, Jan. 2012.
- [220] M. M. Heyhat, F. Kowsary, A. M. Rashidi, M. H. Momenpour, and A. Amrollahi, "Experimental investigation of laminar convective heat transfer and pressure drop of water-based Al₂O₃ nanofluids in fully developed flow regime," *Experimental Thermal and Fluid Science*, vol. 44, no. C, pp. 483–489, Jan. 2013.
- [221] M. H. Esfe and S. Saedodin, "An experimental investigation and new correlation of viscosity of ZnO–EG nanofluid at various temperatures and different solid volume fractions," *Experimental Thermal and Fluid Science*, vol. 55, pp. 1–5, Apr. 2014.

- [222] S. E. B. Maïga, C. T. Nguyen, N. Galanis, and G. Roy, "Heat transfer behaviours of nanofluids in a uniformly heated tube," *Superlattices and Microstructures*, vol. 35, no. 3, pp. 543–557, Mar. 2004.
- [223] W. J. Tseng and K.-C. Lin, "Rheology and colloidal structure of aqueous TiO₂ nanoparticle suspensions," *Materials Science and Engineering: A*, vol. 355, no. 1, pp. 186–192, Aug. 2003.
- [224] J. Garg, B. Poudel, M. Chiesa, J. B. Gordon, J. J. Ma, J. B. Wang, Z. F. Ren, Y. T. Kang, H. Ohtani, J. Nanda, G. H. McKinley, and G. Chen, "Enhanced thermal conductivity and viscosity of copper nanoparticles in ethylene glycol nanofluid," *J. Appl. Phys.*, vol. 103, no. 7, p. 4301, Apr. 2008.
- [225] M. Vakili, A. Mohebbi, and H. Hashemipour, "Experimental study on convective heat transfer of TiO₂ nanofluids," *Heat Mass Transfer*, vol. 49, no. 8, pp. 1159–1165, Jun. 2013.
- [226] K. S. Suganthi, N. Anusha, and K. S. Rajan, "Low viscous ZnO–propylene glycol nanofluid: a potential coolant candidate," *J Nanopart Res*, vol. 15, no. 10, pp. 1986–16, Sep. 2013.
- [227] D. Venerus, J. Buongiorno, R. Christianson, J. Townsend, I. C. Bang, G. Chen, S. J. Chung, M. Chyu, H. Chen, and Y. Ding, "Viscosity measurements on colloidal dispersions (nanofluids) for heat transfer applications," *Applied rheology*, vol. 20, no. 4, 2010.
- [228] C. Chen, M. Ma, K. Jin, J. Z. Liu, L. Shen, Q. Zheng, and Z. Xu, "Nanoscale fluid-structure interaction: Flow resistance and energy transfer between water and carbon nanotubes," *Phys. Rev. E*, vol. 84, no. 4, pp. 046314–8, Oct. 2011.
- [229] P. S. P. T. P Selvakumar, "An Experimental Study on Evacuated Tube Solar Collector using Therminol D-12 as Heat Transfer Fluid Coupled with Parabolic Trough," pp. 1–8, Feb. 2014.
- [230] M. M. Derakhshan, M. A. Akhavan-Behabadi, and S. G. Mohseni, "Experiments on mixed convection heat transfer and performance evaluation of MWCNT–Oil nanofluid flow in horizontal and vertical microfin tubes," *Experimental Thermal and Fluid Science*, vol. 61, no. C, pp. 241–248, Feb. 2015.
- [231] A. O. C. Gómez, A. R. K. Hoffmann, and E. P. B. Filho, "Experimental evaluation of CNT nanofluids in single-phase flow," *International Journal of Heat and Mass Transfer*, vol. 86, pp. –, Dec. 1992.
- [232] "Heat transfer enhancement by using nanofluids in forced convection flows," vol. 26, no. 4, pp. 530–546, Dec. 2004.
- [233] L. S. Sundar, K. V. Sharma, M. T. Naik, and M. K. Singh, "Empirical and theoretical correlations on viscosity of nanofluids_ A review," *Renewable and Sustainable Energy Reviews*, vol. 25, no. C, pp. 670–686, Sep. 2013.
- [234] T. Papanastasiou, G. Georgiou, and A. N. Alexandrou, *Viscous Fluid Flow*, 1st ed. CRC Press, 1999.
- [235] C. Gallegos, *Rheology - Volume I*. Encyclopedia of Life Support Systems (EOLSS), 2010.
- [236] T. Papanastasiou, G. Georgiou, and A. N. Alexandrou, *Viscous Fluid Flow*, 1st ed. CRC Press, 1999.
- [237] K. H. Sweeny and R. D. Geckler, "The Rheology of Suspensions," *J. Appl. Phys.*, vol. 25, no. 9, pp. 1135–1144, 1954.

- [238] "Rheology and Non-Newtonian Fluids," pp. 1–192, Jul. 2013.
- [239] R. K. Dash, K. N. Mehta, and G. Jayaraman, "Casson fluid flow in a pipe filled with a homogeneous porous medium," *International Journal of Engineering Science*, vol. 34, no. 10, pp. 1145–1156, 1996.
- [240] T. F. Tadros, *Rheology of Dispersions*. John Wiley & Sons, 2011.
- [241] G. Natale, M. C. Heuzey, P. J. Carreau, G. Ausias, and J. Férec, "Rheological modeling of carbon nanotube suspensions with rod-rod interactions," *AIChE J.*, vol. 60, no. 4, pp. 1476–1487, Dec. 2013.
- [242] K. B. Anoop, S. Kabelac, T. Sundararajan, and S. K. Das, "Rheological and flow characteristics of nanofluids: Influence of electroviscous effects and particle agglomeration," *J. Appl. Phys.*, vol. 106, no. 3, pp. 034909–8, 2009.
- [243] K. B. Anoop, S. K. Das, and S. Kabelac, "Experimental convective heat transfer studies in a turbulent flow regime using alumina-water nanofluids," *QScience Connect*, vol. 231, no. 2013, pp. 39–13, Mar. 2013.
- [244] S. Sen and T. Mukerji, "Diffusion and viscosity in silicate liquids: Percolation and effective medium theories," *Geophysical Research Letters*, vol. 24, no. 9, pp. 1015–1018, May 1997.
- [245] S. Koo and A. S. Sangani, "Effective-medium theories for predicting hydrodynamic transport properties of bidisperse suspensions," *Phys. Fluids*, vol. 14, no. 10, pp. 3522–13, 2002.
- [246] S. M. Dinh and R. C. Armstrong, "A Rheological Equation of State for Semiconcentrated Fiber Suspensions," *J. Rheol.*, vol. 28, no. 3, pp. 207–227, Jan. 1984.
- [247] C. I. Mendoza and I. Santamaría-Holek, "The rheology of hard sphere suspensions at arbitrary volume fractions: An improved differential viscosity model," *J. Chem. Phys.*, vol. 130, no. 4, pp. 044904–8, 2009.
- [248] E. S. G. Shaqfeh and G. H. Fredrickson, "The hydrodynamic stress in a suspension of rods," *Physics of Fluids A: Fluid Dynamics*, vol. 2, no. 1, pp. 7–24, Jan. 1990.
- [249] D. A. G. Bruggeman, "Berechnung verschiedener physikalischer Konstanten von heterogenen Substanzen. I. Dielektrizitätskonstanten und Leitfähigkeiten der Mischkörper aus isotropen Substanzen," *Ann. Phys.*, vol. 416, no. 7, pp. 636–664, 1935.
- [250] C. R. Sandstrom, *Interactions and Orientation in Concentrated Suspensions of Rigid Rods*. 1993.
- [251] C. Servais, A. Luciani, and J.-A. E. Månson, "Fiber-fiber interaction in concentrated suspensions: Dispersed fiber bundles," *J. Rheol.*, vol. 43, no. 4, pp. 1005–1018, Jul. 1999.
- [252] S. Le Corre, "Rheology of highly concentrated planar fiber suspensions," *J. Rheol.*, vol. 49, no. 5, pp. 1029–, n/a 2005.
- [253] A. W. K. Ma, K. M. Yearsley, F. Chinesta, and M. R. Mackley, "A review of the microstructure and rheology of carbon nanotube suspensions," *Proceedings of the Institution of Mechanical Engineers, Part N: Journal of Nanoengineering and Nanosystems*, vol. 222, no. 3, pp. 71–94, Jan. 2008.
- [254] F. Chinesta, "From Single-Scale to Two-Scales Kinetic Theory Descriptions of Rods Suspensions," *Archives of Computational Methods in Engineering*, vol. 20, no. 1, pp. 1–29, Feb. 2013.
- [255] M. Doi and S. F. Edwards, *The Theory of Polymer Dynamics*. Oxford

- University Press, 1988.
- [256] H. S. Hsich, "Dynamics of polymeric liquids, volume 2: Kinetic theory, R. Byron Bird, Charles F. Curtiss, Robert C. Armstrong, and Ole Hassager, Wiley-Interscience, New York, 1987, 437 pp. Price: \$65.00.," *Journal of Polymer Science Part C: Polymer Letters*, vol. 25, no. 12, pp. 511–511, 1987.
- [257] J. Férec, G. Ausias, M. C. Heuzey, and P. J. Carreau, "Modeling fiber interactions in semiconcentrated fiber suspensions," *J. Rheol.*, vol. 53, no. 1, pp. 49–72, Jan. 2009.
- [258] J. F. Brady and G. Bossis, "Stokesian Dynamics [electronic resource].," 1988.
- [259] H. A. BARNES, M. F. EDWARDS, and L. V. WOODCOCK, "Applications of Computer-Simulations to Dense Suspension Rheology," *Chemical Engineering Science*, vol. 42, no. 4, pp. 591–608, 1987.
- [260] P. Singh, T. I. Hesla, and D. D. Joseph, "Distributed Lagrange multiplier method for particulate flows with collisions," *International Journal of Multiphase Flow*, vol. 29, no. 3, pp. 495–509, Mar. 2003.
- [261] S. Childress, *An Introduction to Theoretical Fluid Mechanics*. Courant Institute of Mathematical Sciences, 2009.
- [262] J. W. S. B. Rayleigh, *The Theory of Sound*, no. 1. Macmillan, 1877.
- [263] I. M. Krieger, "Rheology of monodisperse latices," *Advances in Colloid and Interface Science*, vol. 3, no. 2, pp. 111–136, 1972.
- [264] E. J. Tozzi, *Hydrodynamics, rheology and conduction in suspensions of arbitrarily shaped fibers*. University of Wisconsin--Madison, 2008.
- [265] I. BALBERG, C. H. ANDERSON, S. ALEXANDER, and N. WAGNER, "Excluded Volume and Its Relation to the Onset of Percolation," *Physical Review B*, vol. 30, no. 7, pp. 3933–3943, 1984.
- [266] K. D. Sattler, *Handbook of Nanophysics*. CRC Press, 2010.
- [267] S. R. Broadbent and J. M. Hammersley, "Percolation processes. I. Crystals and Mazes," presented at the Proceedings of the Cambridge Philosophical Society, 1957, vol. 53, no. 3, pp. 629–641.
- [268] A. V. Kyrlyuk and P. van der Schoot, "Continuum percolation of carbon nanotubes in polymeric and colloidal media.," *Proc. Natl. Acad. Sci. U.S.A.*, vol. 105, no. 24, pp. 8221–8226, Jun. 2008.
- [269] D. J. Shaw, "Introduction to colloid and surface chemistry," 1992.
- [270] B. Derjaguin and L. Landau, "Theory of the stability of strongly charged lyophobic sols and of the adhesion of strongly charged particles in solutions of electrolytes," *Progress in Surface Science*, vol. 43, no. 1, pp. 30–59, 1993.
- [271] E. J. W. V. and OVERBEEK (J. Th. G, K. van NES, and J. T. G. OVERBEEK, *Theory of the Stability of Lyophobic Colloids. The Interaction of Sol Particles Having an Electric Double Layer. By E.J.W. Verwey and J. Th. G. Overbeek ... with the Collaboration of K. Van Nes*. 1948.
- [272] C. Schneider, "The Surface Charge of Soft and Hard Sphere Colloidal Particles-Experimental Investigation and Comparison to Theory," 2011.
- [273] R. Heyd, *Nanofluids for Heat Transfer*. 2011.
- [274] J. Huang, X. Wang, Q. Long, and X. Wen, "Influence of pH on the stability characteristics of nanofluids," *2009 Symposium on Photonics and Optoelectronics*, pp. 1–4, 2009.

- [275] S. K. Das, N. Putra, and W. Roetzel, "Pool boiling characteristics of nano-fluids," *International Journal of Heat and Mass Transfer*, vol. 46, no. 5, pp. 851–862, 2003.
- [276] Y. Xuan, "Aggregation Structure and Thermal Conductivity of Nanofluids," pp. 1–6, May 2003.
- [277] X. Cao, J. Chen, S. Wen, C. Peng, M. Shen, and X. Shi, "Effect of surface charge of polyethyleneimine-modified multiwalled carbon nanotubes on the improvement of polymerase chain reaction," *Nanoscale*, vol. 3, no. 4, pp. 1741–1747, 2011.
- [278] C. T. Nguyen, F. Desgranges, G. Roy, N. Galanis, T. Maré, S. Boucher, and H. Angue Mintsa, "Temperature and particle-size dependent viscosity data for water-based nanofluids – Hysteresis phenomenon," *International Journal of Heat and Fluid Flow*, vol. 28, no. 6, pp. 1492–1506, Dec. 2007.
- [279] S. Zhiyao, W. Tingting, X. Fumin, and L. Ruijie, "A simple formula for predicting settling velocity of sediment particles," *Water Science and Engineering*, vol. 1, no. 1, pp. 37–43, 2008.
- [280] S. M. Peker and S. S. Helvacı, *Solid-Liquid Two Phase Flow*. Elsevier Science, 2011.
- [281] G. G. Stokes, *On the Effect of the Internal Friction of Fluids on the Motion of Pendulums*. Cambridge: Cambridge University Press, 2009, pp. 1–10.
- [282] D. Fromer and D. Lerche, "An experimental approach to the study of the sedimentation of dispersed particles in a centrifugal field," *Archive of Applied Mechanics*, vol. 72, no. 2, pp. 85–95, Apr. 2002.
- [283] F. Balboa Usabiaga, B. Kallemov, B. Delmotte, A. Pal Singh Bhalla, B. E. Griffith, and A. Donev, "Hydrodynamics of Suspensions of Passive and Active Rigid Particles: A Rigid Multiblob Approach," *arXiv.org*, vol. 1602. p. arXiv:1602.02170, Feb-2016.
- [284] C. D. Robinson, "Some Factors Influencing Sedimentation," *Ind. Eng. Chem.*, vol. 18, no. 8, pp. 869–871, Aug. 1926.
- [285] J. C. Winterwerp, "On the flocculation and settling velocity of estuarine mud," *Continental Shelf Research*, vol. 22, no. 9, pp. 1339–1360, Jun. 2002.
- [286] J. M. Coulson, "Coulson And Richardson's Chemical Engineering, Volume 2," *disp*, 1962.
- [287] F. H. Bark, "Hydrodynamics of Suspensions. By M. UNGARISH. Springer, 1993. 322 pp. DM 138.," *J. Fluid Mech.*, vol. 290, pp. 406–408, 1995.
- [288] J. F. Richardson and W. N. Zaki, "Sedimentation and fluidisation: Part I," *Chemical Engineering Research and Design*, vol. 75, pp. S82–S100, Dec. 1997.
- [289] G. Anestis and W. Schneider, "Application of the theory of kinematic waves to the centrifugation of suspensions," *Ingenieur-Archiv*, vol. 53, no. 6, pp. 399–407, 1983.
- [290] D. Lerche, "Dispersion Stability and Particle Characterization by Sedimentation Kinetics in a Centrifugal Field," *Journal of Dispersion Science and Technology*, vol. 23, no. 5, pp. 699–709, Feb. 2013.
- [291] G. K. Batchelor, "Sedimentation in a dilute dispersion of spheres," *J. Fluid Mech.*, vol. 52, no. 2, pp. 245–268, n/a 1972.
- [292] A. T. Corey, *Influence of shape on the fall velocity of sand grains*

- [unpublished M. Sc. thesis]: Colorado A&M College. Fort Collins, 1949.
- [293] H. Yu, Y. Qu, Z. Dong, W. J. Li, Y. Wang, W. Ren, and Z. Cui, *Separation of mixed SWNTs and MWNTs by centrifugal force - an experimental study*. IEEE, 2007, pp. 1212–1216.
- [294] R. H. Davis and K. H. Birdsell, “Hindered settling of semidilute monodisperse and polydisperse suspensions,” *AIChE J.*, vol. 34, no. 1, pp. 123–129, Jan. 1988.
- [295] J. Labille and J. Brant, “Stability of nanoparticles in water,” *Nanomedicine*, vol. 5, no. 6, pp. 985–998, Aug. 2010.
- [296] “Nanoscale and Microscale Thermophysical Engineering,” pp. 1–17, Jan. 2013.
- [297] J. L. Bahr, E. T. Mickelson, and M. J. Bronikowski, “Dissolution of small diameter single-wall carbon nanotubes in organic solvents?,” *Chemical Communications*, no. 2, pp. 193–194, 2001.
- [298] K. Esumi, M. Ishigami, A. Nakajima, K. Sawada, and H. Honda, *Chemical treatment of carbon nanotubes*, vol. 34, no. 2. Carbon, 1996, pp. 279–281.
- [299] M. A. Hamon, H. Hu, P. Bhowmik, S. Niyogi, B. Zhao, M. E. Itkis, and R. C. Haddon, “End-group and defect analysis of soluble single-walled carbon nanotubes,” *Chemical Physics Letters*, vol. 347, no. 1, pp. 8–12, Oct. 2001.
- [300] J. Chen, A. M. Rao, S. Lyuksyutov, M. E. Itkis, M. A. Hamon, H. Hu, R. W. Cohn, P. C. Eklund, D. T. Colbert, R. E. Smalley, and R. C. Haddon, “Dissolution of Full-Length Single-Walled Carbon Nanotubes,” *J. Phys. Chem. B*, vol. 105, no. 13, pp. 2525–2528, Apr. 2001.
- [301] S. Shenogin, A. Bodapati, L. Xue, R. Ozisik, and P. Keblinski, “Effect of chemical functionalization on thermal transport of carbon nanotube composites,” *Appl. Phys. Lett.*, vol. 85, no. 1, p. 2229, Sep. 2004.
- [302] J. P. Davim, *Design of Experiments in Production Engineering*. Cham: Springer, 2015.
- [303] J. J. Louviere, D. A. Hensher, and J. D. Swait, *Stated Choice Methods*. Cambridge University Press, 2000.
- [304] M. W. Marshall, S. Popa-Nita, and J. G. Shapter, “Measurement of functionalised carbon nanotube carboxylic acid groups using a simple chemical process,” *Carbon*, vol. 44, no. 7, pp. 1137–1141, Jun. 2006.
- [305] M. A. Turgunov, J. O. Oh, and S. H. Yoon, “Surface Modification of Multiwall Carbon Nanotubes by Sulfuric Acid and Nitric Acid,” presented at the Materials 2014, 2014, pp. 22–25.
- [306] S. A. Shamsuddin, N. H. A. Halim, N. Deraman, and U. Hashim, “The characterization study of functionalized multi-wall carbon nanotubes purified by acid oxidation,” presented at the 2011 IEEE Regional Symposium on Micro and Nanoelectronics, RSM 2011 - Programme and Abstracts, 2011, pp. 263–265.
- [307] C. Warakulwit, J. Majimel, M. H. Delville, P. Garrigue, J. Limtrakul, and A. Kuhn, “Controlled purification, solubilisation and cutting of carbon nanotubes using phosphomolybdic acid,” *Journal of Materials Chemistry*, vol. 18, no. 34, pp. 4056–4061, Sep. 2008.
- [308] Y. Tian, H. Jiang, J. V. Pfaler, Z. Zhu, A. G. Nasibulin, T. Nikitin, B. Aitchison, L. Khriachtchev, D. P. Brown, and E. I. Kauppinen, “Analysis of

- the Size Distribution of Single-Walled Carbon Nanotubes Using Optical Absorption Spectroscopy," *J. Phys. Chem. Lett.*, vol. 1, no. 7, pp. 1143–1148, Apr. 2010.
- [309] H. Xu, X. Cheng, J. Zhong, J. Meng, M. Yang, F. Jia, Z. Xu, and H. Kong, "Characterization of multiwalled carbon nanotubes dispersing in water and association with biological effects," *Journal of Nanomaterials*, vol. 2011, Oct. 2011.
- [310] C. Bantz, O. Koshkina, T. Lang, H.-J. Galla, C. J. Kirkpatrick, R. H. Stauber, and M. Maskos, "The surface properties of nanoparticles determine the agglomeration state and the size of the particles under physiological conditions," *Beilstein J. Nanotechnol.*, vol. 5, no. 1, pp. 1774–1786, 2014.
- [311] H. Hu, A. Yu, E. Kim, B. Zhao, M. E. Itkis, E. Bekyarova, and R. C. Haddon, "Influence of the Zeta Potential on the Dispersability and Purification of Single-Walled Carbon Nanotubes," *J. Phys. Chem. B*, vol. 109, no. 23, pp. 11520–11524, Jan. 2013.
- [312] "Spectrochemical Analysis," pp. 1–9, Nov. 2007.
- [313] D. Lerche and T. Sobisch, "Consolidation of concentrated dispersions of nano- and microparticles determined by analytical centrifugation," *Powder Technology*, vol. 174, no. 1, pp. 46–49, Feb. 2007.
- [314] M. A. Atieh, O. Y. Bakather, B. Al-Tawbini, A. A. Bukhari, F. A. Abuilaiwi, and M. B. Fettouhi, "Effect of Carboxylic Functional Group Functionalized on Carbon Nanotubes Surface on the Removal of Lead from Water," *Bioinorganic Chemistry and Applications*, vol. 2010, no. 11, pp. 1–9, 2010.
- [315] P.-C. Ma, S.-Y. Mo, B.-Z. Tang, and J.-K. Kim, "Dispersion, interfacial interaction and re-agglomeration of functionalized carbon nanotubes in epoxy composites," *Carbon*, vol. 48, no. 6, pp. 1824–1834, May 2010.
- [316] A. Choudhury and P. Kar, "Doping effect of carboxylic acid group functionalized multi-walled carbon nanotube on polyaniline," *Composites Part B*, vol. 42, no. 6, pp. 1641–1647, Sep. 2011.
- [317] R. J. Zasoski, "Zeta potential," in *Encyclopedia of Soil Science*, no. 644, Dordrecht: Springer Netherlands, 2008, pp. 841–845.
- [318] J. M. P. Q. Delgado, "Experimental data of solubility at different temperatures: a simple technique," *Heat Mass Transfer*, vol. 43, no. 12, pp. 1311–1316, Nov. 2006.
- [319] A. V. Delgado, F. González-Caballero, R. J. Hunter, L. K. Koopal, J. Lyklema, International Union of Pure and Applied Chemistry, Physical and Biophysical Chemistry Division IUPAC Technical Report, "Measurement and interpretation of electrokinetic phenomena," *J Colloid Interface Sci*, vol. 309, no. 2, pp. 194–224, May 2007.
- [320] E. J. W. Verwey, "Theory of the stability of lyophobic colloids," *J Phys Colloid Chem*, vol. 51, no. 3, pp. 631–636, May 1947.
- [321] M. Zahn, Y. Ohki, D. B. Fenneman, R. J. Gripshover, and V. H. Gehman, "Dielectric Properties of Water and Water/Ethylene Glycol Mixtures for Use in Pulsed Power System Design," *Proceedings of the IEEE*, vol. 74, no. 9, pp. 1182–1221, Jan. 1986.
- [322] G. Akerlof, "Dielectric constants of some organic solvent-water mixtures at various temperatures," *Journal of the American Chemical Society*, vol. 54, no. 11, pp. 4125–4139, 1932.

- [323] K. Y. Chu and A. R. Thompson, "Densities and Refractive Indices of Glycol Ether-Water Solutions.," *Journal of Chemical & Engineering Data*, vol. 5, no. 2, pp. 147–149, 1960.
- [324] J. H. Lehman, M. Terrones, E. Mansfield, K. E. Hurst, and V. Meunier, "Evaluating the characteristics of multiwall carbon nanotubes," *Carbon*, vol. 49, no. 8, pp. 2581–2602, Jul. 2011.
- [325] T. Yiamsawas, O. Mahian, A. S. Dalkilic, S. Kaewnai, and S. Wongwises, "Experimental studies on the viscosity of TiO₂ and Al₂O₃ nanoparticles suspended in a mixture of ethylene glycol and water for high temperature applications," *Applied Energy*, vol. 111, no. C, pp. 40–45, Nov. 2013.
- [326] P. Mishra, S. Mukherjee, S. Nayak, and A. Panda, "A brief review on viscosity of nanofluids," *Int Nano Lett*, pp. 1–12, 2014.
- [327] M. Kole and T. K. Dey, "Thermal conductivity and viscosity of Al₂O₃ nanofluid based on car engine coolant," *J. Phys. D: Appl. Phys.*, vol. 43, no. 31, p. 315501, Aug. 2010.
- [328] N. S. Shanker, M. C. S. Reddy, and V. B. Rao, "On Prediction Of Viscosity Of Nanofluids For Low Volume Fractions Of Nanoparticles," *International Journal of Engineering*, vol. 1, no. 8, 2012.
- [329] L. Wang and J. Fan, "Nanofluids Research: Key Issues," *Nanoscale Res Lett*, vol. 5, no. 8, pp. 1241–1252, Jun. 2010.
- [330] G. C. xe9, J. Comtet, A. N. X. s, L. X. R. Bocquet, A. Siria, G. Ducouret, F. X. O. Lequeux, N. Lenoir, G. Ovarlez, and A. Colin, "Shear thinning in non-Brownian suspensions," *Soft Matter*, pp. 1–15, Dec. 2017.
- [331] E. Michaelides, C. T. Crowe, and J. D. Schwarzkopf, *Multiphase Flow Handbook, Second Edition*. CRC Press, 2016.
- [332] S. Ghasemi and A. Karimipour, "Experimental investigation of the effects of temperature and mass fraction on the dynamic viscosity of CuO-paraffin nanofluid," *Applied Thermal Engineering*, vol. 128, pp. 189–197, Jan. 2018.
- [333] S. T. Huxtable, D. G. Cahill, S. Shenogin, L. Xue, R. Ozisik, P. Barone, M. Usrey, M. S. Strano, G. Siddons, M. Shim, and P. Keblinski, "Interfacial heat flow in carbon nanotube suspensions," *Nature Materials*, vol. 2, pp. 731 EP –.
- [334] C. R. WILDEMUTH and M. C. WILLIAMS, "Viscosity of Suspensions Modeled with a Shear-Dependent Maximum Packing Fraction," *Rheol Acta*, vol. 23, no. 6, pp. 627–635, 1984.
- [335] J. Z. Q. Zhou, P. H. T. Uhlherr, and F. T. Luo, "Yield stress and maximum packing fraction of concentrated suspensions," *Rheol Acta*, vol. 34, no. 6, pp. 544–561, 1995.
- [336] D. Quemada, "Rheology of concentrated disperse systems and minimum energy dissipation principle," *Rheol Acta*, vol. 16, no. 1, pp. 82–94, 1977.
- [337] R. Mondragón, J. Enrique Julia, A. Barba, and J. C. Jarque, "Determination of the packing fraction of silica nanoparticles from the rheological and viscoelastic measurements of nanofluids," *Chemical Engineering Science*, vol. 80, pp. 119–127, Oct. 2012.
- [338] K. Kalidasan and P. R. Kanna, "Effective utilization of MWCNT-water nanofluid for the enhancement of laminar natural convection inside the open square enclosure," *Journal of the Taiwan Institute of Chemical*

- Engineers*, vol. 65, no. C, pp. 331–340, Aug. 2016.
- [339] P. Amani and K. Vajravelu, “Intelligent modeling of rheological and thermophysical properties of green covalently functionalized graphene nanofluids containing nanoplatelets,” *International Journal of Heat and Mass Transfer*, vol. 120, pp. 95–105, May 2018.
- [340] T. Yousefi, F. Veysi, E. Shojaeizadeh, and S. Zinadini, “An experimental investigation on the effect of Al₂O₃-H₂O nanofluid on the efficiency of flat-plate solar collectors,” *Renewable Energy*, vol. 39, no. 1, pp. 293–298, Apr. 2012.
- [341] J. Jaccard, “Interaction Effects in Factorial Analysis of Variance,” 1998.
- [342] B. C. Lamas, “Nanofluids development and characterization for heat exchanging intensification,” 2013.

APPENDIX

A. Effective Viscosity Experimental Layout

MWCNTs	Base Fluid	Volume Fraction [%]	Temperature [K]	Shear Rate [s ⁻¹]	Runs
D20-40 L1-2	30%EG+70%DW	0,25	283 to 313	85,4 to 305,1	1 to 49
		0,50			50 to 98
		0,75			99 to 147
		1,00			148 to 196
		1,50			197 to 245
D20-40 L1-2	60%EG+40%DW	0,25	283 to 313	85,4 to 305,1	246 to 294
		0,50			295 to 343
		0,75			344 to 392
		1,00			393 to 441
		1,50			442 to 490
D20-40 L5-15	30%EG+70%DW	0,25	283 to 313	85,4 to 305,1	491 to 539
		0,50			540 to 588
		0,75			589 to 637
		1,00			638 to 686
		1,50			687 to 735
D20-40 L5-15	60%EG+40%DW	0,25	283 to 313	85,4 to 305,1	736 to 784
		0,50			785 to 833
		0,75			834 to 882
		1,00			883 to 931
		1,50			932 to 980
D20-40 L10-30	30%EG+70%DW	0,25	283 to 313	85,4 to 305,1	981 to 1029
		0,50			1030 to 1078
		0,75			1079 to 1127
		1,00			1128 to 1176
		1,50			1177 to 1225
D20-40 L10-30	60%EG+40%DW	0,25	283 to 313	85,4 to 305,1	1226 to 1274
		0,50			1275 to 1323
		0,75			1324 to 1372
		1,00			1373 to 1421
		1,50			1422 to 1470
D60-100 L1-2	30%EG+70%DW	0,25	283 to 313	85,4 to 305,1	1471 to 1519
		0,50			1520 to 1568
		0,75			1569 to 1617
		1,00			1618 to 1666
		1,50			1667 to 1715
D60-100 L1-2	60%EG+40%DW	0,25	283 to 313	85,4 to 305,1	1716 to 1764
		0,50			1765 to 1813
		0,75			1814 to 1862
		1,00			1863 to 1911
		1,50			1912 to 1960
D60-100 L5-15	30%EG+70%DW	0,25	283 to 313	85,4 to 305,1	1961 to 2009
		0,50			2010 to 2058
		0,75			2059 to 2107
		1,00			2108 to 2156
		1,50			2157 to 2205
D60-100 L5-15	60%EG+40%DW	0,25	283 to 313	85,4 to 305,1	2206 to 2254
		0,50			2255 to 2303
		0,75			2304 to 2352
		1,00			2353 to 2401
		1,50			2402 to 2450
D50-80 L10-20	30%EG+70%DW	0,25	283 to 313	85,4 to 305,1	2451 to 2499
		0,50			2500 to 2548
		0,75			2549 to 2597
		1,00			2598 to 2646
		1,50			2647 to 2695
D50-80 L10-20	60%EG+40%DW	0,25	283 to 313	85,4 to 305,1	2696 to 2744
		0,50			2745 to 2793
		0,75			2794 to 2842
		1,00			2843 to 2891
		1,50			2892 to 2940

B. Base Fluids Thermal and Transport Properties

Table B.1 - Thermal and transport properties of 30%EG+70%DW [1]

Base Fluid: 30%EG + 70%DW				
Temperature	Viscosity	Density	Specific Heat	Thermal Conductivity
[K]	[mPa.s]	[kg/m ³]	[kJ/kg K]	[W/m K]
283,15	2,950	1050,0	3,617	0,442
293,15	2,202	1046,0	3,648	0,453
298,15	1,927	1043,9	3,663	0,459
303,15	1,696	1041,5	3,678	0,464
313,15	1,346	1037,6	3,704	0,473
323,15	1,088	1033,5	3,734	0,481
333,15	0,900	1027,6	3,780	0,492

Table B.2 - Thermal and transport properties of 60%EG+40%DW [1]

Base Fluid: 60%EG + 40%DW				
Temperature	Viscosity	Density	Specific Heat	Thermal Conductivity
[K]	[mPa.s]	[kg/m ³]	[kJ/kg K]	[W/m K]
283,15	7,850	1091,9	3,044	0,340
293,15	5,402	1087,0	3,085	0,349
298,15	4,547	1084,3	3,107	0,352
303,15	3,860	1081,4	3,130	0,355
313,15	2,850	1076,3	3,174	0,360
323,15	2,170	1071,9	3,216	0,365
333,15	1,690	1064,9	3,255	0,371

C. Apparatus For The Viscosity Measurement

In Figure 1, it is schematically represented the double jacketed small sampler adapter used for the effective viscosity measurement. This enables the control of the sampler temperature, through a Brookfield circulating temperature bath, maintaining the sampler temperature constant during the measurements. Maintaining a steady temperature is detrimental since temperature gradients through the sampler can lead to erratic measurements. All the test were carried during the night to eliminate any possible source of noise in the measurements.

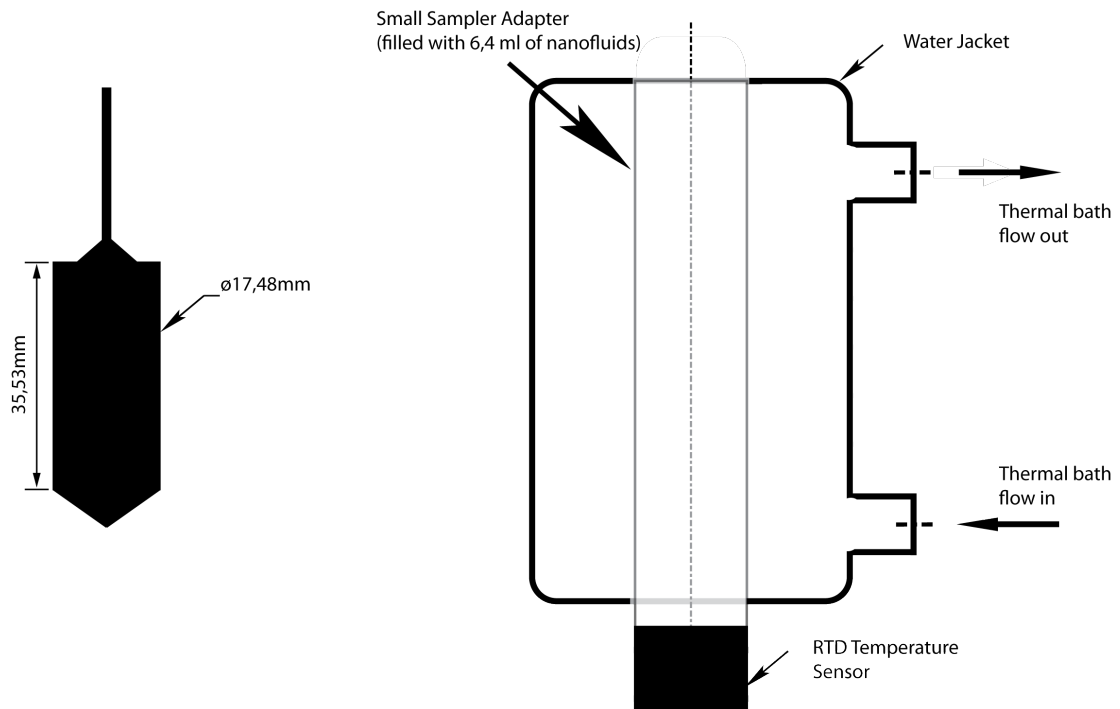


Figure C.1 – Schematic illustration of the double jacketed small sampler adapter for the measurement of the effective viscosity.

D. Experimental Uncertainties Analysis

Any things that can be measured have an associated error. Even under ideal conditions, repeated measurements of a reference standard, will give different readings. The measurement of the rheology properties of fluids requires not only one device but also a group of devices to measure the temperature, density, specific heat, etc. Therefore, to increase the confidence on the experimental measurements, one must consider the accuracy of each individual measuring devices [2].

Volume Fraction Experimental Uncertainties

As described in Equation 3.19, the evaluation of the volume fraction is a function of the measurement of carbon nanotubes mass and the base fluid volume. Thus the uncertainty of these measurements is given as [3] :

$$\Delta\phi = \sqrt{\left(\frac{\partial\phi}{\partial m_{MWCNT}}\right)^2 \Delta m_{MWCNT}^2 + \left(\frac{\partial\phi}{\partial V_{bf}}\right)^2 \Delta V_{bf}^2} \quad \text{Eq. 1.1}$$

which, considering Eq. 3.19 it becomes:

$$\Delta\phi = \sqrt{\left(\frac{\rho_{MWCNT} V_{bf}}{(m_{MWCNT} \rho_{MWCNT} + V_{bf})^2}\right)^2 \Delta m_{MWCNT}^2 + \left(\frac{m_{MWCNT} \rho_{MWCNT}}{(m_{MWCNT} \rho_{MWCNT} + V_{bf})^2}\right)^2 \Delta V_{bf}^2} \quad \text{Eq. 1.2}$$

where,

$$\Delta V_{bf} = \Delta V_{DW} + \Delta V_{EG} = 2\Delta V = 1ml \quad \text{Eq. 1.3}$$

$$\Delta m_{MWCNT} = 0,001g \quad \text{Eq. 1.4}$$

Diameter and Length Distribution Uncertainties

The diameter and length distribution of the bulk and dispersed MWCNTs were measured through SEM image analysis. However, as mention on Chapter 3, a SEM image is a projection of a 3D structure in a 2D plan. Therefore, any estimation of the uncertainty of this analysis is extremely difficult to achieve. Nevertheless, it was considered that the MWCNTs sizes comply within a normal distribution, enabling to estimate the 95% confidence interval of the measured samples. To this end, the standard deviation of the measured diameter and lengths sizes can be expressed as:

$$\sigma = \sqrt{\frac{1}{N-1} \sum_{i=1}^N (X_i - \bar{X})^2} \quad \text{Eq. 1.5}$$

where \bar{X} is the sizes means, and N is the sample size.

From this, the samples 95% confidence interval may be expressed as:

$$[\bar{X} - 2\sigma; \bar{X} + 2\sigma] \quad \text{Eq. 1.6}$$

and the estimated 95% confidence interval for the expected mean size is given by:

$$\bar{X}_{expected} = \bar{X} \pm \Delta\bar{X} \quad \text{Eq. 1.7}$$

where

$$\Delta\bar{X} = Z \frac{\sigma}{\sqrt{N}} \quad \text{Eq. 1.8}$$

where $Z=1,96$ (see normal distribution table) and N is the samples size.

Experimental Zeta Potential Uncertainties

As mention on section 4.2.1, a *Malvern ZS Nano S analyser* was used to evaluate the Zeta potential of the dispersed samples of MWCNTs. For each sample, five measurements were taken and the average calculated. Nevertheless, in each run, the equipment provide several measurements and a dedicated software automatically provide the mean standard deviation and the mean standard error. Therefore, the uncertainty of this measurement is the average of the five mean standard error estimated by the equipment. In Table XXX is provided the mean standard error of each run and the overall mean uncertainty of each sample.

Table D.1 – Standard error of the Zeta potential measurements for each run and the overall mean.

Base Fluid	MWCNTs	$\Delta\xi_1$	$\Delta\xi_2$	$\Delta\xi_3$	$\Delta\xi_4$	$\Delta\xi_5$	$\Delta\bar{\xi}$
30%EG + 70%DW	D20-40 L1-2	9,9	9,7	10,3	8,8	9,4	9,6
	D20-40 L5-15	11,4	9,9	8,8	3,8	9,6	8,7
	D20-40 L10-30	6,4	7,0	7,3	7,5	7,0	7,0
	D60-100 L1-2	8,3	7,1	8,0	7,6	7,6	7,7
	D60-100 L5-15	9,0	8,3	8,9	8,8	10,9	9,2
	D50-80 L10-20	6,8	7,4	6,7	6,7	7,0	6,9
60%EG + 40%DW	D20-40 L1-2	10,9	9,0	8,4	7,9	8,3	8,9
	D20-40 L5-15	9,5	9,5	8,8	7,9	9,6	9,1
	D20-40 L10-30	8,8	10,9	8,0	9,4	8,9	9,2
	D60-100 L1-2	7,0	8,2	7,3	8,2	7,4	7,6
	D60-100 L5-15	7,2	7,7	8,5	7,8	9,7	8,2
	D50-80 L10-20	9,1	10,0	11,3	9,4	9,9	10,0

Experimental Phase Separation Rate Uncertainties

The phase separation rate was evaluated by a *Stability Analyser LUMiSizer 6120* as explained in detail in Section 4.2.1.. The standard deviation error of the mean phase separation rate at the highest RCF, was used as the experimental uncertainty, and was calculated by the dedicated instrument software. Nevertheless, these results were used to extrapolate the phase separation rate for earth gravity (RCF=1). Considering a linear correlation between phase separation and RCF, the mean standard deviation was estimated through the following expression:

$$\Delta\bar{y} = \sqrt{\frac{\sum_{i=1}^N (y_i - m_c x_i)^2}{N - 2}} \quad \text{Eq. 1.9}$$

Experimental Density Uncertainties

As envisaged in Section 4.3, the evaluation of the samples density was achieved by a U-tube digital density meter. From these measurements, the standard deviation error of the mean density was calculated and it was considered as the experimental uncertainties.

Experimental Viscosity Uncertainties

As mention of Section 5.2.1, the Brookfield DV-III Plus rheometer has a declared accuracy of 2% of the full-scale range of the selected spindle/speed combination. Despite the experimental results present a good repeatability of the measurements, a t-Student distribution was considered to estimate the limits of the confidence interval of the experimental viscosity mean. The t-Student distribution was considered since the variance of the sample is an unknown parameter. Therefore, the standard deviation of the effective viscosity mean can be expressed as:

$$\sigma = \sqrt{\frac{1}{N - 1} \sum_{i=1}^N (\mu_i - \bar{\mu})^2} \quad \text{Eq. 1.10}$$

where $\bar{\mu}$ is the viscosity mean, and N the sample size ($N \geq 10$).

The estimated 95% confidence interval for the expected viscosity mean for 9 degree of freedom, is given by:

$$\bar{x}_{expected} = \bar{\mu} \pm \Delta\bar{\mu} \quad \text{Eq. 1.11}$$

where,

$$\Delta\bar{\mu} = t_{9,95} \frac{\sigma}{\sqrt{N}} \quad \text{Eq. 1.12}$$

and $t_{9,95} = 2,292$.

E. Functionalized MWCNTs Size Distributions

D20-40 L1-2

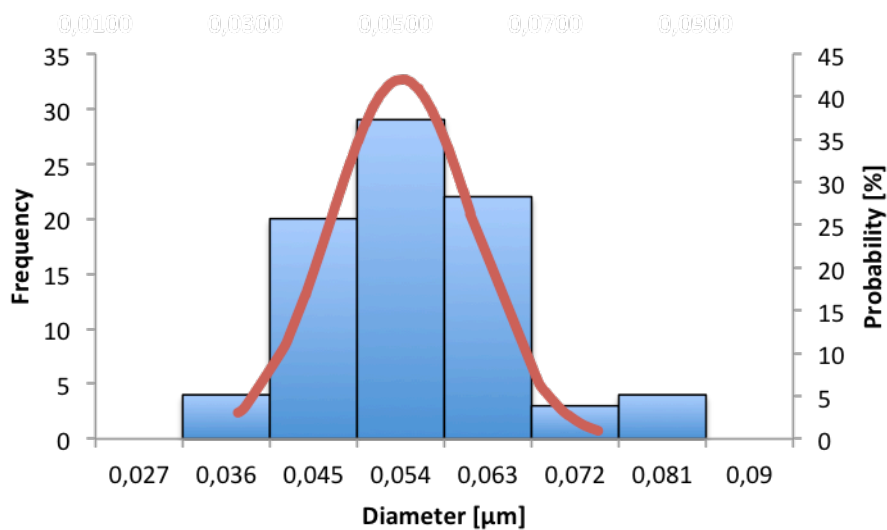


Figure E.1 – Diameter distribution of the dispersed D20-40 L1-2 MWCNT

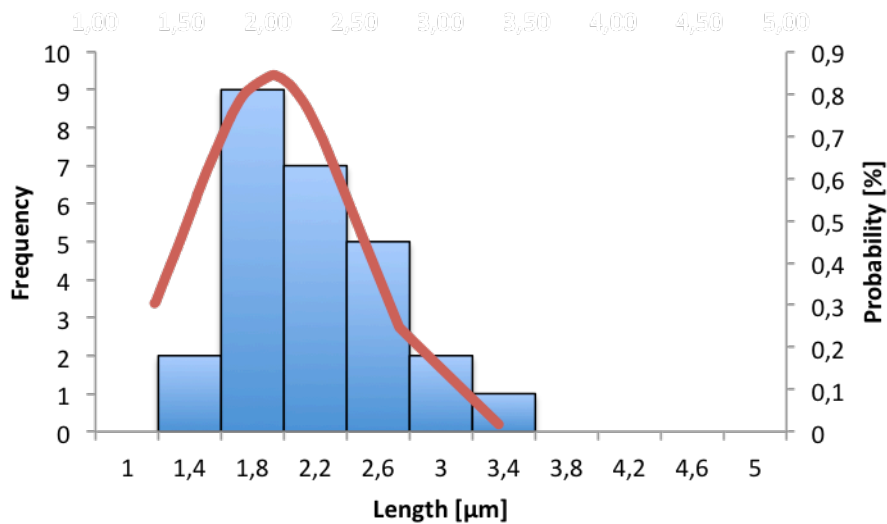


Figure E.2 – Length distribution of the dispersed D20-40 L1-2 MWCNT

D20-40 L5-15

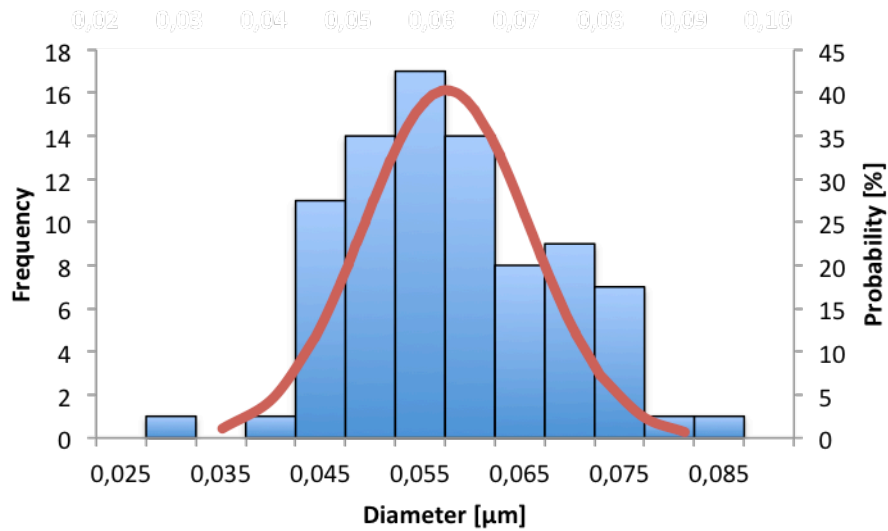


Figure E.3 – Diameter distribution of the dispersed D20-40 L5-15 MWCNT

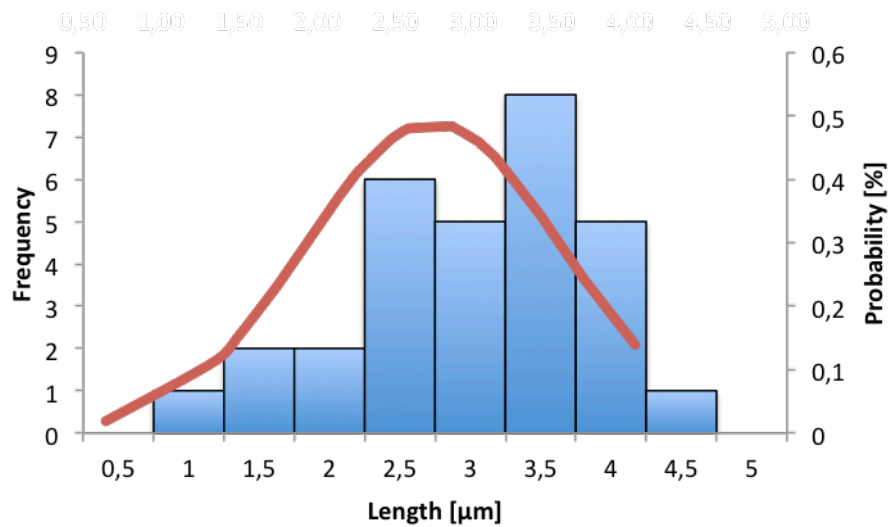


Figure E.4 – Length distribution of the dispersed D20-40 L5-15 MWCNT

D20-40 L10-30

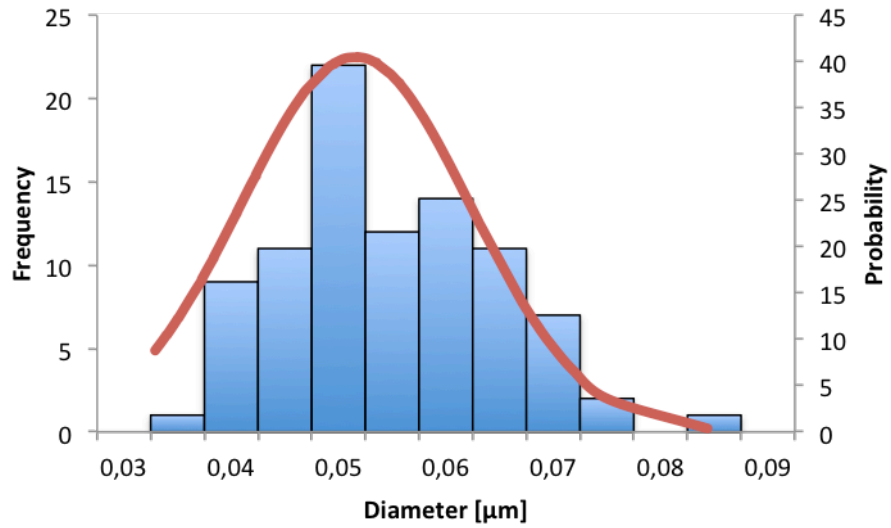


Figure E.5 – Diameter distribution of the dispersed D20-40 L10-30 MWCNT

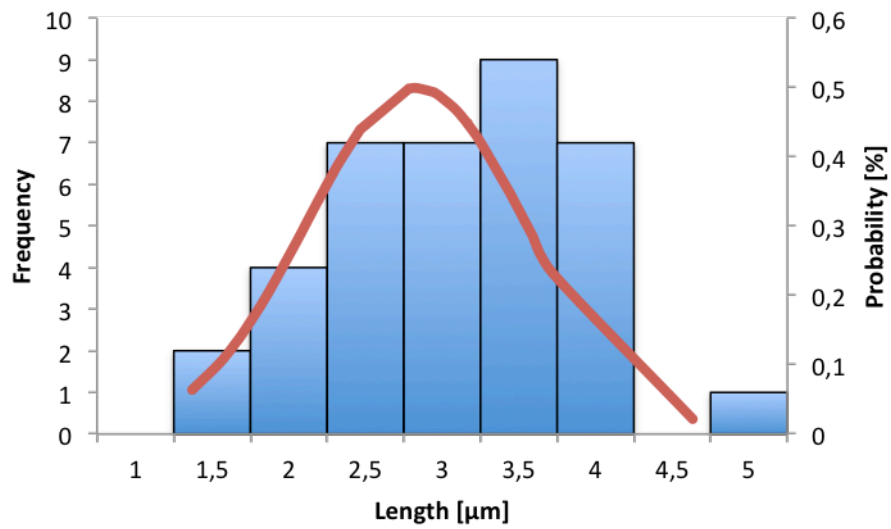


Figure E.6 – Length distribution of the dispersed D20-40 L10-30 MWCNT

D60-100 L1-2

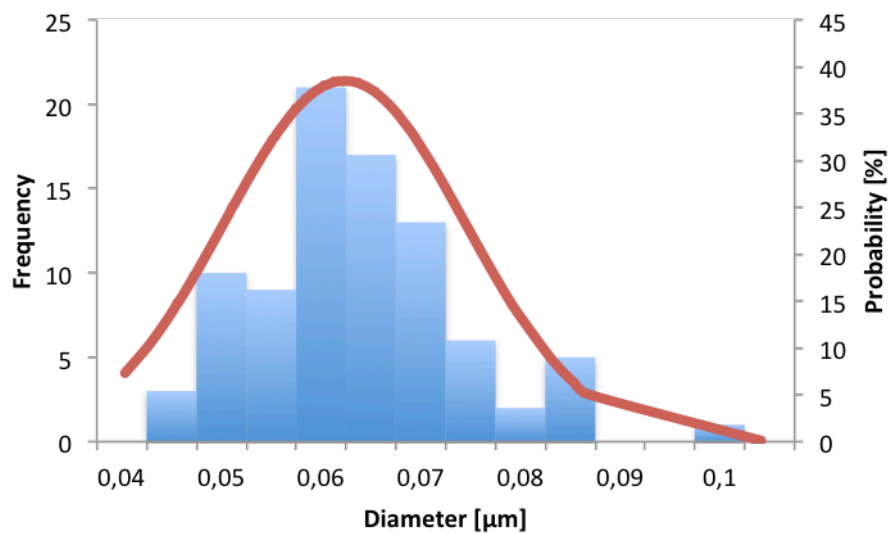


Figure E.7 – Diameter distribution of the dispersed D60-100 L1-2 MWCNT

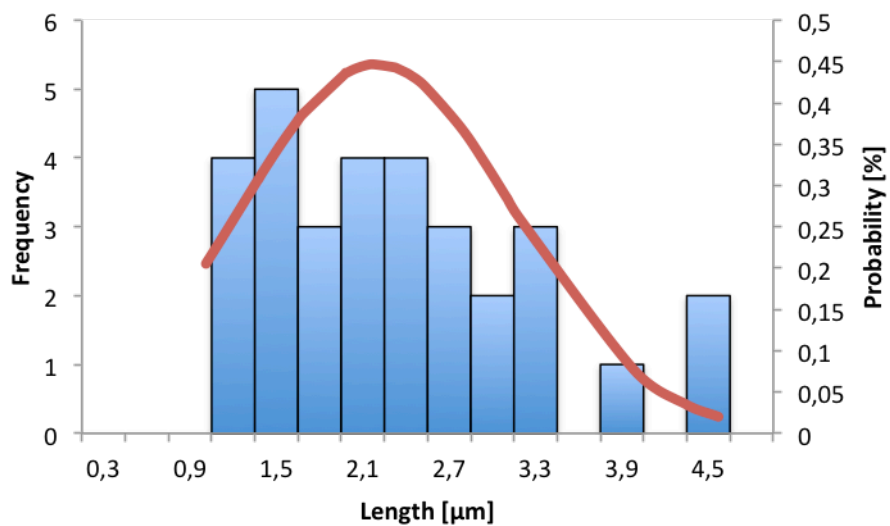


Figure E.8 – Length distribution of the dispersed D60-100 L1-2 MWCNT

D60-100 L5-15

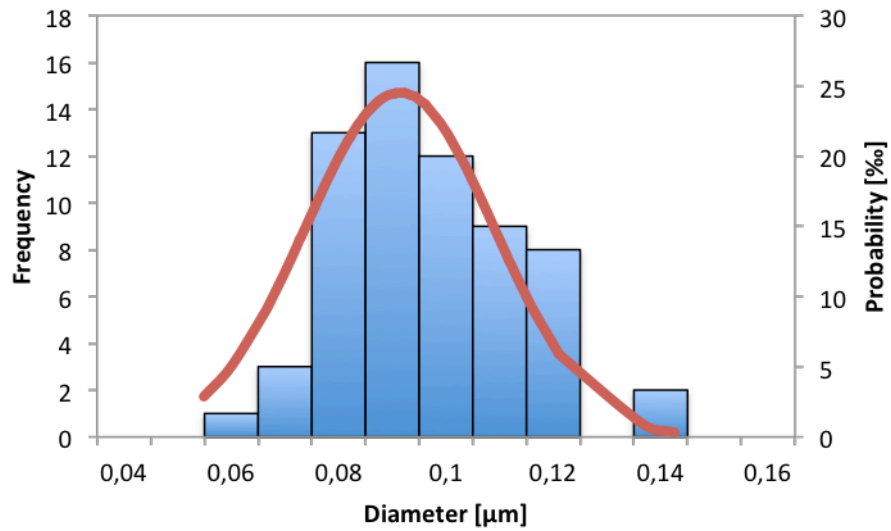


Figure E.9 – Diameter distribution of the dispersed D60-100 L5-15 MWCNT

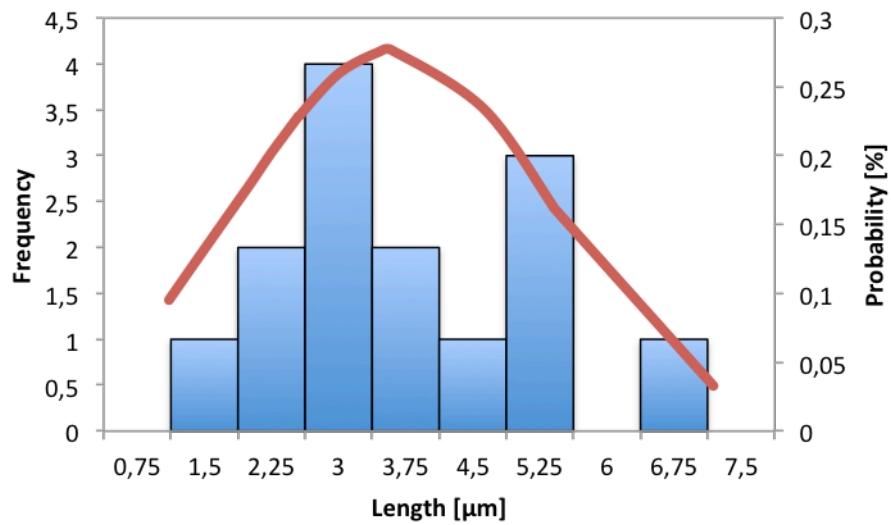


Figure E.10 – Length distribution of the dispersed D60-100 L5-15 MWCNT

D50-80 L10-20

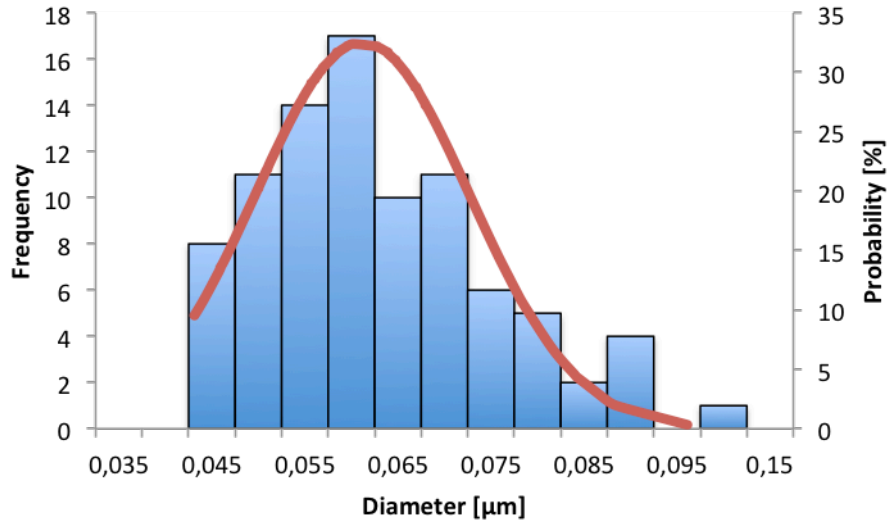


Figure E.11 – Diameter distribution of the dispersed D50-80 L10-20 MWCNT

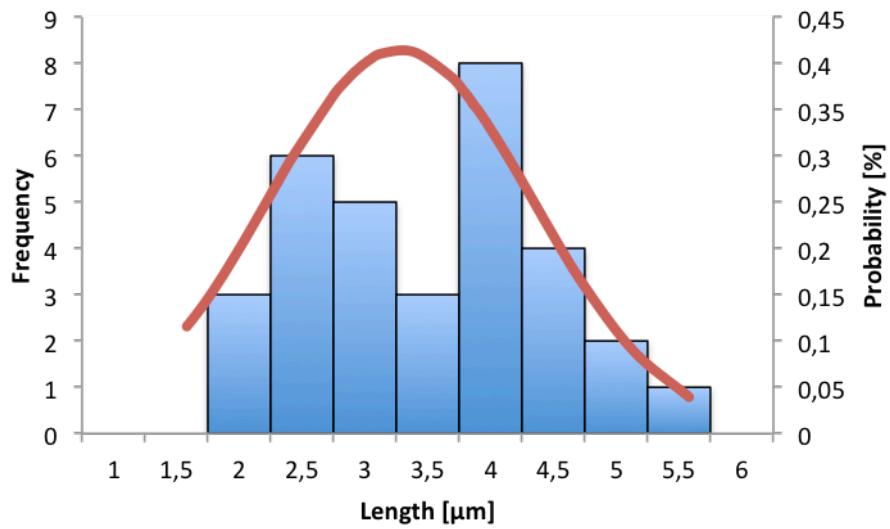


Figure E.12 – Length distribution of the dispersed D50-80 L10-20 MWCNT

F. Thermo Gravimetric Analysis (TGA)

D20-40 L1-2

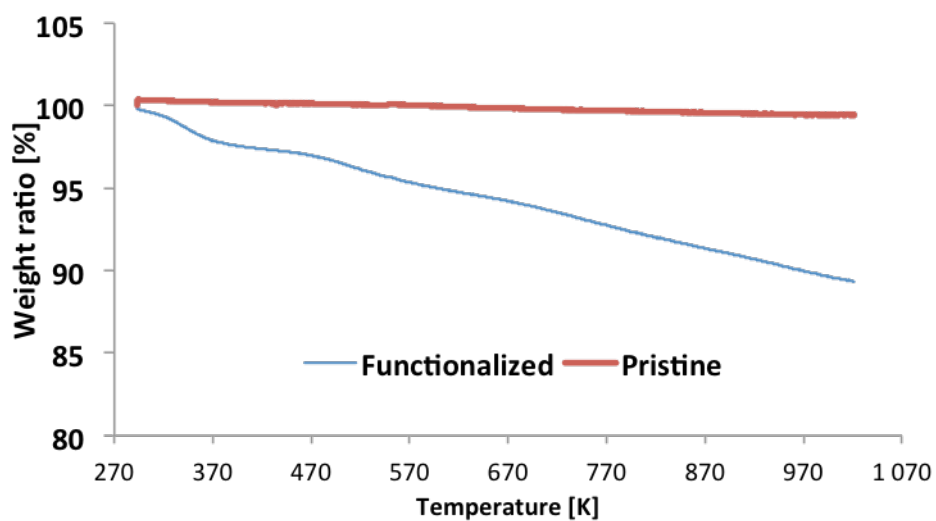


Figure F.1 - Thermo gravimetric analysis of functionalized and pristine MWCNTs D20-40 L1-2

D20-40 L5-15

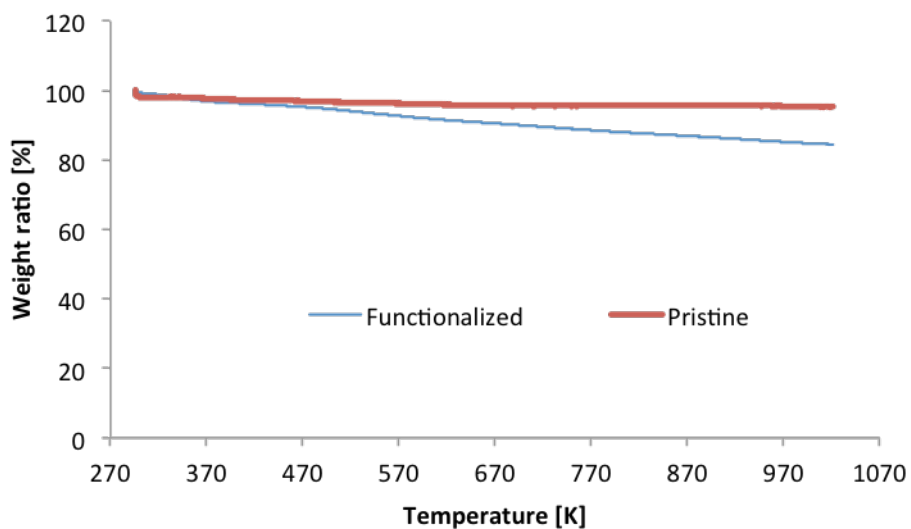


Figure F.2 - Thermo gravimetric analysis of functionalized and pristine MWCNTs D20-40 L5-15

D20-40 L10-30

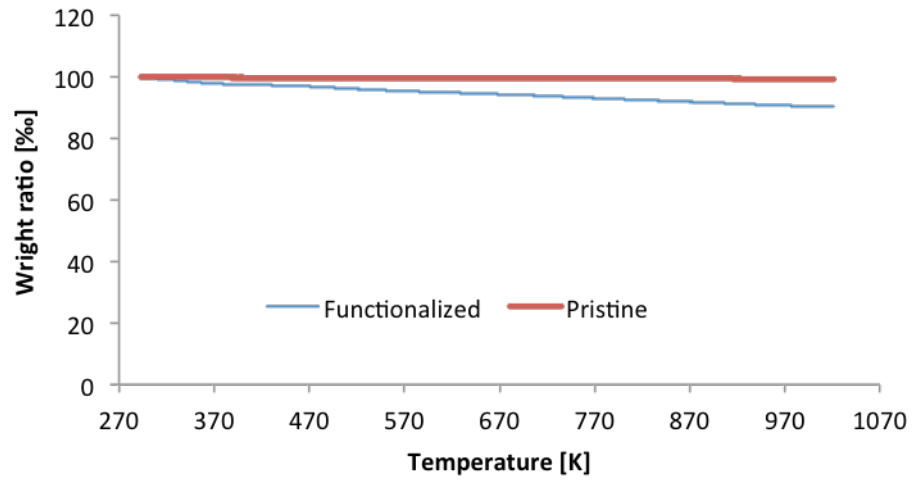


Figure F.3 – Thermo gravimetric analysis of functionalized and pristine MWCNTs D20-40 L10-30

D60-100 L1-2

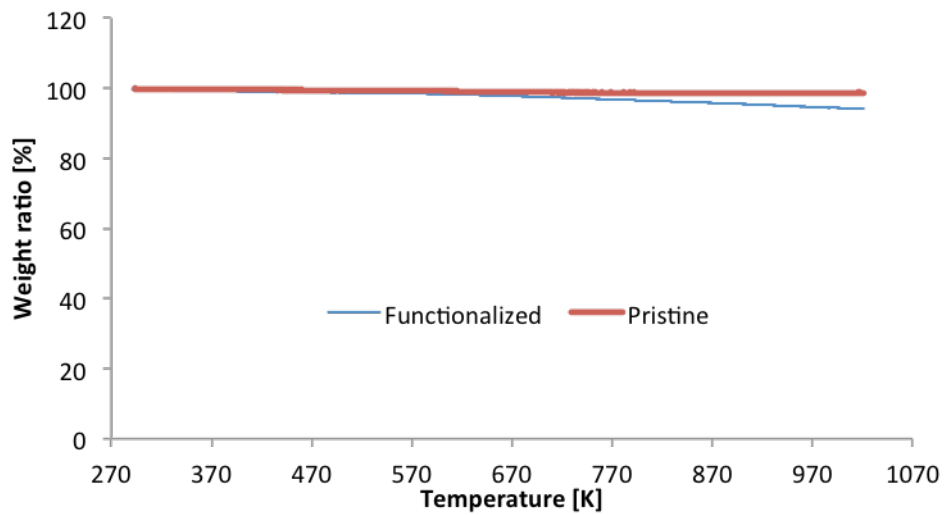


Figure F.4 – Thermo gravimetric analysis of functionalized and pristine MWCNTs D60-100 L1-2

D60-100 L5-15

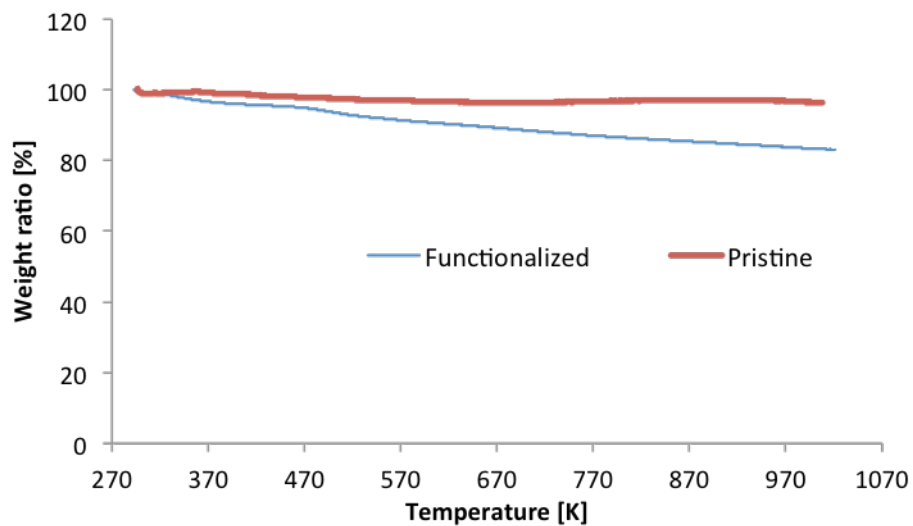


Figure F.5 - Thermo gravimetric analysis of functionalized and pristine MWCNTs D60-100 L5-15

D50-80 L10-20

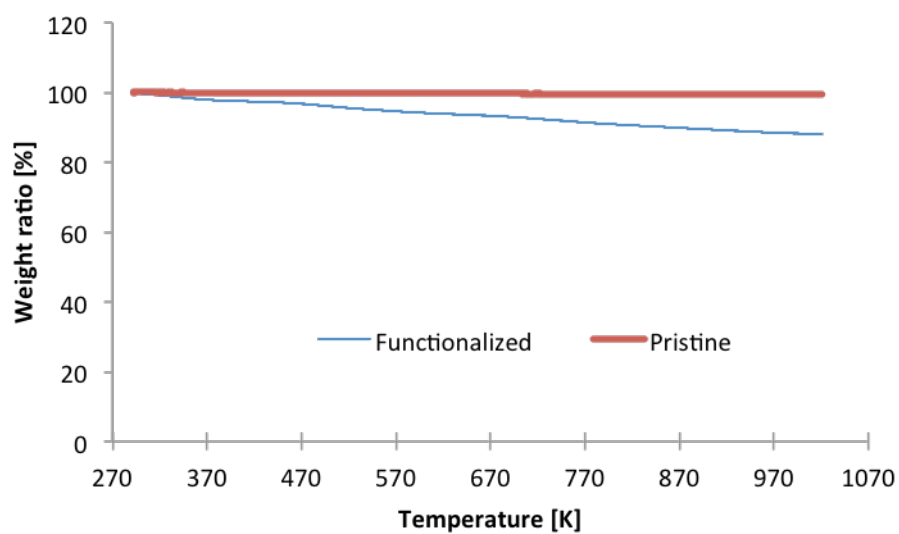


Figure F.6 - Thermo gravimetric analysis of functionalized and pristine MWCNTs D50-80 L10-20

G. Phase Separation Rate

D20-40 L1-2 + 30%EG+70%DW @ RCF = 500 G's

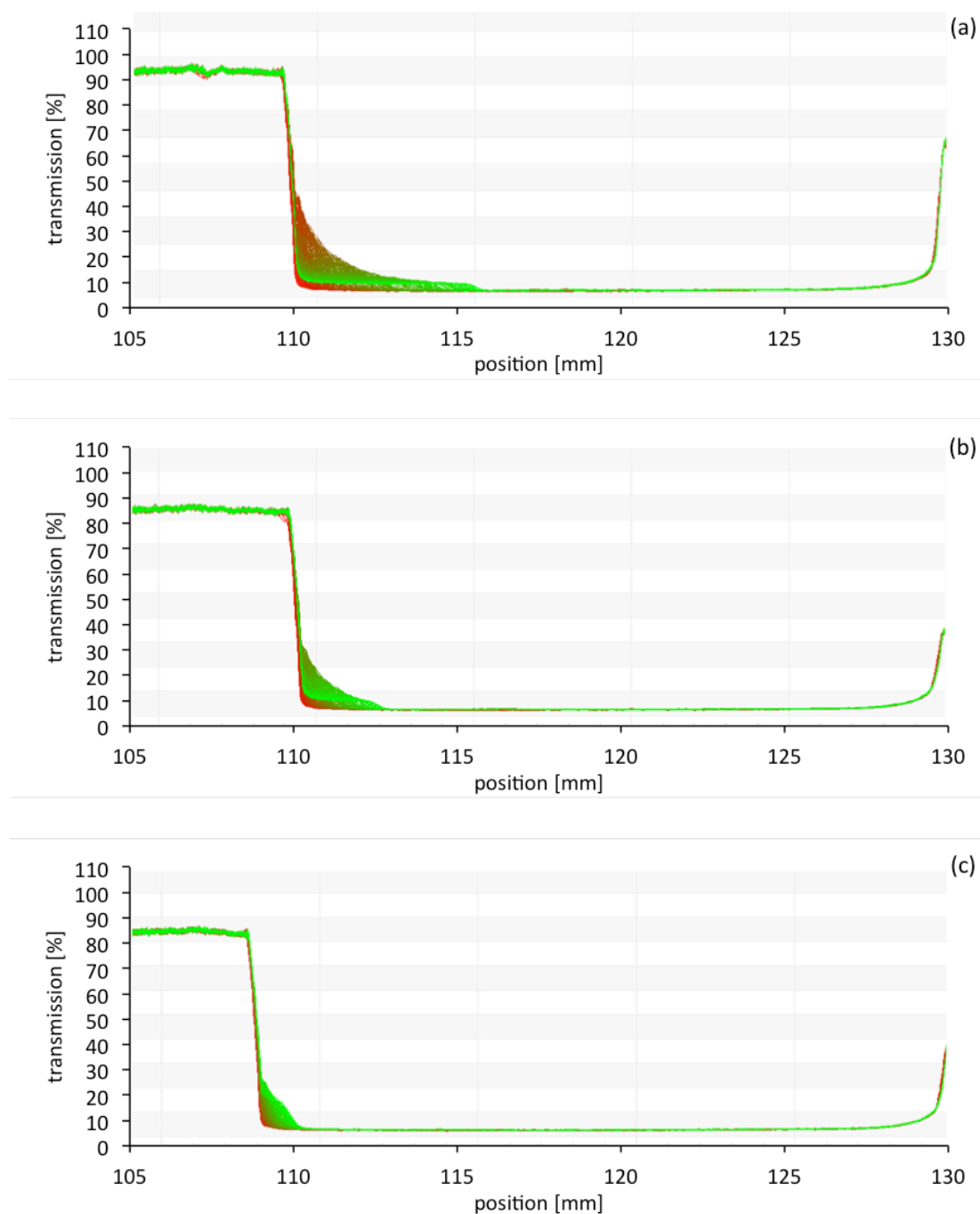


Figure G.1 - Transmission profile evolution of 30EG%+70%DW D20-40 L1-2 (a) 0,25%vol. (b) 0,75%vol. (c) 1,5%vol. @ RCF=500 G's

D20-40 L1-2 + 60%EG+40%DW @ RCF = 500 G's

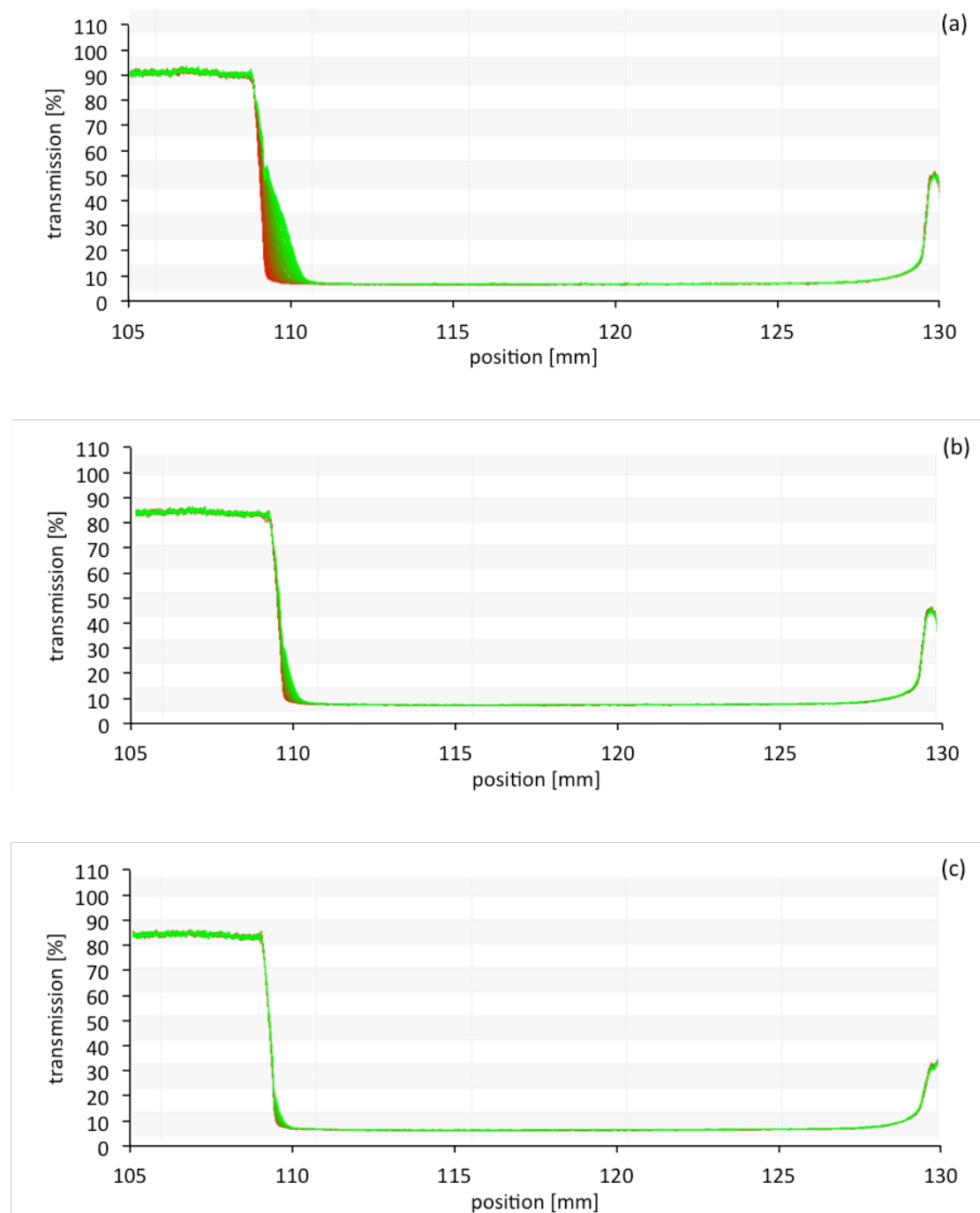


Figure G.2 - Transmission profile evolution of 60EG%+40%DW D20-40 L1-2 (a) 0,25%vol. (b) 0,75%vol. (c) 1,5%vol. @ RCF=500 G's

D20-40 L5-15 + 30%EG+70%DW @ RCF = 500 G's

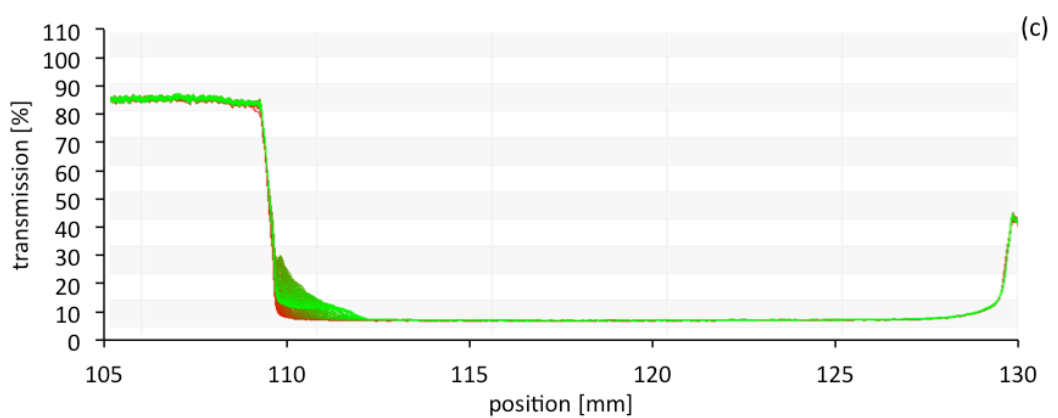
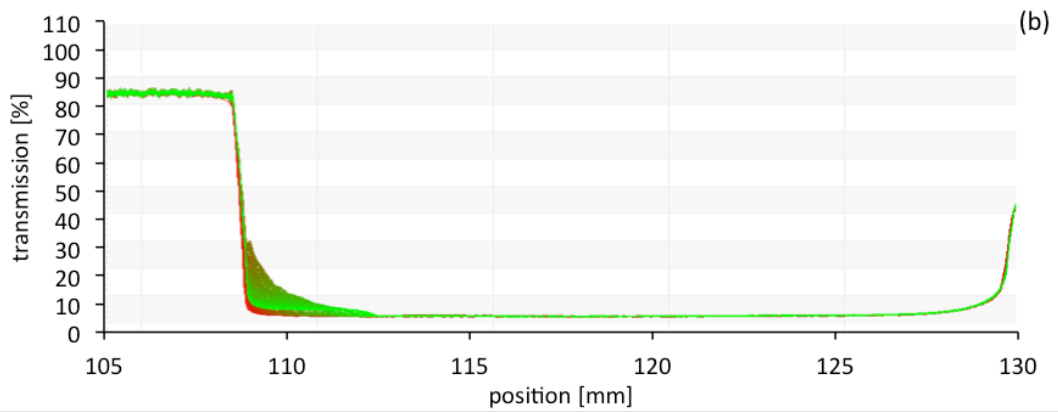
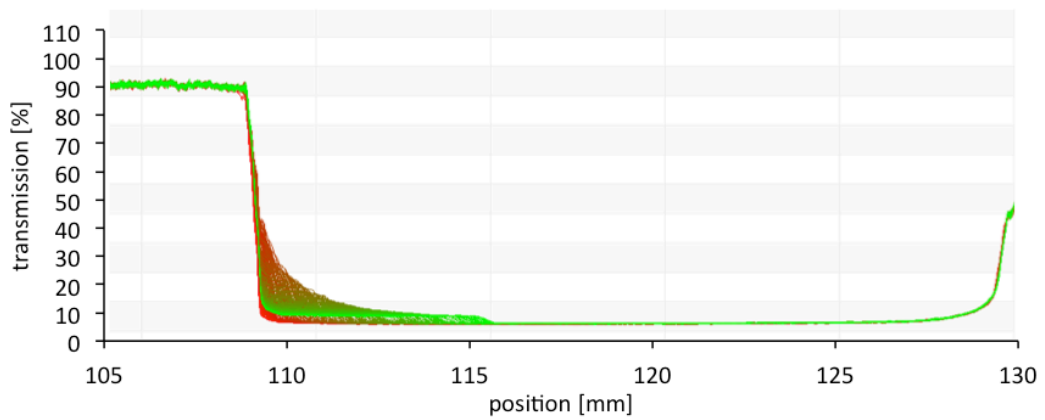


Figure G.3 - Transmission profile evolution of 30EG%+70%DW D20-40 L5-15 (a) 0,25%vol. (b) 0,75%vol. (c) 1,5%vol. @ RCF=500 G's

D20-40 L5-15 + 60%EG+40%DW @ RCF = 500 G's

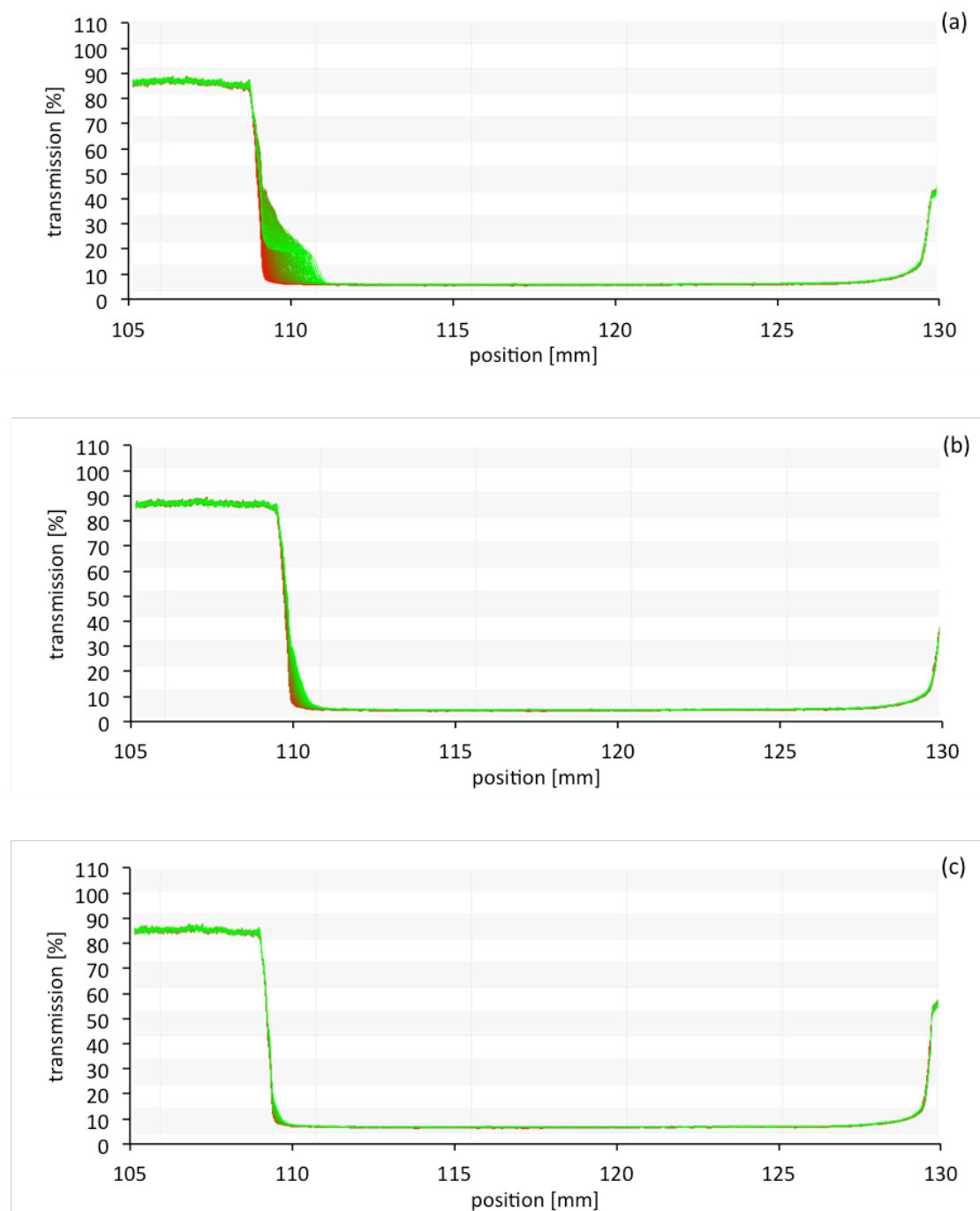


Figure G.4 - Transmission profile evolution of 60EG%+40%DW D20-40 L5-15 (a) 0,25%vol. (b) 0,75%vol. (c) 1,5%vol. @ RCF=500 G's

D20-10 L10-30 + 30%EG+70%DW @ 500G's

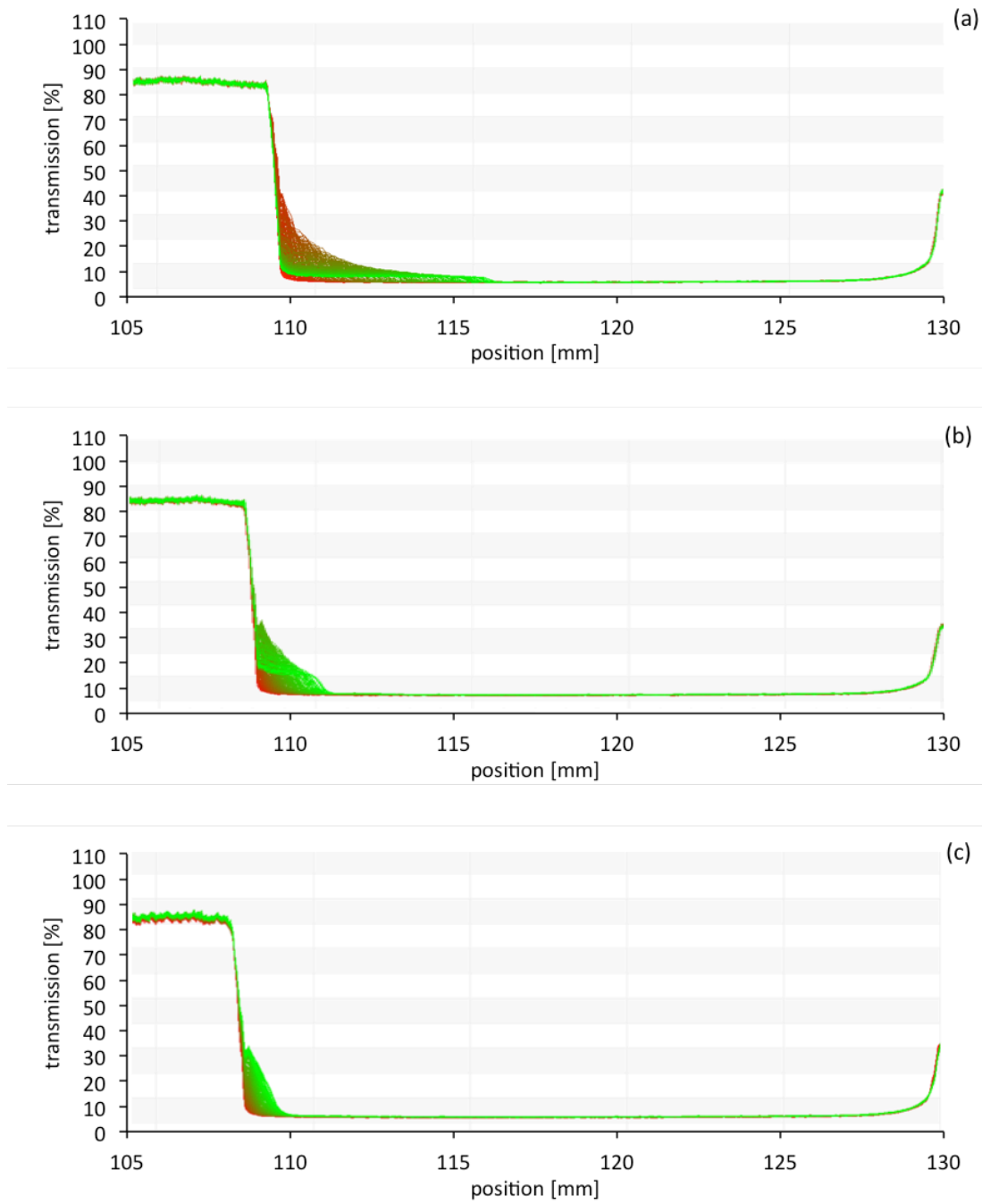


Figure G.5 - Transmission profile evolution of 30EG%+70%DW D20-40 L10-30 (a) 0,25%vol. (b) 0,75%vol. (c) 1,5%vol. @ RCF=500 G's

D20-10 L10-30 + 60%EG+40%DW @ 500G's

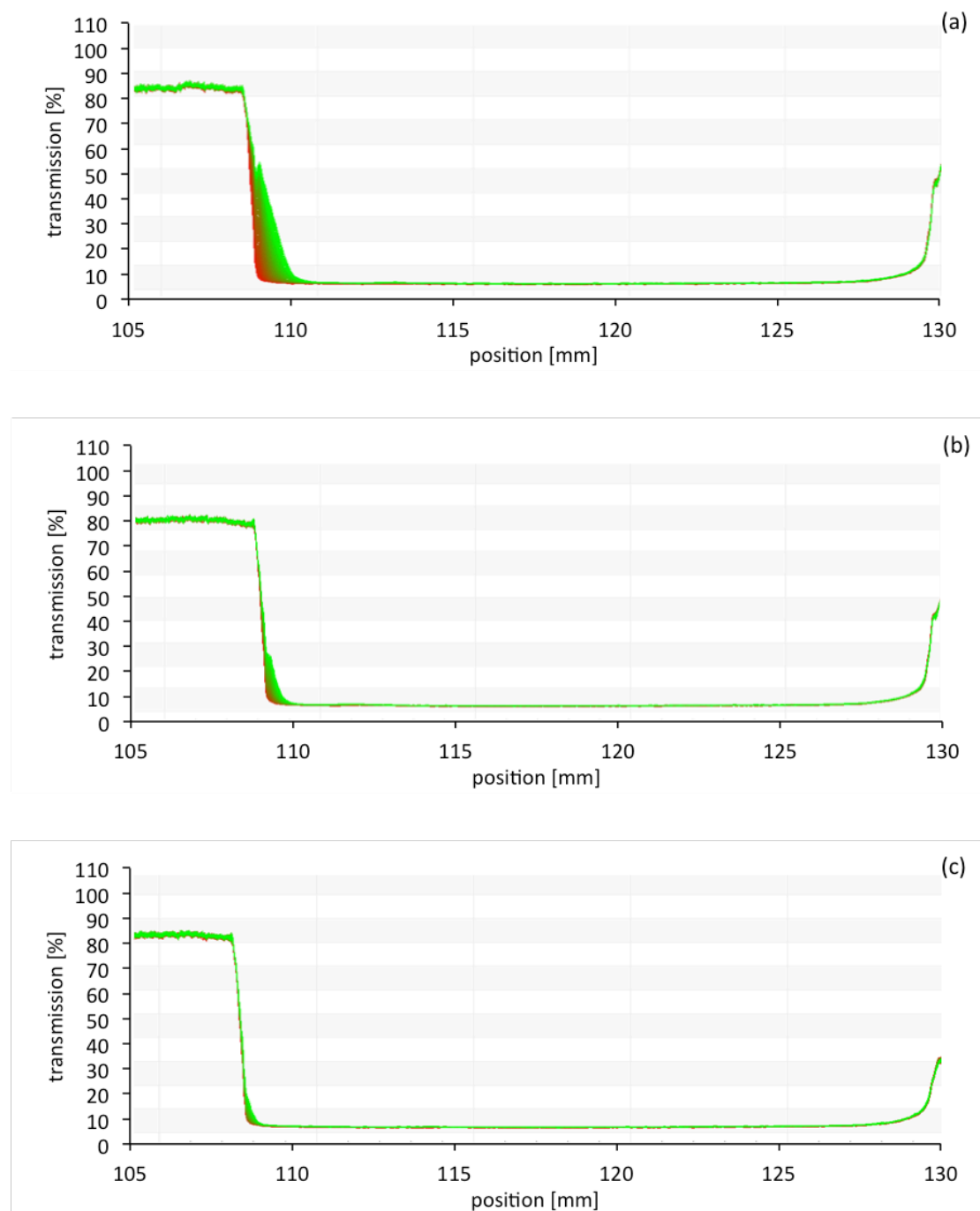


Figure G.6 - Transmission profile evolution of 60EG%+40%DW D20-40 L10-30 (a) 0,25%vol. (b) 0,75%vol. (c) 1,5%vol. @ RCF=500 G's

D60-100 L1-2 + 30%EG+70%DW @ 500G's

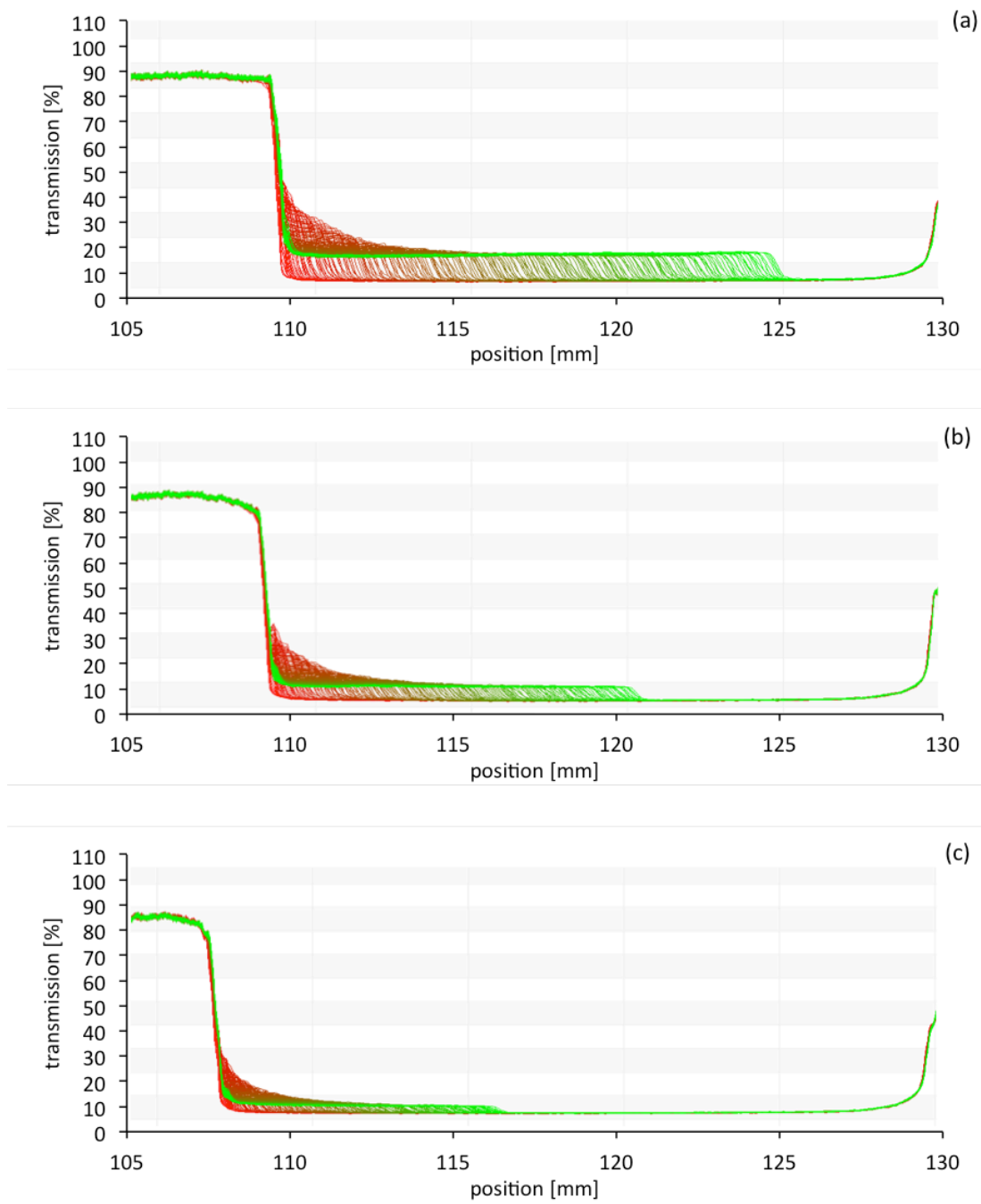


Figure G.7 - Transmission profile evolution of 30EG%+70%DW D60-100 L1-2 (a) 0,25%vol. (b) 0,75%vol. (c) 1,5%vol. @ RCF=500 G's

D60-100 L1-2 + 60%EG+40%DW @ 500G's

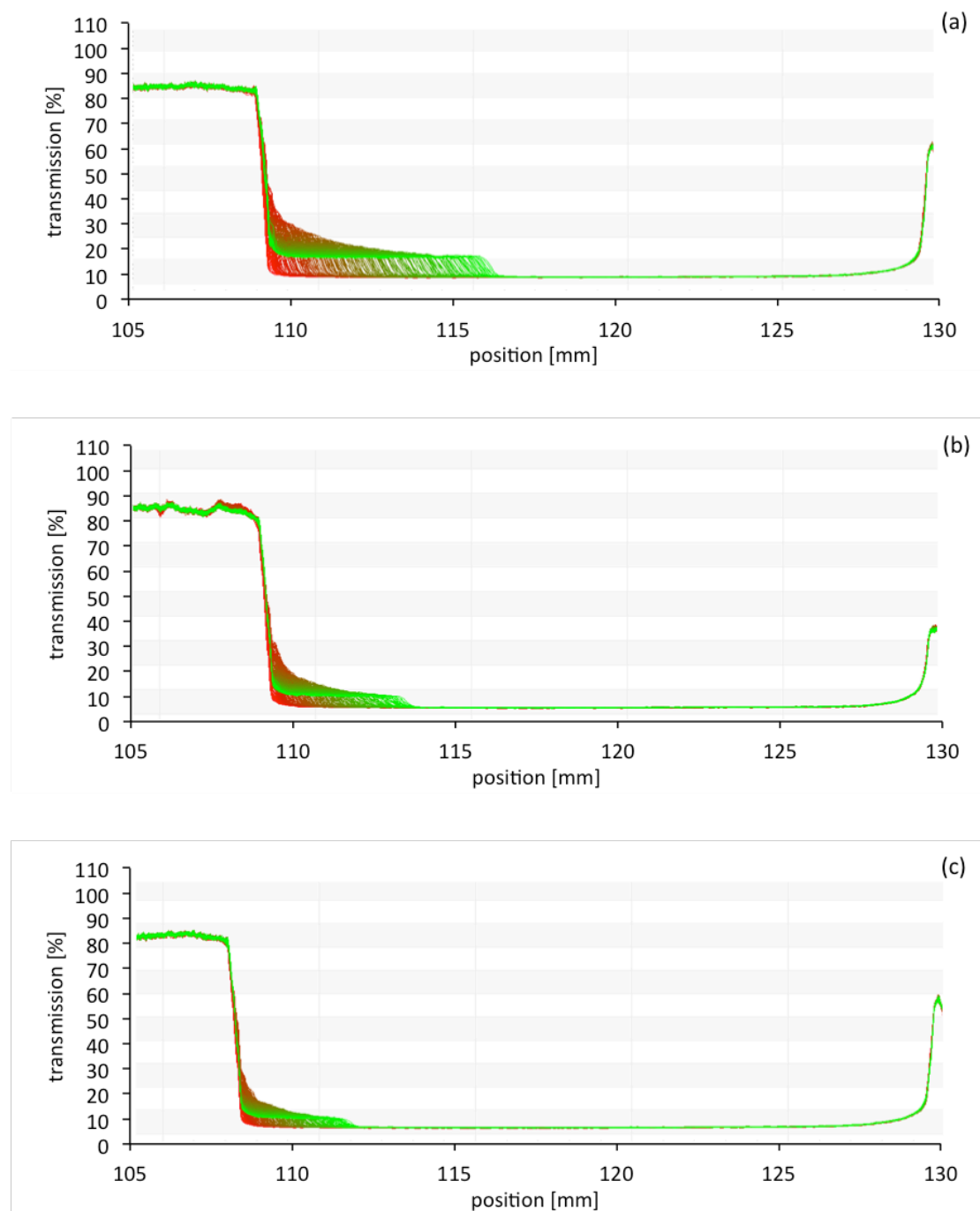


Figure G.8 - Transmission profile evolution of 60EG%+40%DW D60-100 L1-2 (a) 0,25%vol. (b) 0,75%vol. (c) 1,5%vol. @ RCF=500 G's

D60-100 L5-15 + 30%EG+70%DW @ 500G's

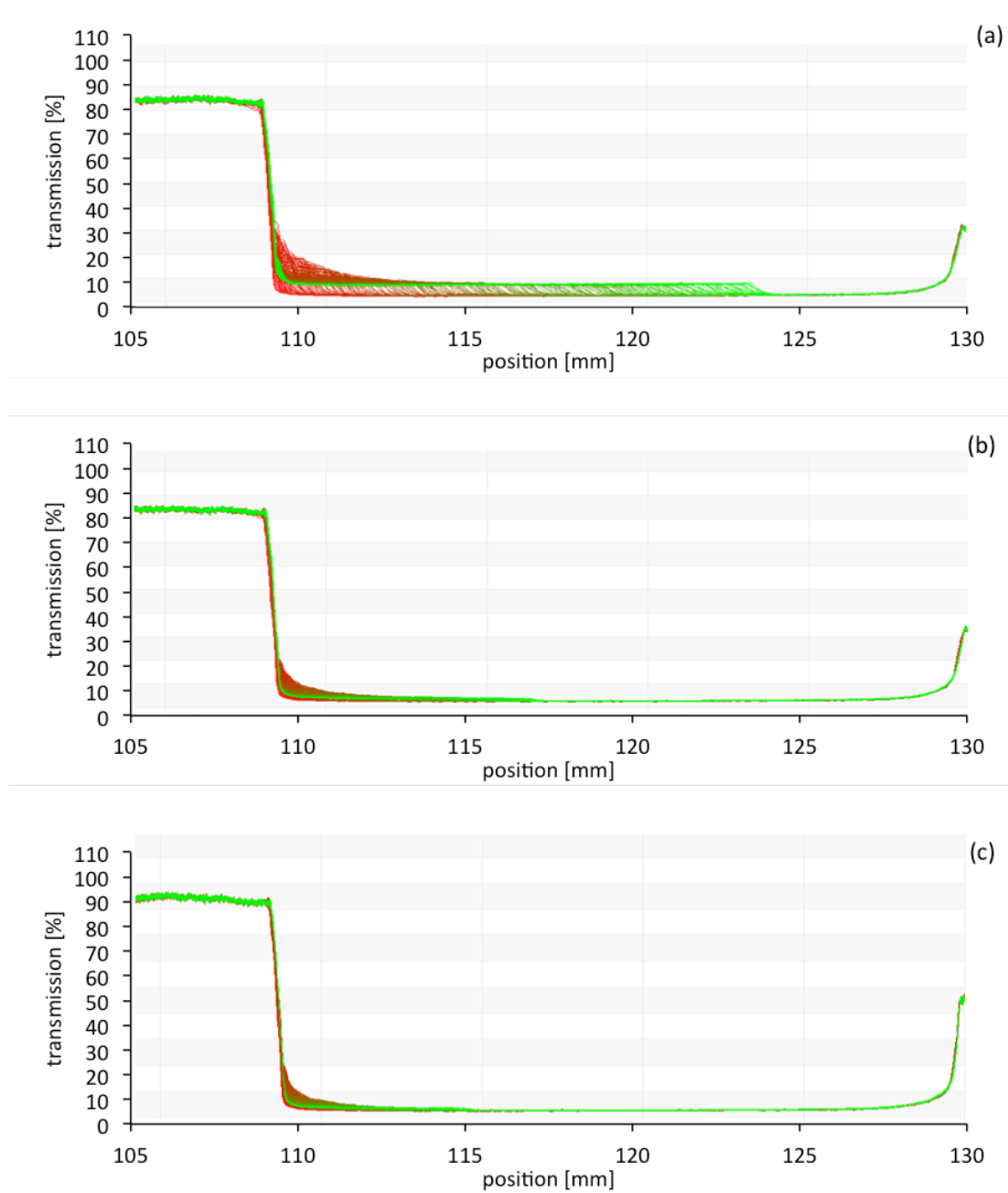


Figure G.9 - Transmission profile evolution of 30EG%+70%DW D60-100 L5-15 (a) 0,25%vol. (b) 0,75%vol. (c) 1,5%vol. @ RCF=500 G's

D60-100 L5-15 + 60%EG+40%DW @ 500G's

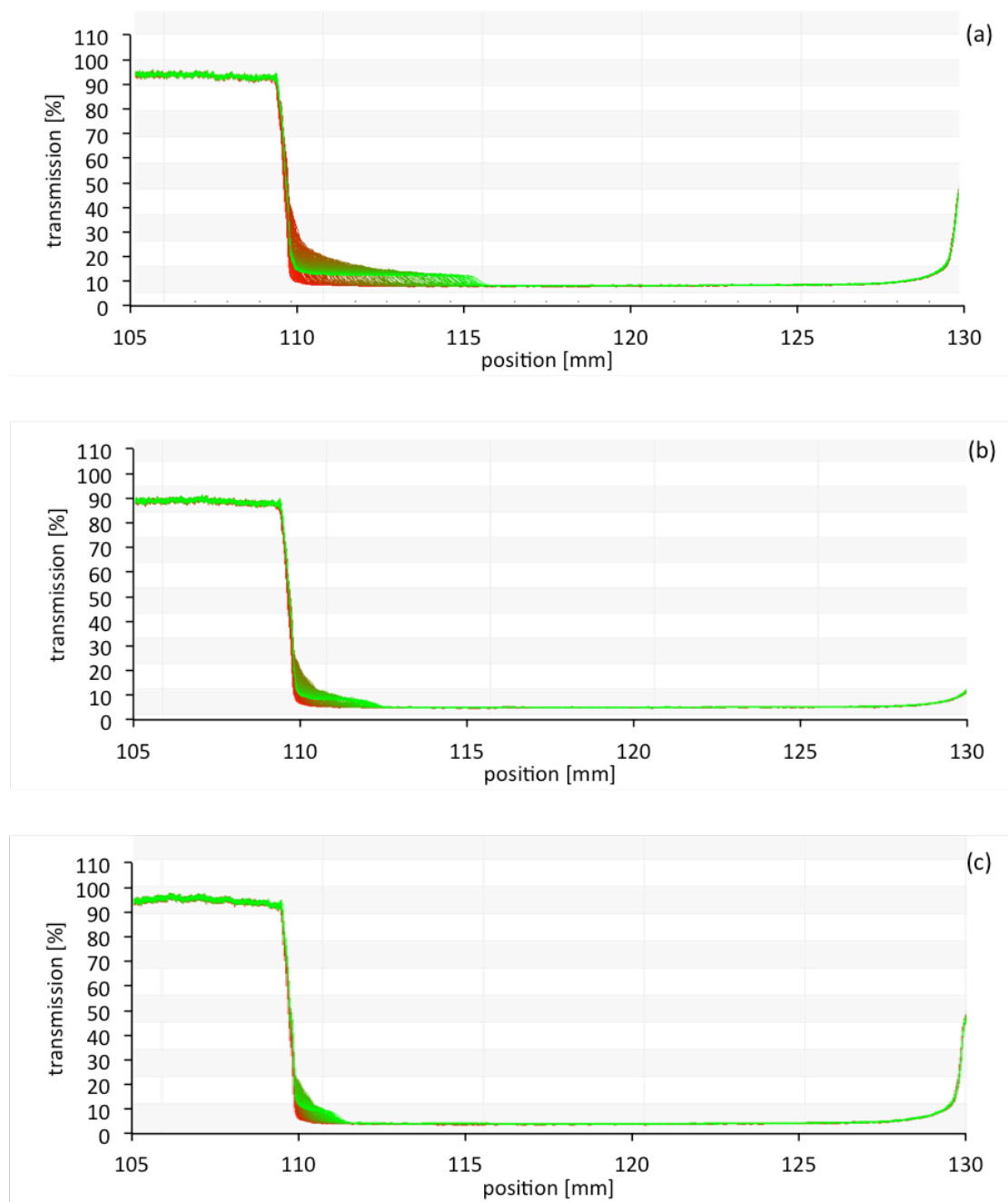


Figure G.10 - Transmission profile evolution of 60EG+40%DW D60-100 L5-15 (a) 0,25%vol. (b) 0,75%vol. (c) 1,5%vol. @ RCF=500 G's

D50-80 L10-20 + 30%EG+70%DW @ 500G's

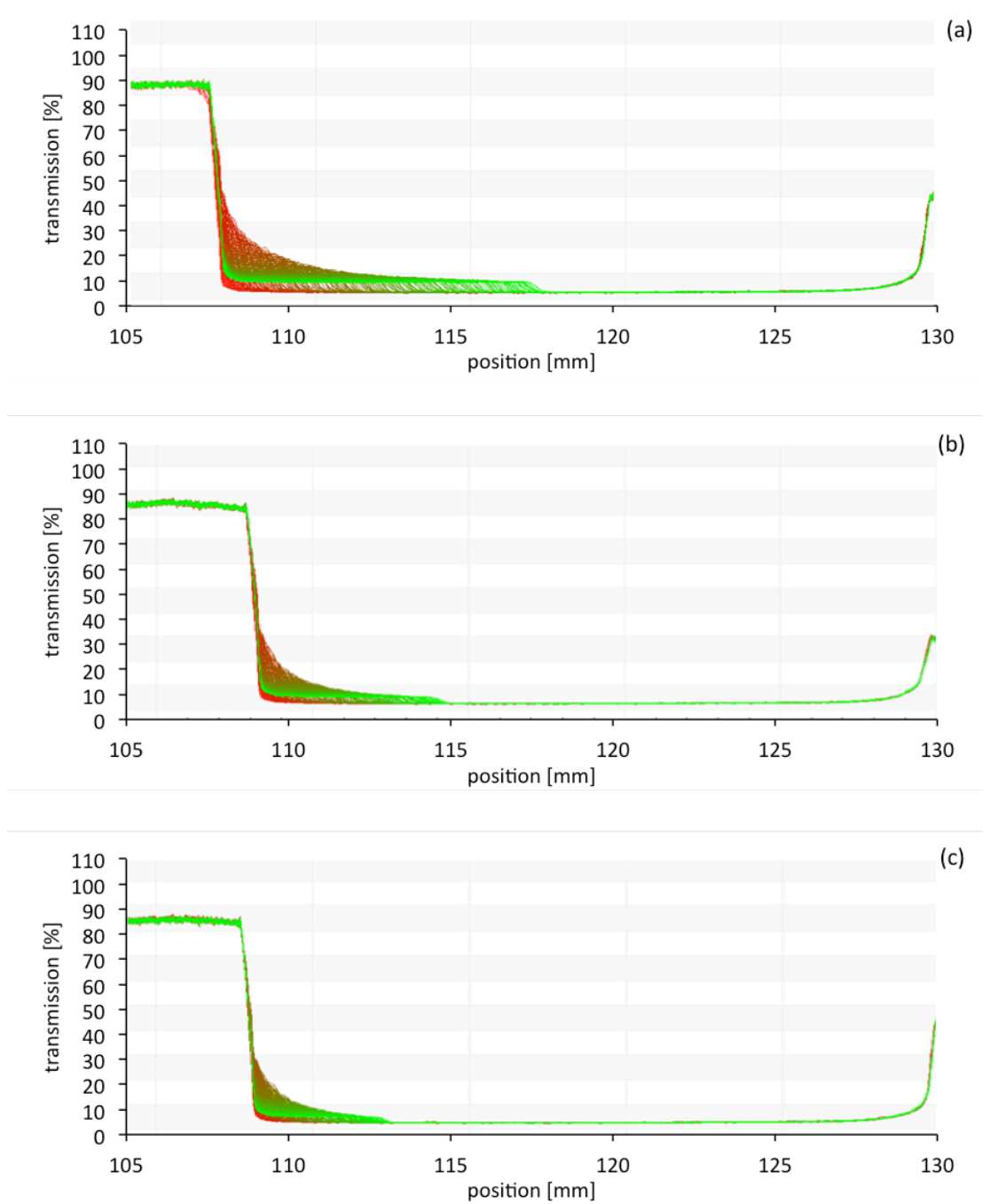


Figure G.11 - Transmission profile evolution of 30EG+70%DW D50-80 L10-20 (a) 0,25%vol. (b) 0,75%vol. (c) 1,5%vol. @ RCF=500 G's

D50-80 L10-20 + 60%EG+40%DW @ 500G's

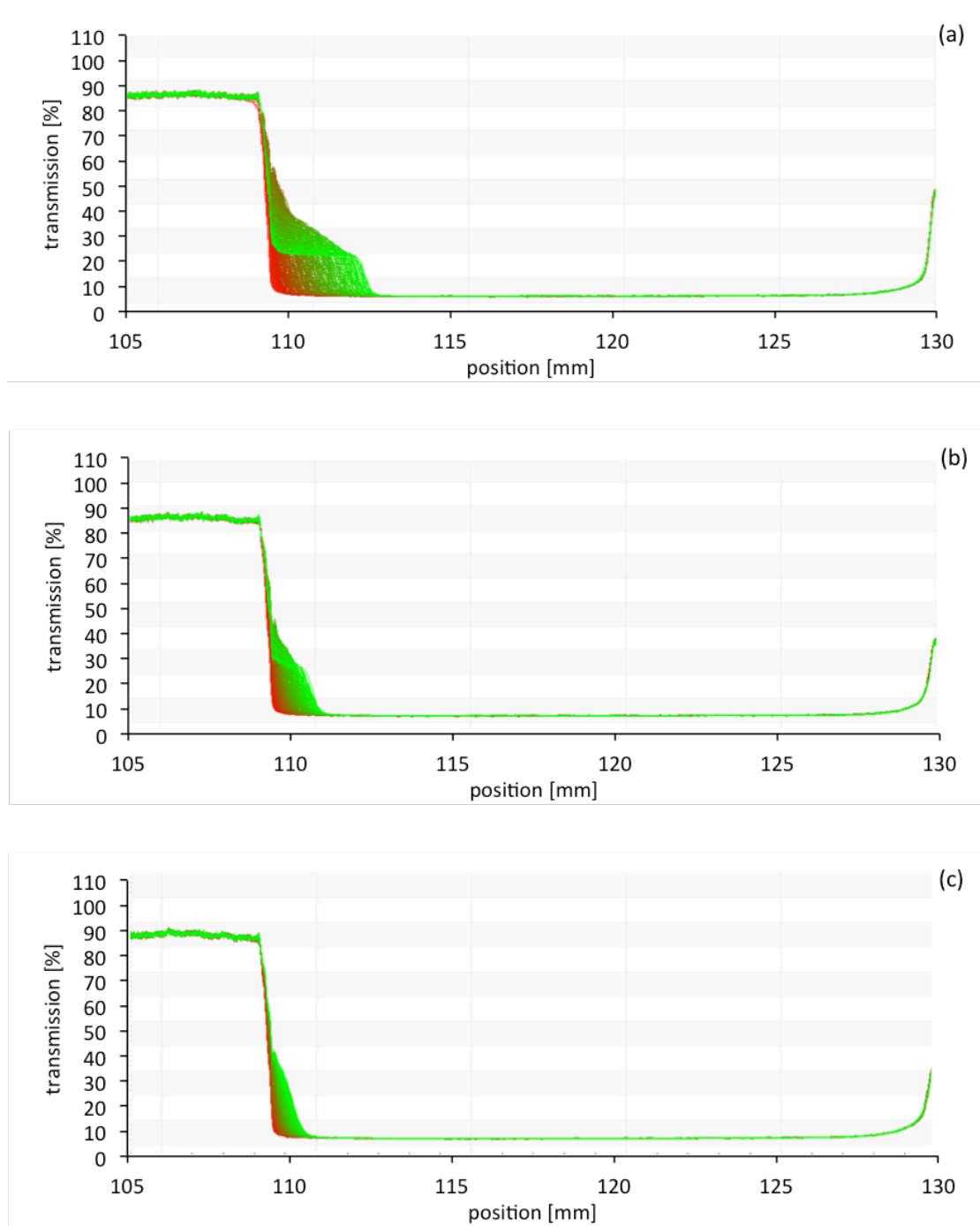


Figure G.12 - Transmission profile evolution of 60EG%+40%DW D50-80 L10-20 (a) 0,25%vol. (b) 0,75%vol. (c) 1,5%vol. @ RCF=500 G's

D20-40 L1-2 + 30%EG+70%DW @ RCF = 1000 G's

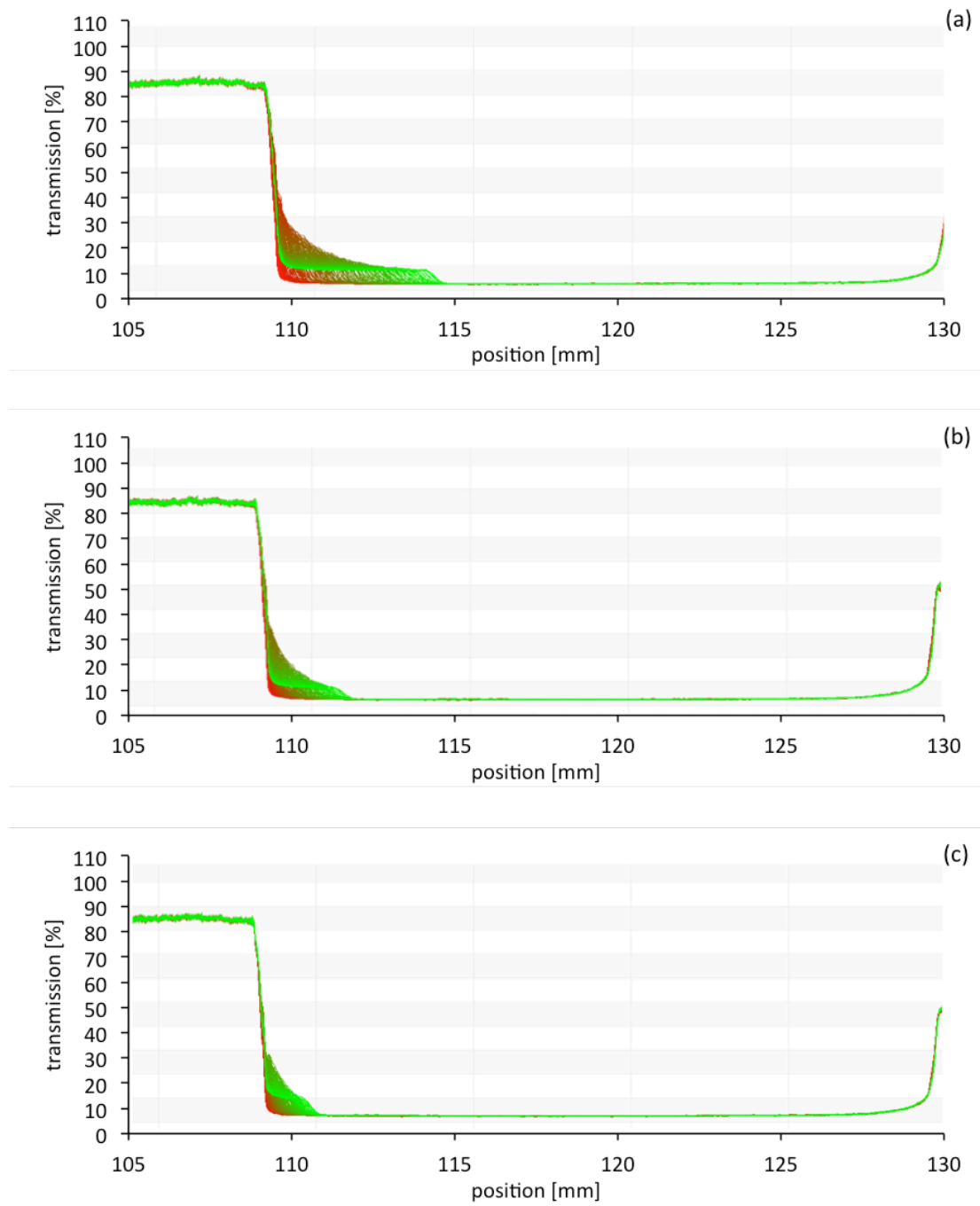


Figure G.13 - Transmission profile evolution of 30EG+70%DW D20-40 L1-2 (a) 0,25%vol. (b) 0,75%vol. (c) 1,5%vol. @ RCF=1000 G's

D20-40 L1-2 + 60%EG+40%DW @ RCF = 1000 G's

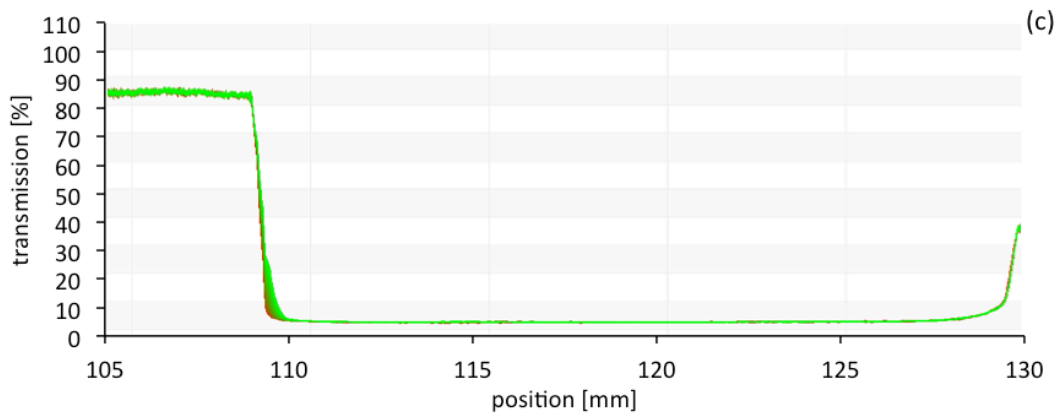
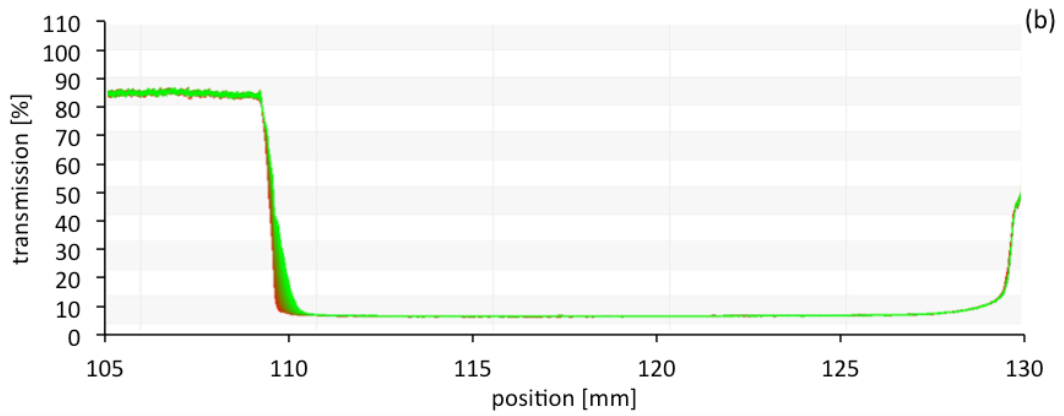
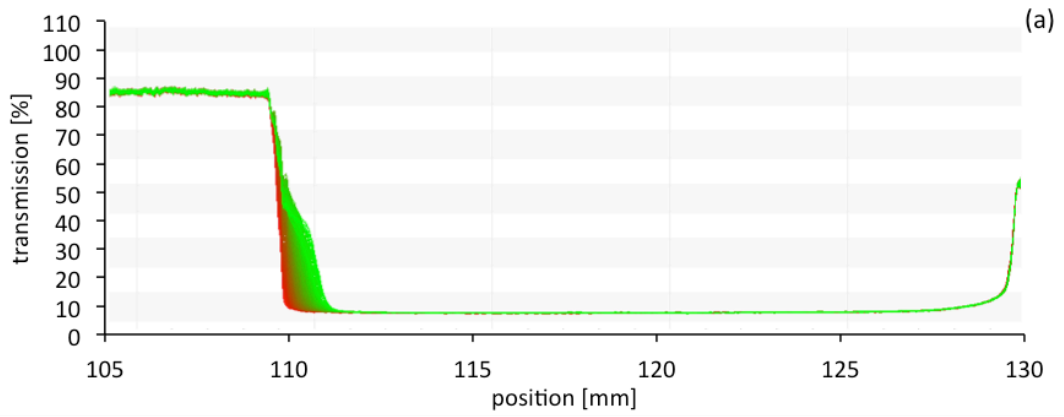


Figure G.14 - Transmission profile evolution of 60EG%+40%DW D20-40 L1-2 (a) 0,25%vol. (b) 0,75%vol. (c) 1,5%vol. @ RCF=1000 G's

D20-40 L5-15 + 30%EG+70%DW @ RCF = 1000 G's

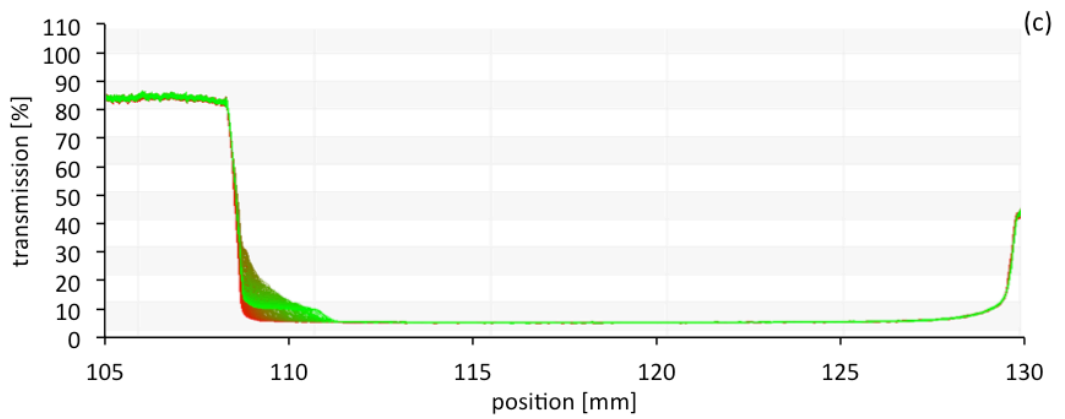
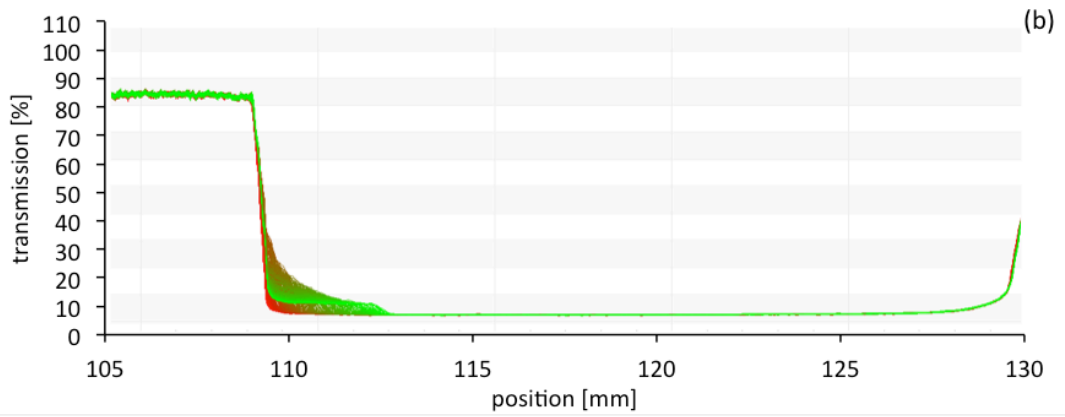
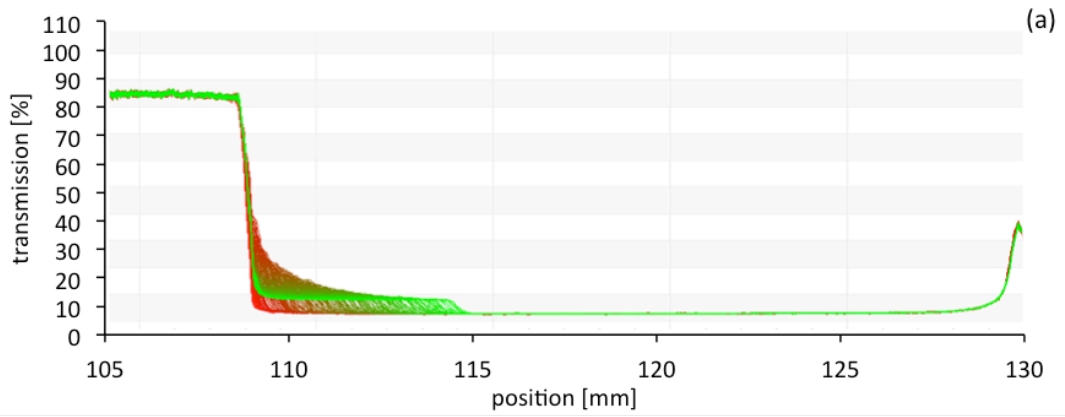


Figure G.15 - Transmission profile evolution of 30EG+70%DW D20-40 L5-15 (a) 0,25%vol. (b) 0,75%vol. (c) 1,5%vol. @ RCF=1000 G's

D20-40 L5-15 + 60%EG+40%DW @ RCF = 1000 G's

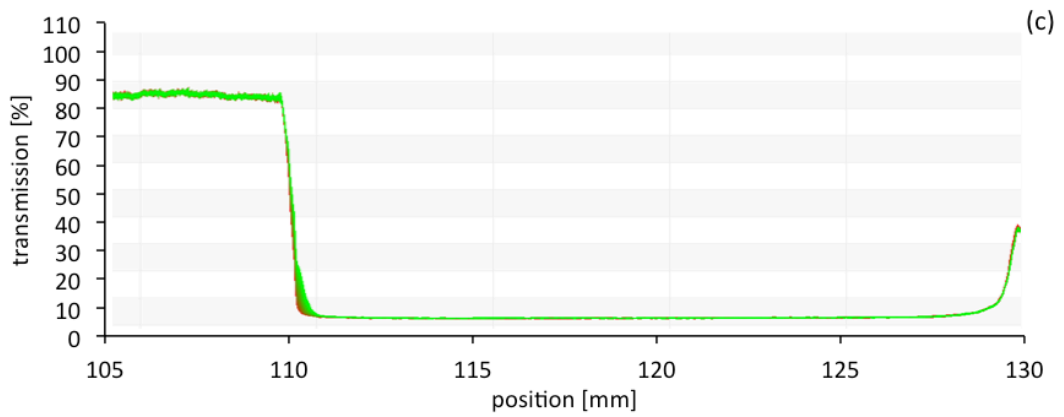
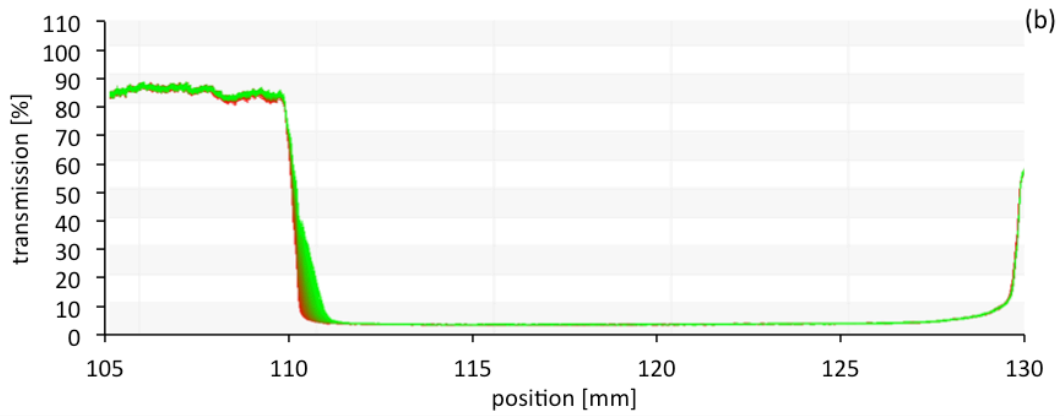
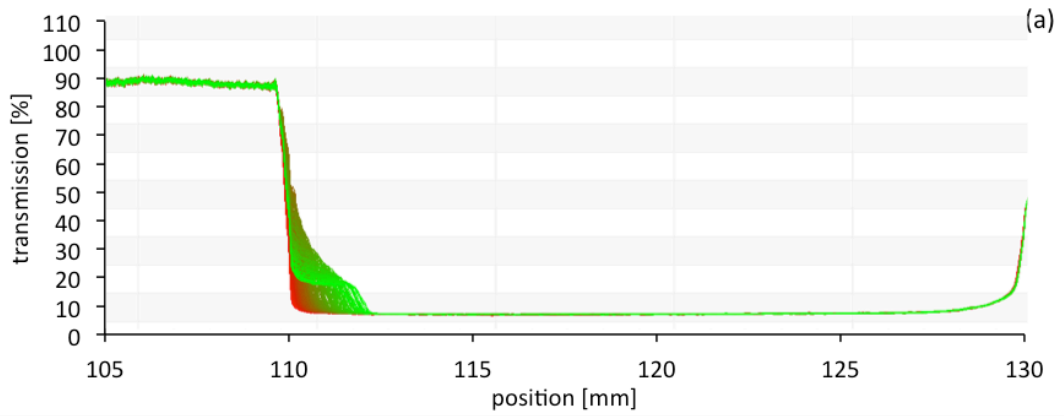


Figure G.16 - Transmission profile evolution of 60EG+40%DW D20-40 L5-15 (a) 0,25%vol. (b) 0,75%vol. (c) 1,5%vol. @ RCF=1000 G's

D20-10 L10-30 + 30%EG+70%DW @ 1000 G's

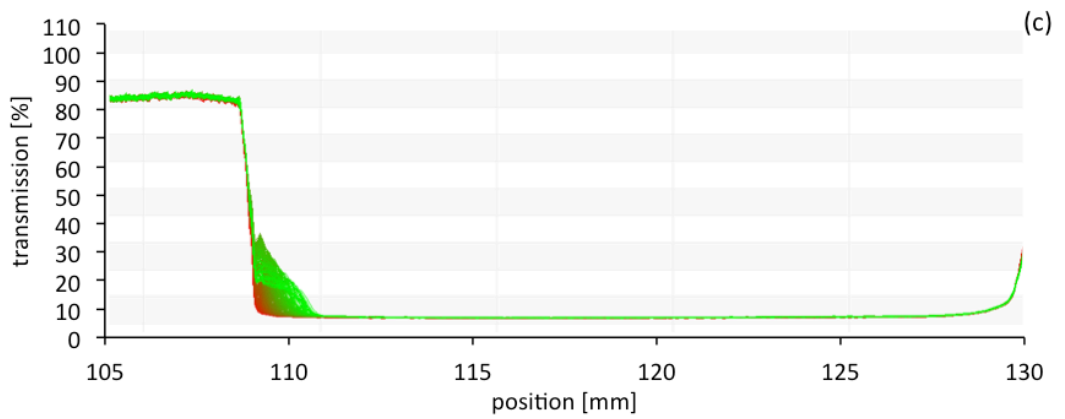
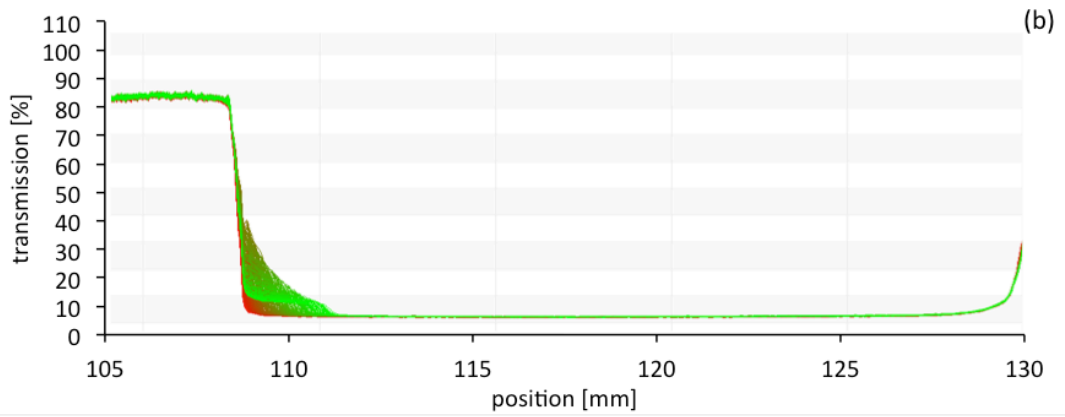
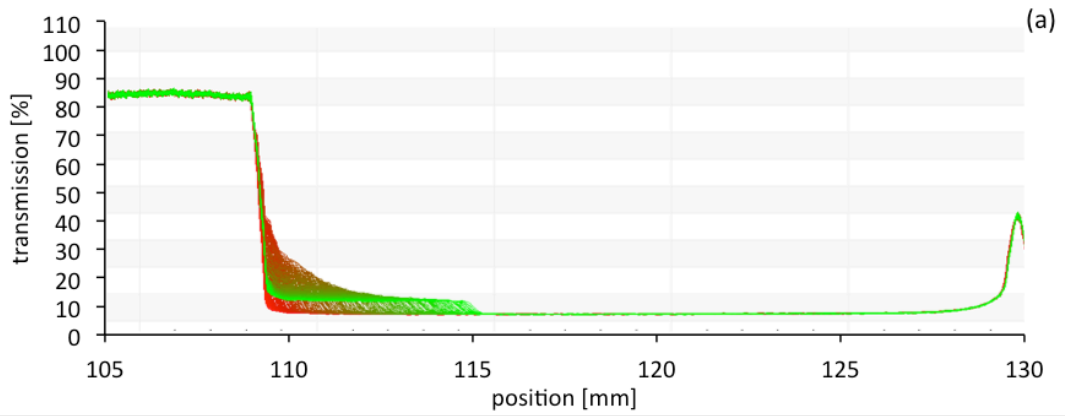


Figure G.17 - Transmission profile evolution of 30EG+70%DW D20-40 L10-30 (a) 0,25%vol. (b) 0,75%vol. (c) 1,5%vol. @ RCF=1000 G's

D20-10 L10-30 + 60%EG+40%DW @ 1000 G's

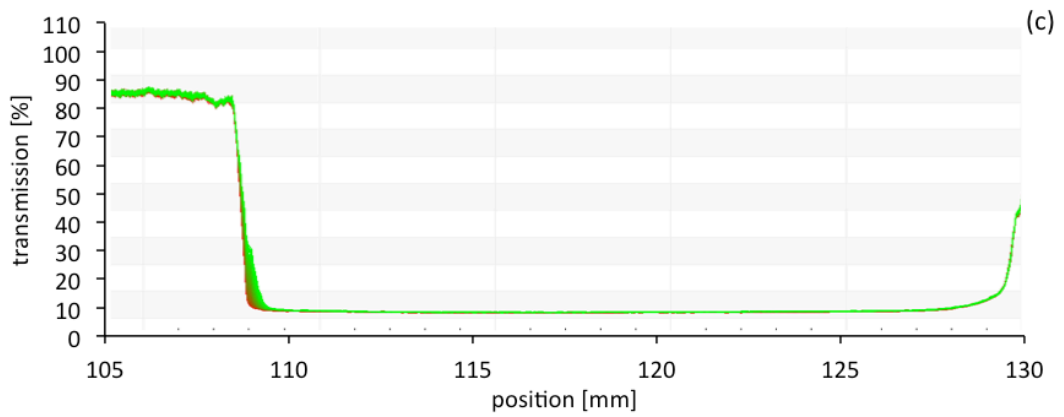
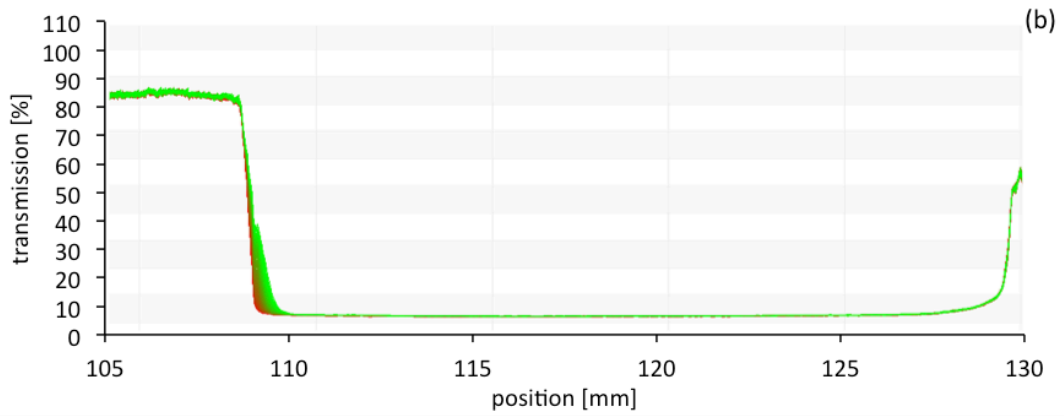
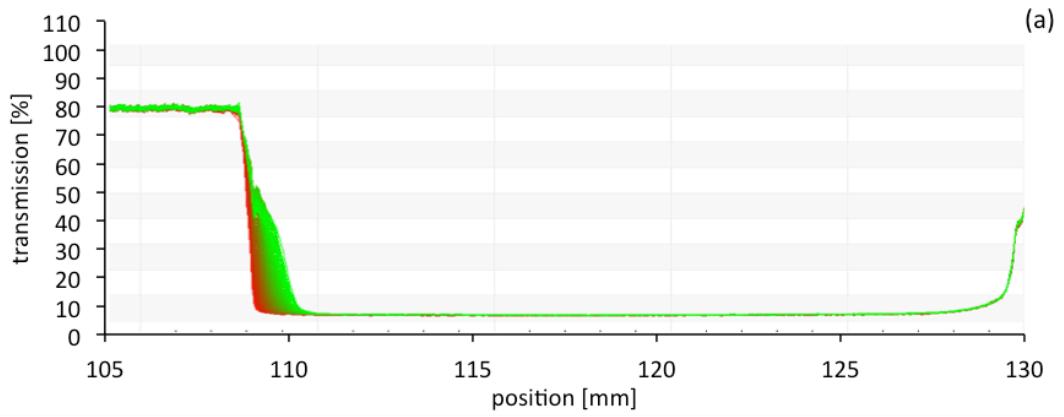


Figure G.18 - Transmission profile evolution of 60EG%+40%DW D20-40 L10-30 (a) 0,25%vol. (b) 0,75%vol. (c) 1,5%vol. @ RCF=1000 G's

D60-100 L1-2 + 30%EG+70%DW @ 1000 G's

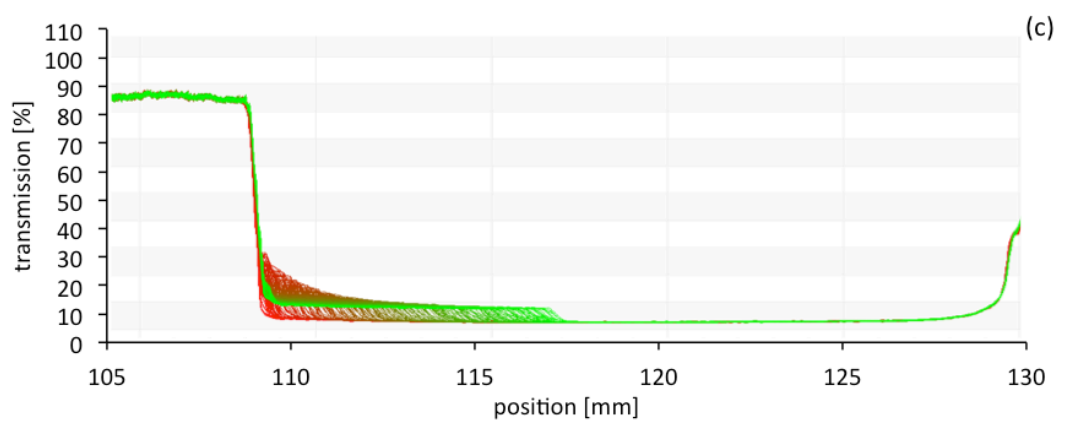
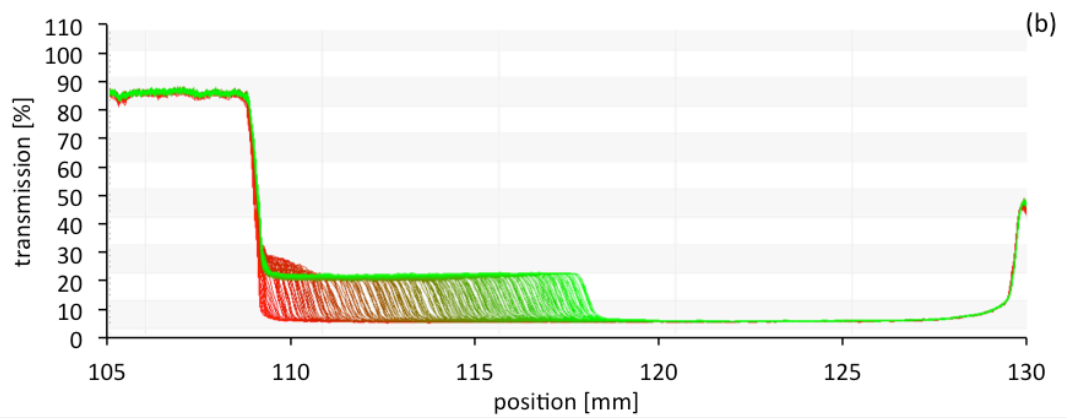
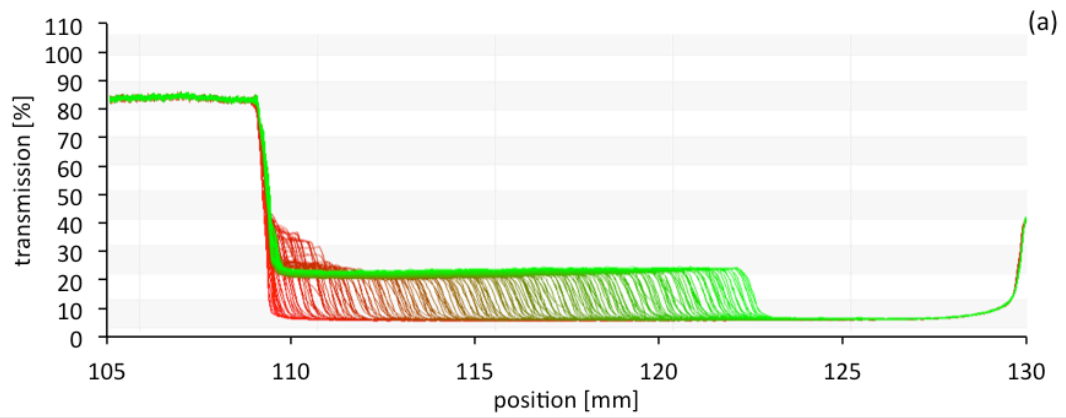


Figure G.19 - Transmission profile evolution of 30EG%+70%DW D60-100 L1-2 (a) 0,25%vol. (b) 0,75%vol. (c) 1,5%vol. @ RCF=1000 G's

D60-100 L1-2 + 60%EG+40%DW @ 1000 G's

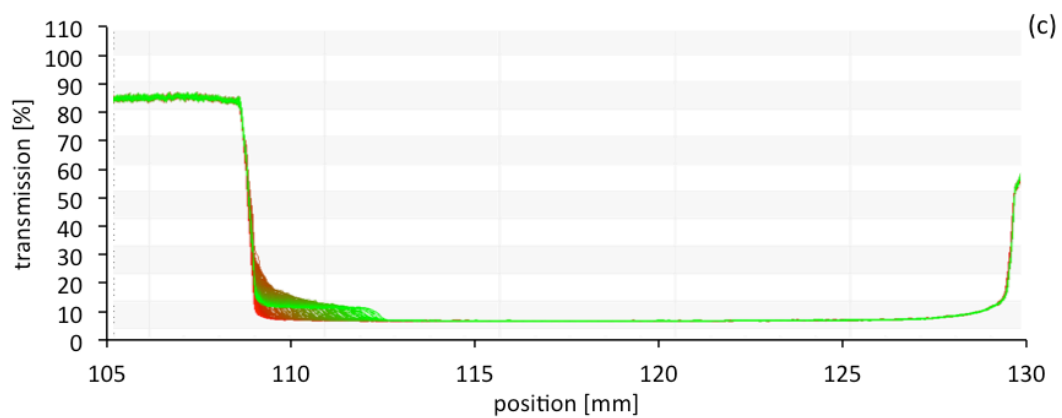
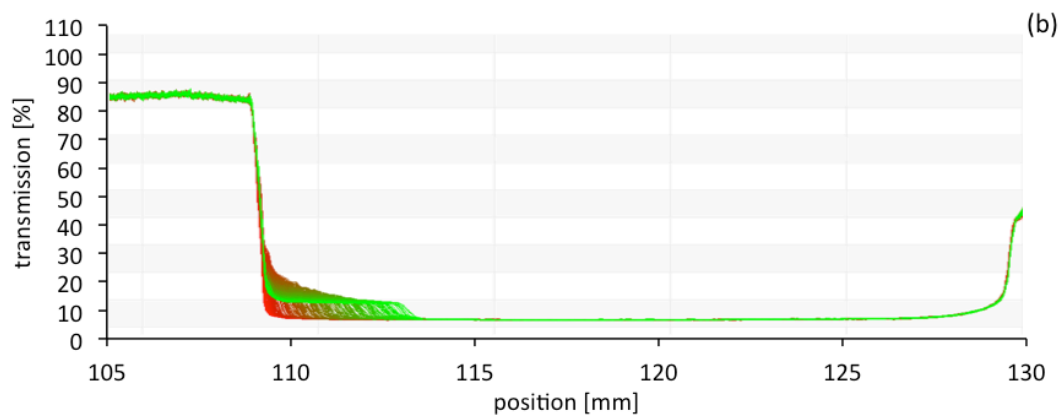
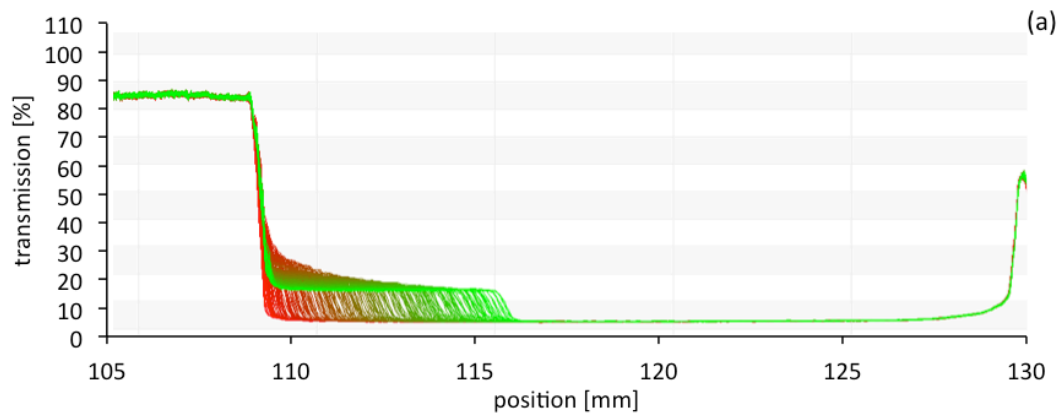


Figure G.20 - Transmission profile evolution of 60EG%+40%DW D60-100 L1-2 (a) 0,25%vol. (b) 0,75%vol. (c) 1,5%vol. @ RCF=1000 G's

D60-100 L5-15 + 30%EG+70%DW @ 1000 G's

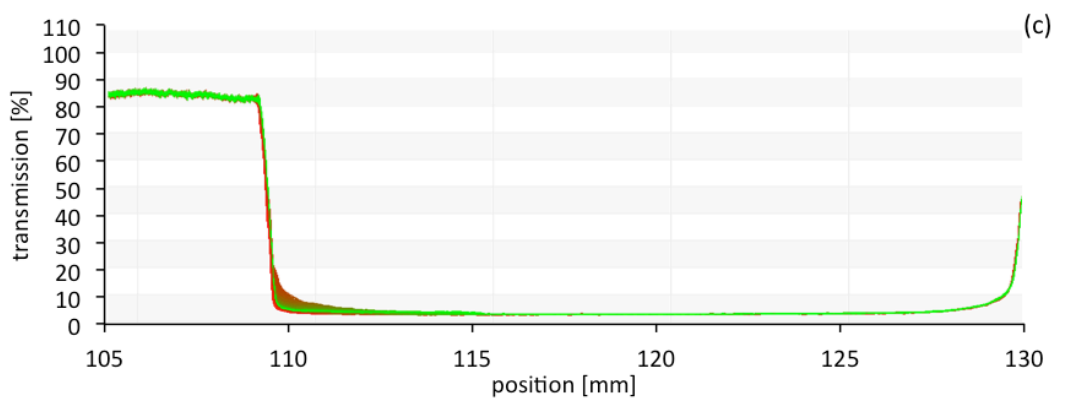
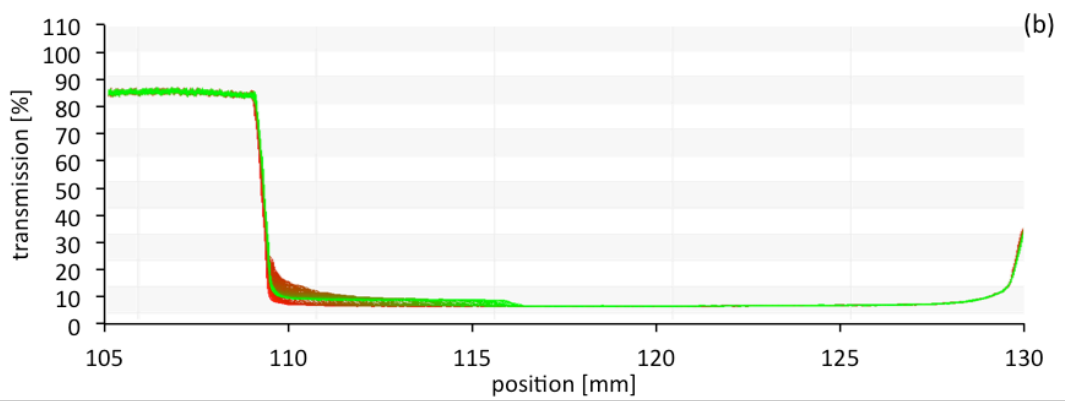
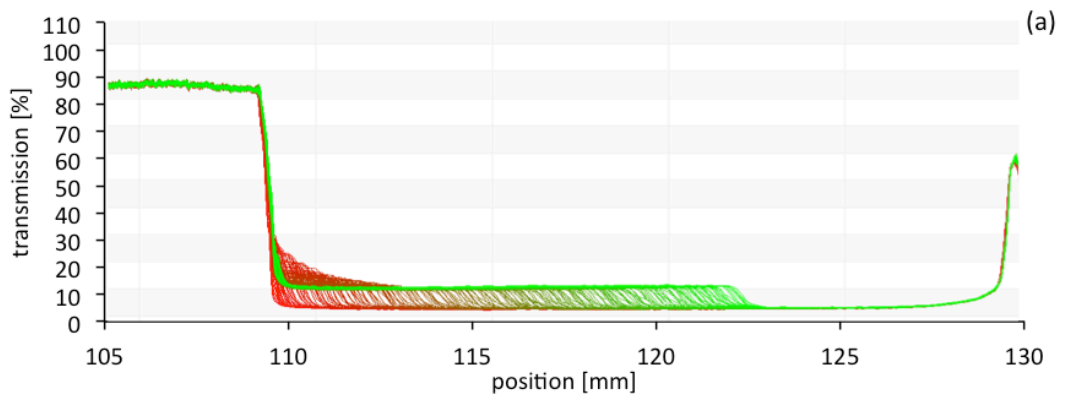


Figure G.21 - Transmission profile evolution of 30EG+70%DW D60-100 L5-15 (a) 0,25%vol. (b) 0,75%vol. (c) 1,5%vol. @ RCF=1000 G's

D60-100 L5-15 + 60%EG+40%DW @ 1000 G's

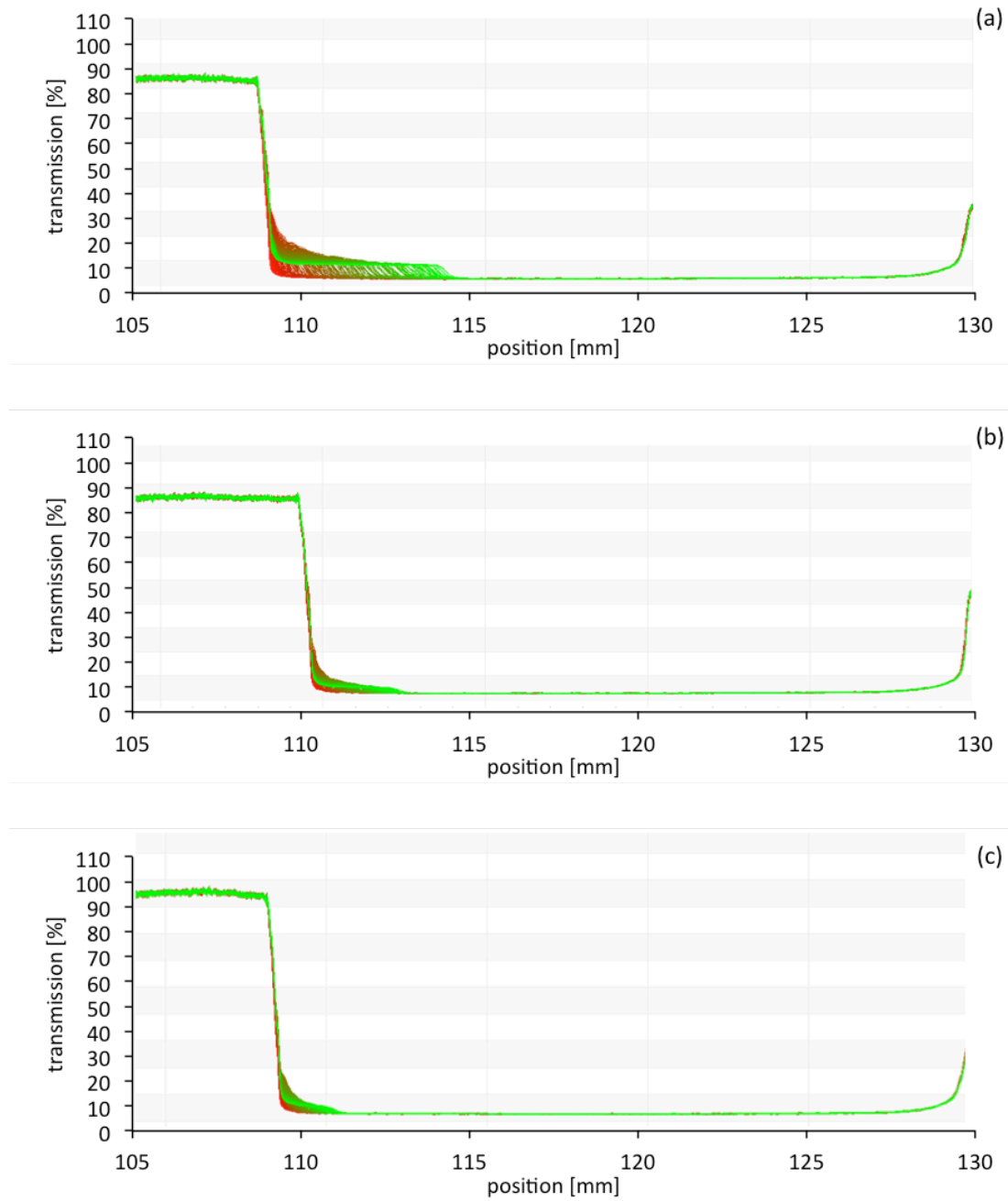


Figure G.22 - Transmission profile evolution of 60EG+40%DW D60-100 L5-15 (a) 0,25%vol. (b) 0,75%vol. (c) 1,5%vol. @ RCF=1000 G's

D50-80 L10-20 + 30%EG+70%DW @ 1000 G's

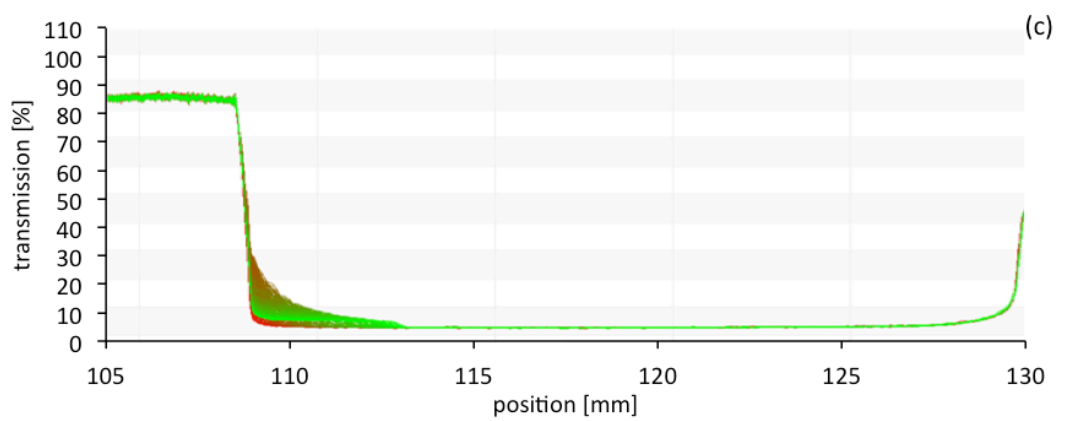
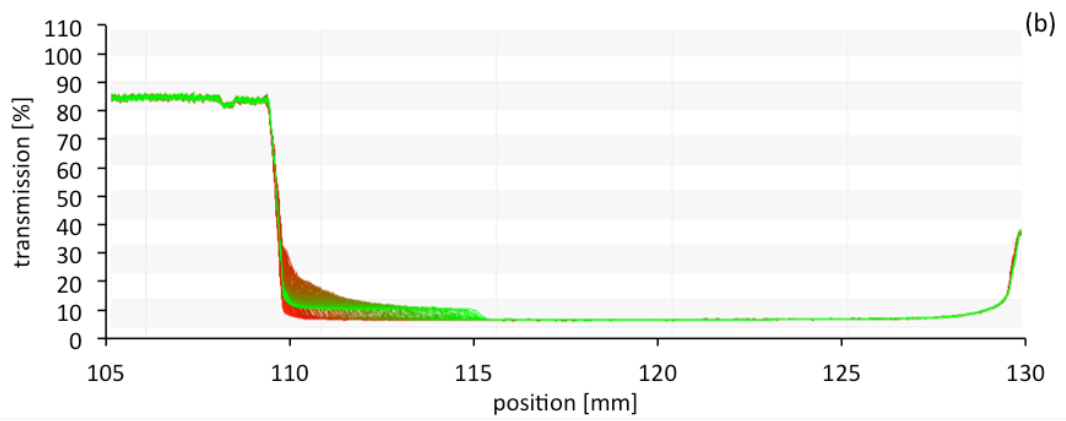
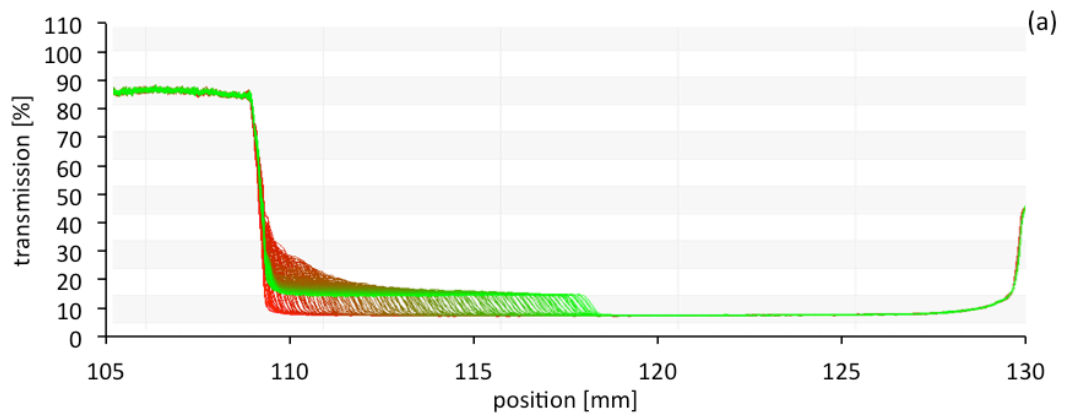


Figure G.23 - Transmission profile evolution of 30EG+70%DW D50-80 L10-20 (a) 0,25%vol. (b) 0,75%vol. (c) 1,5%vol. @ RCF=1000 G's

D50-80 L10-20 + 60%EG+40%DW @ 1000 G's

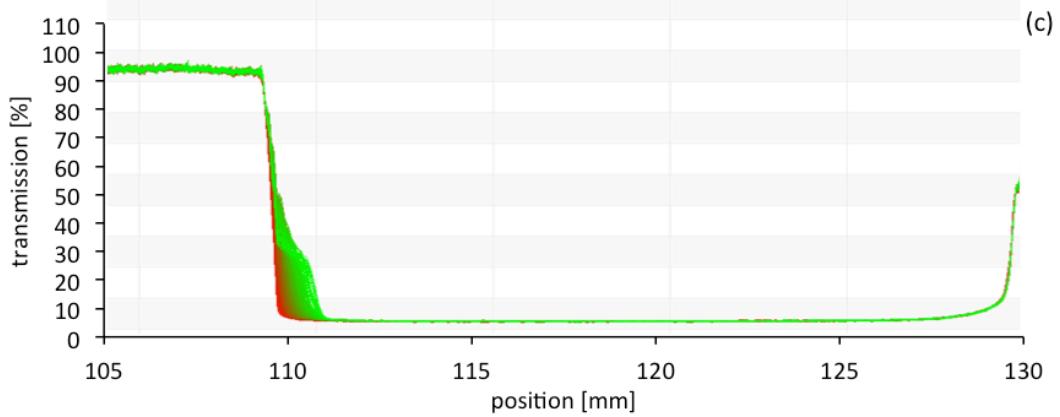
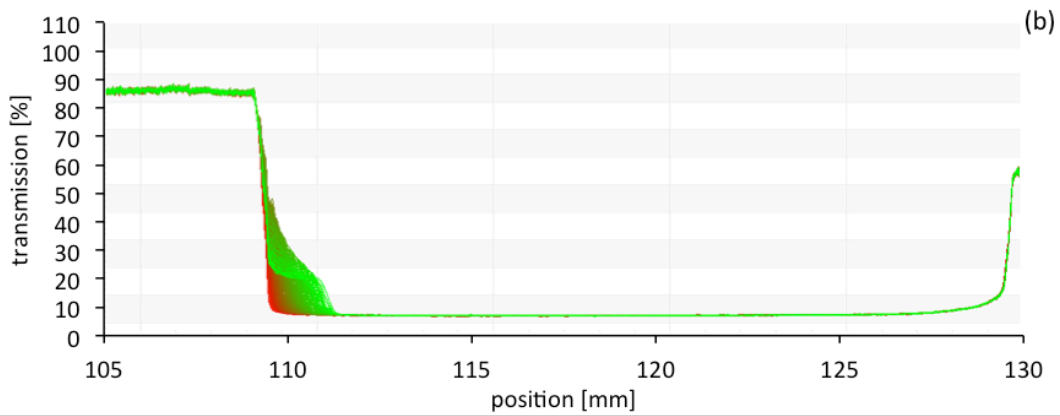
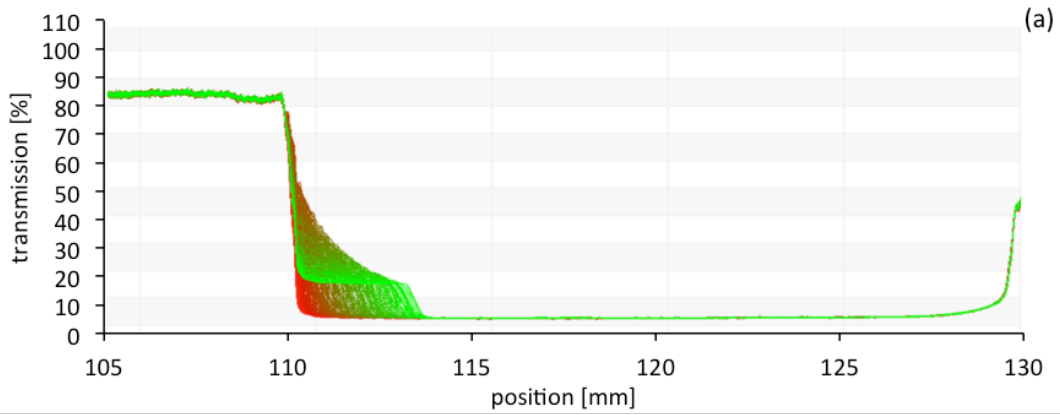


Figure G.24 - Transmission profile evolution of 60EG%+40%DW D50-80 L10-20 (a) 0,25%vol. (b) 0,75%vol. (c) 1,5%vol. @ RCF=1000 G's

D20-40 L1-2 + 30%EG+70%DW @ RCF = 2000 G's

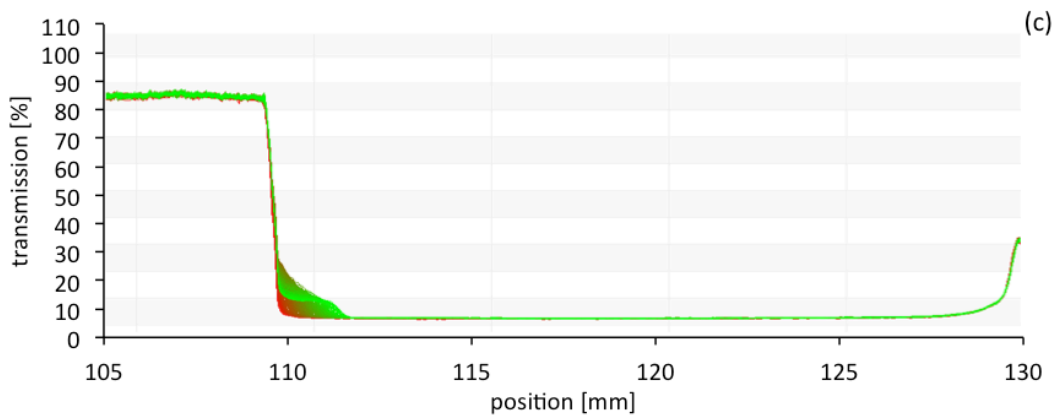
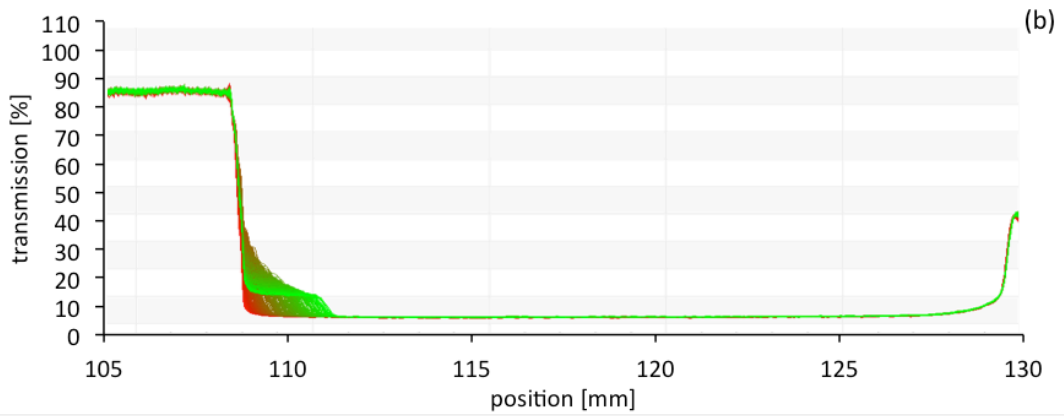
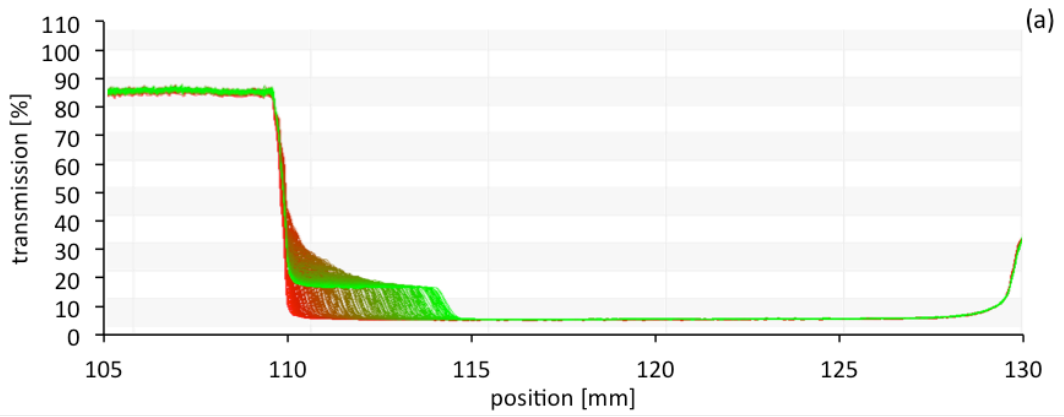


Figure G.25 - Transmission profile evolution of 30EG+70%DW D20-40 L1-2 (a) 0,25%vol. (b) 0,75%vol. (c) 1,5%vol. @ RCF=2000 G's

D20-40 L1-2 + 60%EG+40%DW @ RCF = 2000 G's

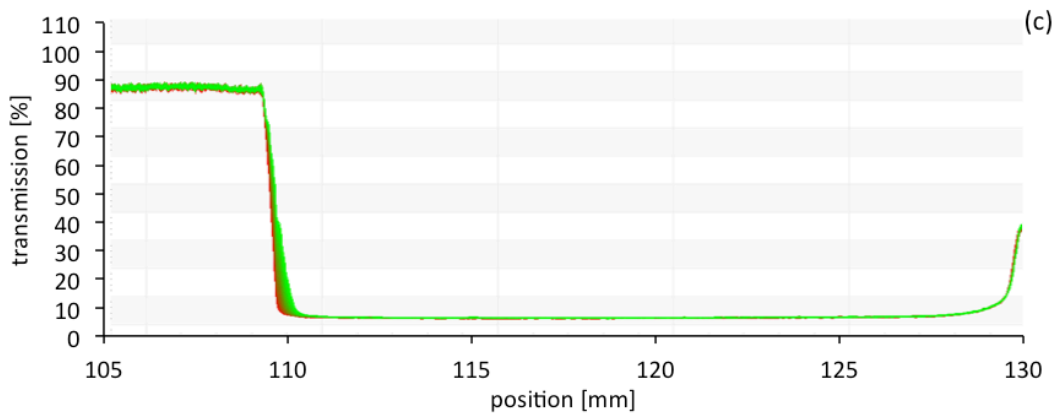
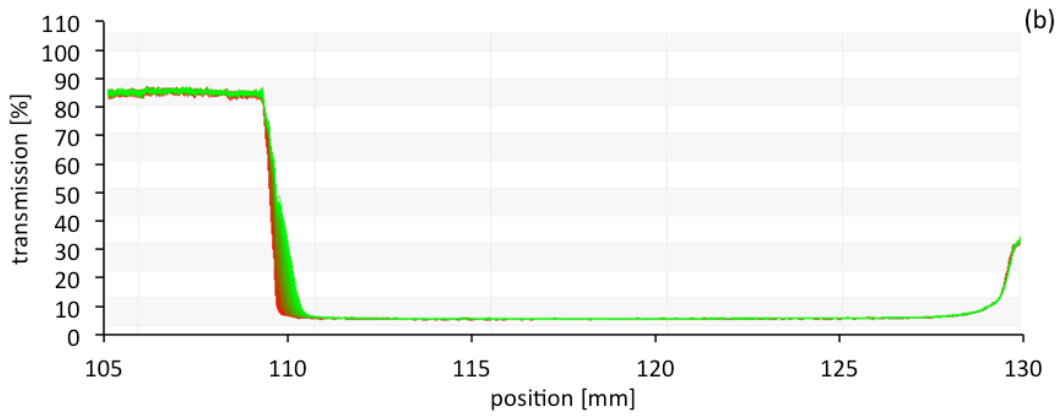
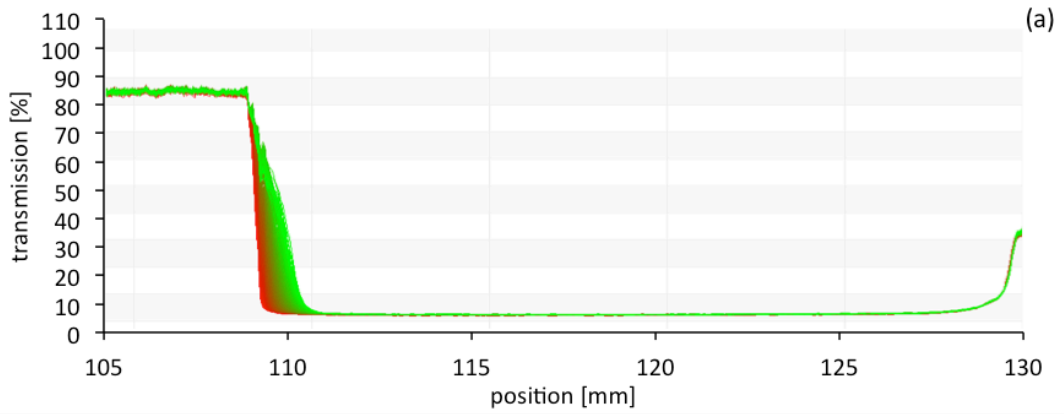


Figure G.26 - Transmission profile evolution of 60EG%+40%DW D20-40 L1-2 (a) 0,25%vol. (b) 0,75%vol. (c) 1,5%vol. @ RCF=2000 G's

D20-40 L5-15 + 30%EG+70%DW @ RCF = 2000 G's

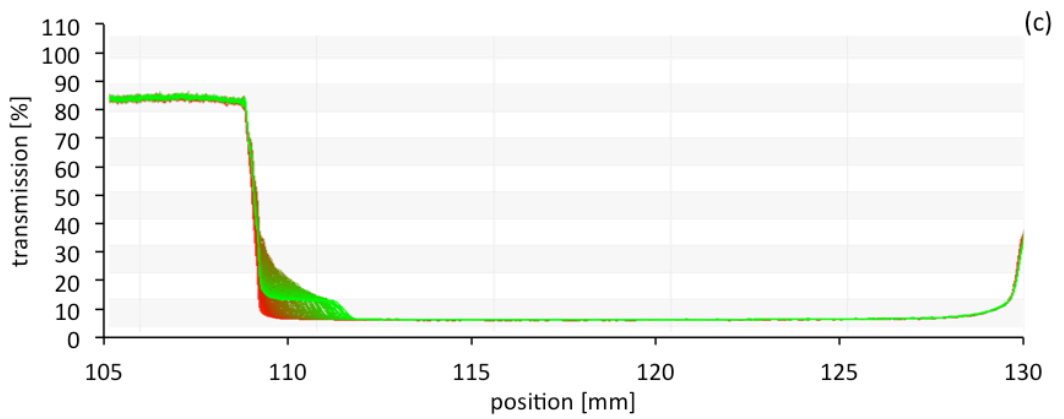
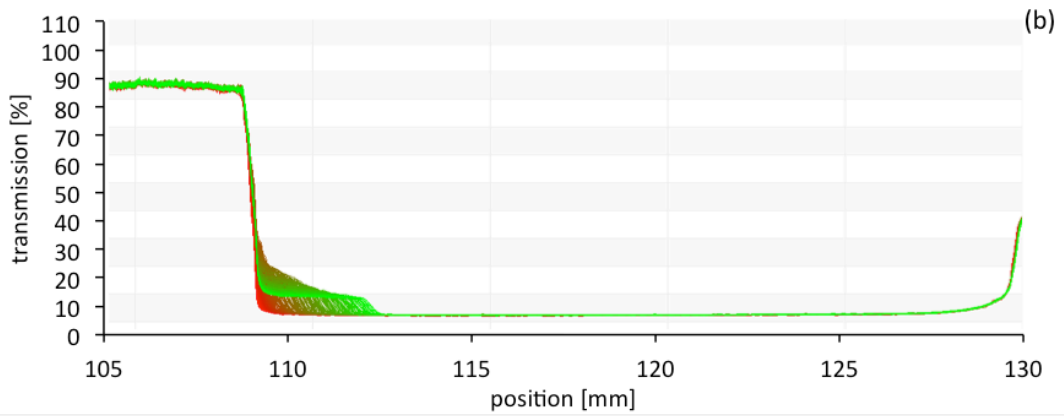
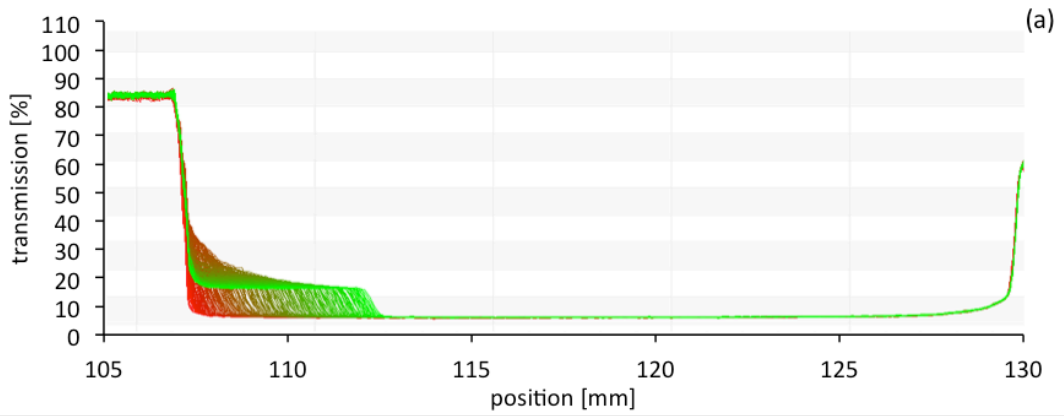


Figure G.27 - Transmission profile evolution of 30EG%+70%DW D20-40 L5-15 (a) 0,25%vol. (b) 0,75%vol. (c) 1,5%vol. @ RCF=2000 G's

D20-40 L5-15 + 60%EG+40%DW @ RCF = 2000 G's

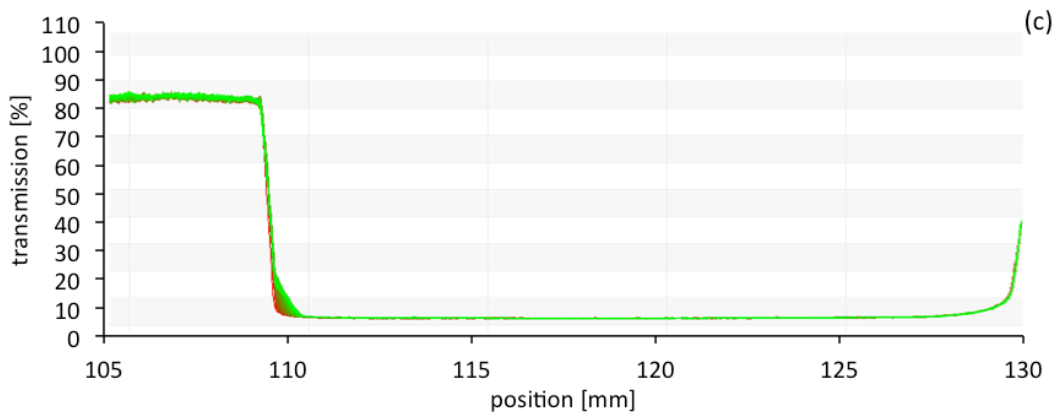
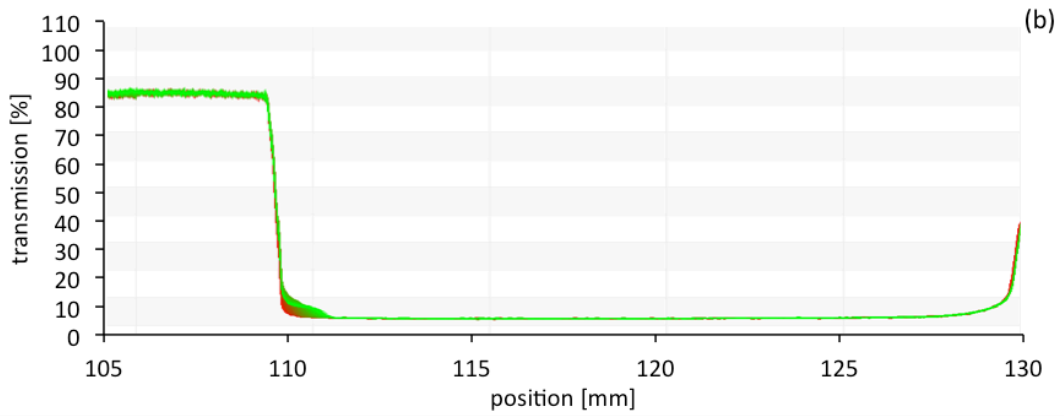
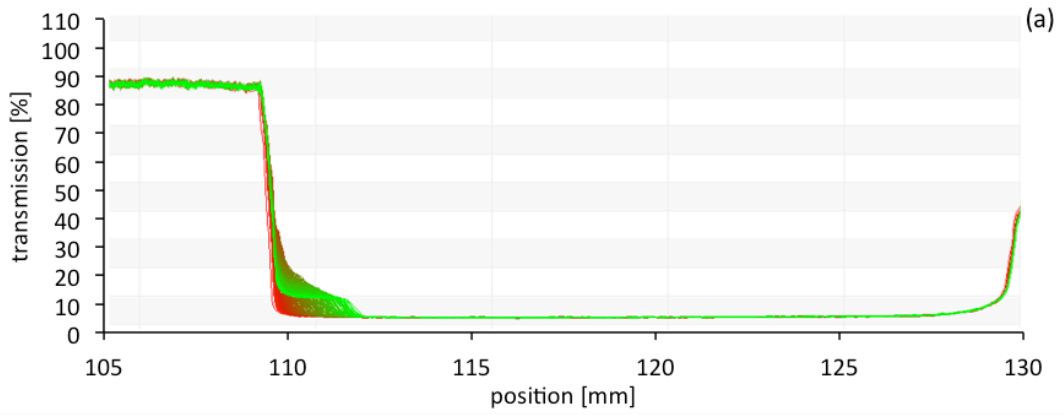


Figure G.28 - Transmission profile evolution of 60EG%+40%DW D20-40 L5-15 (a) 0,25%vol. (b) 0,75%vol. (c) 1,5%vol. @ RCF=2000 G's

D20-10 L10-30 + 30%EG+70%DW @ 2000 G's

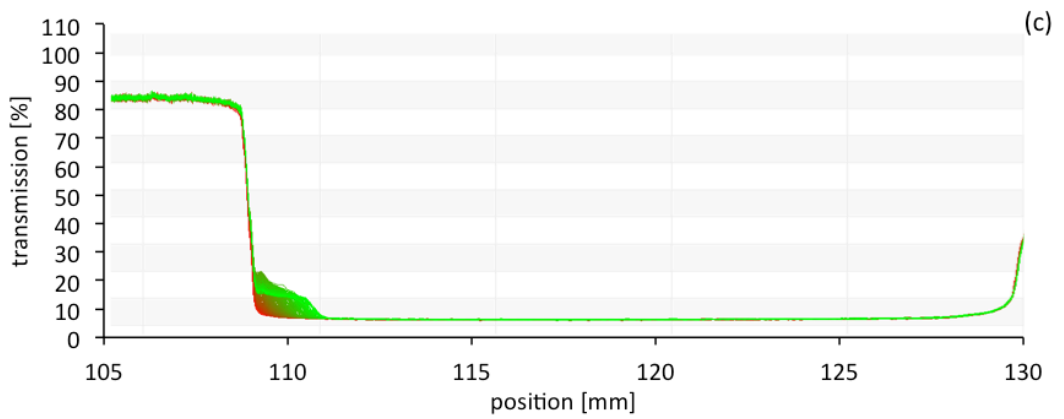
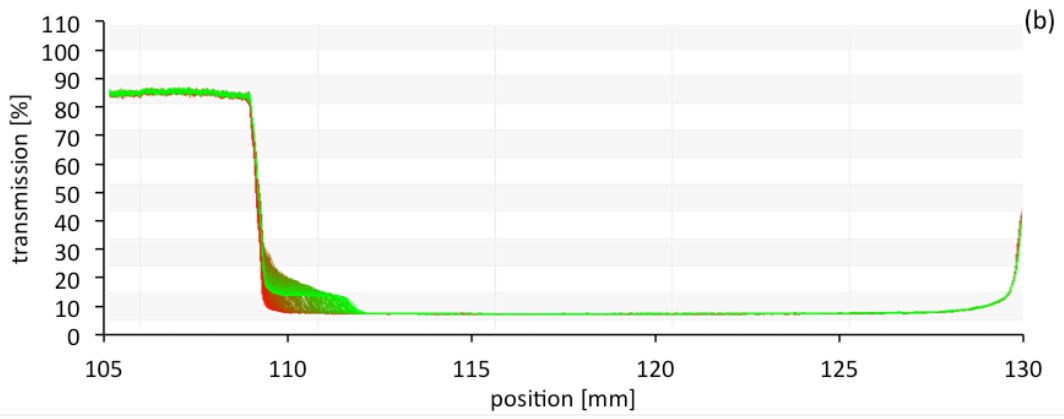
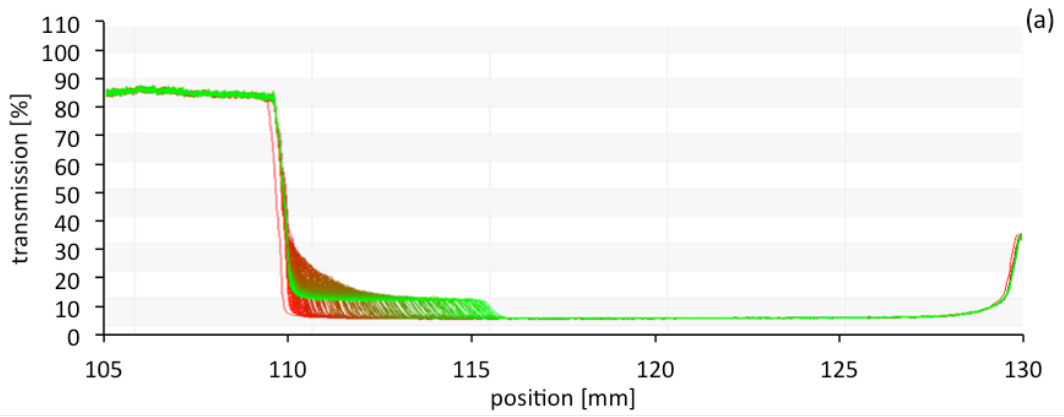


Figure G.29 - Transmission profile evolution of 30EG%+70%DW D20-40 L10-30 (a) 0,25%vol. (b) 0,75%vol. (c) 1,5%vol. @ RCF=2000 G's

D20-10 L10-30 + 60%EG+40%DW @ 2000 G's

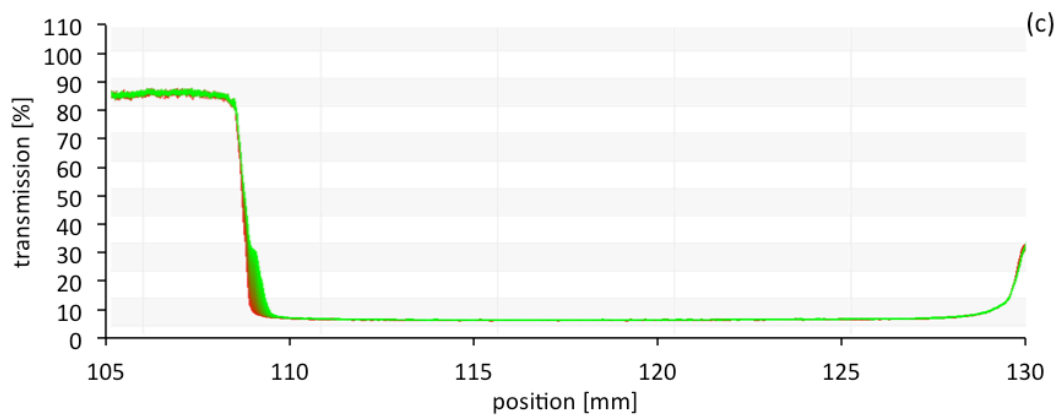
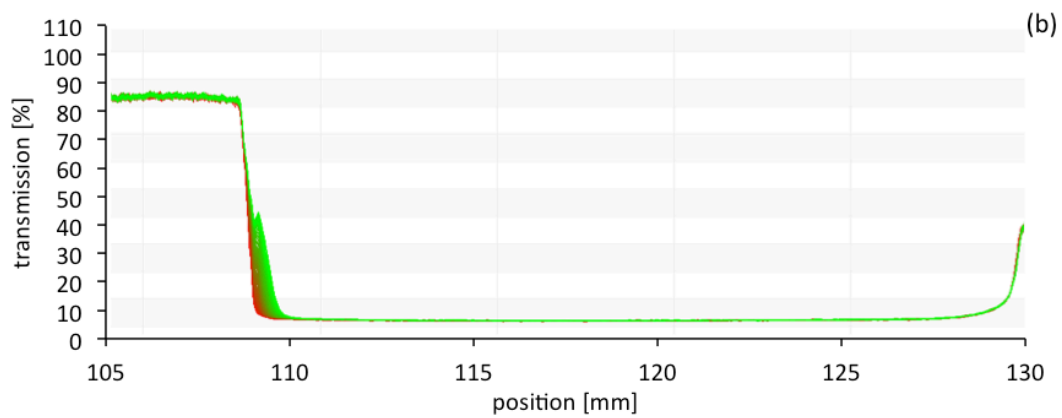
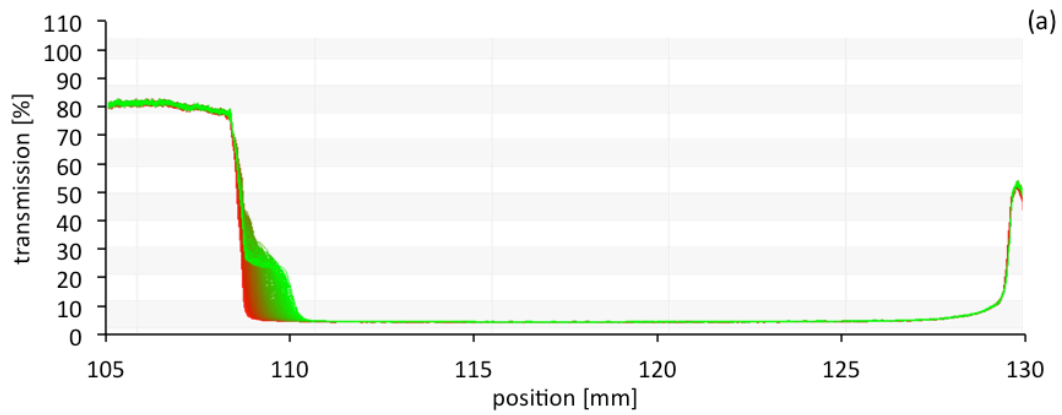


Figure G.30 - Transmission profile evolution of 60EG%+40%DW D20-40 L10-30 (a) 0,25%vol. (b) 0,75%vol. (c) 1,5%vol. @ RCF=2000 G's

D60-100 L1-2 + 30%EG+70%DW @ 2000 G's

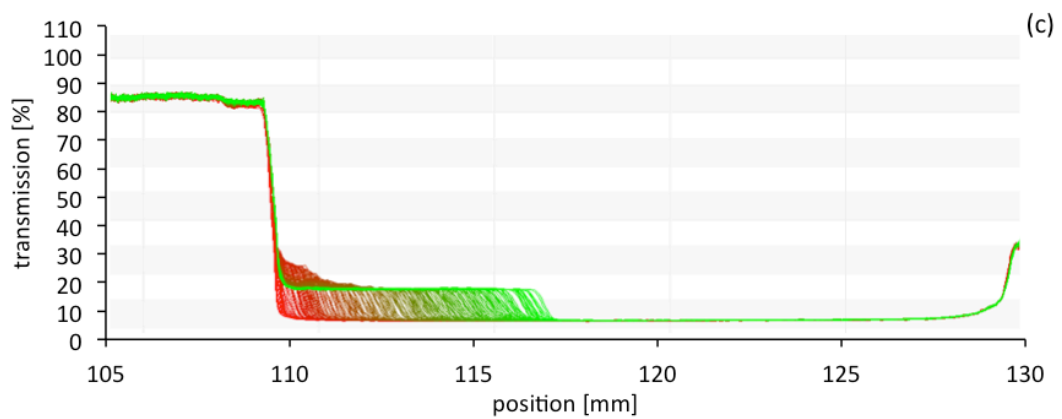
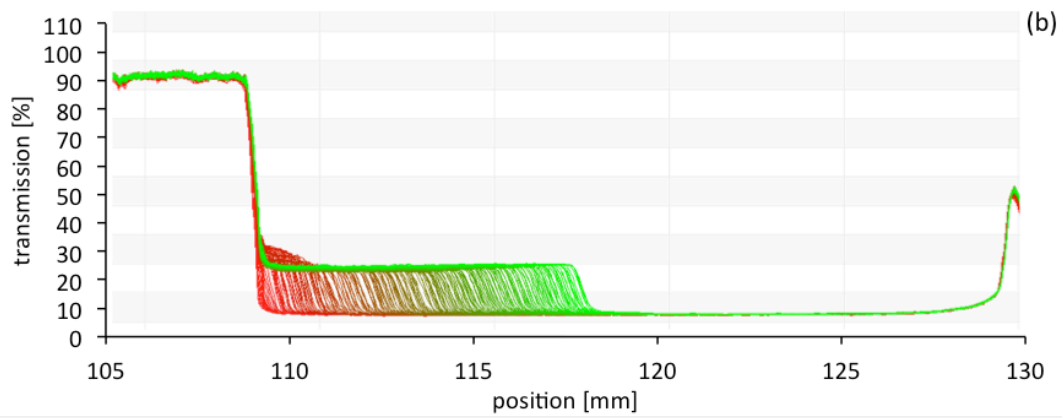
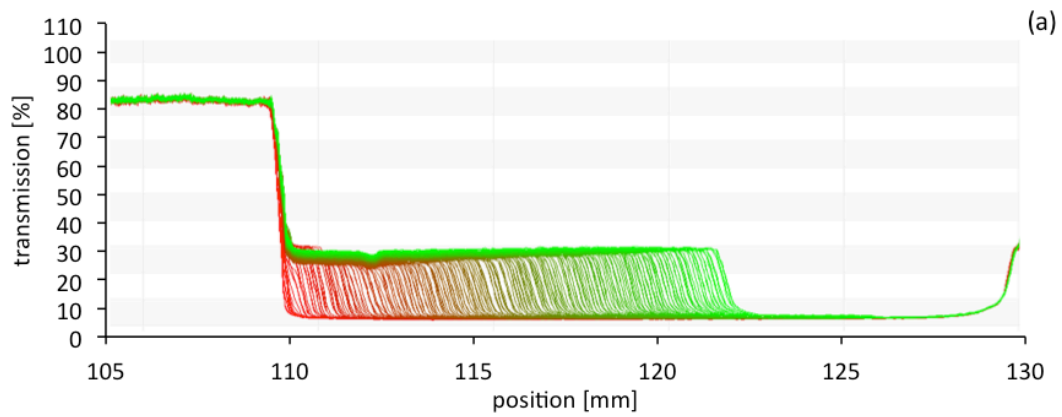


Figure G.31 - Transmission profile evolution of 30EG%+70%DW D60-100 L1-2 (a) 0,25%vol. (b) 0,75%vol. (c) 1,5%vol. @ RCF=2000 G's

D60-100 L1-2 + 60%EG+40%DW @ 2000 G's

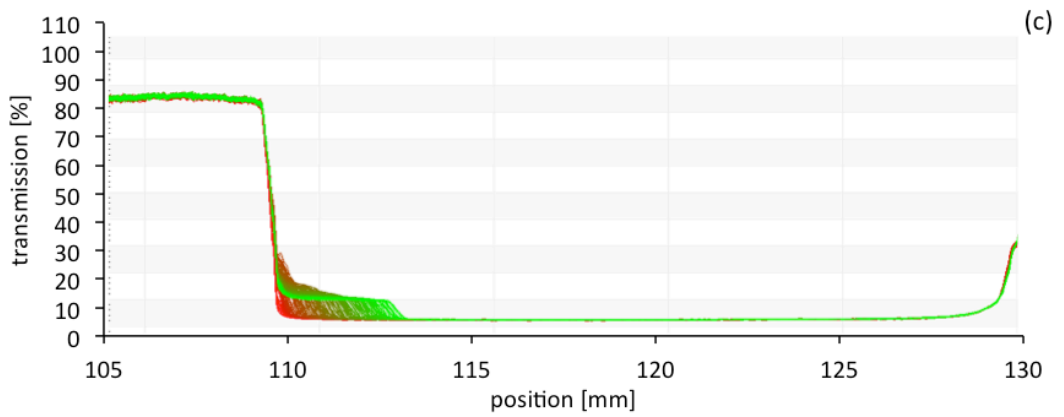
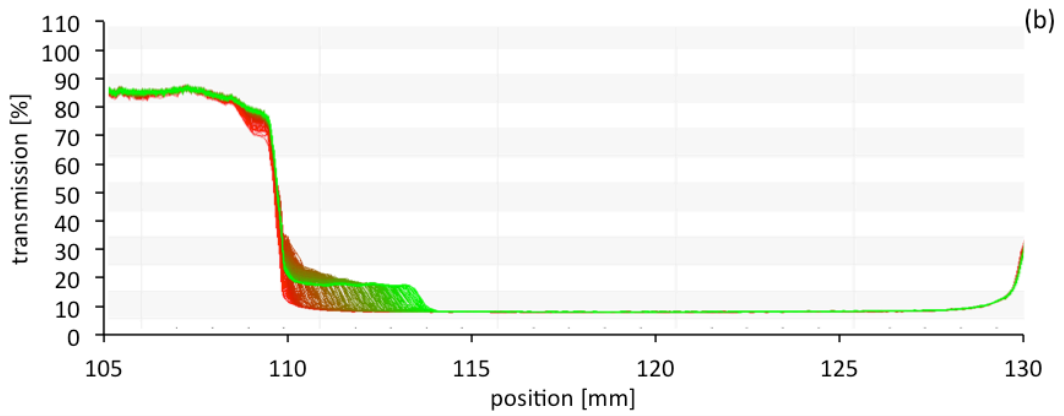
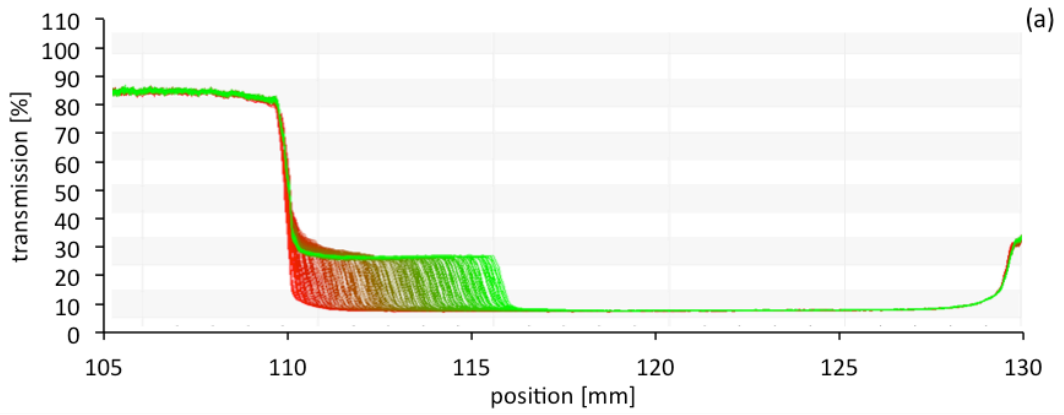


Figure G.32 - Transmission profile evolution of 60EG%+40%DW D60-100 L1-2 (a) 0,25%vol. (b) 0,75%vol. (c) 1,5%vol. @ RCF=2000 G's

D60-100 L5-15 + 30%EG+70%DW @ 2000 G's

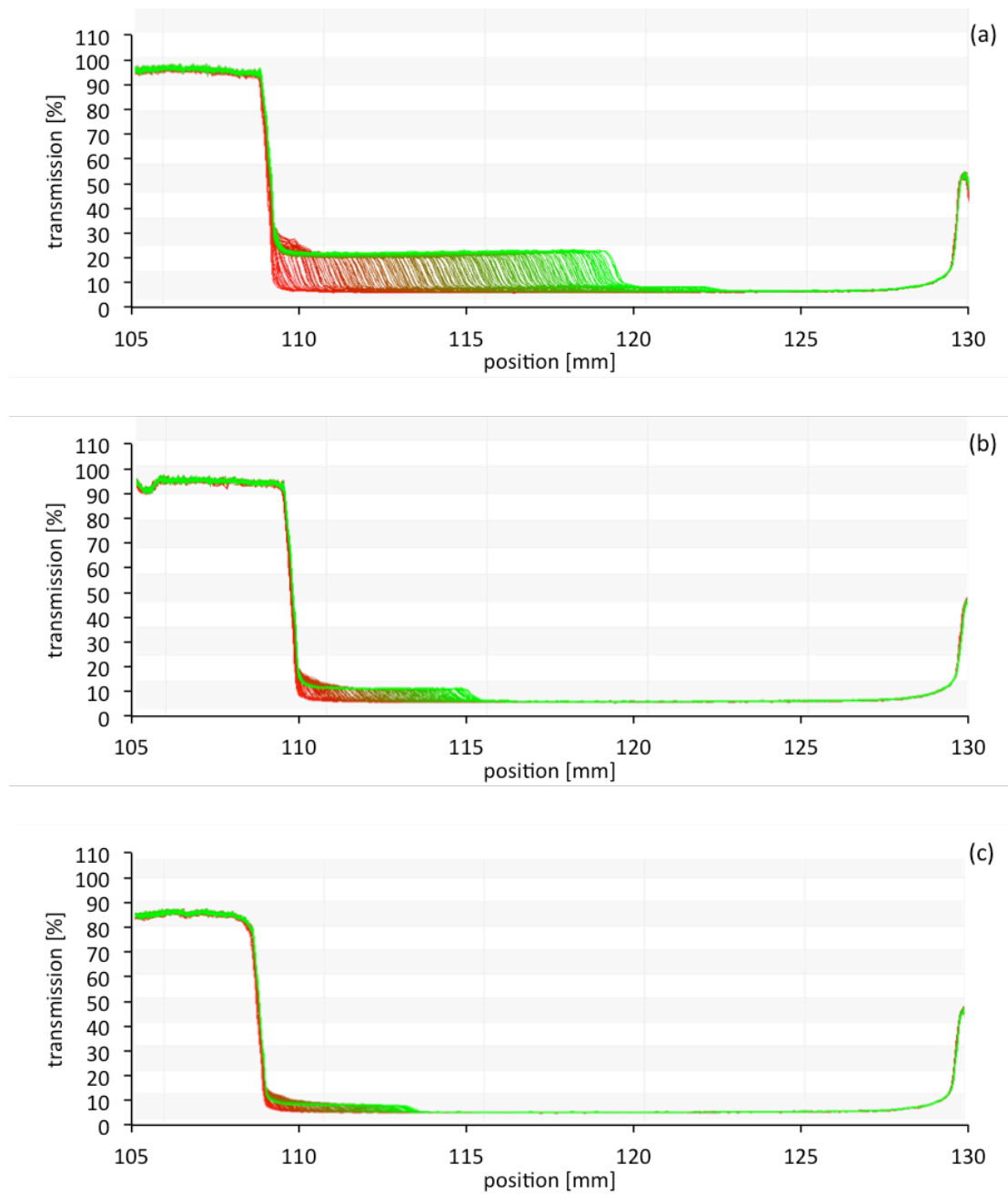


Figure G.33 - Transmission profile evolution of 30EG+70%DW D60-100 L5-15 (a) 0,25%vol. (b) 0,75%vol. (c) 1,5%vol. @ RCF=2000 G's

D60-100 L5-15 + 60%EG+40%DW @ 2000 G's

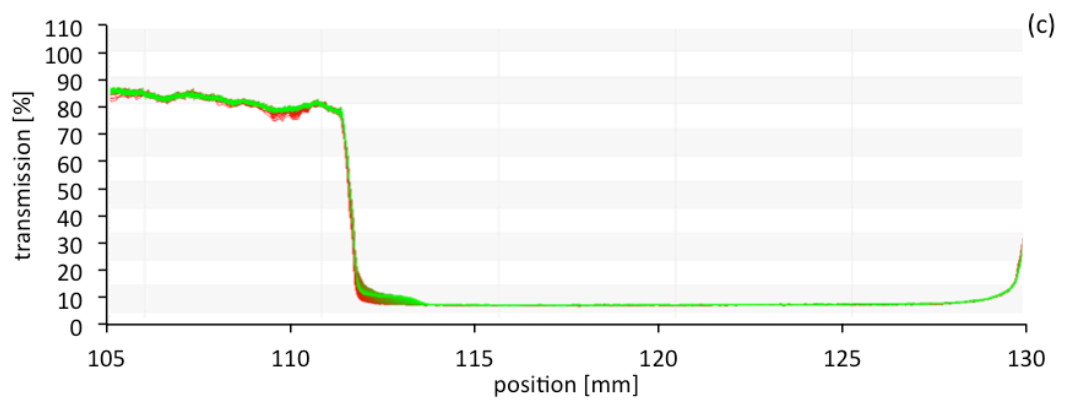
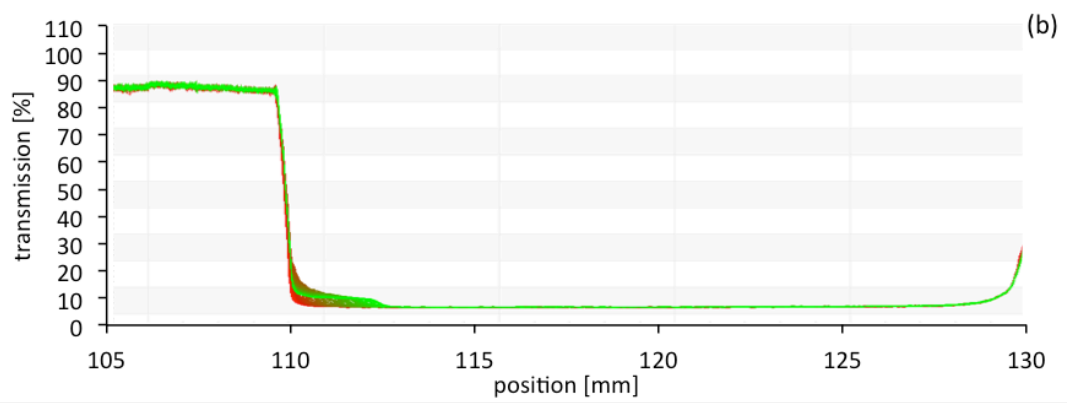
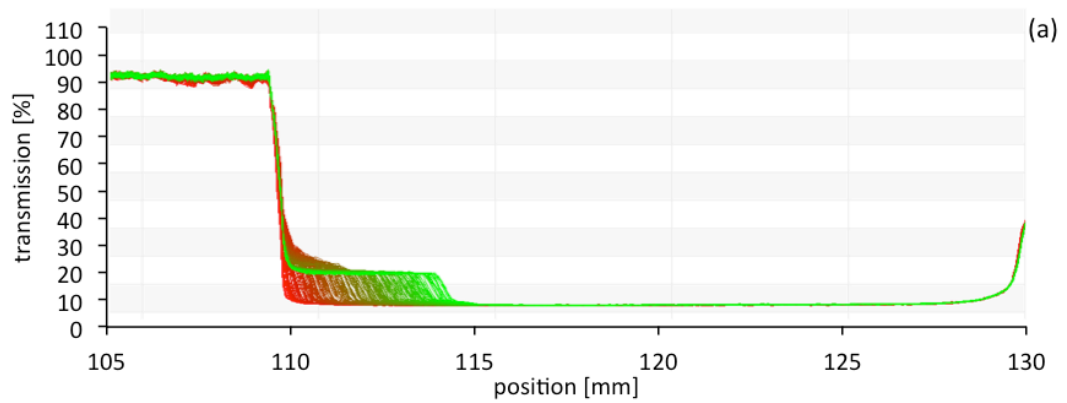


Figure G.34 - Transmission profile evolution of 60EG+40DW D60-100 L5-15 (a) 0,25%vol. (b) 0,75%vol. (c) 1,5%vol. @ RCF=2000 G's

D50-80 L10-20 + 30%EG+70%DW @ 2000 G's

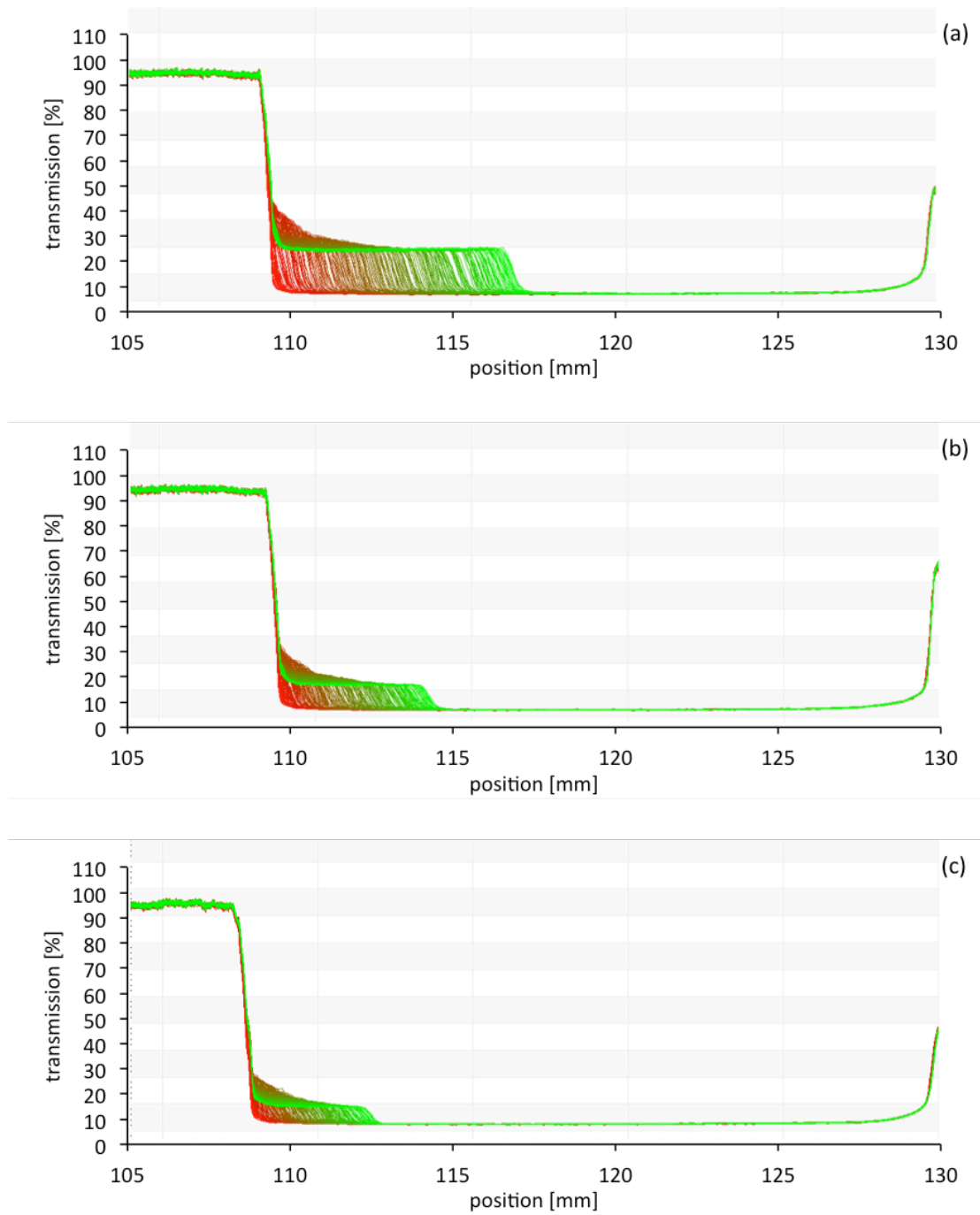


Figure G.35 - Transmission profile evolution of 30EG+70%DW D50-80 L10-20 (a) 0,25%vol. (b) 0,75%vol. (c) 1,5%vol. @ RCF=2000 G's

D50-80 L10-20 + 60%EG+40%DW @ 2000 G's

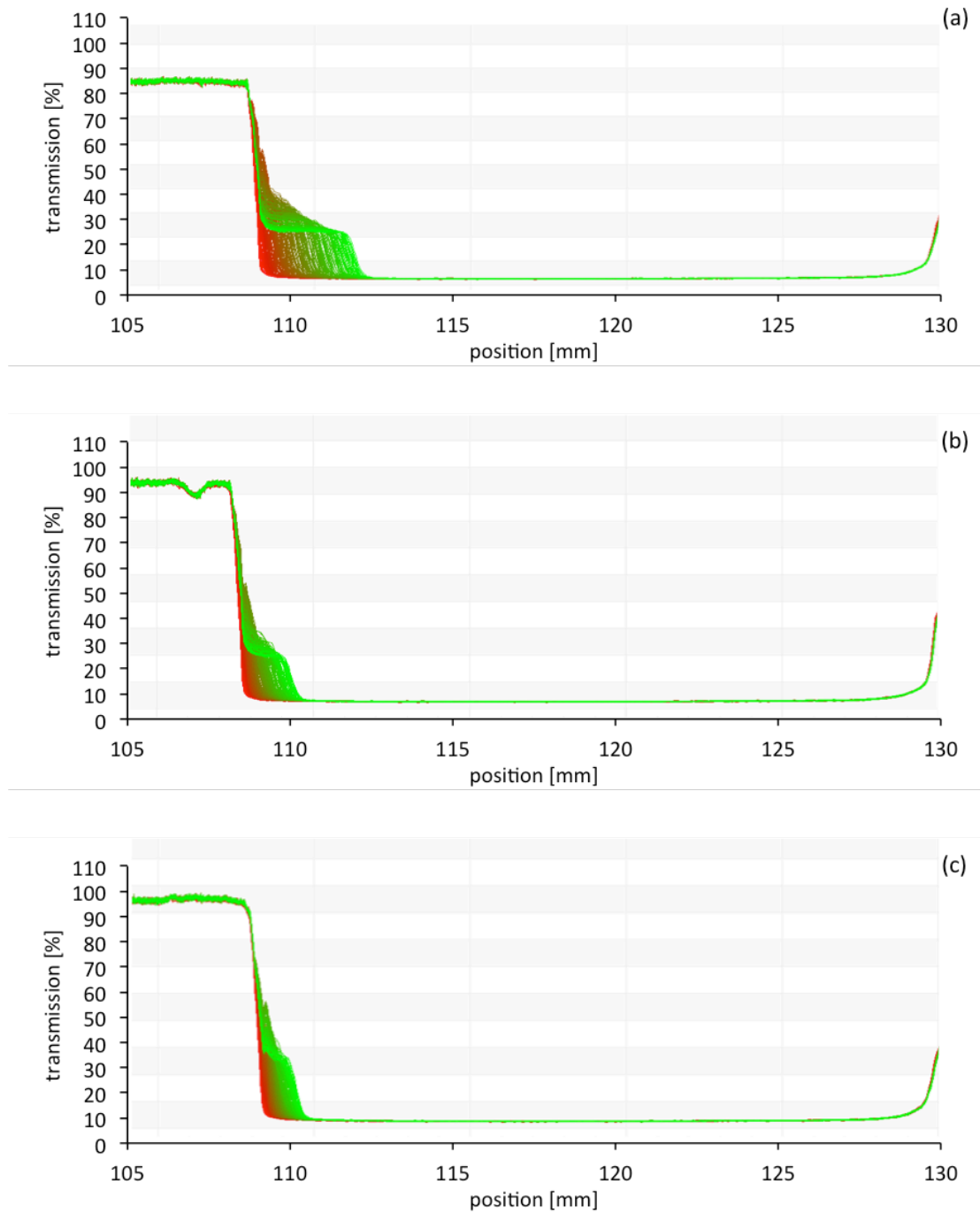


Figure G.36 - Transmission profile evolution of 60EG%+40%DW D50-80 L10-20 (a) 0,25%vol. (b) 0,75%vol. (c) 1,5%vol. @ RCF=2000 G's

H. Phase Separation Rate

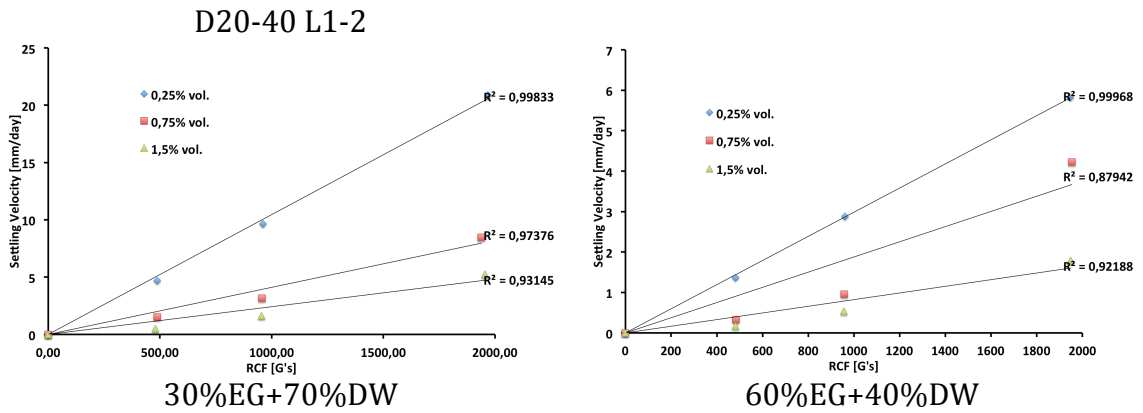


Figure H.1 - Settling velocity (phase separation) as a function of the RCF for different concentrations of D20-40 L1-2 MWCNTs

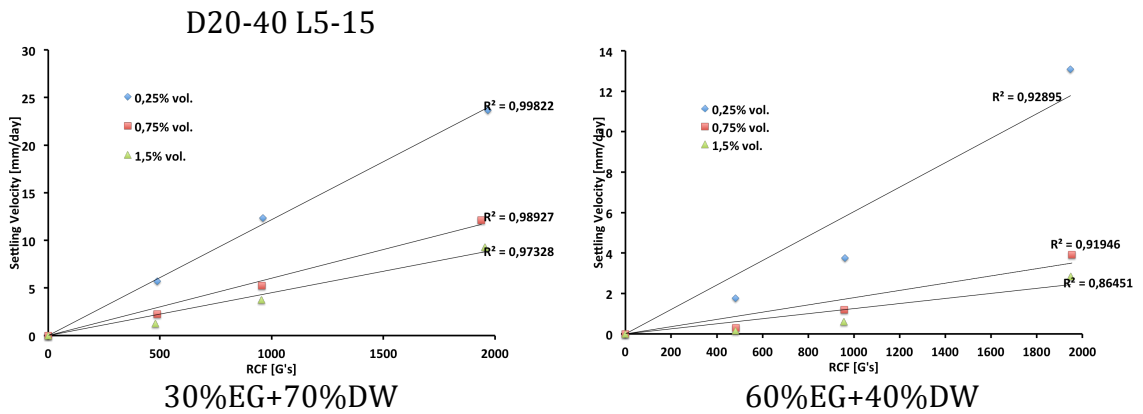


Figure H.2 - Settling velocity (phase separation) as a function of the RCF for different concentrations of D20-40 L5-15 MWCNTs

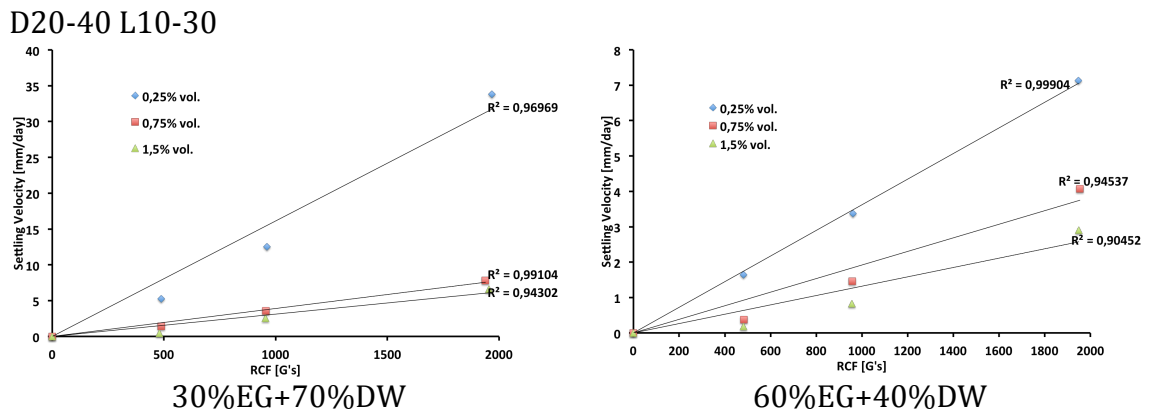
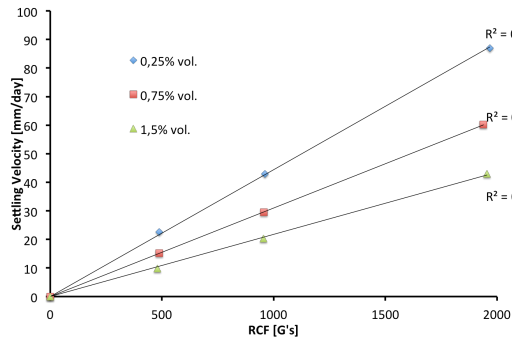
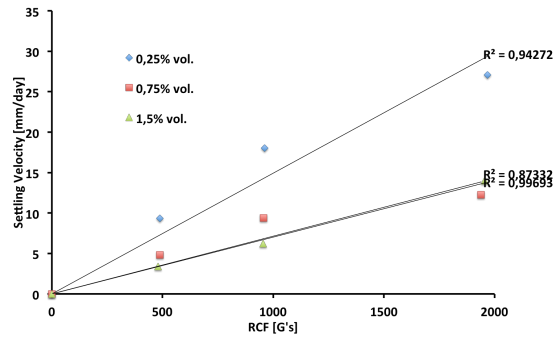


Figure H.3 - Settling velocity (phase separation) as a function of the RCF for different concentrations of D20-40 L1-2 MWCNTs

D60-100 L1-2



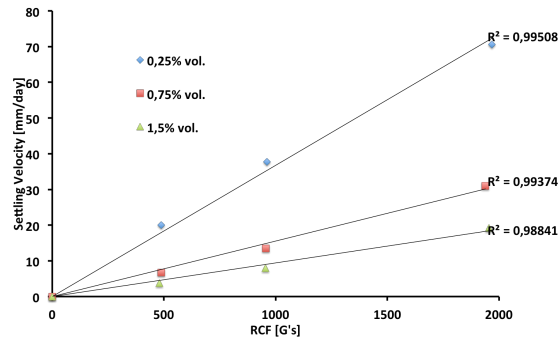
30%EG+70%DW



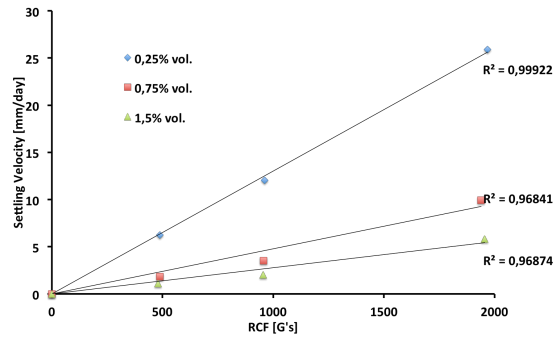
60%EG+40%DW

Figure H.4 - Settling velocity (phase separation) as a function of the RCF for different concentrations of D20-40 L1-2 MWCNTs

D60-100 L5-15



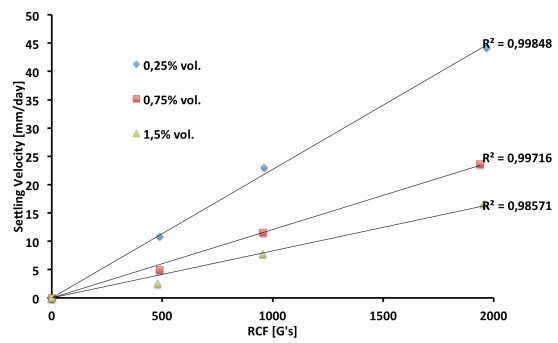
30%EG+70%DW



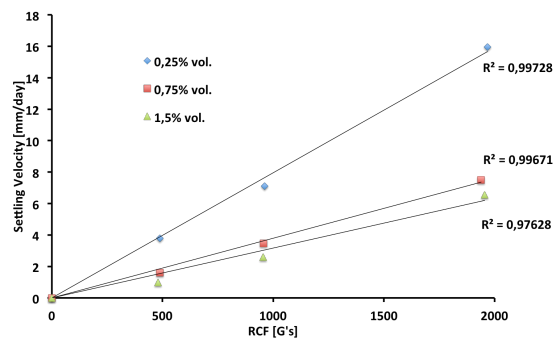
60%EG+40%DW

Figure H.5 - Settling velocity (phase separation) as a function of the RCF for different concentrations of D20-40 L1-2 MWCNTs

D50-80 L10-20



30%EG+70%DW



60%EG+40%DW

Figure H.6 - Settling velocity (phase separation) as a function of the RCF for different concentrations of D20-40 L1-2 MWCNTs

I. FTIR Evaluation

D20-40 L1-2

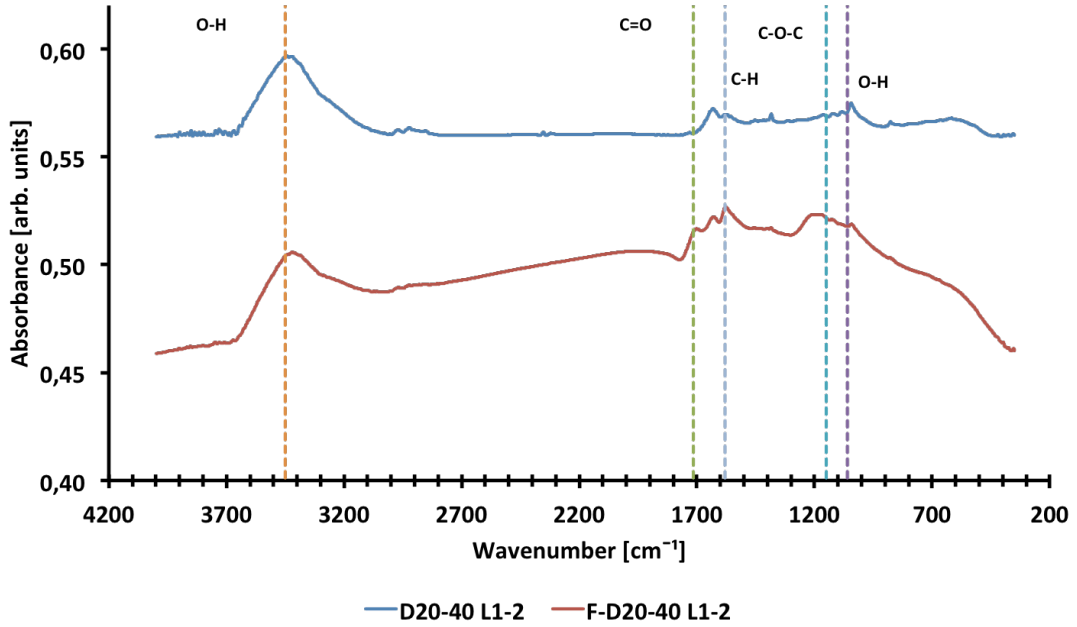


Figure I.1 – FTIR spectrum for bulk and functionalized D20-40 L1-2 MWCNTs

D20-40 L5-15

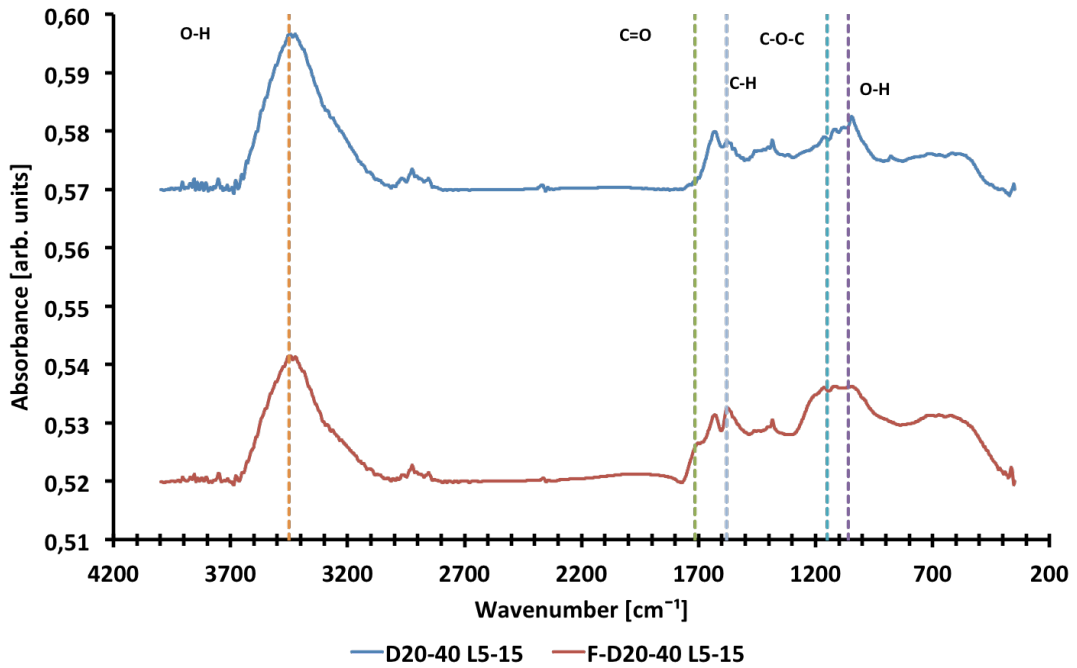


Figure I.2 – FTIR spectrum for bulk and functionalized D20-40 L5-15 MWCNTs

D20-40 L10-30

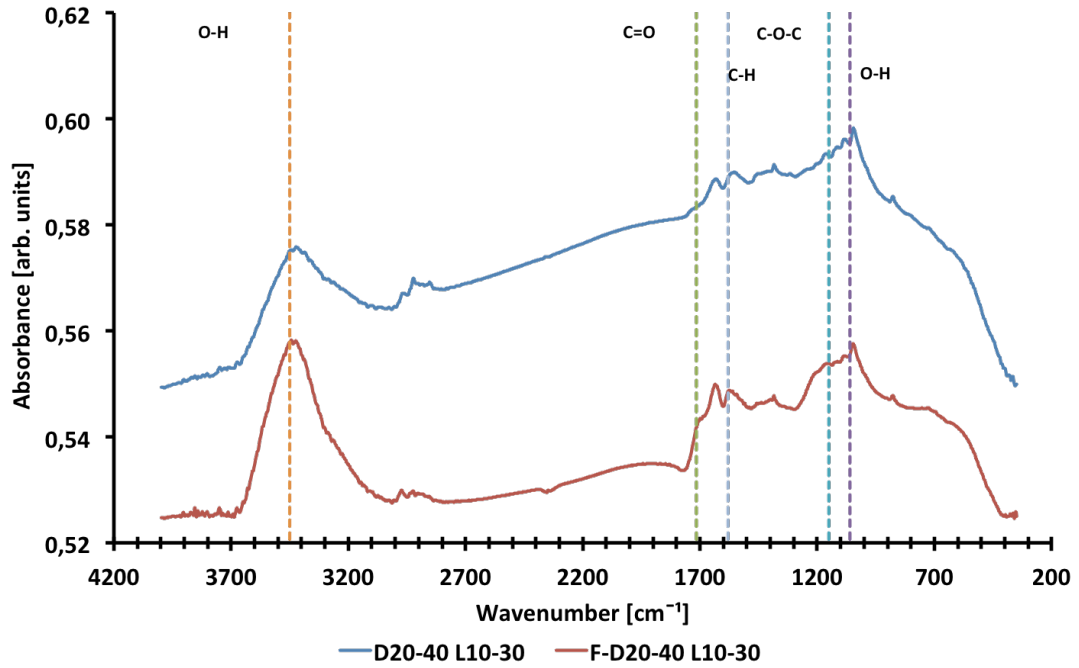


Figure I.3 – FTIR spectrum for bulk and functionalized D20-40 L10-30 MWCNTs

D60-100 L1-2

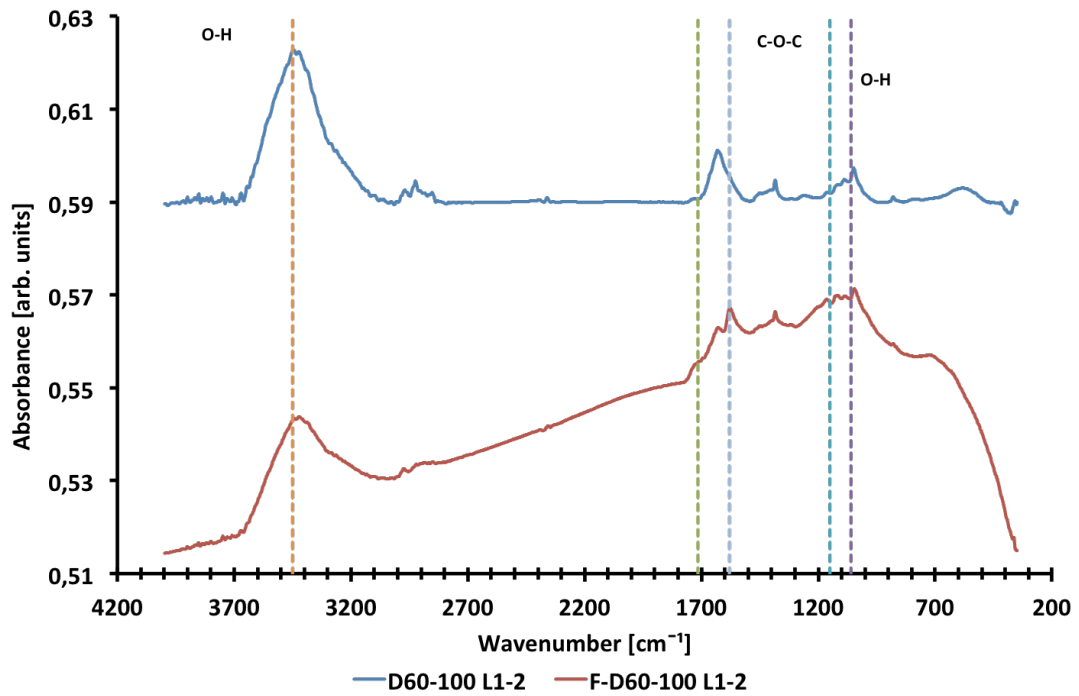


Figure I.4 – FTIR spectrum for bulk and functionalized D60-100 L1-2 MWCNTs

D60-100 L5-15

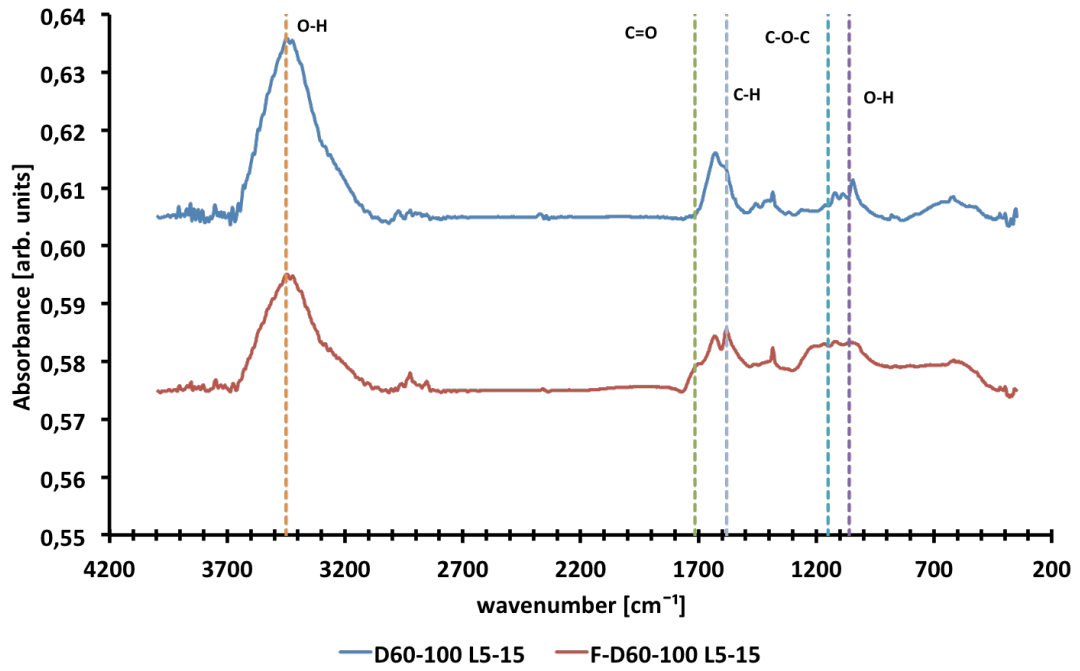


Figure I.5 – FTIR spectrum for bulk and functionalized D20-40 L5-15 MWCNTs

D50-80 L10-20

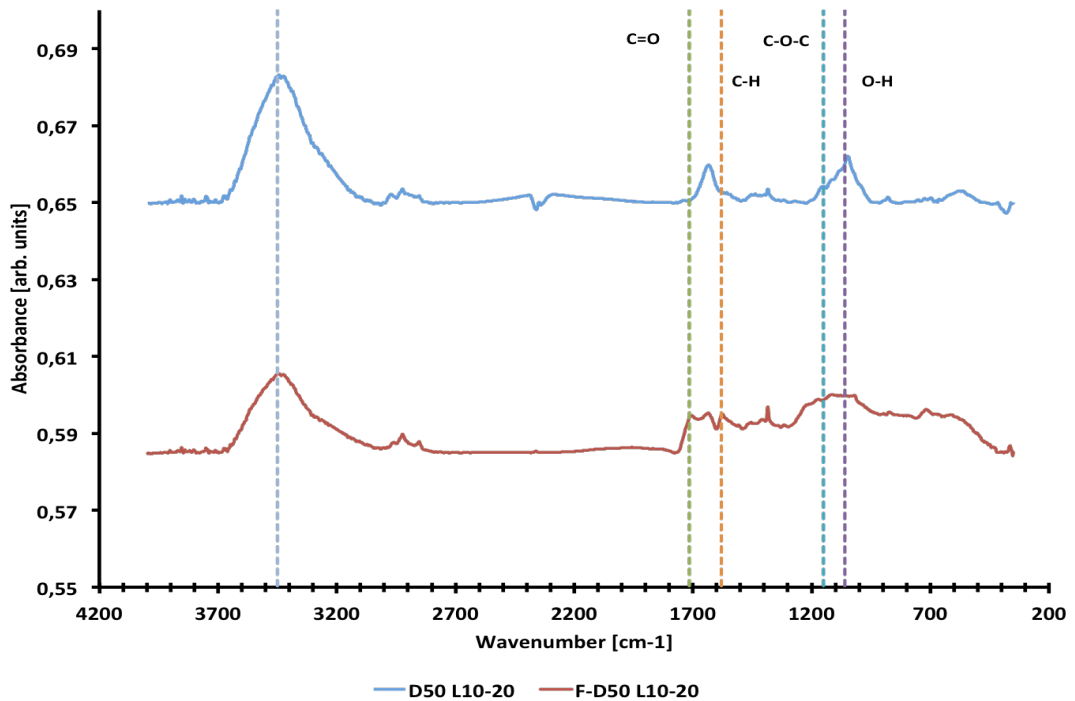


Figure I.6 – FTIR spectrum for bulk and functionalized D50-80 L10-20 MWCNTs

J. Nanofluids Effective Viscosity Tables

MWCNTs Base Fluid % vol. Shear Rate [s ⁻¹]		D20-40 L1-2 30%EG+70%DW 0,25													
		85,4	±	122	±	158,6	±	195,3	±	231,9	±	268,5	±	305,1	±
Temp. [K]	283,15	3,621	0,014	3,614	0,004	3,607	0,005	3,482	0,000	3,491	0,003	3,460	0,003	3,463	0,003
	293,15	2,613	0,015	2,629	0,004	2,618	0,003	2,589	0,002	2,573	0,004	2,601	0,000	2,539	0,003
	298,15	2,256	0,013	2,283	0,007	2,295	0,005	2,267	0,005	2,225	0,004	2,263	0,002	2,264	0,002
	303,15	1,993	0,013	1,989	0,009	2,029	0,005	1,999	0,004	1,925	0,002	1,956	0,000	1,957	0,000
	313,15	1,556	0,014	1,566	0,006	1,580	0,005	1,579	0,005	1,506	0,006	1,521	0,002	1,507	0,002
	323,15	1,262	0,013	1,249	0,007	1,257	0,000	1,261	0,000	1,236	0,005	1,216	0,003	1,170	0,000
	333,15	1,049	0,010	1,035	0,006	1,021	0,000	1,023	0,004	1,018	0,003	0,968	0,001	0,950	0,002

MWCNTs Base Fluid % vol. Shear Rate [s ⁻¹]		D20-40 L1-2 30%EG+70%DW 0,50													
		85,4	±	122	±	158,6	±	195,3	±	231,9	±	268,5	±	305,1	±
Temp. [K]	283,15	3,929	0,018	3,918	0,012	3,862	0,007	3,752	0,006	3,743	0,002	3,675	0,000	3,678	0,003
	293,15	2,881	0,010	2,850	0,007	2,827	0,004	2,789	0,003	2,793	0,004	2,795	0,002	2,756	0,003
	298,15	2,448	0,014	2,447	0,007	2,473	0,004	2,446	0,004	2,385	0,003	2,398	0,000	2,418	0,002
	303,15	2,165	0,011	2,155	0,005	2,191	0,000	2,186	0,003	2,105	0,006	2,110	0,003	2,106	0,003
	313,15	1,685	0,012	1,702	0,007	1,712	0,006	1,717	0,004	1,642	0,006	1,653	0,003	1,643	0,003
	323,15	1,342	0,010	1,343	0,005	1,368	0,000	1,369	0,002	1,331	0,004	1,330	0,000	1,278	0,004
	333,15	1,101	0,014	1,158	0,004	1,119	0,005	1,110	0,003	1,077	0,003	1,050	0,003	1,005	0,003

MWCNTs Base Fluid % vol. Shear Rate [s ⁻¹]		D20-40 L1-2 30%EG+70%DW 0,75													
		85,4	±	122	±	158,6	±	195,3	±	231,9	±	268,5	±	305,1	±
Temp. [K]	283,15	4,544	0,024	4,621	0,007	4,600	0,003	4,483	0,002	4,453	0,004	4,377	0,002	4,339	0,006
	293,15	3,185	0,019	3,197	0,007	3,228	0,006	3,181	0,000	3,188	0,000	3,176	0,000	3,153	0,002
	298,15	2,732	0,020	2,779	0,008	2,805	0,004	2,800	0,000	2,731	0,003	2,744	0,003	2,777	0,001
	303,15	2,422	0,029	2,423	0,007	2,469	0,005	2,504	0,000	2,397	0,002	2,414	0,004	2,417	0,006
	313,15	1,845	0,020	1,844	0,007	1,906	0,011	1,953	0,009	1,857	0,005	1,859	0,003	1,859	0,006
	323,15	1,471	0,020	1,478	0,013	1,505	0,000	1,541	0,010	1,506	0,005	1,481	0,011	1,418	0,009
	333,15	1,231	0,022	1,224	0,013	1,223	0,009	1,274	0,006	1,220	0,007	1,168	0,005	1,096	0,009

MWCNTs Base Fluid % vol. Shear Rate [s ⁻¹]		D20-40 L1-2 30%EG+70%DW 1,00													
		85,4	±	122	±	158,6	±	195,3	±	231,9	±	268,5	±	305,1	±
Temp. [K]	283,15	4,654	0,016	4,706	0,011	4,692	0,005	4,514	0,000	4,476	0,003	4,366	0,001	4,364	0,002
	293,15	3,342	0,024	3,362	0,010	3,402	0,003	3,340	0,003	3,255	0,001	3,245	0,000	3,198	0,002
	298,15	2,840	0,018	2,868	0,005	2,955	0,009	1,341	0,019	2,836	0,002	2,823	0,000	2,868	0,058
	303,15	2,508	0,018	2,536	0,008	2,586	0,004	2,612	0,004	2,509	0,004	2,508	0,002	2,528	0,001
	313,15	1,949	0,017	1,932	0,009	2,004	0,006	2,032	0,004	1,993	0,004	1,971	0,003	1,966	0,002
	323,15	1,603	0,116	1,581	0,010	1,594	0,000	1,617	0,004	1,621	0,004	1,599	0,000	1,529	0,001
	333,15	1,341	0,019	1,333	0,010	1,328	0,006	1,319	0,003	1,316	0,004	1,248	0,003	1,202	0,002

MWCNTs Base Fluid % vol. Shear Rate [s ⁻¹]		D20-40 L1-2 30%EG+70%DW 1,50													
		85,4	±	122	±	158,6	±	195,3	±	231,9	±	268,5	±	305,1	±
Temp. [K]	283,15	5,549	0,014	5,532	0,005	5,478	0,005	5,253	0,004	5,135	0,000	5,038	0,001	5,035	0,000
	293,15	3,988	0,017	3,958	0,006	3,921	0,000	3,872	0,000	3,837	0,000	3,791	0,003	3,724	0,000
	298,15	3,440	0,017	3,433	0,007	3,442	0,002	3,400	0,000	3,299	0,000	3,291	0,000	3,288	0,001
	303,15	3,026	0,017	3,030	0,007	3,047	0,003	3,036	0,007	2,899	0,004	2,912	0,002	2,899	0,003
	313,15	2,332	0,018	2,332	0,007	2,391	0,005	2,407	0,002	2,286	0,000	2,279	0,000	2,261	0,000
	323,15	1,903	0,015	1,891	0,008	1,925	0,000	1,937	0,008	1,883	0,000	1,831	0,000	1,751	0,002
	333,15	1,619	0,017	1,576	0,006	1,588	0,006	1,641	0,004	1,541	0,011	1,474	0,001	1,386	0,000

MWCNTs Base Fluid % vol. Shear Rate [s ⁻¹]		D20-40 L5-15 30%EG+70%DW 0,25													
		85,4	±	122	±	158,6	±	195,3	±	231,9	±	268,5	±	305,1	±
Temp. [K]	283,15	4,168	0,026	4,237	0,014	4,226	0,004	4,099	0,002	4,074	0,004	4,004	0,002	3,986	0,002
	293,15	2,982	0,025	2,977	0,005	3,019	0,005	2,983	0,000	2,993	0,002	2,992	0,000	2,969	0,001
	298,15	2,577	0,019	2,573	0,008	2,628	0,006	2,634	0,004	2,386	0,123	2,178	0,120	2,200	0,133
	303,15	2,034	0,081	2,047	0,065	2,040	0,069	2,023	0,096	1,925	0,101	1,931	0,102	1,933	0,116
	313,15	1,566	0,061	1,620	0,044	1,624	0,046	1,626	0,057	1,527	0,065	1,515	0,070	1,519	0,078
	323,15	1,247	0,060	1,302	0,046	1,305	0,000	1,311	0,051	1,244	0,052	1,218	0,052	1,174	0,056
	333,15	1,049	0,065	1,091	0,028	1,079	0,035	1,082	0,034	1,033	0,042	0,969	0,041	0,944	0,024

MWCNTs Base Fluid % vol. Shear Rate [s ⁻¹]		D20-40 L5-15 30%EG+70%DW 0,50													
		85,4	±	122	±	158,6	±	195,3	±	231,9	±	268,5	±	305,1	±
Temp. [K]	283,15	3,811	0,017	3,775	0,025	3,719	0,008	3,594	0,004	3,562	0,022	3,524	0,020	3,480	0,022
	293,15	2,894	0,107	2,811	0,048	2,748	0,037	2,692	0,016	2,654	0,006	2,649	0,008	2,618	0,006
	298,15	2,589	0,612	2,456	0,051	2,427	0,034	2,384	0,016	2,290	0,009	2,300	0,003	2,305	0,016
	303,15	2,225	0,139	2,172	0,052	2,155	0,038	2,109	0,024	2,018	0,018	2,031	0,010	2,027	0,009
	313,15	1,847	0,584	1,713	0,044	1,711	0,035	1,710	0,035	1,594	0,025	1,590	0,019	1,584	0,016
	323,15	1,441	0,273	1,377	0,046	1,373	0,005	1,365	0,034	1,301	0,027	1,270	0,027	1,217	0,019
	333,15	1,350	1,061	1,147	0,041	1,137	0,036	1,124	0,034	1,069	0,024	1,007	0,019	0,964	0,017

MWCNTs Base Fluid % vol. Shear Rate [s ⁻¹]		D20-40 L5-15 30%EG+70%DW 0,75													
		85,4	±	122	±	158,6	±	195,3	±	231,9	±	268,5	±	305,1	±
Temp. [K]	283,15	4,108	0,004	3,942	0,010	3,887	0,013	3,727	0,012	3,679	0,018	3,638	0,026	3,592	0,014
	293,15	3,061	0,237	2,976	0,006	2,909	0,003	2,806	0,004	2,755	0,023	2,739	0,015	2,706	0,010
	298,15	2,726	0,543	2,644	0,020	2,575	0,020	0,000	0,000	2,395	0,007	2,388	0,004	2,391	0,011
	303,15	2,413	0,330	2,341	0,021	2,314	0,011	2,253	0,013	2,117	0,011	2,122	0,014	2,102	0,016
	313,15	1,851	0,047	1,886	0,038	1,879	0,034	1,835	0,028	1,710	0,020	1,683	0,004	1,671	0,002
	323,15	1,508	0,069	1,539	0,029	1,527	0,005	1,513	0,029	1,411	0,015	1,368	0,005	1,297	0,007
	333,15	1,417	0,809	1,304	0,027	1,300	0,027	1,269	0,031	1,182	0,019	1,092	0,020	1,026	0,009

MWCNTs Base Fluid % vol. Shear Rate [s ⁻¹]		D20-40 L5-15 30%EG+70%DW 1,00													
		85,4	±	122	±	158,6	±	195,3	±	231,9	±	268,5	±	305,1	±
Temp. [K]	283,15	4,343	0,010	4,244	0,021	4,180	0,030	4,035	0,031	3,989	0,025	3,934	0,019	3,895	0,018
	293,15	3,248	0,190	3,208	0,033	3,159	0,024	3,073	0,011	3,011	0,012	3,008	0,016	2,953	0,025
	298,15	3,005	0,739	2,874	0,007	2,799	0,024	1,540	0,914	2,634	0,015	2,620	0,024	2,615	0,023
	303,15	2,575	0,177	2,542	0,017	2,508	0,006	2,427	0,018	2,319	0,004	2,317	0,011	2,306	0,010
	313,15	2,054	0,184	2,036	0,029	2,026	0,025	1,984	0,007	1,857	0,014	1,843	0,007	1,836	0,003
	323,15	1,627	0,048	1,653	0,030	1,638	0,000	1,620	0,020	1,521	0,007	1,504	0,004	1,444	0,005
	333,15	1,540	0,914	1,413	0,037	1,385	0,024	1,351	0,022	1,272	0,013	1,190	0,019	0,806	0,003

MWCNTs Base Fluid % vol. Shear Rate [s ⁻¹]		D20-40 L5-15 30%EG+70%DW 1,50													
		85,4	±	122	±	158,6	±	195,3	±	231,9	±	268,5	±	305,1	±
Temp. [K]	283,15	5,217	0,010	5,045	0,022	4,943	0,027	4,744	0,020	4,652	0,034	4,573	0,029	4,524	0,029
	293,15	3,951	0,014	3,798	0,014	3,691	0,031	3,565	0,027	3,514	0,028	3,490	0,021	3,428	0,027
	298,15	3,618	0,854	3,330	0,022	3,263	0,011	0,000	0,000	3,055	0,030	3,037	0,020	3,045	0,017
	303,15	3,037	0,197	2,985	0,020	2,915	0,015	2,848	0,005	2,706	0,011	2,704	0,014	2,694	0,018
	313,15	2,570	0,687	2,387	0,008	2,372	0,006	2,333	0,010	2,168	0,005	2,145	0,016	2,136	0,009
	323,15	1,988	0,122	1,957	0,010	1,962	0,000	1,918	0,010	1,798	0,004	1,761	0,011	1,686	0,009
	333,15	1,712	0,188	1,667	0,026	1,645	0,030	1,608	0,015	1,523	0,011	1,435	0,005	1,344	0,007

MWCNTs Base Fluid % vol. Shear Rate [s ⁻¹]		D20-40 L10-30 30%EG+70%DW 0,25													
		85,4	±	122	±	158,6	±	195,3	±	231,9	±	268,5	±	305,1	±
Temp. [K]	283,15	3,275	0,023	3,248	0,010	3,199	0,005	3,165	0,004	3,167	0,000	3,122	0,003	3,089	0,003
	293,15	2,415	0,027	2,405	0,010	2,395	0,005	2,401	0,006	2,381	0,003	2,378	0,003	2,369	0,005
	298,15	2,108	0,027	2,108	0,009	2,109	0,005	2,160	0,006	2,077	0,004	2,057	0,004	2,075	0,005
	303,15	1,852	0,027	1,829	0,011	1,855	0,005	1,889	0,010	1,853	0,016	1,849	0,014	1,861	0,016
	313,15	1,458	0,024	1,474	0,013	1,483	0,007	1,507	0,005	1,471	0,007	1,465	0,014	1,497	0,030
	323,15	1,173	0,029	1,201	0,020	1,187	0,005	1,260	0,021	1,224	0,019	1,227	0,025	1,229	0,025
	333,15	1,085	0,034	1,075	0,014	1,123	0,048	1,207	0,045	1,151	0,045	1,074	0,045	1,008	0,029

MWCNTs Base Fluid % vol.		D20-40 L10-30 30%EG+70%DW 0,50													
Shear Rate [s ⁻¹]		85,4	±	122	±	158,6	±	195,3	±	231,9	±	268,5	±	305,1	±
Temp. [K]	283,15	3,528	0,018	3,508	0,005	3,536	0,003	3,424	0,005	3,394	0,004	3,339	0,000	3,324	0,002
	293,15	2,767	0,413	2,580	0,009	2,565	0,006	2,578	0,004	2,578	0,003	2,526	0,003	2,484	0,004
	298,15	2,300	0,014	2,287	0,006	2,255	0,005	2,268	0,005	2,202	0,002	2,209	0,003	2,225	0,007
	303,15	2,191	0,508	1,973	0,007	2,009	0,007	2,040	0,005	1,966	0,011	1,977	0,007	1,998	0,010
	313,15	1,772	0,661	1,573	0,007	1,575	0,007	1,685	0,016	1,600	0,015	1,620	0,021	1,603	0,014
	323,15	1,292	0,183	1,269	0,010	1,307	0,000	1,286	0,008	1,298	0,016	1,314	0,022	1,296	0,020
	333,15	0,998	0,036	1,059	0,009	1,063	0,005	1,055	0,004	1,067	0,007	1,014	0,010	0,944	0,016

MWCNTs Base Fluid % vol.		D20-40 L10-30 30%EG+70%DW 0,75													
Shear Rate [s ⁻¹]		85,4	±	122	±	158,6	±	195,3	±	231,9	±	268,5	±	305,1	±
Temp. [K]	283,15	4,104	0,021	4,150	0,006	4,216	0,005	4,072	0,007	4,024	0,004	3,979	0,000	3,960	0,002
	293,15	2,997	0,024	3,001	0,006	2,984	0,005	3,007	0,005	2,960	0,004	2,952	0,005	2,908	0,009
	298,15	2,642	0,016	2,606	0,008	2,611	0,007	2,600	0,000	2,585	0,005	2,554	0,004	2,563	0,004
	303,15	2,339	0,016	2,326	0,022	2,343	0,030	2,321	0,018	2,319	0,017	2,274	0,007	2,255	0,013
	313,15	1,821	0,014	1,795	0,010	1,869	0,009	1,805	0,006	1,783	0,008	1,813	0,011	1,784	0,005
	323,15	1,497	0,034	1,475	0,018	1,492	0,000	1,562	0,009	1,399	0,011	1,443	0,007	1,408	0,013
	333,15	1,254	0,035	1,233	0,025	1,232	0,008	1,306	0,020	1,270	0,015	1,177	0,020	1,109	0,013

MWCNTs Base Fluid % vol.		D20-40 L10-30 30%EG+70%DW 1,00													
Shear Rate [s ⁻¹]		85,4	±	122	±	158,6	±	195,3	±	231,9	±	268,5	±	305,1	±
Temp. [K]	283,15	4,381	0,020	4,372	0,015	4,395	0,003	4,239	0,004	4,215	0,002	4,127	0,000	4,106	0,003
	293,15	3,201	0,024	3,227	0,004	3,177	0,004	3,125	0,006	3,115	0,003	3,111	0,001	3,077	0,002
	298,15	2,844	0,316	2,775	0,007	2,804	0,003	1,293	0,041	2,696	0,004	2,686	0,000	2,692	0,000
	303,15	2,393	0,025	2,421	0,008	2,472	0,005	2,449	0,003	2,364	0,004	2,368	0,003	2,372	0,003
	313,15	1,862	0,018	1,875	0,008	1,916	0,003	1,930	0,000	1,830	0,004	1,852	0,003	1,852	0,003
	323,15	1,514	0,018	1,519	0,009	1,523	0,000	1,528	0,004	1,478	0,004	1,485	0,003	1,431	0,003
	333,15	1,293	0,041	1,282	0,007	1,284	0,006	1,271	0,002	1,215	0,004	1,153	0,003	1,122	0,002

MWCNTs Base Fluid % vol.		D20-40 L10-30 30%EG+70%DW 1,50													
Shear Rate [s ⁻¹]		85,4	±	122	±	158,6	±	195,3	±	231,9	±	268,5	±	305,1	±
Temp. [K]	283,15	5,821	0,014	5,908	0,004	5,794	0,004	5,604	0,002	5,515	0,002	5,430	0,003	5,346	0,003
	293,15	4,288	0,018	4,268	0,010	4,258	0,007	4,146	0,004	4,080	0,003	4,074	0,003	3,984	0,010
	298,15	3,696	0,017	3,691	0,013	3,697	0,007	3,697	0,000	3,529	0,007	3,504	0,002	3,521	0,006
	303,15	3,241	0,020	3,243	0,011	3,216	0,007	3,252	0,006	3,100	0,006	3,104	0,011	3,117	0,009
	313,15	2,520	0,020	2,512	0,009	2,564	0,007	2,619	0,009	2,464	0,010	2,465	0,008	2,470	0,017
	323,15	2,104	0,046	2,058	0,009	2,073	0,000	2,115	0,016	2,092	0,013	2,041	0,014	1,948	0,010
	333,15	2,257	0,216	1,798	0,030	1,846	0,016	1,946	0,041	1,824	0,034	1,674	0,025	1,569	0,014

MWCNTs Base Fluid % vol.		D60-100 L1-2 30%EG+70%DW 0,25													
Shear Rate [s ⁻¹]		85,4	±	122	±	158,6	±	195,3	±	231,9	±	268,5	±	305,1	±
Temp. [K]	283,15	3,252	0,026	3,221	0,009	3,260	0,008	3,232	0,005	3,200	0,003	3,170	0,003	3,139	0,004
	293,15	2,354	0,030	2,328	0,013	2,341	0,007	2,357	0,004	2,328	0,003	2,350	0,003	2,368	0,002
	298,15	2,034	0,029	2,050	0,007	2,066	0,008	2,072	0,009	2,020	0,004	2,042	0,003	2,051	0,003
	303,15	1,829	0,022	1,820	0,009	1,830	0,005	1,869	0,005	1,774	0,006	1,781	0,002	1,808	0,002
	313,15	1,403	0,021	1,400	0,010	1,414	0,006	1,489	0,000	1,407	0,005	1,414	0,007	1,398	0,003
	323,15	1,136	0,017	1,122	0,008	1,134	0,000	1,162	0,005	1,162	0,004	1,154	0,002	1,097	0,002
	333,15	0,897	0,022	0,929	0,008	0,931	0,008	0,958	0,005	0,950	0,004	0,915	0,003	0,917	0,007

MWCNTs Base Fluid % vol.		D60-100 L1-2 30%EG+70%DW 0,50													
Shear Rate [s ⁻¹]		85,4	±	122	±	158,6	±	195,3	±	231,9	±	268,5	±	305,1	±
Temp. [K]	283,15	3,589	0,020	3,588	0,008	3,583	0,010	3,511	0,002	3,478	0,004	3,447	0,005	3,393	0,004
	293,15	2,688	0,026	2,650	0,007	2,673	0,007	2,616	0,004	2,616	0,004	2,634	0,008	2,600	0,007
	298,15	2,300	0,018	2,292	0,008	2,292	0,009	2,323	0,004	2,266	0,004	2,268	0,003	2,281	0,004
	303,15	2,024	0,022	1,994	0,006	2,010	0,008	2,061	0,004	1,982	0,007	2,004	0,007	1,997	0,003
	313,15	1,556	0,025	1,557	0,007	1,581	0,006	1,670	0,008	1,586	0,006	1,578	0,006	1,592	0,011
	323,15	1,300	0,015	1,283	0,005	1,294	0,000	1,352	0,005	1,299	0,007	1,293	0,011	1,254	0,016
	333,15	1,086	0,016	1,076	0,007	1,080	0,005	1,117	0,011	1,103	0,010	1,048	0,013	0,945	0,011

MWCNTs Base Fluid % vol.		D60-100 L1-2 30%EG+70%DW 0,75													
Shear Rate [s ⁻¹]		85,4	±	122	±	158,6	±	195,3	±	231,9	±	268,5	±	305,1	±
Temp. [K]	283,15	4,140	0,024	4,187	0,009	4,130	0,005	4,038	0,007	4,047	0,003	3,955	0,000	3,916	0,000
	293,15	2,940	0,025	2,996	0,012	3,007	0,007	2,949	0,006	2,927	0,003	2,923	0,000	2,902	0,001
	298,15	2,513	0,023	2,587	0,019	2,663	0,005	0,000	0,000	2,528	0,002	2,518	0,002	2,554	0,003
	303,15	2,177	0,024	2,268	0,011	2,349	0,007	2,321	0,005	2,204	0,005	2,238	0,003	2,212	0,000
	313,15	1,673	0,028	1,723	0,009	1,825	0,010	1,832	0,005	1,719	0,007	1,738	0,003	1,735	0,000
	323,15	1,346	0,027	1,359	0,011	1,451	0,000	1,471	0,005	1,403	0,004	1,360	0,006	1,333	0,002
	333,15	1,120	0,035	1,105	0,012	1,170	0,007	1,181	0,007	1,149	0,004	1,083	0,003	0,959	0,003

MWCNTs Base Fluid % vol.		D60-100 L1-2 30%EG+70%DW 1,00													
Shear Rate [s ⁻¹]		85,4	±	122	±	158,6	±	195,3	±	231,9	±	268,5	±	305,1	±
Temp. [K]	283,15	4,729	0,024	4,764	0,007	4,702	0,007	4,621	0,003	4,526	0,003	4,473	0,003	4,429	0,002
	293,15	3,408	0,018	3,451	0,009	3,440	0,011	3,374	0,004	3,328	0,003	3,310	0,005	3,272	0,002
	298,15	2,915	0,024	2,954	0,011	2,982	0,007	2,924	0,032	2,858	0,004	2,880	0,006	2,878	0,002
	303,15	2,517	0,028	2,568	0,009	2,639	0,005	2,587	0,007	2,507	0,008	2,493	0,007	2,515	0,006
	313,15	1,942	0,026	1,955	0,008	2,057	0,006	2,068	0,008	1,954	0,011	1,943	0,011	1,962	0,006
	323,15	1,563	0,026	1,549	0,010	1,616	0,005	1,658	0,014	1,577	0,012	1,559	0,009	1,507	0,008
	333,15	1,294	0,032	1,294	0,016	1,328	0,013	1,347	0,010	1,319	0,016	1,234	0,014	1,065	0,007

MWCNTs Base Fluid % vol.		D60-100 L1-2 30%EG+70%DW 1,50													
Shear Rate [s ⁻¹]		85,4	±	122	±	158,6	±	195,3	±	231,9	±	268,5	±	305,1	±
Temp. [K]	283,15	5,607	0,020	5,605	0,011	5,553	0,022	5,388	0,034	5,337	0,036	5,209	0,028	5,129	0,013
	293,15	3,966	0,028	4,043	0,018	3,982	0,011	3,919	0,005	3,844	0,012	3,851	0,029	3,809	0,023
	298,15	3,363	0,073	3,508	0,013	3,479	0,008	0,000	0,000	3,314	0,003	3,281	0,002	3,307	0,015
	303,15	2,963	0,034	3,072	0,050	3,087	0,025	3,058	0,006	2,911	0,006	2,913	0,004	2,908	0,006
	313,15	2,472	1,179	2,337	0,043	2,419	0,030	2,418	0,019	2,266	0,012	2,281	0,006	2,262	0,012
	323,15	1,780	0,084	1,832	0,058	1,926	0,005	1,935	0,034	1,838	0,027	1,797	0,009	1,717	0,013
	333,15	1,564	0,570	1,509	0,053	1,569	0,040	1,564	0,035	1,481	0,033	1,406	0,020	1,252	0,003

MWCNTs Base Fluid % vol.		D60-100 L5-15 30%EG+70%DW 0,25													
Shear Rate [s ⁻¹]		85,4	±	122	±	158,6	±	195,3	±	231,9	±	268,5	±	305,1	±
Temp. [K]	283,15	3,367	0,011	3,361	0,008	3,266	0,005	3,177	0,010	3,168	0,006	3,139	0,022	3,106	0,028
	293,15	2,573	0,334	2,504	0,027	2,476	0,003	2,417	0,009	2,378	0,011	2,370	0,004	2,340	0,010
	298,15	2,251	0,368	2,232	0,013	2,210	0,010	2,143	0,014	2,053	0,003	2,047	0,003	2,050	0,010
	303,15	2,074	0,573	1,984	0,038	1,963	0,017	1,915	0,016	1,814	0,011	1,819	0,006	1,807	0,019
	313,15	1,663	0,825	1,588	0,039	1,580	0,027	1,563	0,013	1,459	0,015	1,442	0,009	1,437	0,006
	323,15	1,216	0,133	1,268	0,038	1,275	0,000	1,264	0,032	1,192	0,015	1,169	0,023	1,119	0,004
	333,15	1,156	0,797	1,072	0,024	1,060	0,035	1,052	0,021	0,996	0,025	0,932	0,017	0,910	0,007

MWCNTs Base Fluid % vol.		D60-100 L5-15 30%EG+70%DW 0,50													
Shear Rate [s ⁻¹]		85,4	±	122	±	158,6	±	195,3	±	231,9	±	268,5	±	305,1	±
Temp. [K]	283,15	3,456	0,012	3,481	0,011	3,387	0,016	3,267	0,028	3,249	0,030	3,206	0,016	3,180	0,027
	293,15	2,637	0,212	2,617	0,040	2,533	0,018	2,437	0,003	2,400	0,005	2,394	0,012	2,362	0,026
	298,15	2,427	0,962	2,234	0,026	2,235	0,021	2,168	0,014	2,081	0,003	2,077	0,007	2,090	0,015
	303,15	1,938	0,079	1,995	0,038	1,990	0,031	1,939	0,013	1,820	0,015	1,825	0,008	1,836	0,008
	313,15	1,759	1,201	1,620	0,047	1,607	0,033	1,591	0,025	1,488	0,030	1,468	0,019	1,457	0,017
	323,15	1,192	0,066	1,300	0,040	1,291	0,000	1,290	0,026	1,222	0,021	1,189	0,016	1,140	0,015
	333,15	1,071	0,466	1,093	0,032	1,067	0,031	1,065	0,029	1,014	0,026	0,946	0,016	0,916	0,012

MWCNTs Base Fluid % vol.		D60-100 L5-15 30%EG+70%DW 0,75													
Shear Rate [s ⁻¹]		85,4	±	122	±	158,6	±	195,3	±	231,9	±	268,5	±	305,1	±
Temp. [K]	283,15	3,711	0,007	3,684	0,008	3,615	0,017	3,492	0,029	3,465	0,005	3,436	0,016	3,411	0,022
	293,15	2,728	0,093	2,766	0,015	2,696	0,016	2,607	0,006	2,570	0,003	2,567	0,009	2,540	0,012
	298,15	2,415	0,284	2,455	0,021	2,404	0,015	0,000	0,000	2,250	0,011	2,232	0,012	2,246	0,005
	303,15	2,176	0,510	2,145	0,041	2,142	0,038	2,088	0,039	1,977	0,011	1,976	0,008	1,969	0,004
	313,15	1,651	0,111	1,718	0,036	1,734	0,044	1,694	0,018	1,586	0,019	1,568	0,023	1,563	0,012
	323,15	1,302	0,024	1,391	0,047	1,391	0,000	1,378	0,029	1,290	0,023	1,270	0,023	1,216	0,016
	333,15	1,212	0,734	1,163	0,030	1,159	0,034	1,141	0,029	1,076	0,025	1,017	0,022	0,968	0,011

MWCNTs Base Fluid % vol.		D60-100 L5-15 30%EG+70%DW 1,00													
Shear Rate [s ⁻¹]		85,4	±	122	±	158,6	±	195,3	±	231,9	±	268,5	±	305,1	±
Temp. [K]	283,15	4,406	0,007	4,349	0,028	4,273	0,031	4,119	0,024	4,073	0,025	4,011	0,032	3,981	0,044
	293,15	3,260	0,079	3,243	0,010	3,145	0,024	3,049	0,016	3,012	0,030	2,992	0,015	2,950	0,028
	298,15	2,895	0,281	2,835	0,041	2,776	0,029	1,388	0,303	2,608	0,014	2,595	0,001	2,607	0,004
	303,15	2,536	0,226	2,481	0,011	2,478	0,004	2,416	0,018	2,300	0,007	2,298	0,004	2,300	0,003
	313,15	2,258	1,581	1,985	0,032	2,004	0,026	1,974	0,020	1,838	0,012	1,815	0,005	1,816	0,006
	323,15	1,740	0,800	1,647	0,035	1,648	0,000	1,625	0,026	1,540	0,030	1,486	0,010	1,427	0,007
	333,15	1,388	0,303	1,408	0,048	1,385	0,045	1,355	0,031	1,274	0,025	1,193	0,019	1,129	0,011

MWCNTs Base Fluid % vol.		D60-100 L5-15 30%EG+70%DW 1,50													
Shear Rate [s ⁻¹]		85,4	±	122	±	158,6	±	195,3	±	231,9	±	268,5	±	305,1	±
Temp. [K]	283,15	9,387	0,011	9,015	0,053	8,530	0,035	7,944	0,028	7,623	0,022	7,305	0,020	7,062	0,012
	293,15	6,287	0,033	6,212	0,044	6,142	0,058	5,981	0,042	5,834	0,029	5,752	0,027	5,629	0,027
	298,15	5,844	0,014	5,841	0,025	5,762	0,042	0,000	0,000	5,316	0,029	5,173	0,035	5,107	0,023
	303,15	5,441	0,054	5,335	0,027	5,265	0,022	5,115	0,034	4,796	0,038	4,695	0,042	4,557	0,025
	313,15	4,587	0,039	4,637	0,041	4,649	0,035	4,580	0,045	4,275	0,038	4,197	0,027	4,086	0,042
	323,15	4,746	0,102	4,814	0,033	4,802	0,000	4,668	0,050	4,279	0,032	4,041	0,049	3,722	0,036
	333,15	5,350	0,123	5,124	0,023	4,866	0,022	4,559	0,033	4,149	0,031	3,762	0,041	3,202	0,029

MWCNTs Base Fluid % vol.		D50-80 L10-20 30%EG+70%DW 0,25													
Shear Rate [s ⁻¹]		85,4	±	122	±	158,6	±	195,3	±	231,9	±	268,5	±	305,1	±
Temp. [K]	283,15	3,629	0,020	3,632	0,017	3,617	0,009	3,558	0,004	3,524	0,006	3,490	0,011	3,476	0,025
	293,15	2,684	0,116	2,670	0,053	2,622	0,022	2,593	0,020	2,593	0,015	2,599	0,004	2,563	0,003
	298,15	2,322	0,023	2,315	0,049	2,324	0,034	2,286	0,012	2,256	0,014	2,256	0,011	2,266	0,003
	303,15	2,090	0,161	2,045	0,052	2,059	0,043	2,027	0,026	1,980	0,019	2,000	0,016	1,992	0,011
	313,15	1,583	0,019	1,608	0,052	1,624	0,047	1,628	0,039	1,567	0,030	1,566	0,020	1,569	0,008
	323,15	1,298	0,065	1,304	0,049	1,304	0,005	1,304	0,037	1,271	0,033	1,261	0,027	1,206	0,021
	333,15	1,089	0,013	1,087	0,046	1,071	0,041	1,066	0,036	1,052	0,030	0,993	0,023	0,902	0,018

MWCNTs Base Fluid % vol.		D50-80 L10-20 30%EG+70%DW 0,50													
Shear Rate [s ⁻¹]		85,4	±	122	±	158,6	±	195,3	±	231,9	±	268,5	±	305,1	±
Temp. [K]	283,15	4,340	0,022	4,375	0,013	4,448	0,004	4,322	0,014	4,256	0,017	4,175	0,022	4,119	0,025
	293,15	3,174	0,023	3,169	0,057	3,146	0,019	3,131	0,008	3,112	0,005	3,087	0,003	3,069	0,004
	298,15	2,760	0,033	2,758	0,053	2,755	0,034	2,777	0,018	2,720	0,020	2,675	0,006	2,664	0,003
	303,15	2,462	0,027	2,453	0,058	2,437	0,044	2,434	0,025	2,385	0,019	2,380	0,003	2,333	0,010
	313,15	1,941	0,121	1,897	0,062	1,909	0,054	1,931	0,045	1,848	0,011	1,858	0,021	1,845	0,011
	323,15	1,621	0,400	1,541	0,058	1,537	0,005	1,552	0,044	1,483	0,034	1,467	0,028	1,406	0,020
	333,15	1,350	0,330	1,278	0,057	1,265	0,049	1,283	0,040	1,231	0,034	1,141	0,023	1,017	0,022

MWCNTs Base Fluid % vol.		D50-80 L10-20 30%EG+70%DW 0,75													
Shear Rate [s ⁻¹]		85,4	±	122	±	158,6	±	195,3	±	231,9	±	268,5	±	305,1	±
Temp. [K]	283,15	4,227	0,018	4,242	0,041	4,239	0,006	4,098	0,002	4,066	0,007	4,043	0,026	3,994	0,032
	293,15	3,120	0,019	3,081	0,028	3,063	0,029	3,050	0,010	3,020	0,012	2,986	0,005	2,939	0,003
	298,15	2,728	0,063	2,725	0,059	2,720	0,028	0,000	0,000	2,627	0,012	2,608	0,008	2,605	0,004
	303,15	2,402	0,023	2,407	0,051	2,393	0,045	2,366	0,037	2,308	0,019	2,306	0,011	2,294	0,005
	313,15	1,906	0,015	1,892	0,056	1,925	0,047	1,883	0,040	1,780	0,026	1,815	0,011	1,810	0,010
	323,15	1,549	0,014	1,548	0,049	1,535	0,005	1,498	0,040	1,432	0,027	1,429	0,026	1,392	0,010
	333,15	1,294	0,015	1,297	0,049	1,275	0,043	1,208	0,043	1,163	0,032	1,115	0,028	1,001	0,019

MWCNTs Base Fluid % vol.		D50-80 L10-20 30%EG+70%DW 1,00													
Shear Rate [s ⁻¹]		85,4	±	122	±	158,6	±	195,3	±	231,9	±	268,5	±	305,1	±
Temp. [K]	283,15	7,917	0,190	6,462	0,123	5,642	0,061	5,089	0,035	4,803	0,012	4,616	0,009	4,540	0,007
	293,15	3,533	0,024	3,499	0,027	3,376	0,005	3,279	0,004	3,242	0,005	3,276	0,009	3,262	0,011
	298,15	2,891	0,020	2,942	0,017	2,942	0,014	1,137	0,034	2,899	0,023	2,888	0,040	2,950	0,049
	303,15	2,512	0,023	2,573	0,030	2,665	0,050	2,710	0,058	2,599	0,066	2,661	0,065	2,664	0,063
	313,15	1,837	0,035	2,017	0,062	2,068	0,024	2,154	0,042	2,040	0,048	1,991	0,031	2,104	0,032
	323,15	1,489	0,144	1,499	0,010	1,613	0,005	1,654	0,032	1,607	0,027	1,681	0,048	1,611	0,040
	333,15	1,137	0,034	1,216	0,033	1,307	0,018	1,367	0,027	1,339	0,042	1,285	0,028	1,269	0,041

MWCNTs Base Fluid % vol.		D50-80 L10-20 30%EG+70%DW 1,50													
Shear Rate [s ⁻¹]		85,4	±	122	±	158,6	±	195,3	±	231,9	±	268,5	±	305,1	±
Temp. [K]	283,15	4,718	0,023	4,700	0,025	4,672	0,020	4,516	0,024	4,447	0,017	4,360	0,030	4,279	0,016
	293,15	3,541	0,083	3,476	0,022	3,388	0,017	3,348	0,006	3,313	0,001	3,250	0,005	3,231	0,009
	298,15	3,050	0,036	3,009	0,032	2,980	0,027	0,000	0,000	2,865	0,013	2,841	0,002	2,831	0,003
	303,15	2,866	0,898	2,665	0,051	2,657	0,044	2,627	0,026	2,547	0,010	2,513	0,006	2,525	0,004
	313,15	2,190	0,430	2,093	0,044	2,101	0,036	2,106	0,025	2,015	0,017	1,987	0,014	1,982	0,009
	323,15	1,840	0,474	1,725	0,056	1,707	0,005	1,704	0,039	1,659	0,027	1,606	0,017	1,538	0,016
	333,15	1,503	0,278	1,442	0,052	1,410	0,047	1,399	0,042	1,357	0,032	1,270	0,025	1,118	0,017

MWCNTs Base Fluid % vol.		D20-40 L1-2 60%EG+40%DW 0,25													
Shear Rate [s ⁻¹]		85,4	±	122	±	158,6	±	195,3	±	231,9	±	268,5	±	305,1	±
Temp. [K]	283,15	9,382	0,012	9,283	0,006	9,306	0,000	9,264	0,002	9,208	0,000	9,165	0,003	9,145	0,003
	293,15	6,303	0,167	6,302	0,006	6,250	0,003	6,203	0,000	6,161	0,000	6,104	0,002	6,066	0,002
	298,15	5,349	0,019	5,338	0,007	5,212	0,002	5,217	0,004	5,163	0,003	5,162	0,000	5,134	0,003
	303,15	4,488	0,027	4,542	0,007	4,436	0,007	4,435	0,002	4,364	0,003	4,377	0,000	4,380	0,000
	313,15	3,247	0,023	3,301	0,008	3,297	0,004	3,239	0,005	3,219	0,004	3,213	0,000	3,204	0,001
	323,15	2,379	0,019	2,433	0,011	2,494	0,000	2,481	0,004	2,404	0,000	2,381	0,003	2,412	0,004
	333,15	1,830	0,031	1,858	0,011	1,946	0,008	1,933	0,004	1,835	0,005	1,864	0,006	1,705	0,003

MWCNTs Base Fluid % vol.		D20-40 L1-2 60%EG+40%DW 0,50													
Shear Rate [s ⁻¹]		85,4	±	122	±	158,6	±	195,3	±	231,9	±	268,5	±	305,1	±
Temp. [K]	283,15	9,772	0,027	9,803	0,008	9,849	0,006	9,777	0,006	9,697	0,007	9,679	0,011	9,663	0,009
	293,15	6,390	0,027	6,508	0,006	6,480	0,003	6,512	0,000	6,422	0,000	6,392	0,005	6,406	0,002
	298,15	5,247	0,027	5,400	0,009	5,379	0,003	5,414	0,004	5,372	0,005	5,357	0,003	5,287	0,002
	303,15	4,371	0,027	4,473	0,011	4,548	0,002	4,603	0,004	4,571	0,001	4,582	0,002	4,531	0,002
	313,15	3,113	0,031	3,206	0,007	3,260	0,008	3,230	0,004	3,306	0,004	3,312	0,002	3,305	0,005
	323,15	2,292	0,034	2,364	0,011	2,409	0,000	2,495	0,004	2,494	0,006	2,474	0,009	2,504	0,007
	333,15	1,741	0,032	1,839	0,009	1,890	0,007	1,956	0,002	1,882	0,003	1,927	0,003	1,957	0,003

MWCNTs Base Fluid % vol.		D20-40 L1-2 60%EG+40%DW 0,75													
Shear Rate [s ⁻¹]		85,4	±	122	±	158,6	±	195,3	±	231,9	±	268,5	±	305,1	±
Temp. [K]	283,15	10,660	0,010	10,553	0,006	10,564	0,005	10,473	0,004	10,398	0,000	10,321	0,000	10,266	0,000
	293,15	7,239	0,023	7,140	0,006	7,045	0,000	7,015	0,000	6,883	0,000	6,809	0,000	6,824	0,000
	298,15	6,097	0,024	6,091	0,004	5,933	0,003	0,000	0,000	5,849	0,004	5,858	0,002	5,750	0,003
	303,15	4,968	0,455	5,161	0,008	5,003	0,004	5,029	0,003	4,922	0,002	4,928	0,000	4,931	0,002
	313,15	3,771	0,025	3,772	0,007	3,735	0,007	3,620	0,002	3,615	0,003	3,616	0,004	3,621	0,004
	323,15	2,755	0,022	2,804	0,008	2,805	0,000	2,796	0,007	2,745	0,004	2,699	0,005	2,706	0,004
	333,15	2,086	0,026	2,137	0,010	2,186	0,006	2,192	0,013	2,113	0,009	2,093	0,002	1,899	0,004

MWCNTs Base Fluid % vol.		D20-40 L1-2 60%EG+40%DW 1,00													
Shear Rate [s ⁻¹]		85,4	±	122	±	158,6	±	195,3	±	231,9	±	268,5	±	305,1	±
Temp. [K]	283,15	11,443	0,020	11,184	0,020	10,978	0,014	10,781	0,004	10,677	0,009	10,553	0,005	10,457	0,004
	293,15	7,512	0,032	7,403	0,004	7,263	0,005	7,169	0,002	7,044	0,003	6,983	0,002	6,990	0,003
	298,15	6,243	0,020	6,276	0,005	6,157	0,000	2,223	0,087	6,020	0,003	5,954	0,003	5,898	0,001
	303,15	5,309	0,017	5,332	0,008	5,182	0,000	5,126	0,000	5,065	0,003	5,064	0,002	5,045	0,000
	313,15	3,861	0,030	3,855	0,005	3,846	0,007	3,738	0,003	3,755	0,007	3,759	0,003	3,724	0,005
	323,15	2,920	0,021	2,945	0,007	2,971	0,000	2,956	0,004	2,886	0,004	2,850	0,003	2,877	0,011
	333,15	2,223	0,087	2,293	0,007	2,305	0,003	2,365	0,019	2,227	0,011	2,266	0,016	2,063	0,015

MWCNTs Base Fluid % vol.		D20-40 L1-2 60%EG+40%DW 1,50													
Shear Rate [s ⁻¹]		85,4	±	122	±	158,6	±	195,3	±	231,9	±	268,5	±	305,1	±
Temp. [K]	283,15	14,120	0,041	13,730	0,006	13,714	0,002	13,549	0,002	13,377	0,005	13,339	0,000	13,194	0,000
	293,15	9,394	0,026	9,146	0,007	8,915	0,002	8,825	0,002	8,732	0,000	8,656	0,002	8,626	0,002
	298,15	7,838	0,017	7,745	0,004	7,591	0,000	0,000	0,000	7,344	0,000	7,274	0,003	7,227	0,001
	303,15	6,582	0,023	6,580	0,007	6,402	0,005	6,393	0,000	6,266	0,000	6,221	0,003	6,162	0,000
	313,15	4,809	0,021	4,775	0,008	4,749	0,006	4,617	0,003	4,581	0,000	4,565	0,002	4,528	0,001
	323,15	3,606	0,016	3,589	0,007	3,579	0,000	3,543	0,002	3,490	0,000	3,427	0,000	3,446	0,000
	333,15	2,709	0,024	2,747	0,008	2,779	0,003	2,770	0,010	2,646	0,005	2,675	0,003	2,686	0,005

MWCNTs Base Fluid % vol.		D20-40 L5-15 60%EG+40%DW 0,25													
Shear Rate [s ⁻¹]		85,4	±	122	±	158,6	±	195,3	±	231,9	±	268,5	±	305,1	±
Temp. [K]	283,15	9,567	0,019	9,445	0,009	9,506	0,004	9,538	0,003	9,499	0,004	9,469	0,006	9,446	0,008
	293,15	6,539	0,012	6,563	0,008	6,463	0,000	6,405	0,000	6,364	0,000	6,352	0,003	6,317	0,008
	298,15	5,425	0,012	5,446	0,010	5,396	0,002	5,411	0,004	5,350	0,005	5,350	0,003	5,405	0,075
	303,15	4,570	0,020	4,619	0,007	4,584	0,005	4,618	0,004	4,521	0,011	4,547	0,008	4,545	0,004
	313,15	3,312	0,015	3,323	0,008	3,321	0,009	3,284	0,007	3,315	0,007	3,281	0,011	3,287	0,007
	323,15	2,448	0,034	2,497	0,011	2,499	0,000	2,540	0,016	2,483	0,010	2,432	0,009	2,497	0,005
	333,15	1,880	0,019	1,921	0,008	2,016	0,015	1,988	0,009	1,911	0,008	1,884	0,006	1,931	0,013

MWCNTs Base Fluid % vol.		D20-40 L5-15 60%EG+40%DW 0,50													
Shear Rate [s ⁻¹]		85,4	±	122	±	158,6	±	195,3	±	231,9	±	268,5	±	305,1	±
Temp. [K]	283,15	10,437	0,013	10,337	0,008	10,424	0,006	10,372	0,002	10,314	0,004	10,222	0,001	10,181	0,004
	293,15	6,966	0,019	6,987	0,011	6,896	0,005	6,878	0,005	6,811	0,006	6,745	0,005	6,691	0,010
	298,15	5,874	0,019	5,856	0,011	5,818	0,008	5,837	0,009	5,774	0,005	5,729	0,010	5,701	0,014
	303,15	5,333	0,152	5,079	0,046	5,073	0,018	5,036	0,020	4,931	0,015	4,919	0,018	4,944	0,013
	313,15	4,059	0,126	3,685	0,022	3,781	0,030	3,720	0,027	3,727	0,033	3,717	0,021	3,636	0,029
	323,15	3,067	0,100	2,943	0,042	2,826	0,000	2,888	0,032	2,848	0,036	2,887	0,035	2,844	0,027
	333,15	2,407	0,257	2,151	0,048	2,315	0,050	2,395	0,047	2,249	0,031	2,308	0,022	2,219	0,024

MWCNTs Base Fluid % vol.		D20-40 L5-15 60%EG+40%DW 0,75													
Shear Rate [s ⁻¹]		85,4	±	122	±	158,6	±	195,3	±	231,9	±	268,5	±	305,1	±
Temp. [K]	283,15	12,082	0,020	11,933	0,007	11,906	0,000	11,783	0,004	11,703	0,001	11,588	0,002	11,520	0,024
	293,15	8,328	0,028	8,126	0,008	7,963	0,004	7,880	0,004	7,762	0,000	7,746	0,000	8,261	0,001
	298,15	6,984	0,140	6,861	0,006	6,703	0,003	6,700	0,000	6,598	0,001	6,515	0,002	6,460	0,003
	303,15	6,697	2,385	5,859	0,008	5,699	0,005	5,687	0,002	5,588	0,004	5,592	0,002	5,518	0,000
	313,15	4,206	0,025	4,169	0,008	4,191	0,005	4,092	0,004	4,082	0,000	4,126	0,005	4,085	0,003
	323,15	3,136	0,019	3,137	0,008	3,165	0,000	3,158	0,005	3,113	0,012	3,091	0,010	3,109	0,006
	333,15	2,399	0,021	2,392	0,009	2,424	0,006	2,449	0,004	2,384	0,009	2,402	0,010	2,418	0,008

MWCNTs Base Fluid % vol.		D20-40 L5-15 60%EG+40%DW 1,00													
Shear Rate [s ⁻¹]		85,4	±	122	±	158,6	±	195,3	±	231,9	±	268,5	±	305,1	±
Temp. [K]	283,15	17,696	0,013	17,150	0,013	16,877	0,008	16,730	0,004	16,511	0,005	15,034	0,000	13,194	0,000
	293,15	12,895	1,848	11,852	0,008	11,588	0,004	11,440	0,004	11,263	0,005	11,172	0,001	11,077	0,002
	298,15	10,436	0,017	10,216	0,007	9,918	0,002	9,928	0,026	9,617	0,001	9,515	0,001	9,398	0,001
	303,15	8,837	0,016	8,701	0,006	8,396	0,005	8,230	0,004	8,045	0,004	8,012	0,001	7,948	0,003
	313,15	6,378	0,019	6,319	0,011	6,227	0,005	5,977	0,000	5,969	0,003	5,952	0,003	5,861	0,001
	323,15	4,836	0,040	4,741	0,010	4,685	0,000	4,655	0,011	4,571	0,005	4,529	0,005	4,622	0,004
	333,15	3,928	0,026	3,917	0,010	3,970	0,020	4,026	0,017	3,904	0,021	4,020	0,023	3,840	0,011

MWCNTs Base Fluid % vol.		D20-40 L5-15 60%EG+40%DW 1,50													
Shear Rate [s ⁻¹]		85,4	±	122	±	158,6	±	195,3	±	231,9	±	268,5	±	305,1	±
Temp. [K]	283,15	13,147	0,006	12,812	0,021	12,670	0,017	12,470	0,012	12,322	0,010	12,164	0,005	12,065	0,005
	293,15	9,202	0,074	8,837	0,040	8,573	0,044	8,439	0,026	8,302	0,021	8,212	0,021	8,151	0,013
	298,15	7,853	0,054	7,475	0,047	7,221	0,044	7,000	0,000	7,031	0,034	6,999	0,019	6,925	0,018
	303,15	6,771	0,239	6,419	0,046	6,163	0,034	6,095	0,047	5,986	0,038	5,980	0,022	5,932	0,020
	313,15	5,068	0,200	4,842	0,011	4,684	0,047	4,502	0,044	4,483	0,045	4,470	0,035	4,396	0,032
	323,15	3,972	0,732	3,743	0,015	3,624	0,000	3,531	0,009	3,422	0,022	3,367	0,018	3,381	0,025
	333,15	2,977	0,110	2,937	0,012	2,874	0,004	2,794	0,015	2,635	0,023	2,656	0,020	2,634	0,022

MWCNTs Base Fluid % vol.		D20-40 L10-30 60%EG+40%DW 0,25													
Shear Rate [s ⁻¹]		85,4	±	122	±	158,6	±	195,3	±	231,9	±	268,5	±	305,1	±
Temp. [K]	283,15	8,978	0,021	8,962	0,007	8,976	0,008	8,999	0,018	8,934	0,009	8,870	0,005	8,874	0,010
	293,15	6,139	0,030	6,156	0,011	6,097	0,005	6,121	0,006	6,091	0,005	6,021	0,003	5,974	0,007
	298,15	5,095	0,174	5,235	0,023	5,122	0,008	5,140	0,013	5,125	0,010	5,091	0,011	5,067	0,007
	303,15	4,391	0,038	4,364	0,006	4,346	0,014	4,445	0,042	4,327	0,004	4,354	0,016	4,358	0,015
	313,15	3,221	0,024	3,232	0,012	3,275	0,023	3,319	0,152	3,188	0,009	3,185	0,013	3,212	0,015
	323,15	2,425	0,043	2,465	0,028	2,442	0,000	2,481	0,015	2,434	0,012	2,403	0,011	2,453	0,011
	333,15	1,833	0,024	1,876	0,010	1,912	0,013	1,966	0,018	1,859	0,006	1,862	0,009	1,759	0,016

MWCNTs Base Fluid % vol.		D20-40 L10-30 60%EG+40%DW 0,50													
Shear Rate [s ⁻¹]		85,4	±	122	±	158,6	±	195,3	±	231,9	±	268,5	±	305,1	±
Temp. [K]	283,15	9,916	0,018	9,775	0,007	9,804	0,000	9,775	0,003	9,738	0,003	9,700	0,000	9,654	0,000
	293,15	7,097	0,874	6,728	0,007	6,626	0,005	6,574	0,000	6,517	0,000	6,433	0,003	6,419	0,000
	298,15	5,667	0,022	5,664	0,007	5,542	0,005	5,566	0,000	5,533	0,000	5,505	0,000	5,451	0,000
	303,15	4,786	0,017	4,792	0,008	4,696	0,003	4,715	0,002	4,691	0,002	4,662	0,002	4,697	0,000
	313,15	3,496	0,022	3,502	0,007	3,479	0,005	3,422	0,000	3,429	0,001	3,427	0,002	3,430	0,000
	323,15	2,500	0,017	2,546	0,007	2,572	0,000	2,601	0,002	2,567	0,000	2,528	0,003	2,589	0,003
	333,15	1,848	0,030	1,929	0,007	1,989	0,005	2,007	0,006	1,950	0,003	1,992	0,000	1,992	0,003

MWCNTs Base Fluid % vol.		D20-40 L10-30 60%EG+40%DW 0,75													
Shear Rate [s ⁻¹]		85,4	±	122	±	158,6	±	195,3	±	231,9	±	268,5	±	305,1	±
Temp. [K]	283,15	11,164	0,016	11,072	0,007	11,087	0,000	10,967	0,004	10,866	0,001	10,777	0,003	10,724	0,001
	293,15	7,583	0,024	7,533	0,007	7,402	0,005	7,318	0,000	7,210	0,000	7,178	0,002	7,151	0,001
	298,15	6,321	0,025	6,359	0,007	6,220	0,000	6,000	0,000	6,121	0,002	6,064	0,000	6,002	0,001
	303,15	5,321	0,019	5,403	0,007	5,267	0,002	5,262	0,004	5,190	0,000	5,208	0,000	5,155	0,001
	313,15	3,853	0,018	3,854	0,006	3,907	0,005	3,833	0,004	3,848	0,003	3,803	0,000	3,769	0,001
	323,15	2,840	0,070	2,885	0,006	2,910	0,000	2,910	0,002	2,853	0,001	2,800	0,002	2,815	0,003
	333,15	2,079	0,025	2,178	0,008	2,236	0,007	2,246	0,004	2,154	0,004	2,189	0,000	2,182	0,001

MWCNTs Base Fluid % vol.		D20-40 L10-30 60%EG+40%DW 1,00													
Shear Rate [s ⁻¹]		85,4	±	122	±	158,6	±	195,3	±	231,9	±	268,5	±	305,1	±
Temp. [K]	283,15	11,894	0,016	11,815	0,000	11,734	0,005	11,578	0,002	11,460	0,003	11,321	0,000	11,233	0,003
	293,15	8,136	0,025	7,987	0,007	7,864	0,002	7,720	0,003	7,607	0,000	7,558	0,002	7,557	0,002
	298,15	6,742	0,027	6,774	0,000	6,627	0,000	2,245	0,025	6,492	0,004	6,393	0,002	6,304	0,001
	303,15	5,740	0,022	5,798	0,007	5,664	0,004	5,605	0,000	5,504	0,000	5,545	0,002	5,455	0,001
	313,15	4,154	0,016	4,253	0,009	4,177	0,005	4,067	0,000	4,032	0,003	4,020	0,001	4,007	0,003
	323,15	3,031	0,020	3,105	0,010	3,154	0,000	3,136	0,002	3,061	0,003	2,989	0,001	3,000	0,001
	333,15	2,245	0,025	2,371	0,008	2,436	0,006	2,444	0,000	2,314	0,003	2,346	0,004	2,353	0,004

MWCNTs Base Fluid % vol.		D20-40 L10-30 30%EG+70%DW 1,50													
Shear Rate [s ⁻¹]		85,4	±	122	±	158,6	±	195,3	±	231,9	±	268,5	±	305,1	±
Temp. [K]	283,15	14,666	0,026	14,646	0,009	14,679	0,007	14,544	0,011	14,435	0,007	14,291	0,012	13,194	0,000
	293,15	9,863	0,029	9,931	0,010	9,848	0,005	9,812	0,007	9,670	0,020	9,623	0,024	9,566	0,009
	298,15	8,206	0,028	8,296	0,030	8,153	0,033	8,000	0,000	8,035	0,031	8,019	0,036	7,928	0,049
	303,15	6,827	0,037	7,040	0,025	6,912	0,029	6,936	0,036	6,843	0,028	6,823	0,025	6,760	0,022
	313,15	4,797	0,038	5,009	0,025	5,061	0,025	4,970	0,028	4,993	0,025	5,024	0,021	4,973	0,016
	323,15	3,506	0,071	3,662	0,012	3,787	0,000	3,739	0,033	3,717	0,018	3,678	0,041	3,725	0,029
	333,15	2,579	0,027	2,771	0,029	2,933	0,025	3,018	0,016	2,878	0,035	2,983	0,023	2,974	0,024

MWCNTs Base Fluid % vol.		D60-100 L1-2 60%EG+40%DW 0,25													
Shear Rate [s ⁻¹]		85,4	±	122	±	158,6	±	195,3	±	231,9	±	268,5	±	305,1	±
Temp. [K]	283,15	9,625	0,023	9,491	0,009	9,647	0,005	9,623	0,004	9,539	0,002	9,498	0,000	9,427	0,003
	293,15	6,555	0,023	6,489	0,008	6,430	0,002	6,457	0,005	6,405	0,003	6,354	0,002	6,327	0,002
	298,15	5,478	0,031	5,528	0,008	5,445	0,004	5,480	0,002	5,444	0,000	5,397	0,005	5,344	0,001
	303,15	4,595	0,023	4,653	0,010	4,587	0,000	4,620	0,004	4,565	0,001	4,610	0,004	4,581	0,002
	313,15	3,291	0,025	3,301	0,007	3,359	0,003	3,268	0,000	3,319	0,003	3,322	0,001	3,345	0,000
	323,15	2,539	0,251	2,470	0,011	2,504	0,000	2,529	0,002	2,466	0,004	2,466	0,000	2,500	0,000
	333,15	1,897	0,018	1,898	0,007	1,899	0,004	1,939	0,003	1,861	0,003	1,890	0,000	1,924	0,003

MWCNTs Base Fluid % vol.		D60-100 L1-2 60%EG+40%DW 0,50													
Shear Rate [s ⁻¹]		85,4	±	122	±	158,6	±	195,3	±	231,9	±	268,5	±	305,1	±
Temp. [K]	283,15	10,213	0,027	10,116	0,000	10,159	0,007	10,136	0,012	10,091	0,012	10,036	0,017	10,020	0,012
	293,15	6,643	0,019	6,610	0,006	6,538	0,003	6,485	0,005	6,436	0,012	6,378	0,017	6,366	0,022
	298,15	5,511	0,018	5,596	0,003	5,517	0,008	5,501	0,008	5,450	0,011	5,433	0,009	5,430	0,078
	303,15	4,620	0,017	4,714	0,005	4,605	0,005	4,650	0,006	4,572	0,005	4,601	0,025	4,717	0,031
	313,15	3,340	0,015	3,480	0,031	3,507	0,039	3,429	0,048	3,393	0,030	3,417	0,041	3,452	0,033
	323,15	2,734	0,107	2,572	0,018	2,561	0,000	2,548	0,027	2,528	0,029	2,495	0,040	2,515	0,047
	333,15	1,918	0,028	1,919	0,032	2,099	0,062	2,088	0,032	1,983	0,028	1,980	0,028	2,008	0,036

MWCNTs Base Fluid % vol.		D60-100 L1-2 60%EG+40%DW 0,75													
Shear Rate [s ⁻¹]		85,4	±	122	±	158,6	±	195,3	±	231,9	±	268,5	±	305,1	±
Temp. [K]	283,15	11,101	0,021	11,088	0,013	11,138	0,012	11,124	0,011	11,083	0,008	10,992	0,008	10,971	0,011
	293,15	7,316	0,018	7,202	0,013	7,120	0,006	7,077	0,005	7,018	0,025	6,982	0,013	6,941	0,027
	298,15	6,118	0,021	6,139	0,017	6,029	0,014	0,000	0,000	6,050	0,026	5,999	0,026	5,926	0,030
	303,15	5,195	0,029	5,181	0,022	5,081	0,046	5,120	0,030	5,031	0,042	5,021	0,032	5,035	0,042
	313,15	3,744	0,069	3,922	0,046	3,802	0,049	3,701	0,057	3,676	0,041	3,652	0,042	3,717	0,054
	323,15	2,754	0,043	2,890	0,065	2,838	0,000	2,894	0,051	2,786	0,026	2,729	0,030	2,754	0,044
	333,15	2,197	0,182	2,124	0,055	2,196	0,032	2,194	0,025	2,102	0,038	2,131	0,025	2,118	0,030

MWCNTs Base Fluid % vol.		D60-100 L1-2 60%EG+40%DW 1,00													
Shear Rate [s ⁻¹]		85,4	±	122	±	158,6	±	195,3	±	231,9	±	268,5	±	305,1	±
Temp. [K]	283,15	13,758	0,092	12,932	0,066	12,455	0,019	12,213	0,005	12,019	0,007	11,849	0,008	11,783	0,007
	293,15	8,191	0,032	7,849	0,027	7,615	0,002	7,519	0,005	7,480	0,016	7,459	0,029	7,498	0,021
	298,15	6,883	0,023	6,692	0,015	6,609	0,044	2,886	0,273	6,522	0,021	6,480	0,028	6,515	0,088
	303,15	5,837	0,030	5,760	0,020	5,498	0,024	5,546	0,021	5,568	0,020	5,587	0,038	5,588	0,027
	313,15	4,151	0,037	4,163	0,015	4,043	0,022	3,887	0,037	4,023	0,051	4,124	0,043	4,079	0,046
	323,15	3,187	0,023	3,196	0,043	3,179	0,000	3,172	0,036	3,074	0,060	3,121	0,035	3,158	0,030
	333,15	2,886	0,273	2,419	0,047	2,541	0,030	2,509	0,036	2,576	0,039	2,576	0,049	2,479	0,043

MWCNTs Base Fluid % vol.		D60-100 L1-2 60%EG+40%DW 1,50													
Shear Rate [s ⁻¹]		85,4	±	122	±	158,6	±	195,3	±	231,9	±	268,5	±	305,1	±
Temp. [K]	283,15	15,347	0,065	14,722	0,008	14,578	0,043	14,333	0,011	13,819	0,031	13,332	0,012	13,003	0,024
	293,15	10,259	0,067	9,906	0,017	9,547	0,010	9,351	0,006	9,318	0,036	9,301	0,005	9,231	0,003
	298,15	9,185	0,103	8,486	0,012	8,136	0,007	0,000	0,000	7,828	0,011	7,795	0,014	7,804	0,017
	303,15	8,881	2,100	7,416	0,011	6,999	0,007	6,952	0,007	6,881	0,021	6,901	0,018	6,919	0,026
	313,15	6,146	0,209	5,459	0,016	5,191	0,002	5,016	0,005	4,996	0,005	5,021	0,006	5,005	0,007
	323,15	4,948	1,072	4,201	0,008	4,055	0,000	3,937	0,006	3,804	0,000	3,730	0,001	3,770	0,005
	333,15	3,505	0,071	3,367	0,006	3,259	0,005	3,183	0,005	3,060	0,003	3,059	0,000	2,980	0,003

MWCNTs Base Fluid % vol.		D60-100 L5-15 60%EG+40%DW 0,25													
Shear Rate [s ⁻¹]		85,4	±	122	±	158,6	±	195,3	±	231,9	±	268,5	±	305,1	±
Temp. [K]	283,15	9,076	0,016	9,040	0,007	9,091	0,005	9,063	0,000	9,050	0,000	9,025	0,001	8,974	0,005
	293,15	6,197	0,024	6,166	0,007	6,097	0,010	6,074	0,000	6,019	0,003	6,004	0,000	5,982	0,003
	298,15	5,196	0,025	5,211	0,009	5,106	0,002	5,113	0,002	5,107	0,003	5,044	0,000	5,081	0,000
	303,15	4,347	0,028	4,412	0,015	4,323	0,008	4,326	0,000	4,289	0,002	4,320	0,000	4,328	0,001
	313,15	3,185	0,030	3,290	0,010	3,257	0,005	3,138	0,005	3,135	0,003	3,164	0,002	3,138	0,002
	323,15	2,382	0,041	2,444	0,013	2,468	0,000	2,427	0,005	2,356	0,006	2,329	0,003	2,353	0,004
	333,15	1,851	0,036	1,872	0,016	1,919	0,008	1,909	0,009	1,803	0,003	1,821	0,005	1,639	0,003

MWCNTs Base Fluid % vol.		D60-100 L5-15 60%EG+40%DW 0,50													
Shear Rate [s ⁻¹]		85,4	±	122	±	158,6	±	195,3	±	231,9	±	268,5	±	305,1	±
Temp. [K]	283,15	9,200	0,020	9,065	0,005	9,052	0,000	9,086	0,003	9,051	0,000	8,996	0,000	8,961	0,000
	293,15	6,298	0,025	6,217	0,012	6,164	0,004	6,129	0,000	6,043	0,001	6,008	0,003	5,969	0,003
	298,15	5,273	0,027	5,247	0,007	5,151	0,006	5,151	0,000	5,154	0,002	5,120	0,000	5,056	0,002
	303,15	4,486	0,019	4,521	0,008	4,392	0,010	4,382	0,003	4,305	0,002	4,324	0,000	4,352	0,002
	313,15	3,248	0,022	3,315	0,009	3,246	0,008	3,203	0,000	3,170	0,003	3,168	0,001	3,171	0,001
	323,15	2,378	0,023	2,471	0,013	2,477	0,000	2,478	0,004	2,388	0,005	2,376	0,003	2,376	0,002
	333,15	1,788	0,033	1,886	0,016	1,947	0,008	1,919	0,002	1,825	0,004	1,836	0,006	1,662	0,001

MWCNTs Base Fluid % vol.		D60-100 L5-15 60%EG+40%DW 0,75													
Shear Rate [s ⁻¹]		85,4	±	122	±	158,6	±	195,3	±	231,9	±	268,5	±	305,1	±
Temp. [K]	283,15	9,907	0,014	9,814	0,003	9,824	0,000	9,740	0,005	9,668	0,000	9,603	0,003	9,527	0,002
	293,15	6,953	0,008	6,642	0,009	6,581	0,005	6,512	0,000	6,399	0,000	6,352	0,003	6,337	0,000
	298,15	5,597	0,023	5,612	0,010	5,534	0,009	0,000	0,000	5,474	0,000	5,417	0,003	5,363	0,003
	303,15	5,162	1,118	4,796	0,009	4,699	0,008	4,728	0,004	4,660	0,001	4,680	0,002	4,648	0,002
	313,15	3,433	0,025	3,489	0,014	3,480	0,006	3,382	0,002	3,396	0,000	3,411	0,004	3,405	0,003
	323,15	2,559	0,035	2,614	0,015	2,636	0,000	2,608	0,006	2,552	0,002	2,530	0,006	2,551	0,003
	333,15	1,951	0,041	2,027	0,010	2,084	0,008	2,034	0,005	1,944	0,007	1,954	0,006	1,838	0,007

MWCNTs Base Fluid % vol.		D60-100 L5-15 60%EG+40%DW 1,00													
Shear Rate [s ⁻¹]		85,4	±	122	±	158,6	±	195,3	±	231,9	±	268,5	±	305,1	±
Temp. [K]	283,15	10,934	0,016	10,828	0,010	10,816	0,005	10,704	0,005	10,621	0,000	10,565	0,000	10,491	0,000
	293,15	7,416	0,201	7,352	0,005	7,212	0,004	7,161	0,002	7,051	0,000	6,977	0,000	6,964	0,000
	298,15	6,209	0,027	6,162	0,009	6,087	0,007	2,114	0,029	6,004	0,000	5,926	0,003	5,879	0,000
	303,15	5,235	0,026	5,265	0,012	5,136	0,008	5,109	0,003	5,051	0,004	5,060	0,002	5,037	0,001
	313,15	3,999	0,439	3,832	0,008	3,807	0,004	3,703	0,003	3,698	0,000	3,708	0,000	3,685	0,002
	323,15	2,797	0,034	2,878	0,009	2,872	0,000	2,839	0,005	2,773	0,001	2,747	0,003	2,760	0,001
	333,15	2,114	0,029	2,242	0,011	2,278	0,009	2,232	0,004	2,146	0,002	2,140	0,003	1,968	0,004

MWCNTs Base Fluid % vol.		D60-100 L5-15 60%EG+40%DW 1,50													
Shear Rate [s ⁻¹]		85,4	±	122	±	158,6	±	195,3	±	231,9	±	268,5	±	305,1	±
Temp. [K]	283,15	17,384	0,016	17,135	0,007	17,028	0,007	16,771	0,003	16,518	0,013	15,034	0,000	13,194	0,000
	293,15	11,587	0,019	11,461	0,014	11,274	0,013	11,154	0,012	10,945	0,016	10,813	0,015	10,702	0,015
	298,15	9,752	0,024	9,689	0,009	9,424	0,009	0,000	0,000	9,147	0,025	9,030	0,020	8,927	0,013
	303,15	7,989	0,041	8,135	0,018	7,915	0,018	7,856	0,014	7,736	0,017	7,690	0,017	7,627	0,024
	313,15	5,882	0,036	5,893	0,016	5,921	0,033	5,687	0,026	5,729	0,029	5,728	0,022	5,671	0,023
	323,15	4,577	0,025	4,606	0,005	4,539	0,000	4,513	0,014	4,429	0,028	4,378	0,018	4,478	0,023
	333,15	4,319	0,043	4,376	0,043	4,432	0,035	4,333	0,030	4,116	0,019	4,199	0,023	3,784	0,026

MWCNTs Base Fluid % vol.		D50-80 L10-20 60%EG+40%DW 0,25													
Shear Rate [s ⁻¹]		85,4	±	122	±	158,6	±	195,3	±	231,9	±	268,5	±	305,1	±
Temp. [K]	283,15	8,653	0,017	8,586	0,007	8,588	0,000	8,574	0,003	8,572	0,000	8,582	0,003	8,538	0,000
	293,15	5,922	0,021	5,914	0,007	5,830	0,005	5,796	0,000	5,777	0,001	5,768	0,002	5,751	0,003
	298,15	4,938	0,022	4,973	0,010	4,872	0,005	4,885	0,004	4,867	0,001	4,846	0,000	4,848	0,002
	303,15	4,147	0,017	4,181	0,007	4,126	0,003	4,158	0,002	4,125	0,003	4,182	0,000	4,142	0,001
	313,15	3,043	0,059	3,039	0,004	3,069	0,005	3,033	0,000	3,033	0,004	3,045	0,001	3,020	0,000
	323,15	2,163	0,024	2,236	0,007	2,252	0,000	2,305	0,004	2,257	0,003	2,242	0,002	2,306	0,000
	333,15	1,578	0,033	1,680	0,005	1,745	0,003	1,779	0,006	1,737	0,004	1,742	0,003	1,775	0,000

MWCNTs Base Fluid % vol.		D50-80 L10-20 60%EG+40%DW 0,50													
Shear Rate [s ⁻¹]		85,4	±	122	±	158,6	±	195,3	±	231,9	±	268,5	±	305,1	±
Temp. [K]	283,15	9,457	0,017	9,331	0,004	9,314	0,002	9,273	0,002	9,260	0,001	9,198	0,000	9,225	0,000
	293,15	6,150	0,538	6,376	0,007	6,333	0,004	6,253	0,000	6,228	0,000	6,210	0,000	6,180	0,002
	298,15	5,303	0,154	5,413	0,008	5,303	0,005	5,281	0,000	5,223	0,002	5,228	0,000	5,239	0,002
	303,15	5,028	1,377	4,588	0,008	4,486	0,003	4,485	0,000	4,438	0,002	4,454	0,000	4,436	0,000
	313,15	3,208	0,024	3,291	0,006	3,346	0,005	3,257	0,004	3,263	0,003	3,268	0,003	3,264	0,002
	323,15	2,347	0,079	2,415	0,008	2,459	0,000	2,514	0,003	2,456	0,001	2,404	0,003	2,463	0,001
	333,15	1,715	0,020	1,846	0,007	1,908	0,005	1,938	0,004	1,869	0,003	1,888	0,003	1,903	0,002

MWCNTs Base Fluid % vol.		D50-80 L10-20 60%EG+40%DW 0,75													
Shear Rate [s ⁻¹]		85,4	±	122	±	158,6	±	195,3	±	231,9	±	268,5	±	305,1	±
Temp. [K]	283,15	9,605	0,016	9,432	0,004	9,388	0,003	9,350	0,000	9,287	0,000	9,280	0,000	9,270	0,000
	293,15	6,609	0,021	6,529	0,007	6,418	0,005	6,353	0,003	6,286	0,000	6,262	0,000	6,203	0,002
	298,15	5,503	0,025	5,510	0,006	5,415	0,007	0,000	0,000	5,343	0,000	5,323	0,002	5,282	0,003
	303,15	4,670	0,024	4,718	0,011	4,568	0,000	4,576	0,000	4,523	0,000	4,521	0,000	4,534	0,003
	313,15	3,406	0,017	3,371	0,005	3,431	0,005	3,331	0,004	3,329	0,002	3,336	0,000	3,330	0,003
	323,15	2,663	0,510	2,529	0,005	2,582	0,000	2,559	0,005	2,499	0,000	2,481	0,002	2,498	0,003
	333,15	1,899	0,019	1,972	0,009	2,013	0,004	2,046	0,011	1,951	0,007	1,969	0,007	1,950	0,009

MWCNTs Base Fluid % vol.		D50-80 L10-20 60%EG+40%DW 1,00													
Shear Rate [s ⁻¹]		85,4	±	122	±	158,6	±	195,3	±	231,9	±	268,5	±	305,1	±
Temp. [K]	283,15	10,482	0,019	10,364	0,006	10,339	0,000	10,212	0,002	10,133	0,003	10,034	0,000	9,978	0,000
	293,15	7,205	0,022	7,035	0,007	6,935	0,000	6,876	0,002	6,775	0,000	6,701	0,000	6,658	0,000
	298,15	6,040	0,018	5,999	0,009	5,855	0,005	2,026	0,082	5,771	0,002	5,724	0,000	5,663	0,001
	303,15	5,122	0,016	5,101	0,013	4,969	0,000	4,950	0,002	4,864	0,002	4,861	0,001	4,840	0,002
	313,15	4,529	2,387	3,736	0,007	3,674	0,006	3,590	0,000	3,586	0,001	3,578	0,003	3,561	0,000
	323,15	2,691	0,023	2,841	0,008	2,782	0,000	2,757	0,007	2,696	0,003	2,657	0,003	2,676	0,000
	333,15	2,026	0,082	2,141	0,008	2,184	0,006	2,137	0,006	2,049	0,005	2,074	0,002	2,086	0,004

MWCNTs Base Fluid % vol.		D50-80 L10-20 60%EG+40%DW																																
Shear Rate [s ⁻¹]		85,4		±		122		±		158,6		±		195,3		±		231,9		±		268,5		±		305,1		±						
Temp. [K]	283,15	11,842	0,010	11,652	0,006	11,524	0,003	11,333	0,000	11,213	0,000	11,056	0,000	11,027	0,002																			
	293,15	8,186	0,020	7,942	0,005	7,793	0,000	7,626	0,006	7,522	0,004	7,445	0,002	7,410	0,002																			
	298,15	6,859	0,015	6,775	0,006	6,588	0,000	0,000	0,000	6,408	0,000	6,328	0,000	6,238	0,000																			
	303,15	5,751	0,018	5,781	0,007	5,613	0,005	5,561	0,000	5,469	0,003	5,475	0,003	5,421	0,000																			
	313,15	4,207	0,021	4,206	0,010	4,143	0,003	4,033	0,000	4,001	0,003	4,012	0,001	3,964	0,002																			
	323,15	3,090	0,027	3,101	0,007	3,136	0,000	3,109	0,003	3,023	0,003	2,987	0,000	3,030	0,002																			
	333,15	2,464	0,480	2,375	0,008	2,451	0,011	2,449	0,004	2,315	0,003	2,324	0,002	2,351	0,001																			

K. Patent

Description

STABLE CARBON NANOFUID, OBTAINING METHODS AND USES THEREOF

Technical domain

[0001] The present disclosure relates to an engineering methodology for the intensive, large scale production of stable, long-term, homogeneous and highly dispersed carbon nanoparticle suspensions in polar liquids.

Technical background

[0002] Since its discovery, carbon nanoparticles have incited much attention, specifically to develop and produce new carbon-based nanocomposites (Ramesh, G., & Prabhu, N. (2011). *Nanoscale Research Letters*, 6(1), 334; Li, Y., Zhou, J. A. E., Tung, S., Schneider, E., & Xi, S. (2009). *Powder Technology*, 196(2), 89–101). The combination of the properties of carbon nanoparticles with common materials, originate new composite materials with enhanced properties namely, thermal, electrical and mechanical properties. These new materials may possibly be used in a variety of applications, such as: in polymer reinforcement; as electrode additive materials for batteries and capacitors; as light absorbing elements; conductive ink and as enhanced heat transfer fluids.

[0003] Carbon nanoparticles embrace any carbon particle with at least one nanoscale dimension. These nanoparticles can be arranged in spherical, ring, cone, tapering cone, tubular or sheet-like geometries with single or multi layers of carbon atoms. However, due to the atomic configurations of the carbon atoms ($1s^2 2s^2 2p^2$), instantaneous bonding among nanoparticles may occur creating clusters of nanoparticles. These agglomerates are a drawback to produce homogeneous and stable suspensions of carbon nanoparticles in fluids. To overcome the strong Van der Waals bonds, and to obtain non-agglomerated nanoparticles, the dispersion process of carbon nanoparticles in a base material involves a two-step method: the production of carbon nanoparticles in powders; and its dispersion in a base material. Despite the production

of carbon nanoparticles are well understood and industrialised, its dispersion in a base material is still challenging, requiring a process to break the strong Van der Waals forces without damaging the carbon nanoparticle structure in order to keep their exceptional properties.

[0004] The production of suspension of carbon nanoparticles in liquid phase materials, also known as nanofluids, is a promising industry with many potential applications that can be categorized into: heat transfer applications; automotive applications; paints and ink; glues; and additives. Such areas of potential applications require a methodology to customize the preparation for each application and/or base material. However, the production of carbon nanoparticles tend to form aggregates immediately after being produced.

[0005] The document US 2007/0253888 provides a methodology to prepare a carbon nanofluid through functionalization of the surface of carbon nanotubes and dispersing it by ultrasonication.

[0006] The document US 2014/0191164 A1 provides a methodology to dispersed carbon nanofibers in a liquid by controlling the content of oxygen. The document WO 2010/051102 A2 and the US7871533 B1 provide a methodology to disperse carbon nanotubes in different matrixes with different types of surfactants and dispersion processes.

[0007] As seen, some attempts have been made to increase the dispersibility of carbon nanoparticles in liquid phase materials.

[0008] These facts are disclosed in order to illustrate the technical problem addressed by the present disclosure.

General Description

[0009] As described, carbon nanoparticles have a drawback associated to the form aggregates immediately after being produced. Therefore, the present disclosure relates to carbon nanoparticles with an improvement of solubility and dispersibility of carbon nanoparticles in a given fluid, in particular a polar fluid.

[0010] Several attempts have been made to increase the dispersibility of carbon nanoparticles in liquid phase materials. To keep the suspension stable for long periods of time, without its deterioration, is still an engineering challenge. In this regard, to convert laboratory scale nanofluids to a safe commercial product, the characteristics of the suspension such as: homogeneity; pH (neutral or close to); carbon nanoparticles integrity; high temperature resistance; long term stability have to be guaranteed and stable. By “stable” it is understood a suspension which can maintain its properties, have no agglomeration and no sedimentation for at least one-year time. Moreover, prior art generalises the production methodology independent of the liquid phase material properties. Such leads to a problem in delivering the amount of necessary energy to overcome the Van der Waals forces and disentangle the carbon nanoparticles clusters, since liquids with different viscosities and densities will have different energy necessities.

[0011] The present disclosure solves the above described problems of solubility and dispersibility of carbon nanoparticles in a given fluid by providing a methodology for the continuous production of dispersed carbon nanoparticles in a polar fluid. The suspension of carbon nanoparticles into fluids have two major issues to solve: carbon nanoparticles have a hydrophobic surface, therefore a functionalization treatment of carbon nanoparticle is required in order to increase their wettability and promote the bonding of the fluid atoms with the carbon nanoparticles; secondly, it is necessary a precise control the amount of energy required to disentangle the clusters of carbon nanoparticles without damaging them, guarantee the homogeneity and long shelf life of the suspension.

[0012] The present disclosure illustrates and describes a methodology for continuous production of long-term, stable and homogenous dispersions of carbon nanoparticles, in fluids. In some embodiments, the wettability of the carbon nanoparticles is increased by chemical functionalization.

[0013] In this disclosure, functionalized carbon nanoparticles are continuously and homogeneously dispersed in polar fluids through mechanical agitation in a closed loop reactor producing a stable nanofluid. The fluids composition and dispersion

parameters are also revealed. Therefore, this disclosure provides the methodology for the large scale production of carbon-based nanofluids with the ability to be used as an additive, a heat transfer fluid or as an ink.

[0014] The present disclosure relates to a methodology for the continuous production of a carbon nanoparticle suspension in a polar fluid, solving the previously identified problems. The disclosed production methodology described below is not limited to carbon nanoparticles being possible to be used with other nanoparticles and fluids.

[0015] In an embodiment, this methodology is not limited to carbon nanoparticles or carbon nanotubes.

[0016] In an embodiment, this disclosure relates to functionalization treatments applied to the carbon nanoparticles introducing a plurality of functionalized groups into the surface of the nanoparticle to promote steric repulsion between individual nanoparticles; the functionalized carbon nanoparticles that are obtained are dispersed in a solvent matrix composed by a single fluid or a mixture of fluids with at least one fluid having polar characteristics.

[0017] In an embodiment and in order to guarantee the homogeneity of the suspension, the mixture is subjected to a process of mechanical agitation controlled in a dedicated reactor; the carbon nanofluids produced may be used in different applications.

[0018] In an embodiment the carbon nanofluid may be used as a heat transfer fluid for a radiator or as an additive solution to optimize the properties of solid materials that required a polar fluid in its constitution or preparation, such as concrete with water.

[0019] The present disclosure presents several advantages:

- provides an innovative methodology adequate to the continuous, large scale production of nanofluids (homogenously dispersed carbon nanoparticle in a solvent medium), showing chemical and physical stability for long periods of time even when exposed to harsh working conditions;

- provides the precise control of the energy supplied to the system during the mechanical agitation process. An excessive energy amount will damage the nanoparticles original structure, reducing their ability to enhance the nanofluid properties, a restrained energy delivery will not prevent the formation of nanoparticle clusters resulting in unstable nanofluids.

[0020] This disclosure also relates to a method to produce continuously long-term suspensions of carbon nanoparticles in polar fluids. This method comprises several steps such as:

- selecting a plurality of carbon nanoparticles;
- functionalizing the surface of the carbon nanoparticles wherein at least a carboxylic acid group, hydroxyl group, carbonyl group, ester groups and their combinations; is introduced onto de surface of the carbon nanoparticles;
- selecting a fluidic matrix or a mixture of fluids with at least one fluid with polar properties; and
- combining the carbon nanoparticles into the matrix by means of a specific and dedicated high-capacity flow-through ultrasonic reactor, through a mechanical agitation process to de-agglomeration of the carbon nanoparticles bundles into an evenly dispersed suspension.

[0021] In an embodiment, the fluidic matrix may comprise at least one or a mixture of: acetaldehyde, acetic acid, acetone, acetonitrile, 1,2-butanediol, 1,3-butanediol, 1,4-butanediol, 2-butoxyethanol, butyric acid, diethanolamine, diethylenetriamine, dimethylformamide, dimethoxyethane, dimethyl sulfoxide, 1,4-dioxane, ethanol, ethylamine, ethylene glycol, formic acid, furfuryl alcohol, glycerol, methanol, methyl diethanolamine, methyl isocyanide, 1-propanol, 1,3-propanediol, 1,5-pentanediol, 2-propanol, propanoic acid, propylene glycol, pyridine, tetrahydrofuran, triethylene glycol, water and mixtures thereof.

[0022] In an embodiment, the long-term carbon fluid now disclosed is stable for periods ranging from 1 hour - 5 years; 12 hours – 1 year; 7 days – 1 month; 15 days – 1 month.

[0023] In an embodiment, the mechanical agitation process comprises a stirrer and an ultrasonic operation in a closed loop reactor.

[0024] In an embodiment, the carbon nanoparticles comprise solid particles with at least one dimension in nanoscale.

[0025] In an embodiment, the carbon nanoparticles also comprise a spherical, tubular, simple sheet geometry and a single, double or multi walled configuration.

[0026] In an embodiment, the functionalization comprises treating the carbon nanoparticles with strong acids solutions, by plasma activation and/or by polymeric solutions; in particular the strong acid solutions may comprise a mixture of 302 grams of H_2SO_4 and 1104 grams of HNO_3 for each 20 grams of carbon nanoparticle. Furthermore, the method now disclosed may also comprise a step of accelerating the oxidation of the carbon nanoparticles through heating the mixture of carbon nanoparticles and strong acidic solution, in particular at 130°C (403 K) for 30 minutes; and a step of cooling the mixture, in particular to a room temperature and leaving to rest for 24 hours.

[0027] The method now disclosed may further comprise:

- a step of washing the mixture with pure water and centrifugation until a pH level of, at least, 5 is reach;
- a drying step of the mixture of purified nanoparticles at 100°C (373 K) until all the content of fluid evaporates and a powder is formed.

[0028] In an embodiment, the continuous preparation of a suspension of carbon nanoparticles in a fluidic matrix comprises:

- mixing the purified carbon nanoparticles in a fluidic matrix, and
- de-agglomerate the nanoparticles through mechanical agitation process.

[0029] In an embodiment, the mixing process may comprise a mixture of a volume fraction of carbon nanoparticles ranging from 0.001 to 8 % (V/V) in the fluidic matrix.

[0030] In an embodiment, the de-agglomeration of the nanoparticles may be conducted by through mechanical agitation process comprises:

- mixing the solution with a mechanical stirrer for at least 15 minutes, and
- applying ultrasounds through a closed loop ultrasonic process.

[0031] In an embodiment, the ultrasonic process of the method disclosed comprises the application of a low-intensity probe, with a wave amplitude ranging from 10 to 35 μm and a frequency range from 20 to 80 kHz. This ultrasonic process comprises continuously application of a ultrasound energy to the mixture until reaching 250 J/ml. The mixture subjected to the ultrasonic process is kept at constant temperature, such that the fluid viscosity ranges from 0.001 and 0.04 N.s/m².

[0032] The present disclosure also relates to a carbon based nanofluids, which may be used as a heat transfer fluid. The carbon based nanofluids is capable of serving as an additive agent to increase the thermal properties of polymeric fluids; a printing ink; a paint; an electric conductive layer; a protective coating; an additive for Li Ion battery electrode and cathode.

[0033] The present disclosure relates to a stable carbon nanofluid obtainable by the application of a ultrasonic current up to 250 J/ml comprising:

a polar matrix fluid and a plurality of carbon nanoparticles, wherein up to 8% ($v_{\text{carbon nanoparticles}}/v_{\text{nanofluid}}$) of the carbon nanoparticles comprise a reactive group selected from the following list: carboxylic acid group, hydroxyl group, carbonyl group, ester groups and combinations thereof;

wherein the reactive group ratio may be obtained by several method such as X-ray photoelectron spectroscopy (XPS) and is not less than 10 %; i.e. the reactive group ratio obtained by X-ray photoelectron spectroscopy is not less than 10 % ($((\text{Intensity}_{\text{Chemical treated CNT}} - \text{Intensity}_{\text{Bulk CNT}})/(\text{Intensity}_{\text{Chemical treated CNT}}) \times 100)$);

wherein the viscosity of the stable carbon nanofluid is between 0.001-0.04 Pa.s at 20 °C; preferably 0.002-0.0204 Pa.s at 20 °C;

wherein said nanofluid has a long-term stability.

[0034] In an embodiment, the long-term stability of the carbon nanofluid may be more than 1 year, preferably more than 2 years, more preferably more than 5 years.

[0035] In an embodiment, the stable carbon nanofluid may be obtainable by an ultrasonic energy between 100-250 J/ml; preferably 200–300 J/ml.

[0036] In an embodiment, the viscosity of the stable carbon nanofluid may be between 0.001-0.040 Pa.s at 20 °C; preferably 0.002-0.021 Pa.s at 20 °C.

[0037] In an embodiment, the stable carbon nanofluid may comprise up to 6% ($v_{\text{carbon nanoparticles}}/v_{\text{nanofluid}}$) of carbon nanoparticles, preferably up to 4% ($v_{\text{carbon nanoparticles}}/v_{\text{nanofluid}}$) of carbon nanoparticles, more preferably up to 2% ($v_{\text{carbon nanoparticles}}/v_{\text{nanofluid}}$) of carbon nanoparticles.

[0038] In an embodiment, the carbon nanoparticles of the stable carbon nanofluid now disclosed may be spherical, tubular, simple sheet, single walled, double walled, multi walled or combinations thereof.

[0039] In an embodiment, the reactive group ratio attached in the carbon nanoparticle surface is at least 10 % ($(\text{Intensity}_{\text{Chemical treated CNT}} - \text{Intensity}_{\text{Bulk CNT}})/(\text{Intensity}_{\text{Chemical treated CNT}}) \times 100$) higher than the bulk carbon nanoparticles, preferably up to 20% ($(\text{Intensity}_{\text{Chemical treated CNT}} - \text{Intensity}_{\text{Bulk CNT}})/(\text{Intensity}_{\text{Chemical treated CNT}}) \times 100$) higher than the bulk carbon nanoparticle, more preferably up to 15% ($(\text{Intensity}_{\text{Chemical treated CNT}} - \text{Intensity}_{\text{Bulk CNT}})/(\text{Intensity}_{\text{Chemical treated CNT}}) \times 100$) higher than the bulk carbon nanoparticle.

[0040] In an embodiment, the polar matrix fluid is selected from the following list: acetaldehyde, acetic acid, acetone, acetonitrile, 1,2-butanediol, 1,3-butanediol, 1,4-butanediol, 2-butoxyethanol, butyric acid, diethanolamine, diethylenetriamine, dimethylformamide, dimethoxyethane, dimethyl sulfoxide, 1,4-dioxane, ethanol,

ethylamine, ethylene glycol, formic acid, furfuryl alcohol, glycerol, methanol, methyl diethanolamine, methyl isocyanide, 1-propanol, 1,3-propanediol, 1,5-pentanediol, 2-propanol, propanoic acid, propylene glycol, pyridine, tetrahydrofuran, triethylene glycol, water and combinations thereof.

[0041] In an embodiment, said fluid is obtainable by the application of an ultrasonic energy comprising an amplitude of 17-25; preferably 19-24, more preferably 20-22.

[0042] In an embodiment, said fluid is obtainable by the application of an ultrasonic energy comprising a frequency of 17-25 Hz; more preferably 18-20 Hz.

[0043] This disclosure also relates to an electric conductive layer, an additive agent, a heat transfer fluid, a printing ink, a paint, a protective coating comprising the stable carbon nanofluid now disclosed.

[0044] This disclosure also relates a method for preparing the stable carbon nanofluid now disclosed and comprising the following steps:

selecting a plurality of carbon nanoparticles;

functionalizing the carbon nanoparticle surface with a reactive group selected from the following list: carboxylic acid group, hydroxyl group, carbonyl group, ester groups and combinations thereof;

dispersing the plurality of carbon functionalized nanoparticles in a polar matrix fluid;

submitting the dispersed mixture to an ultrasonication.

[0045] In an embodiment, the carbon nanoparticle functionalization may comprise adding a strong acid or a strong oxidant or a reactive plasma,

[0046] In an embodiment, the strong acid may be HNO_3 , H_2SO_4 , HClO_3 , HClO_4 , or mixtures thereof;

[0047] In an embodiment, the strong oxidant may be KMnO_4 , O_3 , or mixtures thereof.

[0048] In an embodiment, the carbon nanoparticle functionalization is carried out by heating the mixture of carbon nanoparticle and strong acid at 130 °C for 30 minutes.

Throughout the description and claims the word “comprise” and variations of the word, are not intended to exclude other technical features, additives, components, or steps. Additional objectives, advantages and features of the solution will become apparent to those skilled in the art upon examination of the description or may be learned by practice of the solution.

Brief description of the drawings

[0049] The following figures provide preferred embodiments for the present disclosure and should not be seen as limiting the scope of the disclosure.

[0050] **Figure 1:** SEM images of some carbon nanoparticles **(a)** before **(b)** after functionalization.

[0051] **Figure 2:** Schematic diagram of the developed reactor to continuously disperse carbon nanoparticles into polar fluids wherein 2 represents an industrial ultrasonic system; 21 represents the ultrasonic processor; 22 represents the ultrasonic transducer; 23 represents low intensity ultrasonic probe; 3 represents a flow cell; 31 represents a tank/reservoir; 32 represents the tank 31 inner wall; 33 represents the tank 31 outer wall; 331 represents the tank 31 inlet feedthrough; 332 represents the tank 31 outlet feedthrough; 34 represents limpet coils; 341 represents the inlet of the external coil 31; 342 represents the outlet of the external coil 31; 4 represents a batch reactor; 41 represents a tank/reservoir; 42 represents the inner wall of tank 41; 43 represents the outer wall of tank 41 ; 431 represents a inlet feedthrough for tank 41; 44 represents limpet coils; 441 represents limpet coils 44 inlet; 442 represents limpet coils 44 outlet; 45 and 46 represent feedthrough for tank 3; 5 represents a control valve; 6 represents three way valve; 7 represents variable flow pump; 8 represents low meter; 9 represents the collection tank/reservoir; 911 represents XX; 911 represents is tank 9 inlet feedthrough; 91 represents the outer wall of tank 9; 92 represents the outer wall of tank 9.

[0052] **Figure 3:** Thermal conductivity of carbon based nanofluids with different concentrations of carbon nanotubes of type D50L10 **(a)** EG 30%vol+H₂O 70%vol base fluid and **(b)** EG 60%vol + H₂O 40%vol base fluid.

[0053] **Figure 4:** Viscosity of carbon based nanofluids with different concentrations of carbon nanotubes of type D50L10 **(a)** EG 30% vol + H₂O 70% vol base fluid and **(b)** EG 60% vol + H₂O 40% vol base fluid.

[0054] **Figure 5:** Specific heat of carbon based nanofluids with different concentrations of carbon nanotubes of type D50L10.

[0055] **Figure 6:** Density of carbon based nanofluids with different concentrations of carbon nanotubes of type D50L10.

[0056] **Figure 7:** Shelf life of two carbon based nanofluids, with three different concentrations of carbon nanotubes and six geometries.

[0057] **Figure 8:** Zeta potential of carbon based nanofluids with different concentrations of carbon nanotubes of type D50L10.

Detailed description

[0058] The present disclosure is related to a dedicated methodology for the extensive production of carbon based nanofluids and the compositions thereof. The nanofluids of the present disclosure comprise, but are not limited to, carbon nanoparticles, such as carbon nanotubes, carbon nanorods, spherical carbon nanoparticles or carbon sheets, and at least one fluid with polar characteristics. However, the scope of the present disclosure is not limited to these types of nanoparticles, fluids and materials.

[0059] As used in this disclosure, the terms “nanoparticles” or “nanomaterial” refers to a material that has a discrete shape with at least one nanoscale dimension (width, diameter, height) or inferior to 1 micron (μm). Moreover, the “nanoparticle” now disclosed has an aspect ratio (e.g. length : diameter; length : width) of 1, 1 to 10, 10 to 17, 17 to 33, 33 to 50, 50 to 83, 83 to 125, 125 to 166, 166 to 250, 250 to 375, 375 to 750, 750 to 1500, or 1500 to 15000.

[0060] In some embodiments, the nanoparticles have at least a diameter from 1 to 15 nm, 15 to 20, 20 to 30, 20 to 40, 40 to 60, 50 to 80, 60 to 100 nm or higher.

[0061] In some embodiments, the nanoparticles having a non-spherical geometry have at least one dimension of 1 to 2, 2 to 5, 5 to 15 and 10 to 30 μm or higher.

[0062] In some embodiments, the nanoparticle can have a tubular, cylindrical, ellipsoidal, rod, parallelepiped, pyramidal or sheet like geometry.

[0063] In some embodiments, the carbon nanoparticles are carbon nanotubes with a single-walled, double walled or multi walled configuration.

[0064] In some embodiments, the nanoparticles can be an arrangement of carbons in a single or multi-layer configurations.

[0065] In some embodiments, the nanofluids can have a diversity of nanoparticle geometries and dimensions, however, having a prevalent geometry, dimension and wall configuration.

[0066] In some embodiments, the surface of the carbon nanoparticles is chemically functionalized by ways of covalent and/or non-covalent techniques. The non-covalent functionalization is characterized by employing π - π stacking or hydrophobic interactions onto carbon nanoparticle surface, and is achieved with aromatic compounds, surfactants, polymers, and/or biopolymers. The covalent functionalization is characterized by an oxidative damage of the carbon nanoparticle surface, leaving "holes" with oxygenated functional groups attached, such as, carboxylic (COOH) and hydroxyl (OH) acid, ketone, alcohol and/or ester groups. This oxidative process is achieved by immersing carbon nanoparticles into a strong acid solution, composed of at least one of the following acids, HNO₃, H₂SO₄, HClO₃, HClO₄ or a mixture of them; or strong oxidants, such as KMnO₄, O₃ or a reactive plasma. The functional groups attached to the surface of the carbon nanoparticles has the peculiarity of having both hydrogen acceptors and hydrogen donors. This will reduce the hydrophobic surface characteristics of the carbon nanoparticle, while balancing the repulsion/attraction Van der Waals forces. Moreover, carboxylic and hydroxyl groups have polar properties, increasing the solubility of functionalized carbon nanoparticles in polar fluids.

[0067] In an embodiment, the nanofluids can have a diversity of base fluids with polar characteristics namely, but is not limited to: acetaldehyde, acetic acid, acetone, acetonitrile, 1,2-butanediol, 1,3-butanediol, 1,4-butanediol, 2-butoxyethanol, butyric acid, diethanolamine, diethylenetriamine, dimethylformamide, dimethoxyethane,

dimethyl sulfoxide, 1,4-dioxane, ethanol, ethylamine, ethylene glycol, formic acid, furfuryl alcohol, glycerol, methanol, methyl diethanolamine, methyl isocyanide, 1-propanol, 1,3-propanediol, 1,5-pentanediol, 2-propanol, propanoic acid, propylene glycol, pyridine, tetrahydrofuran, triethylene glycol, water, mixtures of fluids with at least one polar fluid, and mixtures thereof.

[0068] In an embodiment, the functionalization process is achieved by immersing the carbon nanoparticles into a mixture of strong acid solution composed by 25% volume of HNO_3 and 75% volume of H_2SO_4 . The volume ratio of the acidic solution to volume of raw carbon nanoparticles has to be proximally in the range of 1 part by volume of nanoparticles to 174 parts by volume of acid solution, or more preferably, in the range of 1 part by volume of nanoparticle to 87 parts of acidic solution. The mixture is heated to a temperature between 120 °C to 150 °C (393 to 423 K) but more preferable at 130 °C (403 K), in order to accelerate the oxidation process and minimize the structural damage on the carbon nanoparticles surface. After 30 minutes at that temperature, the heater is turned off and the solution is cooled to room temperature. The functionalized carbon nanoparticles with carboxyl groups (COOH), are then washed with pure water in order to stop the oxidation reaction. Afterwards, the mixture is centrifuge to accelerate the carbon nanoparticle sedimentation. The washing and centrifugation process is repeated until a pH level in the range of 5 to 7 is reached. Next, the functionalized carbon nanoparticles are dried in an oven at 100 °C (373 K) in order to evaporate the remaining water and form a dry powder. The functionalized carbon nanoparticles are then blended and dispersed in the base fluid by a mechanical agitation process. This energy-induced agitation process is the most critical step in the production of the nanofluids and has to be precisely controlled, otherwise it will not be possible to ensure the structural integrity of the carbon nanoparticles. Additionally, density and viscosity measurements are performed and compared with known values in order to guarantee the success of the dispersion process.

[0069] Should be noted that, despite the fact that in the above embodiments carbon nanoparticles are functionalized by ways of a strong acid solution, other

functionalization techniques and solutions can be adopted, to the extent that they provide an increase of the wettability of the carbon nanoparticle.

[0070] In another embodiment, is provided a method for the preparation of a dispersion of carbon nanoparticles in fluids to serve as an additive agent.

[0071] The carbon nanoparticles or carbon nanotubes are functionalized by a strong acid mixture composed by 25% by volume of nitric acid and a 75% by volume of sulphuric acid. The content of raw carbon nanoparticles or carbon nanotubes has to be proximally in the range of 1 part by volume of carbon nanoparticles to 174 parts by volume of acid solution, or more preferably, in the range of 1 part by volume of nanoparticle to 87 parts by volume of acidic solution. The mixture is heated to a temperature between 120 °C to 150 °C (393 to 423 K) for 30 minutes for the oxidation reaction to occur, afterward the heater is turned off and the mixture is cooled to room temperature. The functionalized carbon nanoparticles or carbon nanotubes with carboxyl groups (COOH), are then washed with pure water in order to stop the oxidation reaction. Afterwards, the mixture is centrifuge in order to accelerate the carbon nanoparticles or carbon nanotubes sedimentation. The washing and centrifugation process is repeated until a pH level in the range of 5 to 7 is reached. Next, the functionalized carbon nanoparticles or carbon nanotubes are dried in an oven at 100°C (373 K) in order to evaporate the remaining water and form a dry powder. The functionalized carbon nanoparticles or carbon nanotubes are then blended and dispersed by a mechanical agitation process, in a base fluid accordingly to the final application of the additive. This energy-induced agitation process is the most critical step in the production of nanofluids and has to be precisely controlled, otherwise will not be possible to ensure the structural integrity of the carbon nanotubes. Additionally, density and viscosity measurements are performed and compared with known values in order to guarantee the success of the dispersion process.

[0072] The mechanical agitation process is performed by ways of mechanical stirrer and ultrasonic agitation operations. The high-capacity flow-through ultrasonic reactor system Fig. 2, is manly composed by an ultrasonic system 2 with a flow cell 3, a mixture

tank 4, and a collection tank 9. The batch reactor 4 is composed by a tank 41 with an external limpet coil 44 to maintain the required temperature of the base fluid, and a mechanical mixer 47. The tank outer wall 43 has an inlet 431 that is connected with the flow cell 3, and an outlet 432 that is connected to the control valve 5. The inlet feedthrough 45 is used to fill the tank 41 with the desired amount of nanoparticles and the feedthrough 46 is used to fill the tank with the required amount of base fluid. The external limpet coil has an inlet 441 where a heat transfer fluid enters filling the coil and exits via the outlet 442 back to a temperature control unit. The ultrasonic system 2 comprises an industrial ultrasonic processor 21 with an ultrasonic frequency of at least 20 KHz and with adjustable amplitude, connected to an ultrasonic transducer 22; and an ultrasonic low intensity probe 23. The ultrasonic probe 23 is hermetic sealed in the flow cell 3 to avoid any leak and to maintain the system pressurised. The flow cell 3 is composed by a tank 31 with an external limpet coil 34 to maintain a required base fluid temperature. The tank outer walls 33 have an inlet feedthrough 331 where de base fluid enters passing through the ultrasonic probe 23 and exits via the outlet feedthrough 332 for the batch reactor 4. The external limpet coil 34 have an inlet 341 where a heat transfer fluids enters filling the coils and exits via the outlet 342 back to a temperature control unit. The collection tank outer wall 91 has an inlet 911 where the fluid enters to the collection tank 9 from the 3-way valve 6. A variable flow rate pump 7 is used to recirculate the fluids throughout the system and the flow rate is monitoring by a flow meter 8.

[0073] In the above-described system, the temperature control system 44 and 34 is not limited to a specific device or technique and can be modify by a trained person in the art of heat exchanging processes.

[0074] In one or more embodiments of the present disclosure, a specific volume of base fluid is dumped into the mixture tank 4, follow by the amount of nanoparticles desired to achieve the chosen volume fraction.

[0075] The present disclosure relates to a methodology to produce long-term stable suspension of carbon nanoparticles in a polar base fluid. This suspension can have a variety of applications, as a final product or as an additive to others materials or

process. These suspensions are composed by 92 to 99.999 % vol. of base fluid and 0.001 to 8 % vol. of carbon nanoparticles. The preferable composition of the carbon based nano-suspension is directly dependent on its final application. This tailoring service has to be made from those skilled on the art of the preparation of suspensions of carbon nanoparticles or carbon nanotubes in polar fluids acquainted with the effects on the suspensions properties.

[0076] In accordance with the methodology described above, a preferable composition of a water based heat transfer fluid or water based additive agent is, for example, a composition containing 98 to 99.75 % vol. of water and 0.25 to 2 % vol. of carbon nanoparticles. The composition may contain other polar or non-polar fluids in addition to the based polar fluid.

[0077] The preparation of a nanofluid is divided into two steps: the functionalization of the nanoparticle surfaces and the blending of the functionalized carbon nanoparticles with de polar fluid. The first step has been already described above; the second step is a quite more complex and has to be precisely controlled. As described above, the carbon nanoparticles are dispersed by mechanical agitation as illustrated on Fig. 2. This ultrasonic energy induced agitation process is the most critical step in the production of nanofluids and has to be precisely controlled, otherwise the carbon nanoparticles will not be homogeneously dispersed and some damages on the nanoparticles structure may occur. Since the velocity of the ultrasonic waves strongly depends on the medium, since different fluid viscosities will affect the wave velocity. Therefore, for a consistent operation of the ultrasonic dispersion for different types of fluids as well as for different carbon nanoparticles concentrations (different viscosities and densities), the agitation process has to be controlled as a function of the delivered energy per volume of fluid while maintaining a low viscosity. Moreover, the ultrasonication must be applied by a low-intensity probe, otherwise the carbon nanoparticle structure will be damaged. The amplitude of the ultrasound wave, has to be within an interval of 10 to 35 μm , but preferable at 17 μm . During the agitation process the temperature of the samples must be kept constant. For high viscosity

fluids this temperature must be tailored in order to reach a viscosity within an interval of 0.001 and 0.04 N.s/m².

Nanofluid properties assessment

[0078] The structural integrity of the carbon nanoparticles and the dispersion rate were evaluated by means of a Scanning Electron Microscopy (SEM). This technique allows the assessment of the nanoparticle dimensions while evaluating the structural damages caused by the functionalization and mechanical agitation processes. Fig. 1 illustrates two SEM images of carbon nanotubes prior to functionalization (a) and after functionalization (b); it is clear in Fig.1a that the carbon nanotubes are aggregated in bundles composed by several tubes; in contrast, after the functionalization (Fig.1b) it is clear that the carbon nanotubes are separated.

[0079] The thermal conductivity (k) of the carbon based nanofluids was evaluated by means of a transient hot wire system. Fig. 3 illustrates the thermal conductivity for two different base fluids (a) 30% vol. of ethylene glycol with 70% vol. of H₂O and (b) 60%vol. of ethylene glycol with 40% vol. of H₂O, with 5 different concentrations of carbon nanotubes (0.25; 0.50; 0.75; 1.0; 1.5 % vol) and five temperatures (10 (283), 20 (293), 25 (298), 30 (303), 40 (313), 50 (323) °C (K)).

[0080] The zeta potential measurements were conducted in a Malvern ZS Nano S analyser at 20°C (293 K). Since the electro-kinetic potential is independent of the nanoparticle volume fraction and temperature, the measurements were conducted for six different types of carbon nanotubes (different aspect ratio) dispersed in two distinct base fluids (30%vol. of ethylene glycol with 70%vol. of H₂O and 60%vol. of ethylene glycol with 40%vol. of H₂O) as illustrated in. Fig. 7.

Shelf Life Measurements

[0081] The colloidal stability of the nanofluids was evaluated by a Space and Time-resolve Extinction Profiles (STEP) method. This innovative method imposes an intensive centrifugal force to the samples while records the kinetics of any concentration changes due to sedimentation or phase separation. These tests were conducted by a LUMiSizer analyser, and this equipment registers the settling velocity of the nanoparticles and one of the outcome results is the shelf life. Fig. 6 illustrates the shelf life for the two base fluids (30% vol. of ethylene glycol with 70% vol. of H₂O and 60% vol. of ethylene glycol with 40% vol. of H₂O), with three different concentrations of carbon nanotubes (0.25; 0.75; 1.5 % vol) at 20 °C (293 K).

[0082] The viscosity (μ) measurements were evaluated by a Brookfield shear rate control rheometer DVIII. The produced nanofluids were subjected to different shear rates and the viscosities were recorded. Fig. 4, illustrates the viscosity of the two base fluids (a) 30% vol. of ethylene glycol with 70% vol. of H₂O and (b) 60% vol. of ethylene glycol with 40% vol. of H₂O, with five different concentrations of carbon nanotubes (0.25; 0.50; 0.75; 1.0; 1.5 %vol) and at six temperatures (10 (283), 20 (293), 25 (298), 30 (303), 40 (313), 50 (323) °C (K)).

[0083] The specific heat (cP) measurements were evaluated by a Perkin Elmer differential scanning calorimeter (DSC) 4000. The produced nanofluids were subjected to a heating ramp of 5 °C/min from 5 to 70 °C (278 to 343 K) and the heat flow was recorded. Fig. 5 illustrates the specific heat results at ten temperatures, for three different concentration of carbon nanotubes (0.25, 0.75 and 1.5 % vol.) and two base fluids (a) 30% vol. of ethylene glycol with 70% vol. of H₂O and (b) 60% vol. of ethylene glycol with 40% vol. of H₂O.

[0084] The present disclosure will now be described with reference to a number of examples. However, the disclosure is not limited to the examples.

Functionalization (chemical treatment)

[0085] Six different geometries of commercial available carbon nanotube manufacture by Cheaptubes Inc. a nanoparticle supplier has been used as raw material; a commercially available concentrated nitric and sulphuric acids were used to perform

the surface functionalization of the carbon nanotubes. In Table 1, it is described the nanotubes' geometrical characteristics, the concentrations of each chemical reagent, and the pH level achieved after the washing process.

Table 2 – Nanoparticle geometry and functionalization parameters.

Name	Nanoparticle	Geometry		Functionalization reagents content				T [°C]	pH level
		Diameter [nm]	Length [µm]	Nanoparticle [g]	Nitric acid [g]	Sulphuric acid [g]	Acids per nanoparticle ratio		
D50L10	Carbon nanotubes	50-80	10-20	20	302	1104	70	120-150	~5
D60L5	Carbon nanotubes	60-100	5-15	20	302	1104	~70	120-150	~5
D60L1	Carbon nanotubes	60-100	1-2	20	302	1104	70	120-150	~5
D20L10	Carbon nanotubes	20-40	10-30	20	302	1104	~70	120-150	~5
D20L5	Carbon nanotubes	20-40	5-15	20	302	1104	70	120-150	~5
D20L1	Carbon nanotubes	20-40	1-2	20	302	1104	~70	120-150	~5

[0086] As depicted in Table 1, the ratio of acid mixture regarding the mass of the carbon nanotubes, must be proximally 70, otherwise the functionalization will not be sufficient to attach significant carboxylic groups onto the surface of the carbon nanotubes. Additionally, the functionalization time must be well controlled; otherwise the carbon nanotube surface can withstand some damages. In order to control the functionalization time, the temperature of the mixture must be kept between 120 °C to 150 °C (393 to 423 K) for 30 minutes, but preferably at 130 °C (403K) for 30 minutes. Afterwards, the mixture is cooled down to room temperature and diluted with distilled water. The dilution process is repeated until a pH level of proximally 5 to 7 is reached. The functionalized carbon nanotubes are then dried in an oven and then triturated to form a powder. The functionalization of the surface of the carbon nanotubes are not limited to this technique, the main goal is to increase the content of oxygen attached to the surface of the carbon nanotubes. This process must be executed by a skilled person on functionalization of nanoparticles.

Example 1 - Production and Composition of Nanofluids (NF30EG)

[0087] The nanofluids *NF30EG* are composed by dispersing multiwalled carbon nanotubes *D50L10* in a mixture of 30% vol. of ethylene glycol and 70% vol. of water. The carbon nanotubes are dispersed in the ethylene glycol/water mixture by ways of mechanical agitation previously described and illustrate on Fig. 2. This energy-induced process must be precisely controlled, otherwise carbon nanotubes will not be uniformly dispersed and may be damaged. The velocity of the ultrasonic waves depends strongly on the medium, since different densities (viscosities) will affect the wave velocity. Therefore, the ultrasonic operation must be carefully tailored regarding the nanofluid density and volume. Therefore, the ultrasonic operation must be controlled as a function of energy per volume of fluid, otherwise for different concentrations of carbon nanotubes, i.e. different densities (viscosities), the dispersion will not be homogeneous and the process will not be reliable. Moreover, the ultrasonic operation must be applied by a low-intensity horn probe, otherwise some damages could be induced on the carbon nanotube structure. The amplitude of the ultrasound wave should to be proximally 17 μm . Throughout the agitation process the samples temperature must be kept constant. For high viscosity fluids this temperature should be tailored in order to reach a viscosity within an interval of 0.001 - 0.04 Pa.s at 20 °C. The content of carbon nanotubes in the dispersion liquid and the ultrasonic operation parameters are described in Table 2.

Table 3 - Ultrasonic operation parameters

Base Fluid: 30%vol. Ethylene Glycol + 70%vol. Water				
Content of CNT (% vol.)	Process Agitation Energy [J/ml]	Amplitude [μ]	Frequency [kHz]	Sample Temperature [$^{\circ}$ C (K)]
0.25	~250	~17	20	~20 (293)
0.5	~250	~17	20	~25 (298)
0.75	~250	~17	20	~30 (303)
1.0	~250	~17	20	~35 (308)
1.5	~250	~17	20	~45 (318)

[0088] Next, the NF30EG Nanofluids will be subjected to a full experimental characterization, such as thermal and stability properties as describe previously. In Table 3, it is presented the carbon nanotube volume fraction (%vol.), the density (ρ), specific heat (c_p), viscosity (μ), thermal conductivity (k), Zeta potential (Zeta) and shelf-life (Life). All measurements were evaluated at 20 $^{\circ}$ C (293.15 K).

Table 4 – Thermal properties and stability results

Content of CNT (% vol.)	Specific heat (c_p) [J/kg.K]	Viscosity (μ) [Pa.s]	Thermal conductivity (k) [W/m.K]	Zeta potential (Zeta) [mV]	Shelf-life (Life) [Years]	Freeze Protection [$^{\circ}$ C (K)]
0.25	4.533	0.00310	0.468	>60	~5	-20 (253)
0.5	4.448	0.00313	0.473		~5,5	-20 (253)
0.75	4.380	0.00317	0.482		~7	-20 (253)
1.0	4.361	0.00328	0.501		~7,5	-20 (253)
1.5	4.339	0.00471	0.534		~8	-20 (253)

[0089] In Table 4, it is depicted the percentage of increasing of the thermal properties, relatively to the base fluid. The maximum variation recorded for all the thermal properties was for a volume fraction of 0.015 (1.5 % vol.), the thermal conductivity and the relative viscosity increased 18.5 and 91.77 %, respectively; the specific heat was decrease 4.33%. As seen, the production of nanofluids with small amounts of carbon nanotubes according to the present disclosure, results in a significant variation of the thermal properties.

Table 5 - Thermal properties variation versus carbon nanotube volume fraction concentration

Base Fluid: 30%vol. Ethylene Glycol + 70%vol. Water			
Content of CNT (% vol.)	Specific heat (cp) [%]	Viscosity (μ) [%]	Thermal conductivity (k) [%]
0.25	-0.05	26.22	1.96
0.5	-1.93	27.44	3.05
0.75	-3.43	29.07	5.01
1.0	-3.85	33.55	9.15
1.5	-4.33	91.77	18.50

Example 2 - Production and Composition of Nanofluids (NF60EG)

[0090] The nanofluids NF60EG are composed by dispersing multiwalled carbon nanotubes D50L10 in a mixture of 60% vol. of ethylene glycol and 40% vol. of water. The carbon nanotubes are dispersed in the ethylene glycol/water mixture by ways of mechanical agitation previously described and illustrate on Fig. 2. This energy-induced process must be precisely controlled, otherwise carbon nanotubes will not be uniformly dispersed and may be damaged. The velocity of the ultrasonic waves depends strongly on the medium, since different densities (viscosities) will affect the wave velocity. Therefore, the ultrasonic operation must be carefully tailored regarding the nanofluid density and volume. Therefore, the ultrasonic operation must be controlled as a function of energy per volume of fluid, otherwise for different concentrations of carbon nanotubes, i.e. different densities (viscosities), the dispersion will not be homogeneous and the process will not be reliable, for example by the application in time of an ultrasonic energy between 100-250 J/ml; preferably 200–300 J/ml. Moreover, the ultrasonic operation must be applied by a low-intensity or horn probe, otherwise some damages could be induced on the carbon nanotube structure. The amplitude of the ultrasound wave should to be proximally 17 μ m. Throughout the agitation process the samples temperature must be kept constant. For high viscosity fluids this temperature should be tailored in order to reach a viscosity within an

interval of 0.001 and 0.04 N.s/m². The content of carbon nanotubes in the dispersion liquid and the ultrasonic operation parameters are described in Table 5.

Table 6 - Ultrasonication operation parameters

Base Fluid: 60%vol. Ethylene Glycol + 40%vol. Water				
Content of CNT (% vol.)	Process Agitation Energy [J/ml]	Amplitude	Frequency [Hz]	Sample Temperature [°C (K)]
0.25	~250	~17	20	~27 (300)
0.5	~250	~17	20	~32 (305)
0.75	~250	~17	20	~37 (310)
1.0	~250	~17	20	~43 (315)
1.5	~250	~17	20	~47 (320)

[0091] Next, the NF30EG Nanofluids are subjected to thermal properties and stability evaluation as describe previously. In Table 7 is represented the carbon nanotube volume fraction (vol. %), the density (ρ), specific heat (c_p), viscosity (μ), thermal conductivity (k), Zeta potential (Zeta), shelf-life (Life) and freeze protection. All measurements were evaluated at 20°C (293.15 K).

Table 7 - Thermal properties and stability results

Base Fluid: 60%vol. Ethylene Glycol + 40%vol. Water						
Content of CNT (% vol.)	Specific heat (c_p) [J/kg.K]	Viscosity (μ) [Pa.s]	Thermal conductivity (k) [W/m.K]	Zeta potential (Zeta) [mV]	Shelf-life (Life) [years]	Freeze Protection [°C (K)]
0.25	3.642	0.00681	0.353	68.36	8	-50 (223)
0.5	3.594	0.00716	0.364		12	-50 (223)
0.75	3.521	0.00915	0.373		16	-50 (223)
1.0	3.519	0.0103	0.384		17	-50 (223)
1.5	3.502	0.0206	0.409		19	-50 (223)

[0092] In Table 8, is depicted the thermal properties variation ratio due to the present of the carbon nanotubes. The maximum variation recorded for all the thermal properties was for a volume fraction of 0.015 (1.5 % vol.), the thermal conductivity and the relative viscosity increased 16.2 and 266.22 %, respectively; the specific heat was decrease 4.34%. As seen, the production of nanofluids with small amounts of carbon nanotubes according with the present disclosure, result in a significant variation of the thermal properties.

Table 8 – Thermal properties variation versus carbon nanotube volume fraction concentration

Base Fluid: 60%vol. Ethylene Glycol + 40%vol. Water			
Content of CNT (% vol.)	Specific heat (c _p) [%]	Viscosity (μ) [%]	Thermal conductivity (k) [%]
0.25	-0.33	21.07	0.28
0.5	-1.67	27.29	3.40
0.75	-3.78	62.67	5.97
1.0	-3.84	83.11	9.09
1.5	-4.34	266.22	16.19

Table 8 – Stability of the long-term carbon fluid of the present disclosure

30% Ethylene Glicol + Water						
Content of CNT (% vol.)	Specific heat (c _p) [J/kg.K]	Viscosity (μ) [Pa.s]	Thermal conductivity (k) [W/m.K]	Zeta potential (Zeta) [m.V]	Shelf-life (Life) [Years]	Freeze Protection [°C (K)]
0.25	4.533	0.00310	0.468	>60	~5	-20 (253)
0.5	4.448	0.00313	0.473		~5,5	-20 (253)
0.75	4.380	0.00317	0.482		~7	-20 (253)
1.0	4.361	0.00328	0.501		~7,5	-20 (253)
1.5	4.339	0.00471	0.534		~8	-20 (253)

Table 9 – Stability of the long-term carbon fluid of the present disclosure

Base Fluid: 60%vol. Ethylene Glycol + 40%vol. Water						
Content of CNT (% vol.)	Specific heat (C _p) [J/kg.K]	Viscosity (μ) [Pa.s]	Thermal conductivity (k) [W/m.K]	Zeta potential (Zeta) [mV]	Shelf-life (Life) [years]	Freeze Protection [°C (K)]
0.25	3.642	0.00681	0.353	68.36	8	-50 (223)
0.5	3.594	0.00716	0.364		12	-50 (223)
0.75	3.521	0.00915	0.373		16	-50 (223)
1.0	3.519	0.0103	0.384		17	-50 (223)
1.5	3.502	0.0206	0.409		19	-50 (223)

[0093] The disclosure should not be seen in any way restricted to the embodiments described and a person with ordinary skill in the art will foresee many possibilities to modifications thereof.

[0094] The above described embodiments are combinable. The following claims further set out particular embodiments of the disclosure.

Date: 30 July 2018

CLAIMS

1. A stable carbon nanofluid obtainable by the application of an ultrasonic current up to 250 J/ml comprising
 - a polar matrix fluid and a plurality of carbon nanoparticles,
 - wherein up to 8% ($v_{\text{carbon nanoparticles}}/v_{\text{nanofluid}}$) of the carbon nanoparticles comprise a reactive group selected from the following list: carboxylic acid group, hydroxyl group, carbonyl group, ester groups and combinations thereof;
 - wherein the reactive group ratio is not less than 10 %;
 - wherein the viscosity of the stable carbon nanofluid is between 0.001-0.04 Pa.s at 20 °C; preferably 0.002 - 0.0204 Pa.s at 20 °C;
 - wherein said nanofluid has a long-term stability.
2. Stable carbon nanofluid according to the previous claim wherein the long-term stability is more than 1 year, preferably more than 2 years, more preferably 5 years.
3. Stable carbon nanofluid according to the previous claims obtainable by the application of an ultrasonic energy between 100-250 J/ml; preferably 200–300 J/ml.
4. Stable carbon nanofluid according to the previous claims wherein the viscosity of the stable carbon nanofluid is between 0.001-0.040 Pa.s at 20 °C; preferably 0.002 to 0.021 Pa.s at 20 °C.
5. Stable carbon nanofluid according to the previous claims comprising up to 6% ($v_{\text{carbon nanoparticles}}/v_{\text{nanofluid}}$) of carbon nanoparticles, preferably up to 4% ($v_{\text{carbon nanoparticles}}/v_{\text{nanofluid}}$) of carbon nanoparticles, more preferably up to 2% ($v_{\text{carbon nanoparticles}}/v_{\text{nanofluid}}$) of carbon nanoparticles.

6. Stable carbon nanofluid according to the previous claims wherein the carbon nanoparticles are spherical, tubular, simple sheet, single walled, double walled, multi walled or combinations thereof.
7. Stable carbon nanofluid produced according to the previous claims 1 wherein the reactive group ratio attached in the carbon nanoparticle surface is at least 10 % higher than the bulk carbon nanoparticles, preferably up to 20% of the carbon nanoparticle, more preferably up to 15% higher of the bulk carbon nanoparticle.
8. Stable carbon nanofluid according to the previous claims wherein the polar matrix fluid is selected from the following list: acetaldehyde, acetic acid, acetone, acetonitrile, 1,2-butanediol, 1,3-butanediol, 1,4-butanediol, 2-butoxyethanol, butyric acid, diethanolamine, diethylenetriamine, dimethylformamide, dimethoxyethane, dimethyl sulfoxide, 1,4-dioxane, ethanol, ethylamine, ethylene glycol, formic acid, furfuryl alcohol, glycerol, methanol, methyl diethanolamine, methyl isocyanide, 1-propanol, 1,3-propanediol, 1,5-pentanediol, 2-propanol, propanoic acid, propylene glycol, pyridine, tetrahydrofuran, triethylene glycol, water, combinations thereof.
9. Stable carbon nanofluid according to the previous claims wherein the fluid is obtainable by the application of an ultrasonic energy comprising an amplitude of 17-25; preferably 19-24, more preferably 20-22.
10. Stable carbon nanofluid according to the previous claims wherein the fluid is obtainable by the application of an ultrasonic energy comprising a frequency of 17-25 Hz; more preferably 18-20 Hz.
11. An electric conductive layer, an additive agent, a heat transfer fluid, a printing ink, a paint, a protective coating comprising the stable carbon nanofluid according to any one of the previous claims.
12. A method for preparing a stable carbon nanofluid comprising the following steps:

selecting a plurality of carbon nanoparticles;

functionalizing the carbon nanoparticle surface with a reactive group selected from the following list: carboxylic acid group, hydroxyl group, carbonyl group, ester groups and combinations thereof;

dispersing the plurality of carbon functionalized nanoparticles in a polar matrix fluid;

submitting the dispersed mixture to an ultrasonication.

13. Method according to claim 12 wherein the carbon nanoparticle functionalization comprises adding a strong acid or a strong oxidant or a reactive plasma.

14. Method according to claim 12-13 wherein the carbon nanoparticle functionalization is carried out by heating the mixture of carbon nanoparticle and strong acid at 130 °C for 30 minutes.

15. Method according to claims 12-14 wherein the strong acid is HNO_3 , H_2SO_4 , HClO_3 , HClO_4 , or mixtures thereof.

16. Method according to claim 13 wherein the strong oxidant is KMnO_4 , O_3 , or mixtures thereof.

Date: 30 July 2018

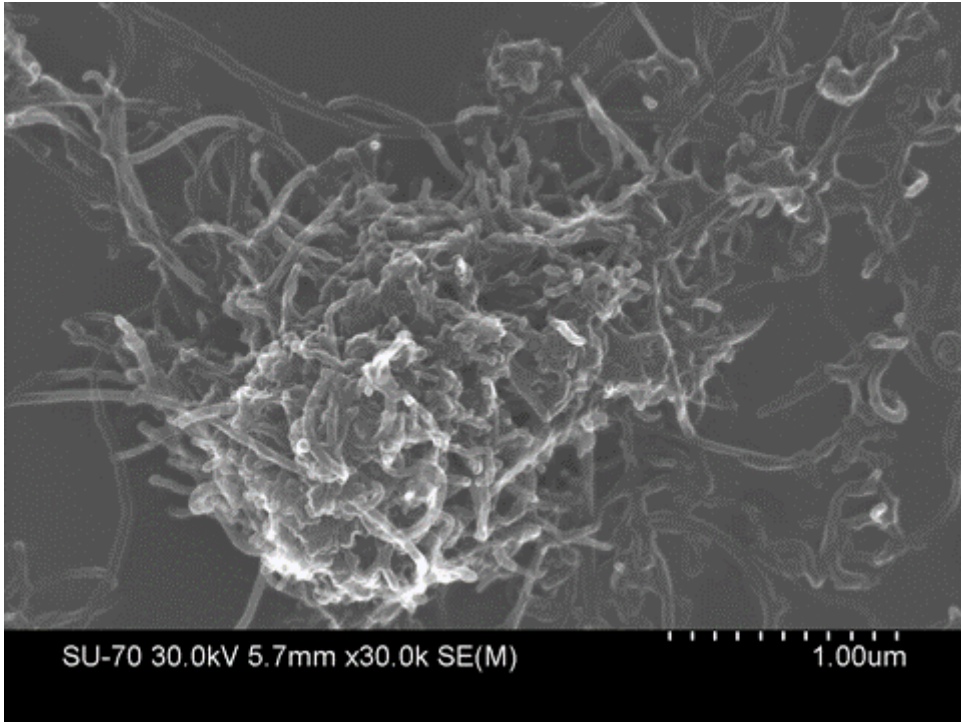


Fig. 1A



Fig. 1B

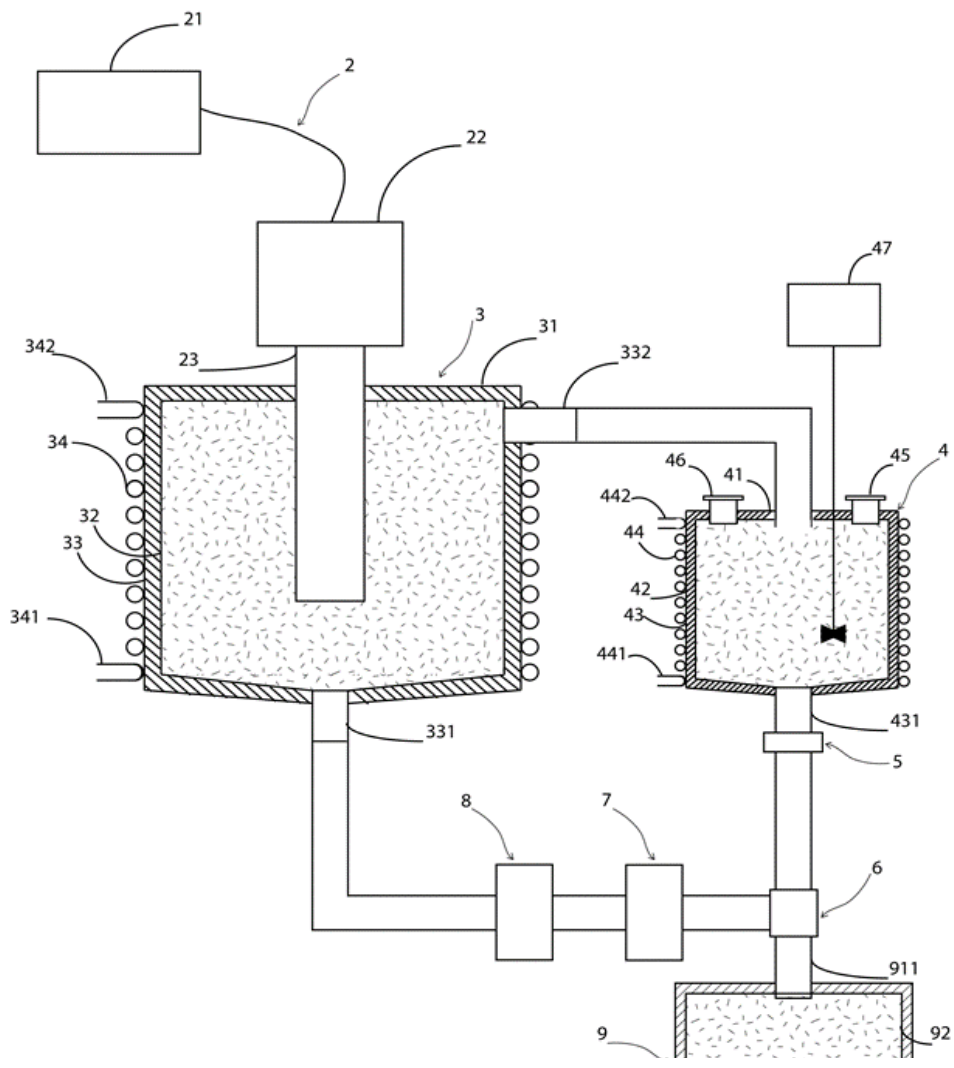


Fig. 2

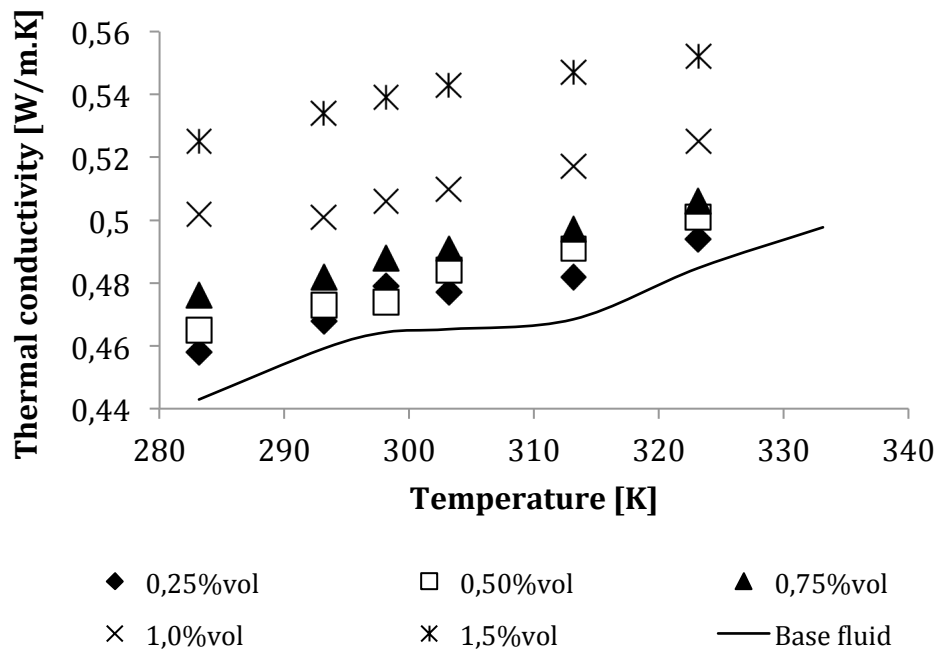


Fig. 3A

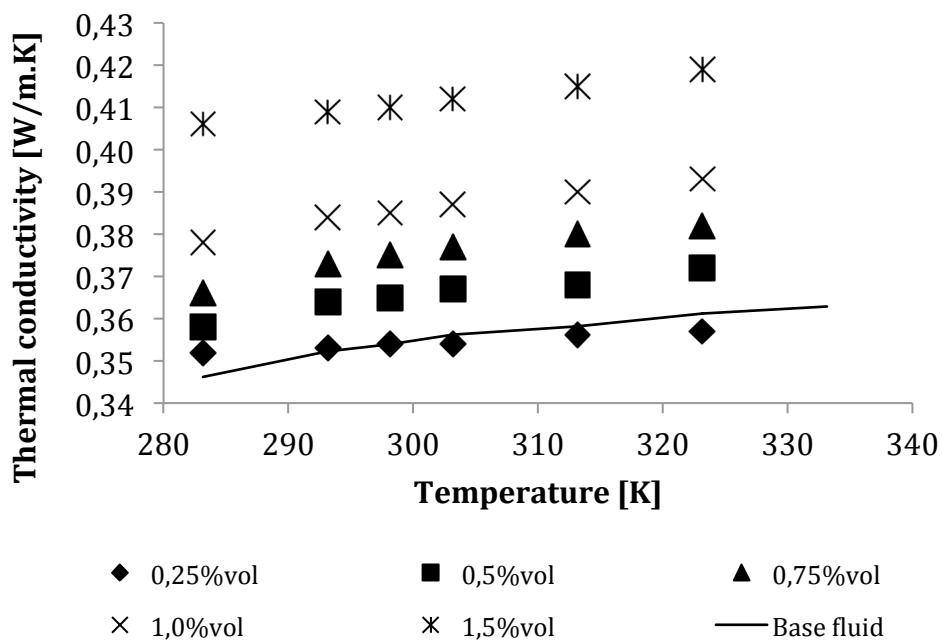


Fig. 3B

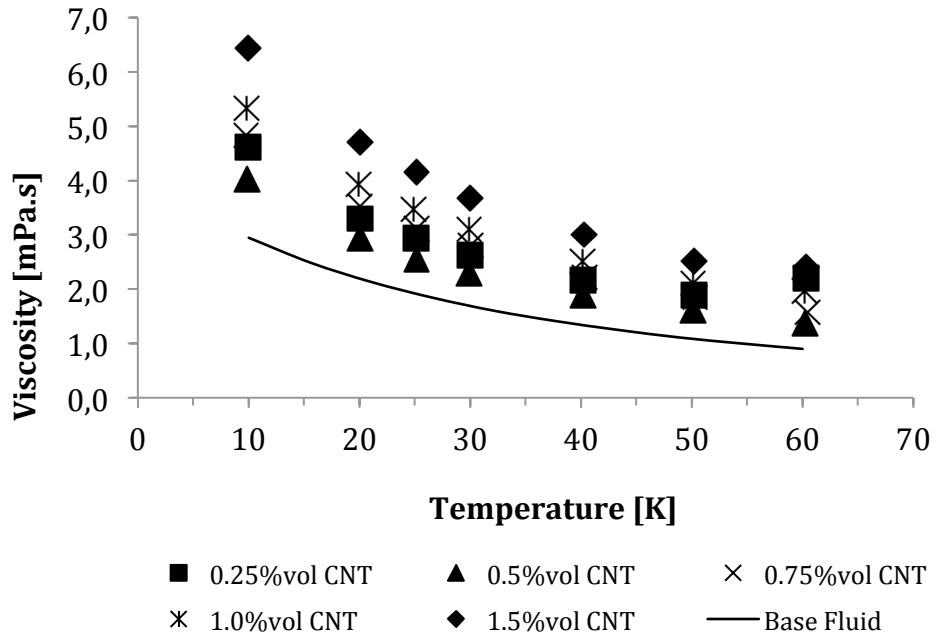


Fig. 4A

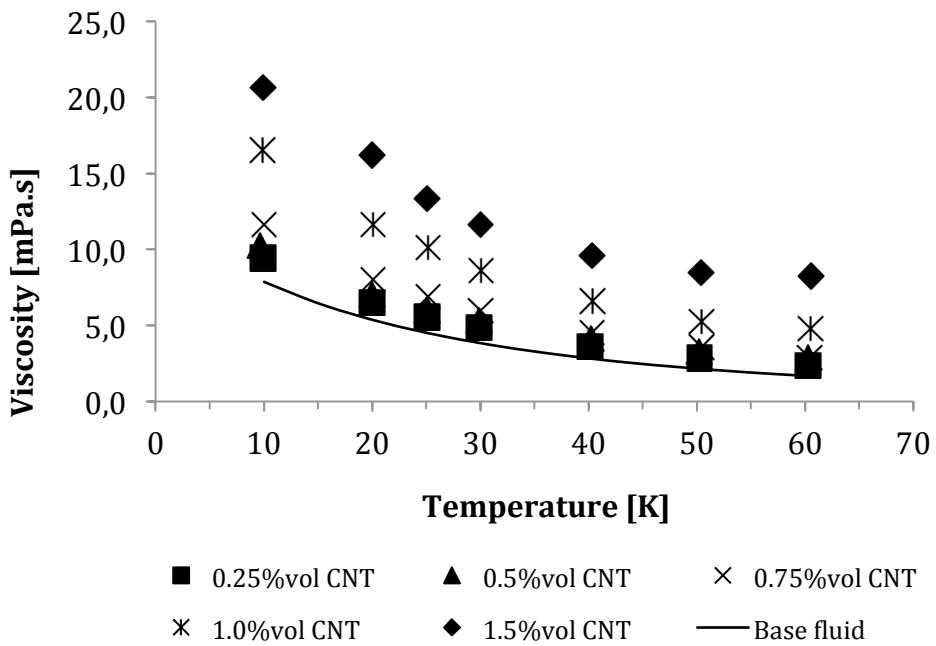


Fig. 4B

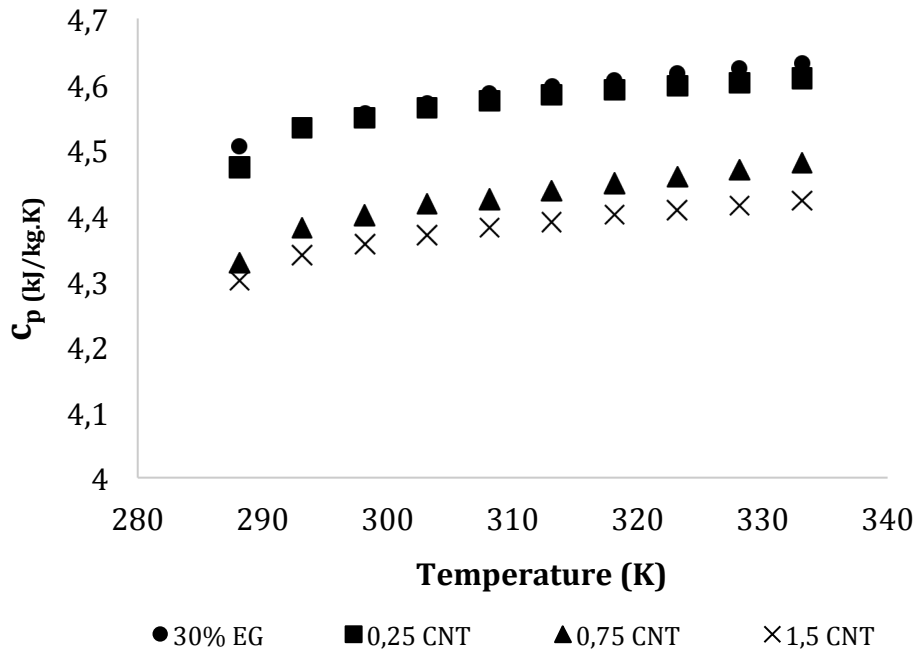


Fig. 5A

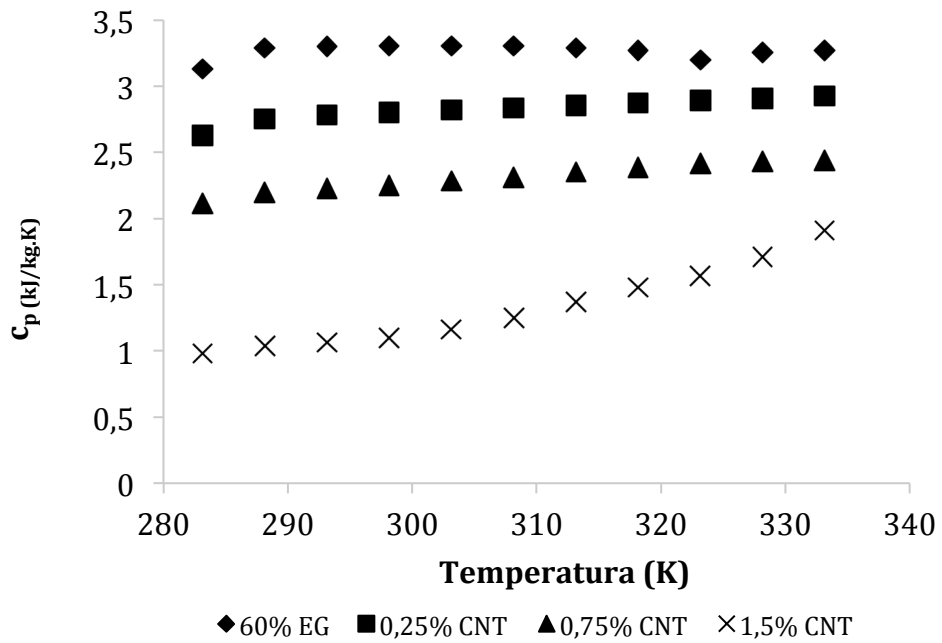


Fig. 5B

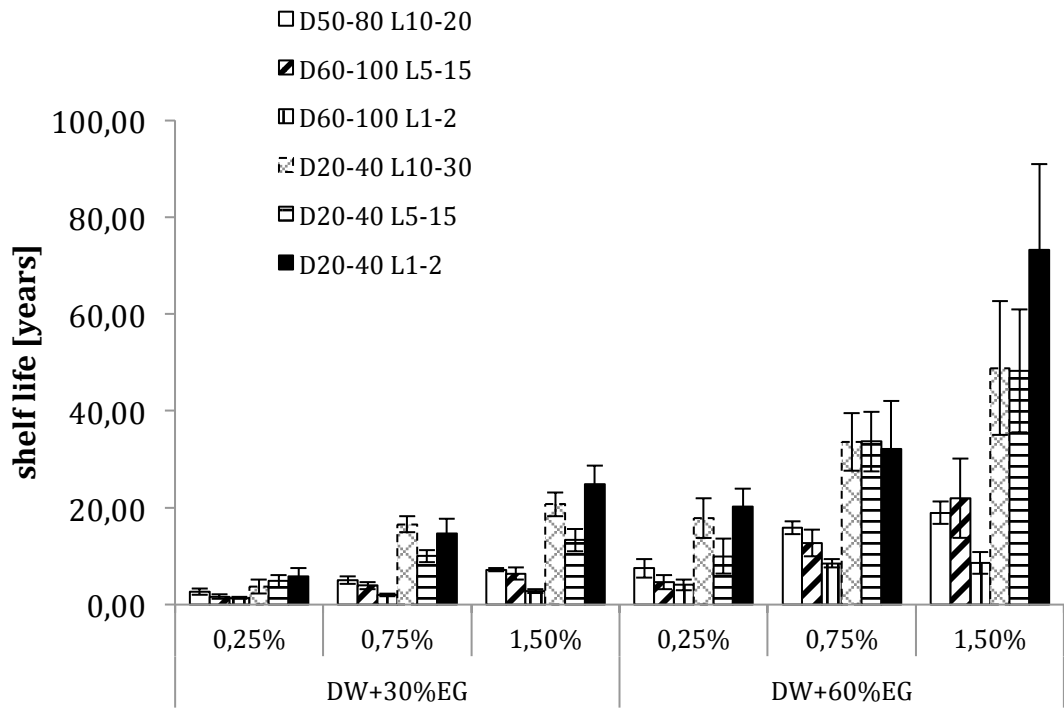


Fig. 6

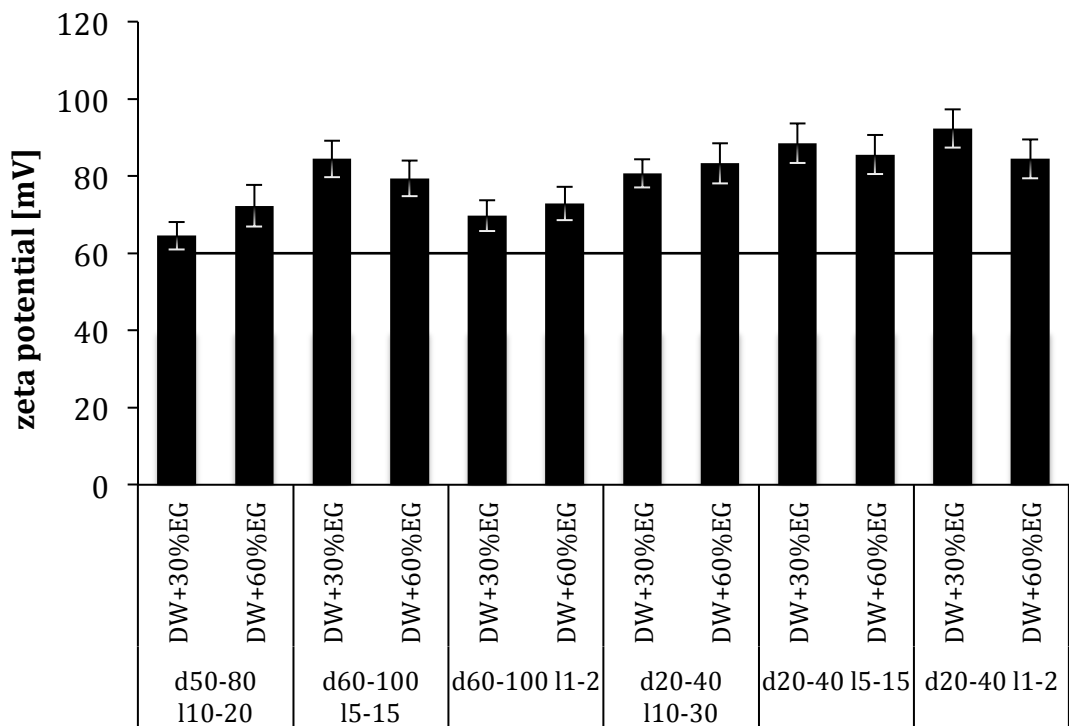


Fig. 7

L. Business Plan

In order to promote and simplify its industrial dissemination, the author decided to take this nano technology to the best Portuguese entrepreneurial acceleration program named COHiTEC developed by COTEC Portugal and lecture at Porto Business School. COHiTEC is a program in technology commercialization aimed at supporting the valorization of the knowledge produced at Portuguese R&D institutions. The outcome from this program was a complete business plan for developing an advanced heat transfer fluid for the automotive industry, named CARBONFLUIDS®

Business Plan for the nFLUID®

by


CARB  FLUIDS®

Table of Contents

APPENDIX.....	Error! Bookmark not defined.
A. Effective Viscosity Experimental Layout.....	1
B. Base Fluids Thermal and Transport Properties.....	2
C. Apparatus For The Viscosity Measurement.....	3
D. Experimental Uncertainties Analysis.....	4
Volume Fraction Experimental Uncertainties.....	4
Diameter and Length Distribution Uncertainties.....	4
Experimental Zeta Potential Uncertainties.....	5
Experimental Phase Separation Rate Uncertainties.....	6
Experimental Density Uncertainties.....	6
Experimental Viscosity Uncertainties.....	6
E. Functionalized MWCNTs Size Distributions.....	7
F. Thermo Gravimetric Analysis (TGA).....	13
G. Phase Separation Rate.....	16
H. Phase Separation Rate.....	52
I. FTIR Evaluation.....	54
J. Nanofluids Effective Viscosity Tables.....	57
K. Business Plan.....	68
1. Executive Summary.....	13
2. Business Opportunity (Problem).....	15
3. Solution.....	17
4. Technology and IP.....	20
4.1 Patent Process.....	22
5. Industry and Competition.....	28
6. Market Analysis.....	31
7. Business Model and Strategy.....	34
7.1 - Production in-house.....	34
7.2 - Partnering with existing players and use the nFluid as an additive.....	34
8. Marketing and Sales Plan.....	37
8.1 Production in-house.....	37
8.2 Partnerships.....	38
9. Milestones and Roadmap.....	39
9.1 Period (2008 - 2014):.....	39
9.2 Phase 1(a): Early stage R&D (Current situation):.....	39

9.3 Phase 1(b): Field Test	40
9.4 Phase 2(a): Final Product development	40
9.5 Phase 2(b): Product launch	40
10. Risk Analysis	42
11. Financial Forecast and Funding Needs	43
11.1- Capex	43
11.2 Assumptions	46
11.2 Investment required	47
12. Team and Management Structure	48
References	50

1. Executive Summary

In the last four years, CARBOnFLUIDS has been developing the nFluid, which is a mixture of a thermal fluid with carbon nanoparticles. The addition of such carbon nanoparticles enhances the properties of the thermal fluid and can be used in a heat or cooling systems. The nFluid detains higher thermal conductivity (+18%) and excellent thermo-physical properties unlike commonly used coolant fluids. Furthermore nFluid can be customizable to detain a higher rate of heat transfer (16%), according to the customer needs and/or applications.

The applications of the nFluid are diverse, however, it will be directed to the automotive industry, more specifically to commercial vehicles, like logistics and transportation vehicles, since it can produce savings from 1% to 2% on fuel consumption. This is a market of 300 million vehicles that is growing at a rate of 5.5% and uses up to 36 liters of coolant solution per vehicle. However, CARBOnFLUIDS's target will be countries with high income that have high fuel prices, like Canada, Japan, South Korea, Australia and others located in Europe, which represent over 48 million vehicles.

The nFluid is currently in the second stage of development, as it is in the process of characterization and field testing. Once these procedures are completed, CARBOnFLUIDS will formally apply for the international patent of the

production process of nFluid and then start production for commercialization. This will be done by either in-house production or with partnerships.

The investment required is 2.8 million euros with an expected payback of 4 years. It is also expected that by the 5th year, CARBOnFLUIDS will have sales on the value of 48 million euros and that by year seven the growth rate of sales will stabilize with double digit values.

Research and Development activities are expected to continue to further develop the nFluid to improve the fluid and find new opportunities to entry other markets to explore.

2. Business Opportunity (Problem)

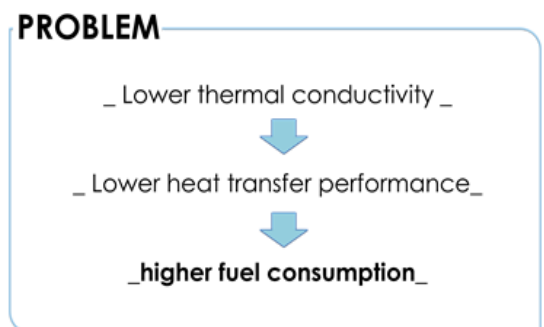
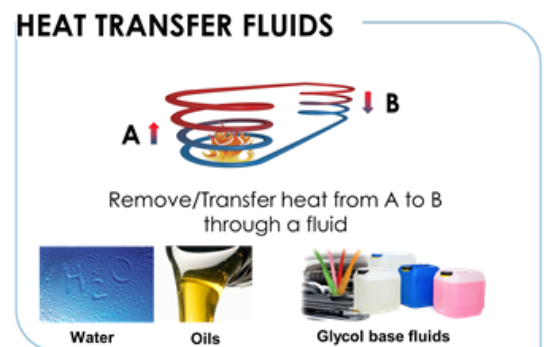
The continuous development in industrial process increases the demand for new technological solutions to improve the effectiveness of heat transfer, mainly in what concerns energy consumption. However, the performance of these devices strongly depends on their cooling technology. Therefore, improving these technologies is detrimental to achieve a higher level of sustainability.

Heat transfer fluids are the most common media to transfer heat, from a body A to a body B, and have a global application, ranging from the automotive industry, solar panels, batteries, medical instruments, energy systems (as HVAC) to microelectronics. However, such fluids detains some problems, such as poor thermo-physical

properties, poor thermal conductivity, low heat transfer coefficient, and low heat transfer performance, being one of the major barrier for the development of compact and energy efficient heat exchangers.

Considering all the industries, the one that presents less barriers to entry in the market is the automotive industry. The current solutions used in the automotive industry (over 1 billion vehicles growing at a rate of 5.5% per year) possess some unattractive characteristics, including poor thermo-physical properties (low thermal conductivity and inefficiency heat transfer performance) and the escalating the cost of energy. However, increases in the cost of energy and raw materials drives a need to improve the key properties of the existing solutions.

Therefore, a fluid with better thermal properties while maintaining the freeze protection can work better than current cooling fluids to maintain the system environment at an optimal working temperature; also, since the heat oscillations is one of the key driver to reduce fuel consumption and the system lifespan, a better thermal-property fluid can also help to extend the usage time of

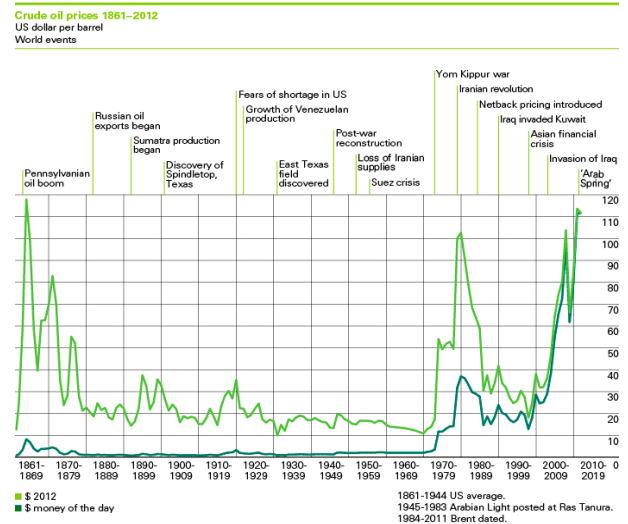


systems.

By improving these properties and optimizing the operational temperature of engines, fuel consumption level could be reduced. This is important because in the last two decades the price of oil has been rising from \$16.75 to \$91.17¹, which has become an increasing pain for the users of traditional automotive vehicles (diesel and gasoline). This tendency is expected to continue as the price is fixed by OPEC (oil cartel) and it is produced in countries with high social and political instability, like Venezuela, Nigeria, Iraq, etc. This affects all end user drivers, transportation companies, and logistic companies.

Another problem that the automotive industry faces, from the manufacturer's point of view, is the need to save costs to either offer better returns to investors or provide less expensive products to customers. Existing solutions oblige manufacturers to use a determined amount of raw materials of radiator systems, which translate into a determined amount of cost; if new solutions could reduce this amount of raw materials used in systems, it would translate into cost reduction and might potentially become a standard pushed by manufacturer to consumers through the redesign of vehicles, which used new compact radiator system with better thermal-property fluids. Additionally, this reduction of the radiator's size will reduce aerodynamic drag as well as reduce the weight, which could lead to further reduction in fuel consumption.

Water is by far the best heat transfer fluid; however, when temperature goes below 0°C, water can freeze inside the system leading to a system malfunction. A similar problem can happen when the temperature of the system increase over the boiling point, creating water vapor and making the engine



¹ BP (2012) Crude oil prices 1961-2012. Available from: <http://www.bp.com/en/global/corporate/about-bp/energy-economics/statistical-review-of-world-energy-2013/review-by-energy-type/oil/oil-prices.html> [Accessed on 15th June 2014]

overheating, which could permanently damage the car engine. In order to mitigate this problem, car manufactures advised to use other cooling solutions which can endure temperatures below -40°C and above 120°C .

To conclude, the energy crisis and environmentalism act as a stimulus to the increasing need for products or measures that result in energy saving. Also, the transportation energy consumption accounts for more than 60% of the total petroleum and liquid fuels consumed worldwide. Hence, the transportation sector is really in need of new solutions to mitigate this imminent problem; thermal-fluid with enhanced thermal properties can provide opportunities to diminish the fuel consumption of vehicles.

3. Solution


The nFluid is a heat transfer fluid that combines the enhanced thermo-physical properties of carbon nanoparticles with the flowability of liquids, achieving a fluid with a 20% higher thermal performance, 18% higher thermal-conductivity, and a long-term suspension stability (>5 years). By improving the thermal properties of cooling solutions, many of the problems, associated with the lack of efficiency of the heat transfer systems, can be solved.

Carbon nanoparticles have been the subject of study in last decade, resulting in thousands of research papers over the past 15 years, and their special material properties (great hardness, high thermal conductivity, and chemical and thermal stability) are well understood. CARBOnFLUIDS's researchers have been studying the use of these carbon nanoparticles to improve heat transfer fluids since 2001, resulting in the nFluid. This fluid was subjected to a full laboratory characterization as well as to a laboratory proof of concept resulting in a scientific publication on "Heat and Mass Transfer" journal ², proving the ability of nanofluids for enhancing the performance of cooling applications.

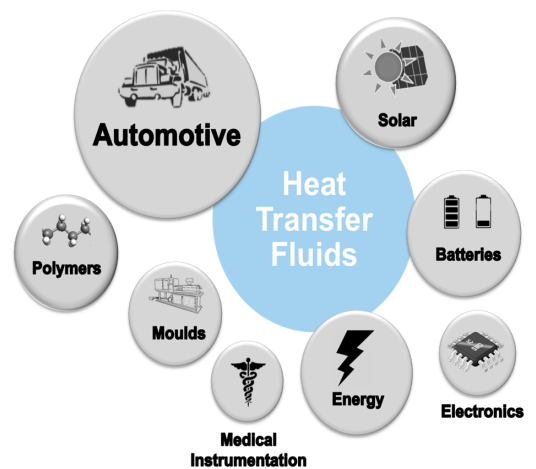
This technology can be applied to many other applications than automotive coolant, like in the energy sector, solar panels, polymers, medical instruments, electronics, etc., which the CARBOnFLUIDS team expect to continue developing to create new opportunities and markets. The better performance of nFluid as a thermal fluid could also lead to miniaturization, which could save, not only raw materials (to manufacturers), but also improve other characteristics of the products where is being applied; for example, in the automotive industry, the use of the nFluid and fluids with similar properties as a standard could result in smaller radiators, therefore, a reduction in aerodynamic drag.

According to a US Department of Energy (DOE) research entitled "Effects of Nanofluids on Heavy Vehicle Cooling Systems" ³, fluids with similar characteristics as the nFluid can help to save up to 2.5% in fuel consumption

SOLUTION nFLUID®



- _ 18% higher thermal conductivity
- _ 20% higher heat transfer
- _ Long-term stability >5 years
- _ Developing common materials
- _ Savings on Fuel Consumption of 1~2 %



² Abreu, B. Lamas, L., Fonseca, A., Martins, N. and Oliveira, M. (2014) [Experimental characterization of convective heat transfer with MWCNT based nanofluids under laminar flow conditions](#). *Heat and Mass Transfer*. Vol. 50 (1), pp. 65-74.

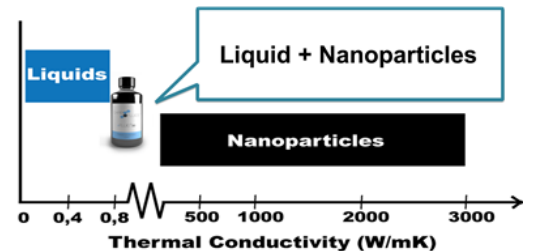
³ Presentation from the U.S. DOE Office of Vehicle Technologies "Mega" Merit Review 2008 on February 25, 2008 in Bethesda, Maryland

with a reduction of 5% on the size of the radiator. When considering the prices of fuel in Portugal 1.30€/L - 1.40€/L, it can be observed that this is a significant amount (up to 3 cents saved per liter according to current use). Even 1% saving in fuel consumption can make a difference, especially in heavy users, such as transportation (including public transports) and logistic companies. Furthermore, the nFluid thermal properties could also allow manufacturers to reduce the amount of raw materials used in the production of radiators. Because the thermal properties of nFluid will be more effective, the radiator area needed to cool down the systems can be reduced compared to current solutions.

This results have been obtained mostly from theoretical models and research from other institutions like the US department of Energy and the Argonne National Laboratory (the creators of nanofluids). However, all the experimental data that we state were determined experimentally following the international standards methodology. The proof of concept was made in a laboratory apparatus; however, a proof-of-concept in a real environment is still needed.

4. Technology and IP

nFluid heat transfer fluid is a hydrocarbon-based heat transfer fluid designed for use in closed-loop, liquid phase, and cooling system **up to 120°C (250°F)**. This fluid is specially formulated with carbon nanoparticles to offer **long-life stability**, **greater heat transfer performance**, enhanced **durability**, and high **thermal stability**.



- **Stability:** There are several types of stability on suspensions of nanoparticles in fluids, the nFluid retains all of them: thermal stability, long-term suspension stability and enhanced durability (carbon is one of the strongest materials known).
- **Customization:** nFluid can be tailored to specific conditions to reach the best performance of your system. Additionally, the fluid can be used without the needs for any system modification.
- **Potential:** The enhanced thermo-physical properties of the fluids provides the opportunity for the miniaturization of heat transfer system as well as the development of novel heat transfer technologies.

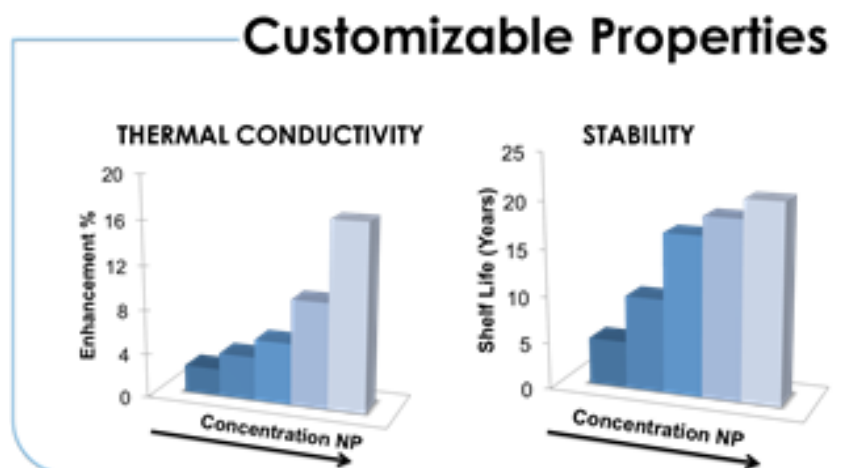


Fig. 1 and 2 present the thermal conductivities (k) and the viscosities for different types of nFluid compared with fluids without the nanoparticles. Such results clearly highlight the higher thermal conductivity of the nFluid (as compared with other commercially available thermal fluids - $k=0.38$ W/mK) and enhancement of the thermal conductivity of the different nFluids ($k_{\text{enhancement}}$ up to 16%).

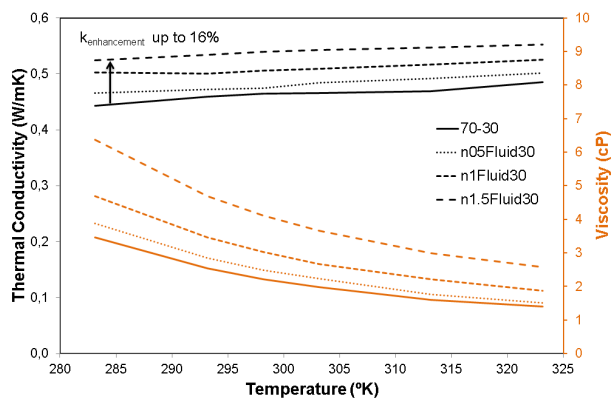


Fig 1 . Thermal conductivity and viscosity of the base fluid, with 30% ethylene glycol, compared with three different nFluid.

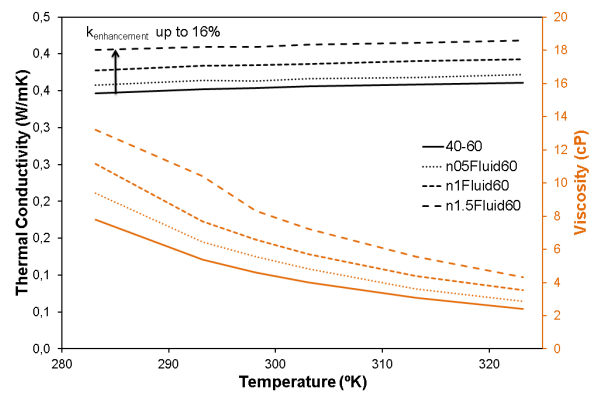


Fig 2 . Thermal conductivity and viscosity of the base fluid, with 60% ethylene glycol, compared with three different nFluid.

The research team already has performed the first laboratory-level proof of concept and the results are strongly encouraging. Even with very lower concentration of nanoparticles, the thermal performance of nFluids is 17% better than the same fluid without the nanoparticles. However, the team is preparing new protocols to perform new tests for the real use proof of concept.

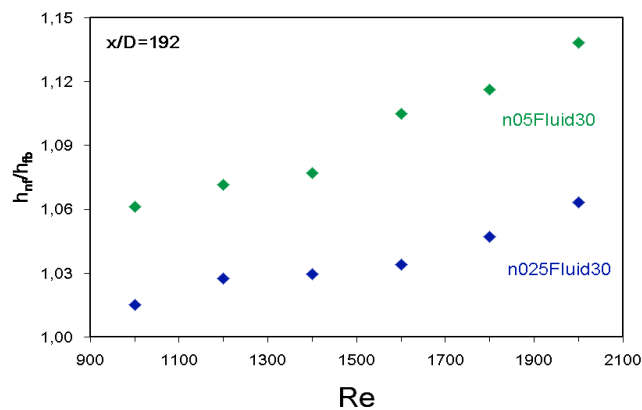


Fig 3 . Proof of concept: heat transfer coefficient for the n025Fluid30 and

the n50Fluid30 nanofluids, relative to base fluid at different Reynolds number, at an axial distance $x/D=192$.

The research team has been developing this innovative nFluid for more than 6 years and it has also build a clear path for the product development, even though we are still at the stages of development. Currently, the remaining technology and product development difficulties are “*real environment testing*” (Field Testing). However, when considering the technology itself, nFluid is almost fully developed. Hence, CARBOnFLUIDS has great confidence in this technology.

About IP, since the combination of fluid and nanoparticle is not a new idea, it will be more difficult for us to patent it based on materials or combinations. Nevertheless, the “process” of producing thermal-fluid, like receipt, is more likely to be patented. As a result, our team is now working on protection of our production process, including the composition, energy used, and the time. The following table shows some features of nFluid:

Typical Properties	nFluid30	nFluid60
Composition	DI water + EthyleneGlycol +NP	DI water + EthyleneGlycol +NP
Aparence	Black	Black
Odor	Odorless	Odorless
Boilling Point (°C)	>120	>120
Freezing Point (°C)	-15	-40
Specific Heat @20°C (kJ/kg*K)	3,64	3,08
Thermal Conductivity @20°C (W/mk)	0,53	0,41
Viscosity @20° (cP)	4,7	10,39

4.1 Patent Process

There are a few patents regarding to the use of nanoparticles, namely carbon nanotubes, in base fluids to improve the heat transfer properties of base fluids. However, to achieve such properties they use surfactants and dispersants which can compromise the thermo-physical properties of the suspensions.

1. US Patent 033975, Mclellan et al, provisional application filed 9/09/2011;

2. US Patent 0220840 Alvarado et al, provisional application filed 11/03/2010 - "Fluid Viscosity and Heat Transfer Via Optimized Energizing of Multi-Walled Carbon Nanotube-Based Fluids "
3. US Patent 0095911 Morita et al, provisional application filed 10/01/2008 - "Heat transport medium"
4. GB Patent 001557 Pick et al, provisional applications filed 19/06/2009 - "A method of making carbon nanotube dispersions for the enhancement of the properties of fluids"
5. US Patent 0100578 Withers James C et al, provisional applications filed 29/01/2002 - "Nano carbon materials for enhancing thermal transfer in fluids"
6. US Patent 16888 Zhang et al, provisional applications filed 24/12/2003 - "Enhancing thermal conductivity of fluids with graphite nanoparticles and carbon nanotube"
7. US Patent 051102 Rouse et al, provisional application filed 9/09/2009 (WO2010051102 A2) - "Carbon nanotubes dispersions"
8. US Patent 0253888 Liu et al, provisional application filed 28/04/2006 - "A method for preparing carbon nanofluids"

Despite the large number of patents and literature about carbon nanofluids with promising results to heat transfer applications, until now there isn't any proven method capable of engineer a stable long-term carbon nanofluid.

The nFluid is an engineered nanofluid to be used as advanced heat transfer fluid. The main objective is to disperse and stabilize the functionalized carbon nanotubes in a conventional heat transfer fluid, in order to produce a homogeneous and stable long-term nanofluid with enhanced thermal performance. The patentable technology provides a detailed process to engineer a homogeneous and stable fluid without the addition of any surfactant or another reagent and/or solvent. The embodiments of the patent comprise a water base fluid multiple concentrations of functionalized carbon nanotubes. For all the embodiments, the specific mechanical energy and how it is induced in the mixture is disclosed in order to kept structural damage to a minimum, especially the tube type nanoparticles. The patent also provides the techniques that must

be employed to inquire the shelf life and quality control of the nFluids, which are of major importance in order to be used in real applications.

1. US Patent 033975 - the invention is directed to nanofluids comprising nanomaterials, methods to prepare the nanofluids, and products prepared by the methods and indicate that the thermal conductivity of mixtures of water, 50-90% of ethylene glycol and polyvinylpyrrolidone could be improved in the presence of alumina, silver and gold nanoparticles and carbon nanotubes. **However, nanofluids prepared with emulsifiers can only be applied to low temperature applications, since the emulsifiers evaporate at low temperatures. Furthermore, it is unclear how the nanofluid self-life is determined, without details there is no guarantee that the suspension will remain stable. Another issue is related with the thermal conductivity measurements, it is known that the thermal conductivity is temperature sensitive, however there is no information regarding to the temperature of the thermal conductivity measurements. Additionally, there is little information in how these suspensions are produced, this is a critical step to assure that the suspension will remain stable.**

2. US Patent 0220840 - corroborated that the addition of multiwalled carbon nanotubes into a mixture of water and Gum Arabic improved the heat transfer capability of the base fluid. The maximum demonstrated enhancement of an aqueous fluid in thermal conductivity is 20% and in convective heat Transfer is 32%. The thermal conductivity enhancement increased considerably at bulk temperatures greater than 24 DEG C. The percentage enhancement in convective heat transfer in a tube increases with axial distance. The resultant optimized fluid is also described. **However, the use of surfactants and/or stabilizers, as Gum Arabic, influences the thermo-physical properties of suspensions, owing the risk of failure at high temperature applications. Additionally, since the nanofluid is intent for industrial uses it is only guarantee that it will remain stable for one month, which in a practical perspective it is not acceptable.**

3. US Patent 0095911 - relates to a heat transport medium used in a heat exchanger; wherein the heat transport medium improves heat conductivity

without increasing kinetic viscosity by stably dispersing carbon nanotubes in base liquid; specially water and ethylene glycol. Carbon nanotubes are stably dispersed in the base liquid by including sodium carboxyl methyl cellulose which has average molecular weight given by GPC measuring method is 6000-30000. Therefore, the heat transport medium improves heat conductivity without increasing kinetic viscosity. pH can be kept in proper range. Furthermore, a chemical reaction by the dispersant is prevented. **However, the use of dispersants strongly influence the thermo-physical properties of the suspension. Besides, the mixture description misses some details of utmost importance, such as the sonication intensity and amplitude, or the overall mechanical energy induced into the mixture, these details are of utmost importance to guarantee the stabilization of the suspension and to minimize the structural damage of the carbon nanotubes.**

4. GB Patent 001557 - indicated that the addition of carbon nanotubes in lubricating oil, improved the thermal and electric conductivity. **However, the mixture description misses some details, such as the intensity, amplitude of the ultrasonic induced energy. These details are of utmost importance to guarantee highly homogeneous and stability of the nanofluid, and to minimize the structural damage of the carbon nanotubes. Also, it is unclear the procedure for the thermal conductivity measurements, as well as the temperatures at which the measurements are performed, since thermal conductivity is temperature dependent. Furthermore, the applied method to study the stability of the dispersion over time is not taught.**

5. US Patent 0100578 - indicated a novel fluid heat transfer agent suitable for use in a closed heat transfer system, for example, wherein energy is transferred between an evaporator and a condenser in heat exchange relationship with the heat transfer agent that is caused to flow from one to the other. The novel heat transfer agent is a complex comprising a body of heat transfer fluid, for example, ethylene glycol or water, having suspended therein carbon nanoparticles in a quantity sufficient to enhance the thermal conductivity of the body of heat transfers fluid, per se. The carbon nanoparticles are selected from carbon in the form of sp² type and sp³ type bonding and preferably comprise nanotubes or

fullerenes and may have a coupling agent bonded thereto or enclosed therein when the nanotube or fullerene forms a hollow capsule.; The coupling agent may be a polar organic group covalently bonded to the carbon nanoparticles and miscible in the fluid medium that the addition of carbon nanotubes in heat transfer fluids enhanced the thermal conductivity. **However, the mixture process misses some details, such as: the base fluid volume for the volume fraction of nanoparticles, the percentage of each fluid in water/ethylene glycol mixtures and the energy induced by the ultra-sonication process/magnetic stirrer to the nanofluids. Furthermore, the method to study the dispersion stability of the nanofluid over time is not taught.**

6. US Patent 16888 - indicated that the addition of carbon nanomaterials into heat transfer fluids and petroleum liquid medium enhanced the thermal conductivity. To confer long term stability, the use of one or more chemical dispersants is preferred. The thermal conductivity enhancement, compared to the fluid without carbon nanomaterial, is somehow proportional to the amount of carbon nanomaterials (carbon nanotubes and/or graphite) added. **However, the mixture procedure misses some details, such as the intensity, amplitude of the ultrasonic induced energy. These details are of utmost importance to guarantee a homogeneous and stable suspension, and to minimize the structural damage of the carbon nanotubes. Furthermore, in all of the embodiments of the invention they use dispersants which strongly influences the thermo-physical properties of the suspension. Moreover, the applied method to study the suspension stability over time is not taught.**

7. US Patent 051102 - indicated the efficient dispersion of carbon nanotubes in various media and methods of using the same in such applications as inks, coatings, and composites and in various electrical and electronic articles. A dispersant is used which has the formula $P-(U-Y)_s$ where P is a metal or metal-free phthalocyanine, Y is a compatibilizing moiety with a molecular weight between 500 and 5000 g/mol, U is a linking moiety covalently bonding Y to P, and s is an integer between 1 and 4 the method disperse carbon nanotubes into an organic or aqueous. **However, the mixture description misses some of**

utmost importance details, such as the intensity of the ultrasonic induced energy, these details are of utmost importance to guarantee a stable and homogeneous suspension, and to minimize the structural damage of the carbon nanotubes. Furthermore, in all of the embodiments the invention uses dispersants. The use of such surfactants influences the thermo-physical properties of the suspension.

8. US Patent 0253888 - provide a method to prepare a carbon nanofluid. The method includes providing a base fluid, providing a number of carbon nanotubes, combining the carbon nanotubes with the base fluid, dispersing the carbon nanotubes substantially evenly in the base fluid through a physical agitation operation, and cooling a system performing the physical agitation operation during the physical agitation operation. The present invention also provides a carbon nanofluid capable of serving as a heat transfer fluid. The carbon nanofluid includes about 99.8 to about 98% by volume of a base fluid, and from about 0.2 to about 2.0% by volume of functionalized carbon nanotubes substantially evenly-dispersed in the base fluid. However, the mixture description misses some important details such as, the intensity, amplitude and sample volume for the ultra-sonication operation. These details are of utmost importance to guarantee the stability and the homogeneity of the nanoparticles dispersed in the base fluid, and to minimize the structural damage of the carbon nanotubes. Moreover, they don't perform any test that guarantee the homogeneity of the nanofluid as well as the stability over time.

The patent process of the nFluid will be based on the production process, rather than in the product itself. The application is currently being prepared and will be submitted once the field testing is completed with satisfactory results and the financial resources are in place. This is because there are product with similar composition, but different characteristics. By patenting the technology, internationally, CARBOnFLUIDS will have a competitive advantage, as the exclusive rights to it and will be able to either produce it, license or both.

5. Industry and Competition

Thermo-fluids are a growing industry, especially, since its applications are extensive. However, not all thermo fluids can be applied to the same areas and some require to meet certain standards. In the case of the nFluid, it will be applied initially to the Automotive industry; this is because, compared to other industries, the entry barriers of the automotive industry are not as high as the others. In this industry relevant information is available and certification procedures are accessible, especially in countries with well established procedures and regulations. For certification of the nFluid, the team already has a safety and regulation technician, which will proceed with the Material Safety Data Sheet (MSDS) and will certificate all the measured properties with respect to the international standards methodologies. However, depending on the local laws this certification can be optional and not a must.

When addressing heavy users of this industry (transport and logistics companies) some concerns may appear. Companies in this segment may require products that are approved by the vehicle's manufacturer in order to keep the guarantee of their vehicles. For any solution to be approved by the manufacturer, it requires to be tested and analyzed, which can take up to five years. However, the alternative for this approval, by either internal or external lab, in comply with the SDMD 15 and BSY standards, as they address the minimum requirements to make a quality coolant solution and can take up to 2 months.

Another issue for new entrants, in this industry, is the power that established players have. Existing companies in the automotive industry have an extensive network of distribution and production, as well as an already developed relations with retailers and other distributors. Therefore competing directly with these players may not be the best approach for a product that cannot compete on price or differentiate in the market as rivalry is high. Some of the alternatives that already exist are:

- PAR antifreeze
- ARBO antifreeze

- OEM premium extended life
- Shell HD Preminum

Currently, there are many alternatives in the market, enabling customers to choose according to price, brand, or perceived benefits. This excess of supply have resulted in the commoditization of coolants. Differentiation could be achieve by developing better products that can create value to final consumers and result in higher profits, which could be done by focusing in the needs of specific niches of the market.

There are other liquids that can serve as cooling fluids (substitutes), but they are either not certified nor have the thermal properties required to do the job. An example is water; however, it may create other problems in the system such as corrosion at a faster rate and freeze or boiling problems. Substitutes are more common in countries with low education/low income/low regulatory enforcement, such as developing countries, where CARBOnFLUIDS is not expected to operate (at least initially). In contrast, there is a wide range of universal coolants that can be used to different situation without harming, as much, the system. These coolants are available in low cost retailers, like Walmart, that sell universal coolants as they are cheaper and 'do the job'.

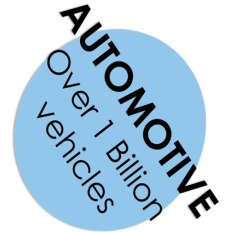
To compete in this industry, CARBOnFLUDs intends to differentiate the nFluid, by addressing savings on fuel consumption and the potential extension of the vehicle's lifespan to transport and logistic companies, as they are the heavy users of the industry and these issues are relevant to them.

The bargaining power of suppliers is limited, since there are many alternatives and the established players in the industry are big In contrast, the carbon nanoparticles used in the production process of nFluids are still an expensive material, but as more suppliers have appeared and their scale of production has increased the price of these material has been decreasing. However, there are big differences in prices from one supplier to another, as values that range from 200€ per kilogram to 100€ per gram. The price of carbon nanoparticles are expected to have an impact in the costs of production, at least in the initial stages of production, which emphasizes the need to follow a strategy of differentiation, as previously mentioned.

The cooling fluids industry is an industry that is mature, with players already placed with a well-developed structure. Therefore, to compete in this market new entrants have to seek gaps in the market, which can be entering in markets that are not served by these competitors, reduce costs or offering benefits that can translate into value to customer.

6. Market Analysis

The Automotive industry is big in volume; it is also estimated that there are over one billion vehicles circulating worldwide currently. In 2010, according to Ward's Automotive Group, the total vehicles in the world was 1,015,260,827 (70% cars - 30% commercial vehicles), being more concentrated in Western Europe, North America, and the Far East. The industry is growing at a rate of 5.5%, mostly due to the improvement of conditions in developing countries like China and India.



Automobiles use cooling fluid to keep the engine at a constant working temperature (avoiding overheating or freezing). Therefore, it is an important component in the maintenance of vehicles and it is recommended to change this fluid every five years or every 150,000 Km, in both new and existing vehicles. In contrast, cooling solutions have become commoditized, which can jeopardize the entry of new competitors, especially if they neglect focus on price nor offer something that creates significant value to persuade consumers.

The nFluid has high production costs, when compared with competitors, therefore, the criteria to choose an addressable market should include economic environment and cultural openness because nFluid is a new product at a premium price. CARBOnFLUIDS can only enter the market where customers perceive the benefits that nFluid provides and are "willing" to pay a premium for it. Consequently, the nFluid has to be directed to countries with higher disposable income, a more proactive culture towards cost savings in the long run and high fuel prices.

The countries that have these characteristics are Canada, Japan, South Korea, Austria, Belgium, Denmark, Finland, France, Germany, Iceland, Ireland, Luxembourg, Malta, Netherlands, Norway, Spain, Sweden, Switzerland, United Kingdom, and Australia. Countries like U.S.A. (not included), Japan and South Korea have low taxation in fuel, which make them less attractive, as it would take longer to for the nFluid to produce savings to customers. The countries selected represent 31.19% (800 million vehicles approx.) of the total vehicles in the

world and the structure present some changes (85% cars - 15% commercial vehicles).

When analyzing the automotive market within the selected markets, it can be observed that commercial vehicles have a higher attractiveness, especially related to logistics and transportation, as they have higher level of usage, therefore, CARBOnFLUIDS would have a higher volume of sales, as customers will have a better perception of nFluid's benefits in fuel consumption. This segment has over 48 million vehicles that use up to 36 liters of coolant solution each.

By replacing existing cooling solutions for the nFluid, vehicles will reduce the time that the thermostat and the fan are working, which could lead to fuel saving of about 1% or 2%. By using the following formula, it can be calculated from which Kilometer a vehicle can start saving by using nFluid

$$\text{BreakevenDistance}(km) \times \text{FuelConsumption} \left(\frac{\text{Fuel Liter}}{km} \right) \times \text{FuelPrice} \left(\frac{\text{€}}{\text{Fuel Liter}} \right)$$

$$= \text{RadiatorFluidUsage}(\text{Liter}) \times \text{PriceDifference} \left(\frac{\text{€}}{\text{Fuel Liter}} \right)$$

Efficiency increase	breakeven point distance
1%	106,000 Km
2%	53,000 Km

For these calculations it was considered that each truck has capacity for 36 liters, a cost of 1.20 €/liter to 1.43€/liter for fuel, a competitors price of 8 €/liter of coolant solution and a rate of fuel consumption of 0.1 liter of fuel per kilometer. It is estimated that the average Small and Medium Enterprise (SME) has around 150 trucks.





High thermal performance fluid



Better temperature control



1~2% Savings on fuel consumption

It is expected that in in the first year, by continuing to work closer to potential customers, the nFluid will be applied to at least 4,000 vehicles and it is expected that high growth will continue in the first five years, serving 86,000 vehicles by the end of the fifth year.

7. Business Model and Strategy

The CARBOnFLUIDS team is currently finishing the documentation and analysis of the fluid as it is working on the 'proof of concept' of nFluid as a coolant solution. Once, the proof of concept is completed, CARBOnFLUIDS will proceed to apply for patent protection of the production methodology for the nFluid. This is important, as it will protect the Intellectual Property giving the exclusive rights of the production of this fluid to CARBOnFLUIDS.

The CARBOnFLUIDS has two business model from where to choose varying in the levels of risk and potential rewards. These are **Production in-house** and **Partnering with existing players using the nFluid as an additive** to improve existing solutions from partners.

7.1 - Production in-house

This is the preferred option of CARBOnFLUIDS, however, it is also the one that bears more risk. For this option, the expected initial investment is the highest, as there is the need to acquire equipment and provide the conditions for production (e.g. clean room). This option will also require more work from CARBOnFLUIDS team, as it will need to develop relations with suppliers, distributors (principal), and customers to have success. However, due to the benefits that the liquid can provide this strategy is feasible; even if the costs are higher than current solutions, it can provide higher savings in other areas.

7.2 - Partnering with existing players and use the nFluid as an additive

This option has less risks in comparison with the previous one, as it will share the risk with the partners. It also has been studied during the elaboration of this report, having the attention of companies like Bosch. However, for these partnerships to be effective CARBOnFLUIDS must have the patent and provide more complete proof of concept. Otherwise it is highly probable that any deal may not be achievable.

Currently CARBOnFLUIDS has contacted OCSiAI, the largest

"...And we think that along with our expertise in CNT manufacture and customer network we could create a good collaboration... We can join our efforts to get this product to the market..."

Andrey Senyut Managing
Director @ OCSiAI

carbon nanoparticle producer in USA, who is interested in the development of the nFluid and its applications.

These players already have relations with a network of suppliers and sellers, which CARBOnFLUIDS can leverage and get the product to the market faster. This strategy may also result in other applications for nFluid due to the experience of these partners. In contrast, it is also expected that the returns may be also less than in the previous option.

For any of these options, it is very important that CARBOnFLUIDS addresses the benefits and advantages of its product to customers, as they will be paying a premium (when compared with competition) for a product that can be considered, to some extent, a 'commodity'.

CARBOnFLUIDS will be limited to its cost of production regardless of the business model chosen, which is around 7.10€/Liter. This value is high when compared to other competitors in the industry (especially because they usually mix the solution with distilled water), to the point of being similar to the price of competitors to the end user. However, the nFluid will be competing with the premium cooling fluids, therefore, it can charge a similar price, resulting on a positive margin contribution. Also, it is believed that with the increasing of production for double, the production cost will be decrease of about 30% (this would be more feasible to archive in a shorter term if partnerships are in place).

When considering the scenario of partnering with other companies of the industry, it is expected that it will be a feasible strategy, even to other segments, as in theory it is possible to mix the nFluid with other solutions that exist in the market. This mix is expected to be better than the original product (but not as effective as pure nFluid) resulting in a lower cost and with little modifications.

The cost structure is expected to be similar to that of other thermo fluid producer, such as Eastman, BASF, and DOW. This means that gross margins will be above 30% (47%), R&D 5% (2.5%), and Marketing expenses 4% (3%) as percentage of sales⁴. Therefore, considering a cost of production of 7.10€/Liter (excluding labor) and the gross margin of the industry being 30% the intended

⁴ Average values of the industry of thermofluids are shown and in brackets those expected to be practiced by CARBOnFLUIDS

selling price is 15 €/Liter (gross profit of 75% - considering as Cost of Goods Sold, the raw materials and energy needed) to absorb the cost of labor not included and the fixed costs. The figures are higher than competition as scale of production and reach are lower, however, it is expected that nFluid will also improve performance more than their solutions.

Through calculations it can be shown that the prices compensate in the long run, since the efficiencies it creates in the system, regarding fuel consumption, can be observed as followed:

In contrast, as nFluid gains scale of production, its both prices and cost of goods sold per unit are expected to decrease in terms of absolute value, as there will be opportunities to access economies of scales and nano-carbon particles are expected to be more accessible (commoditized), which will increase the accessibility to the end user to products that contain nFluid and even sell coolant solutions made only with nFluid.

The initial investment will be high due to the conditions required for the production of the liquid, for example, a 'clean room' is required due to the nature of the nanoparticles accounting for 60,000€. The total investment required will be 2.8 million euros and it is expected that each production line (to increase production capacity) will cost 74,000€, able to produce an extra 38,720 liters per year

8. Marketing and Sales Plan

The nFluid is directed to companies that require solutions to control in an effective manner the temperature of objects or systems. Therefore, companies in the sector of selling anti-freeze solutions for the automotive industry (commercial vehicles). The plan will vary according to the strategy that is selected from those previously mentioned:

8.1 Production in-house

In this type of approach, the CARBOnFLUIDS will deal directly with distributors, based on their insights and contact with customers and have a wider distribution network than CARBOnFLUIDS, they will play a key role defining strategies for this type of market. However, the priority will always be to deal directly with B2B customers, mainly logistics and transportation (including public transportation) by leveraging on the benefits it provides to these companies, its increasing portfolio of customers and word of mouth (if achievable). It is estimated that the average SME has 150 trucks and that the adherence to nFluid won't be 100% of the trucks for each company, since the price is high and they may want to test it in a portion of their fleet. However, CARBOnFLUIDS believes that in the first year can achieve the figure of 4,000 trucks out of the 48 million of the served market, especially from the countries located in Europe. These assumption is rectified by the feedback received from companies that CARBOnFluids has contacted.

The marketing budget is estimated to be 3% of sales that can be used to create promotions, increase allowance of distributors, pay commission on sales or any other tactic that could lead to an increase on sales and that is aligned with the strategic objectives of the company.

"If you can improved the fuel consumption even by 1%, the fuel savings will be huge."

João Soares
Transdev, Lda

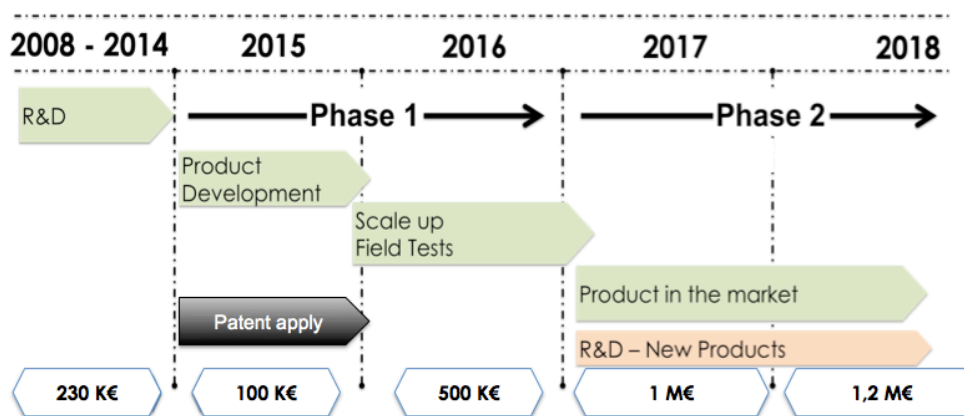
8.2 Partnerships

This will be a B2B approach and will consist on addressing players that are already established in the market (especially those seeking a competitive advantage) that produce liquids with similar solutions or even suppliers. The idea is that nFluid could be used by them as an alternative to their current products (increasing their range) and preparing them for the challenges of the future, like the miniaturization of current systems (radiators) or an additive to increase the performance of existing products (this will require further testing). The aim is not to compete with their current range, but to provide a more effective alternative, as these companies have the resources, network, experience, and distribution channels to sell this type of products to the final customer (B2C).

The approach to companies through this method will be done based on results from comparing their current solutions with nFluid and a blend of nFluid and their solution. In this way CARBOnFLUIDS can provide hard data of the improvements it can provide and quantify the benefits and costs to these companies. Depending on the option chosen the price will vary according to the cost of production and the quantities supplied.

9. Milestones and Roadmap

When analyzing the customers, products, competitors, the strategy and characteristics of the team, it can be developed a roadmap to implement act on in stages (see appendix I). These stages are the following:



9.1 Period (2008 - 2014):

This stage represent the historic performance of CARBOnFLUIDS in the development of the nFluid as it currently developed. This stage has been financed mainly by the Fundação para a Ciência e Tecnologia and University of Aveiro, as part of its research activities and the doctorate course of CARBOnFLUIDS researchers.

9.2 Phase 1(a): Early stage R&D (Current situation):

This stage of the project is to the CARBOnFLUIDS's current situation. This includes the characterization of the product, by analyzing all its properties, as potential partners and investors that are interested in the project, have requested this type of information. This procedure is also important and relevant in the certification process needed to enter the market of coolant fluids.

The second part of this stage will consist in the application for patent. The application process is being already addressed, but it is not yet completed as it is required for the characterization to be at a further stage. It is expected that this item will start to be formally addressed in the last quarter of the present year.

It is important to mention that during this stage of the project the team will be composed by the researchers of the project and it will not require any extra staff, since this is part of the processes on this stage are part of their competencies and they are familiar with the process and development of the nFluid. It is expected that a 100,000 € will be needed during this stage to complete the tasks in this process.

9.3 Phase 1(b): Field Test

This stage is expected to start as early as 2015 and to last for the whole year. It will be divided into tasks according to the deepness of the analysis of the fluid to its application to radiators through the scale up of Field Testing.

During this period contacts with potential customers will start, to archive the number of trucks targeted for year 1 (4,000 trucks) and even part of year 2 of operations. The purpose is to validate the product to the market conditions, by addressing issues such as certification, scalability and other conditions.

It is also expected, that the formal application for the international patent has been already delivered and that it is started to be analyzed by the Patent Cooperation Treaty (PCT).

The budget for this stage is 500,000 € (including the costs associated with the patent application).

9.4 Phase 2(a): Final Product development

During this stage the results obtained in the previous one (Field Testing) and study the application and feasibility to the market. Through this stage, the efforts to increase contact with distributors, customers and/or partnerships by hiring staff dedicated to these tasks and allocating a budget (3% of sales approx.) that could help the product have a higher reach.

The estimated budget for this stage is 1,000,000 €, which include the items related to the production, cash for unexpected expenses and part of the initial operational expenses.

9.5 Phase 2(b): Product launch

This stage the product will be accessible to the final consumer, either through distributors or partnerships. At this stage is expected that the

CARBOnFLUIDS will be producing positive results and that research and development will continue to improve the nFluid and to find new applications for it.

10. Risk Analysis

The thermo-fluid has characteristics that have not been achieved by other laboratories. Hence, the patent protection is important to the continuity of our project. However, there are risks regarding whether or not it will be approved, especially since it uses a combination of existing procedures, which are patented, to elaborate the product. Currently, our patent registration process is being prepared and capital will be raised to proceed.

During the first year, the organization will be limited to use the minimum equipment to produce the nFluid in a reasonable scale. However, if this equipment suffers damages or becomes inoperational, the production will stop causing delays on deliveries. Therefore, to minimize this risk and to keep a sustainable strategy, the CARBOnFLUIDS will acquire more equipment in the first year generating extra capacity and based on the growth projections from the first years' experience.

There may also be issues with Legal and Regulatory issues that may arise from the use of the product, such as environmental (mainly disposal of the product after use) and other requirements that may arise during the certification. Hence, we also pay attention on regulation problems to reduce related risks.

The industry may not be as receptive as they currently are. This is because the proof of concept is still a work in process and the final results may not meet the current expectations of the parties interested in the product. However, the results obtained so far, are satisfactory and it is expected that this trend will continue.

There are some financial risks, like market risk (interest rates and currency), credit risk, and liquidity risk (funding) that can affect the company negatively; therefore, they should be considered and addressed to reduce these risks.

The interest rate is currently low when observing data from the BCE; however, when approaching commercial banks the reality is different, the cost of debt available to companies is high and many guarantees are required, which make this a high risk to startups, like CARBOnFLUIDS, especially when

considering this a source for funding. Therefore, equity is the only consideration at this stage.

Currency and changes in fiscal policy can also be a source of risk, as one of the components used in the process of creating the nFluid (the carbon nano particles) is imported from China. This exposes the CARBOnFLUIDS to import taxes (23% aprox.) and changes currency value due to exchange rates. However, the risk of exchange rates is relatively low, since the price is set up in U.S. dollars, which is stable in comparison with other currencies.

11. Financial Forecast and Funding Needs

For this project, at this stage, the main cost of investment is related to the patent, including application fee and maintenance fee and the final Field Testing for characterization and certification of the product; also, the time for patent application is also an implicit cost. The longer it takes, the longer time to market for our product.

11.1- Capex

Initially there will be expenses related with the purchase of assets, more specifically, equipment and the creation of conditions for production. The following table shows this items in detail:

The administrative expenses are related to the use of administration, which will be mainly related to the Responsible Researcher, Administrative and Sales person. This will be important in the coordination of efforts, communications and sales pitch.

Lab Material		Administrative Equipment	
Security closet	5,000 €	Pc/MAC	1,000 €
Material's closet	1,000 €	Smartphone	200 €
		Mesa+cadeira+estante	300 €
		Impressoras	300 €
		Desks	400 €
		Chairs (5)	300 €
		Total per person	2,500 €
		Total expense (3 people)	7,500 €

Closet for storing nanoparticles	5,000 €
Gloves	300 €
Lab coat	600 €
Masks	1,000 €
Other basic equipment	1,000 €
Clean Room	46,000 €
Total expense	59,900€

This refers to the basic equipment that is required to produce the nFluid. It is important to say that the clean room is the highest expense and it is also the most important to guarantee the safety of the staff and the immediate environment. This is also an expense that has to be done by a third party,

as it has to be certified and need specific conditions for preparation of the lab. This item also includes materials that will be used by staff, like masks, lab coat, as well as safety equipment.

The success of the company cannot only rely on one single product unless it continues to innovate it and find new applications if possible. The current project has been the result of research and development and the team of scientist responsible is integrated in the organization, for which they can evolve the current product to improve it and apply it to other applications that have been already been studied, like fluid for solar panels, cooling for machinery in production plants, etc.

Equipamentos R&D \ QC	
Homogenizador	4,000 €
Ultrasound bath	2,000 €
Viscometer	3,500 €
Water bath	4,500 €
pH meter	8 €
Hoods	8,000 €
Balance	2,000 €
Stove	10,000 €
Total expenses	34,008 €

Equipments Production	
Centrifuge (2x)	10,000 €
Ultrasonds	14,000 €
Hotte (2x)	15,000 €
Furnances	15,000 €
Tanks	5,000 €

Mixture tank	5,000 €
Vehicles	15,000 €
Total expense	79,000€

The equipment for production is composed of basic and essential equipment, that are more common across any lab or business. The car in the plan is proposed for the purpose of sales and representation, with the possibility of reducing this cost by working with dealerships and get a second hand car approved by them

11.2 Assumptions

The assumptions to work the finance are the following:

- **Sales are expected to growth** at a rate of 120% for the first year, 150% for the second year, 130% for the third year and 70% for the fifth year, as the product can be beneficial to drivers, especially professionals of driving. It is expected that the growth for the automotive industry will become more stable by year seventh or eighth of operations, but to continue in the double digits. This amount is not higher, due to the price it has, and it could become more if the partnership option is chosen, as establish players have better knowledge on where to allocate the product and which customers would be more interested.
- The **capital expenditure** is expected to occur according to the demand, as it will be related to production capacity.
- The **Cost of Goods Sold** is estimated to be 7.10 €/Liter based on experiences of the research team. However, this value can decrease up to 30% if production doubles, which can also improve the Income Statement. Based on this the price establish will be 15 €/Liter as explained before.
- The **inflation** expected is around 1% per year, which will affect the Cost of Goods Sold, and other operational costs, like salaries. The **salaries** considered for the seven team members required as a minimum to complement the skills of the current team.
- Expenses related to **R&D** are expected to be 2.5% of sales and **marketing** expenses 3% of sales, based on proxies' analysis. From similar analysis is expected that the receivables will be 13% of sales, payables 6% of sales and inventory 14% of sales.
- The **tax rate** considered was 26.5% for corporate tax and 23.75% for taxes related to staff and salaries.

The forecasted financial statements, based on these assumptions and projections are in the appendix 2

11.2 Investment required

After analyzing the financials and considering the macroeconomic factors it is expected that the most feasible way to raise capital is through equity, since commercial banks required many guarantees and when they supply with capital they do so at an elevated cost, practicing rates of up to 10%. This cost could jeopardize the performance of the company on an initial stage, limiting room for development and growth.

The amount that it will be required on an initial phase will include the capital expenditures and some of the operational expenses for the first years. Therefore it is estimated to be:

Description	Amount
+ Administrative Equipment	7,500 €
+ Lab Material	59,900 €
+ Equipamentos R&D \ QC	34,008 €
+ Equipments Production	79,000 €
+ Extra production capacity (9 production lines)	666,000 €
= TOTAL CAPEX	846,408 €
+ Expenses of development	600,000 €
+ Expenses associated with Patent	150,000 €
+ Capital for initial operations and unexpected expenses	368,000 €
= TOTAL CAPITAL	2,810,816 €


12. Team and Management Structure


The CARBOnFLUIDS team is composed by three researches, Bruno Abreu, Bruno Lamas and Maria Fonseca; two business managers Alberto Diniz and Zih-Siang, with the support of Armando Azevedo and Helder Freitas as Business Consultants. The individual curriculum of each members are in the Appendix 2

Regarding the research team, their experience in developing thermal-fluid is their field of expertise and they have been working on the development of this technology for more than four years, which provides the team a strong insight into this nanoparticle-based fluid technology. During this period the scientific part of team has published as significant amount of articles that resulted from their experience and research in this field.


On the other hand, the management team counts with experience from both professional work and academic development, especially, from MBA training and education. The team will complement their decision making in the business process with the insights from the Business Consultants to address weaknesses, such as lack of entrepreneurship experience and market's insight, in order to elaborate a better roadmap.

Bruno Abreu		
Academic	Doctorate in Mechanical Engineering Universidade de Aveiro – 2013	
	Degree and Master in Mechanical Engineering Universidade de Aveiro – 2010	
Professional Experience	Researcher - Universidade de Aveiro 2012 – Present	
Galp Energia 2010		
	Researcher - Universidade de Aveiro 2008 – 2009	

Maria Fonseca		
Academic	Doctorate in Physics Universidade de Aveiro – 2007	
	Degree in Physic Engineering Universidade de Aveiro – 2001	
Professional Experience	Researcher - Universidade de Aveiro 2001 – Present	
Teacher at ISDOM 2013 – Present		

Bruno Lamas		
Academic	Post-doctoral researcher Universidade de Aveiro – 2014	
	Doctorate in Mechanical Engineering Universidade de Aveiro – 2013	
Professional Experience	Energy efficiency researcher - Galp Energia 2009	
Researcher - Universidade de Aveiro 2011 – Present		
	Master of Science in Petroleum Engineering Heriot-Watt University 2014 - Present	

Alberto Diniz		
Academic	BSc (Hons) Business Management University of Hull (UK) - 2006	
	Master in Marketing Faculty of Economy of University of Porto - 2011	
Professional Experience	Masters Business Administration Porto Business School – 2014	
IMPA – Economistas e Consultores, Lda, 2006 – 2008		
	Bayswater, S.A. – Tourism Management 2009 – Present	

Zih-Siang		
Academic	Degree in Electrical and Computer Engineering National Taiwan University (TW) - 2011	
	Masters Business Administration Porto Business School – 2014	
Professional Experience	Academia Sinica – telecommunication research 2012 – 2013	

Bruno Abreu, Bruno Lamas and Maria Fonseca will continue developing the company's strategy with continuous support from the same consultants for clarifications and improvements on their business model (or others with similar characteristics). However, due to their current responsibilities and schedules, the team will be complemented with staff that will be hired. The professionals to employ are estimated to be seven, from either business, scientific or production background. The final team's configuration will be the following:

- **Staff type 1: R&D Researchers PhD** – One researchers with doctoral degree will give support and coordinate the proof of concept and also the research and development department. They will also support the consulting department.
- **Staff type 2: Researchers** – Two research engineer preferable with a chemical degree and with some research or industry experience will be hired. He will be supporting the PhDs in all the R&D activities and also in quality control.
- **Staff type 3: Production Engineer** – A engineer preferable with a mechanics or industrial managing degree will support all the production process and also in collaboration with the research engineering be responsible for the quality control department. He will also be responsible for the application of quality standards
- **Staff type 4: Manufacturing technician** – A technician to make and control all the machinery and process in the production department. He will be responsible for producing the products from their raw material form until the packing and expedition of the end product.
- **Staff type 5: Financial Controller/Administrative** – An employee with managing and accounting skills- He will be responsible with all the bureaucracy regarding accounting, paperwork and a secretary work.
- **Staff type 6: Sales & Marketing** – An employee with sales experience. He will be responsible for all the sales and also for defining the marketing plan for the products. He will also be responsible for establishing strategic relationships with future partners.

Once the existing team is complemented with the skills and capabilities of the new recruits, it is expected that better results will be achieved in both production and sales, as these are components that should be addressed to the operability of the company.

References

- [1] R. A. A.-C. E. American Society of Heating, *2009 ASHRAE Handbook*. American Society of Heating, 2009.
- [2] R. W. Miller, *Flow Measurement Engineering Handbook*. McGraw-Hill Education, 1996.
- [3] J. H. Williams, *Guide to the Expression of Uncertainty in Measurement (the GUM)*. IOP Publishing, 2016.